uOttawa

L'Université canadienne
Canada's university

FACULTÉ DES ÉTUDES SUPÉRIEURES ET POSTOCTORALES

uOttawa

L'Université canadienne
Canada's university

FACULTY OF GRADUATE AND POSDOCTORAL STUDIES

Jennifer Scott

AUTEUR DE LA THÈSE / AUTHOR OF THESIS

Ph.D. (Chemistry)

GRADE / DEGREE

Department of Chemistry

FACULTÉ, ÉCOLE, DÉPARTEMENT / FACULTY, SCHOOL, DEPARTMENT

Unanticipated Ability of the Bis-iminopyridine Ligand to Participate in the Reactivity of Transition Metal Complexes: Synthetic and Structural Investigations of Bis-iminopyridine-$FeCl_2$ and Related Complexes

TITRE DE LA THÈSE / TITLE OF THESIS

Sandor Gambarotta

DIRECTEUR (DIRECTRICE) DE LA THÈSE / THESIS SUPERVISOR

CO-DIRECTEUR (CO-DIRECTRICE) DE LA THÈSE / THESIS CO-SUPERVISOR

EXAMINATEURS (EXAMINATRICES) DE LA THÈSE / THESIS EXAMINERS

S. Berry

D. Richeson

P. Chirik

D. Fogg

Gary W. Slater

Le Doyen de la Faculté des études supérieures et postdoctorales / Dean of the Faculty of Graduate and Postdoctoral Studies

Unanticipated Ability of the Bis-iminopyridine Ligand to Participate in the Reactivity of Transition Metal Complexes: Synthetic and Structural Investigations of Bis-iminopyridine-$FeCl_2$ and Related Complexes

Jennifer L. Scott

Thesis submitted to the
Faculty of Graduate and Postdoctoral Studies
in partial fulfillment of the requirements for the degree of

Doctorate in Philosophy
in
Chemistry

Ottawa-Carleton Chemistry Institute
University of Ottawa

Candidate
Jennifer L. Scott

Supervisor
Professor Sandro Gambarotta

Your file Votre référence
ISBN: 978-0-494-34147-6
Our file Notre référence
ISBN: 978-0-494-34147-6

Abstract

The discovery by Brookhart and Gibson that late transition metals supported by diimine ligands could sustain high activity for ethylene polymerization deposed the long-standing practice of employing only early metal d^0 catalytic systems. This thesis focuses on our studies towards elucidation of the mechanism and determination of the nature of the active species responsible for the exceptional catalytic behaviour of the bis-iminopyridine-Fe derivative. Alkylation of the catalyst precursor in Chapter 2 with a bulky, stable alkyl has shown a pronounced ability of the ligand system to be involved in the reactivity of the metal center, resulting in numerous transformations to the ligand backbone, including alkylation of the pyridine ring and the imine-C atom, deprotonation of the ketimine methyl groups, and dimerization and reduction. In Chapter 3, alkylation of the catalyst precursor with a more reactive alkyl led to reduction of the system by two electrons, with the ligand system being the recipient of the additional electrons at the expense of the metal center. Unexpectedly, the reduced system is also active for ethylene polymerization, producing polymer with the same activity and polymer quality as the divalent precursor, suggesting that activation of the catalyst involves an initial two electron reduction of the system. Further studies in Chapter 4, exploring activation of the complex with aluminum alkyls, have observed reduction of the metal center and transmetallation of the reduced ligand from Fe to Al as a possible deactivation pathway.

The ability of the ligand to accept negative charge and assemble multi-nuclear structures leads to the proposed active species as a zwitterionic, cationic Fe alkyl.

Expanding the reactivity studies to complexes of Cr in Chapter 5 highlights increased catalytic activity upon reduction towards a pseudo-monovalent Cr complex. Once again, the ligand accepts the added electron density and this ability to host electrons in the π^* orbital appears to be the rationale behind the catalytic activity experienced by the later-metal systems.

Chapters 6 and 7 develop the reduction chemistry of bis-iminopyridine complexes of Fe and Cr respectively, revealing several dinitrogen complexes of Fe, and ultimately reduction and partial hydrogenation of a bridging Cr-N_2 complex towards complete cleavage of the N-N triple bond. Chapter 8 introduces two new Co-N_2 complexes and describes a spontaneous reductive coupling of the dianionic version of the ligand upon complexation to Co, forming a dimeric, double dinitrogen complex.

Incorporating the knowledge acquired in preceding chapters, two potential ligand scaffolds (dipyrroles and Schiff base pyrroles) were explored in Chapter 9 as supporting ligands for late metal polymerization catalysts. Although the results of catalytic testing remain preliminary, the pyrrole ligands continue to be of interest due to their ability to assemble heteropolymetallic clusters with potential for small molecule activation.

Expect the Unexpected.

Acknowledgements

When I began graduate work at the University of Ottawa, seemingly eons ago, I had absolutely no idea what I was getting myself into. Introductory words, upon my entrance to the lab, were, "Here's your fire extinguisher, welcome to the Gambarotta lab."

As this chapter of my life comes to an end, I have numerous people to thank for helping me get through relatively unscathed. First and foremost, I'd like to thank Sandro, my supervisor. He has always kept the door open and is always there to listen, bounce ideas off, and definitely never at a loss for new experiments to try; his sense of adventure is contagious! I'd like to thank him for all the opportunities he's given me and his constant faith in my ability to succeed. His encouragement, honesty and advice are very much appreciated.

Throughout the years and the cycles of labmates there has never been a dull moment and many of them have helped me along the way. However, there are three people I'd like to single out who have survived the majority of this time with me, including those frequent moments of temporary insanity. Indu has done so much for me and I can't thank her enough, particularly for her help and collaboration with this thesis. She constantly puts others before herself and her selfless nature and smiling face are an inspiration to all who have worked with her. She is also the best cook I've ever met and one of my best friends. I'd like to thank Ilia for all his amazing patience and all of his help, especially for solving most of the crystal structures in this thesis. He is the best teacher I've ever had and the Gambarotta lab would not have survived without him! And Pat, who is the best friend a person could ask for and I'm very thankful to have shared this experience with him. He taught me a lot about chemistry, but more about life and the importance of friendship. Even though I don't say it, I'll never forget our times together and I only hope there will be more in the future. Also, thanks to Elena for help with ligand synthesis. And to all the people I've had the pleasure of working with (Terri, Harminder, Claire, Davide, Athi, Hiro, Bala, Sougandi, Amir, Khalid, Indira, and all of the others) its been a blast!

Graduate school would not have been the same without all the fun times, courtesy of the CGSA and all of the friends I've met along the way: the Matts, the Marcs, the Joes,

the Pats; the Kathys, Ludi, Heather, Jay, Larisa, etc...I know there are more and I'm sorry if I haven't mentioned everyone! And of course, my running group: Nat, Pat and especially Gan, who stuck around the longest. Those were the best of times and I miss them all very much. I could not have done this without them.

And last, but definitely not least, I'd like to thank my family. They have been there, in the background, throughout the whole process with their encouragement. My parents have always been there for me and taught me that I could achieve whatever I wanted in life. I'd also like to thank my best friends and sisters, Kelly and Joanne. I'm very grateful for their entertaining phone calls and best wishes during my time in Ottawa; they make me feel like I haven't left home. But most importantly, I'd like to thank my husband Fred, who has probably had the most trying time of this thesis. Despite my moments, he showed faith and support for what I wanted to achieve. He is my rock and is always there to bring me back to the real world and focus on the important things in life. Thanks for understanding and believing in me.

List of Publications

(1) Vidyaratne, I.; Scott, J.; Gambarotta, S.; Budzelaar, P. H. M.; Korobkov, I. *Inorg. Chem.* ASAP.

(2) Vidyaratne, I.; Scott, J.; Gambarotta, S.; Korobkov, I.; Duchateau, R. R. J. *Organometallics* **2007**, *26*, 3201.

(3) Scott, J., Gambarotta, S., Korobkov, I., Knijnenburg, Q., de Bruin, B., Budzelaar, P. *J. Am. Chem. Soc.* **2005**, *127*, 17204-17206.

(4) Heiser, D. E., Pelascini, F., Kramer, D., Scott, J., Gambarotta, S., McCahill, J., Stephan, D. W., Okuda, J., Mulhaupt, R. *Macromol. Symp. 2006, 236*, 156-160.

(5) Scott, J., Gambarotta, S., Korobkov, I., Budzelaar, P. *Organometallics* **2005**, *24*, 6298-6300.

(6) Scott, J., Gambarotta, S., Korobkov, I., Budzelaar, P. *J. Am. Chem. Soc.* **2005**, *127*, 13019-13029.

(7) Scott, J., Gambarotta, S., Korobkov, I. *Can. J. Chem.* **2005**, *83*, 279-285. (special issue dedicated to Dinitrogen Chemistry)

(8) Gambarotta, S., Scott, J. *Angew. Chem. Int. Ed. Eng.* **2004**, *43*, 5298-5308.

(9) Scott, J., Gambarotta, S., Yap, G., Rancourt, D. G. *Organometallics* **2003**, *22*, 2325-2330.

Table of Contents

List of Common Abbreviations

acac	acetylacetonate
Ar	aromatic group (in all cases, Ar = 2,6-$^{i}Pr_2C_6H_3$)
Bz	benzyl
Cp	cyclopentadienyl, C_5H_5
Et	ethyl
Et_2O	ether
GPC	gel permeation chromatogram
HS	high spin
^{i}Bu	isobutyl
^{i}Pr	isopropyl
IR	infrared
IS	intermediate spin
L	ligand (in all cases, L = 2,6-[2,6-(^{i}Pr)$_2$PhN=C(CH_3)]$_2$(C_5H_3N))
LA	Lewis acid
LS	low spin
M	metal atom
MAO	methylaluminoxane
Me	methyl
Mw	molecular weight
nacnac	β-diketiminate
NMR	nuclear magnetic resonance
PE	polyethylene
Ph	phenyl
R	alkyl group
THF	tetrahydrofuran
TIP	temperature independent paramagnetism
TMA	trimethylaluminum
TMS	tetramethylsilane
X	halogen

List of Figures

List of Tables

Chapter One

Introduction

Polyethylene: A Brief History of its Discovery[1]

Occasions of serendipity are particularly abundant when it comes to scientific research. Louis Pasteur expressed this idea fittingly when he stated "where observation is concerned, chance favours only the prepared mind".[1e] The history of polyethylene (PE) is no exception, given that most of the major breakthroughs have transpired through unforeseen events. Were it not for the instincts and inquisitiveness of the early polyethylene pioneers, the world could be a very different place today.

Polyethylene made its debut in 1898 in the lab of the German chemist Hans von Pechmann, naively christened polymethylene after the repeating $-CH_2-$ units. Colleagues Eugen Bamberger and Friedrich Tschirner isolated the white, waxy substance while heating diazomethane.[1] However, as the saying goes, necessity drives invention and the need for a synthetic polymer was not great enough at the turn of the century to warrant further study. Thus, full appreciation of polyethylene was postponed 35 years until its second, entirely coincidental, discovery.

The year was 1933 and Britain's ICI (Imperial Chemical Industries) was undertaking widespread research into high pressure reactions intended for the dyestuffs industry. The reaction between benzaldehyde and ethylene at 1700 atm yielded an unexpected sample of polyethylene (after having accidentally been left over the weekend). Realizing the potential of such a material, discoverers Eric Fawcett and

Reginald Gibson undertook numerous attempts to reproduce the reaction, unluckily resulting in an explosion and subsequent fire due to a burst pressure joint near the oil thermostat. Due to the dangerous nature of the high pressure reactions, ICI management immediately cancelled all high pressure research until the advent of safer apparatuses.

In 1935, armed with the latest in high pressure equipment, Micheal Perrin of ICI revived the polyethylene research. Withdrawing to an isolated building (incidentally with thicker walls) a whopping 8g of polyethylene was produced on their first attempt. Numerous subsequent efforts, however, yielded less than satisfactory results, demonstrating once again the poor reproducibility of this chemistry. Approximately 200 reactions later, it was discovered that trace amounts of oxygen present in the ethylene feed were needed to initiate the radical polymerization process, forming large amounts of branched (or low density) polyethylene (LDPE). Commercial production of LDPE began in 1939, the year Germany launched their attack on Poland, marking the beginning of World War II. The timing could not have been more fortuitous, for LDPE proved extremely important as an insulator in air and ship borne radar cables, technology that ultimately enabled the triumph of Britain in the Battle of the Atlantic.[1]

Chance prevailed yet again with the discovery of high density polyethylene (HDPE). Unlike the soft, limited-use LDPE, HDPE was much stiffer, stronger and heat resistant, thereby drastically increasing the number of potential applications. In 1951, Hogan and Banks at Phillips Petroleum unintentionally invented the first low-pressure method for the linear polymerization of ethylene over a Cr-oxide supported catalyst.[2] Roughly two years later, Karl Ziegler, a non-polymer chemist, published the equally exciting formation of HDPE with a completely different low-pressure catalytic system based on titanium-halides and aluminum alkyls, a discovery that would earn him the 1963 Nobel Prize in Chemistry (shared with Giulio Natta).[3]

The simultaneous discoveries of the Phillips and Ziegler catalysts led to the commercialization of both processes by the end of the 1950's. Although Ziegler's catalyst required much lower pressures of ethylene, the Phillip's Cr catalyst was much cheaper, thereby superseding the need for more specialized equipment. Regrettably, the new plastics were plagued by problems of cracking and softness, leading to the manufacture of a plethora of useless, off-specific plastic. The growing mass of squandered polymer

threatened the extinction of numerous chemical companies. Salvation came in the form of a plastic hoop approximately one meter in diameter: the hula-hoop. Wham-O Toy Company bought the dejected polymer, saving the companies from bankruptcy and enabling research to progress towards the development of improved polymers and catalyst systems.[1]

The breakthroughs depicted herein highlight the fortuitous induction of polyethylene to the world. As Louis Pasteur said, "chance favours the prepared mind". This could not be truer of the intuition, curiosity and determination displayed by chemists in the development of ethylene polymerization.

Ziegler-Natta Polymerization of Ethylene

At the time of the discovery of his catalytic system, Karl Zielger was director of the Kaiser Wilhelm (later Max Planck) Institute for Coal Research at Mülheim an der Ruhr, presumably conducting research in an unrelated field. An organic chemist at heart, however, he found it much more appealing to study the organic chemistry of aluminum alkyls. Prior to the historic discovery, he and his student, Erhard Holzkamp, were attempting the preparation of higher aluminum alkyls by heating triethylaluminum in the presence of ethylene when they inadvertently isolated butene.[1] Realizing the importance of this outcome, an intensive investigation ensued, eventually recognizing the presence of trace colloidal Ni in the reactor as the perpetrator. Prompted by these results, the chemistry of organoaluminum compounds with various transition metal salts was developed, displaying facile polymerization of ethylene to linear polymers at atmospheric pressure. Of the reactions tested, the system produced by the reaction of aluminum alkyls with titanium tetrachloride proved the most valuable. Consequently, a whole new area of research was established, encouraging many others to explore the chemistry of organometallic compounds in catalysis and shaping the direction of polymerization research for years to come.[4]

Despite the onslaught of research, attempts to discern mechanistic details of the polymerization were plagued by the heterogeneous nature of the catalytic system. The most accepted proposal that emerged was suggested by Cossee and Arlman.[5] It was proposed that upon combining the titanium halide and the aluminum alkyl in diesel oil or

petrol, the $TiCl_4$ becomes reduced to $TiCl_3$, which precipitates out as α-$TiCl_3$ crystallites. $TiCl_3$ on the surface of the particles reacts with the aluminum alkyls to generate easily accessible Ti-C bonds through halide exchange. The presence of a vacant site on the exposed Ti center encourages approach and side-on π-bonding of an ethylene monomer. The proximity of the Ti-C bond to the activated ethylene molecule facilitates insertion of the monomer into the metal-alkyl bond via a cyclic transition state, thereby lengthening the alkyl group by two carbon units and regenerating the adjacent vacant site. Repeated coordination and insertion of ethylene into the growing polymer chain constitutes the chain propagation mechanism suggested by Cossee and Arlman, shown in Scheme 1.1.[5] Various available chain termination pathways will be discussed in a subsequent section of the introduction.

Scheme 1.1

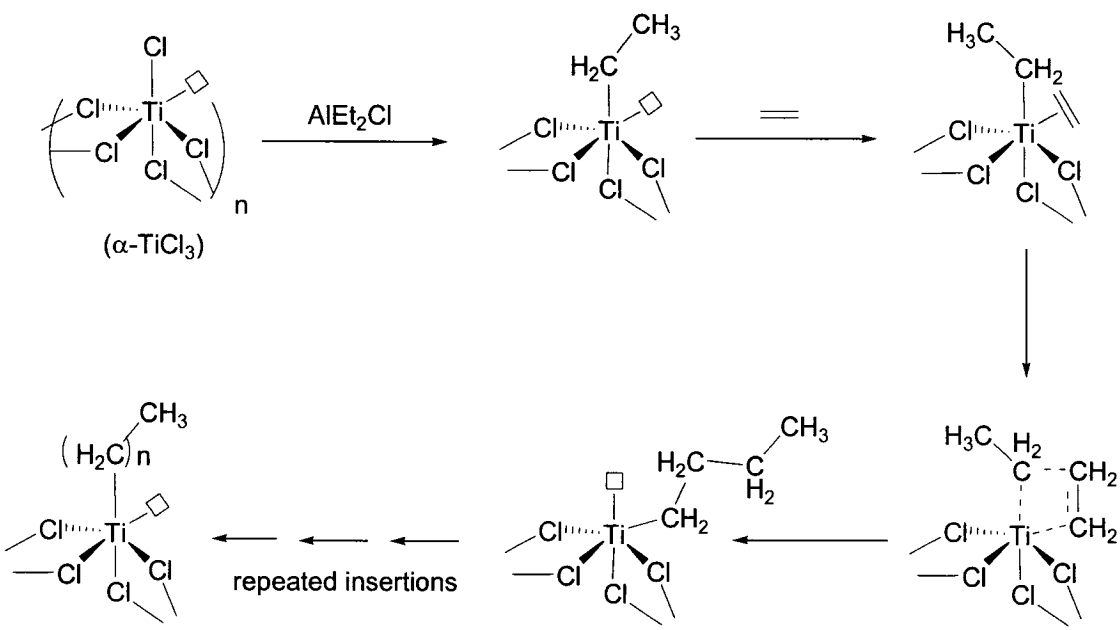

Homogeneous Single-Site Catalysts for Ethylene Polymerization

Although of historical and commercial significance, the catalytic system discovered by Ziegler was not without fault. The resulting polymer was consistently beset with wide molecular weight distributions, perhaps due to the participation of more than

one catalytic species throughout the polymerization. Hence came a very important stage in the evolution of PE; the introduction of homogeneous, single-site catalysts.[4] These species were discrete chemical compounds with nearly identical catalytic behaviour and promoted greater control over the resulting molecular weight distributions. The first complexes emerged in 1957 by Breslow, Newburg and Natta.[6] Their titanocene Cp_2TiCl_2/AlR_2Cl system afforded polymers with a more distinct structure not obtainable using Ziegler's heterogeneous system. Although the activities were much too low to be of commercial significance, the distinct, homogeneous nature of the catalysts furnished a greater opportunity for studying the polymerization process.

Research in ethylene polymerization has since focused on two main areas: 1) studies aimed at determining the mechanism of olefin polymerization by transition metal catalysts, and 2) exploiting the newly gained knowledge towards the design of new and improved catalytic systems. Subsequent studies by numerous groups have since contributed significantly to our knowledge of cocatalyst function, generation of the active species and the mechanism of olefin insertion.[4]

Mechanism of Ethylene Polymerization

The isolation of discrete cationic metal alkyls proved extremely important for the development of the mechanism of polymerization. By studying the reactivity of the cationic metal alkyls with H_2 and olefins, valuable insights into chain initiation, propagation and termination were obtained. Compiling the research in olefin polymerization to date, a generally accepted mechanism can be described for the activation of the catalyst and insertion and polymerization of the monomer.[4] Scheme 1.2 displays the activation of a typical Group 4 metallocene catalyst with an aluminum alkyl and the ensuing polymerization of ethylene. The sequence of events upon addition of activator is most likely chloride abstraction and subsequent alkylation of the metal center, followed by cationization with AlR_3 to produce a cationic metal alkyl 'active' species. This species can either be present as a contact ion pair or a solvent-separated ion pair. The contact ion pair is regarded as the dormant state, in which the co-catalyst is actually bonded to the catalyst through an alkyl bridge. The solvent-separated ion pair, on the other hand, is the catalytically active species, in which the cationic active metal center

and the anionic co-catalyst are completely separated, opening a vacant site on the metal center. An equilibrium exists between the two states in the catalyst system.[4,7]

Scheme 1.2

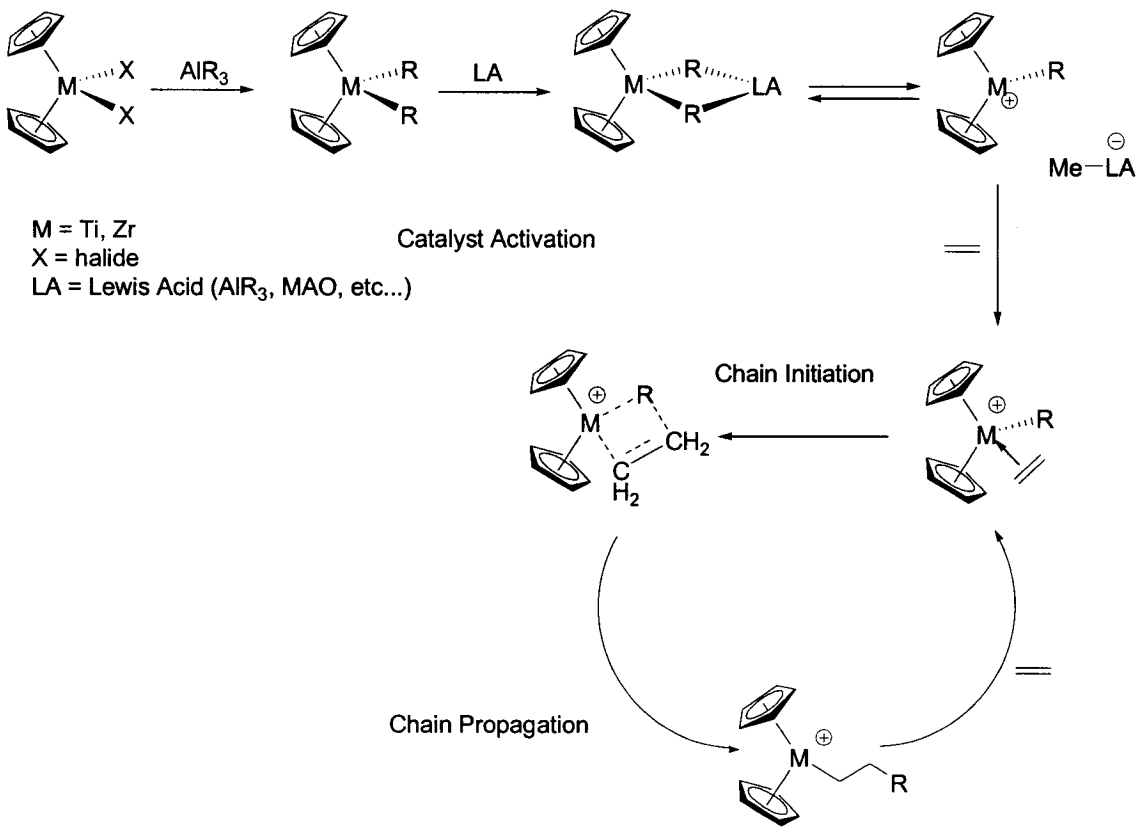

Cationization of the metal center enhances the Lewis acidity of the electron deficient d^0 metal center and encourages approach and side-on coordination of the ethylene molecule to the newly-vacant coordination site. The position of the activated monomer adjacent to the M-C bond supports the formation of a four-membered cyclic transition state, promoting insertion of the olefin into the M-C bond. From here, polymerization proceeds via subsequent cycles of fixation and insertion of the ethylene monomer into the growing alkyl chain.[4] The length and final structure of the resulting polymer depend on the catalyst system and cannot be predicted.

A cationic metal alkyl active species was suggested as early as 1961 by Shilov;[8] an idea that was supported by the electrochemical studies of Dyachkovskii describing

ethylene insertion at a cationic metal alkyl center.[9] Eisch, however, was the first to structurally characterize the insertion product from the reaction of $Cp_2TiCl_2/AlMeCl_2$ with $Me_3SiC{\equiv}CC_6H_5$ in 1985.[10] Nevertheless, a structurally characterized cationic metal alkyl had never been isolated to support these claims.

Expanding research beyond aluminum-based co-catalysts, Jordan *et al.* were the first to isolate and structurally characterize a cationic metal alkyl species from the reaction of Cp_2ZrMe_2 with an equimolar amount of $AgB(C_6H_5)_4$.[11] Fascinatingly, polymerization proceeded upon addition of ethylene and in the absence of added co-catalyst, substantiating the identity of the active species as a coordinatively unsaturated cationic metal alkyl. It is therefore understood that the main role of the aluminum co-catalyst in the homogeneous metallocene system is ultimately that of promoting the formation of a cationic metal alkyl.[4]

The Role of the Activator

Initially, various Lewis acidic aluminum alkyls, or aluminum alkyl halides, were employed as activators in homogeneous metallocene catalytic systems. Despite improving the quality of the polymer and also the understanding of the polymerization mechanism, the activity of these systems remained too poor to be considered for commercial applications. The main role of the co-catalyst is the generation of the active species via alkylation and abstraction of a halide or alkyl from the metal center to give a coordinatively unsaturated cationic metal alkyl. Besides the use of aluminum alkyls to afford the active species, other methods of cationic metal alkyl formation were discovered, such as abstracting a methyl group from an already alkylated metal center via protonation with $[HNR_3][B(C_6H_5)_4]$[4,12] or via reaction with a strong Lewis acid like $B(C_6F_5)_3$[13] or a trityl borate salt, $[(C_6H_5)_3C][B(C_6F_5)_4]$.[14] In each of these cases, the presence of a large anionic borate unit promotes formation of a solvent-separated ion pair and the presence of a vacant site adjacent to the M-C bond.

The success and consequent enthusiasm generated by the use of these and other Lewis acids galvanized research in homogeneous metallocene catalysis. The culmination was reached with the completely coincidental discovery of MAO. Upon the accidental addition of water to $Cp_2TiEtCl/AlEtCl_2$, Reichert and Meyer noticed a considerable

enhancement of the rate of ethylene polymerization.[15] Similar effects were noticed by Long and Breslow in the comparable system, $Cp_2TiCl_2/AlMe_2Cl$.[16] The extraordinary results were attributed to the formation of dimeric aluminoxane, ClMeAl-O-AlMeCl, which is expected to be a stronger Lewis acid than $AlMe_2Cl$ and therefore a more efficient activator. In 1980, Kaminski and Sinn performed the controlled addition of H_2O to the otherwise-inactive halogen-free $Cp_2ZrMe_2/AlMe_3$ system, achieving the highest levels of catalytic activity ever seen for ethylene polymerization (increased by orders of magnitude compared to the original system).[17] These results led to the discovery of the highly efficient activator methyl aluminoxane (MAO). The MAO-activated systems offered higher productivities and polymer with narrower polydispersities, translating to lower costs and cleaner polymer and making MAO the preferred catalyst activator to this day.[4]

Although the use of MAO as a cocatalyst has become ubiquitous, the poorly characterized structure of MAO complicates mechanistic studies and makes determination of the active species much more difficult.[18] It is believed to be composed of –MeAlO- units in a polymeric array, with variable amounts of free $AlMe_3$. Similarities to other aluminum activators allow alkylation of the metal centers, and the Lewis acidic properties of MAO encourage halide or alkyl abstraction from the metal center to create a vacant site. It is believed that the extended structure of the anionic MAO helps it to remain separated from the metal center, maintaining the cationic nature of the active species with consequent increased activity of polymerization.[18] Unfortunately, large amounts of MAO are generally necessary to activate the catalysts (1000-15000 equivalents), which is a severe drawback in terms of financial considerations. On the positive side, MAO is an excellent scavenger of water, the presence of which in trace amounts could abate or even destroy the catalyst.[18]

Chain Termination Pathways

The growth of the polymer chain can be interrupted on the metal center in a number of ways (Scheme 1.3). The most common chain termination pathway involves β-hydride transfer (or elimination) from the polymer chain to either the coordinated monomer or the metal center.[19] In recent years, another mechanism has been observed in

some early and late metal systems, in which the growing chain is transferred to the Al center of the cocatalyst, termed chain transfer to aluminum.[19a,20-22] This pathway could either be the sole termination pathway at play, or may occur in combination with β-H transfer. In each case, the active metal catalyst is regenerated after elimination of the polymer chain.

Scheme 1.3

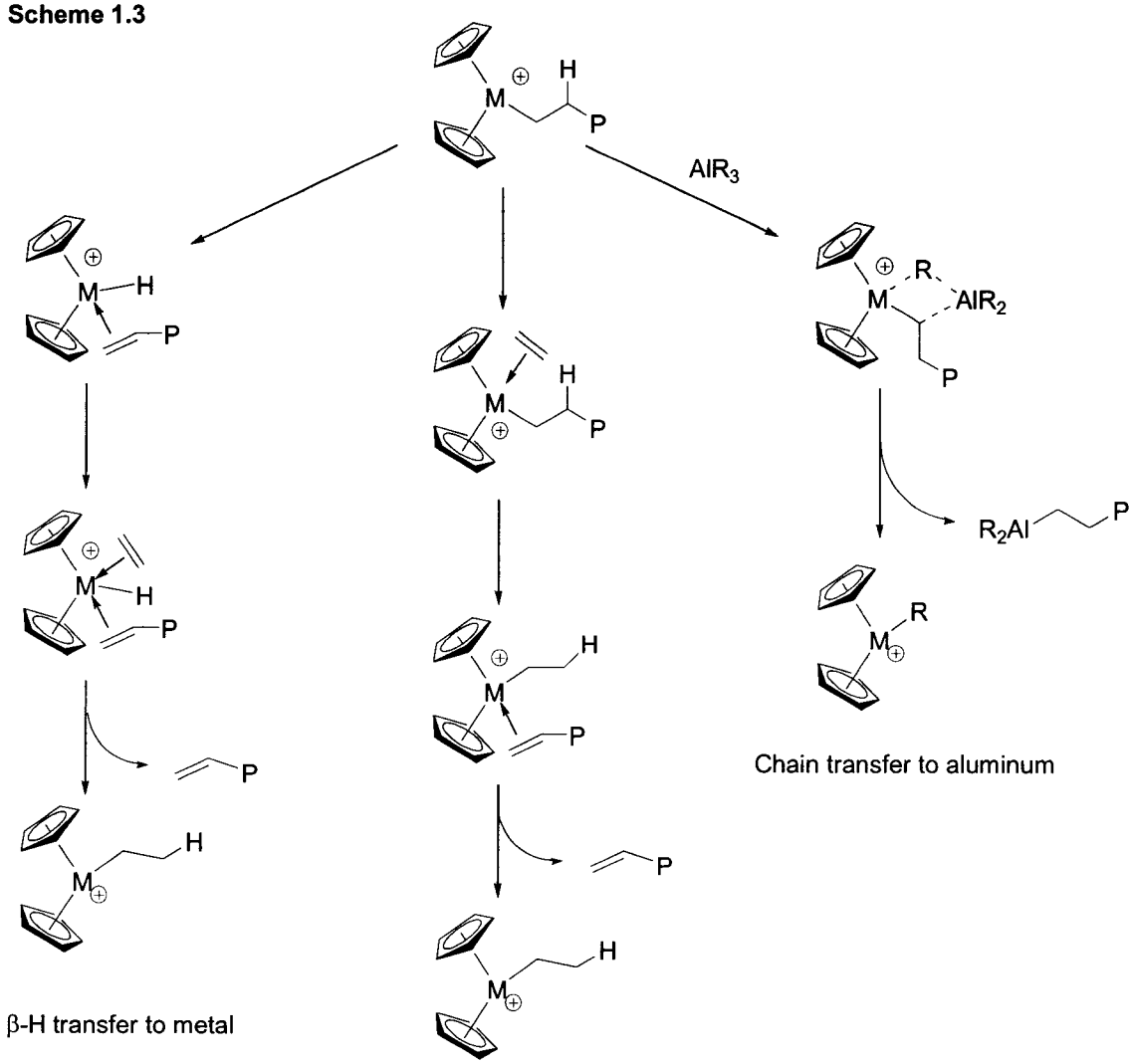

The resulting polymer chain is characterized according to its length, nature of the end groups and the amount of branching, and these characteristics are the result of the relative rates of chain propagation, termination and branching throughout the

polymerization.[4] Chain termination is an important factor when it comes to the microstructure of the resulting polymer. The appearance of the end-groups in the resultant polymer is an indication of the mechanism, being either fully saturated for chain transfer to Al or 50% olefinic for β-hydride elimination.

Design of New Catalysts

Over the years, single-site catalysis research has progressed through modifications to the ligand environment, increasing our understanding of the polymerization mechanisms while maintaining a high level of catalytic activity.[4] Chart 1.1 highlights a handful of the interesting systems to emerge during the evolution of single-site catalyst research. The first major adaptation of the cyclopentadienyl ligand environment was the installation of a bridging atom between two Cp rings (either Si or C, displayed by complex **1.1**).[23] These new ligands, termed ansa-metallocenes, infused important stereochemical control to the resulting polymer structure when employing racemic versions of the ligand (mainly important for stereospecific propylene polymerization).[24] The 1980's saw the emergence of the next generation of Ziegler-Natta catalysts, labeled as non-metallocenes and yet based on the presence of one Cp ring, incorporating alkoxy or amido cyclopentadienyl systems (complex **1.2**).[25] Bercaw *et al.* were the first to introduce the dialkylsilyl-bridged-alkylimido Cp ligands, or constrained geometry ligands, forcing the angle of the bidentate ligand to be less than 115°.[25a] The rationale behind the geometry constraints was based on the more open nature of the metal center for increased monomer incorporation. Under the technological name "INSITE" (DOW), new families of ethylene-olefin copolymers emerged, characterized by narrow polydispersities and long chain branching.[25bc]

Chart 1.1

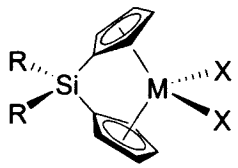

1.1

M = Ti, Zr
X = CH_3, Cl, Br
R = CH_3, C_2H_5, n-C_3H_7
Ref. 23

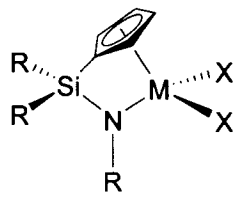

1.2

M = Ti, Zr
Ref. 25bc

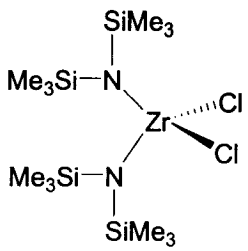

1.3

Ref. 26

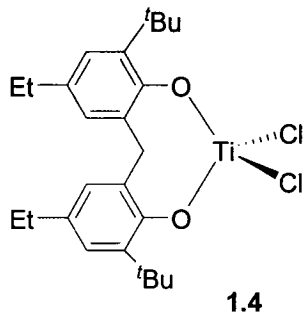

1.4

Ref. 27

The next evolution in ligand design was initiated following the observation that non-Cp complexes, such as simple bis-amido-Zr (**1.3** in Chart 1.1), could also polymerize ethylene in the presence of MAO with competitive activity and producing excellent polymers.[26] Soon after, Schaverien introduced Ti chelating-phenoxide complexes as catalysts for ethylene and propylene polymerization (**1.4**)[27] and several other groups followed suit.[28] These findings marked the new era of the so-called non-Cp, or alternative, Ziegler-Natta catalysts. The main issues surrounding this research were of course the appropriate selection of donor atoms, the fine tuning of steric hindrance, the influence of ligand architecture on polymer quality and catalyst activity, among other characteristics. The rejuvenated enthusiasm and consequent flourishing activity led to the discovery of a large variety of diversified systems and numerous reviews have been published on the subject.[4]

Late Transition Metals as Olefin Polymerization Precatalysts

The use of first row late transition metal complexes as catalysts for olefin polymerization is an interesting alternative to the ubiquitous presence of group 4 systems described previously. Cheaper, and in some cases more environmentally benign (Fe), late metal systems assemble a new set of characteristics that contrast to the previously-established prerequisites for a successful catalyst system. The successful use of late metals[21,29-31] for classical cationic Ziegler-Natta catalysis has broken the paradigm in this field requiring early metals in high oxidation states sporting high Lewis acidity. Unlike the electrophilic d^0 metals, late metals carry more electron density in proximity to the core, presumably diminishing the attraction of the weakly basic ethylene molecule. In addition, the lability of the metal-alkyl bond among late metals makes their catalysts more susceptible to β-H elimination.

Prior to the mid-nineties, only a few examples of late transition metal catalysts existed. Nonetheless, their vulnerability towards β-H elimination made them an attractive option for ethylene oligomerization. For example, Shell had already been exploiting a Ni oligomerization catalyst (shown as complex **1.5** in Chart 1.2) for years in the Shell Higher Olefins Process (SHOP).[29] In 1992, a cationic Co(III) complex was described which unconventionally polymerized ethylene to high molecular weight, low polydispersity polymers, albeit with low activities (**1.6**).[30] A huge evolutionary leap occurred in the mid-90's with the discovery of a family of late transition metal systems as active catalysts for ethylene polymerization (Chart 1.2). Johnson, Killian and Brookhart introduced diimine complexes of Group 10 (**1.7**)[31] that became the first examples of late transition metals able to polymerize ethylene and higher olefins to high molecular weight polymers with increased activities. The long established paradigm assigning solely electron deficient early metals to polymerize olefins had been challenged, initiating the study of more late metal imino systems. The largest, most important discovery was pioneered simultaneously by the groups of Brookhart and Gibson.[21] Separately, the first ever Fe based ethylene polymerization system was published, supported by a bis-iminopyridine ligand backbone (**1.8**), producing highly linear, high molecular weight polymers with activities that rivaled those of the metallocenes. This breakthrough propelled research towards understanding the unique abilities of this system to sustain

catalytic activity at a late metal center and spurred the development of other transition metal systems based on this ligand.

Chart 1.2

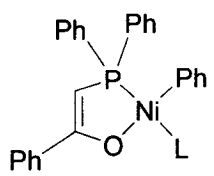

1.5

$L = PPh_3$, C_5H_5N
Ref. 29

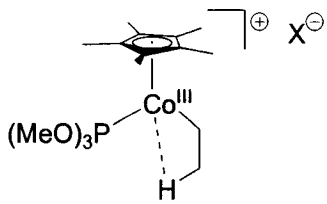

1.6

$X = BF_4$, $B[3,5\text{-}(CF_3)_2C_6H2]_4$
Ref. 30

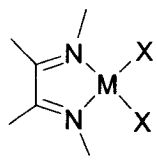

1.7

M = Ni, Pd
X = Cl, Br
Ref. 31

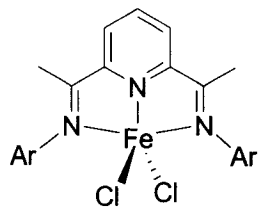

1.8

Ar = 2,6-$^{i}Pr_2C_6H_3$
Ref. 21

Although the bis-iminopyridine ligand had been known for some time in traditional coordination chemistry,[32] its popularity as a supporting ligand for late transition metal olefin polymerization catalysts was rejuvenated by the Brookhart and Gibson discoveries.[21] When bound to late transition metals (Fe, Co) the resulting complexes were capable of a high level of catalytic activity and the resulting polymers were high molecular weight and very linear in nature. In particular, the Fe-derivative portrayed the highest level of catalytic activity for ethylene polymerization when activated with MAO, ranging from 600 to 20,600 g/mmol·h·atm, and produced high molecular weight polymers (148,000 – 611,000). The analogous Co system displayed activities approximately an order of magnitude less than the Fe system and achieved lower molecular weight polymers (14,000 – 257,000). The perspectives for commercialization introduced by these results were particularly attractive since they offered a cheaper and more environmentally friendly option (Fe) for the polyolefins industry. The anticipated onslaught of research into these and other transition metal analogues opened a Pandora's Box of ligand transformations *(vide infra)* and ultimately engendered more questions than previously imagined pertaining to the role assumed by the ligand and the mechanism operating during the polymerization.

The Bis-iminopyridine Ligand

Central to the findings described above was the utilization of a simple ligand, a neutral tridentate Schiff base, buried and forgotten in the ancient coordination chemistry of late metals.[32] The synthesis of the ligand is a relatively straight-forward acid-catalyzed condensation between the corresponding aniline and diacetyl pyridine (Scheme 1.4).[21] An excess of aniline is used to ensure complete conversion to the desired product, as is often the case in Schiff base syntheses.

Scheme 1.4

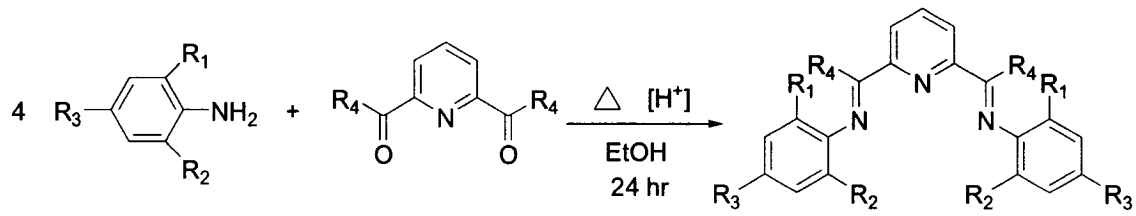

The ligand was regarded as particularly promising and, as shown in the following chapters, has attracted considerable interest in the literature. In fact, there are several important characteristics of the ligand system with respect to steric and electronic effects that were expected to lead to increased control during ethylene polymerization. The use of three strong N-donor atoms ensures tridentate meridional coordination of the ligand to the metal center with the aryl groups on the imine function situated perpendicular to the planar backbone formed by the pyridine ring and the imino groups. The presence of substituents in the *ortho*-positions of the aryl rings instills flexibility with respect to steric bulk and protection of the active metal center. Larger substituents can hinder rotation of the aryl ring about the N-C bond, in turn introducing added stabilization at the metal center. Other possibilities involve altering the group attached to the imino-C atom. The most popular arrangement involves a methyl group, but the aldimine version has also been synthesized,[21,22] as well as other derivatives containing larger groups like phenyls[33] or even heteroatom substituents.[33bc,34]

From an electronic perspective, the ligand has several advantages. Not only can the presence of electron withdrawing or donating groups on the imino-aryl rings or the pyridine ring introduce a degree of electronic control, but the presence of a planar

conjugated backbone with low lying π* orbitals may also confer interesting electronic properties to the systems.[35]

Coordination of the ligand to the metal center occurs without difficulty, resulting in a pentacoordinate, square pyramidal metal center retaining two chlorine ligands (the differences between the Fe and Co structures are minor). Scheme 1.5 shows an example of the possible complexes.

Scheme 1.5

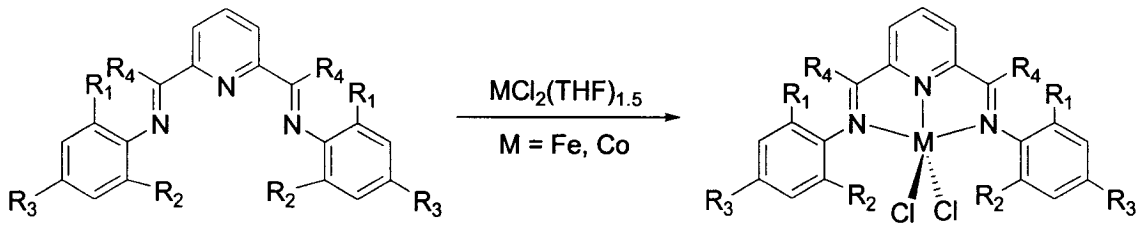

Ethylene Polymerization by Bis-iminopyridine Fe and Co complexes

The first results published by Brookhart and Gibson concerning the polymerization of ethylene by the Fe and Co systems involved a standard polymerization study.[21,22] The sample system chosen for discussion is shown in Scheme 1.5, where R_1 = R_2 = ^{i}Pr, R_3 = H and R_4 = Me[a] and the conditions employed during the testing include the use of toluene as a solvent, 500 equivalents of MAO as the cocatalyst, room temperature, 1 bar ethylene pressure and a reaction time of 30 minutes. Variations to the reaction conditions will be discussed later in the text.

Upon addition of MAO and ethylene to the solution of catalyst in toluene, an immediate exotherm was observed, highlighting a lack of induction period. The activity of the catalyst peaks near the onset of polymerization, decreasing with time to a final value only 10-20% of the initial activity. These particular observations appear to be standard for all conditions and modifications to the ligand backbone. Under the conditions outlined above, the Fe system achieves an activity of approximately 650 g/mmol·h·atm, compared to the Co analogue activity of 450 g/mmol·h·atm. Both systems

[a] Throughout the remainder of the thesis, the abbreviation 'Ar' will refer to an aryl ring containing these substituents [Ar = 2,6-^{i}Pr$_2$C$_6$H$_3$].

produce highly linear polyethylene. A GPC of the polymer indicates a difference between the two metal systems. The polymer obtained by the Fe precatalyst displays a bimodal distribution of the molecular weight (peaks at ~3,000 and 46,000, shown in Figure 1.1), whereas the cobalt precatalyst produces polymer with a single molecular weight peak centered at 14,000. The polydispersity index is large for both samples; however, when taken separately, the lower molecular weight fraction of the Fe polymer has an individually smaller PDI compared to the higher molecular weight fraction.

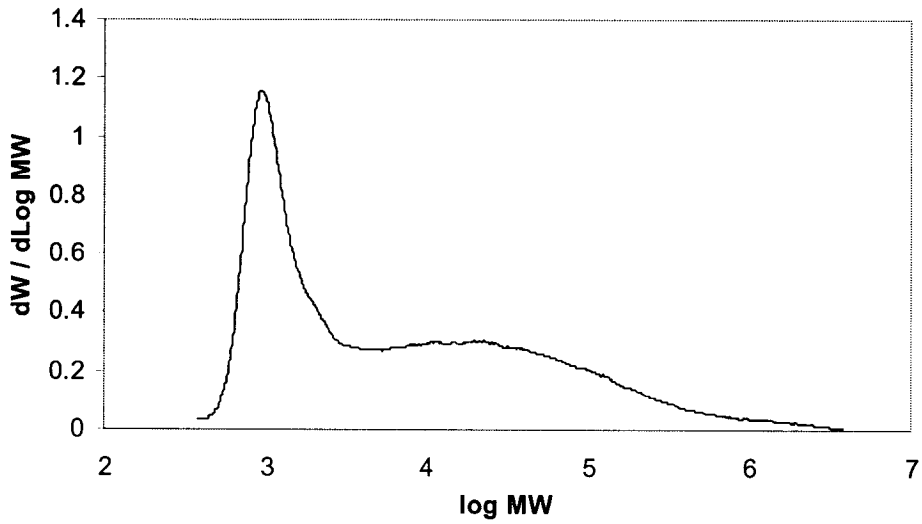

Figure 1.1: Gel permeation chromatogram of polymer from $LFeCl_2$/MAO

End group analysis is an important technique for determining the mechanism of chain termination operating during the catalytic cycle.[36] Comparing the polymer samples obtained from the separate metal centers highlights a distinct difference in the preferred chain termination pathway followed by each metal system.[22] Even within the Fe system, two different polymer samples are obtained and can be separated by Soxlet extraction. End-group analysis of the single polymer sample produced by Co reveals a 1:1 ratio of vinyl to saturated ends, indicative of chain termination via β-H transfer to monomer or metal. Similar observations can be made on the high molecular weight fraction from the Fe system. On the other hand, the low molecular weight fraction is almost exclusively

composed of fully saturated ends, a positive consequence of chain termination via chain transfer to aluminum. The bimodal nature of the Fe polymer may either be the result of two separate active centers during catalysis, or a change in the active center with time. Indeed, the ratio of the fractions does change over time.[22] Early in the polymerization, the lower molecular weight fraction is the main termination mechanism. As time progresses, the number of aluminum species available for chain transfer decreases, resulting in a subsequent decrease in the rate of chain transfer to aluminum. On the other hand, the rate of β-H transfer remains the same throughout the run. Therefore, after a longer reaction time, the amount of high molecular weight polymer is larger. Embedding of the catalytic Fe center in the polymer after a prolonged catalytic run may also explain the change in molecular weight distribution over time, making transfer of the growing chain to an aluminum center more difficult.

Regardless of the structural similarities between the Fe and Co precatalysts, the difference in catalytic activities and resulting polymer indicate that the Fe and Co systems follow different chain termination pathways, suggesting the formation of different active species in each case. In addition, the Fe precatalyst engages in more than one chain termination pathway and therefore may also involve the formation of two separate active species.

Modifications to the Catalytic System

Over the course of catalytic testing of these remarkable catalytic systems, several trends were observed upon adjusting variables such as ligand substituents, type and concentration of co-catalyst, pressure of ethylene and temperature of the system.[22] Not only were the activities of the catalyst affected, but the nature of the resulting polymer was also influenced by subtle changes to the system, including molecular weight, molecular weight distribution and end-group ratios, while still maintaining a high degree of linearity. Alterations to the electronics and sterics of the ligand system play a large role with respect to the isolated products.

The most obvious steric modification introduced into these systems consists of variations in the *ortho*-groups on the aryl rings. Many exploratory studies have been undertaken in this direction and reveal that a decrease of the steric bulk leads to an

increase in the activity of the catalyst, as well as to a decrease in the molecular weight of the polymer, to the extent of obtaining oligomers in the absence of *ortho*-groups ($R^2 = R^3 = H$).[37] Increasing steric bulk with the presence of a cyclopentyl group in the *ortho*-position actually stabilizes the system even more, retaining more activity at higher temperatures.[38] The presence of only one bulky *ortho*-substituent per aryl ring also results in oligomerization.[39] Interestingly, the use of an asymmetric ligand, in which one aryl group has steric bulk (in the form of ^{i}Pr groups) and the other bears no substituents, also results in oligomerization, whereas an increase of the sterics by addition of two *ortho*-methyl groups to the unsubstituted aryl ring results in polymerization. However, making the second aryl group asymmetric by incorporating only one *ortho*-methyl group produces polymers and oligomers simultaneously.[40] Complete removal of one imine function by condensing only one side of the diacetyl pyridine also gives catalysts for the oligomerization of ethylene.[41] The combination of these results indicate that the active center is stabilized by the presence of steric bulk in the *ortho*-positions, in turn hindering the process of chain transfer and therefore achieving higher molecular weight of the polymer. On the other hand, decreased steric bulk increases the activity of the catalyst, opening up the active center and increasing the rate of chain propagation as well as chain termination.

Although the substituent on the imino function has no direct effect on the metal center, a combination of electronic and steric factors may still be found when altering the group. In going from a ketimine (R_4 = Me) to an aldimine (R_4 = H) a large decrease in reactivity, as well as molecular weight, is observed.[22] The differences could be related to the freedom of rotation of the aryl ring. Therefore, the rate of propagation is decreased more than the rate of termination.

In an interesting study, Gibson *et al.* incorporated a heteroatom imino substituent, R_4 = XR, onto the Fe system.[34] When X = O and R = Me, the catalyst was inactive under the normal conditions. This result was explained by assuming reversible binding of the Lewis acid cocatalyst to the oxygen atom, somehow resulting in catalyst destabilization. In changing the heteroatom from oxygen to sulfur, the catalyst remains active for ethylene polymerization, although with lower activity and producing polymer of lower molecular weight. It appears the softer nature of the sulfur atom may lead to weaker

bonding to the activator. Increasing the steric bulk around the heteroatom to prevent activator binding (with R = 2,6-$Me_2C_6H_3$) also results in active catalysts, with the oxygen derivative giving a somewhat low activity but an increase in the polymer molecular weight. The sulfur derivative, on the other hand, combines the electronic effects of the soft donor and the steric effects of the aryl ring to form a catalyst with comparable, if not higher, activity. More importantly, the presence of the sulfur group leads to an increase in the catalyst lifetime.

Varying the concentration of the MAO activator has been also analyzed in detail and displays an increase in the activity of the catalyst as a function of the activator concentration,[22] evidently the result of an increase in the number of active sites being generated. The distribution of molecular weights in the polymer is also affected by an increase in the concentration. The close analysis of a gel permeation chromatogram of a polymer produced by these catalysts clearly shows that as the concentration of MAO is increased, the lower molecular weight peak grows, due to chain transfer to aluminum. This can be explained by the fact that increasing the concentration of MAO invariably increases the amount of free TMA in the system. By increasing the number of aluminum centers available for chain transfer chain termination becomes increasingly probable. Consequently, a decrease in the concentration to 250:1 [Al:Fe] gives a unimodal molecular weight distribution, completely comprised of high molecular weight polymer.

Varying the identity of the cocatalyst also has an effect on the polymerization. The use of aluminum alkyls leads to a slight decrease in the activity of the catalyst, and the activity decreases with time at a much faster rate than with MAO,[22] presumably a result of decreased catalyst stability. Also, chain transfer to aluminum becomes the major chain transfer mechanism, displaying almost complete suppression of the β-H transfer pathway and a narrower polydispersity of the lower molecular weight fraction. However, increasing the concentration of the aluminum alkyl activator eventually decreases the activity of the catalyst, either by catalyst decomposition or formation of stable contact ion pairs, thereby blocking the coordination site necessary for coordination and insertion of ethylene on the cationic metal center. The use of chlorinated aluminum alkyls was found to deactivate the system, perhaps through the similar formation of stable μ-chloro Al-Fe complexes.[22]

Increasing the pressure of the ethylene feed gives a higher yield of polymer and more of the higher molecular weight fraction, while maintaining the activity.[22] The yield of polymer increases linearly with the increase in pressure, indicating that chain propagation is first order in ethylene concentration. Since the rate of β-H transfer is also first order in ethylene, the fraction of high molecular weight polymer from β-H transfer increases while the lower molecular weight polymer from chain transfer to Al remains constant.

Variations in the temperature of the catalytic run can also affect the results. The catalytic system is more productive at lower temperatures, since an increase in the reactor temperature leads to a decrease in the activity and the molecular weight.[22] This may be due to decreased stability of the presumed Fe-alkyl intermediate at higher temperatures. Decomposition may occur via reductive elimination (β-hydride elimination followed by reduction); a common pathway for late transition metal alkyls that may be exacerbated by the increased temperature of the reaction medium.

Finally, it is interesting to examine the influence of reaction time on the catalytic cycle. Running the reaction for a shorter period of time shows that the lower molecular weight fraction is produced early on in the polymerization.[22] The rate of chain transfer to Al is therefore greater than β-H transfer. However, as the reaction time increases, the chain termination pathway tends to favour β-H transfer. The concentration of Al co-catalyst is at its highest at the beginning of the polymerization. As the aluminum centers become occupied with polymer and the catalyst becomes imbedded in the growing polymer chains, the rate of chain transfer to aluminum decreases; a victim of diffusion-controlled chain transfer. The rate of β-H transfer however, remains constant throughout the run. Therefore, after longer reaction times, the amount of vinyl-ended polymer, or the higher molecular weight fraction, increases.

Mechanistic Studies of the Bis-iminopyridine Catalytic Systems

Despite the variety of polymerization studies, involving modifications to the ligand and variations in the reaction conditions, important questions remain regarding the reaction mechanism. The elucidation of the reaction mechanism is not a purely academic exercise but is essential to gain control over the polymerization and in turn over the

quality of the polymer produced by the reaction. For one, the ability of a late metal center to attract and coordinate a free ethylene monomer in a sufficiently labile fashion to enable catalytic transformations was originally thought to be a difficult event, considering the increased electron density at the metal center compared to the early metal systems. Also, late transition metal alkyls are known to be susceptible to reductive elimination; a condition non-conducive to the formation of high molecular weight polymers. Fundamental questions regarding the mechanism must therefore be answered in order to design more improved late transition metal catalyst systems.

As discussed above, analysis of the polymer samples has proven extremely helpful in determining the mechanism of chain transfer acting in these systems. Many groups have pursued intensive investigations on these complexes, with the goal of isolating and characterizing active species of the catalytic system, or any possible intermediates of the activation step. The use of a cocatalyst in these systems is paramount and the role of MAO in activating the catalyst is generally assumed to be that of an alkylating and cationizing agent. Activation of the late metal bis-iminopyridine systems is therefore believed to follow the same general mechanism, generating a 14 electron cationic metal alkyl as the active species which then follows the typical polymerization mechanism of Ziegler-Natta catalysts (described by the Cossee-Arlman mechanism of coordination/insertion of ethylene into the growing chain).[5] Despite numerous efforts,[42-45] and plentiful theoretical investigations,[46] isolation of the active species in the Fe system remained elusive.

One of the main goals of this thesis was the determination of the active species in the bis-iminopyridine Fe precatalyst. However, in the interests of chronological order and heightened anticipation, a full discussion of the Fe system is detailed later in the introduction and continued in Chapters 2, 3 and 4. The ability of the bis-iminopyridine ligand to support catalytic activity with late metals encouraged testing of this ligand system with other transition metals. Studies completed with V,[47] Cr,[48] and Mn[48,49] in our laboratory displayed very interesting characteristics with regards to the ligand system, ultimately proving its non-ancillary nature. The knowledge gained not only by our group, but also by several others, in studying numerous complexes of the bis-iminopyridine ligand have suggested that activation of the Fe-analogue may not follow the typical

Cossee-Arlman mechanism as previously envisaged. As such, a detailed investigation of the behaviour of this fascinating ligand system is included throughout the introduction prior to the discussion of the Fe catalyst.

The Vanadium System

The non-ancillary nature of the ligand backbone was unequivocally demonstrated during studies of the V(III) analogue.[47] Akin to its late metal congeners, the VCl_3 complex displayed a high level of catalytic activity for ethylene polymerization when activated by MAO. However, reaction of the precursor with MeLi or MAO in the absence of ethylene did not generate the expected V-alkyl product. Instead, the ligand system became the object of nucleophilic attack, undergoing methylation at the *ortho*-position of the pyridine ring. The result was the formation of a monoanionic ligand and the creation of a vacant coordination site at the metal center (Scheme 1.6). The activity and polymer quality obtained by the new pentacoordinate species was identical to the VCl_3 precursor, suggesting the presence of the same active species in both cases.

Scheme 1.6

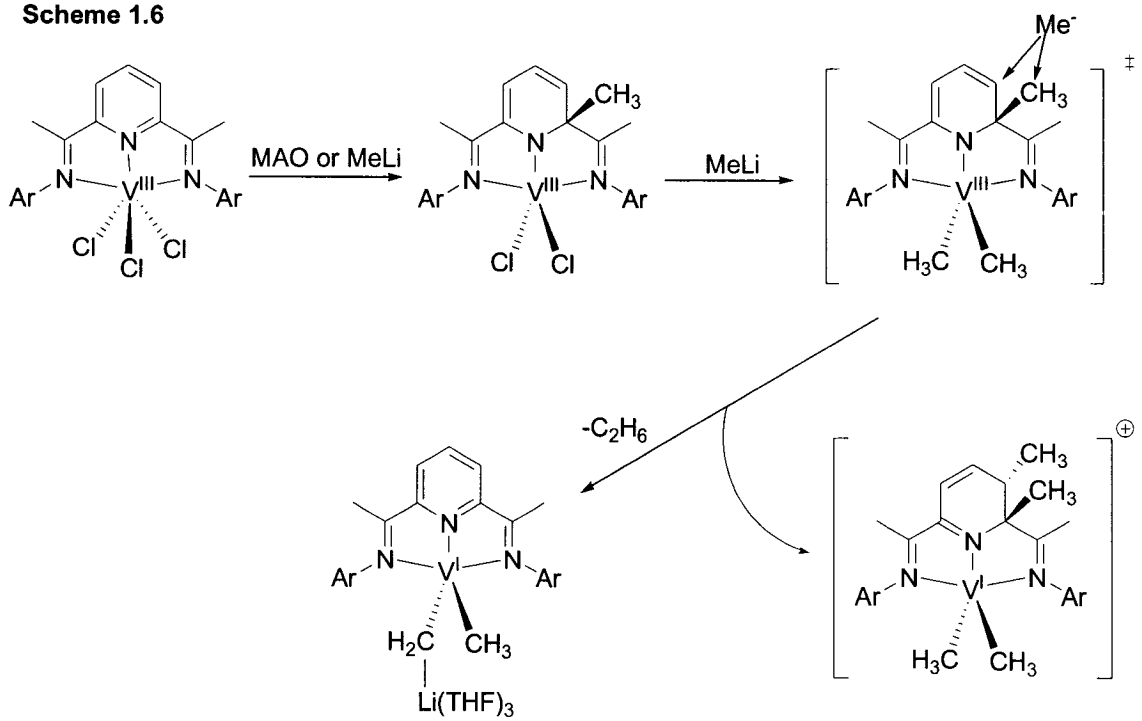

Further reaction with excess MeLi not only alkylated the metal center, but the pyridine ring as well, once again demonstrating the susceptibility of the pyridine ring to nucleophilic attack. Two monovalent, anionic V dialkyls were isolated from the reaction mixture, a consequence of Me-group attack at either the *ortho*-Me group or the *meta*-position of the pyridine ring (Scheme 1.6). In either case, the second attack by a carbanion resulted in a two electron reduction of the metal center and subsequent catalyst deactivation. These observations provided the first indication of possible direct involvement of the ligand.

The Chromium System

The capacity of the ligand to support catalytic activity for both early and late transition metals advised a further investigation into the behaviour of the analogous mid-transition metals, such as Cr and Mn. The rationale behind the choice of these two metals is somewhat contrasting. Chromium is the element used by industry for the Phillips catalytic process.[2] Instead, manganese seems to be the most reluctant metal in terms of providing polymerization catalysts. Given the spectacular performance of complexes of the bis-iminopyridine ligand system, an investigation on the Cr and Mn derivatives seems to be appropriate.

Surprisingly, the bis-iminopyridine-$CrCl_3$ complex displayed unexpectedly low catalytic activity for ethylene polymerization (MAO activation, room temperature and 1 atm pressure of ethylene).[48] A slew of similar Cr-bis-iminopyridine complexes, obtained by varying ligand substituents and ligand symmetries, were tested independently by the groups of Small[50] and Esteruelas.[33a] Conditions could be optimized to achieve extremely high levels of catalytic activity, similar to those of the Fe-'supercatalyst'. The divalent Cr complex was also tested for catalytic activity for the polymerization of ethylene, as well as for propylene.[33a,50,51] Separate studies investigating a possible relationship between both oxidation states in the catalytic cycle have resulted in varying opinions. UV-VIS studies of Small suggest reduction of the trivalent complex upon activation with the aluminum co-catalyst, towards the divalent precursor,[50] whereas Esteruelas proposed that the original trivalent state is preserved in the catalytically active species.[33a]

Parallel studies were undertaken in our lab to examine the reactivity of the trivalent complex with different alkylating agents, unveiling a recurring penchant for reduction to the divalent state.[48] Reacting the trichloride complex with BzMgCl introduced a series of unprecedented ligand transformations, resulting in a dinuclear complex of two divalent Cr alkyls supported by a dimerized hexadentate dianionic ligand (Scheme 1.7). The intricate reaction can be rationalized in three steps: 1) one electron reduction of the metal center by the first equivalent of alkyl; 2) alkylation of the metal center and the *para*-position of the pyridine ring by two more equivalents of BzMgCl; and 3) cycloaddition of two separate units through C-C bond formation between the pyridine *meta*-carbons.

Scheme 1.7

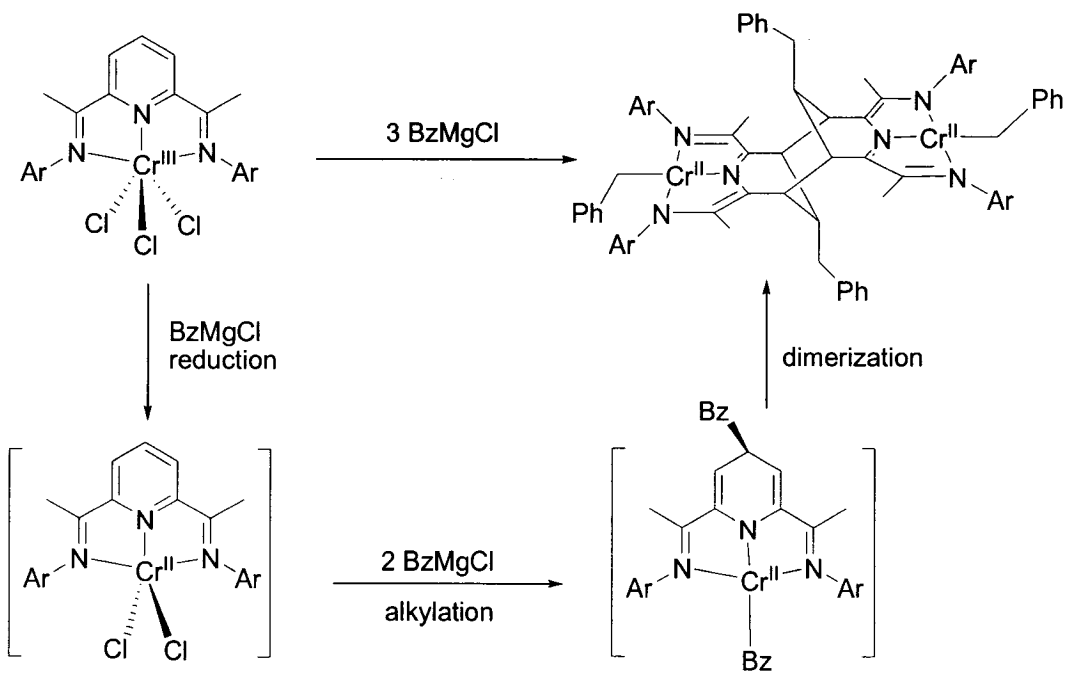

Reduction of the metal center is similar to that observed in the vanadium case[47] and also, as we shall see later, for numerous other metals. Although the subsequent alkylation of the metal center is relatively straight-forward, nucleophilic attack of the pyridine *para*-C is not nearly so obvious. Whether the alkylation is the direct result of attack at the *para*-position, or whether it is due to migration of the alkyl from the metal

center has not been determined. The driving force for the subsequent dimerization may be explained in terms of spin density accretion at the *meta*-Cs following pyridine alkylation.

Addition of $AlMe_3$ to the trivalent Cr complex also resulted in reduction of the metal center by one electron (Scheme 1.8).[48] The remaining Cl atoms are found bridging two separate $AlMe_3$ moieties. Although reduction of the trivalent precursor to Cr(II) may be the primary mechanism upon activation, formation of this particular species appears to be a deactivation pathway, since polymerization of ethylene does not proceed under the usual conditions.

Scheme 1.8

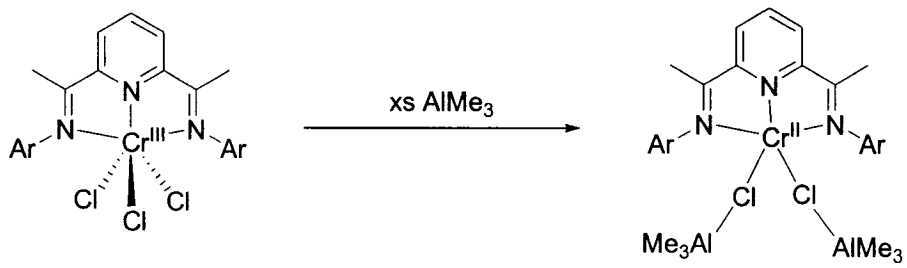

The Manganese System

Despite the similar geometry and high spin electronic configuration as the Fe and Co congeners,[21] the Mn congener is not an active catalyst precursor for ethylene polymerization under mild reaction conditions.[48,49] Regardless, a thorough investigation ensued, prompted by the desire for an increased understanding of this system. The reaction of $LMnCl_2$ with 2 MeLi led directly to reduction and alkylation of the metal center to $LMn^{I}Me$ (Scheme 1.9).[49] Results to date suggest that facile reduction of the metal center appears to be a general trend in the chemistry of this ligand system. On the other hand, addition of 2 equivalents of $LiCH_2SiMe_3$ resulted in the isolation of two products.[48] In the first complex, the divalent metal center is tetracoordinated to the alkyl and the ligand, which has become dianionic by deprotonation of both iminomethyl groups. An ether-solvated Li countercation completes the structure. The second product is a Mn dimer in which each metal center has been alkylated and reduced by one electron (Scheme 1.9). The dimerization is realized by C-C bond formation between two former methyl imino groups which, as a result of the reaction, have been deprotonated by the

alkylating agent. Deprotonation of the second methyl group by another equivalent of alkyl may lead instead to the other byproduct of this unusual reaction.

Scheme 1.9

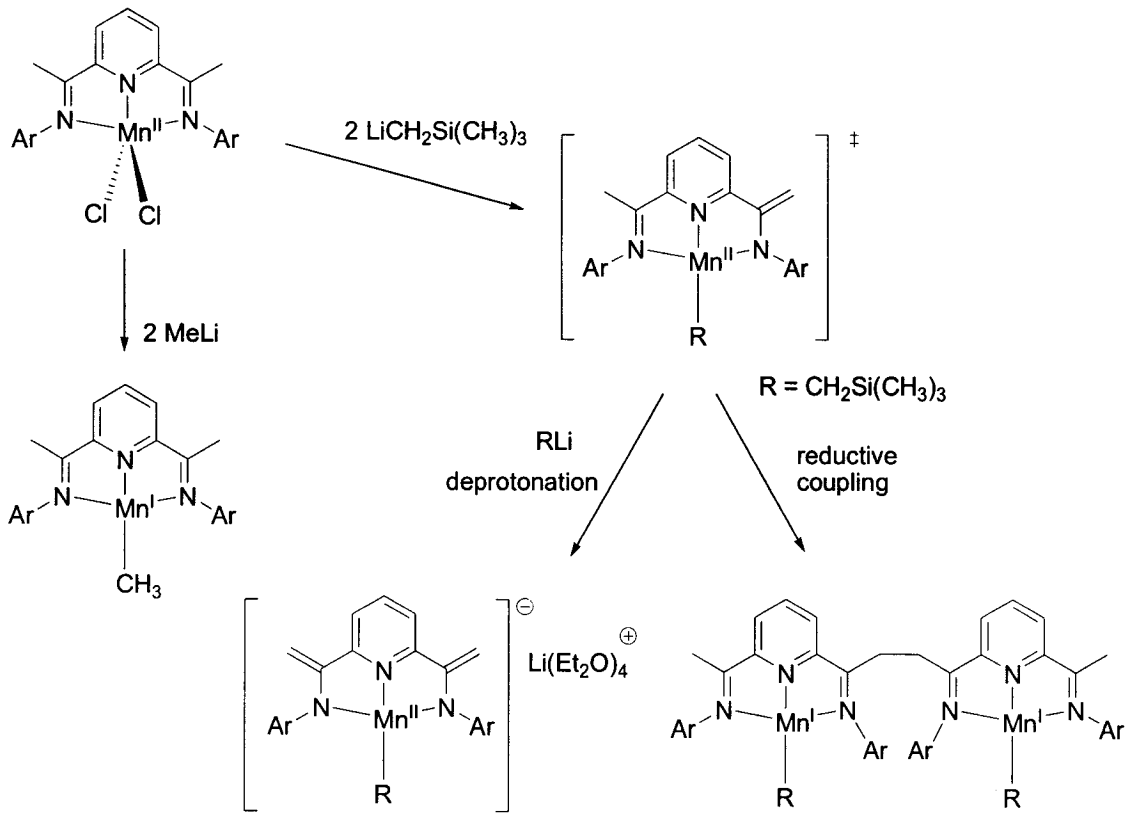

The transformations observed with the Mn system illustrate not only the stabilizing ability of the ligand towards rare, low-valent states, but also the possibility of deprotonating the imino methyl groups to form novel dianionic ligands or dimerized neutral ligands. The results delineated thus far show the unique ability of the ligand to undergo a variety of transformations and to engage in internal redox processes with the metal center upon addition of activators or alkylating agents. The deciding factors favouring one transformation over another were unknown at the time this work was undertaken, but appear to be related to the nature of the metal center and the strength of the alkylating agent.

The Cobalt System

Despite structural similarities, the Fe and Co precatalysts of the bis-iminopyridine ligand behave differently towards ethylene polymerization.[21] Upon activation with MAO the Co congener displays a lower catalytic activity for ethylene polymerization than the Fe derivative under the same conditions, producing highly linear polyethylene of a much lower molecular weight. GPC analysis of the polymer displays a unimodal distribution of molecular weights with a large polydispersity, compared to the bimodal distribution of molecular weights for the polymer made by the Fe catalyst. The lower molecular weight fraction of this polymer consists mainly of saturated ends, with low levels of vinyl unsaturation, indicative of a main termination pathway involving chain transfer to Al, with fewer incidental β-H transfer events. On the other hand, the polymer generated by the Co catalyst, as well as the smaller, high molecular weight fraction of the polymer generated by the Fe derivative, contain a 1:1 ratio of vinyl to saturated ends, due to dominant chain termination via β-H transfer to the monomer or metal center.[22] The difference in polymer quality suggests a profound difference in the structure and nature of the active site performing the polymerization. In agreement with this statement, mechanistic studies of both systems have lead to different conclusions, and the results of the Co derivative are discussed below.

According to the established Ziegler-Natta polymerization mechanism, the active species in the $LCo^{II}Cl_2$ catalyst precursor is expected to be a 15 electron cationic metal alkyl, $LCo^{II}R^+$. Simultaneous studies by the groups of Gal and Gibson towards isolation of the active species describe the addition of MAO or MeLi to the divalent precursor to afford reduction of the metal center to the monovalent species, $LCo^{I}Cl$ (Scheme 1.10).[52] Alternatively, the monovalent complex can be formed by direct reduction of $LCo^{II}Cl_2$ with metallic Zn. Alkylation of the metal center proceeds in a subsequent step with a second equivalent of MeLi, or via reaction with other nucleophilic alkyls (MeMgBr, Bz_2Mg, $LiCH_2TMS$), to form $LCo^{I}R$ (Scheme 1.10). Although none of the alkyl derivatives are active for ethylene polymerization *per se*, once activated by MAO they exhibit identical activities and polymer qualities as the divalent precursor. Reduction of the catalyst by one electron has therefore been established as the first step towards

activation of the catalyst with MAO, discounting the formation of a cationic Co^{II} alkyl as the active species and raising questions about the possible chain initiation mechanism.

Scheme 1.10

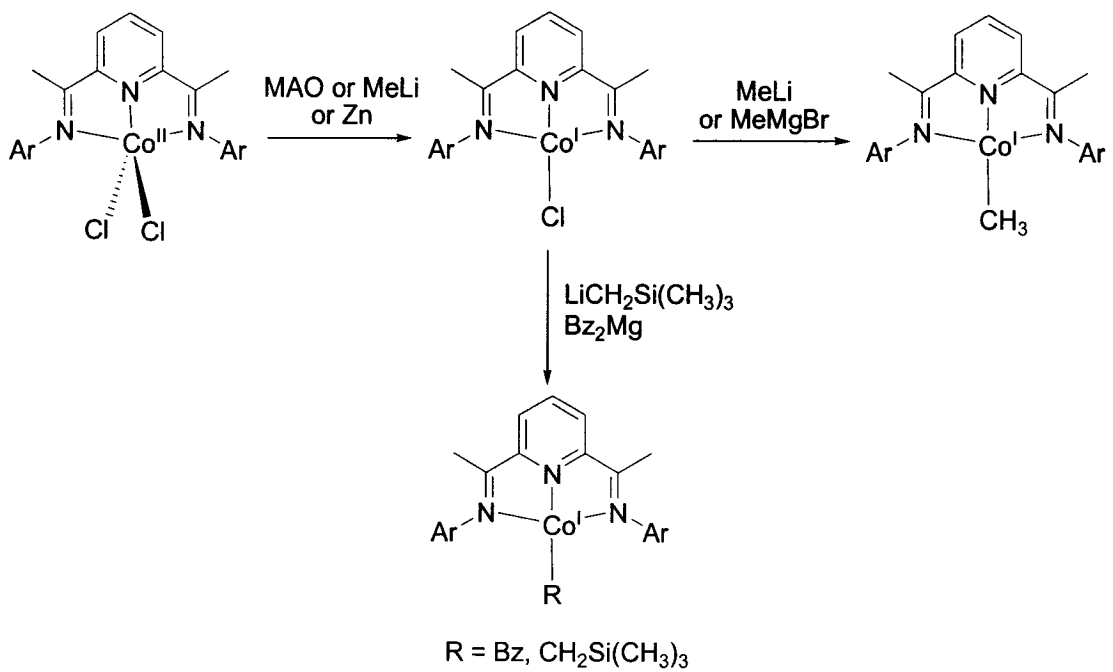

Prying further into the mechanism, addition of the Lewis acid $B(C_6F_5)_3$ to $LCo^{I}Me$ leads to methide abstraction and dinitrogen fixation by the resulting cationic Co^{I} center (Scheme 1.11).[52b] In the presence of ethylene, the end-on dinitrogen unit is replaced by a π-bound ethylene molecule and polymerization proceeds, albeit with extremely low activity (11 g PE/mmol·h·atm). The conclusions that can be drawn thus far are that the active species initially formed upon activation by MAO is a cationic Co^{I} species, as opposed to a Co-alkyl. Erker *et al.* reported similar observations, including Cl abstraction from $LCo^{I}Cl$ by addition of $Li[B(C_6F_5)_4]$ and trapping of a cationic Co^{I} species devoid of an alkyl and yet capable of polymerizing ethylene in very low yields (Scheme 1.11).[53] The possibility that the observed activity is the result of trace alkyls present in the reaction mixture has not been excluded. Nevertheless, these results question the identity of the active species and the pre-established necessity for transition metal σ-bound alkyls to initiate polymerization in late transition metal systems.

Scheme 1.11

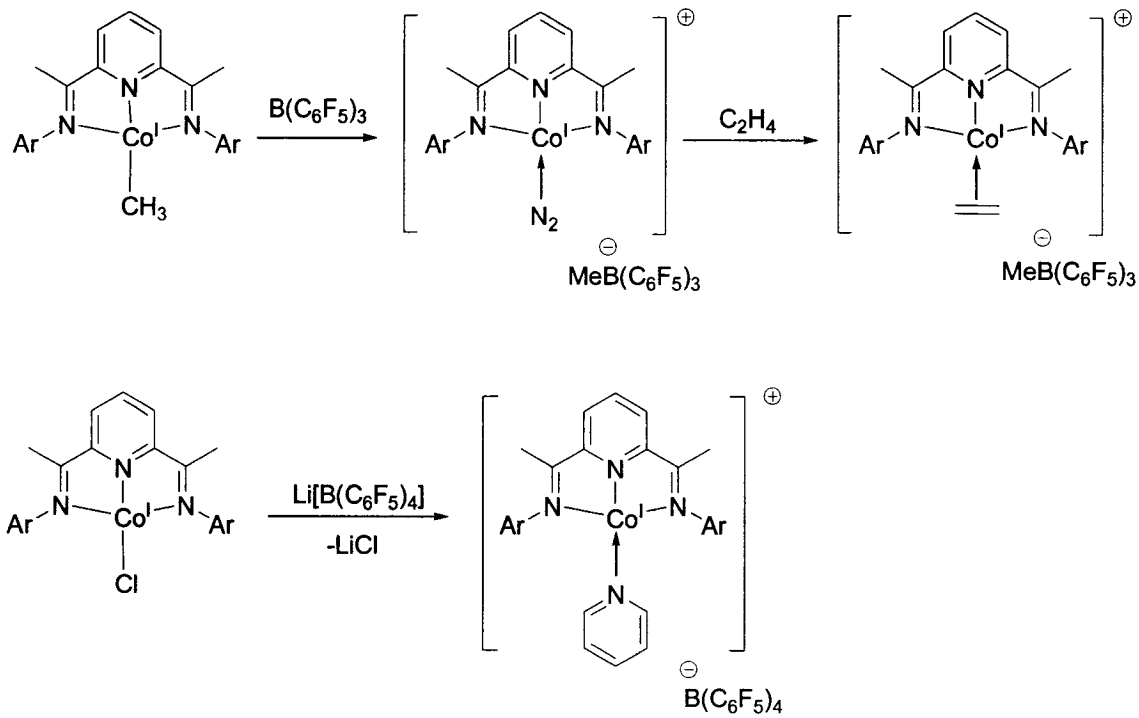

Numerous pathways can be envisaged for the initiation of the polymer chain, including reaction of the bound ethylene molecule with a Lewis acid to generate a zwitterionic Co(III) species, formation of a metallacyclopentane by oxidative coupling of two ethylene units, or even C-H bond activation of the coordinated ethylene to form a Co(III) vinyl hydride, among others.[52-54] Recently, two Zr systems employing similar silylamido-cyclopentadienyl ligands have also challenged the traditional Ziegler-Natta paradigm by polymerizing ethylene in the absence of an apparent transition metal σ-alkyl.[55] In these cases, the initial C-C bond forming step is believed to proceed via alkyl transfer from the countercation-bound methyl group, originally abstracted from the metal center by the activator, to the coordinated ethylene. Gibson *et al.* completed an interesting study involving deuterium labeling of the metal-bound methyl group in $LCo^{I}Me$, demonstrating incorporation of $-CD_3$ to the saturated ends of the resulting polymer.[54] Therefore, initiation of polymerization involves incorporation of the alkyl groups from the cocatalyst, most likely proceeding via nucleophilic attack of the pre-abstracted methide on the Co center and coordination of the Lewis acid to the bound ethylene,

oxidizing the metal center to Co(III) in the process (Scheme 1.12). Chain propagation may then proceed by ethylene insertion into either Co-C bond.

Scheme 1.12

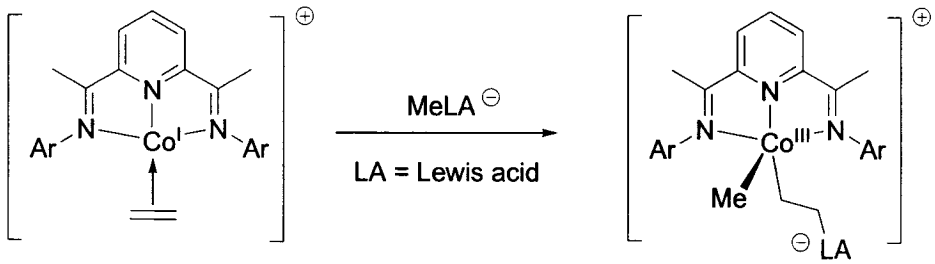

Besides activation by MAO or $B(C_6F_5)_3$, polymerization of ethylene by $LCo^{I}Me$ could also be triggered by addition of $Li[B(C_6F_5)_4]$.[33b] A plausible ligand specific activation mode was offered by Erker, describing interaction of the Li cation with one arm of the ligand, creating a vacant site at the metal center for approach of an ethylene unit (Scheme 1.13). The lability of the imino N atom is not without precedent, as shown by the modified ligand, where π-bonding to the aryl group stabilizes the complex.[33bc] It is therefore conceivable that ethylene could also act as a suitable stabilizing donor for the metal center.

Scheme 1.13

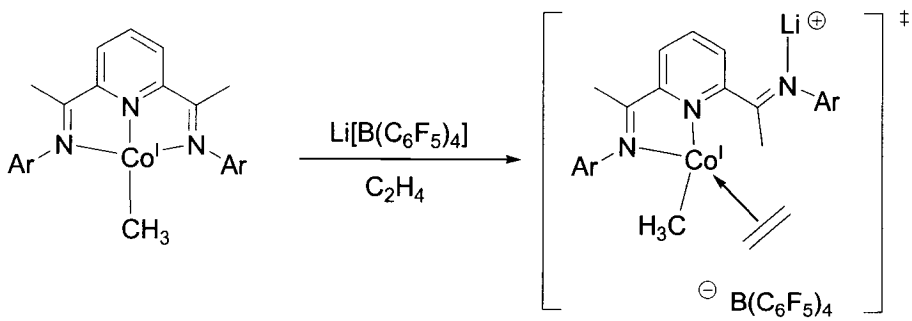

The experimental observations presented above illustrate an unexpected activation mode for the Co-bis-iminopyridine precatalyst. Contrary to the formation of a cationic divalent Co alkyl as the active species, activation with MAO affords instead one electron reduction of the metal center to give an alkyl-free Co(I) cationic unit. The unusual

activation pathway implies an alternative mechanism of ethylene polymerization than previously assumed and raises questions as to the mechanism involved in catalysis by the Fe derivative.

The Aluminum System

Preliminary studies by Gibson[56] and Grassi[57] exploring the reaction between the bis-iminopyridine ligand and aluminum activators once again demonstrated the complex nature of these systems. Upon simple coordination of the ligand to $AlMe_3$, one of the imino functions on the ligand backbone becomes alkylated (Scheme 1.14). In an effort to assess the reactivity of the bis-iminopyridine-Al complexes as cationic aluminum alkyls for ethylene polymerization, $B(C_6F_5)_3$ was added to the imino-alkylated adduct to abstract a methyl group.[56] Small amounts of solid polyethylene were isolated after ethylene was passed over the resulting cationic Al alkyl.

Scheme 1.14

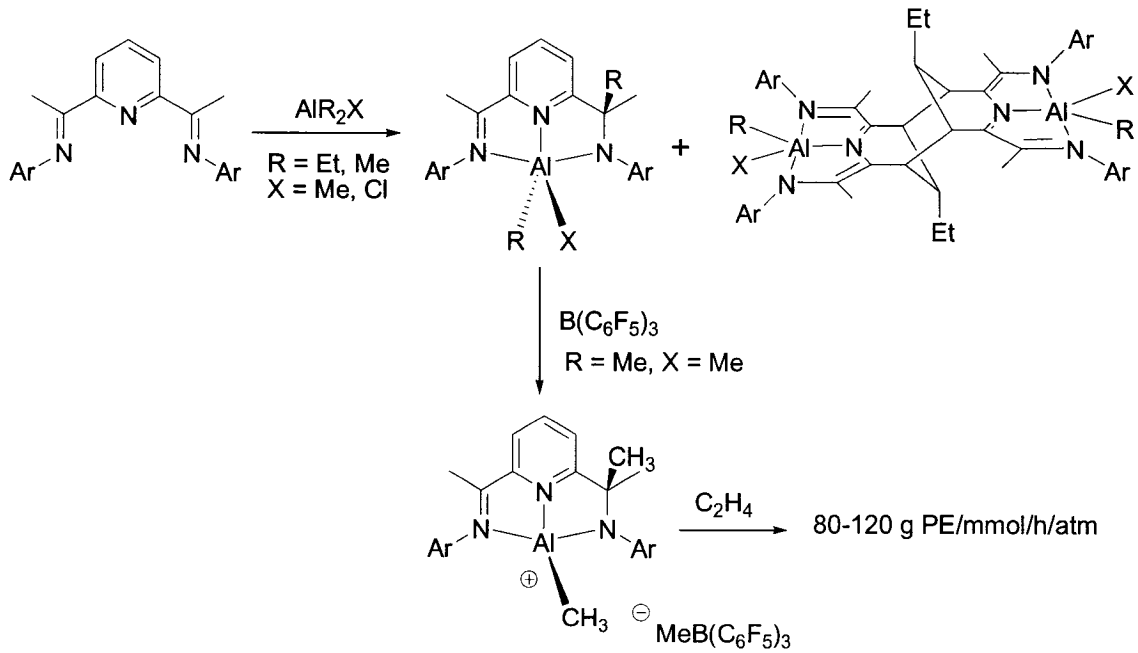

Budzelaar *et al.* completed a more in-depth study of the reactivity between various aluminum activators and the ligand system.[58] NMR studies revealed the presence of several products upon addition of the aluminum complexes to the ligand. Besides

alkylation at the imino-C atom, other products included alkylation of the *ortho* and *para*-positions of the pyridine ring. Another unexpected product from the reaction with $AlEt_2Cl$ was a strange dimer whose dinuclear structure is realized through C-C bond formation between adjacent *meta*-carbons from two identical units (Scheme 1.14). The Al center remains coordinated to an alkyl moiety, a Cl atom and the ligand, which has in turn been alkylated at the *para*-position of the pyridine ring. These observations are analogous to the reactivity witnessed on chromium.[48] The trend emerging from the chemistry summarized above is that the ligand becomes susceptible towards nucleophilic attack by alkylating agents at various positions of the ligand backbone. To better elucidate this point, reactivity studies were therefore attempted with various alkylating agents in the absence of transition metals.

Ligand Alkylation

Addition of MeLi to a suspension of the free ligand in ether resulted in methylation of the pyridine nitrogen atom and tri-coordination of the ligand to the Li cation, affording both a dinuclear[59] and mononuclear[60] species (Scheme 1.15). The dinuclear complex features a Li-C bond from the first Li cation to the *para*-carbon of the pyridine ring of the second unit. The tetra-coordination of the second Li is completed by a molecule of ether, preventing further aggregation.

Nucleophilic attack at the relatively electron-rich N atom of the pyridine ring was unprecedented and is obviously not preferred over alkylations at other positions. The N-methylation appears to be reversible, seeing that reaction with a mild electrophile like ^{i}PrBr abstracts the Me group and reverts the structure back to that of free ligand (Scheme 1.15).[59] Moderate heating of either the mononuclear or dinuclear species afforded mono-deprotonation of one of the two imino-methyl groups and consequent anionization of the ligand.[59,60] Deuterium labeling studies have shown that deprotonation of the ketimine wings is not due to methyl migration through the ligand, but rather to primary dissociation and subsequent attack by a Li-bound Me group.[61]

Scheme 1.15

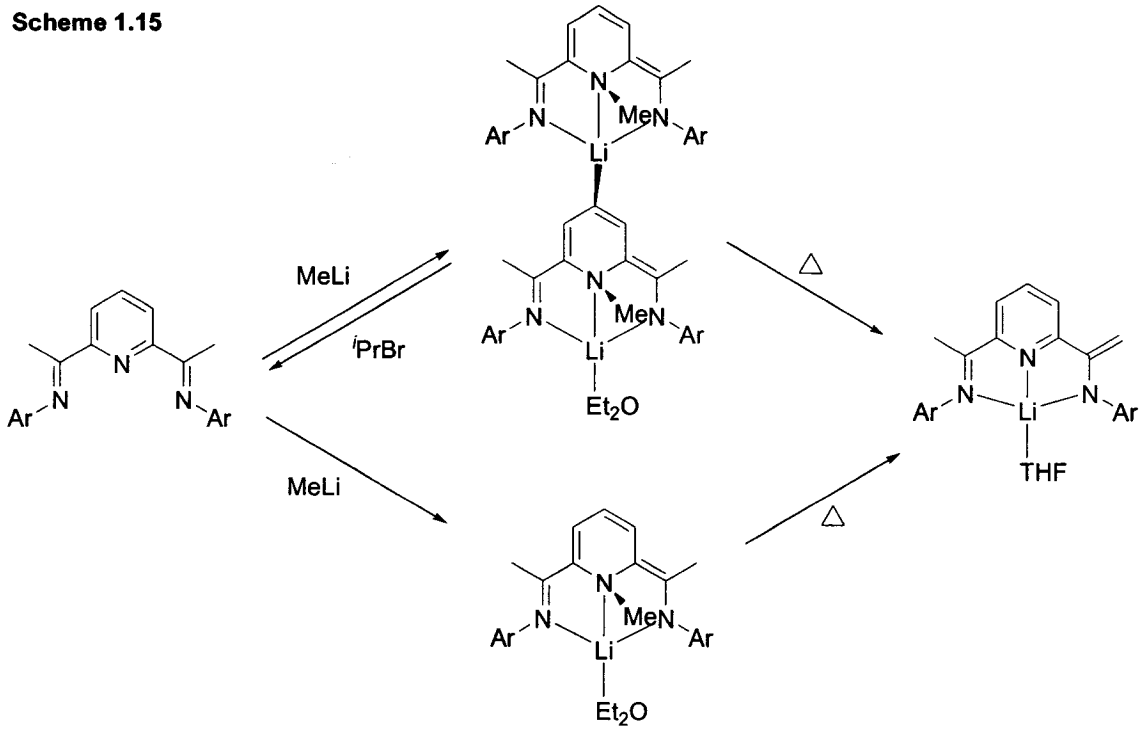

Reversible nucleophilic attack at the pyridine N atom has been uncovered as a recurring theme in a recent paper by Gibson, concerning reaction of the ligand with other main group alkyls, like MgR_2 and ZnR_2, where R = Me, Et, ^{i}Pr.[61] Unlike the MeLi product, deprotonation of the imino-methyl groups is not an observed reaction pathway. However, tautomerization may occur, where methyl migration from the N atom to the *ortho*-position of the pyridine ring is found to be largely driven by steric factors. Perhaps most intriguing is the perceived involvement of single electron transfer (SET) in the mechanism of ligand alkylation, akin to the related chemistry of α-diimine[62] ligands (Scheme 1.16). EPR studies have uncovered the presence of a radical intermediate.

Scheme 1.16

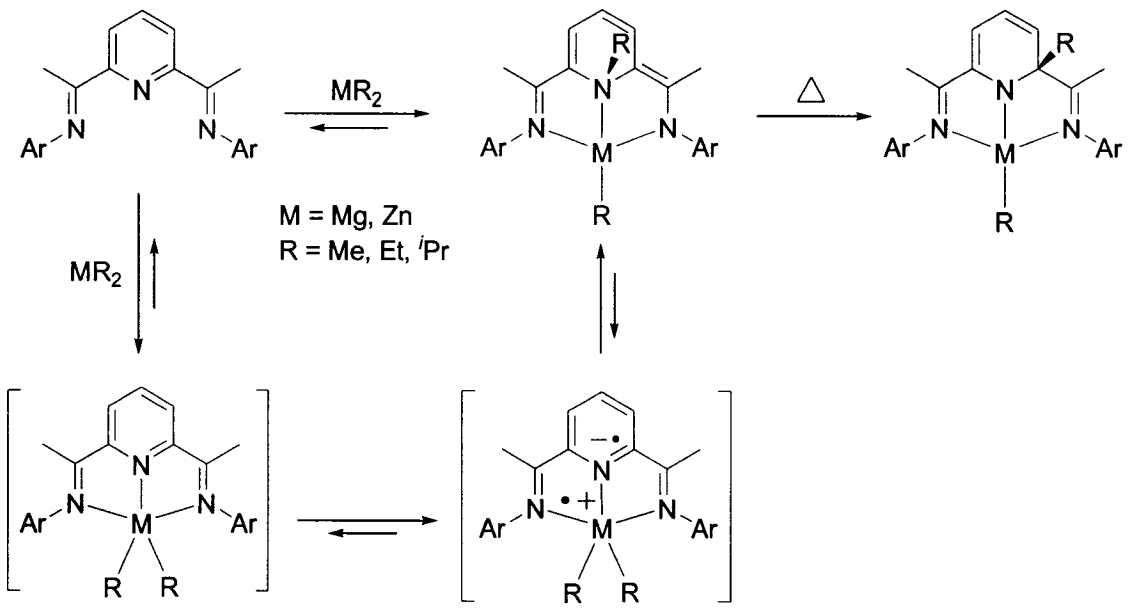

The potential of the deprotonated mono-anionic organolithium complex as a supporting ligand for ethylene polymerization catalysts was intriguing. However, the reaction is complex and not suitable for large scale preparation, due to the low yield and presence of other intractable products.[59-61] Therefore, the use of a different alkylating agent was attempted, namely $LiCH_2Si(CH_3)_3$. Addition of one equivalent of $LiCH_2Si(CH_3)_3$ to a suspension of the intact ligand in THF lead to the isolation of a novel dianionic ligand, in which both ketimine methyl groups have been deprotonated (Scheme 1.17).[63] This behaviour may explain the related outcome upon addition of $LiCH_2Si(CH_3)_3$ to the $MnCl_2$ derivative, as previously discussed (Scheme 1.9).[48] Incidentally, this simple preparation has allowed the rational preparation of the dianionic form of the ligand in very large scale, therefore opening new perspectives for the chemistry of these systems.

Scheme 1.17

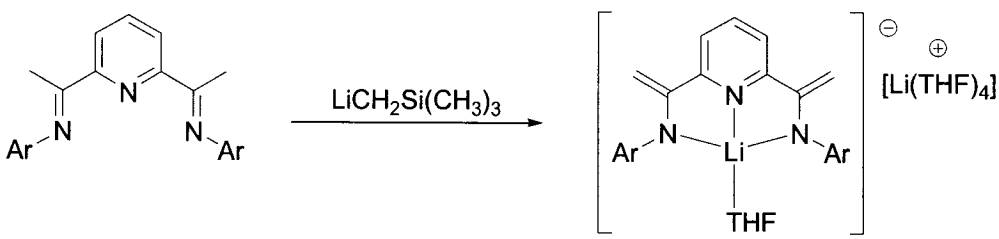

The Dianionic Ligand as a Supporting Ligand for Lanthanide Metals

The preparation of the modified dianionic ligand has encouraged a series of reactivity studies to evaluate the coordination chemistry and catalytic activity of the dianionic ligand supporting various transition metals. Nowhere has its use been more significant than in the chemistry of the lanthanides (La, Nd), fueled by the surprising inability to form complexes with the intact ligand and the hopes that anionization of the ligand may improve binding to the metal center. Addition of the dilithium diamido ligand to $LnCl_3(THF)_3$ (Ln = Nd, Cl) resulted in facile formation of the expected metathesis products, maintaining the metal center in the trivalent state (Scheme 1.18).[63,64] The Nd complex could also be recrystallized as an anionic DME adduct.

Scheme 1.18

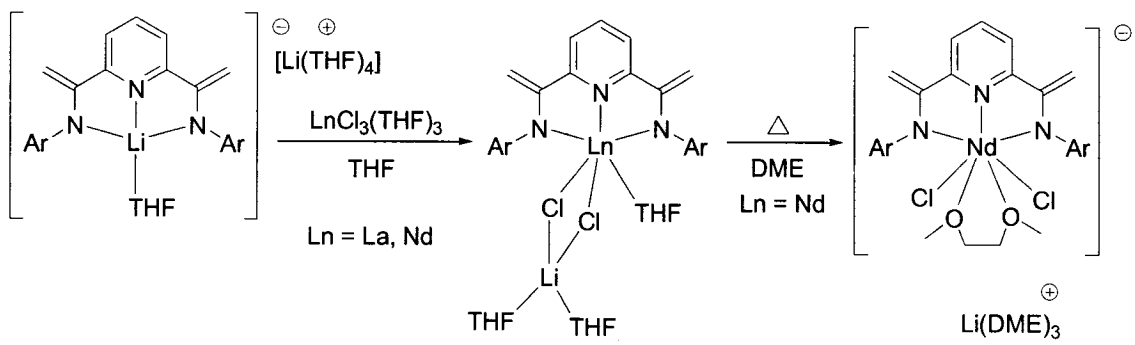

The importance of lanthanide complexes as stereospecific butadiene polymerization catalysts encouraged further reactivity testing. The Nd complex displays an excellent catalytic activity for butadiene polymerization, forming cis-polybutadiene with good yields and high selectivity.[63] Attempted alkylations with a variety of Grignard and organolithium reagents led only to intractable materials. In one attempt a successful alkylation was achieved with allylMgBr on the DME-Nd adduct. The allyl unit and a Br atom replaced both Cl atoms (Scheme 1.19).[63] The Li countercation was maintained outside the coordination sphere of the metal center. Interestingly, the allyl adduct was not a highly active catalyst for butadiene polymerization.

Scheme 1.19

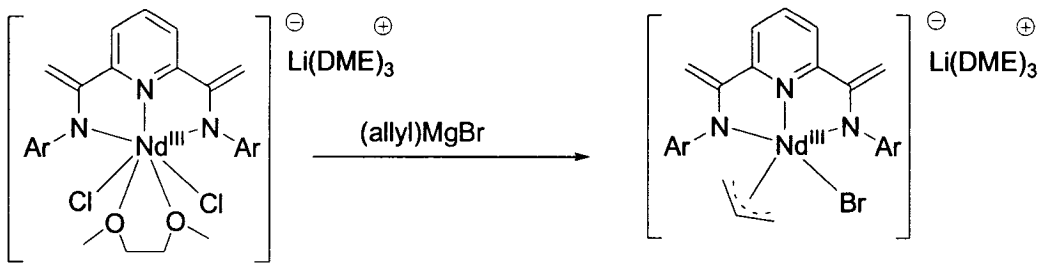

One question regarding the use of the new dianionic ligand was whether it could stabilize low-valent metal centers as well as the neutral ligand. As expected, reduction of the above dichloride complexes does not lead to the formation of rare divalent Nd centers. Instead, the ligand is the recipient of the electron, undergoing C-C bond formation between the methyl groups of two identical units[64] to form a similar dimeric structure to that observed in the chemistry of Mn (Scheme 1.20).[48]

Scheme 1.20

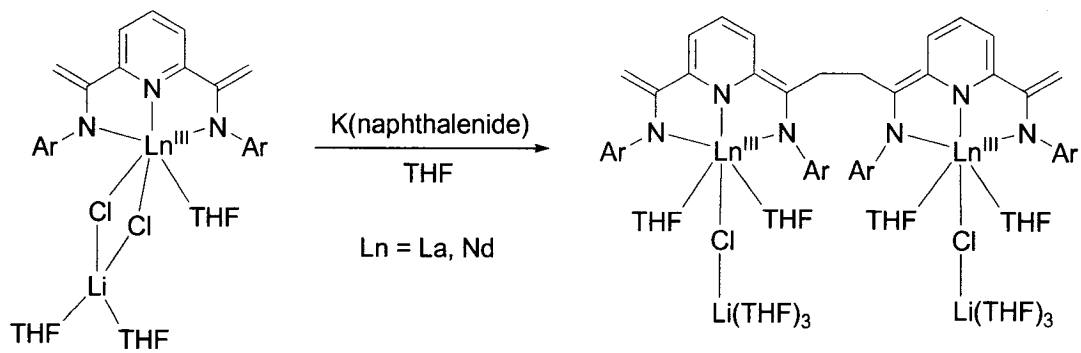

Electronic Properties of the Ligand System

In regards to supporting catalytic activity towards ethylene polymerization, the bis-iminopyridine ligand is a truly fascinating system, having gained attention by transforming stereotypically benign late transition metals into unprecedented catalytic systems.[21] Studies to date have unveiled unique chemical properties of the ligand, revealing pronounced non-ancillary behaviour through direct involvement in the reactivity of the metal center. The ligand system has been shown to undergo a variety of transformations, including alkylation at all positions of the pyridine ring,[47,58-61] alkylation

of the imino-C atom,[56-58] deprotonation of one[59-61] or both ketimine methyl groups,[48,63,64] and even dimerization through the ketimine methyl groups[48,64] or the *meta*-positions of the pyridine ring.[48,58] However, it is the distinctive electronic properties of the ligand that differentiate it from other systems. Certain electronic variations in the ligand backbone result in termination of the catalytic activity, therefore highlighting an unusually enhanced dependence on the electronic configuration of the ligand core. For example, if the *para*-hydrogen atom on the pyridine ring is replaced with a chloride, the catalytic activity of the Fe catalyst decreases tremendously.[65]

In 2000, the first study on the electronic configuration of the ligand was published, involving octahedral diligated complexes of various first row transition metals.[35a] It concluded that the ligand could bind either in a neutral fashion, or in a one electron reduced form. In a following paper, computational studies revealed a low-lying π^* orbital on the ligand and the propensity for electron transfer from the metal t_{2g} orbital to the LUMO of the ligand.[35b] The metal-to-ligand charge transfer (MLCT) could be characterized crystallographically by an elongation in the C=N bond lengths, as well as by a small and yet visible contraction of the C_{imine}-C_{ortho} bond distances. The number of electrons transferred could be quantified by comparing the ligand deformations to a Zn reference complex. However, difficulties arise when determining whether the electron has been transferred completely to the ligand system from the metal center, or whether a more accurate description of the bonding situation is but an increased level of back-donation from the metal center to the ligand. Distinguishing between the strongly back-donating MLCT model and a purely biradical model is not possible by crystallographic methods since in most cases, the overall bonding is the result of the two bonding possibilities. The percentage of participation of one over the other will depend on the nature, oxidation state and spin state of the metal center. Therefore, the degree of reduction, as determined by the metal center, could dictate the nature of the transformation, with certain transformations occurring more frequently than others. It will depend on the energy difference in the metal d orbitals vs the LUMO of the ligand, as well as any electron-pair repulsions in paired d-electrons. Variations in the degree of reduction of the ligand may help to explain the multitude of transformations outlined thus far.

In an attempt to verify the electron accepting ability of the ligand, reduction reactions were carried out in our lab. Reduction of the free ligand with metallic Li led to the formation of two rare organotrilithium compounds (Scheme 1.21).[66] The first complex contains an intact ligand bound to three Li cations and displays a magnetic moment of 1.30 μ_B. Although the value is slightly lower than expected for one unpaired electron, an explanation may be provided by the existence of an antiferromagnetic exchange between the radical anions, the existence of which are confirmed by a complex 25-line EPR spectrum centered around g = 2.001. The second species, also composed of three lithium centers, has undergone deprotonation at one of the imine methyl groups and hence is not paramagnetic in nature. Conversion of the first product to the second product occurs readily upon heating, and implies a formal one electron oxidation through the loss of one H atom. In accord, reduction with Li(naphthalenide) led only to the second product (Scheme 1.21). Besides being a weaker reducing agent, the basicity of Li(naphthalanide) may also promote deprotonation over reduction. Regardless, the reduction of the ligand with Li has undeniably shown the exceptional ability of the ligand to accommodate up to three electrons in its delocalized π-system.

Scheme 1.21

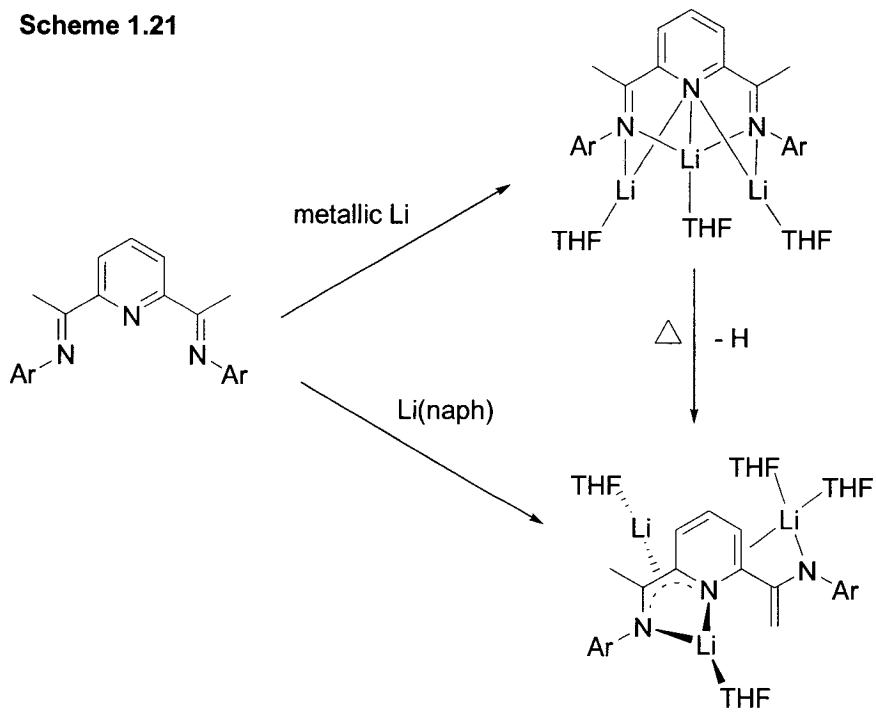

The inherent electron accepting ability of the ligand may lead to the appearance of low-valency at the metal center. An interesting example of this phenomenon involves a pseudo-divalent Nd complex prepared in our lab. During an attempt to prepare a highly reactive Nd(II) species, metallic Nd and I_2 were reacted in the presence of the ligand. The isolated product is characterized by an intact ligand surrounding the metal center, which is also coordinated to two iodide atoms and a molecule of THF (Scheme 1.22).[64] From the formal point of view, the metal center appears to be in the +2 oxidation state. However, the magnetic behaviour of the complex clearly indicates that the complex actually consists of a Nd(III) center antiferromagnetically coupled to a ligand radical anion. In this case, the ligand is the recipient of one electron from the metal center, to be delocalized throughout the π-system.

Scheme 1.22

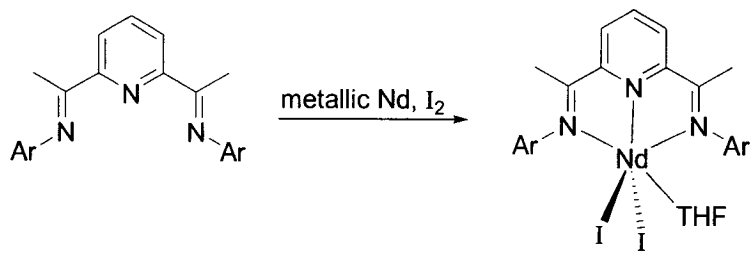

The electron accepting ability of the ligand is not limited to lanthanides and lithium complexes. Calculations by Budzelaar have highlighted that the Co center in the one-electron reduced precursor to ethylene polymerization is indeed a divalent Co center antiferromagnetically coupled to a ligand radical anion.[67] The phenomenon of ligand reduction at the expense of the metal center appears to be a trend, and as such, examples permeate the chapters of this thesis.

The Iron System

Although the bis-iminopyridine Fe system displays a higher level of catalytic activity than any other derivative, up until recently less was known concerning its mode of activation. Under the assumption of a straight forward Ziegler-Natta mechanism of operation, several theoretical studies have been published despite the absence of

experimentally isolated intermediates.[46] Disagreements abound, however, concerning the spin state of Fe in the active center (a 14 electron cationic Fe alkyl). On the basis of DFT calculations, Ziegler predicted a low spin state for the active Fe center,[46a] while Morokuma[46c] and Zhakarov[46d] proposed a high spin species. In parallel, attempts were made to experimentally isolate intermediates from the activation process. However, the anticipated lability of the Fe dialkyl intermediate hampered efforts, apparently due to facile reductive elimination, as experienced for numerous other Fe dialkyls.[68]

Shifting attention towards the isolation of a halogenated cationic species as a precursor to the monoalkyl cationic center, Gibson *et al.* reacted the $LFeCl_2$ complex with $AgSbF_6$.[42] As expected, the Ag reagent abstracted one chloride, forming a cationic metal center stabilized by the presence of a donor molecule in the empty coordination site (Scheme 1.23). The presence of donor molecules may be eliminated with the use of a dichelating monoanionic ligand, such as *acac*. The fully saturated, donor-free cation was generated via reaction with Ag(*acac*) followed by $NaBPh_4$.

Scheme 1.23

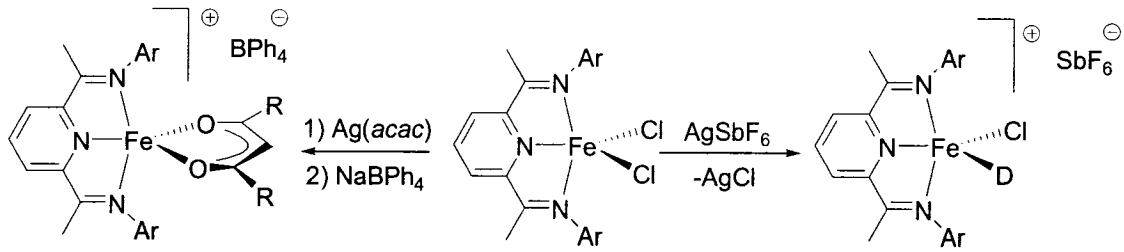

D = donor molecule

The cationic complex is not active for the polymerization of ethylene unless further activated with MAO. However, in the presence of MAO, activities comparable to the original $FeCl_2$ complex were obtained, as well as nearly identical polymers, indicating participation of the same active species.[42] Although the results of Gibson do not provide information with regards to activation of the catalyst with MAO, they do illustrate the possibility of forming a cationic Fe(II) complex.

The group of Talsi completed an intensive investigation of the reaction of $LFeCl_2$ with MAO and $AlMe_3$ monitored by ^{1}H-NMR and ^{2}H-NMR.[44] Unfortunately, the

paramagnetic nature of Fe in these compounds prevents unambiguous assignment of the resonances. Peak assignments were therefore made based on intensity and line width, which correlates well with distance from the paramagnetic center. Talsi's studies, in combination with mass spectrometry experiments by Repo,[45] led to the suggestion that a bimetallic species of Fe and Al may be formed. In addition, complete replacement of the chloro groups with methyl groups was observed as a result of an increased concentration of the cocatalyst. The nature of MAO as a stronger Lewis acid than AlR_3 is illustrated nicely in the experiment outlined in Scheme 1.24. MAO is capable of abstracting a methyl group from the metal center to form an ion pair, whereas addition of $AlMe_3$ results in neutral bridging structures and a coordinatively saturated metal center.[44,45]

Scheme 1.24

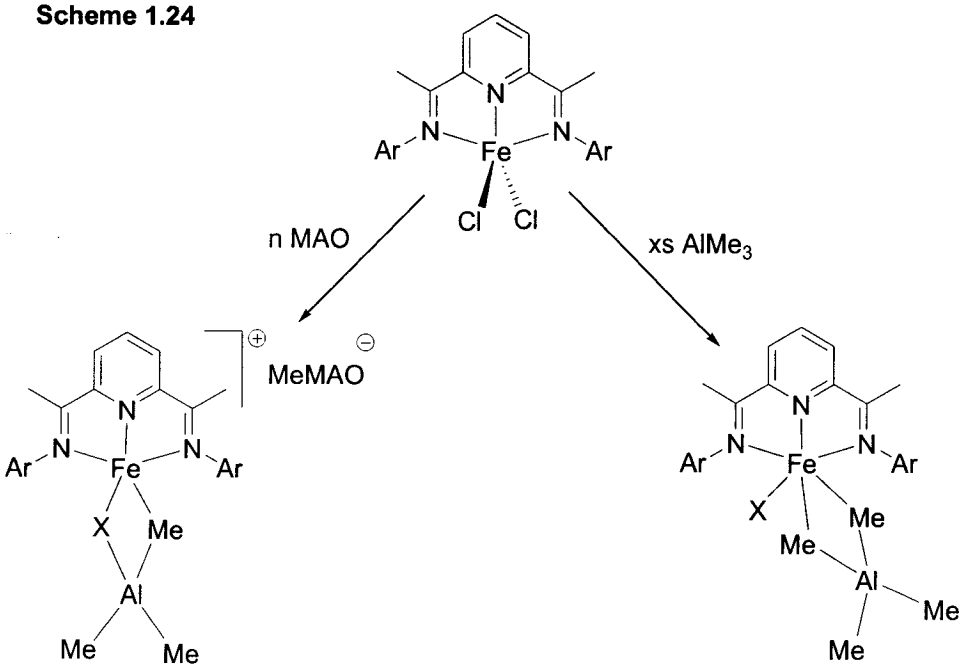

The species characterized by NMR may actually be considered as the dormant states in the mechanism (due to the lack of empty coordination site). De-coordination of the Lewis acidic $AlMe_3$ would generate a coordinatively unsaturated cationic divalent metal alkyl as the high-energy intermediate that propagates polymerization. The

equilibrium between the dormant and active states is the factor directing the catalytic cycles.

In addition to controversies regarding the spin state of Fe in the catalytically active species, the oxidation state of the Fe center also became the center of a debate. Contrary to Talsi and Repo's conclusion of a divalent active Fe center,[44,45] Gibson proposed the formation of a trivalent active site upon addition of MAO, based on comparative Mossbauer and EPR studies involving complexes of both oxidation states.[43] Nevertheless, structural characterization of an actual active site or intermediate had not been achieved by this point.

Aim of the Thesis

The preceding pages of this introduction have highlighted the unique and diverse properties of the bis-iminopyridine ligand. Despite the wealth of information gathered for other transition metal systems, the most active and promising catalyst, Fe, remains poorly understood. The ambiguity of the mechanistic studies and the lack of concrete results furnished by other groups encouraged us to pursue research aimed towards understanding the system. The lofty goal of our curiosity-driven research was the isolation of the active species responsible for the high activity displayed by the catalyst. In an attempt to furnish the desired results, reactivity studies were undertaken involving reaction of the $FeCl_2$ precursor with various alkylating agents and aluminum activators. Concomitant to our work, other groups were pursing similar chemistry, publishing observations which mainly furthered our results. A discussion of their work has been included in the following chapters where deemed appropriate. Therefore, the first few chapters deal with the reactivity of the Fe-bis-iminopyridine catalyst. Subsequent chapters expand our knowledge of the unique bis-iminopyridine ligand and its derivatives on Co and Cr, culminating in an extensive list of possible Fe-dinitrogen complexes and dinitrogen cleavage by a reduced Cr complex. The last chapter tests the ability of a different N-based ligand to support catalytic activity for late transition metals.

Chapter 2 outlines the multitude of transformations occurring upon alkylation with $LiCH_2Si(CH_3)_3$, including dialkylation of the metal center, alkylation of the *ortho-*

position of the pyridine ring and the imino-C atom, deprotonation of both imino-methyl groups and even reduction and dimerization towards a dinuclear mono-valent Fe alkyl.

In **Chapter 3**, the reactivity of the precursor in the presence of MeLi is explored. Reduction by two electrons appears to be a prerequisite for formation of the active species.

The intriguing observations regarding reaction with aluminum alkyls are included in **Chapter 4**. Although our ultimate goal of isolating the active species was not fully realized, the isolated deactivation products, as well as analysis of results from the previous chapters, have aided in suggesting a possible reaction mechanism for the system.

Chapter 5 follows an in-depth study of the Cr-bis-iminopyridine system, describing the formation of a formally monovalent Cr complex exhibiting greater catalytic activity for ethylene polymerization than the tri- or divalent congeners. Reactivity studies with various alkylating agents and aluminum activators have isolated several products, including a similar deactivation product as seen with the Fe precursor.

The theme of dinitrogen fixation is explored in **Chapter 6**, where reduction of the $FeCl_2$ precursor leads to the isolation of various nitrogen-bound products. Unfortunately, despite increased amounts of reducing agent, the dinitrogen moieties refused to be reduced, instead adding electrons to the ligand backbone.

The culmination of dinitrogen chemistry is realized in **Chapter 7**, describing dinitrogen activation and cleavage upon reduction of the bis-iminopyridine Cr complexes and highlighting the difference in reactivity between the mid and late transition metals to facilitate this transformation.

Chapter 8 explores the complexation of $CoCl_2$ with the doubly-deprotonated dianionic version of the ligand, leading to spontaneous dimerization of the ligand and reduction of the metal center by one electron, as well as labile dinitrogen fixation.

Finally, **Chapter 9** explores the use of another ligand system for late transition metals. Although the catalytic activity of these new systems is non-existent, the macrocylic structures assembled are of academic interest and are promising for future work.

References

(1) Information for this section was obtained from a number of different sources, see: (a) Seymour, R. B.; Cheng, T. *History of Polyolefins: The World's Most Widely Used Polymers* D. Riedel Publsihing Company, Dordrecht, **1986**. (b) McMillan, F. M. *The Chain Straighteners* McMillan, London, **1979**, 203. (c) http://www.rsc.org/Education/EiC/issues/2005_Jan/infochem.asp. (d) http://www.rsc.org/ConferencesAndEvents/RSCEvents/Landmarks/Polyethylene.asp. (e) Louis Pasteur, Lecture, University of Lille (December 7th, 1854).

(2) Hogan, J. P.; Banks, R. L. Phillips Petroleum Co., U.S. Patent No. 2825721, 1958.

(3) (a) Ziegler, K.; Krupp, F.; Zosel, K. *Angew. Chem.* **1955**, *67*, 425. (b) Ziegler, K.; Holzkamp, E.; Breil, H.; Martin, H. *Angew. Chem.* **1955**, *67*, 426. (c) Ziegler, K.; Breil, H.; Holzkamp, E.; Martin, H. DE 973626, **1953** [*Chem. Abstr.* **1960**, *54*, 14794.

(4) Selected Reviews: (a) Stille, J. K. *Chem. Rev.* **1958**, *58*, 541. (b) Bajgur, C. S.; Sivaram, S. *Current Science* **2000**, *78*, 1325. (c) Hlatky, G. G. *Chem. Rev.* **2000**, *100*, 1347. (d) Gibson, V. C.; Spitzmesser, S. K. *Chem. Rev.* **2003**, *103*, 283. (e) Chen, E. Y.-X.; Marks, T. J. *Chem. Rev.* **2000**, *100*, 1391. (f) Böhm, L. L. *Angew. Chem. Int. Ed.* **2003**, *42*, 5010. (g) Boor, J. *Ziegler-Natta Catalysts and Polymerization* Academic Press, New York, 1979. (h) Kaminsky, W. (ed.) *Metalorganic Catalysts for Synthesis and Polymerizations* Springer, Berlin, **1999**. (i) Gavens, P. D.; Bottreel, M.; Keeland, J. W.; McMeeking, J. *Comprehensive Organometallic Chemistry* Eds Wilkinson, G.; Stone, F. G. A.; Abel, E. W., Pergamon, Oxford, **1982**, *vol. 3*, 475.

(5) (a) Cossee, P. *J. Catal.* **1964**, *3*, 80. (b) Arlman, E. J. *J. Catal.* **1964**, *3*, 89. (c) Cossee, P.; Arlman, E. J. *J. Catal.* **1964**, *3*, 99.

(6) (a) Breslow, D. S.; Newburg, N. R. *J. Am. Chem. Soc.* **1957**, *79*, 5072. (b) Natta, G.; Pino, P.; Mazzanti, G.; Lanzo, R. *Chim. Ind. (Milan)* **1957**, *39*, 1032.

(7) Bochmann, M.; Lancaster, S. J. *Angew. Chem.. Int. Ed. Eng.* **1994**, *33*, 1634. (b) Tritto, I.; Donetti, R.; Sacchi, M. C.; Locatelli, P.; Zannoni, G. *Macromolecules* **1997**, *30*, 1247. (c) Petros, R. A.; Norton, J. R. *Organometallics* **2004**,*23*, 5105. (d) Mynott, R.; Fink, G.; Fenzl, W. *Angew. Makromol. Chem.* **1987**, *154*, 1. (e) Fink, G.; Rottler, R. *Angew. Makromol. Chem.* **1981**, *94*, 25. (f) Fink, G.; Rottler, R.; Kreiter, C. G. *Angew. Makromol. Chem.* **1981**, *96*, 1.

(8) Zefirova, A. K.; Shilov, A. E. *Dokl. Akad. Nauk. SSSR* **1961**, *136*, 599.

(9) Dyachkovskii, F. S.; Shilova, A. K.; Shilov, A. E. *J. Polym. Science. Part C* **1967**, *16*, 2333.

(10) Eisch, J. J.; Piotrowski, A. M.; Brownstein, S. K.; Gabe, E. J.; Lee, F. L. *J. Am. Chem. Soc.* **1985**, *107*, 7219.

(11) (a) Jordan, R. F.; Dasher, W. E.; Echols, S. F. *J. Am. Chem. Soc.* **1986**, *108*, 1718. b) Jordan, R.F.; Bajgur, C. S.; Willett, R.; Scott, B. *J. Am. Chem. Soc.* **1986**, *108*, 7410.

(12) Taube, R.; Krukowka, L. *J. Organomet. Chem.* **1988**, *347*, C9.

(13) Yang, X.; Stern, C. L.; Marks, T. J. *J. Am. Chem. Soc.* **1991**, *113*, 3623.

(14) Chien, J. C. W.; Tsai, W. M.; Rausch, M. D. *J. Am. Chem. Soc.* **1991**, *113*, 8570.

(15) Reichert, K. H.; Meyer, K. R. *Makromol. Chem.* **1973**, *169*, 163.

(16) Long, P. W.; Breslow, D. S. *Liebigs Ann. Chem.* **1975**,463.

(17) Sinn, H.; Kaminsky, W. *Adv. Organomet. Chem.* **1980**, *18*, 99.

(18) Negureanu, L.; Hall, R. W.; Butler, L. G.; Simeral, L. A. *J. Am. Chem. Soc.* **2006**, *128*, 16816; and references therein.

(19) (a) Thorshaug, K.; Stovneng, J. A.; Rytter, E.; Ystenes, M. *Macromolecules* **1998**, *31*, 7149. (b) Busico, V.; Cipullo, R.; Chadwick, J. C.; Modder, J. F.; Sudmeijer, O. *Macromolecules* **1994**, *27*, 7538. (c) Stehling, U.; Diebold, J.; Kirsten, R.; Röll, W.; Brintzinger, H. H.; Jüngling, S.; Mülhaupt, R.; Langhauser, F. *Organometallics* **1994**, *13*, 964. (d) Tsutsui, T.; Mizuno, A.; Kashiwa, N. *Polymer* **1989**, *30*, 428. (e) Brintzinger, H. H.; Fischer, D.; Mülhaupt, R.; Rieger, B.; Waymouth, R. M. *Angew. Chem., Int. Ed. Engl.* **1995**, *34*, 1143.

(20) (a) Chien, J. C. W.; Wang, B.-P. *J. Polym. Sci. A* **1990**, *28*, 15. (b) Naga, N.; Mizunuma, K. *Macromol. Chem. Phys.* **1998**, *199*, 113. (c) Thorshaug, K.; Rytter, E.; Ystenes, M. *Macromol. Rapid Commun.* **1997**, *18*, 715. (d) D'Agnillo, L.; Soares, J. B. P.; Penlidis, A. *Macromol. Chem. Phys.* **1998**, *199*, 955. (e) Murtuza, S.; Casagrande, O. L., Jr.; Jordan, R. F. *Organometallics* **2002**, *21*, 1882. (f) Shin, D. G.; Byun, D.-J.; Kim, S. Y., US 0041779, **2001**. (g) Rogers, J. S.; Bazan, G. C. *Chem. Commun.* **2000**, 1209. (h) Bazan, G. C.; Rogers, J. S.; Fang, C. C. *Organometallics* **2001**,*20*, 2059. (i) Mullins, M. J.; Boone, H. W.; Nickias, P. N.; Snelgrove, V., (Dow Chemical Co.), WO 02/42313, **2002**. (j) Simon, L. C.; Mauler, R. S.; De Souza, R. F. *J. Polym. Sci. A* **1999**, *37*, 4656. (k) Bambirra, S.; van Leusen, D.; Meetsma, A.; Hessen, B.; Teuben, J. H. *Chem. Commun.* **2003**, 522. (l) Samsel, E. G.; Eisenberg, D. C., (Ethyl Corporation), EP 0574854, **1993**. (m) Britovsek, G. J. P.; Cohen, S. A.; Gibson, V. C.; van Meurs, M. *J. Am. Chem. Soc.* **2004** *126*, 10701. (n) Britovsek, G. J. P.; Cohen, S. A.; Gibson, V. C.; Maddox, P. J.; van Meurs, M. *Angew. Chem. Int. Ed.* **2002**, *41*, 489.

(21) (a) Small, B. L.; Brookhart, M.; Bennett, A. M. A. *J. Am. Chem. Soc.* **1998**, *120*, 4049. (b) Britovsek, G. J. P.; Gibson, V. C.; Kimberley, B. S.; Maddox, P. J.; McTavish, S. J.; Solan, G. A.; White, A. J. P.; Williams, D. J. *Chem. Commun.* **1998**, 849.

(22) Britovsek, G. J. P.; Bruce, M.; Gibson, V. C.; Kimberley, B. S.; Maddox, P. J.; Mastroianni, S.; McTavish, S. J.; Redshaw, C.; Solan, G. A.; Strömberg, S.; White, A. J. P.; Williams, D. J. *J. Am. Chem. Soc.* **1999**, *121*, 8728.

(23) (a) Bajgur, C. S.; Tikkanen, W.; Petersen, J. L. *Inorg. Chem.* **1985**, *24*, 2539. (b) For more examples see the reviews in ref. 4.

(24) (a) Wild, F. R. W. P.; Wasincionek, M.; Huttener, G.; Brintzinger, H. H. *J. Organomet. Chem.*, **1985**, *288*, 63. (b) Coates, G. W. *Chem. Rev.* **2000**, *100*, 1223.

(25) (a) Shapiro, P. J.; Bunel, E.; Schaefer, W. P.; Bercaw, J. E. *Organometallics* **1990**, *9*, 867. (b) Cannich, J. A. M.; Turner, H. W., Exxon Chemical Patents, Pat. Appn WO-A92, 1992 (*Chem. Abstr.* **1993**, *118*, 81615. (c) Chum, P. S.; Kao, C. I.; Knight, G. W. *Plast. Eng.* **1995**, June 21. (d) Okuda, J. *Chem. Ber.* **1990**, *123*, 1649. (e) Hughes, A. K.; Meetsma, A.; Teuben, J. H. *Organometallics* **1993**, *12*, 1936. (f) McKnight, A. L.; Waymouth, R. M. *Chem. Rev.* **1998**, *98*, 2587.

(26) (a) Andersen, R. A. *Inorg. Chem.* **1979**, *18*, 2928. (b) Cannich, J. A. M.; Turner, H. W., (Exxon) PCT Int. Appl. WO 92/12162, July 23, **1992**.

(27) van der Linden, A.; Schaverien, C. J.; Meijboom, N.; Ganter, C.; Orpen, A. G. *J. Am. Chem. Soc.* **1995**, *117*, 3008.

(28) (a) Sernetz, F. G.; Mulhaupt, R.; Fokken, S.; Okuda, J. *Macromolecules* **1997**, *30*, 1562. (b) Fokken, S.; Spaniol, T. P.; Okuda, J.; Sernetz, F. G.; Mulhaupt, R. *Organometallics* **1997**, *16*, 4240. (c) Kakugo, M.; Miyatake, T.; Mizunuma, K. *Macromol. Chem., Macromol. Symp.* **1993**, *66*, 203.

(29) (a) Klabunde, V.; Ittel, S. D. *J. Mol. Catal.* **1987**, *41*, 123. (b) Desjardins, S. Y.; Cavell, K. J.; Hoare, J. L.; Skelton, B. W.; Sobojew, A. N.; White, A. H.; Keim, W. *J. Organomet. Chem.* **1997**, *544*, 163.

(30) (a) Brookhart, M.; Grant, B.; Volpe, A. F., Jr. *Organometallics* **1992**, *11*, 3920. (b) Brookhart, M.; DeSimone, J. M.; Grant, B. E.; Tanner, M. J. *Macromolecules* **1995**, *28*, 5378.

(31) (a) Johnson, L. K.; Killian, C. M.; Brookhart, M. S. *J. Am. Chem. Soc.* **1995**, *117*, 6414. (b) Killian, C. M.; Tempel, D. J.; Johnson, L. K.; Brookhart, M. S. *J. Am. Chem. Soc.* **1996**, *118*, 11664.

(32) (a) Lions, F.; Martin, K. V. *J. Am. Chem. Soc.* **1957**, *79*, 2733. (b) Sacconi, L.; Morassi, R.; Midollini, S. *J. Chem. Soc. (A)* **1968**, 510. (c) Alyea, E. C.; Merell, P. H. *Synth. React. Inorg. Met.-Org. Chem.* **1974**, *4*, 535.

(33) (a) Esteruelas, M. A.; López, A. M.; Méndez, L.; Oliván, M.; Oñate, E. *Organometallics* **2003**, *22*, 395., (b) Kleigrewe, N.; Steffen, W.; Blomker, T.; Kehr, G.; Frohlich, R.; Wibbeling, B.; Erker, G.; Wasilke, J.-C.; Wu, G.; Bazan, G. C. *J. Am. Chem. Soc.* **2005**, *127*, 13955. (c) Archer, A. M.; Bouwkamp, M. W.; Cortez, M.-P.; Lobkovsky, E.; Chirik, P. J. *Organometallics* **2006**, *25*, 4269.

(34) Smit, T. M.; Tomov, A. K.; Gibson, V. C.; White, A. J. P.; Williams, D. J. *Inorg. Chem.* **2004**, *43*, 6511.

(35) (a) de Bruin, B.; Bill, E.; Bothe, E.; Weyhermüller, T.; Wieghardt, K. *Inorg. Chem.* **2000**, *39*, 2936. (b) Budzelaar, P. H. M.; de Bruin, B.; Gal, A. W.; Wieghardt, K.; van Lenthe, J. H. *Inorg. Chem.* **2001**, *40*, 4649.

(36) Roberts, G. C. K. *NMR of Macromolecules: A Practical Approach*; IRC Press, Oxford, U.K., **1993**.

(37) De Boer, E. J. M.; Deuling, H. H.; van der Heijden, H.; Meijboorn, M.; van Oort, B. A.; van Zon, A. WO01/58874, **2001**.

(38) Ivanchev, S. S.; Yakimansky, A. V.; Rogozin, D. G. *Polymer* **2004**, *45*, 6453.

(39) (a) Small, B. L.; Brookhart, M. *J. Am. Chem. Soc.* **1998**,*120*, 7143. (b) Britovsek, G. J. P.; Mastroianni, S.; Solan, G. A.; Baugh, S. P. D.; Redshaw, C.; Gibson, V. C.; White, A. J. P.; Williams, D. J.; Elsegood, M. R. J. *Chem. Eur. J.* **2000**, *6*, 2221. (c) Ma, Z.; Sun, W.-H.; Li, Z.-L.; Shao, C.-X.; Hu, Y.-L. *Chin. J. Polym. Sci.* **2002**, *20*, 205.

(40) Bianchini, C.; Giambastiani, G.; Guerrero, I. R.; Meli, A.; Passaglia, E.; Gragnoli, T. *Organometallics* **2004**, *23*, 6078.

(41) (a) Bluhm, M. E.; Folli, C.; Döring, M. *J. Mol. Cat. A* **2004**, *212*, 13. (b) Fernandes, S.; Bellabarba, R. M.; Ribeiro, A. F. G.; Gomes, P. T.; Ascenso, J. R.; Mano, J. F.; Dias, A. R.; Marques, M. M. *Polymer Int.* **2002**, *51*, 1301.

(42) Britovsek, G. J. P.; Gibson, V. C.; Spitzmesser, S. K.; Tellmann, K. P.; White, A. J. P.; Williams, D. J. *J. Chem. Soc., Dalton Trans.* **2002**, 1159.

(43) Britovsek, G. J. P.; Clentsmith, G. K. B.; Gibson, V. C.; Goodgame, D. M. L.; McTavish, S. J.; Pankhurst, Q. A. *Catal. Commun.* **2002**, *3*, 207.

(44) (a) Bryliakov, K. P.; Semikolenova, N. V.; Zudin, V. N.; Zakharov, V. A.; Talsi, E. P. *Catal. Commun.* **2004**, *5*, 45. (b) Bryliakov, K. P.; Semikolenova, N. V.; Zakharov, V. A.; Talsi, E. P. *Organometallics* **2004**, *23*, 5375.

(45) Castro, P. M.; Lahtinen, P.; Axenov, K.; Viidanoja, J.; Kotiaho, T.; Leskelä, M.; Repo, T. *Organometallics* **2005**, *24*, 3664.

(46) (a) Deng, L.; Margl, P.; Ziegler, T. *J. Am. Chem. Soc.* **1999**, *121*, 6479. (b) Griffiths, E. A. H.; Britovsek, G. J. P.; Gibson, V. C.; Gould, I. R. *Chem. Commun.* **1999**, 1333. (c) Khoroshun, D. V.; Musaev, D. G.; Vreven, T.; Morokuma, K. *Organometallics* **2001**, *20*, 2007. (d) Zakharov, I. I.; Zakharov, V. A. *Macromol. Theory Simul.* **2004**, *13*, 583.

(47) Reardon, D.; Conan, F.; Gambarotta, S.; Yap, G.; Wang, Q. *J. Am. Chem. Soc.* **1999**, *121*, 9318.

(48) Sugiyama, H.; Aharonian, G.; Gambarotta, S.; Yap, G. P. A.; Budzelaar, P. H. M. *J. Am. Chem. Soc.* **2002**, *124*, 12268.

(49) Reardon, D.; Aharonian, G.; Gambarotta, S.; Yap, G. P. A. *Organometallics* **2002**, *21*, 786.

(50) Small, B. L.; Carney, M. J.; Holman, D. M.; O'Rourke, C. E.; Halfen, J. A. *Macromolecules* **2004**, *37*, 4375.

(51) Devore, D.; Feng, S. S.; Frazier, K. A.; Patton, J. T. (Dow Chemical) WO0069923, 2000.

(52) (a) Kooistra, T. M.; Knijnenburg, Q.; Smits, J. M. M.; Horton, A. D.; Budzelaar, P. H. M.; Gal, A. W. *Angew. Chem. Int. Ed.* **2001**, *40*, 4719. (b) Gibson, V. C.; Humphries, M. J.; Tellmann, K. P.; Wass, D. F.; White, A. J. P.; Williams, D. J. *Chem. Commun.* **2001**, 2252.

(53) Steffen, W.; Blömker, T.; Kleigrewe, N.; Kehr, G.; Fröhlich, R.; Erker, G. *Chem. Commun.* **2004**, 1188.

(54) Humphries, M. J.; Tellmann, K. P.; Gibson, V. C.; White, A. J. P.; Williams, D. J. *Organometallics* **2005**, *24*, 2039.

(55) (a) Cano, J.; Royo, P.; Lanfranchi, M.; Pellinghelli, M. A.; Tiripicchio, A. *Angew. Chem. Int. Ed.* **2001**, *40*, 2495. (b) Jin, J.; Wilson, D. R.; Y.-X., E. *Chem. Commun.* **2002**, 708.

(56) Bruce, M.; Gibson, V. C.; Redshaw, C.; Solan, G. A.; White, A. J. P.; Williams, D. J. *Chem. Commun.* **1998**, 2523.

(57) Milione, S.; Cavallo, C.; Tedesco, C.; Grassi, A. *J. Chem. Soc. Dalton Trans.* **2002**, 1839.

(58) (a) Knijnenburg, Q.; Smits, J. M. M.; Budzelaar, P. H. M. *C. R. Chimie* **2004**, *7*, 865. (b) Knijnenburg, Q.; Smits, J. M. M.; Budzelaar, P. H. M *Organometallics* **2006**, *25*, 1036.

(59) Khorobkov, I.; Gambarotta, S.; Yap, G. P. A. *Organometallics* **2002**, *21*, 3088.

(60) Clentsmith, G. K. B.; Gibson, V. C.; Hitchcock, P. B.; Kimberley, B. S.; Rees, C. W. *Chem. Commun.* **2002**, 1498.

(61) Blackmore, I. J.; Gibson, V. C.; Hitchcock, P. B.; Rees, C. W.; Williams, D. J.; White, A. J. P. *J. Am. Chem. Soc.* **2005**, *127*, 6012.

(62) (a) van Koten, G.; Jastrzebski, J. T. B. H.; Vrieze, K. *J. Organomet. Chem.* **1983**, *250*, 49. (b) Kaupp, M.; Stoll, H.; Preuss, H.; Kaim, W.; Stahl, T.; van Koten, G.; Wissing, E.; Smeets, W. J. J.; Spek, A. L. *J. Am. Chem. Soc.* **1991**, *113*, 5606. (c) Kaim, W. *Acc. Chem. Res.* **1985**, *18*, 160. (d) Ashby, E. C. *Acc. Chem. Res.* **1988**, *21*, 414. (e) Wissing, E.; Kaupp, M.; Boersma, J.; Spek, A. L.; van Koten, G. *Organometallics* **1994**, *13*, 2349.

(63) Sugiyama, H.; Gambarotta, S.; Yap, G. P. A.; Wilson, D. R.; Thiele, S. K.-H. *Organometallics* **2004**, *23*, 5054.

(64) Sugiyama, H.; Korobkov, I.; Gambarotta, S.; Möller, A.; Budzelaar, P. H. M. *Inorg. Chem.* **2004**, *43*, 5771.

(65) Pelascini, F.; Wesolek, M.; Peruch, F.; Lutz, P. J. *Eur. J. Inorg. Chem.* **2006**, *2006*, 4309.

(66) Enright, D.; Gambarotta, S.; Yap, G. P. A.; Budzelaar, P. H. M. *Angew. Chem. Int. Ed.* **2002**, *41*, 3873.

(67) Knijnenburg, Q.; Hetterscheid, D.; Kooistra, T. M.; Budzelaar, P. H. M. *Eur. J. Inorg. Chem.* **2004**, 1204.

(68) Lau, W.; Huffman, J. C.; Kochi, J. K. *Organometallics* **1982**, *1*, 155.

Chapter Two

Alkylation of the Bis-iminopyridine-$FeCl_2$ Precursor with $LiCH_2SiMe_3$

Introduction

Regardless of the catalytic system considered for olefin polymerization, the metal-carbon σ-bond is at the foundation of this remarkable transformation. Although disagreements abound with respect to the role of the activator, the presence of a cationic metal center and the oxidation state of the metal in the catalytically active species, the essential event in polymerization is the formation of a metal carbon σ-bond.[1] Hence, the most obvious preliminary step towards determining the mechanism of polymerization almost always revolves around M-C σ-bond formation and the factors which determine both the reactivity and stability of this particular function. The importance of the M-C bond has in turn boosted attention towards the preparation, characterization and reactivity of homoleptic organo-transition metal complexes, in the interests of preparing single component catalysts which do not require pyrophoric and dangerous aluminum or expensive borane activators.

Unlike the main group metals, the formation of a transition metal alkyl is not a trivial matter by any means. Throughout the early years, numerous attempts to isolate seemingly simple complexes such as diethyliron or diethylcobalt were unsuccessful, misleadingly promoting the idea that transition metal alkyls are not thermodynamically stable.[2] Contrary to this notion, however, transition metal alkyls are no less stable than

main group alkyls,[3] but their stability pivots mainly on kinetic considerations as opposed to thermodynamic constraints. Unfortunately, transition metal alkyls suffer from facile decomposition pathways, the most important being β-hydride elimination. In this process, the β-hydrogen of the alkyl is transferred to the metal center through a four-membered transition state, forming a metal-hydride σ-bond and a weakly π-bound terminal C=C double bond. In the case of first row transition metals, the metal center is easily reduced by elimination of the hydride atom, generally resulting in the metal in its elemental form.[2] One way to overcome this drawback is with the use of an alkyl free of β-hydrogens, such as $-CH_2Si(CH_3)_3$ or the neopentyl analogue. Only in this way have homoleptic Fe-alkyl systems been isolated.[4]

Contrary to the bleak outlook described above for Fe-C bonds, Fe-alkyls can be stabilized by using ancillary ligands, like phosphines,[5] cyclopentadienyl and CO,[6] which on one hand greatly enhances the stability of the metal carbon bond, while on the other substantially quenches the reactivity. More related to this work are the Fe-alkyls supported by diamine or diimine ligands.[7] These complexes may be prepared relatively easily from the original ligated dichloride precursors. Although similar in nature to the $FeCl_2$-bis-iminopyridine catalyst,[8] these species do not display the high degree of catalytic activity for ethylene polymerization and are nonetheless susceptible to facile reduction to the zero or monovalent state. It is therefore conceivable that, given the outstanding activity of the bis-iminopyridine Fe catalyst,[8] the ligand provides the M-C bond with the appropriate stability to disfavour termination pathways while maintaining the high reactivity necessary for catalytic efficiency.

The attempts to isolate a dialkyl species from the bis-iminopyridine $FeCl_2$ complex are described herein and involve the use of $LiCH_2Si(CH_3)_3$ as the alkylating agent. Although $LiCH_2Si(CH_3)_3$ is not present in the actual catalytic run, and will therefore not be involved in the polymerization, it was hoped that the lack of β-hydrogens will provide the M-C bond with sufficient stability to be isolated. Given the complexity of the behaviour of this non-innocent ligand and its frequent involvement in the reactivity of the metal carbon bond, it will be important to monitor the alkylation of the Fe complex. As seen in Chapter 1, alkylation of similar systems by several different alkylating agents has led to nucleophilic attack at every position of the pyridine ring[9-12]

and also the imine-carbon atom.[12,13] Alkylation has also resulted in deprotonation of either one[11bc,14] or both[10,12,15,16] ketimine methyl groups and initiated two separate dimerization pathways, either through the methyl imine groups,[10,12,13,17,18] or through the pyridine *meta*-carbons.[10,13c] The only instance in which the ligand was not attacked during the alkylation was with the bis-iminopyridine-$CoCl_2$ precursor.[19] However, in this case, the metal center is reduced by one electron prior to alkylation. Needless to say, alkylation of the bis-iminopyridine systems has never been straightforward, and as such, simple dialkylation of the $LFeCl_2$ precursor would be rather surprising. For this reason, the use of $LiCH_2Si(CH_3)_3$ is even more advisable, as it increases the chance of isolating characterizable products from the reaction mixture and will hopefully aid in uncovering the secret behind the high activity displayed by the Fe system versus other transition metals.

The aim of this study was to understand the chemistry of the Fe-C functionality in the bis-iminopyridine Fe catalyst. Concurrent with the publication of this work, the groups of Chirik[20] and Campora[21] independently published reports detailing the formation of the Fe-dialkyl species from reaction of the bis-iminopyridine-$FeCl_2$ precursor with $LiCH_2Si(CH_3)_3$. Herein, we describe the extended results of the alkylation of the bis-iminopyridine-$FeCl_2$ catalyst with $LiCH_2Si(CH_3)_3$.

Experimental Section

All operations were performed under a nitrogen atmosphere using standard Schlenk techniques or in a purified nitrogen-filled dry-box. The THF complex of $FeCl_2$ was prepared according to the standard procedure. The ligand 2,6-[2,6-(^{i}Pr)$_2$PhN=C(CH_3)]$_2$(C_5H_3N),[8] the mono-[11] and di-deprotonated[15,18] derivatives and $LiCH_2Si(CH_3)_3$[22] were prepared following published procedures. Infrared spectra were recorded on a Mattson 9000 and Nicolet 750-Magna FT-IR instrument from Nujol mulls prepared in a dry box. Samples for magnetic susceptibility measurements were weighed inside a dry box equipped with an analytical balance and sealed into calibrated tubes and the measurements were carried out at room temperature with a Gouy balance (Johnson Matthey). Magnetic moments were calculated following standard methods and corrections for underlying diamagnetism were applied to the data. Elemental analyses

were performed on a Perkin-Elmer 2400 CHN analyzer. Data for X-ray crystal structure determinations were obtained with a Bruker diffractometer equipped with a Smart CCD area detector.

Preparation of {2,6-[2,6-(^{i}Pr)$_2$PhN=C(CH$_3$)]$_2$(C$_5$H$_3$N)}FeCl$_2$.

A suspension of 2,6-[2,6-(^{i}Pr)$_2$PhN=C(CH$_3$)]$_2$(C$_5$H$_3$N) (2.05 g, 4.26 mmol) in THF was added to a suspension of FeCl$_2$(THF)$_{1.5}$ (1.00 g, 4.26 mmol) in THF and the resulting dark blue mixture was stirred overnight. After evaporating the THF in vacuum, the residue was dissolved in an appropriate amount of CH_2Cl_2, concentrated and layered with hexane. Dark blue crystals of the bis-iminopyridine-$FeCl_2$ starting complex were grown while sitting at room temperature for 2 days: 84% yield. Although this procedure is very similar to published procedures[8] and prepares the identical compound, this synthesis strictly avoids the use of water or alcohols, and as such, ensures a 'dry' starting complex for further reactions. Full characterization of the material can be found in reference 8.

Preparation of {2,6-[2,6-(^{i}Pr)$_2$PhN=C(CH$_3$)]$_2$-(2-CH$_2$SiMe$_3$)}(C$_5$H$_3$N)Fe(CH$_2$SiMe$_3$) (2.1).

A suspension of FeCl$_2$(THF)$_{1.5}$ (0.200 g, 0.85 mmol) and 2,6-[2,6-(^{i}Pr)$_2$PhN=C(CH$_3$)]$_2$(C$_5$H$_3$N) (0.410 g, 0.85 mmol) in approximately 10 mL of THF was stirred for four hours affording the usual dark blue colour. The suspension was cooled to -35°C and mixed with a cooled solution of LiCH$_2$SiMe$_3$ (0.168 g, 1.78 mmol) in THF. The colour of the solution instantly changed from royal blue to dark reddish-orange upon mixing. The solution was stirred for approximately one minute to ensure complete mixing and evaporated to dryness, maintaining a cold temperature throughout the procedure. Cold hexane was added to the dark brown residue and a dark reddish-orange suspension was centrifuged to remove a substantial amount of insoluble material. The resulting solution was allowed to stand at -35°C for 24 hours, upon which time the mother liquor was removed from small dark crystals (recognized later as a small amount of **2.2**), concentrated and put back in the freezer for two days, resulting in the crystallization of **2.1** as dark red crystals (0.212 g, 0.30 mmol, 35% yield). Anal. Calcd. (found) for C$_{41}$H$_{65}$FeN$_3$Si$_2$ (%): C, 69.16 (69.05); H, 9.20 (9.18); N, 5.90 (5.87). IR (Nujol mull,

cm^{-1}): ν 3066 (w), 2929 (s), 1614 (m), 1568 (s), 1498 (s), 1363 (m), 1352 (m), 1321 (s), 1288 (m), 1242 (m), 1195 (m), 1143 (m), 1099 (w), 1056 (w), 1043 (w), 970 (w), 946 (w), 937 (w), 881 (s), 850 (s,b), 813 (m,b), 773 (m), 721 (m,b), 700 (m). [μ_{eff} = 5.6 μ_B].

Preparation of {2,6-[2,6-(^{i}Pr)$_2$PhN=C(CH$_3$)]$_2$}(C$_5$H$_3$N)Fe(CH$_2$SiMe$_3$)$_2$ (2.2).

Method A. The preparation was carried out as above except the remaining hexane-insoluble solids were dissolved in ether. The colour became dark purple and the mixture was centrifuged to separate a dark purple solution from a small amount of colourless solids. The ether solution was concentrated and kept at -35°C for 2 days, upon which crystals of **2.2** suitable for X-ray analysis were isolated (0.180 g, 0.25 mmol, 30% yield). Anal. Calcd. (found) for $C_{41}H_{65}FeN_3Si_2$ (%): C, 69.16 (69.13); H, 9.20 (9.15); N, 5.90 (5.83). IR (Nujol mull, cm^{-1}): ν 2931 (s), 2865 (s), 1645 (w), 1585 (w), 1548 (w), 1282 (s), 1259 (m), 1263 (s), 1193 (w), 1155 (m), 1135 (m), 1110 (w), 1097 (w), 973 (s), 916 (w), 894 (w), 850 (s,b), 823 (s), 775 (m), 727 (m,b). [μ_{eff} = 5.6 μ_B].

Method B. A solution of LiCH$_2$SiMe$_3$ (0.168 g, 1.78 mmol) in ether (5 mL) was added to a suspension of FeCl$_2$(THF)$_{1.5}$ (0.200 g, 0.85 mmol) in ether (5 mL) at -35°C. The mixture began to turn yellow with swirling. The mixture was kept at -35°C with periodic swirling for approximately two minutes. The resulting brownish-yellow suspension was added to a cooled suspension of 2,6-[2,6-(^{i}Pr)$_2$PhN=C(CH$_3$)]$_2$(C$_5$H$_3$N) (0.410 g, 0.85 mmol) in ether (10 mL). The colour instantly became dark purple and the mixture was stirred for two minutes to ensure complete mixing. The reaction was then centrifuged to remove a dark purple solution from insoluble white precipitates. Upon concentrating and freezing at -35°C, dark purple block crystals of **2.2** were obtained (0.357 g, 0.50 mmol, 59% yield).

Method C. A solution of LiCH$_2$SiMe$_3$ (0.170 g, 1.80 mmol) in THF (5 mL) was added to a suspension of {2,6-[2,6-(^{i}Pr)$_2$PhN=C(CH$_3$)]$_2$(C$_5$H$_3$N)}FeCl$_2$ (0.500 g, 0.82 mmol) in 10 mL of THF at -35°C. The colour slowly changed from dark blue to dark brownish-red and the suspension slowly dissolved into solution upon stirring. After stirring for approximately 30 minutes, the solvent was evaporated and cold hexane was added to the brown residue. The resulting suspension was centrifuged and a dark olive-green solution (from which **2.4** crystallized) was separated from the dark precipitates. Diethyl ether was

added to the precipitates and the solution was centrifuged to separate a dark purple solution from white precipitates. Concentration of the solution and standing in the freezer for two days afforded crystals of **2.2** (0.304 g, 0.427 mmol, 52% yield).

Preparation of {2-[2,6-(^{i}Pr)$_2$PhN=C(CH$_3$)]-6-[2,6-(^{i}Pr)$_2$PhNC(CH$_3$)(CH$_2$SiMe$_3$)] (C$_5$H$_3$N)}Fe(CH$_2$SiMe$_3$) (2.3).

A procedure identical to that described for complex **2.1** was followed. Crystals of **2.3** grew out of the same hexane solution as **2.1** but could be physically separated with the help of a stereo-microscope due to their very distinct rectangular shape (0.055 g, 0.08 mmol, 10 % yield). Anal. Calcd. (found) for $C_{41}H_{65}FeN_3Si_2$ (%): C, 69.16 (69.10); H, 9.20 (9.18); N, 5.90 (5.87).

Transformation of 2.3 to 2.2.

Addition of diethyl ether (10 mL) to crystals of **2.3** (0.055 g, 0.08 mmol) afforded a dark purple solution from which dark purple crystals of **2.2** were isolated after freezing at -35°C for two days (0.035 g, 0.05 mmol, 62% yield).

Preparation of {[2,6-[2,6-(^{i}Pr)$_2$PhN-C=(CH$_2$)]$_2$(C$_5$H$_3$N)}Fe(μ-Cl)Li(THF)$_3$ (2.4).

Method A. To a suspension of {2,6-[2,6-(^{i}Pr)$_2$PhN=C(CH$_3$)]$_2$(C$_5$H$_3$N)}FeCl$_2$ (0.500 g, 0.82 mmol) in THF (10 mL) a solution of LiCH$_2$SiMe$_3$ (0.170 g, 1.80 mmol) in THF (5 mL) was added at -35°C. The colour slowly changed from dark blue to dark brownish-red and the solids slowly dissolved with stirring. After stirring for approximately 30 minutes, the solvent was evaporated and cold hexane was added to the brown residue. The resulting suspension was centrifuged and a dark olive-green solution was separated from dark precipitates (identified as **2.2** upon recrystallization in ether, 65% yield). The solution was placed in the freezer overnight and then the mother liquor was removed from a small amount of crystallized **2.2** and placed back in the freezer. Dark orange crystals of **2.4** were grown from the hexane solution after standing at -35°C for 2 days (0.098 g, 0.12 mmol, 15% yield). Anal. Calcd. (found) for $C_{45}H_{66}ClFeLiN_3O_3$ (%): C, 67.96 (67.93); H, 8.37 (8.31); N, 5.28 (5.24). IR (Nujol mull, cm^{-1}): ν 2918 (s), 2854 (s), 1644 (m), 1572 (s), 1322 (m), 1279 (s), 1249 (m), 1236 (s), 1210 (w), 1193 (w), 1154

(m), 1134 (m), 1107 (m,b), 1047 (s), 1005 (m), 972 (s), 890 (m), 848 (s,b), 822 (s), 773 (s), 727 (s). [μ_{eff} = 5.8 μ_B].

Method B. A solution of {[2,6-{[2,6-(^{i}Pr)$_2$C$_6$H$_3$]N-C=(CH$_2$)}$_2$(C$_5$H$_3$N)]Li(THF)}{Li(THF)$_4$} (0.727 g, 0.85 mmol) in THF was added to a suspension of $FeCl_2(THF)_{1.5}$ (0.200 g, 0.85 mmol) in THF (35 mL) at -35°C. The colour of the suspension was dark brownish-red. After stirring for approximately 30 minutes, the solvent was evaporated and cold hexane was added to the brown residue. The suspension was centrifuged to eliminate a small amount of lightly-coloured material. Dark orange crystals of **2.4** were grown from the hexane solution upon standing at -35°C for 2 days (0.379 g, 0.48 mmol, 56% yield).

Preparation of [{2,6-[2,6-(^{i}Pr)$_2$PhN-C=(CH$_2$)]$_2$(C$_5$H$_3$N)}FeCH$_2$Si(CH$_3$)$_3$][Li(THF)$_4$] (2.6).

A solution of $LiCH_2SiMe_3$ (0.168 g, 1.78 mmol) in ether was added to a suspension of $FeCl_2(THF)_{1.5}$ (0.200 g, 0.85 mmol) in ether at -35°C. The mixture was stirred for approximately two minutes, upon which time the colour gradually became darker yellow-brown. At this time, a solution of {2-[2,6-(^{i}Pr)$_2$PhN-C=(CH$_2$)]-6-[2,6-(^{i}Pr)$_2$PhN-CCH$_3$](C$_5$H$_3$N)}Li(THF) (0.476 g, 0.85 mmol) in ether, also kept at -35°C, was added. The colour of the mixture became dark royal blue and stirring was continued for one hour. The ether was evaporated and the resulting mass solubilized in THF. After centrifugation and concentration, the THF solution was layered with hexane affording, after standing for two days, reddish-brown crystals of **2.6** (0.430 g, 0.47 mmol, 55% total yield). Anal. Calcd. (found) for $C_{53}H_{86}SiN_3FeLiO_4$ (%): C, 69.18 (68.77); H, 9.42 (9.68); N, 4.57 (5.01). IR (Nujol mull, cm^{-1}): ν 2952 (s), 2855 (s), 1561 (s), 1523 (w), 1468 (s), 1434 (m), 1377 (m), 1367 (m), 1356 (m), 1320 (m), 1309 (w), 1283 (w), 1252 (m), 1228 (w), 1209 (w), 1176 (w), 1125 (w), 1101 (w), 1083 (w), 1040 (s), 1003 (m), 968 (w), 935 (w), 916 (w), 887 (s), 868 (s), 812 (m), 771 (m), 760 (m), 746 (m), 722 (m). [μ_{eff} = 5.6 μ_B].

X-ray Crystallography

All of the compounds **2.1-2.6** consistently yielded crystals that diffracted weakly, and the results presented are the best of several trials. The crystals were mounted on thin glass fibers using paraffin oil and cooled to the data collection temperature. Data were collected on a Bruker AXS SMART 1k CCD diffractometer. Data for the compounds **2.1** and **2.6** were collected with a sequence of 0.3° ω scans at 0, 120, and 240° in φ. To obtain acceptable redundancy data for compound **2.3**, the sequence of 0.3° ω scans at 0, 90, 180, and 270° in φ was used. Initial unit cell parameters were determined from 50 data frames collected at different sections of the Ewald sphere. Semiempirical absorption corrections based on equivalent reflections were applied.[23] Systematic absences in the diffraction data-set and unit-cell parameters were consistent with monoclinic $P2_1/n$ for **2.1**, orthorhombic *Pbca* for **2.2**, triclinic $P\bar{1}$ for **2.3,** monoclinic $P2_1/n$ for **2.4** and monoclinic $P2_1/c$ for **2.6**. Solutions in centrosymmetric space groups for all of the compounds yielded chemically reasonable and computationally stable results of refinement. The structures were solved by direct methods, completed with difference Fourier synthesis, and refined with full-matrix least-squares procedures based on F^2. The compound molecules were located in common positions in the structures of all the complexes. All non-hydrogen atoms were refined with anisotropic displacement coefficients. All hydrogen atoms were treated as idealized contributions. All scattering factors are contained in several versions of the SHELXTL program library, with the latest version used being v.6.12.[24] Crystallographic data and relevant bond distances and angles are reported in Tables 2.1-2.3.

Table 2.1. Crystal Data and Structure Analysis Results of Complexes 2.1-2.4 and 2.6

	2.1	**2.2**	**2.3**	**2.4**	**2.6**
formula	$C_{41}H_{65}FeN_3Si_2$	$C_{41}H_{65}FeN_3Si_2$	$C_{41}H_{65}FeN_3Si_2$	$C_{45}H_{66}ClFeLiN_3O_3$	$C_{53}H_{86}N_3FeLiO_4Si$
Mw	711.99	711.99	711.99	795.25	920.13
crystal system	Monoclinic	Orthorhombic	Triclinic	Monoclinic	Monoclinic
space group	P2(1)/n	Pbca	P-1	P2(1)/n	P2(1)/c
a (Å)	9.8426(12)	15.942(5)	9.610(3)	11.574(3)	15.998(19)
b (Å)	18.821(2)	20.104(6)	10.865(3)	18.331(5)	27.61(3)
c (Å)	22.748(3)	26.360(8)	22.115(7)	21.787(5)	24.90(3)
α (deg)	90	90	89.135(5)	90	90
β (deg)	91.684(2)	90	85.805(6)	96.094(5)	97.75(2)
γ (deg)	90	90	66.610(5)	90	90
V (Å^3)	4212.1(9)	8449(5)	2113.5(12)	4596.3(19)	10902(22)
Z	4	8	2	4	4
radiation (Kα, Å)	0.71073	0.71073	0.71073	0.71073	0.71073
T (K)	206(2)	208(2)	208(2)	208(2)	213
D_{calcd} (g cm^{-3})	1.124	1.120	1.119	1.149	1.121
μ_{calcd} (mm^{-1})	0.445	0.443	0.443	0.425	0.342
F_{000}	1548	3088	772	1708	4000
R, R_w[2] [a]	0.0623, 0.1399	0.0593, 0.1463	0.0721, 0.1272	0.0783, 0.1540	0.0688, 0.1518
GoF	1.036	1.091	1.011	1.065	1.008

[a] $R = \Sigma||F_0| - |F_c||/\Sigma|F|$, $R_w = [\Sigma(|F_0| - |F_c|)^2/\Sigma wF_0^2\}^{1/2}$

Table 2.2. Selected Bond Distances (Å) and Angles (deg) of Complexes 2.1-2.3

2.1	2.2	2.3
Fe(1)-N(1) = 2.224(3)	Fe(1)-N(1) = 2.271(3)	Fe(1)-N(1) = 2.433(3)
Fe(1)-N(2) = 2.015(2)	Fe(1)-N(2) = 2.018(3)	Fe(1)-N(2) = 2.130(3)
Fe(1)-N(3) = 2.160(3)	Fe(1)-N(3) = 2.213(3)	Fe(1)-N(3) = 1.960(3)
Fe(1)-C(41) = 2.036(3)	Fe(1)-C(34) = 2.061(3)	Fe(1)-C(38) = 2.045(4)
C(1)-C(2) = 1.499(5)	Fe(1)-C(38) = 2.062(4)	C(1)-C(2) = 1.499(6)
N(2)-C(3) = 1.473(4)	C(1)-C(2) = 1.506(5)	N(3)-C(8) = 1.477(5)
C(3)-C(4) = 1.516(4)	C(8)-C(9) = 1.498(5)	C(8)-C(9) = 1.533(5)
C(4)-C(5) = 1.338(5)	N(1)-C(2) = 1.305(4)	N(1)-Fe(1)-N(2) = 69.27(12)
C(5)-C(6) = 1.429(5)	N(3)-C(8) = 1.304(4)	N(1)-Fe(1)-N(3) = 145.82(13)
C(6)-C(7) = 1.371(4)	N(1)-Fe(1)-N(2) = 72.78(11)	N(1)-Fe(1)-C(38) = 99.55(15)
C(7)-N(2) = 1.366(4)	N(2)-Fe(1)-N(3) = 73.92(11)	N(2)-Fe(1)-N(3) = 78.49(13)
C(8)-C(9) = 1.489(5)	N(1)-Fe(1)-N(3) = 140.80(10)	N(2)-Fe(1)-C(38) = 156.75(16)
N(1)-Fe(1)-N(2) = 75.94(10)	N(1)-Fe(1)-C(34) = 94.01(12)	N(3)-Fe(1)-C(38) = 114.62(16)
N(1)-Fe(1)-N(3) = 121.88(10)	N(2)-Fe(1)-C(34) = 140.17(13)	
N(1)-Fe(1)-C(41) = 115.74(13)	N(3)-Fe(1)-C(34) = 98.50(13)	
N(2)-Fe(1)-N(3) = 78.37(11)	N(1)-Fe(1)-C(38) = 105.96(13))	
N(2)-Fe(1)-C(41) = 140.44(13)	N(2)-Fe(1)-C(38) = 107.68(13)	
N(3)-Fe(1)-C(41) = 117.27(13)	N(3)-Fe(1)-C(38) = 103.37(13)	
	C(34)-Fe(1)-C(38) = 112.09(15)	

Table 2.3. Selected Bond Distances (Å) and Angles (deg) of Complexes 2.4-2.6

2.4	2.5	2.6
Fe(1)-N(1) = 2.013(6)	Fe(1)-C(34) = 2.05	Fe(1)-N(1) = 2.094(4)
Fe(1)-N(2) = 2.095(6)	N(1)-C(2) = 1.31	Fe(1)-N(2) = 2.138(4)
Fe(1)-N(3) = 2.022(6)	C(1)-C(2) = 1.50	Fe(1)-N(3) = 2.078(4)
Fe(1)-Cl(1) = 2.318(2)	N(3)-C(8) = 1.31	Fe(1)-C(34) = 2.068(5)
N(1)-C(2) = 1.380(9)	C(8)-C(9) = 1.49	N(1)-C(2) = 1.360(6)
C(1)-C(2) = 1.362(10)		N(3)-C(8) = 1.354(6)
N(3)-C(8) = 1.375(9)		C(1)-C(2) = 1.337(7)
C(8)-C(9) = 1.344(10)		C(8)-C(9) = 1.356(7)
Cl(1)-Li(1) = 2.362(13)		N(1)-Fe(1)-N(3) = 145.67(15)
N(1)-Fe(1)-N(2) = 75.7(3)		N(2)-Fe(1)-C(34) = 155.4(2)
N(1)-Fe(1)-N(3) = 151.3(3)		N(1)-Fe(1)-C(34) = 107.1(2)
N(1)-Fe(1)-Cl(1) = 104.25(19)		N(2)-Fe(1)-N(3) = 74.08(16)
N(2)-Fe(1)-N(3) = 75.7(3)		N(1)-C(2)-C(1) = 127.6(5)
N(2)-Fe(1)-Cl = 177.48(18)		Fe(1)-C(34)-Si(1) = 128.6(3)
N(3)-Fe(1)-Cl(1) = 104.44(19)		
Fe(1)-Cl(1)-Li(1) = 171.0(4)		

Complex 2.1. Complex **2.1** consists of an Fe atom coordinated to the three nitrogen atoms of the ligand system [Fe(1)-N(1) = 2.224(3) Å, Fe(1)-N(2) = 2.015(2) Å, Fe(1)-N(3) = 2.160(3) Å] which has been alkylated at one of the two pyridine ring *ortho*-positions (Figure 2.1). One silylated-alkyl group is also attached to Fe [Fe(1)-C(41) = 2.036(3) Å], providing the metal center with a severely distorted tetrahedral coordination geometry [N(1)-Fe(1)-N(2) = 75.94(10)°, N(1)-Fe(1)-N(3) = 121.88(10)°, N(1)-Fe(1)-C(41) = 115.74(13)°, N(2)-Fe(1)-N(3) = 78.37(11)°, N(2)-Fe(1)-C(41) = 140.44(13)°, N(3)-Fe(1)-C(41) = 117.27(13)°]. The consequence of the pyridine ring alkylation and resulting loss of aromaticity can be noticed in the ring deviation from planarity and the expected variation in bond lengths compared to the precursor[8] [N(2)-C(3) = 1.473(4) Å, C(3)-C(4) = 1.516(4) Å, C(4)-C(5) = 1.338(5) Å, C(5)-C(6) = 1.429(5) Å, C(6)-C(7) = 1.371(4) Å, C(7)-N(2) = 1.366(4) Å]. The other geometrical parameters of the ligand do not show significant features and are comparable to those of the vanadium catalyst that underwent a similar distortion upon alkylation with MAO.[9]

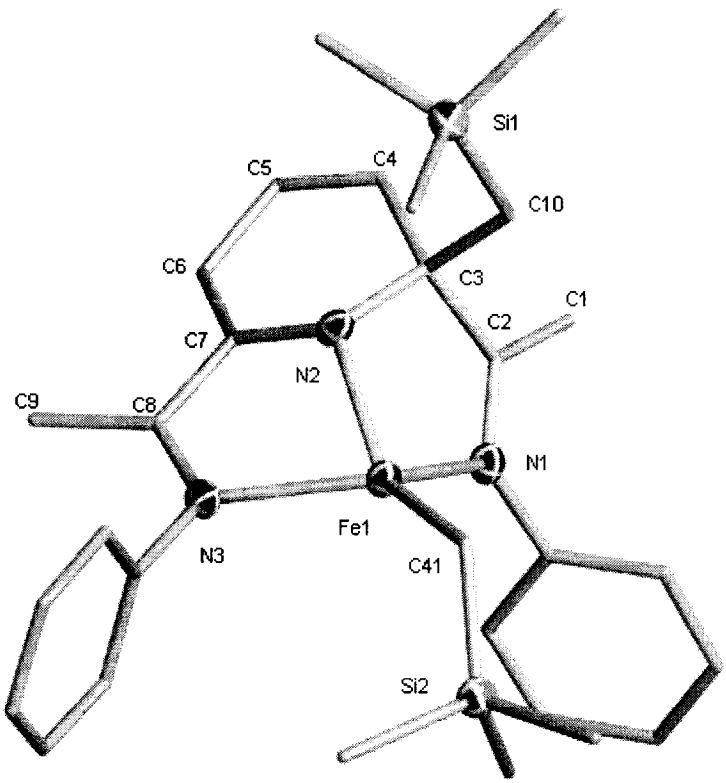

Figure 2.1. Partial thermal ellipsoid plot for **2.1** with the ellipsoids drawn at the 30% probability level. Hydrogen atoms have been omitted for clarity.

Complex 2.2. The structure showed a pentacoordinated Fe atom bound to the three nitrogen atoms of the intact ligand [Fe(1)-N(1) = 2.271(3) Å, Fe(1)-N(2) = 2.018(3) Å, Fe(1)-N(3) = 2.213(3) Å] and two alkyl units [Fe(1)-C(34) = 2.061(3) Å, Fe(1)-C(38) = 2.062(4) Å] (Figure 2.2). The overall coordination geometry around the metal center may be regarded as distorted square pyramidal with the basal plane defined by the three nitrogen atoms of the ligand system and the C atom of one of the two the alkyl groups [N(1)-Fe(1)-N(2) = 72.78(11)°, N(2)-Fe(1)-N(3) = 73.92(11)°, N(3)-Fe(1)-C(34) = 98.50(13)°, C(34)-Fe(1)-N(1) = 94.01(12)°, N(1)-Fe(1)-N(3) = 140.80(10)°, N(2)-Fe(1)-C(34) = 140.17(13)°]. The axial position is occupied by the second alkyl moiety [C(38)-Fe(1)-N(1) = 105.96(13)°, C(38)-Fe(1)-N(2) = 107.68(13)°, C(38)-F(1)e-N(3) = 103.37(13)°, C(38)-Fe(1)-C(34) = 112.09(15)°]. The ligand system is basically intact as a result of the coordination and does not show any significant features with respect to the structures of other MCl_2 derivatives [M = V, Cr, Mn, Fe, Co, Ln].[8-10,18]

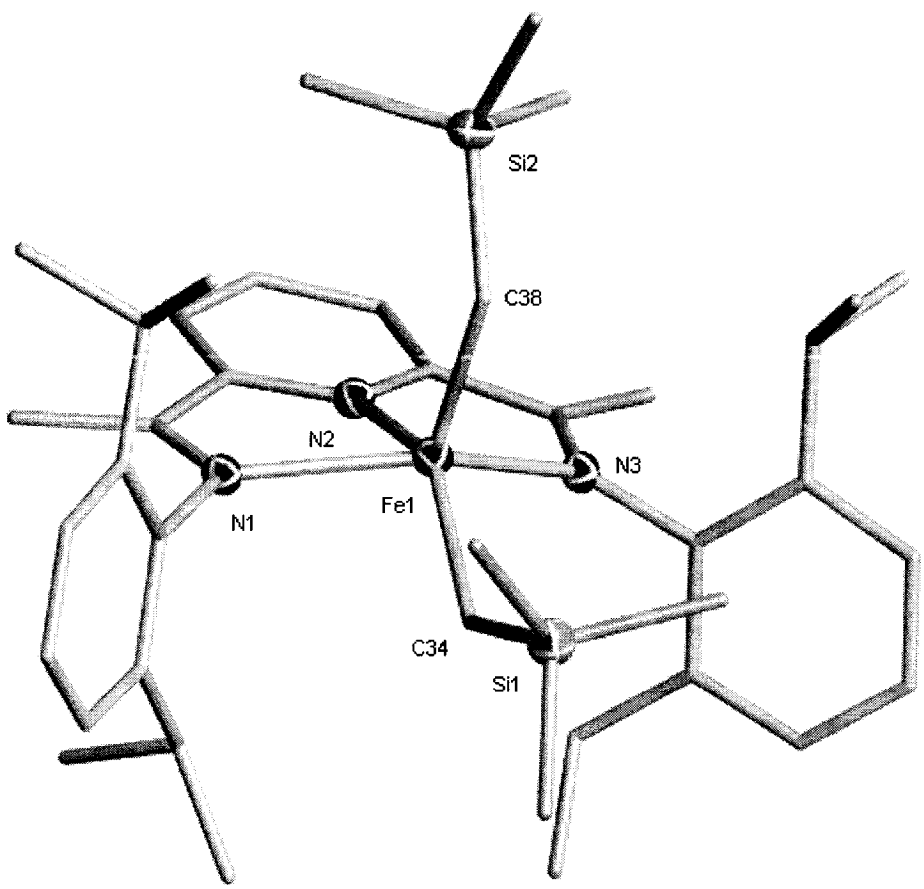

Figure 2.2. Partial thermal ellipsoid plot for **2.2** with the ellipsoids drawn at the 30% probability level. Hydrogen atoms have been omitted for clarity.

Complex 2.3. The structure of **2.3** consists of a tetracoordinate Fe atom surrounded by the ligand system which has undergone alkylation similar to the case of **2.1** (Figure 2.3). However, instead of being attached to the pyridine ring *ortho*-position, the alkyl group is found connected to one of the two former imine C atoms. The coordination sphere of the metal center is defined by the three N atoms of the alkylated ligand system and the C atom of one alkyl group [Fe(1)-N(1) = 2.433(3) Å, Fe(1)-N(2) = 2.130(3) Å, Fe(1)-N(3) = 1.960(3) Å, Fe(1)-C(38) = 2.045(4) Å]. The coordination geometry of Fe is distorted between square planar and tetrahedral [N(1)-Fe(1)-N(2) = 69.27(12)°, N(1)-Fe(1)-N(3) = 145.82(13)°, N(1)-Fe(1)-C(38) = 99.55(15)°, N(2)-Fe(1)-N(3) = 78.49(13)°, N(2)-Fe(1)-C(38) = 156.75(16)°, N(3)-Fe(1)-C(38) = 114.62(16)°]. The alkylation of the ligand C_{imine} atom causes a substantial distortion and deviation from planarity in that region of the molecule. The quaternization of the former imine C atom is reflected in bond distances and angles as expected for the disappearance of the conjugation [N(3)-C(8) = 1.477(5) Å, N(3)-C(8)-C(7) = 108.0(3)°]. The Fe-N distance is also shorter than the others as a result of the acquisition of anionic character of that particular N atom.

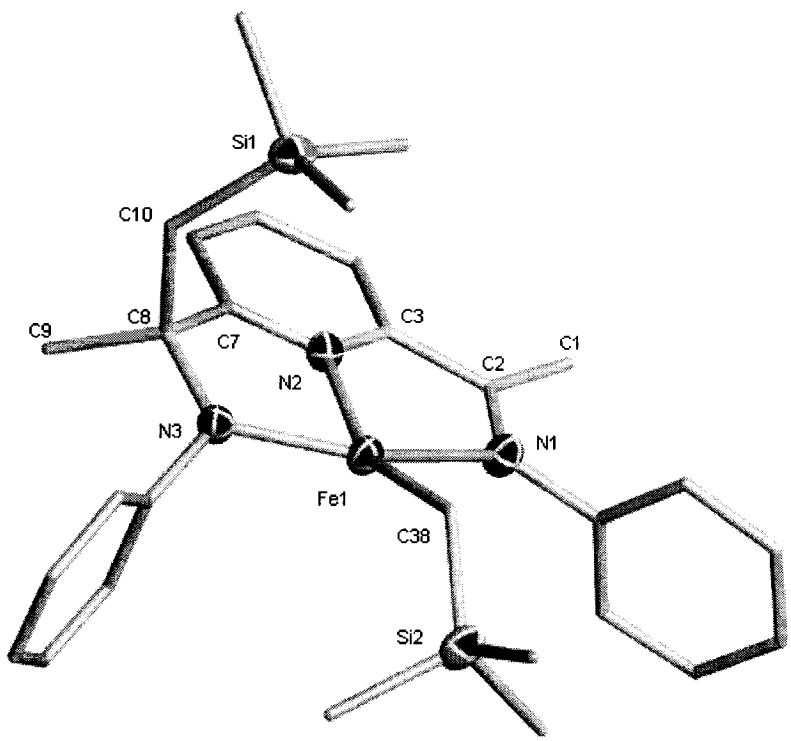

Figure 2.3. Partial thermal ellipsoid plot for **2.3** with the ellipsoids drawn at the 30% probability level. Hydrogen atoms have been omitted for clarity.

Complex 2.4. The molecule consists of a four-coordinate Fe atom (Figure 2.4) bonded to the three nitrogen atoms of the newly-modified ligand [Fe(1)-N(1) = 2.013(6) Å, Fe(1)-N(2) = 2.095(6) Å, Fe(1)-N(3) = 2.022(6) Å] and a chlorine atom [Fe(1)-Cl(1) = 2.318(2) Å]. The chlorine atom bridges one Li cation solvated by three molecules of THF [Cl(1)-Li(1) = 2.362(13) Å]. The Fe center is found in a slightly distorted square planar geometry [N(1)-Fe(1)-N(2) = 75.7(3)°, N(2)-Fe(1)-N(3) =75.7(3)°, N(3)-Fe(1)-Cl(1) = 104.44(19)°, Cl(1)-Fe(1)-N(1) = 104.25(19)°, N(1)-Fe(1)-N(3) = 151.3(3)°, N(2)-Fe(1)-Cl(1) = 177.48(18)°]. The ligand system displays very short distances between the imino-C's and the ketimine methyl-C's [C(1)-C(2) = 1.362(10) Å, C(8)-C(9) = 1.344(10) Å], typically indicating that the former Me group has been deprotonated with consequent formation of a $C{=}CH_2$ function. In turn, there is a parallel increase in the adjacent $C{=}N_{imine}$ bond lengths [N(1)-C(2) = 1.380(9) Å, N(3)-C(8) = 1.375(9) Å].

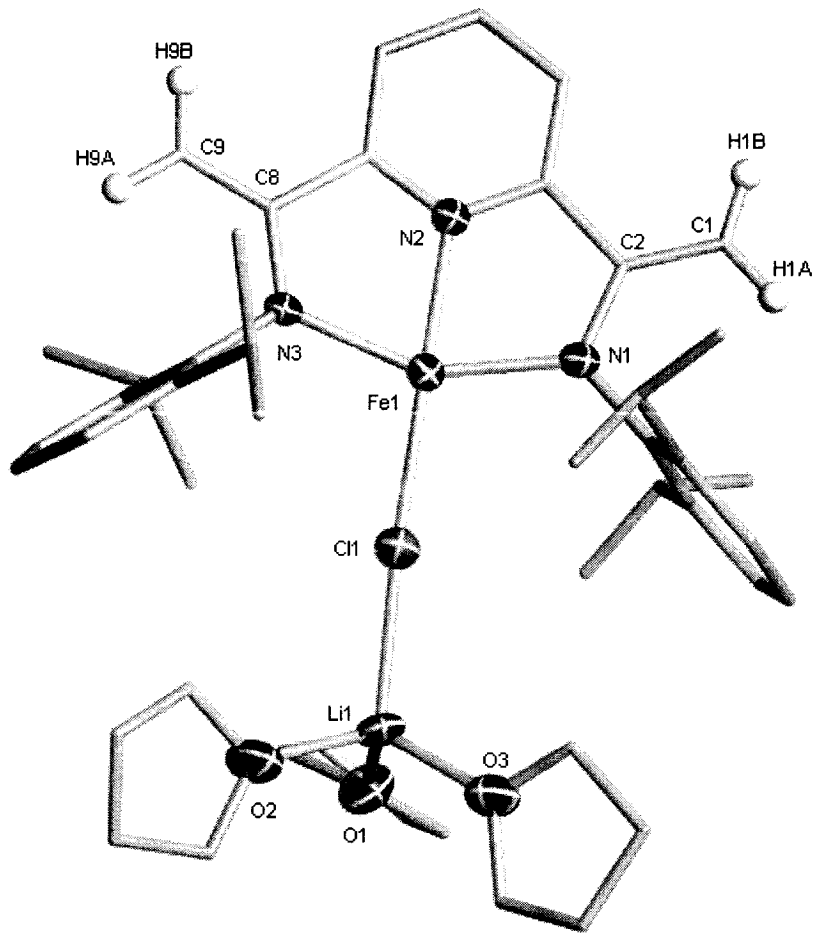

Figure 2.4. Partial thermal ellipsoid plot for **2.4** with the ellipsoids drawn at the 30% probability level. Most hydrogen atoms have been omitted for clarity.

Complex 2.5. Despite numerous attempts, the diffraction data of complex **2.5** was never good enough for a complete anisotropic refinement. However, the connectivity could be established in one case, and a representative structure is shown in Figure 2.5. The complex is a symmetry generated dimer, with identical Fe centers surrounded by the ligand system and an alkyl group [Fe(1)-C(34) = 2.05 Å] in a distorted square planar arrangement. The bimetallic nature is realized by a C-C bond between the ketimine methyl C's of two equal units. Other ligand features are as expected for the ligand in its intact state.

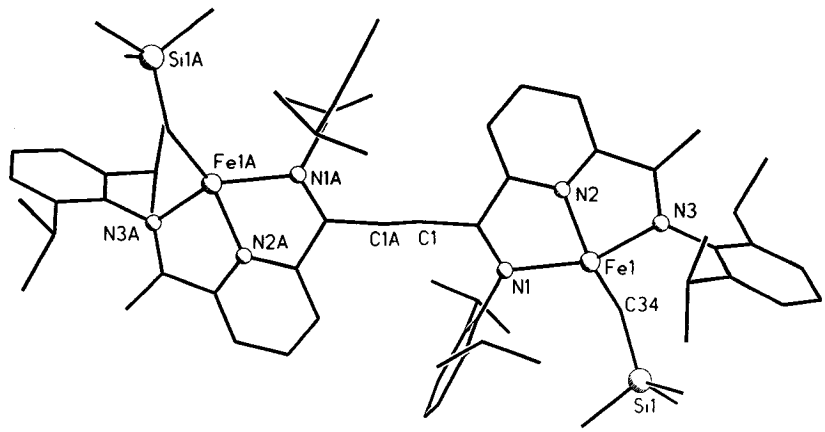

Figure 2.5. Ball and stick drawing of **2.5**.

Complex 2.6. The crystal structure of **2.6** (Figure 2.6) is very similar to **2.4** except for the alkyl unit and lithium cation solvated by four molecules of THF and unconnected to the Fe-containing anion. The bond distances and angles of the distorted square planar atom are very comparable [Fe(1)-N(1) = 2.094(4) Å, Fe(1)-N(2) = 2.138(4) Å, Fe(1)-N(3) = 2.078(4) Å]. The Fe-C distance [Fe(1)-C(34) = 2.068(5) Å] also compares well with those of **2.1, 2.2, 2.3,** and **2.5**. The coordination geometry around the Fe center displays a significant deviation from planarity [C(34)-Fe(1)-N(2) = 155.41(18)°; N(1)-Fe(1)-N(3) = 145.67(15)°, N(1)-Fe(1)-N(2) = 73.34(17)°]. The dianionic character of the ligand system is witnessed by the short C-C distances [C(1)-C(2) = 1.337(7) Å, C(8)-C(9) = 1.356(7) Å] formed by the C atom attached to the imine functions, describing a definite C-C double bond character. By the same token, the C-N distances are elongated compared to the those found in complex **2.2** [N(1)-C(2) = 1.360(6) Å, N(3)-C(8) = 1.354(6) Å].

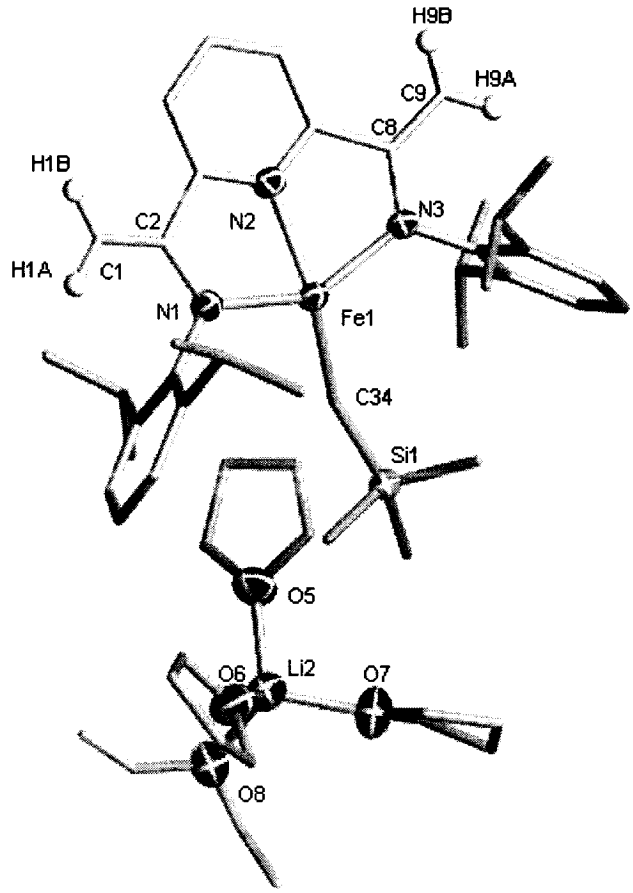

Figure 2.6. Partial thermal ellipsoid plot for **2.6** with the ellipsoids drawn at the 30% probability level. Most hydrogen atoms have been omitted for clarity.

Results and Discussion

The reaction of $LiCH_2SiMe_3$ with the dark blue 2,6-[2,6-(^{i}Pr)$_2$PhN=C(CH_3)]$_2$(C_5H_3N)$FeCl_2$, prepared *in situ* by reacting the neutral 2,6-[2,6-(^{i}Pr)$_2$PhN=C(CH_3)]$_2$(C_5H_3N) ligand with $FeCl_2(THF)_{1.5}$, was carried out in THF at -35°C (Scheme 2.1). Dark red crystals of the divalent {2,6-[2,6-(^{i}Pr)$_2$PhN=C(CH_3)]$_2$-2-CH_2SiMe_3}(C_5H_3N)Fe(CH_2SiMe_3) (**2.1**) were isolated after separation from the insoluble materials and fractional crystallization in pure hexane. In turn, the hexane-insoluble fraction was recrystallized from cold ether, affording large, dark purple crystals of {2,6-[2,6-(^{i}Pr)$_2$PhN=C(CH_3)]$_2$}(C_5H_3N)Fe(CH_2SiMe_3)$_2$ (**2.2**) (Scheme 2.1). The formulae and connectivity of both complexes have been elucidated by X-ray crystal structures (Figures 2.1 and 2.2).

Scheme 2.1

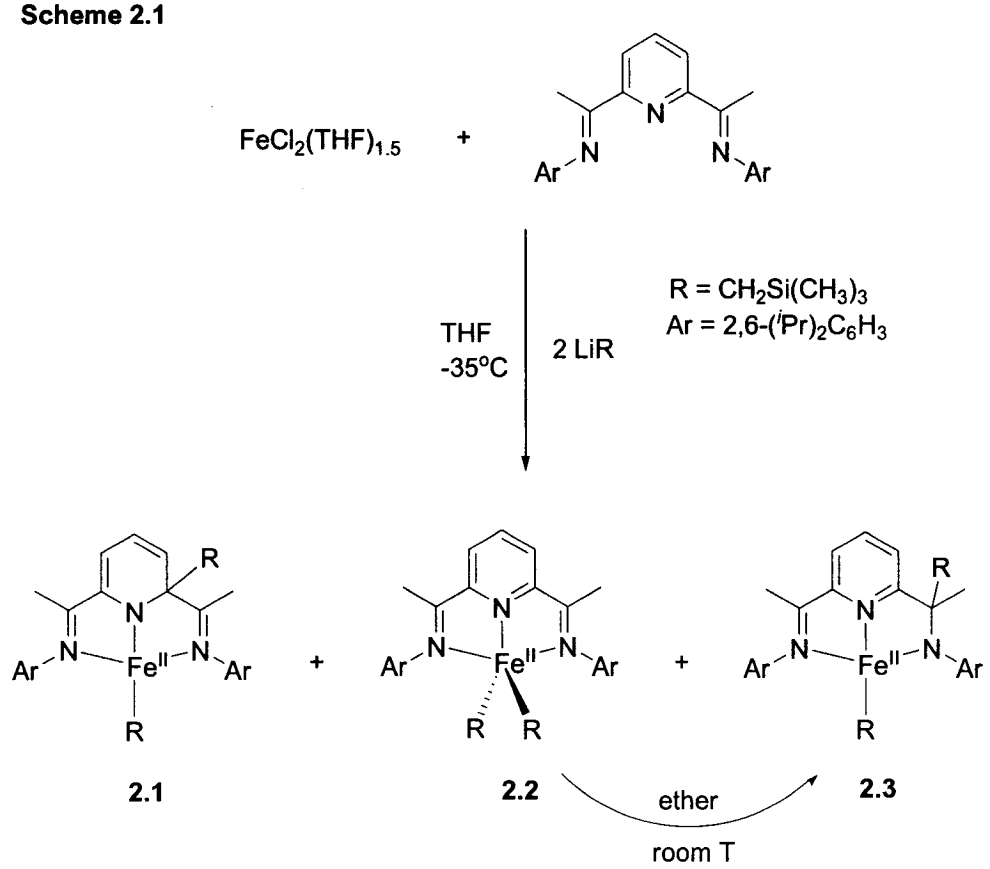

The formation of complex **2.1** is the result of two distinct processes. The first is the alkylation of the pyridine ring *ortho*-position. Similar to the case of the vanadium analogue,[9] this may be explained by the presence of a substantial displacement of negative charge from the ring *ortho*-carbon atom in the starting 2,6-[2,6-(^{i}Pr)$_2$PhN=C(CH$_3$)]$_2$(C$_5$H$_3$N)FeCl$_2$ adduct, which makes this particular position more susceptible to nucleophilic attack. The *ortho*-alkylation has a major impact on the molecular structure since the consequent anionization of the neutral ligand requires dissociation of one of the two chlorine atoms attached to the Fe atom with a decrease in the metal coordination number. The second process is a straightforward replacement of the remaining chlorine atom by the second alkylating agent, leading to a severely distorted tetrahedral geometry of the metal center. The connectivity, as summarized in Scheme 2.1, unambiguously assigns the divalent state to the Fe center. The magnetic moment of 5.6 μ_B measured at room temperature is also in reasonable agreement with the

presence of four unpaired electrons in an Fe(II) d^6 high-spin configuration with some TIP contribution.

Single crystals of **2.2** displayed identical cell parameters and structure to those recently reported by Chirik[20] and Campora.[21] At first glance, the formation of complex **2.2** seems to be the result of a straightforward chloride replacement of 2,6-[2,6-(^{i}Pr)$_2$PhN=C(CH$_3$)]$_2$(C$_5$H$_3$N)FeCl$_2$. However, the yield of **2.2** can be substantially improved (up to 30% increase) and the formation of **2.1** virtually eliminated (it was no longer present among the products isolable from the reaction mixture) when the reaction was carried out by inverting the order of addition of the reagents (beginning with a low temperature reaction between $FeCl_2$ and $LiCH_2SiMe_3$, followed by low temperature addition of the ligand). This suggests, as an alternative possibility, that the formation of **2.2** might also be the result of the direct reaction of $LiCH_2SiMe_3$ with free $FeCl_2$, *followed* by complexation of the diimine ligand. The presumed presence of free $FeCl_2$ in the reaction mixture leading to the mixture of **2.1** and **2.2** may be caused by a ligand dissociation equilibrium from 2,6-[2,6-(^{i}Pr)$_2$PhN=C(CH$_3$)]$_2$(C$_5$H$_3$N)FeCl$_2$, as observed for example in the chemistry of the lanthanides.[15,18] This point is further substantiated by the observation that transmetallation reactions are readily obtainable with this ligand system. For example, simple mixing at room temperature of 2,6-[2,6-(^{i}Pr)$_2$PhN=C(CH$_3$)]$_2$(C$_5$H$_3$N)FeCl$_2$ with $CoCl_2$ in THF affords the corresponding $CoCl_2$ adduct and $FeCl_2$.[25] Another possibility is that the very poor solubility of both unreacted $FeCl_2$ and of the complex could make the presence of $FeCl_2$ unavoidable during its *in situ* preparation. Even in this case, the room temperature solid state magnetic moment of **2.2** [μ_{eff} = 5.6 μ_B] compares well with that of both the starting 2,6-[2,6-(^{i}Pr)$_2$PhN=C(CH$_3$)]$_2$(C$_5$H$_3$N)FeCl$_2$[8] and **2.1**, thus confirming that the metal has remained in its divalent state. Finally, it should be observed that neither **2.1** nor **2.2** can be formed by reaction of $LiCH_2SiMe_3$ with the ligand *followed* by reaction with $FeCl_2$. The lithium alkyl Me_3SiCH_2Li instantly reacts with the ligand at either room or low temperature to produce the dianionic ligand.[15,18] The reaction of the dianion with $FeCl_2$ forms a different product (see below).

We have observed that, during the formation of **2.1**, variable amounts of well-formed crystals of a similar colour but different shape occasionally appear, provided that

the entire work-up is carried out at a temperature below -20°C. Manual separation of the crystals afforded the new complex {2-[2,6-(^{i}Pr)$_2$PhN=C(CH$_3$)]-6-[2,6-(^{i}Pr)$_2$PhNC(CH$_3$)(CH$_2$SiMe$_3$)](C$_5$H$_3$N)}Fe(CH$_2$SiMe$_3$) (**2.3**) (Figure 2.3) in analytically pure form.

Similar to the case of **2.1** and **2.2**, the formation of complex **2.3** also requires the intervention of two alkyl groups. However, one has been attached to one of the two imine-C atoms, similar to that witnessed with Al,[13] while the metal center bears the second in a severely distorted tetrahedral geometry. Nucleophilic attack at the imino-C atom disrupts the aromaticity in that area of the ligand backbone and consequently results in another monoanionic ligand, establishing the +2 oxidation state of the metal center. During attempts to recrystallize **2.3**, we have observed that the dark red colour becomes purple when dissolved at room temperature in ether. Crystallization from ether afforded a good yield of **2.2**, thus indicating that simple dissolution of **2.3** in ether is sufficient for the conversion, which requires migration of the alkyl group from the imine-carbon atom towards the metal center. This transformation denotes that, depending on the reaction conditions, **2.3** might be an intermediate in the formation of **2.2**, which is apparently thermodynamically more stable but kinetically less favoured. Complex **2.2** appears to be reasonably robust towards an excess of alkylating agent. This is a significant departure from the behaviour of the vanadium analogue,[9] where removal of the alkyl group from the *ortho*-position of the pyridine ring can be achieved via treatment with an excess of alkylating agent.[9] In the case of the vanadium complex, this process triggers a two-electron reduction of the metal center, which in turn is responsible for catalyst de-activation. Nonetheless, **2.2** is not *thermally* robust and *reversibly* changes colour from purple to brown upon heating before fully decomposing. We found no evidence for thermal transformations of **2.1**. Even though, based on the above observations, **2.1** appears to be more stable than **2.2**, we have not been able to detect the formation of **2.1** in the decomposition of **2.2**.

The reaction of 2,6-[2,6-(^{i}Pr)$_2$PhN=C(CH$_3$)]$_2$(C$_5$H$_3$N)FeCl$_2$ with two equivalents of LiCH$_2$SiMe$_3$ followed a surprisingly different course when it was carried out using the *pre-formed complex* re-suspended in THF (Scheme 2.2) rather than the *in situ*-generated species. In this case, we found no evidence for the formation of either **2.1** or **2.3**. The reaction, which is completely reproducible, afforded a substantial yield of **2.2** (52%) and

a smaller amount of a new dark orange by-product {[2,6-[2,6-(^{i}Pr)$_2$PhN-C=(CH$_2$)]$_2$ (C$_5$H$_3$N)}Fe(μ-Cl)Li(THF)$_3$ (**2.4**) which was isolated and purified by fractional crystallization.

Scheme 2.2

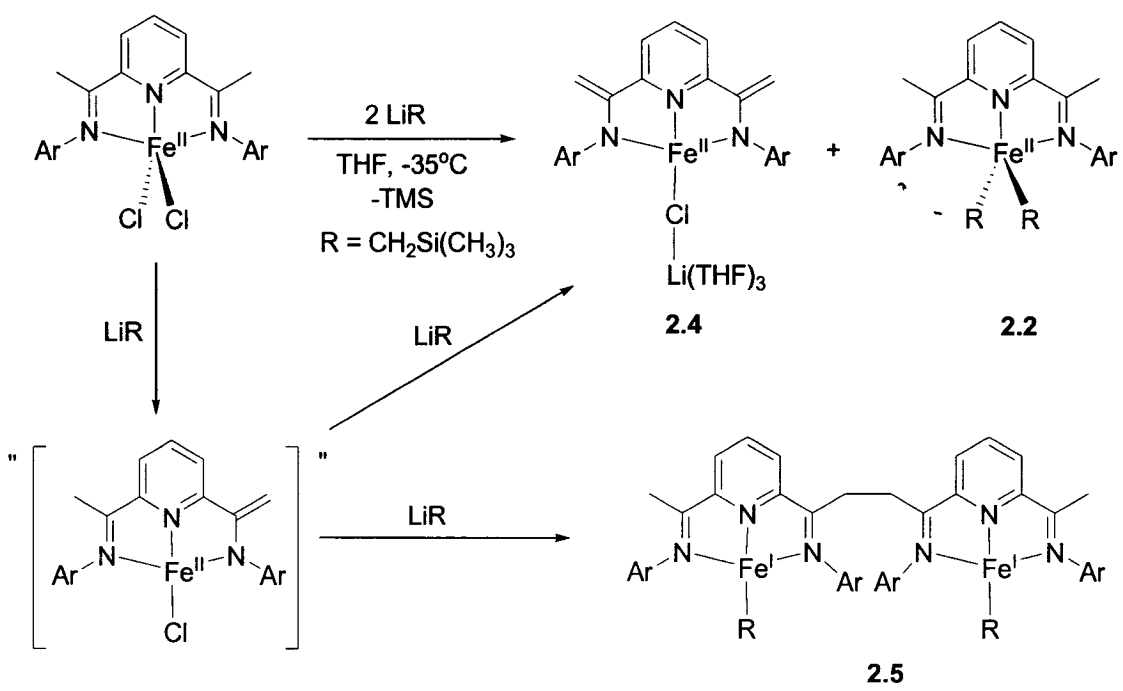

Complex **2.4** can also be conveniently prepared (56% isolated crystalline material) via direct reaction of the dianionic form of the ligand (obtained either *in situ* or in crystalline form from the high yield reaction with two equivalents of LiCH$_2$SiMe$_3$ at either low or room temperature) with FeCl$_2$. In all reactions involving ligand deprotonation it was always possible to detect the formation of tetramethylsilane in the reaction mixtures by GC-MS experiments. Evidently, the formation of **2.4** indicates the existence of an alternative alkylation pathway.

The room temperature magnetic moment of **2.4** in the solid state [μ_{eff} = 5.8 μ_B] compares well with the other complexes reported in this work[12] and is in agreement with a d^6 high spin Fe(II) center in a distorted square planar geometry. The connectivity of **2.4**, as yielded by the X-ray structure (Figure 2.4), clearly shows that the two former imine methyl groups have been deprotonated to produce two ene-amido functions and hence a

dianionic ligand (Scheme 2.2). There are precedents for this type of behaviour in the chemistry of this ligand system with several metal ions, including manganese,[10] lithium[15] and the lanthanides.[15]

Recent results by Chirik[16] have also shown the propensity of the methyl groups to be deprotonated simply by the addition of strong base alkali metal amides, MNR_2, to the dichloride precursor (Scheme 2.3). The Fe center is then stabilized by coordination to either the newly formed HNR_2 weak base (when R = Me) or to two molecules of THF present in the reaction mixture. Addition of pyridine or CN^tBu to the products results in immediate substitution of the weakly bound amine or THF molecules for the stronger ligands. Interestingly, addition of amine, $HNMe_2$, to the dialkyl (complex **2.2**) also leads to deprotonation of the methyl groups and replacement of the alkyl groups by the amine ligand. Deuterium labeling studies[16] have shown that in this case the deprotonation is promoted by a transient Fe-amide-alkyl species.

Scheme 2.3

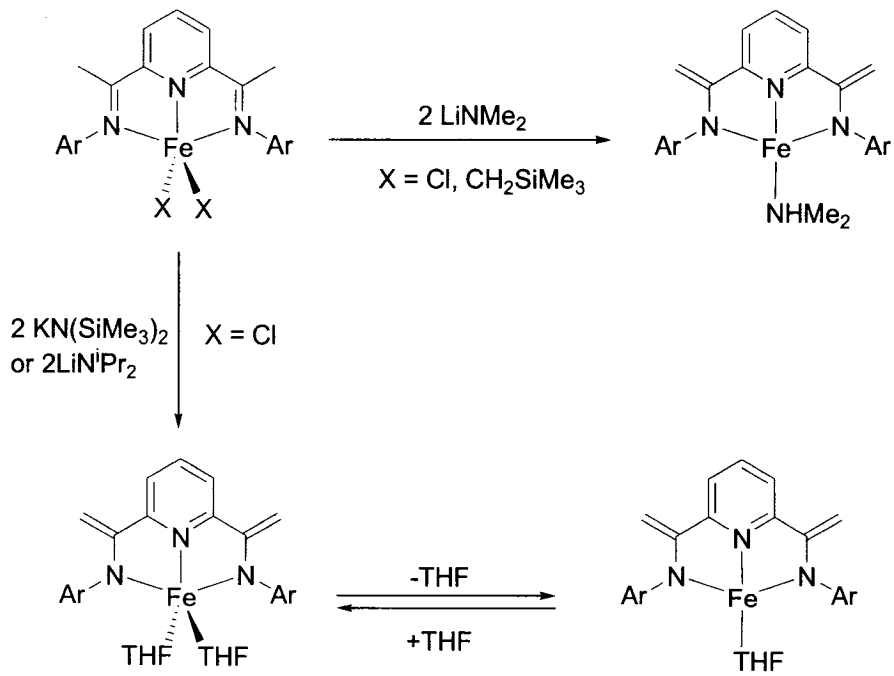

We have previously reported that in some cases, depending on the electronic configuration of the metal, the formation of mono-deprotonated or doubly-deprotonated species similar to **2.4** leads to a curious dimerization reaction via radical coupling of two

$C{=}CH_2$ moieties.[10,17,18] This coupling (Scheme 2.2) requires electrons to be provided to the ligand system, which can be obtained either from an external reducing agent (as in the case of the lanthanides)[18] or at the expense of the $C{=}CH_2$ bond, in turn triggering a one electron reduction of the metal center.[10,17] In the preparation of complexes **2.2** and **2.4**, we occasionally observed the formation of a small, yet significant, amount of dark crystals of a new dimeric species $\{[\{[2,6\text{-}(^{i}Pr)_2C_6H_5]N\text{-}C{=}(CH_2)\}(C_5H_3N)\{[2,6\text{-}(^{i}Pr)_2C_6H_5]N{=}CCH_2\}]Fe(CH_2SiMe_3)\}_2$ (**2.5**) (Figure 2.5). Unfortunately, no further purification was possible due to the low yield and poor solubility of this complex, regrettably preventing complete characterization. Only in one case was the quality of the crystals sufficient to allow a crystal structure determination.[26] Although the poor quality of the diffraction data did not allow a full anisotropic refinement, the connectivity and main features of this new compound were at least demonstrated. The complex is dinuclear with the same arrangement previously observed in Co,[17] Ln,[18] and Mn[10] chemistry, in which the dimerization is realized via the formation of a new C-C bond between two identical ketimine groups. The salient features are the tetracoordination of the Fe atom, the dinuclear structure and the non-deprotonation of the residual carbon group attached to the imine function [C-C = 1.49 Å]. Given the presence of the alkyl group attached to the Fe atom, the oxidation state of the metal center can be regarded as monovalent from the *formal* point of view. The fact that a monovalent Fe is generated at the expense of the ligand system is in line with the behaviour of the Co derivatives.[17] Reduction of the metal center upon alkylation with $LiCH_2SiMe_3$ was also described by Chirik.[20] In this case, the use of smaller aryl substituents, namely ethyl groups in the *ortho* and *para*-positions, led to a mixture of products containing the expected dialkyl and a reduced monovalent alkyl (with an intact ligand) in a 1:4 ratio.

Further attempts to clarify the genesis of complex **2.5** and to make this species available in larger scale were carried out with a number of experiments at both low and room temperature and by changing the sequence of addition of the reagents. In an attempt to follow synthetic pathways successful with other metals, reduction was probed by treating **2.4** with either NaH or K(naphthalenide).[10,17,18] However, only intractable materials systematically resulted from these efforts. On the other hand, given that only one of the two imine Me groups has undergo deprotonation to form complex **2.5**, we have

synthesized the mono-deprotonated lithium salt of the ligand [{[2,6-(^{i}Pr)$_2$C$_6$H$_5$]N-C=(CH$_2$)}(C$_5$H$_3$N){[2,6-(^{i}Pr)$_2$C$_6$H$_5$]N=CCH$_2$}]Li.[11b] Low-temperature addition of this anion to $FeCl_2$, followed by addition of two equivalents of $LiCH_2SiMe_3$, once again afforded only intractable materials. However, the low-temperature treatment of $FeCl_2$ with $LiCH_2SiMe_3$, presumably forming an *in situ* FeR_2 species, followed by addition of the ligand mono-lithium salt gave a new complex [{[2,6-[2,6-(^{i}Pr)$_2$PhN-C=(CH$_2$)]$_2$(C$_5$H$_3$N)}Fe(CH$_2$SiMe$_3$)][Li(THF)] (**2.6**) in acceptable yield (Scheme 2.4). The magnetic moment in solid state of this new species is in line with those of the other compounds reported in this chapter.

Scheme 2.4

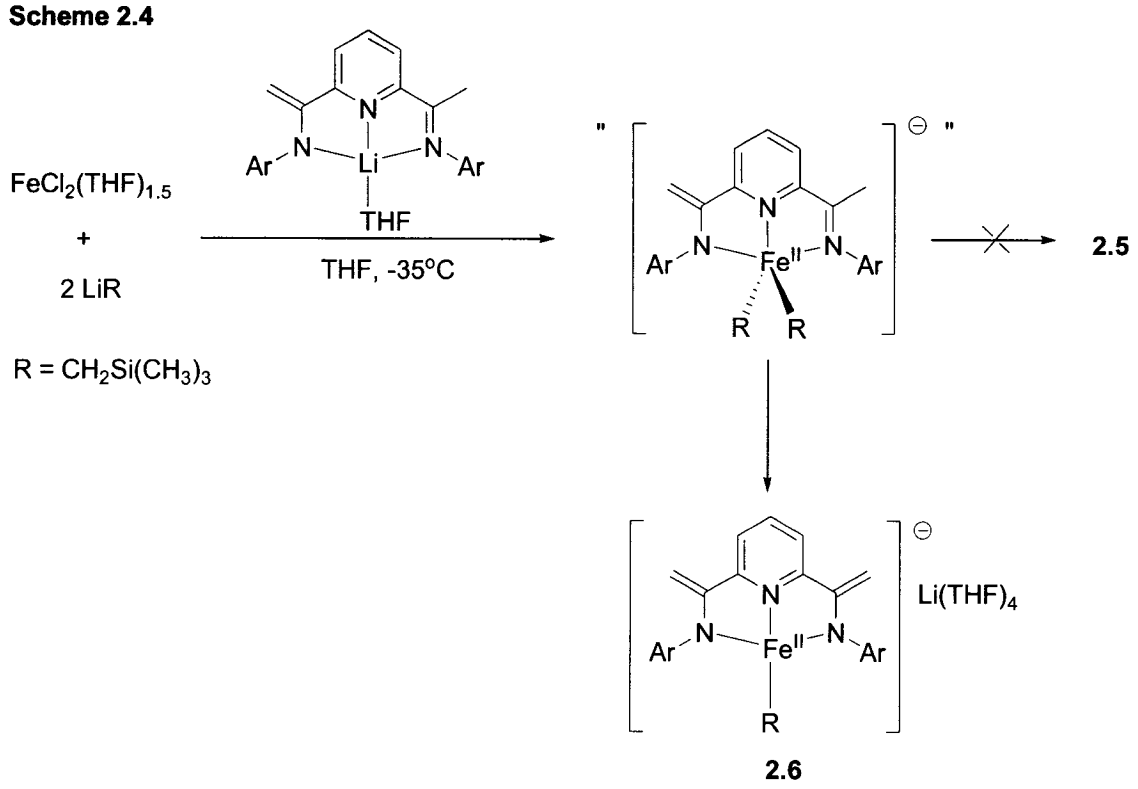

The basic structure of **2.6** (Figure 2.6) is very similar to complex **2.4**, besides the coordination of an alkyl to the metal center and the presence of the Li countercation solvent-separated from the metal anion. In all probability, the reaction proceeds via formation of an intermediate adduct of FeR_2 with the mono-deprotonated ligand. The failure of this species to give reductive dimerization towards **2.5**, instead of deprotonating the second ketimine group to give complex **2.6**, is puzzling. It suggests that a residual

chlorine atom attached to Fe is important for the reductive dimerization and that the formation of the Fe-C bond in **2.5** occurs after the reduction of the metal center. Therefore, under normal reaction conditions, kinetics governs the reaction in Scheme 2.2, where deprotonation of the second methyl unit occurs at a faster rate than reductive dimerization, thus forming complex **2.4** instead of **2.5**.

Polymerization Results

The catalytic testing of each complex was performed under identical conditions for the purpose of comparison. A pre-weighed amount of catalyst was dissolved in 100 mL of toluene in a Schlenk flask under N_2. A solution of 500 equivalents of MAO in toluene was added to the catalyst and allowed to stir for 10 minutes. The nitrogen was evacuated and ethylene added at 1 atmosphere of pressure. The reactions were run for 30 minutes under a continuous flow of ethylene and quenched by addition of MeOH and HCl. The resulting polymer was collected by filtration and dried thoroughly prior to obtaining the mass. Table 2.4 outlines the results of the catalytic testing and also includes the $LFeCl_2$ precursor for comparison.

Table 2.4. Polymerization Results

Complex	Temp. (°C)	Mass of Catalyst (g)	MAO (equivs)	Run time (mins)	Yield PE (g)	Activity gPE/mmol cat·hr·atm
2.1	23	0.008	500	30	2.80(±0.15)	509
2.2	23	0.010	500	30	3.32	474
2.4	23	0.005	500	30	4.30	1433
2.5	23	0.007	500	30	3.60	654
2.6	23	0.006	500	30	3.30	1015
$LFeCl_2$[a]	23	0.007	500	30	3.90	678

[a] L = 2,6-[2,6-(^{i}Pr)$_2$PhN=C(CH_3)]$_2$(C_5H_3N)

There are interesting implications as far as the catalytic activity of these species is concerned. At room temperature and atmospheric pressure, all complexes display high catalytic activity very similar to that of the $FeCl_2$ adduct, in spite of their tetracoordination (except for **2.2**) and high spin state. Complexes **2.4** and **2.6** are twice as active comparably. However, the polyethylene samples display very different natures and

their GPC's are overlaid in Figure 2.7. Complexes **2.1** and **2.2** form identical types of polyethylene showing a reasonably narrow distribution at low molecular weights and a minor amount of broadly dispersed PE at very high molecular weights, very similar to the polyethylene produced by the $LFeCl_2$ precursor under identical conditions (Figure 2.7, dark blue line and dark green line). In contrast, the formally monovalent **2.5** produces only broadly dispersed high molecular weight PE (Figure 2.7, orange line) while complexes **2.4** and **2.6** show an intermediate behaviour in the sense that the two types of PE are present in comparable amounts in the sample (Figure 2.7, pink and turquoise lines).

Recalling Chapter 1, the low molecular weight polymer contains fully saturated ends, indicative of a chain termination pathway via chain transfer to aluminum. On the contrary, the high molecular weight fraction contains a ratio of 1:1 vinyl to saturated ends, the result of β-hydride transfer as the main termination mechanism.[27] The bimodal nature of the GPC is either due to the presence of two separate active species or is the result of a change in the active species throughout the polymerization run. The results suggest that the activation of complexes **2.1** and **2.2** and the $LFeCl_2$ precursor involve the formation of the same active species and are therefore related in the catalytic cycle. However, the PE produced by **2.5** contains only the high molecular weight type of polymer, and therefore β-hydride transfer is the only chain termination pathway functioning in this case. The suppression of the low molecular weight peak suggests that only one active species is generated by complex **2.5**, that which is responsible for the formation of the higher molecular weight polymer. The molecular weight distributions of the polymers produced by complexes **2.4** and **2.6** appear to be intermediate between the precursor and complex **2.5**. This behaviour indicates that complexes **2.4** and **2.6** may follow a similar activation pathway as the precursor but may also be susceptible to dimerization and reduction towards a monovalent Fe species during the catalytic cycle, presumably a consequence of the double bonds.[10,17,18] Also, **2.1** and **2.2** might be able to produce analogues of **2.4** and ultimately of **2.5** while in the presence of large amounts of alkylating agent. The reason for the remarkable difference between the samples of PE produced by complexes in the two different oxidation states is unclear. It may well be related to the different electronic configurations of the two oxidation states, which in turn

relates to the relative stability of the intermediates involved in the chain propagation and termination steps.[28] At this stage, it is interesting to observe that the monovalent species **2.5** is indeed catalytically very active and that all species generated by the alkylation of the $FeCl_2$ adduct are catalytically active. The fact that the catalysts are present as high spin tetracoordinate Fe(II) complexes dispels the myth that species such as these would not be good catalysts for ethylene polymerization.[7a,34]

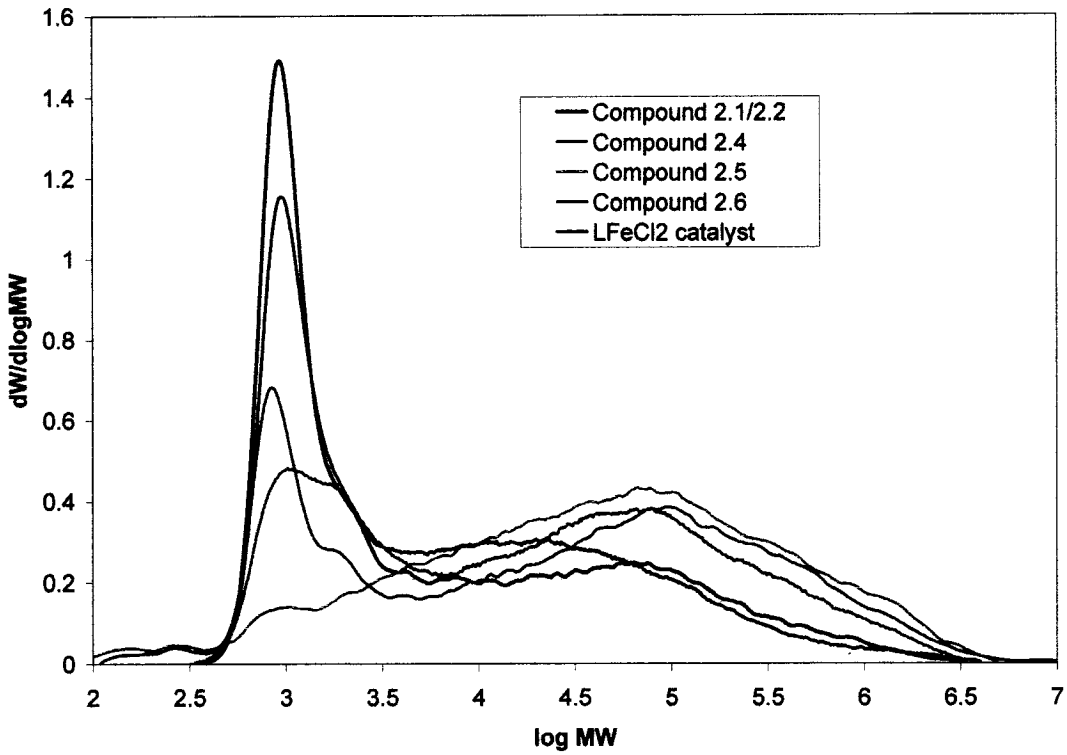

Figure 2.7. Gel permeation chromatogram of **2.1** and **2.2** (Mn. 1,860, Mw = 66,100, Ms 741,700, PD = 35.54), of **2.5** (Mn = 3,250, Mw = 219,000, Mz = 1,207,000, PD = 67.38), of **2.4** (Mn = 2,620, Mw = 207,300, Mz = 2,061,000, PD = 79.12) and of **2.6** (Mn = 3,250, Mw = 219,000, Mz = 1,207,000, PD = 67.38).

Calculations

In collaboration with Peter Budzelaar, density functional calculations on model complexes (see below) were performed[12] with the TURBOMOLE program[29] in combination with the OPTIMIZE routine of Baker and co-workers.[30] Because they give interesting insight into the chemistry presented above, the results have been included herein. All relevant structures were fully optimized as minima or transition states at the

restricted or unrestricted B3-LYP[31] level, employing the standard SV(P) basis sets.[32] All stationary points were characterized by vibrational analyses using analytic or numerical second derivatives, and thermal corrections (ZPE, enthalpy, entropy; 273 K, 1 bar) were calculated from these using standard formulae of statistical thermodynamics. Improved electronic energies were calculated at the SV(P) optimized geometries using the TZVPP basis set on all atoms;[33] these improved energies were combined with the (U)B3-LYP/SV(P) thermal corrections to arrive at the final free energies.

Extensive calculations were carried out on model complex L'FeMe$_2$ (**2.2a**) and its alkyl-shifted isomers [L'-2-Me]FeMe (**2.1a**, *ortho*-alkylated complex) and [L'-*i*-Me]FeMe (**2.3a**, imino-alkylated complex), where L' is a model ligand bearing only Me groups at the imine nitrogens. In addition, an isomer [L'-N-Me]FeMe (the product of alkyl migration to the pyridine nitrogen) was included because this might be an intermediate in alkyl transfers between metal and ligand. Finally, the Fe^{I} complex L'FeMe (**2.5a**) was included as a model for half of complex **2.5**. Geometries for spin states from S = 0 to 3 (for Fe^{II}) or $^1/_2$ to $^5/_2$ (for Fe^{I}) were fully optimized for each of the above-mentioned species. For the triplet and quintet states only, the geometries of the full complexes **2.1**, **2.2**, **2.3** and [L-N-R]FeR (L-N-R = pyridine ring N-alkylated; R = CH_2SiMe_3) were also fully optimized; larger basis sets and thermal corrections were not feasible here.

DFT calculations on simplified models **2.1a-2.3a** (bearing just Me groups at Fe and the imine nitrogens) indicate that for each of the Fe^{II} species considered, the IS (triplet, S = 1) and HS (quintet, S = 2) states are close in energy, with the LS (singlet, S = 0) state always being significantly higher (Table 2.5). These results agree with our experimental observation of a paramagnetic ground state for **2.1** and **2.2**. They might also be relevant to the nature of the active species in the Fe polymerization system. The spin state of the catalytically active species has been at the center of a theoretical debate. The active species in the catalytic cycle (generated by mixing $LFeCl_2$ with MAO) has commonly been assumed to be $LFeR^+$. Initial theoretical work by Ziegler *et al.* on this system[34] indicated that the HS state was too high in energy to be accessible for $LFeR_2$ and $LFeR^+$, and would anyhow not be able to perform polymerization. Therefore, it was concluded that the LS state was probably involved in the polymerization, although participation of the IS state could not be excluded. The results of separate calculations by

Morokuma[35] and Zakharov[36] instead indicated that the LS state is highest in energy, while IS and HS states are close. Our calculations are more in line with these results. Given that our *experiments* indicate that $LFeR_2$ is already HS, and that our *calculations* indicate an even larger preference for the IS/HS states for $LFeR^+$ than for $LFeR_2$, we tentatively conclude that any $LFeR^+$ species involved in polymerization will *not* be low-spin. Of course, it remains possible that the catalytic cycle of this system does not involve $LFeR^+$ at all.[36] In the Fe^{II} complexes studied here, IS or HS states are preferred in which the diiminopyridine ligand appears to be electronically innocent, i.e. the complexes truly contain Fe^{II}. In contrast, for the formally monovalent L'FeMe **2.5a** (model for one half of dimer **2.5**) the energies of S = $^1/_2$, $^3/_2$ and $^5/_2$ states are predicted to be all very close in energy (within a few kcal/mol). The S = $^1/_2$ state is best described as containing IS Fe^{II} antiferromagnetically coupled to a ligand radical anion, i.e. analogous to the situation in the diamagnetic formally Co^I alkyls LCoR.[37]

Table 2.5. Calculated relative free energies (kcal/mol) of L'FeMe$_2$ and isomers in different spin states

Complex	S=0 (LS)	S=1 (IS)	S=2 (HS)	S=3
L'FeCl$_2$	23.58	15.56	0.00	12.10
L'FeMe$_2$ (**2.2a**)	13.56	9.33	5.79	15.35
[2-Me-L']FeMe (**2.1a**)	36.20	15.33	11.66	33.25
[*i*-Me-L']FeMe (**2.3a**)	16.64	0.00	5.31	21.97
[N-Me-L']FeMe[a]	37.15	16.28	10.48	43.24
L'FeMe$^+$	24.13	8.49	0.00	32.70
	S=$^1/_2$	S=$^3/_2$	S=$^5/_2$	
L'FeMe	1.25	5.03	0.00	

[a] Adduct with Me group at pyridine nitrogen

It is interesting to observe that the extent of simplification used for the calculation changes the relative order of stability of the complexes. According to the calculations on the simplified model systems, the IS state of imine adduct **2.3a** is the most stable of all species considered: it is lower than the corresponding HS state (by 6 kcal/mol) and all other isomers considered (by 4-17 kcal/mol). This disagrees with the experimental observations and indicates that steric effects play an important role here. Indeed, geometry optimization of the full systems **2.1-2.3** changes the order of stability

completely. The estimated free energies of all HS states are now lower than those of the corresponding IS states (Table 2.6, last column). Dialkyl **2.2** is lowest in energy, followed by the 2-adduct **2.1** at 4 kcal/mol and the imine adduct **2.3** at 6 kcal/mol. This revised stability order agrees well with experiment. However, it also indicates that if the bulky alkyls were to be exchanged for smaller Me or *n*-alkyl groups (as could happen during initiation with MAO), the Fe dialkyl might no longer be the most stable isomer, with the imine adduct becoming at least as favourable. In view of the remarkable ease of alkyl shift between the imine moiety and the metal atom observed in the present work, it seems that some form of ligand alkylation might well be important in activation of the Fe complex.

Table 2.6. Effect of steric bulk on alkyl transfer energetics (IS and HS states only; kcal/mol)

System		ΔE_{model}	ΔG_{model}	ΔE_{full}	ΔG_{full} (est)[a]
$LFeR_2$ (**2.2**)	IS	10.75	9.33	4.28	8.16
	HS	12.10	5.79	1.42	0.00
[2-R-L]FeR (**2.1**)	IS	16.94	15.33	14.10	17.81
	HS	13.34	11.66	0.00	4.08
[*i*-R-L]FeR (**2.3**)	IS	0.00	0.00	4.85	11.89
	HS	6.79	5.31	0.17	6.16
[N-R-L]FeR	IS	16.69	16.28	18.30	25.20
	HS	11.07	10.48	5.13	12.35

[a] Obtained by combining the SV(P) energies for the full system with thermal and basis set (SV(P)→TZVPP) corrections for the model system.

Conclusion

In conclusion, the remarkably complex behaviour of the bis-iminopyridine Fe catalyst in the presence of alkylating agents has been unveiled. As previously observed with several other transition metals, the non-innocent behaviour of this ligand system dominates during the alkylation procedure. Different from the other cases however, the mobility of the alkyl groups and the variety of transformations does not affect the redox chemistry to a large degree. The reduction of the metal center, which is a rather common feature in the case of other metals, seems to be confined exclusively to the dimerization pathway via coupling of two deprotonated imine C atoms. Otherwise, the combination of a divalent organo-iron species with this ligand system seems to be reasonably robust once the complex is formed, at least with the particular alkyl used in this study. The catalytic

activity of complexes **2.1** and **2.2** is very similar to that of the $LFeCl_2$ precursor, suggesting the same activation pathway in the catalytic cycle. The fact that the monovalent species also displays very high catalytic activity and produces only one type of PE suggests that the species responsible for the higher molecular weight fraction of PE, that undergoing β-hydride transfer as the main termination pathway, contains the catalyst in a reduced state.

References

(1) See Chapter 1.

(2) Huheey, J. E.; Keiter, E. A.; Keiter, R. L. *Inorganic Chemistry: Principles of Structure and Reactivity;* Harper Collins College Publishers: New York, 1990.

(3) Simões, J. A.; Beauchamp, J. L. *Chem. Rev.* **1990**, *90*, 629.

(4) (a) Machelett, B. *Z. Chem.* **1976**, *16*, 116. (b) Mueller, H.; Seidel, W.; Goerls, H. *J. Organomet. Chem.* **1993**, *445*, 133. (c) Klose, A.; Solari, E.; Floriani, C.; Chiesi-Villa, A.; Rizzoli, C.; Re, N. *J. Am. Chem. Soc.* **1994**, *116*, 9123. (d) Seidel, W.; Mueller, H.; Goerls, H. *Angew. Chem. Int. Ed.* **1995**, *34*, 325. (e) Wehmschulte, R. J.; Power, P. P. *Organometallics* **1995**, *14*, 3264. (f) Viefhaus, T.; Schwarz, W.; Hubler, K.; Locke, K.; Weidlein, J. *Z. Anorg. Allg. Chem.* **2001**, *627*, 715.

(5) (a) Hermes, A. R.; Girolami, G. S. *Organometallics* **1987**, *6*, 763. (b) Chatt, J.; Shaw, B. L. *J. Chem. Soc.* **1961**, 285. (c) Seidel, V. W.; Lattermann, K.-J. *Z. Anorg. Allg. Chem.* **1982**, *488*, 69.

(6) Kerber, R. C. *Comprehensive Organometallic Chemistry II*; Abel, E. W.; Stone, F. G. A.; Wilkinson, G., Eds.; Pergamon, New York, **1995**.

(7) (a) Bart, S. C.; Hawrelak, E. J.; Schmisseur, A. K.; Lobkovsky, E.; Chirik, P. J. *Organometallics* **2004**, *23*, 237. (b) Holland, P. L.; Cundari, T. R.; Perez, L. L.; Eckert, N. A.; Lachicotte, R. J. *J. Am. Chem. Soc.* **2002**, *124*, 14416. (c) Smith, J. M.; Lachicotte, R. J.; Holland, P. L. *Organometallics* **2002**, *21*, 4808. (d) Sciarone, T. J. J.; Meetsma, A.; Hessen, B.; Teuben, J. H. *Chem. Commun.* **2002**, 1580. (e) Kisko, J. L.; Hascall, T.; Parkin, G. *J. Am. Chem. Soc.* **1998**, *120*, 10561. (f) Fryzuk, M. D.; Leznoff, D. B.; Ma, E. S. F.; Rettig, R. J.; Young, V. G. *Organometallics* **1998**, *17*, 2313.

(8) (a) Small, B. L.; Brookhart, M.; Bennett, A. M. A. *J. Am. Chem. Soc.* **1998**, *120*, 4049. (b) Britovsek, G. J. P.; Gibson, V. C.; Kimberley, B. S.; Maddox, P. J.; McTavish, S. J.; Solan, G. A.; White, A. J. P.; Williams, D. J. *Chem. Commun.* **1998**, 849.

(9) Reardon, D.; Conan, F.; Gambarotta, S.; Yap, G. P. A.; Wang, Q. *J. Am. Chem. Soc.* **1999**, *121*, 9318.

(10) (a) Sugiyama, H.; Aharonian, G.; Gambarotta, S.; Yap, G. P. A.; Budzelaar, P. H. M. *J. Am. Chem. Soc.* **2002**, *124*, 12268. (b) Reardon, D.; Aharonian, G.; Gambarotta, S.; Yap, G. P. A. *Organometallics* **2002**, *21*, 786.

(11) (a) Clentsmith, G. K. B.; Gibson, V. C.; Hitchcock, P. B.; Kimberley, B. S.; Rees, C. W. *Chem. Commun.* **2002**, 1498. (b) Khorobkov, I.; Gambarotta, S.; Yap, G. P. A. *Organometallics* **2002**, *21*, 3088. (c) Blackmore, I. J.; Gibson, V. C.; Hitchcock, P. B.; Rees, C. W.; Williams, D. J.; White, A. J. P. *J. Am. Chem. Soc.* **2005**, *127*, 6012.

(12) Scott, J.; Gambarotta, S.; Korobkov, I.; Budzelaar, P. H. M. *J. Am. Chem. Soc.* **2005**, *127*, 13019.

(13) (a) Bruce, M.; Gibson, V. C.; Redshaw, C.; Solan, G. A.; White, A. J. P.; Williams, D. J. *Chem. Commun.* **1998**, 2523. (b) Milione, S.; Cavallo, C.; Tedesco, C.; Grassi, A. *J. Chem. Soc. Dalton Trans.* **2002**, 1839. (c) Knijnenburg, Q.; Smits, J. M. M.; Budzelaar, P. H. M. *C. R. Chimie* **2004**, *7*, 865. (d) Knijnenburg, Q.; Smits, J. M. M.; Budzelaar, P. H. M *Organometallics* **2006**, *25*, 1036.

(14) Enright, D.; Gambarotta, S.; Yap, G. P. A.; Budzelaar, P. H. M. *Angew. Chem. Int. Ed.* **2002**, *41*, 3873.

(15) Sugiyama, H.; Gambarotta, S.; Yap, G. P. A.; Wilson, D. R.; Thiele, S. K.-H. *Organometallics* **2004**, *23*, 5054.

(16) Bouwkamp, M. W.; Lobkovsky, E.; Chirik, P. J. *Inorg. Chem.* **2006**, *45*, 2.

(17) Scott, J.; Gambarotta, S.; Korobkov, I. *Can. J. Chem.* **2005**, *83*, 279.

(18) Sugiyama, H.; Korobkov, I.; Gambarotta, S.; Möller, A.; Budzelaar, P. H. M. *Inorg. Chem.* **2004**, *43*, 5771.

(19) (a) Kooistra, T. M.; Knijnenburg, Q.; Smits, J. M. M.; Horton, A. D.; Budzelaar, P. H. M.; Gal, A. W. *Angew. Chem. Int. Ed.* **2001**, *40*, 4719. (b) Gibson, V. C.; Humphries, M. J.; Tellmann, K. P.; Wass, D. F.; White, A. J. P.; Williams, D. J. *Chem. Commun.* **2001**, 2252. (c) Steffen, W.; Blömker, T.; Kleigrewe, N.; Kehr, G.; Fröhlich, R.; Erker, G. *Chem. Commun.* **2004**, 1188. (d) Kleigrewe, N.; Steffen, W.; Blömker, T.; Kehr, G.; Fröhlich, R.; Wibbeling, B.; Erker, G.; Wasilke, J.-C.; Wu, G.; Bazan, G. C. *J. Am. Chem. Soc.* **2005**, *127*, 13955.

(20) (a) Bouwkamp, M. W.; Bart, S. C.; Hawrelak, E. J.; Trovitch, R. J.; Lobkovsky, E.; Chirik, P. J. *Chem. Commun.* **2005**, 3406. (b) Bowkamp, M. W.; Lobkovsky, E.; Chirik, P. J. *J. Am. Chem. Soc.* **2005**, *127*, 9660.

(21) Cámpora, J.; Naz, A. M.; Palma, P.; Alvarez, E. *Organometallics* **2005**, *24*, 4878.

(22) Tessier-Youngs, C.; Beachley Jr., O. T. *Inorg. Synth.* **1986**, *24*, 95.

(23) Blessing, R. *Acta Crystallogr.* **1995**, *A51*, 33.

(24) Sheldrick, G. M. Bruker AXS, Madison, WI, 2001.

(25) Scott, J. Gambarotta, S. unpublished results.

(26) Crystal data for **2.5**: $C_{74}H_{106}Fe_2N_6Si_2$, M_W = 1247.42, monoclinic, $P2_1/c$, a = 17.41 Å, b = 12.07 Å, c = 18.33 Å, β = 111.1°, V = 3851.8 Å^3.

(27) Britovsek, G. J. P.; Bruce, M.; Gibson, V. C.; Kimberley, B. S.; Maddox, P. J.; Mastroianni, S.; McTavish, S. J.; Redshaw, C.; Solan, G. A.; Strömberg, S.; White, A. J. P.; Williams, D. J. *J. Am. Chem. Soc.* **1999**, *121*, 8728.

(28) Schmid, R.; Ziegler, T. *Organometallics* **2000**, *19*, 2756.

(29) a) Ahlrichs, R.; Baer, M.; Haeser, M.; Horn, H.; Koelmel, C. *Chem. Phys. Lett.* **1989**, *162*, 165; b) Treutler, O.; Ahlrichs, R. *J. Chem. Phys.*, **1995**, *102*, 346; c) Ahlrichs, R.; *et al.* Turbomole Version 5, January **2002**. Theoretical Chemistry Group, University of Karlsruhe.

(30) Baker, J. *J. Comput. Chem.* **1986**, *7*, 385; PQS version 2.4, **2001**, Parallel Quantum Solutions, Fayetteville, Arkansas, USA; the Baker optimizer is available separately from PQS upon request.

(31) a) Lee, C.; Yang, W.; Parr, R. G. *Phys. Rev. B* **1988**, *37*, 785; b) Becke, A. D. *J. Chem. Phys.* **1993**, *98*, 1372; c) Becke, A. D. *J. Chem. Phys.* **1993**, *98*, 5648; Note that the Turbomole functional "b3-lyp" is not identical to the Gaussian "B3LYP" functional.

(32) Schaefer, A.; Horn, H.; Ahlrichs, R. *J. Chem. Phys.* **1992**, *97*, 2571.

(33) Schaefer, A.; Huber, C. Ahlrichs, R. *J. Chem. Phys.* **1994**, *100*, 5829.

(34) Deng, L.; Margl, P.; Ziegler, T. *J. Am. Chem. Soc.* **1999**, *121*, 6479.

(35) Khoroshun, D. V.; Musaev, D. G.; Vreven, T.; Morokuma, K. *Organometallics* **2001**, *20*, 2007.

(36) Zakharov, I. I.; Zakharov, V. A. *Macromol. Theory Simul.* **2004**, *13*, 583.

(37) Knijnenburg, Q.; Hetterscheid, D.; Kooistra, T. M.; Budzelaar, P. H. M. *Eur. J. Inorg. Chem.* **2004**, 1204.

Chapter Three

Alkylation of the Bis-iminopyridine-$FeCl_2$ Catalyst with MeLi

---

Introduction

The discovery by Brookhart and Gibson that late transition metal systems were able to catalyze the polymerization of ethylene with extremely high activities was a major breakthrough in homogeneous single-site catalysis.[1] It has dissolved the archetypal boundaries surrounding the necessity for Group 4, d^0 systems as a prerequisite for highly Lewis acidic/highly active catalytic systems.[2] However, with this valuable information came new queries regarding the nature of the catalytically active species. Did the late metal systems follow the classic Ziegler-Natta mechanism for polymerization?

Subsequent to the Brookhart-Gibson discovery, several research groups attempted extensive theoretical investigations into the Fe system,[3] invariably assuming the formation of a 14 electron, cationic divalent Fe alkyl as the catalytically active species. This in turn raised important questions regarding the metal spin state of the catalytically active species and how it could be controlled. This crucial point was debated in the literature immediately after the discovery, with Ziegler[3a] calculating the low spin state as the most accessible while Morokuma[3c] and Zhakarov[3d] regarded the high spin state as the lowest in energy. However, the calculations, and hence the controversy, were based on a very precise traditional mechanistic paradigm since experimental mechanistic information was not yet available. As new information came to light, the actual oxidation

state of iron in the catalytically active species became the object of debate. A trivalent Fe center was proposed by Gibson based on Mössbauer and EPR studies comparing the Fe(II) and Fe(III) catalysts.[4] However, this proposal was refuted by Talsi *et al.*, whose spectroscopic NMR investigations suggested instead the involvement of a paramagnetic Fe(II) alkyl bridging the aluminum cocatalyst.[5] Supported by the MS studies of Repo[6] specifically targeting the interaction of the Fe catalyst with MAO and AlR_3, Talsi's results show that the nature of the activator determines whether cationic or neutral, *but at all times divalent*, species are formed upon activation.[5]

Although cationic divalent Fe species had previously been generated by Gibson,[7] the first example of an unsaturated cationic Fe(II) *alkyl* was obtained by Chirik *et al.* via cationization of $LFeR_2$ ($R = CH_2Si(CH_3)_3$) with $B(C_6F_5)_3$ (Scheme 3.1).[8] In the presence of ethylene, the cationic species was conclusively shown to afford polymerization without the need for further activation, albeit with a much lower activity and a different polymer quality than the dichloride precursor. Cationization of the dialkyl was also possible with an ammonium borate salt. However, in the presence of THF or ether, the neutral donors become coordinated to the metal center and attenuate the activity of the catalyst. Regardless of whether a cationic alkyl is generated upon activation of the precursor with MAO, these results show that a cationic Fe alkyl is indeed possible and that it can be used to polymerize ethylene in the absence of MAO.[8]

Scheme 3.1

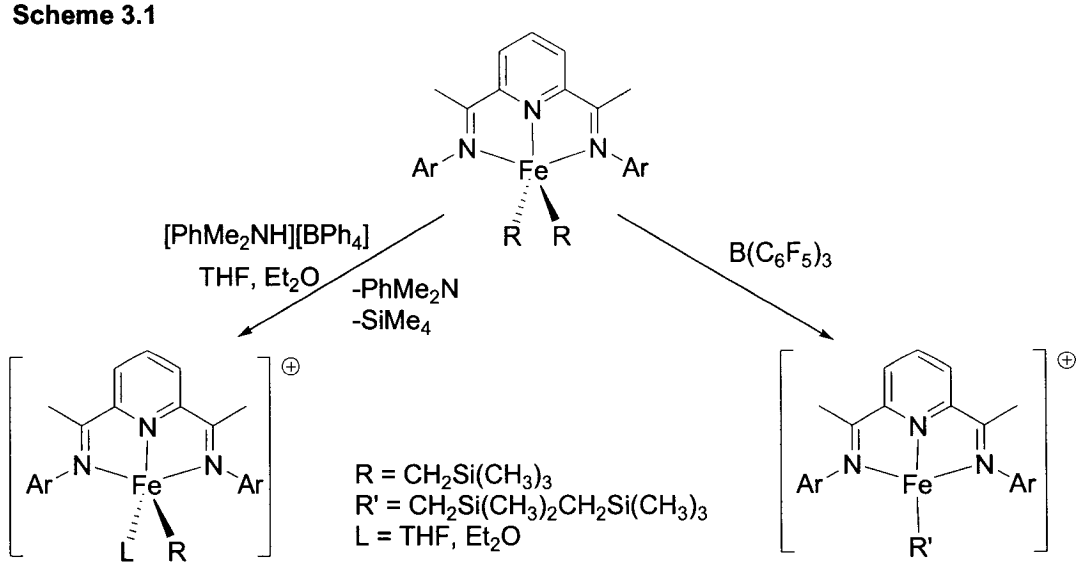

Prior to experimental mechanistic studies, the catalytically active species in the analogous cobalt system was also presumed to be a cationic divalent metal alkyl. However, in their attempt to generate such a species, the groups of Gibson[9] and Gal[10] simultaneously discovered that the first step upon addition of alkylating agent is actually *reduction* of the cobalt center to the monovalent state, followed by alkylation. Activation of these complexes with MAO and exposure to ethylene produces PE with the same activity and polymer quality as the divalent precursor, thereby suggesting that activation with MAO involves an initial one electron reduction to a d^8 Co(I) center.[9,10] Cationized complexes were also shown to polymerize ethylene in the absence of cocatalyst,[9] as well as in the absence of a M-C σ-bond.[11] These observations invalidate the cationic Co(II) alkyl assumption and question the designation of these late metal species as Ziegler-Natta catalysts.

In an attempt to understand the behaviour of the more active Fe-analogue, we investigated the reactivity with different alkylating agents and aluminum activators. Chapter 2 describes the intricate performance of the system upon alkylation with the larger alkyl $LiCH_2Si(CH_3)_3$, illustrating alkylation of the pyridine ring *ortho*-position and the imino-C atom, along with the metal center, as well as deprotonation of both ketimine methyl groups and reductive dimerization.[12] Clearly, the ligand shows an inherent susceptibility to be involved in the reactivity of the M-C bond. Although alkylation with $LiCH_2Si(CH_3)_3$ is clearly not very representative of the actual activation process by MAO, and the bulkier alkyl may lend more stability to the system, the array of results gives a solid indication of the variety of accessible activation routes. Therefore, in this chapter, the reactivity of the $FeCl_2$ precursor is explored in the presence of MeLi, which is a far stronger alkylating agent and more reducing than MAO. Nonetheless, addressing the stability of the Fe-Me bond is central to understanding the activation process of the Fe catalyst.

Concomitant with this study, Chirik group published their findings regarding the reaction of the $FeCl_2$ precursor with MeLi.[13] Upon addition of 2 equivalents of the Li-alkyl to a suspension of $\{2,6\text{-}[2,6\text{-}(^{i}Pr)_2PhN{=}C(CH_3)]_2(C_5H_3N)\}FeCl_2$ in ether, the complex undergoes mono-alkylation and one-electron reduction (Scheme 3.2). The monovalent complex could also be produced via an initial reduction of the dichloride

species with $NaBEt_3H$ or Na(Hg) to the monochloro-complex, followed by a direct salt metathesis with MeLi.[13]

Scheme 3.2

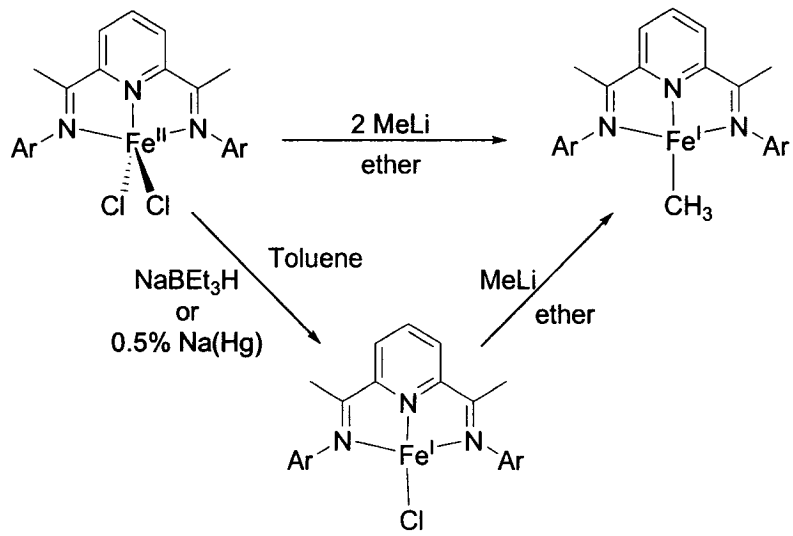

The one electron reduction to a monovalent alkyl is in line with the behaviour of the cobalt catalyst described above[9-11] and appears to be a common reaction pathway for the late metal systems. However, information about the catalytic activity of this species with or without additional activator was not reported and it is therefore unknown whether or not the precursor and the reduced species involve the same active site during the polymerization. However, a dimeric monovalent alkyl was isolated (Chapter 2, complex **2.5**) and shown to be catalytically active upon activation with MAO, producing exclusively the high molecular weight polymer from the β-hydride transfer termination pathway.[12] If participation of the ligand was not an issue and the catalysis results were mainly due to the presence of the metal center in the +1 oxidation state, a similar catalytic performance could be expected from Chirik's monovalent alkyl. However, modification of the ligand backbone through dimerization may also lead to unusual catalyst reactivity.

In this chapter, we describe the reaction of the bis-iminopyridine-$FeCl_2$ complex[1] with 3 equivalents of MeLi, affording a reduced complex with the formal appearance of a *zerovalent* species.[14] The observations described herein expand on the results of Chirik,[13]

creating a more complete picture of the reactivity of the system with strong alkylating agents.

Experimental Section

All operations were performed either under a nitrogen atmosphere using standard Schlenk techniques or in a purified nitrogen-filled dry-box. The complex {2,6-[2,6-(^{i}Pr)$_2$PhN=C(CH$_3$)]$_2$(C$_5$H$_3$N)}FeCl$_2$ was prepared following the procedure outlined in Chapter 2. The solution of MeLi in ether (1.6 M) was purchased from Aldrich and used as is. Infrared spectra were recorded on a Mattson 9000 and Nicolet 750-Magna FT-IR instrument from Nujol mulls prepared in a dry box. Samples for magnetic susceptibility measurements were weighed inside a dry box equipped with an analytical balance and sealed into calibrated tubes and the measurements were carried out at variable temperatures with a SQUID magnetometer. Magnetic moments were calculated following standard methods and corrections for underlying diamagnetism were applied to the data. Elemental analyses were performed on a Perkin-Elmer 2400 CHN analyzer. Data for X-ray crystal structure determinations were obtained with a Bruker diffractometer equipped with a Smart CCD area detector.

Preparation of [{2,6-[2,6-(^{i}Pr)$_2$PhN=C(CH$_3$)]$_2$(C$_5$H$_3$N)}FeCH$_3$][Li(THF)$_4$] (3.1)

A solution of MeLi in ether (1.85 mL from a 1.6M solution, 2.96 mmol) was added to a suspension of {2,6-[2,6-(^{i}Pr)$_2$PhN=C(CH$_3$)]$_2$(C$_5$H$_3$N)}FeCl$_2$ (0.600 g, 0.99 mmol) in ether at -35°C. The colour became dark brownish-red. The ether was evaporated and THF was added, forming a dark red solution. This solution was concentrated and layered with ether, upon which time white solids precipitated and were discarded. The solution was again concentrated and layered with hexanes, forming dark red crystals overnight at room temperature (0.550 g, 0.64 mmol, 64% yield). Anal. Calcd. (found) for C$_{51}$H$_{80}$FeLiN$_3$O$_{4.25}$ (%): C, 70.73 (70.69); H, 9.31 (9.28); N, 4.85 (4.83). Crystal data for **3.1**: C$_{102}$H$_{160}$Fe$_2$Li$_2$N$_6$O$_{8.5}$, Mw = 1731.94, monoclinic, ***P2$_1$***, a = 12.6741(19) Å, b = 17.383(3) Å, c = 24.089(4) Å, β = 97.102(3)°, V = 5266.5(14) Å^3, Z = 2, T = 211 K, F_{000} = 1880, R = 0.0794, wR2 = 0.1804, GoF = 1.019. Alternate unit cell: orthorhombic, a =

11.1 Å, b = 17.8 Å, c = 21.6 Å, V = 4276. Selected bond distances and angles can be found in Table 3.1.

Table 3.1 Selected Bond Distances (Å) and Angles (deg) of Complex 3.1

Fe(1)-N(1) = 1.917(6)	C(2)-C(3) = 1.404(10)
Fe(1)-N(2) = 1.849(6)	C(7)-C(8) = 1.421(11)
Fe(1)-N(3) = 1.915(5)	C(8)-C(9) = 1.515(10)
Fe(1)-C(34) = 2.015(8)	N(1)-Fe(1)-N(2) = 80.7(2)
N(1)-C(2) = 1.356(8)	N(2)-Fe(1)-N(3) = 80.4(3)
N(3)-C(8) = 1.377(9)	N(3)-Fe(1)-C(34) = 99.2(3)
N(2)-C(3) = 1.391(9)	N(1)-Fe(1)-C(34) = 99.6(3)
N(2)-C(7) = 1.372(8)	N(1)-Fe(1)-N(3) = 161.1(3)
C(1)-C(2) = 1.485(11)	N(2)-Fe(1)-C(34) = 178.9(4)

Results and Discussion

The reaction of {2,6-[2,6-(^{i}Pr)$_2$PhN=C(CH$_3$)]$_2$(C$_5$H$_3$N)}FeCl$_2$ with two equivalents of MeLi has recently been reported to afford a monovalent [{2,6-[2,6-(^{i}Pr)$_2$PhN=C(CH$_3$)]$_2$}(C$_5$H$_3$N)Fe-Me] species.[13] Increasing the amount of MeLi to three equivalents allows the isolation of deep-red crystals of a formally zerovalent species [{2,6-[2,6-(^{i}Pr)$_2$PhN=C(CH$_3$)]$_2$}(C$_5$H$_3$N)Fe-Me][Li(THF)$_4$]•(THF)$_{0.25}$ (**3.1**) in 64% yield in analytically pure form as the only isolable product (Scheme 3.3).

Scheme 3.3

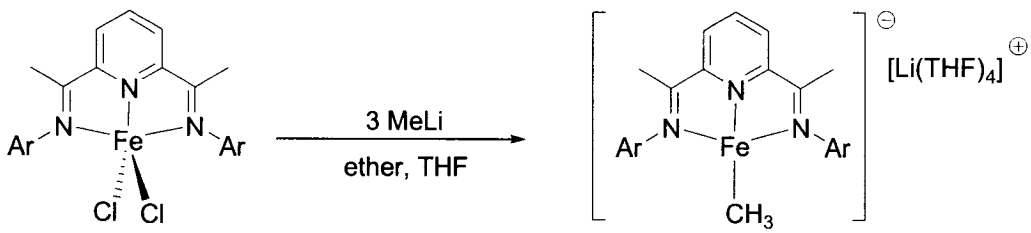

3.1

The formula and connectivity have been confirmed by X-ray diffraction of single crystals grown from a THF solution layered with hexane and can be seen in Figure 3.1 and selected bond distances and angles are listed in Table 3.1. The apparently intact ligand backbone surrounds the metal center in a distorted square planar geometry [Fe(1)-

N(1) = 1.917(6) Å, Fe(1)-N(2) = 1.849(6) Å, Fe(1)-N(3) = 1.915(5) Å], completed by the coordination of a terminal methyl group [Fe(1)-C(34) = 2.015(8) Å, N(1)-Fe(1)-N(2) = 80.7(2)°, N(2)-Fe(1)-N(3) = 80.4(3)°, N(3)-Fe(1)-C(34) = 99.2(3)°, N(1)-Fe(1)-C(34) = 99.6(3), N(1)-Fe(1)-N(3) = 161.1(3)°, N(2)-Fe(1)-C(34) = 178.9(4)°]. A THF-solvated Li countercation lies outside the coordination sphere of the metal center and is not within bonding distance of the anionic moiety. Crystals of a similar structure but different unit cell can also be grown from a cold ether solution. In this case, the resulting ether-solvated Li cation is found bridged to the metal center by the bound methyl group. Disorder of the ether molecules made that area of the molecule extremely difficult to model, and therefore only the unit cell is recorded herein for reference purposes.

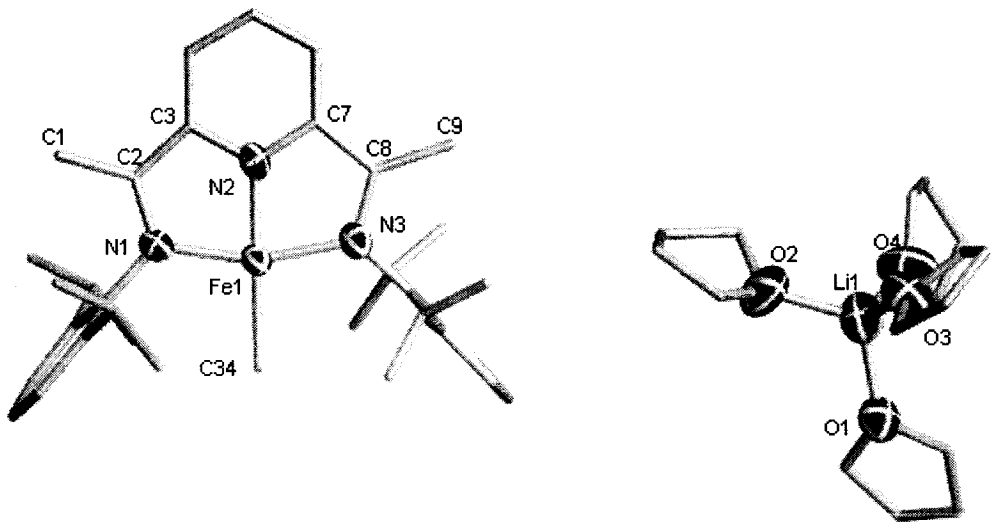

Figure 3.1. Partial thermal ellipsoid plot of **3.1**. Thermal ellipsoids are drawn at the 30% probability level. Hydrogen atoms have been omitted for clarity.

The anionic moiety of the complex is nearly isostructural with the monovalent complex reported by Chirik *et al.*.[13] Contrary to the observations for other metal systems[15] the methyl groups attached to the imine functions have not been deprotonated by the strongly basic MeLi [C(1)-C(2) = 1.485(11) Å, C(8)-C(9) = 1.515(10) Å]. Nonetheless, the metal center has been reduced and the complex appears to contain Fe in its formal zerovalent state. The reduction could be similar to that observed in the case of the more established Co analogue which, upon alkylation, afforded Co(I).[9-11] It is also possible that the reduction may be assisted by the ligand system, as in the case of the

two-electron reduction observed with vanadium in which the first equivalent of MeLi attacks the *ortho*-position of the pyridine ring and is subsequently attacked by a second equivalent, forming ethane and donating two electrons to the system.[16] Although *ortho*-alkylation is a possible reaction pathway for Fe, as shown in Chapter 2,[12] the isolation of the mono-reduced complex by Chirik suggests direct reduction over ligand alkylation. In addition, an internal charge transfer may also occur with this ligand,[17] characterizing **3.1** as a monovalent Fe bound to a radical anion, or even a divalent Fe bound to a ligand dianion. In line with this idea, DFT calculations by Budzelaar *et al.* have shown that the reduced Co(I) catalyst can be more aptly described as a Co(II) center antiferromagnetically coupled to a ligand radical anion.[18] In any case, the formation of **3.1** has required two electrons.

Upon close inspection of the bond distances of **3.1** in comparison to the precursor[1] and Chirik's mono-reduced species,[13] several differences can be noted that support a possible ligand reduction at the expense of the metal center (shown in Table 3.2).[19] First of all, the distances of the ligand N atoms to the metal center have shortened, indicating either increased back-donation to the ligand as a result of a reduced Fe center, or a stronger interaction due to the presence of a dinegative charge on the ligand. Examination of the ligand backbone reveals progressive trends in going from the divalent precursor to the mono- and di-reduced species.[19] The C-N imine bonds lengthen with reduction from an average of about 1.298 Å in the starting complex to 1.367 Å in complex **3.1**, along with the N_{pyr}-C_{ortho} bonds in the pyridine ring, from 1.339 Å to 1.381 Å. Conversely, the C_{imine}-C_{ortho} bond distances are shortened upon reduction, from an average of 1.474 Å to 1.412 Å. The bond length adjustments in the ligand are an indication that the electron density resides in low-lying π^* orbitals on the ligand backbone, as opposed to the metal center.

Table 3.2. Comparative Bond Distances of Selected Complexes (Å)

Complex	Fe-N	N_{imine}-C_{imine}	C_{imine}-C_{ortho}	C_{ortho}-N_{pyr}
	2.222(4)	1.301(7)	1.466(8)	1.356(7)
$LFeCl_2$[a]	2.091(4)	1.295(7)	1.482(8)	1.323(7)
	2.225(5)			
	1.968(5)	1.337(7)	1.432(8)	1.349(7)
LFeMe[b]	1.893(4)	1.332(7)	1.442(8)	1.368(7)
	1.952(5)			
	1.917(6)	1.356(8)	1.404(10)	1.391(9)
3.1	1.849(6)	1.377(9)	1.421(11)	1.372(8)
	1.915(5)			

[a] L = 2,6-[2,6-(^{i}Pr)$_2$PhN=C(CH_3)]$_2$(C_5H_3N)
[b] Reference 13.

The magnetism of **3.1** also supports the formation of a ligand radical over the metal in a reduced state. Assuming a direct reduction of the metal center, the resulting d^8 square planar Fe(0) complex would reasonably be expected to be diamagnetic. However, the species is paramagnetic with a magnetic moment which rises steadily from an intercept of μ_{eff} = 1.3 μ_B at 2-4 K to reach the value of 6.4 μ_B at room temperature (300 K) (Figure 3.2). Although the magnetic behaviour could not be properly simulated, it is possible that, similar to the case of the Nd[17a] and Co[18] congeners, thermal population of ligand orbitals at the expense of the low-valent metal center occurs. Thus, a high-spin Fe(II) coupled to a diradical dianion is probably the most realistic description of this system. However, the occurrence of trace amounts of elemental Fe, perhaps due to complete reduction, cannot be ruled out at this stage.

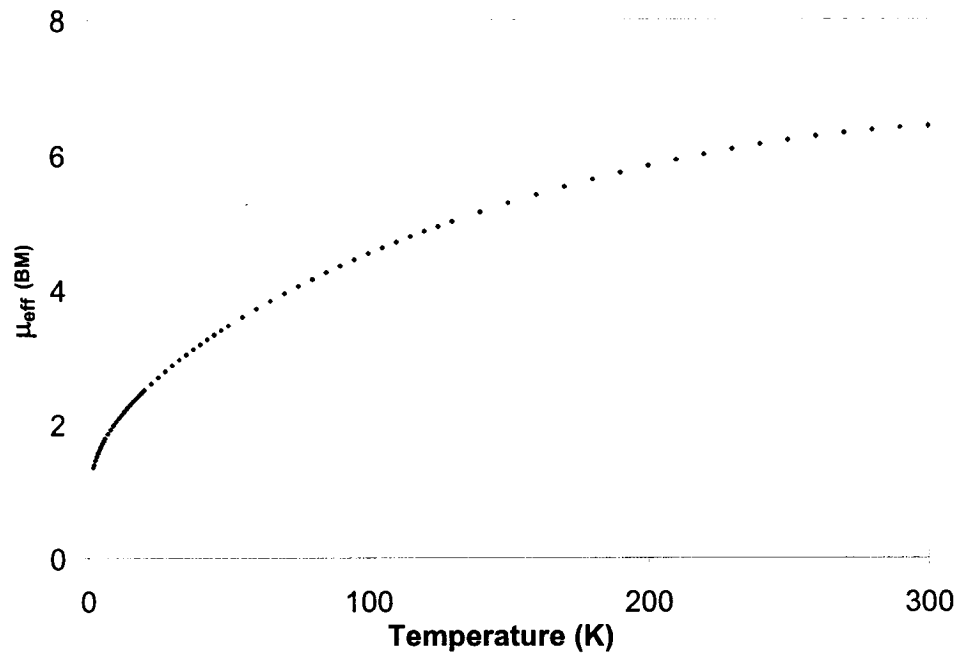

Figure 3.2. Magnetic moment data at variable temperature for complex **3.1**.

In collaboration with Peter Budzelaar, DFT calculations were performed on the isolated anion starting from the crystallographic atomic coordinates and assuming several spin states.[14] A closed-shell genuine Fe(0) description could be ruled out. The singlet state is best described as containing intermediate-spin Fe(II), with each of the Fe unpaired electrons antiferromagnetically coupled to an electron in a ligand π^* orbital, i.e. it has a double-singlet-biradical structure. The triplet and quintet states, which are close in energy to the singlet, are similar but have the spins of one or two of the ligand π^* electrons inverted. Neither the calculated energies, nor the comparison of calculated and experimental geometries allow assignment of the spin state of complex **3.1**. The electronic structure is very similar to that calculated for Co(I)[18] in the sense that it shows a biradical character with unpaired electrons in metal *d* orbitals antiferromagnetically coupled to ligand π^* orbitals. Different from the Co(I) complex however, the Fe metal center uses both d_{xz} and d_{yz} for such biradical couplings, presumably because the *d* orbitals are high in energy due to the presence of the negative charge.[14]

Catalysis Results

When a toluene solution of **3.1** was exposed to ethylene gas, there was no apparent colour change nor polymer formation. However, the addition of 500 equivalents of MAO with exposure to 1 atmosphere of ethylene led to the isolation of large amounts of polyethylene after 30 minutes of reaction. The activity of **3.1** was found to be 600 gPE/mmol·h·atm, which compares well, within experimental error, with the activity obtained for the divalent Fe starting complex under the same conditions (675 gPE/mmol·h·atm). Even more striking is the fact that the polymers produced by **3.1** and the divalent precursor are *very similar* (Figure 3.3) clearly indicating that the catalytically active species is the same in both polymerization reactions. It should also be noted that the polymer produced by the cationic Fe(II) derivative of Chirik[8] is completely different from that obtained in the present case and that activation of **3.1** with $B(C_6F_5)_3$ under the usual reaction conditions did not yield polymer in a significant amount.

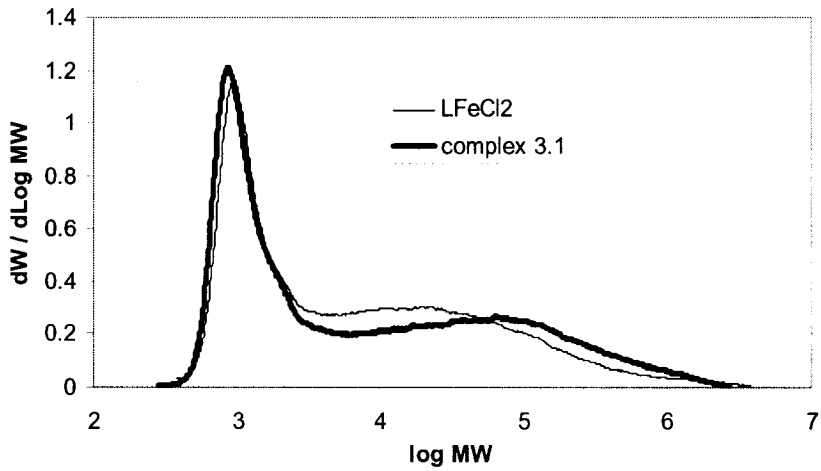

Figure 3.3. Comparative gel permeation chromatogram of the Fe(II) precursor and complex **3.1** (Mn = 1954, Mw = 76377, Mz = 673379, PD = 39.09 determined by high T GPC in 1,2,4-trichlorobenzene).

The evidence reported herein is hard to reconcile with a cationic Ziegler-Natta mechanism for ethylene polymerization with **3.1**, and hence also with the original Brookhart/Gibson $FeCl_2$ precursor. The reduction of the catalyst by two electrons also discounts the oxidation pathway suggested by Gibson upon activation with MAO.[4] Although complex **3.1** still requires an excess of activator to perform polymerization, the

role of the aluminum activator is not likely to be the formation of a cationic species. The removal of the coordinated MeLi unit by the Lewis acid may provide a coordinatively unsaturated "LFe(0)" or "L^{2-}Fe(II)" *neutral* species which, in view of Chirik's results, will most likely give labile coordination with olefin,[20] with polymerization proceeding via a completely different mechanism than expected. Another possibility is coordination of the Lewis acidic TMA to an area of increased electron density on the ligand backbone and formation of a bridging methyl group to the metal center, which could create a zwitterionic pseudo-cationic Fe alkyl into which ethylene insertion could occur. The proximity of the bound Al could also facilitate chain transfer to Al as the primary chain termination pathway observed by this system.[21] Speculation aside, at least one of the activation routes of the $FeCl_2$ precursor involves a two electron reduction of the system.

Conclusion

In conclusion, the addition of a strongly reducing alkylating agent to the $FeCl_2$ precursor results in a two electron reduction of the system. More accurately, the resulting complex contains a divalent Fe center antiferromagnetically coupled to a ligand diradical dianion, where the electrons occupy the ligand π^* orbitals instead of the metal center. Activation of the complex with MAO polymerizes ethylene with the same activity and polymer quality as that achieved by the precursor under similar conditions. Therefore, upon activation of the precursor with MAO, the system undergoes a two electron reduction towards an as yet unidentified active species, most likely discounting a typical Ziegler-Natta polymerization mechanism.

References

(1) (a) Small, B. L.; Brookhart, M.; Bennett, A. M. A. *J. Am. Chem. Soc.* **1998**, *120*, 4049. (b) Britovsek, G. J. P.; Gibson, V. C.; Kimberley, B. S.; Maddox, P. J.; McTavish, S. J.; Solan, G. A.; White, A. J. P.; Williams, D. J. *Chem. Commun.* **1998**, 849.

(2) See Chapter 1.

(3) (a) Deng, L.; Margl, P.; Ziegler, T. *J. Am. Chem. Soc.* **1999**, *121*, 6479. (b) Griffiths, E. A. H.; Britovsek, G. J. P.; Gibson, V. C.; Gould, I. R. *Chem. Commun.* **1999**, 1333. (c) Khoroshun, D. V.; Musaev, D. G.; Vreven, T.; Morokuma, K. *Organometallics* **2001**, *20*, 2007. (d) Zakharov, I. I.; Zakharov, V. A. *Macromol. Theory Simul.* **2004**, *13*, 583.

(4) Britovsek, G. J. P.; Clentsmith, G. K. B.; Gibson, V. C.; Goodgame, D. M. L.; McTavish, S. J.; Pankhurst, Q. A. *Catal. Commun.* **2002**, *3*, 207.

(5) (a) Bryliakov, K. P.; Semikolenova, N. V.; Zudin, V. N.; Zakharov, V. A.; Talsi, E. P. *Catal. Commun.* **2004**, *5*, 45. (b) Bryliakov, K. P.; Semikolenova, N. V.; Zakharov, V. A.; Talsi, E. P. *Organometallics* **2004**, *23*, 5375.

(6) Castro, P. M.; Lahtinen, P.; Axenov, K.; Viidanoja, J.; Kotiaho, T.; Leskelä, M.; Repo, T. *Organometallics* **2005**, *24*, 3664.

(7) Britovsek, G. J. P.; Gibson, V. C.; Spitzmesser, S. K.; Tellmann, K. P.; White, A. J. P.; Williams, D. J. *J. Chem. Soc., Dalton Trans.* **2002**, 1159.

(8) Bouwkamp, M. W.; Lobkovsky, E.; Chirik, P. J. *J. Am. Chem. Soc.* **2005**, *127*, 9660.

(9) Gibson, V. C.; Humphries, M. J.; Tellmann, K. P.; Wass, D. F.; White, A. J. P.; Williams, D. J. *Chem. Commun.* **2001**, 2252.

(10) Kooistra, T. M.; Knijnenburg, Q.; Smits, J. M. M.; Horton, A. D.; Budzelaar, P. H. M.; Gal, A. W. *Angew. Chem. Int. Ed.* **2001**, *40*, 4719.

(11) (a) Steffen, W.; Blomker, T.; Kleigrewe, N.; Kehr, G.; Frolich, R.; Erker, G. *Chem. Commun.* **2004**, 1188. (b) Kleigrewe, N.; Steffen, W.; Blomker, T.; Kehr, G.; Frohlich, R.; Wibbeling, B.; Erker, G.; Wasilke, J.-C.; Wu, G.; Bazan, G. C. *J. Am. Chem. Soc.* **2005**, *127*, 13955.

(12) Scott, J.; Gambarotta, S.; Korobkov, I.; Budzelaar, P. H. M. *J. Am. Chem. Soc.* **2005**, *127*, 13019.

(13) Bouwkamp, M. W.; Bart, S. C.; Hawrelak, E. J.; Trovitch, R. J.; Lobkovsky, E.; Chirik, P. J. *Chem. Commun.* **2005**, 3406.

(14) Scott, J.; Gambarotta, S.; Korobkov, I.; Budzelaar, P. H. M. *Organometallics* **2005**, *24*, 6298.

(15) (a) Khorobkov, I.; Gambarotta, S.; Yap, G. P. A. *Organometallics* **2002**, *21*, 3088. (b) Clentsmith, G. K. B.; Gibson, V. C.; Hitchcock, P. B.; Kimberley, B. S.; Rees, C. W. *Chem. Commun.* **2002**, 1498. (c) Blackmore, I. J.; Gibson, V. C.; Hitchcock,

P. B.; Rees, C. W.; Williams, D. J.; White, A. J. P. *J. Am. Chem. Soc.* **2005**, *127*, 6012.

(16) Reardon, D.; Conan, F.; Gambarotta, S.; Yap, G.; Wang, Q. *J. Am. Chem. Soc.* **1999**, *121*, 9318.

(17) (a) Sugiyama, H.; Korobkov, I.; Gambarotta, S.; Moeller, A.; Budzelaar, P. H. M. *Inorg. Chem.* **2004**, *43*, 5771. (b) Vidyaratne, I.; Gambarotta, S.; Korobkov, I.; Budzelaar, P. H. M. *Inorg. Chem.* **2005**, *44*, 1187.

(18) Knijnenburg, Q.; Hetterscheid, D.; Kooistra, T. M.; Budzelaar, P. H. M. *Eur. J. Inorg. Chem.* **2004**, 1204.

(19) (a) Budzelaar, P. H. M.; de Bruin, B.; Gal, A. W.; Wieghardt, K.; van Lenthe, J. H. *Inorg. Chem.* **2001**. *40*, 4649. (b) Bart, S. C.; Chlopek, K.; Bill, E.; Bouwkamp, M. W.; Lobkovsky, E.; Neese, F.; Wieghardt, K.; Chirik, P. J. *J. Am. Chem. Soc.* **2006**, *128*, 13901.

(20) Bart, S. C.; Lobkovsky, E.; Chirik, P. J. *J. Am. Chem. Soc.* **2004**, *126*, 13794.

(21) Britovsek, G. J. P.; Bruce, M.; Gibson, V. C.; Kimberley, B. S.; Maddox, P. J.; Mastroianni, S.; McTavish, S. J.; Redshaw, C.; Solan, G. A.; Strömberg, S.; White, A. J. P.; Williams, D. J. *J. Am. Chem. Soc.* **1999**, *121*, 8728.

Chapter Four

Activation of the Bis-iminopyridine-$FeCl_2$ Catalyst with Aluminum Alkyls

---

Introduction

In general, a catalytic system for ethylene polymerization is composed of a catalyst precursor (the transition metal complex performing the actual polymerization) and an appropriate Lewis acidic co-catalyst.[1] Among its numerous functions, the co-catalyst's main purpose is to activate the precursor by generating the active species responsible for the polymerization. Common activators include MAO, various trialkyl aluminum compounds, or other boron Lewis acids, like $B(C_6F_5)_3$. Thus, the role of the activator in a typical Ziegler-Natta system is normally regarded to be the formation of an unsaturated cationic metal alkyl, via alkylation of the metal center and abstraction of either an alkyl or a halide to create a vacant coordination site adjacent to the M-C bond. Consequent cationization favours approach and coordination of the incoming monomer to the metal center, creating the conditions for insertion of the monomer into the M-C bond, and hence lengthening of the polymer chain.[1]

Decades of research into Group 4 metal olefin polymerization catalysts support the mechanism described above, as discussed in Chapter 1. However, in the case of the late metal bis-iminopyridine-Fe catalyst[2] the situation appears to be slightly different, perhaps even more complex. Studies aimed towards elucidating the reaction mechanism and identifying the features which enable such a desirable catalytic behaviour have

explored several key issues: 1) the stability of the M-C bond; 2) the role played by the ligand; and 3) the oxidation state and electronic configuration of the metal ion in the catalytically active species.[3-8] The alkylation studies reported in Chapter 2 have outlined a non-anticipated ability of the bis-iminopyridine ligand to engage directly in the reactivity of the M-C bond.[6] In turn, this has resulted in an impressive variety of transformations, including alkylation of the ligand backbone, deprotonation of the methyl groups, and dimerization and reduction. Studies exploring the addition of a more reactive alkyl to the same system (Chapter 3) resulted in a two electron reduction to a formally zerovalent Fe species.[7] However, the ability of the ligand π-system to accept a considerable amount of spin density creates the appearance of low-valency and the species can more accurately be described as a divalent Fe center bound to a ligand diradical dianion. Remarkably, the reduced complex was shown to have the same catalytic activity upon activation with MAO and produce the same polymer as the divalent precursor.[7] These results indicate that activation of the divalent precursor and the reduced species involve transformation to the same active species, and therefore, activation of the precursor involves an initial reduction of the system by two electrons. Thus, it is difficult to anticipate the formation of a cationic Fe(II) alkyl from this point, in turn raising questions regarding the role of the activator in these systems and the nature of active species responsible for the polymerization.

In an attempt to gain further insight into this fascinating system, and perhaps answer the questions posed above, we have herein studied the reaction of the bis-iminopyridine-$FeCl_2$ complex with several aluminum activators, AlR_3 [R = Me, Et, ^{i}Bu]. Unfortunately, in the case of MAO (the preferred activator), efforts have only led to ill-defined species, most likely due to the complex nature of this activator. Studies by Gibson *et al.* have shown that activation of the Fe system by aluminum alkyls results in only a marginal decrease in the catalytic activity and exclusive formation of the low molecular weight polymer formed by chain transfer to the aluminum center.[9] Thus, exploring the mechanism of activation of the Fe-precursor with aluminum alkyls is still a valid route for modeling the behaviour of these catalytically active species. On the other hand, the aluminum alkyl catalytic systems have a shorter catalyst lifetime than their MAO counterpart,[9] most likely the result of decreased catalyst stability. Aware of the

simplification introduced by the use of AlR_3, we still believe that any information would be valuable and the results of our attempts in this direction are presented in this chapter.[10]

Experimental Section

All operations were performed either under a nitrogen atmosphere using standard Schlenk techniques or in a purified nitrogen-filled dry-box. $FeCl_2(THF)_{1.5}$ was prepared following the standard procedure and the ligand 2,6-[2,6-(^{i}Pr)$_2$PhN=C(CH$_3$)]$_2$(C$_5$H$_3$N) was prepared following the published procedure.[2] {2,6-[2,6-(^{i}Pr)$_2$PhN=C(CH$_3$)]$_2$ (C$_5$H$_3$N)}FeCl$_2$ was prepared following the procedure outlined in Chapter 2. The solutions of $AlMe_3$ (2.0 M in toluene), $AlEt_3$ (1.0 M in toluene), $AlMe_2Cl$ (1.0 M in toluene), and Al^{i}Bu$_3$ (1.0 M in toluene) were purchased from Aldrich and used as such. Infrared spectra were recorded on a Mattson 9000 and Nicolet 750-Magna FT-IR instrument from Nujol mulls prepared in a dry box. NMR spectra were recorded on a Varian INOVA 500 spectrometer. Samples for magnetic susceptibility measurements were weighed inside a dry box equipped with an analytical balance and sealed into calibrated tubes and the measurements were carried out at room temperature with a Gouy balance (Johnson Matthey). Magnetic moments were calculated following standard methods and corrections for underlying diamagnetism were applied to the data. Elemental analyses were performed on a Perkin-Elmer 2400 CHN analyzer. Data for X-ray crystal structure determinations were obtained with a Bruker diffractometer equipped with a Smart CCD area detector.

Preparation of {2,6-[2,6-(^{i}Pr)$_2$PhN=C(CH$_3$)]$_2$(C$_5$H$_3$N)}Al(CH$_3$)$_2$ (4.1).

Method A: To a stirring suspension of {2,6-[2,6-(^{i}Pr)$_2$PhN=C(CH$_3$)]$_2$(C$_5$H$_3$N)}FeCl$_2$ (0.500 g, 0.82 mmol) in toluene (20 mL) at -35°C, 10 equivalents of $AlMe_3$ were added (2.0 M, 4.2 mL, 8.2 mmol). The colour changed from royal blue to purple and finally to dark green upon warming to room temperature with stirring over a period of approximately 2 hours. The mixture was stirred overnight and the solvent evaporated *in vacuo*, leaving behind a dark residue. Addition of hexane to the residue allowed removal of an emerald green solution, from which complex **4.3** was isolated. In turn, addition of fresh ether to the remaining residue allowed removal of a dark orange-brown solution,

from which complex **4.2** was isolated. The left-over precipitates (insoluble in hexane or ether) were dissolved in fresh toluene. After centrifugation and removal of the dark brown-orange solution from the remaining dark precipitates, the solution was concentrated and dark orange crystals of **4.1** were grown upon standing at -35°C for several days. (0.23 g, 0.32 mmol, 38% yield). Anal. Calcd. (found) for $C_{49}H_{65}AlN_3$ (%): C, 81.40 (81.06); H, 9.06 (9.12); N, 5.81 (5.56). IR (Nujol mull, cm^{-1}): ν 2912 (s), 2855 (s), 1629 (w), 1597 (m), 1522 (m), 1322 (w), 1269 (s), 1251 (w), 1237 (s), 1211 (w), 1189 (m), 1171 (m), 1101 (w), 1076 (s), 1055 (w), 1036 (m), 937 (s), 883 (w), 863 (m), 831 (m), 815 (w), 803 (s), 777 (s), 761 (w), 727 (s), 683 (s), 661 (s).

Method B: A solution of $AlMe_3$ (2.0 M, 0.35 mL, 0.70 mmol) was added to a suspension of {2,6-[2,6-(^{i}Pr)$_2$PhN=C(CH$_3$)]$_2$(C$_5$H$_3$N)}Fe(CH$_2$SiMe$_3$)$_2$ (**2.2**) (0.10 g, 0.14 mmol) in toluene at -35°C. The colour became dark yellow-brown and turned orange-brown after stirring for approximately 30 minutes. The mixture was stirred overnight, evaporated to dryness and washed with hexane. The residue was dissolved in toluene, centrifuged, concentrated and placed in the freezer to crystallize (0.040 g, 0.050 mmol, 39%).

Method C: The ligand {2,6-[2,6-(^{i}Pr)$_2$PhN=C(CH$_3$)]$_2$(C$_5$H$_3$N)} (0.40 g, 0.83 mmol) was reacted with 1 equivalent of Na (0.019 g, 0.83 mmol) in THF. The resulting dark purple solution was evaporated to dryness and dissolved in toluene. A solution of Me_2AlCl (1.0 M, 0.84 mL, 0.83 mmol) was added at -35°C and the solution became dark orange. Centrifugation and freezing allowed the isolation of orange crystals of **4.1** (0.45 g, 0.62 mmol, 76%). ^{1}H NMR (d_6-benzene), 500MHz, 25°C, δ (ppm): 11.6-10.8 (broad singlet, *p*-C$_5$***H***$_3$N), 8.5 (d, *m*-C$_6$***H***$_3$^{i}Pr$_2$), 7.19 (m, *p*-C$_6$***H***$_3$^{i}Pr$_2$), 7.01 (m, toluene), 5.53-5.16 (broad singlet, *m*-C$_5$***H***$_3$N), 3.59 (s, THF), 3.28 (m, C***H***Me$_2$), 2.91 (m, C***H***Me$_2$), 2.58 (very broad singlet, N=CC***H***$_3$), 2.28 (s, Al-C***H***$_3$), 2.13 (s, toluene), 1.91 (very broad singlet, N=CC***H***$_3$), 1.44 (s, THF), 1.16 (d, J_{HH} = 6.6 Hz, CH(C***H***$_3$)$_2$), 0.90 (m, CH(C***H***$_3$)$_2$). [μ_{eff} = 1.7 μ_B]

Preparation of {2,6-[2,6-(^{i}Pr)$_2$PhN=C(CH$_3$)]$_2$(C$_5$H$_3$N)}AlCl(CH$_3$) (4.2).

The identical procedure was carried out as above for complex **4.1**. However, the brownish-orange ether-soluble portion was concentrated and left sitting at room temperature for two days, upon which time orange plates of **4.2** grew in 30% yield (0.135

g, 0.25 mmol). Anal. Calcd. (found) for $C_{34.35}H_{47.05}AlC_{10.65}N_3$ (%): C, 74.73 (74.67); H, 8.58 (8.62); N, 7.61 (7.10). IR (Nujol mull, cm^{-1}): ν 2913 (s), 2854 (s), 1522 (s), 1463(s), 1376 (s), 1322 (w), 1237 (s), 1181 (m), 1149 (w), 1084 (s), 947 (s), 884 (w), 864 (m), 831 (m), 804 (m), 777 (m), 760 (w), 727 (w), 699 (m), 656 (m), 633 (w).

Preparation of [η^4-{2,6-[2,6-(^{i}Pr)$_2$PhN=C(CH$_3$)]$_2$(C$_5$H$_3$N)}Al$_2$Me$_3$(μ-Cl)][AlMe$_3$(THF)] (4.3).

The procedure for complex **4.1** was followed and the green hexane-soluble portion was concentrated and left at -35°C. Bright emerald green needles of **4.3** grew after a few days (0.044 g, 0.057 mmol, 7%). IR (Nujol mull, cm^{-1}): ν 2949-2861 (b, s), 1611 (w), 1567 (w), 1463 (s), 1405 (w), 1376 (s), 1318 (m), 1253 (w), 1232 (w), 1179 (s), 1161 (m), 1118 (w), 1065 (m), 1018 (s), 943 (w), 918 (w), 869 (m), 814 (m), 804 (m), 759 (w), 722 (m), 708 (m), 681 (s). ^{1}H NMR (C_6D_6), 500MHz, 25°C, δ (ppm): 7.11 (d, 4H, *m*-C$_6$***H***$_3$^{i}Pr$_2$), 7.05 (t, 2H, *p*-C$_6$***H***$_3$^{i}Pr$_2$), 6.66 (broad, 2H, *m*-C$_5$***H***$_3$N), 5.14 (broad, 1H, *p*-C$_5$***H***$_3$N), 3.59 (m, 2H, (CH$_3$)$_2$C***H***), 3.32 (t, 4H, THF), 2.85 (m, 2H, (CH$_3$)$_2$C***H***), 1.62 (s, 6H, NC=C***H***$_3$), 1.35 (d, 6H, (C***H***$_3$)$_2$CH), 1.23 (m, 12H, (C***H***$_3$)$_2$CH), 0.96 (d, 6H, (C***H***$_3$)$_2$CH), 0.88 (m, 4H, THF), -0.23 (s, 9H, Al(C***H***$_3$)$_3$(THF)), -0.39 (s, 6H, -Al(C***H***$_3$)$_2$Cl-), -0.72 (s, 3H, -Al(C***H***$_3$)Cl-).

Preparation of [η^4-{2,6-[2,6-(^{i}Pr)$_2$PhN=C(CH$_3$)]$_2$(C$_5$H$_3$N)}Al$_2$Et$_3$(μ-Cl)]Fe-(η^6-C$_7$H$_8$) (4.4).

{2,6-[2,6-(^{i}Pr)$_2$PhN=C(CH$_3$)]$_2$(C$_5$H$_3$N)}FeCl$_2$ was prepared *in situ* by mixing FeCl$_2$(THF)$_{1.5}$ (0.200 g, 0.85 mmol) with {2,6-[2,6-(^{i}Pr)$_2$PhN=C(CH$_3$)]$_2$(C$_5$H$_3$N)} (0.410 g, 0.85 mmol) in toluene (20 mL) overnight. The dark blue suspension was cooled to -35°C and 5 equivalents of AlEt$_3$ were added by syringe (4.25 mL of a 1.0 M solution in toluene, 4.25 mmol). The colour initially became dark green and then dark orange upon stirring overnight. The toluene was evaporated and hexane was added, removing a dark greenish-brown solution. The remaining precipitates were dissolved in ether, centrifuged to remove any insoluble material, concentrated and left to crystallize at room temperature for 2 days. The crystals were washed with many fractions of fresh hexane to reveal a final yield of 41% for complex **4.4** (0.280 g, 0.34 mmol). Anal. Calcd. (found) for

$C_{46}H_{66}N_3Al_2ClFe$ (%): C, 68.52 (67.98); H, 8.25 (8.01); N, 5.21 (5.02). IR (Nujol mull, cm^{-1}): ν 2918 (s), 2854 (s), 1597 (s), 1584 (s), 1509 (s), 1305 (s), 1272 (m), 1236 (w), 1219 (w), 1192 (m), 1171 (m), 1108 (m), 1073 (w), 1054 (w), 1033 (w), 992 (m), 971 (m), 947 (m), 902 (w), 847 (m), 820 (s), 803 (m), 793 (m), 777 (s), 724 (m), 690 (m). [μ_{eff} = 1.4 μ_B]

Preparation of [η^4-{2,6-[2,6-(^{i}Pr)$_2$PhN=C(CH$_3$)]$_2$(C$_5$H$_3$N)}Al$_2$^{i}Bu$_3$(μ-Cl)]Fe-(η^6-C$_7$H$_8$) (4.5).

The preparation of complex **4.5** is very similar to that of **4.4** described above, starting from the *in situ* preparation of {2,6-[2,6-(^{i}Pr)$_2$PhN=C(CH$_3$)]$_2$(C$_5$H$_3$N)}FeCl$_2$: FeCl$_2$(THF)$_{1.5}$ (0.100 g, 0.42 mmol) mixed with {2,6-[2,6-(^{i}Pr)$_2$PhN=C(CH$_3$)]$_2$(C$_5$H$_3$N)} (0.205 g, 0.42 mmol) in toluene (20 mL) overnight. After cooling to -35°C, 10 equivalents of Al(^{i}Bu)$_3$ (4.26 mL of a 1.0 M solution in toluene, 4.2 mmol) were added to the dark blue suspension. Upon addition, the colour became dark green and everything appeared to go into solution. After approximately 30 minutes of stirring at room temperature, the colour of the solution became very dark orange-brown. The reaction was stirred overnight and toluene was removed by vacuum distillation. Hexane was added to the dark brown sticky mass and the resulting dark brown solution was centrifuged to remove any precipitates, concentrated and left at room temperature. Crystals of **4.5** grew after 24 hours from a concentrated hexane solution (0.194 g, 0.22 mmol, 52% yield). Anal. Calcd. (found) for $C_{46}H_{66}N_3Al_2ClFe$ (%): C, 68.52 (68.42); H, 8.25 (8.37); N, 5.21 (5.18). [μ_{eff} = 1.5 μ_B]

X-ray Crystallography

All of the compounds **4.1-4.5** consistently yielded crystals that diffracted weakly, and the results presented are the best of several trials. The crystals were mounted on thin glass fibers using paraffin oil and cooled to the data collection temperature. Data were collected on a Bruker AXS SMART 1k CCD diffractometer. Data for the compounds **4.1**, **4.3** and **4.5** were collected with a sequence of 0.3° ω scans at 0, 120, and 240° in φ. To obtain acceptable redundancy data for compounds **4.2** and **4.4**, the sequence of 0.3° ω scans at 0, 90, 180, and 270° in φ was used. Initial unit cell parameters were determined

from 50 data frames collected at the different sections of the Ewald sphere. Semi-empirical absorption corrections based on equivalent reflections were applied.[11] Systematic absences in the diffraction data-set and unit-cell parameters were consistent with monoclinic ***Pc*** for **4.1**, triclinic $P\bar{1}$ for **4.2,** monoclinic $P2_1/n$ for **4.3**, triclinic $P\bar{1}$ for **4.4** and monoclinic $P2_1/n$ for **4.5**. Solutions in centrosymmetric space groups for all of the compounds yielded chemically reasonable and computationally stable results of refinement. The structures were solved by direct methods, completed with difference Fourier synthesis, and refined with full-matrix least-squares procedures based on F^2. The compound molecules were located in common positions in the structures of all the complexes. All non-hydrogen atoms were refined with anisotropic displacement coefficients. All hydrogen atoms were treated as idealized contributions. All scattering factors are contained in several versions of the SHELXTL program library; with the latest version used being v.6.12.[12] Crystallographic data and relevant bond distances and angles are reported in Tables 4.1-4.3.

Table 4.1. Crystal Data and Structure Analysis Results for complexes 4.1-4.5

	4.1	**4.2**	**4.3**	**4.4**	**4.5**
formula	$C_{49}H_{65}AlN_3$	$C_{34.35}H_{47.05}AlC_{l0.65}N_3$	$C_{43}H_{69}Al_3ClN_3O$	$C_{92}H_{132}Al_4Cl_2Fe_2N_6$	$C_{52}H_{78}Al_2ClFeN_3$
Mw	723.02	552.02	760.40	1612.56	890.43
crystal system	Monoclinic	Triclinic	Monoclinic	Triclinic	Monoclinic
space group	Pc	P-1	P2(1)/n	P-1	P2(1)/n
a (Å)	10.727(6)	8.888(17)	18.062(4)	10.676(4)	10.872(2)
b (Å)	12.871(7)	9.831(19)	9.0057(18)	19.708(7)	19.267(4)
c (Å)	16.300(9)	20.81(4)	28.311(6)	21.150(7)	23.812(5)
α (deg)	90	83.36(3)	90	82.262(6)	90
β (deg)	98.068(10)	87.92(3)	91.423(4)	89.088(6)	101.081(4)
γ (deg)	90	64.90(3)	90	87.984(6)	90
V (Å^3)	2228(2)	1635(5)	4603.7(16)	4407(3)	4894.9(19)
Z	2	2	4	2	4
radiation (Kα, Å)	0.71073	0.71073	0.71073	0.71073	0.71073
T (K)	213(2)	208(2)	213(2)	207(2)	125(2)
D_{calcd} (g cm^{-3})	1.078	1.121	1.097	1.215	1.208
μ_{calcd} (mm^{-1})	0.080	0.141	0.173	0.477	0.436
F_{000}	786	596	1648	1728	1920
R, $R_w{}^{2\,a}$	0.0758, 0.1360	0.0532, 0.1342	0.0622, 0.1353	0.0673, 0.1660	0.0386, 0.1057
GoF	1.040	1.039	1.021	1.013	1.001

[a] $R = \Sigma||F_0| - |F_c||/\Sigma|F|$, $R_w = [\Sigma(|F_0| - |F_c|)^2/\Sigma wF_0^2\}^{1/2}$

Table 4.2. Selected Bond Distances (Å) and Angles (deg) for complexes 4.1-4.3

4.1	4.2	4.3	4.3 (cont'd)
Al(1)-N(1) = 2.212(8)	Al(1)-N(1) = 2.163(4)	Al(1)-N(1) = 1.993(5)	N(1)-Al(1)-C(34) = 99.9(3)
Al(1)-N(2) = 1.892(8)	Al(1)-N(2) = 1.928(4)	Al(1)-N(2) = 2.003(5)	N(1)-Al(1)-Cl(1) = 103.75(16)
Al(1)-N(3) = 2.163(8)	Al(1)-N(3) = 2.118(4)	Al(1)-N(3) = 1.995(5)	N(2)-Al(1)-N(3) = 80.2(2)
Al(1)-C(34) = 1.982(4)	Al(1)-C(34) = 1.98(2)	Al(1)-C(34) = 1.951(6)	N(2)-Al(1)-C(34) = 176.8(3)
Al(1)-C(35) = 2.007(4)	Al(1)-C(35) = 1.978(15)	Al(1)-Cl(1) = 2.404(2)	N(2)-Al(1)-Cl(1) = 85.69(15)
N(1)-C(2) = 1.297(10)	Al(1)-Cl(1) = 2.185(10)	Al(2)-N(2) = 1.969(5)	N(3)-Al(1)-C(34) = 98.4(3)
N(3)-C(8) = 1.331(11)	Al(1)-Cl(2) = 2.037(5)	Al(2)-Cl(1) = 2.275(3)	N(3)-Al(1)-Cl(1) = 105.14(15)
N(2)-C(3) = 1.371(11)	N(1)-C(2) = 1.315(4)	Al(2)-C(35) = 1.958(8)	C(34)-Al(1)-Cl(1) = 97.5(2)
N(2)-C(7) = 1.381(10)	N(3)-C(8) = 1.318(4)	Al(2)-C(36) = 1.946(7)	N(2)-Al(2)-Cl(1) = 90.10(16)
C(1)-C(2) = 1.501(13)	N(2)-C(3) = 1.384(4)	N(1)-C(2) = 1.323(7)	N(2)-Al(2)-C(35) = 113.0(3)
C(2)-C(3) = 1.425(13)	N(2)-C(7) = 1.368(4)	N(3)-C(8) = 1.333(7)	N(2)-Al(2)-C(36) = 112.0(3)
C(7)-C(8) = 1.416(12)	C(1)-C(2) = 1.499(5)	N(2)-C(3) = 1.458(7)	Cl(1)-Al(2)-C(35) = 106.9(3)
C(8)-C(9) = 1.539(12)	C(2)-C(3) = 1.447(4)	N(2)-C(7) = 1.456(7)	Cl(1)-Al(2)-C(36) = 107.6(3)
N(1)-Al(1)-N(2) = 76.2(4)	C(7)-C(8) = 1.443(4)	C(1)-C(2) = 1.494(8)	C(35)-Al(2)-C(36) = 122.0(4)
N(1)-Al(1)-N(3) = 153.1(3)	C(8)-C(9) = 1.492(4)	C(2)-C(3) = 1.399(9)	Al(1)-N(2)-Al(2) = 101.8(2)
N(1)-Al(1)-C(34) = 97.6(3)	N(1)-Al(1)-N(2) = 75.89(12)	C(3)-C(4) = 1.381(8)	Al(1)-Cl(1)-Al(2) = 82.38(8)
N(1)-Al(1)-C(35) = 95.4(3)	N(1)-Al(1)-N(3) = 147.51(10)	C(4)-C(5) = 1.410(8)	N(2)-C(3)-C(4) = 117.3(6)
N(2)-Al(1)-N(3) = 77.1(3)	N(1)-Al(1)-C(34) = 101.7(8)	C(5)-C(6) = 1.379(8)	C(3)-C(4)-C(5) = 120.2(6)
N(2)-Al(1)-C(34) = 119.0(3)	N(1)-Al(1)-Cl(2) = 95.57(14)	C(6)-C(7) = 1.371(8)	C(4)-C(5)-C(6) = 117.1(6)
N(2)-Al(1)-C(35) = 126.2(3)	N(2)-Al(1)-N(3) = 77.02(12)	C(7)-C(8) = 1.365(8)	C(5)-C(6)-C(7) = 123.0(6)
N(3)-Al(1)-C(34) = 97.6(3)	N(2)-Al(1)-C(34) = 103.7(8)	C(8)-C(9) = 1.506(8)	C(6)-C(7)-N(2) = 115.9(6)
N(3)-Al(1)-C(35) = 98.2(3)	N(2)-Al(1)-Cl(2) = 146.16(16)	N(1)-Al(1)-N(2) = 79.7(2)	C(7)-N(2)-C(3) = 112.2(5)
C(34)-Al(1)-C(35) = 114.72(18)	N(3)-Al(1)-C(34) = 101.8(8)	N(1)-Al(1)-N(3) = 143.2(2)	
	N(3)-Al(1)-Cl(2) = 97.00(17)		
	C(34)-Al(1)-Cl(2) = 110.2(8)		

Table 4.3. Selected Bond Distances (Å) and Angles (deg) for complexes 4.4 and 4.5

4.4	4.4 (cont'd)	4.5	4.5 (cont'd)
Fe(1)-C(5) = 2.278(9)	C(7)-C(8) = 1.393(9)	Fe(1)-C(4) = 2.1492(17)	N(1)-Al(1)-N(3) = 142.75(6)
Fe(1)-C(6) = 1.959(8)	C(8)-C(9) = 1.518(8)	Fe(1)-C(5) = 2.0220(17)	N(1)-Al(1)-C(41) = 103.35(7)
Fe(1)-C(7) = 2.338(9)	N(1)-Al(1)-N(2) = 80.11(17)	Fe(1)-C(6) = 1.9774(17)	N(1)-Al(1)-Cl(1) = 104.75(5)
Fe(1')-C(3) = 2.254(6)	N(1)-Al(1)-N(3) = 140.54(19)	Fe(1)-C(7) = 2.1392(16)	N(2)-Al(1)-N(3) = 77.76(5)
Fe(1')-C(4) = 1.748(10)	N(1)-Al(1)-C(34) = 99.1(2)	Fe(1)-centroid = 1.542(19)	N(2)-Al(1)-C(41) = 172.61(7)
Fe(1')-C(5) = 1.905(9)	N(1)-Al(1)-Cl(1) = 105.80(14)	Al(1)-N(1) = 1.9296(14)	N(2)-Al(1)-Cl(1) = 85.17(4)
Fe(1')-C(6) = 2.146(7)	N(2)-Al(1)-N(3) = 79.55(18)	Al(1)-N(2) = 2.0007(14)	N(3)-Al(1)-C(41) = 94.97(6)
Fe(1)-centroid = 1.565(12)	N(2)-Al(1)-C(34) = 178.4(2)	Al(1)-N(3) = 2.1234(14)	N(3)-Al(1)-Cl(1) = 104.42(4)
Al(1)-N(1) = 1.996(4)	N(2)-Al(1)-Cl(1) = 84.49(15)	Al(1)-C(41) = 1.9801(17)	C(41)-Al(1)-Cl(1) = 98.03(6)
Al(1)-N(2) = 1.993(4)	N(3)-Al(1)-C(34) = 100.4(2)	Al(1)-Cl(1) = 2.3996(7)	N(2)-Al(2)-Cl(1) = 88.82(4)
Al(1)-N(3) = 2.035(5)	N(3)-Al(1)-Cl(1) = 105.45(14)	Al(2)-N(2) = 1.9658(14)	N(2)-Al(2)-C(45) = 115.52(7)
Al(1)-C(34) = 1.974(5)	C(34)-Al(1)-Cl(1) = 97.03(18)	Al(2)-Cl(1) = 2.2964(7)	N(2)-Al(2)-C(49) = 112.05(7)
Al(1)-Cl(1) = 2.430(2)	N(2)-Al(2)-Cl(1) = 89.49(15)	Al(2)-C(45) = 1.9654(18)	Cl(1)-Al(2)-C(45) = 104.13(6)
Al(2)-N(2) = 1.970(5)	N(2)-Al(2)-C(36) = 113.7(5)	Al(2)-C(49) = 1.9732(18)	Cl(1)-Al(2)-C(49) = 108.29(6)
Al(2)-Cl(1) = 2.268(3)	N(2)-Al(2)-C(38) = 126.3(6)	N(1)-C(2) = 1.389(2)	C(45)-Al(2)-C(49) = 121.90(8)
Al(2)-C(36) = 2.005(16)	Cl(1)-Al(2)-C(36) = 101.8(5)	N(3)-C(8) = 1.315(2)	Al(1)-N(2)-Al(2) = 103.10(6)
Al(2)-C(38) = 2.15(2)	Cl(1)-Al(2)-C(38) = 102.8(7)	N(2)-C(3) = 1.4445(19)	Al(1)-Cl(1)-Al(2) = 82.80(2)
N(1)-C(2) = 1.351(7)	C(36)-Al(2)-C(38) = 114.4(8)	N(2)-C(7) = 1.467(2)	N(2)-C(3)-C(4) = 113.87(14)
N(3)-C(8) = 1.322(7)	Al(1)-N(2)-Al(2) = 103.3(2)	C(1)-C(2) = 1.505(2)	C(3)-C(4)-C(5) = 122.40(15)
N(2)-C(3) = 1.449(7)	Al(1)-Cl(1)-Al(2) = 82.73(8)	C(2)-C(3) = 1.355(2)	C(4)-C(5)-C(6) = 116.78(14)
N(2)-C(7) = 1.447(8)	N(2)-C(3)-C(4) = 116.9(5)	C(3)-C(4) = 1.438(2)	C(5)-C(6)-C(7) = 112.20(14)
C(1)-C(2) = 1.503(7)	C(3)-C(4)-C(5) = 122.1(6)	C(4)-C(5) = 1.423(2)	C(6)-C(7)-N(2) = 117.22(14)
C(2)-C(3) = 1.386(8)	C(4)-C(5)-C(6) = 114.6(6)	C(5)-C(6) = 1.422(2)	C(7)-N(2)-C(3) = 108.96(12)
C(3)-C(4) = 1.385(9)	C(5)-C(6)-C(7) = 120.7(6)	C(6)-C(7) = 1.445(2)	
C(4)-C(5) = 1.406(10)	C(6)-C(7)-N(2) = 116.0(6)	C(7)-C(8) = 1.434(2)	
C(5)-C(6) = 1.393(9)	C(7)-N(2)-C(3) = 108.4(5)	C(8)-C(9) = 1.503(2)	
C(6)-C(7) = 1.422(8)		N(1)-Al(1)-N(2) = 82.14(6)	

Complex 4.1. The crystal structure of **4.1** (Figure 4.1) shows an $AlMe_2$ unit bound to the apparently intact ligand [Al(1)-N(1) = 2.212(8) Å, Al(1)-N(2) = 1.892(8) Å, Al(1)-N(3) = 2.163(8) Å, Al(1)-C(34) = 1.982(4) Å, Al(1)-C(35) = 2.007(4) Å] with the Al center adopting a distorted pentacoordinate environment. Although the geometry appears to be trigonal bipyramidal, it is in fact mid-way between trigonal bipyramidal and square pyramidal ($\tau = 0.45$).[13] The two carbon atoms and the N of the pyridine ring lie in a plane perpendicular to the plane defined by the ligand backbone, bisecting at the Al center [N(2)-Al(1)-C(34) = 119.0(3)°, C(34)-Al(1)-C(35) = 114.72(18)°, N(2)-Al(1)-C(35) = 126.2(3)°, N(1)-Al(1)-N(2) = 76.2(4)°, N(1)-Al(1)-C(34) = 97.6(3)°, N(1)-Al(1)-C(35) = 95.4(3)°, N(2)-Al(1)-N(3) = 77.1(3)°, N(3)-Al(1)-C(34) = 97.6(3)°, N(3)-Al(1)-C(35) = 98.2(3)°]. The non-linearity of the two imine N atoms [N(1)-Al(1)-N(3) = 153.1(3)°] prevents definition of the complex as trigonal bipyramidal. Upon close inspection of the ligand backbone, slight deviations from the typical distances can be seen. Taking {2,6-[2,6-(^{i}Pr)$_2$PhN=C(CH_3)]$_2$(C_5H_3N)}$FeCl_2$ as the standard,[2] one of the C_{imine}-N bond distances has been lengthened by 0.03 Å [1.331(11) Å vs 1.298 Å on average]. More strikingly, the C_{imine}-C_{ortho} and N_{pyr}-C_{ortho} bond distances have been shortened and lengthened from the neutral intact ligand, by an average of approximately 0.05 Å and 0.03 Å respectively [1.421 Å vs 1.474 Å and 1.376 Å vs 1.340 Å on average]. Two molecules of toluene are found crystallized in the lattice per unit cell.

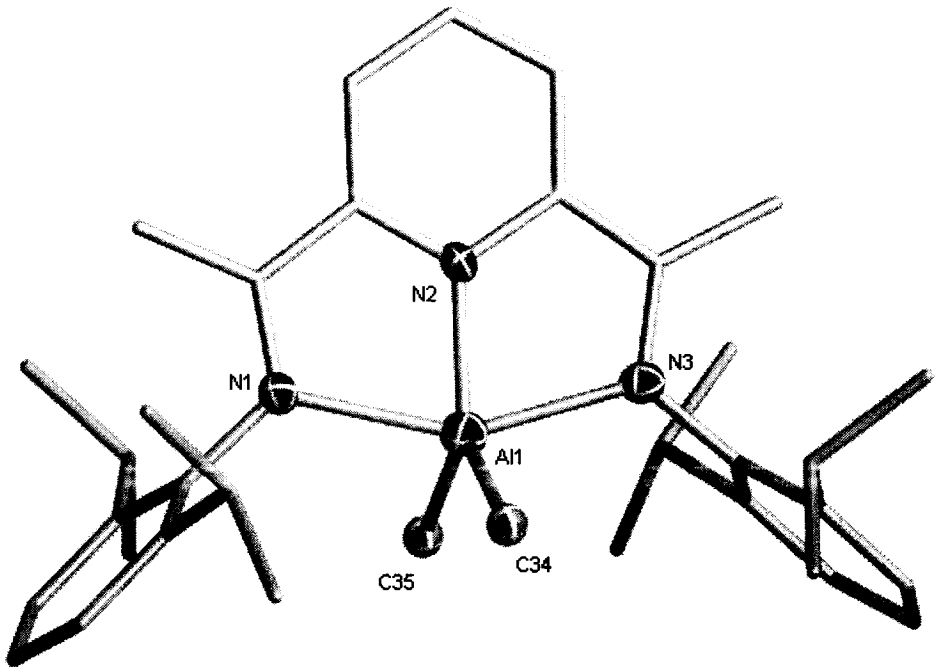

Figure 4.1. Partial thermal ellipsoid plot of **4.1**. Thermal ellipsoids are drawn at the 30% probability level. Hydrogen atoms have been omitted for clarity.

Complex 4.2. Complex **4.2** is structurally very similar to complex **4.1** in that the ligand system surrounds a pentacoordinate Al center [Al(1)-N(1) = 2.163(4) Å, Al(1)-N(2) = 1.928(4) Å, Al(1)-N(3) = 2.118(4) Å]. However, the metal center adopts a distorted square pyramidal geometry and the Al ion is found pushed up from the plane defined by the ligand (Figure 4.2). The model could only be satisfactorily refined when considering a co-crystallization between a mixture of compounds. In this case, the two terminal groups consist of a mixture of methyl and Cl co-crystallized with partial occupancy. The apical position is 55% methyl [Al(1)-C(34) = 1.98(2) Å] and 45% Cl [Al(1)-Cl(1) = 2.185(10) Å], whereas the group in the basal plane is 80% methyl [Al(1)-C(35) = 1.978(15) Å] and only 20% Cl [Al(1)-Cl(2) = 2.037(5) Å]. Figure 4.2 is a representative model of the complex, showing 100% occupancy of an apical methyl and basal Cl for simplicity. The basal plane is defined by the nitrogen atoms of the ligand and the 0.8 Me/0.2 Cl group [N(1)-Al(1)-N(2) = 75.89(12)°, N(2)-Al(1)-N(3) = 77.02(12)°, N(3)-Al(1)-Cl(2) = 97.00(17)°, N(1)-Al(1)-Cl(2) = 95.57(14), N(1)-Al(1)-N(3) = 147.51(10)°, N(2)-Al(1)-

Cl(2) = 146.16(16)°] and the axial site is occupied by the 0.55 Me/0.45 Cl group [N(1)-Al(1)-C(34) = 101.7(8)°, N(2)-Al(1)-C(34) = 103.7(8)°, N(3)-Al(1)-C(34) = 101.8(8)°, C(34)-Al(1)-Cl(2) = 110.2(8)°]. Similar to complex **4.1**, deviations are apparent in the bond distances of the ligand backbone, although to a smaller extent than that observed for complex **4.1**. Compared to $\{2,6\text{-}[2,6\text{-}(^{i}Pr)_2PhN{=}C(CH_3)]_2(C_5H_3N)\}FeCl_2$,[2] the C_{imine}-N distance has been lengthened slightly by approximately 0.02 Å, from 1.298 Å to 1.316 Å on average, and the C_{imine}-C_{ortho} bond length has been shortened by approximately 0.03 Å on average, from 1.474 Å to 1.445 Å. Finally, the C_{ortho}-N_{pyr} distances have also been lengthened by 0.036 Å, from 1.340 Å to 1.376 Å on average.

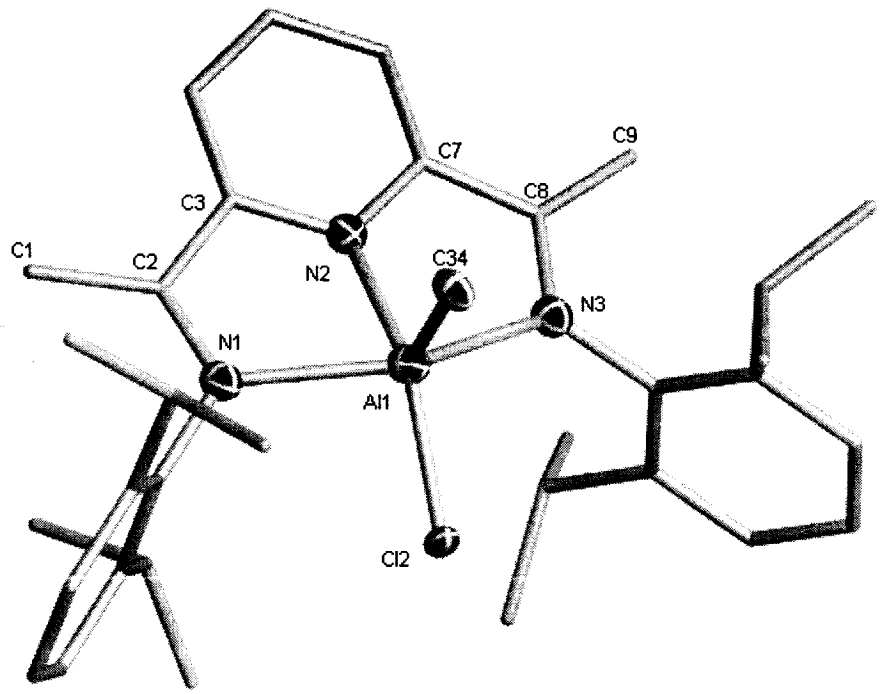

Figure 4.2. Partial thermal ellipsoid plot of **4.2**. Thermal ellipsoids are drawn at the 30% probability level. Hydrogen atoms have been omitted for clarity. The atom at C34 is actually comprised of 45% CH_3/55% Cl and the atom at Cl_2 is actually 20% Cl/80% CH_3.

Complex 4.3. The structure of complex **4.3** consists of two aluminum centers bound to the N atoms of the ligand system (Figure 4.3). One of the aluminum centers is pentacoordinated to the three N atoms [Al(1)-N(1) = 1.993(5) Å, Al(1)-N(2) = 2.003(5) Å, Al(1)-N(3) = 1.995(5) Å], a terminal methyl group [Al(1)-C(34) = 1.951(6) Å] and a

Cl atom [Al(1)-Cl(1) = 2.404(2) Å] in a geometry borderline between square pyramidal and trigonal bipyramidal (τ = 0.56)[13] [N(1)-Al(1)-N(2) = 79.7(2)°, N(1)-Al(1)-N(3) = 143.2(2)°, N(1)-Al(1)-C(34) = 99.9(3)°, N(1)-Al(1)-Cl(1) = 103.75(16)°, N(2)-Al(1)-N(3) = 80.2(2)°, N(2)-Al(1)-C(34) = 176.8(3)°, N(2)-Al(1)-Cl(1) = 85.69(15)°, N(3)-Al(1)-C(34) = 98.4(3)°, N(3)-Al(1)-Cl(1) = 105.14(15)°, C(34)-Al(1)-Cl(1) = 97.5(2)°]. The second Al center is tetrahedrally coordinated to two terminal methyl groups [Al(2)-C(35) = 1.958(8) Å, Al(2)-C(36) = 1.946(7) Å], the Cl atom [Al(2)-Cl(1) = 2.275(3) Å] and the N of the pyridine ring [Al(2)-N(2) = 1.969(5) Å, N(2)-Al(2)-Cl(1) = 90.10(16)°, N(2)-Al(2)-C(35) = 113.0(3)°, N(2)-Al(2)-C(36) = 112.0(3)°, Cl(1)-Al(2)-C(35) = 106.9(3)°, Cl(1)-Al(2)-C(36) = 107.6(3)°, C(35)-Al(2)-C(36) = 122.0(4)°]. The nitrogen of the pyridine ring and the Cl atom form a bridge to the first Al center [Al(1)-N(2)-Al(2) = 101.8(2)°, Al(1)-Cl(1)-Al(2) = 82.38(8)°]. As a result of its tetracoordinate nature, the pyridine N atom is now sp^3 [Al(1)-N(2)-C(3) = 111.6(4)°, Al(1)-N(2)-C(7) = 111.4(4)°, Al(2)-N(2)-C(3) = 109.9(4)°, Al(2)-N(2)-C(7) = 109.5(4)°, C(7)-N(2)-C(3) = 112.2(5)°], and hence the aromaticity of the pyridine ring has been disrupted, taking on a slightly folded conformation [N(2)-C(3)-C(4) = 117.3(6)°, C(3)-C(4)-C(5) = 120.2(6)°, C(4)-C(5)-C(6) = 117.1(6)°, C(5)-C(6)-C(7) = 123.0(6)°, C(6)-C(7)-N(2) = 115.9(6)°]. Bond distances in the ligand backbone have also been modified. The sp^3 nature of the pyridine N atom severely lengthens the N_{pyr}-C_{ortho} bond distances [N(2)-C(3) = 1.458(7) Å, N(2)-C(7) = 1.456(7) Å], suggestive of pure single bonds. Besides a slight lengthening in the C=N imine bonds, the C_{imine}-C_{ortho} bond lengths have shortened by a large extent, from an average of approximately 1.474 Å to 1.382 Å. The crystal structure is complete with a THF-solvated molecule of $AlMe_3$ co-crystallized in the lattice [Al(3)-C(37) = 1.968(7) Å, Al(3)-C(38) = 1.973(6) Å, Al(3)-C(39) = 1.941(8) Å, Al(3)-O(1) = 1.904(6) Å], with the Al center found tetrahedrally coordinated to three terminal methyl groups and a molecule of THF [C(37)-Al(3)-C(38) = 115.8(3)°, C(37)-Al(3)-C(39) = 112.9(4)°, C(37)-Al(3)-O(1) = 103.8(3)°, C(38)-Al(3)-C(39) = 114.5(3)°, C(38)-Al(3)-O(1) = 104.6(3)°, C(39)-Al(3)-O(1) = 103.4(3)°].

(a)

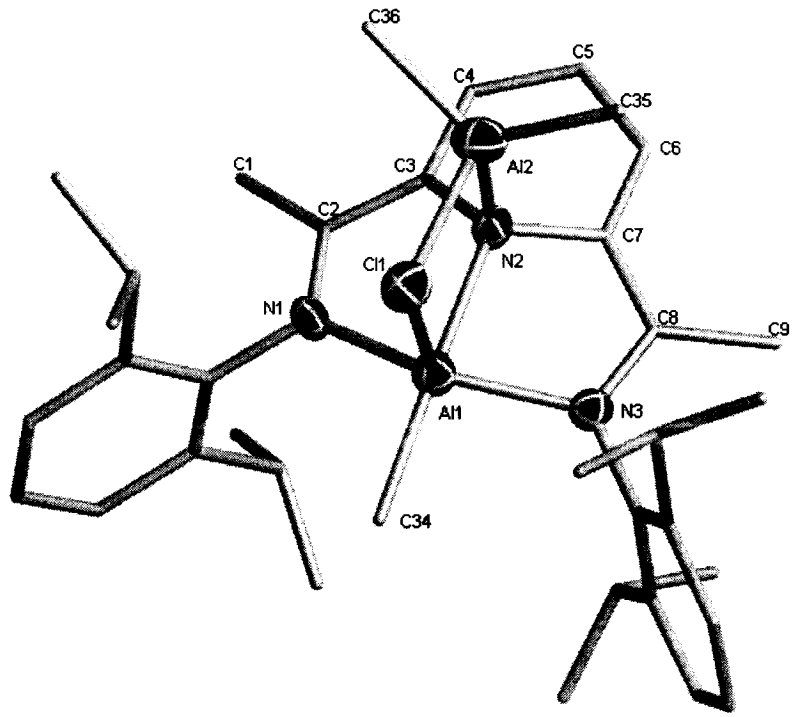

(b)

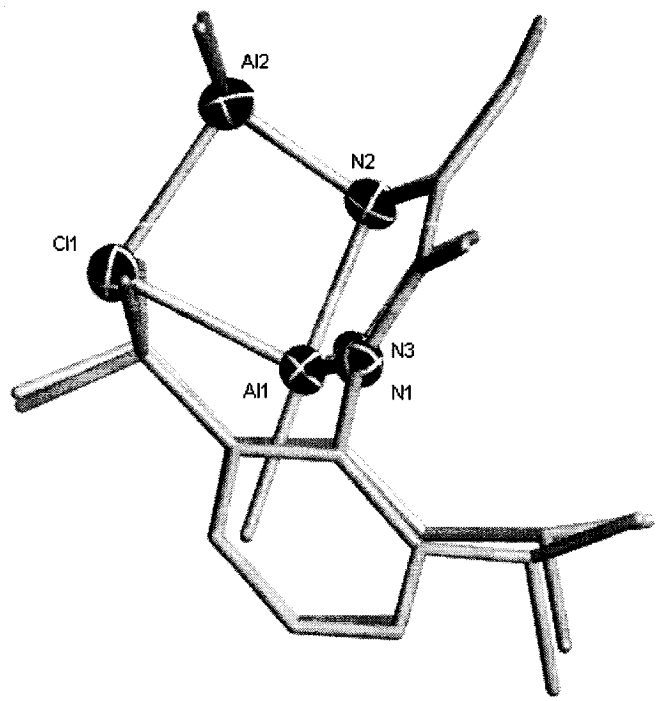

Figure 4.3. Two partial thermal ellipsoid plots of **4.3**. Thermal ellipsoids are drawn at the 30% probability level. The $AlMe_3(THF)$ moiety and all hydrogen atoms have been omitted for clarity.

Complex 4.4. The crystal structure of **4.4** (Figure 4.4) shows a $Et_2Al(\mu\text{-}Cl)AlEt$ unit bound to the N atoms of the folded ligand in an arrangement reminiscent of complex **4.3**. One Al center is surrounded by the three N atoms of the ligand system [Al(1)-N(1) = 1.996(4) Å, Al(1)-N(2) = 1.993(4) Å, Al(1)-N(3) = 2.035(5) Å], a Cl atom [Al(1)-Cl(1) = 2.430(2) Å] and an ethyl group [Al(1)-C(34) = 1.974(5) Å]. The geometry about the metal center is severely distorted trigonal bipyramidal (τ = 0.63).[13] The axial sites are occupied by the N of the pyridine ring and the C of the ethyl group [N(2)-Al(1)-C(34) = 178.4(2)°, N(2)-Al(1)-N(1) = 80.11(17)°, N(2)-Al(1)-N(3) = 79.55(18)°, N(2)-Al(1)-Cl(1) = 84.49(15)°, C(34)-Al(1)-N(1) = 99.1(2)°, C(34)-Al(1)-N(3) = 100.4(2)°, C(34)-Al(1)-Cl(1) = 97.03(18)°]. The other two N atoms and the Cl atom are found in the equatorial positions [N(1)-Al(1)-N(3) = 140.54(19)°, N(1)-Al(1)-Cl(1) = 105.80(14)°, N(3)-Al(1)-Cl(1) = 105.45(14)°]. The second Al center is bridged to the first by the Cl atom [Al(2)-Cl(1) = 2.268(3) Å] and the N of the pyridine ring [Al(2)-N(2) = 1.970(5) Å, Al(1)-N(2)-Al(2) = 103.3(2)°, Al(1)-Cl(1)-Al(2) = 82.73(8)°] and also bound to two ethyl groups [Al(2)-C(36) = 2.005(16) Å, Al(2)-C(38) = 2.15(2) Å] in a tetrahedral geometry [N(2)-Al(2)-Cl(1) = 89.49(15)°, N(2)-Al(2)-C(36) = 113.7(5)°, N(2)-Al(2)-C(38) = 126.3(6)°, Cl(1)-Al(2)-C(36) = 101.8(5)°, Cl(1)-Al(2)-C(38) = 102.8(7)°, C(36)-Al(2)-C(38) = 114.4(8)°]. The asymmetric unit consists of two molecules. Both show an Fe center η^4-coordinated to the pyridine ring of the ligand and η^6-coordinated to a molecule of toluene. The first molecule shows the Fe center (and its corresponding molecule of toluene [Fe(1)-centroid = 1.565(12) Å] disordered over two positions (58%, 42%) and alternately η^4-coordinating one or the other side of the pyridine ring [Fe(1')-C(3) = 2.254(6) Å, Fe(1')-C(4) = 1.748(10) Å, Fe(1')-C(5) = 1.905(9) Å, Fe(1')-C(6) = 2.146(7) Å]. The Fe in the second molecule maintains a common position, but the coordinating toluene is disordered in two positions. In both molecules, the pyridine ring aromaticity has been disrupted, taking on a slightly folded conformation as a result of the η^4 bonding and sp^3 nature of the nitrogen atom [for example: N(2)-C(3)-C(4) = 116.9(5)°, C(3)-C(4)-C(5) = 122.1(6)°, C(4)-C(5)-C(6) = 114.6(6)°, C(5)-C(6)-C(7) = 120.7(6)°, C(6)-C(7)-N(2) = 116.0(6)°, C(7)-N(2)-C(3) = 108.4(5)°]. The nitrogen of the pyridine ring is tetrahedrally bound to both Al atoms [Al(1)-N(2)-C(3) = 113.1(3)°, Al(1)-N(2)-C(7) = 112.8(3)°, Al(2)-N(2)-C(3) = 108.2(3)°, Al(2)-N(2)-C(7) = 111.0(4)°, C(7)-N(2)-C(3) = 108.4(5)°, Al(1)-N(2)-

Al(2) = 103.3(2)°]. Other ligand bond distances have been altered by the disruption, but their deviations are different in the two molecules. The first molecule, in which the Fe center alternates equally between both sides of the pyridine ring, displays symmetric modifications, including a lengthening of the C=N bond by approximately 0.03 Å, from an average of 1.298 Å in $\{2,6\text{-}[2,6\text{-}(^{i}Pr)_2PhN{=}C(CH_3)]_2(C_5H_3N)\}FeCl_2$[2] to 1.335 Å in **4.4**, and a drastic shortening of the C_{imine}-C_{ortho} bond by about 0.08 Å, from an average of 1.474 Å to 1.390 Å. However, the second molecule, in which the Fe center maintains its position η^4-bound to only one side of the pyridine ring, suffers from an asymmetric localization of the bonding electrons. The half of the ligand containing the Fe-bound *ortho*-C contains relatively normal bond distances for C=N [N(4)-C(48) = 1.317(6) Å] and C_{imine}-C_{ortho} bonds [C(48)-C(49) = 1.433(7) Å], characteristic of double and single bonds respectively. However, the other half of the ligand backbone displays the opposite arrangement [N(6)-C(54) = 1.402(6) Å, C(53)-C(54) = 1.351(7) Å].

a)

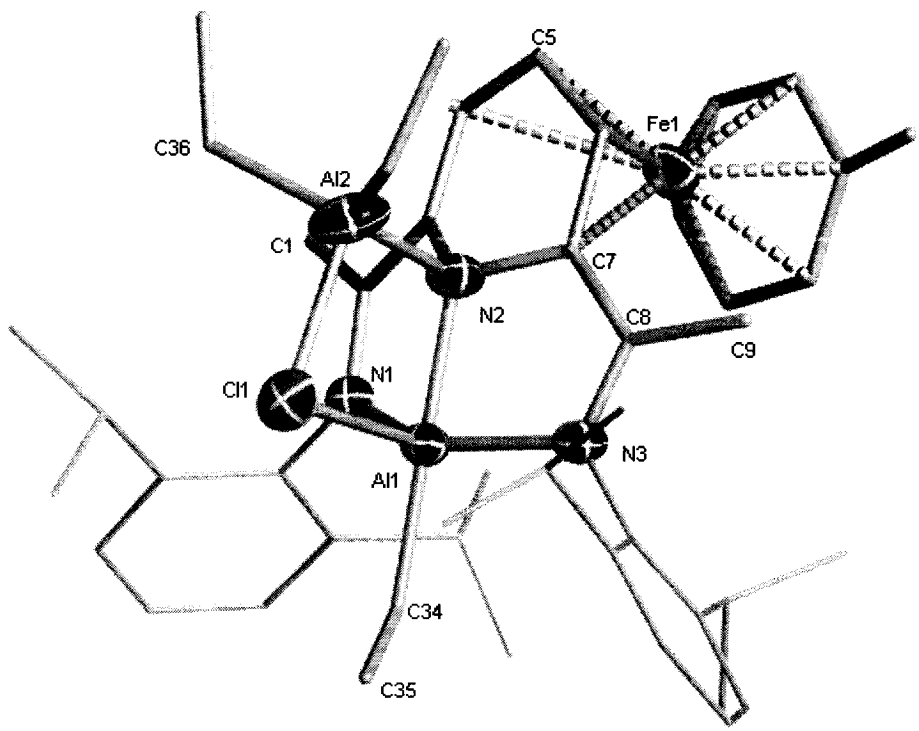

b)

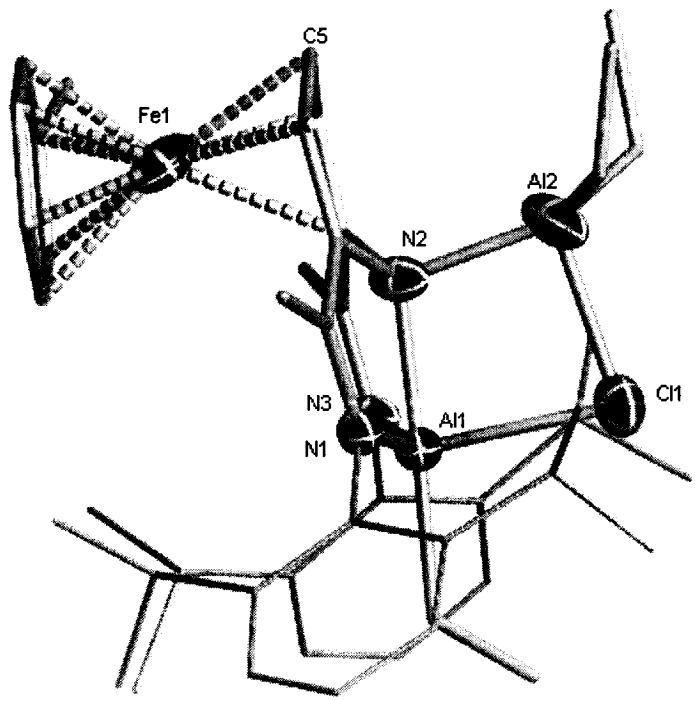

Figure 4.4. Two partial thermal ellipsoid plots of **4.4**. Thermal ellipsoids are drawn at the 30% probability level. Hydrogen atoms have been omitted for clarity.

Complex 4.5. The structure of complex **4.5** is very similar to that of complex **4.4** in that it is trimetallic on only one ligand (Figure 4.5). Once again, the two Al centers are found bridged to each other though the Cl atom and the pyridine N atom [Al(1)-N(2)-Al(2) = 103.10(6)°, Al(1)-Cl(1)-Al(2) = 82.80(2)°]. One Al is tetrahedrally coordinated to two isobutyl groups [Al(2)-C(45) = 1.9654(18) Å, Al(2)-C(49) = 1.9732(18) Å], the Cl atom [Al(2)-Cl(1) = 2.2964(7) Å] and the pyridine N atom [Al(2)-N(2) = 1.9658(14) Å, N(2)-Al(2)-Cl(1) = 88.82(4)°, N(2)-Al(2)-C(45) = 115.52(7)°, N(2)-Al(2)-C(49) = 112.05(7)°, Cl(1)-Al(2)-C(45) = 104.13(6)°, Cl(1)-Al(2)-C(49) = 108.29(6)°, C(45)-Al(2)-C(49) = 121.90(8)°]. The second Al is surrounded by all three N atoms of the ligand system [Al(1)-N(1) = 1.9296(14) Å, Al(1)-N(2) = 2.0007(14) Å, Al(1)-N(3) = 2.1234(14) Å], the Cl atom [Al(1)-Cl(1) = 2.3996(7) Å] and one isobutyl unit [Al(1)-C(41) = 1.9801(17) Å] in a distorted pentacoordinate geometry exactly between trigonal bipyramidal and square pyramidal ($\tau = 0.50$)[13] [N(1)-Al(1)-N(2) = 82.14(6)°, N(1)-Al(1)-N(3) = 142.75(6)°, N(1)-Al(1)-C(41) = 103.35(7)°, N(1)-Al(1)-Cl(1) = 104.75(5)°, N(2)-Al(1)-N(3) = 77.76(5)°,

N(2)-Al(1)-C(41) = 172.61(7)°, N(2)-Al(1)-Cl(1) = 85.17(4)°, N(3)-Al(1)-C(41) = 94.97(6)°, N(3)-Al(1)-Cl(1) = 104.42(4)°, C(41)-Al(1)-Cl(1) = 98.03(6)°]. The ligand system is folded from its original planar structure around the pyridine ring [N(2)-C(3)-C(4) = 113.87(14)°, C(3)-C(4)-C(5) = 122.40(15)°, C(4)-C(5)-C(6) = 116.78(14)°, C(5)-C(6)-C(7) = 112.20(14)°, C(6)-C(7)-N(2) = 117.22(14)°, C(7)-N(2)-C(3) = 108.96(12)°], with the N atom adopting sp^3 geometry [Al(1)-N(2)-C(3) = 110.57(10)°, Al(1)-N(2)-C(7) = 115.23(10)°, Al(2)-N(2)-C(3) = 105.41(9)°, Al(2)-N(2)-C(7) = 113.07(10)°, Al(1)-N(2)-Al(2) = 103.10(6)°]. The other portion of the pyridine ring is found η^4-bound to an Fe atom [Fe(1)-C(4) = 2.1492(17) Å, Fe(1)-C(5) = 2.0220(17) Å, Fe(1)-C(6) = 1.9774(17) Å, Fe(1)-C(7) = 2.1392(16) Å], which is also η^6-bound to a molecule of toluene [Fe(1)-centroid = 1.542(19) Å]. Similar to complexes **4.3** and **4.4**, the C=N and C_{imine}-C_{ortho} distances have been lengthened and shortened respectively. However, the distances on each side of the ligand are definitely not symmetrical [N(1)-C(2) = 1.389(2) Å vs N(3)-C(8) = 1.315(2) Å, and C(2)-C(3) = 1.355(2) Å vs C(7)-C(8) = 1.434(2) Å], indicating a lack of aromaticity in this area of the ligand and localization of the bond order.

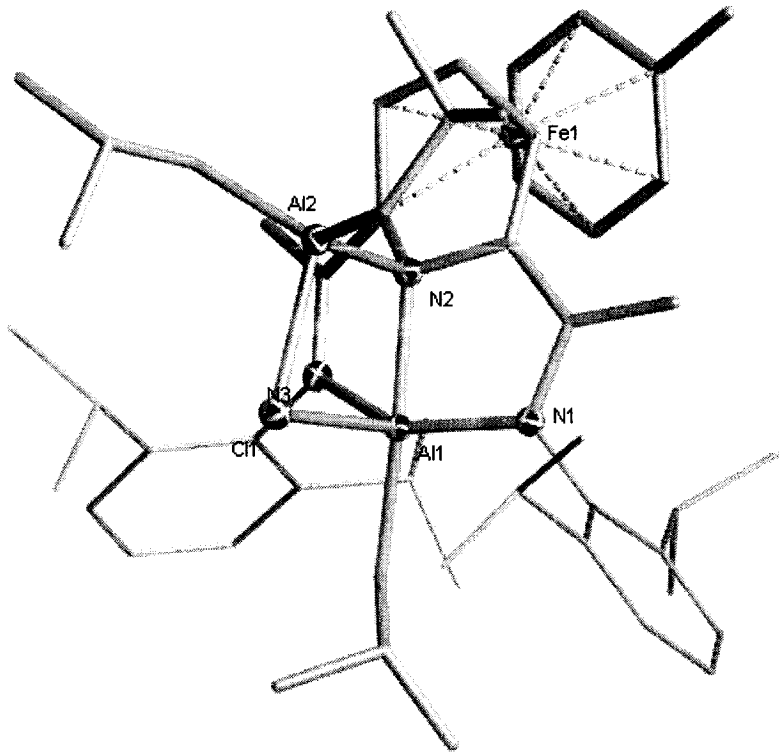

Figure 4.5. Partial thermal ellipsoid plot of **4.5**. Thermal ellipsoids are drawn at the 30% probability level. Hydrogen atoms have been omitted for clarity.

Results

The reaction of $LFeCl_2$ (L= {2,6-[2,6-(^{i}Pr)$_2$PhN=C(CH$_3$)]$_2$(C$_5$H$_3$N)}) with 10 equivalents of $AlMe_3$ was carried out in toluene at -35°C (Scheme 4.1). Upon addition of the aluminum activator, the colour changed instantly from royal blue to purple. Allowing the suspension to warm to room temperature resulted in another colour change to green. Evaporation of the solvent *in vacuo*, followed by separation and fractional crystallization, afforded complexes **4.1**, **4.2** and **4.3**, from toluene, ether and hexane respectively (Scheme 4.1). Complex **4.1** could also be formed in 39% yield from the reaction of {2,6-[2,6-(^{i}Pr)$_2$PhN=C(CH$_3$)]$_2$(C$_5$H$_3$N)}Fe(CH$_2$SiMe$_3$)$_2$ with Me_3Al. The formulae and connectivity of complexes **4.1**, **4.2** and **4.3** have been elucidated by single crystal X-ray diffraction and representative models can be seen in Figures 4.1, 4.2 and 4.3.

Scheme 4.1

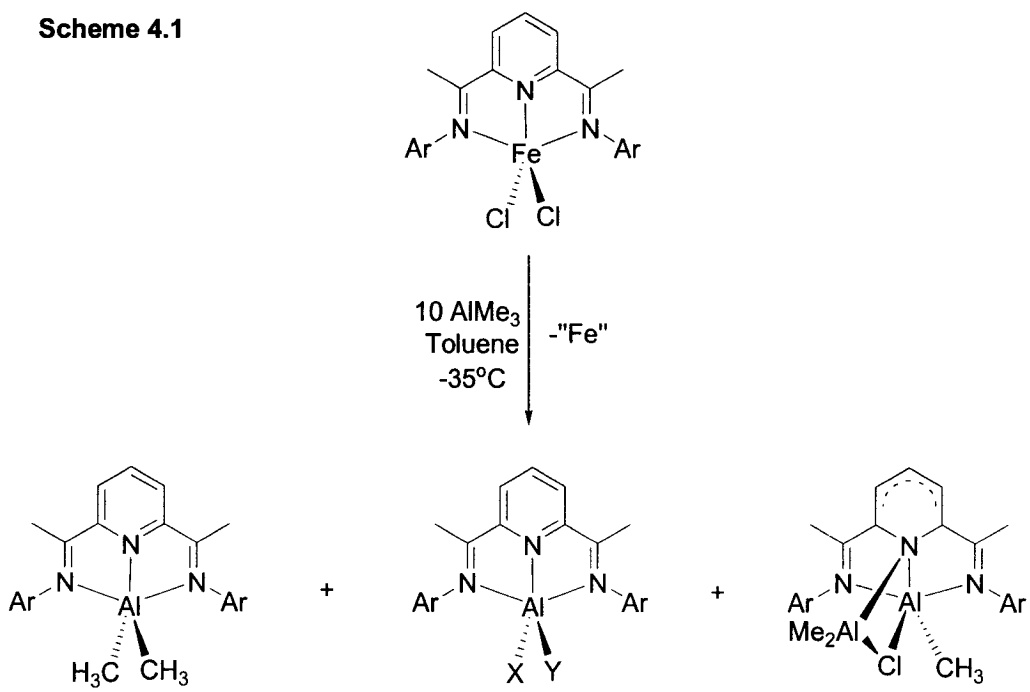

4.1 **4.2** **4.3**

X = 0.8 CH_3, 0.2 Cl
Y = 0.55 CH_3, 0.45 Cl

In each of the complexes **4.1**, **4.2** and **4.3**, there is no Fe atom. Complexes **4.1** and **4.2** appear to be very similar, both consisting of a pentacoordinate Al center surrounded by an apparently intact ligand and two terminal groups. However, complex **4.1** contains

fully occupied methyl groups in the two pendant coordination sites, whereas in complex **4.2**, the two crystallographically distinct sites consist of a combination of methyl and chloride groups in partial occupancy. A positive chlorine test confirms the presence of chloride in complex **4.2** and structural refinement of the crystallographic data suggest a 55%/45% Me/Cl ratio for one site and 80%/20% Me/Cl for the other. Although both sites display partial occupancy, they are not disordered over the two positions. A consequence of chloride coordination to the metal center is a change in the geometry adopted by aluminum. Complex **4.1** assumes a distorted, and yet almost symmetrical, geometry which can be considered somewhat between trigonal bipyramidal and square pyramidal. The geometry about the Al center in complex **4.2**, on the other hand, is square pyramidal. In this case, the terminal group with the higher Cl/Me ratio resides in the apical position.

The formal appearance of these complexes as divalent Al species is obviously deceiving given the established ability of the ligand to embark on electron-transfer interactions.[7,14-17] Thus, **4.1** and **4.2** are more appropriately described as $[(L^{-1})Al^{III}(X)_2]$, with the unpaired electron mainly centered on the one-electron reduced diiminepyridine radical anion. Upon close inspection of the crystal structures, deviations are apparent in the ligand backbone corresponding to reduction of the ligand by one electron, as discussed in Chapter 3.[15bd]

As expected, both species are paramagnetic. However, the degree of paramagnetism was much larger than expected for one unpaired electron. The solid state room temperature magnetic moments measured anywhere from 19.8 μ_{BM} to 4.5 μ_{BM}. The reason for this behaviour is likely to be ascribed to adventitious contamination by elemental Fe amongst the crystals in an approximate ratio of 1:9 Fe:Al (XRF). The small amount of Fe is enough to drastically affect the magnetic weight of the sample and therefore give unrepresentative readings. Washing the crystals with several portions of hexane to remove tiny particles of metallic iron resulted in a more reasonable value of the magnetic moment ($\mu_{eff} = 4.5\ \mu_B$). The NMR spectrum remained non-diagnostic.

Complexes **4.1** and **4.2** provide the second case of a crystallographically characterized paramagnetic Al species, the first having been very recently obtained with the series of (bis-imine)acenaphthene derivatives (dpp-BIAN)AlR_2 (dpp-BIAN = 1,2-bis[(2,6-$^i Pr_2C_6H_3$)imino]acenaphthene ; R = Me, Et, *i*Bu).[18] According to the procedure

reported by Schumann for the preparation of those species,[18] **4.1** could also be conveniently synthesized (79%) via reduction of the ligand in THF with metallic Na followed by addition of Me_2AlCl in toluene. The improved preparation allows clean isolation of the complex in excellent yield with complete absence of elemental Fe. The magnetic moment at room temperature was measured as 1.7 μ_B, as expected for one unpaired electron.

With the help of Dr. Maurel, charge delocalization throughout the ligand backbone in **4.1** was conclusively demonstrated by an EPR spectrum (Figure 4.6), showing the complexity expected for an organic radical.

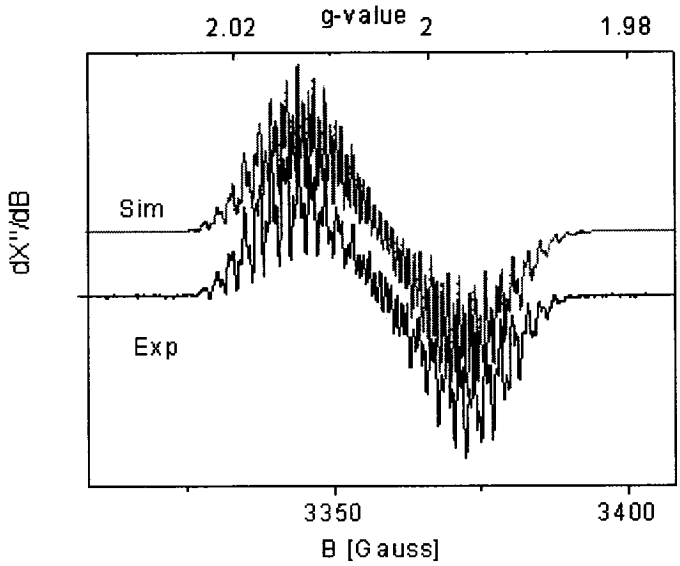

Figure 4.6. Solution X-band EPR spectrum of **4.1** in toluene at 293 K. Conditions: Frequency = 9.4228 GHz, modulation amplitude = 0.01 mT, microwave power = 0.998 mW. The simulation was obtained with the parameters included and explained in the text.

Collaborators from Radboud University Nijmegen (Peter Budzelaar, Quinten Knijnenburg and Bas de Bruin) provided a satisfactory simulation of the experimental spectrum using parameters consistent with a substantial delocalization of the spin density over the diiminepyridine part of the ligand, with hyperfine couplings (HFC's) to aluminum (A^{Al}), the pyridine nitrogen (A^{1N}), two equivalent imine nitrogens (A^{2N}), the pyridine ring proton in *para*-position (A^{1H}), two equivalent *meta*-protons (A^{2H}) and a set

of six equivalent protons (A^{6H}) corresponding to the two equivalent imine methyl groups (see Figure 4.6, Table 4.4).[10] The possibility that A^{H6} could also stem from coupling with the six equivalent protons of the two aluminum-bound methyl groups was clearly ruled out by DFT calculations. From the optimized geometry of **4.1**, the EPR parameters were calculated with both ORCA and ADF. ORCA gave the most satisfactory results, in good agreement with the experimental parameters (Table 4.4).[10]

Table 4.4. Experimental and DFT-EPR properties of 1.[a]

	Nuclear spin I [b]	Exp. (sim.)	ORCA (B3-LYP)	ADF (BP86)
g_{iso}		2.0031	2.0031	2.0034
A^{Al}	5/2	13.39	20.90	17.40
A^{1N}	1	15.45	9.90	7.20
A^{2N}	1	5.50	4.60 [c]	3.20 [c]
A^{1H}	½	17.81	15.80	13.10
A^{2H}	½ (2)	4.94	4.50 [c]	1.70 [c]
A^{6H}	½ (6)	7.50	6.50 [c]	0.48 [c]
A^{Me}	½ (6)	< 0.5	0.11 [c]	0.03 [c]

a) Absolute values of the HFC's in MHz; b) number of equivalent nuclei in brackets; c) Average of non-equivalent atoms in the static DFT structure.

Although complex **4.1** is paramagnetic, an acceptable NMR spectrum was obtained, showing severe shifts and broadening of the proton peaks of the ligand backbone and unreliable integration values. The peak for the pyridine ring *para*-H is found broadened over a full ppm and centered at 11.28 ppm. In the 2D NMR, the resonance is coupled to a similarly wide, but stronger, peak at 5.37 ppm, corresponding to the pyridine *meta*-Hs. The other aryl protons are coupled and found slightly shifted at 8.50 ppm and 7.29 ppm. The high field region of the spectrum displays underlying paramagnetism and a mixture of sharp and broad signals. The imino-Me protons of the backbone are also severely broadened at 2.58 ppm and 1.91 ppm and not coupled to any other signal. The presence of THF peaks at 3.59 ppm and 1.44 ppm as slightly broadened singlets suggests possible coordination of THF to the Al center in the solution state. A consequence of this is a disruption in the symmetry of the complex, resulting in more than one set of coupled isopropyl peaks. The methyl groups on the aluminum center are

present as a sharp singlet at 2.28 ppm, another indication that the electron density remains on the ligand and not at the metal center.

The SOMO of complex **4.1**[10] consists mainly of the diiminepyridine π^* orbital of L^{-1}, with small antibonding contributions from σ^* Al-C orbitals, and nearly zero contribution from aluminum itself (Figure 4.7a). The LUMO of **4.1** consists of a different diiminepyridine π^* orbital, without any other significant contributions (Figure 4.7b). Substantial delocalization of the spin density over the diiminepyridine part of **4.1** is clear from a spin density plot (Figure 4.7c).[10]

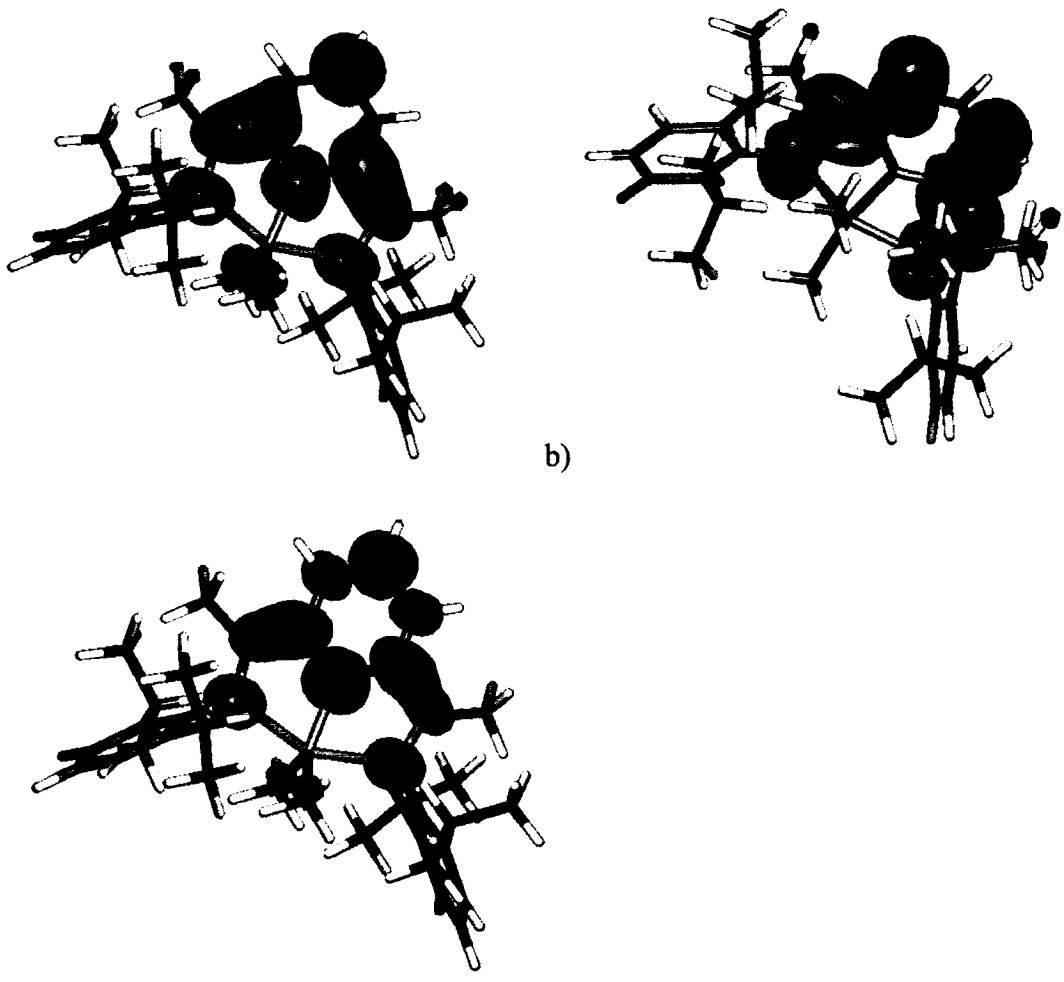

a) b)

c)

Figure 4.7. a) SOMO of complex **4.1**; b) LUMO of complex **4.1**; and c) spin density plot of complex **4.1**.[10]

Complex **4.3** is crystallized separately from the same reaction mixture that furnished complexes **4.1** and **4.2**. The small emerald green crystals could be isolated in 10% yield from a cold hexane solution. The structure (Figure 4.3) consists of an Al dimer, in which one Al center is surrounded by the ligand system, a terminal methyl group, and bridged to the second Al through a Cl atom and the N of the pyridine ring. The tetrahedral coordination sphere of the second Al is completed by two more terminal methyl groups. Like complexes **4.1** and **4.2**, the aluminum centers in **4.3** are most likely present in the trivalent state, requiring the presence of two additional electrons on the ligand, forming a dianionic diradical ligand. The bond distances of the ligand backbone have been modified and are in the expected range for reduction by two electrons, as discussed in Chapter 3.[15bd] The ^{1}H NMR spectrum of complex **4.3** is relatively straight-forward and all of the peaks may be assigned. Although the spectrum displays sharp features characteristic of a diamagnetic species, the *meta* and *para*-protons of the pyridine ring have been shifted to lower ppm values (6.66 ppm and 5.14 ppm) and are slightly broad, most likely a result of slight paramagnetism and added electron density in the ligand π^* orbital. The resonance of the imino-methyl protons is also found slightly lower than in the neutral ligand (1.62 ppm). Three separate ^{i}Pr resonances can be found, due to the unsymmetric nature of the structure (1.35 ppm (6H), 1.23 ppm (12H), 0.96 ppm (6H)). All of the aluminum methyl-bound protons may be found at negative ppm, corresponding to the three aluminum environments in the crystal structure (-0.23 ppm, -0.39 ppm, -0.72 ppm).

To verify the generality of this reaction scheme, the {2,6-[2,6-(^{i}Pr)$_2$PhN=C(CH$_3$)]$_2$(C$_5$H$_3$N)}FeCl$_2$ precursor was reacted with other aluminum alkyls. The reactions with AlEt$_3$ and Al^{i}Bu$_3$ (10 eq) were carried out in toluene at -35°C (Scheme 4.2). After work-up, the reaction mixtures afforded the paramagnetic dark orange complexes [η^4-LAl$_2$R$_3$(μ-Cl)]Fe-(η^6-C$_7$H$_8$) (L = {2,6-[2,6-(^{i}Pr)$_2$PhN=C(CH$_3$)]$_2$(C$_5$H$_3$N)}, R = Et, **4.4** and R = ^{i}Bu, **4.5**) which were isolated in significant yield (41% and 52% respectively). Single crystal X-ray diffraction of both complexes revealed similar structures (Figures 4.4 and 4.5) comprised of a R$_2$Al(μ-Cl)AlR unit bound to the bent ligand center, bearing a striking resemblance to complex **4.3**. However, an atom of Fe can be found partially extruded from the ligand system, η^4-bound to the pyridine ring and η^6-

bound to a molecule of toluene. Both complexes are paramagnetic with rather low values of the magnetic moment at room temperature [μ_{eff} = 1.4 and 1.5 μ_B]. The ^{1}H-NMR spectra consist of broad features in the range normally expected for diamagnetic species. The resonances of the non-equivalent ethyl groups of complex **4.4** attached to the aluminum atoms can tentatively be assigned to two broad singlets at -0.3 ppm, 0.9 ppm, 0.17 ppm and 0.32 ppm. Also clearly recognizable were the resonances of the non-equivalent ^{i}Pr substituents at 3.5 ppm (*ipso* H) and 1.4 ppm (Me groups).

Scheme 4.2

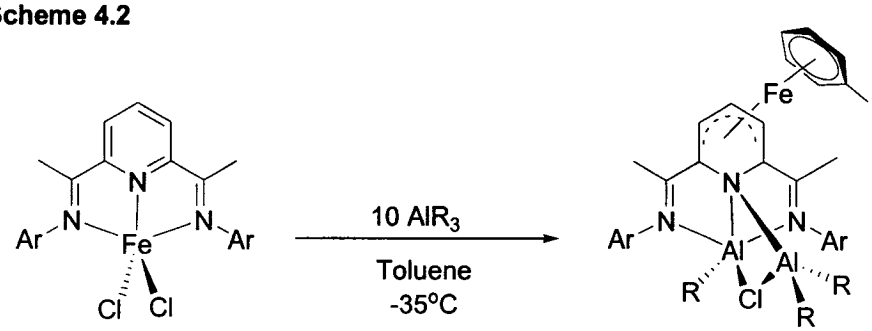

R = Et, **4.4**
R = ^{t}Bu, **4.5**

Given the established ability of this ligand to accept up to three electrons into its π-system,[14,15] there is no doubt that once again the two Al atoms are in their trivalent state and that the ligand is dianionic, thus being the recipient of two of the *four* electrons necessary for the formation of **4.4** and **4.5**. In this event, the Fe atom may be regarded as being present in its *formal* zerovalent state. However, there is the realistic possibility that the ligand may actually be carrying *three* electrons and that Fe may be in the monovalent state.

DFT calculations were carried out by Peter Budzelaar on different spin states of a model compound having Me groups instead of the Et and ^{i}Pr groups of **4.4** and benzene instead of toluene.[10] In both singlet and triplet states the ligand has accepted two electrons from the Al_2Me_3Cl fragment to which it is bound. In the singlet state, these electrons are located in an orbital that is a 1:1 mixture of the original two ligand π^* orbitals. This orbital mixing results in a localization of the imine single and double bonds, and in a concentration of the LAl_2Me_3Cl HOMO on one side of the pyridine ring. Interaction with

the iron-containing fragment then results in a regular 18-electron (arene)$Fe^{(0)}$(butadiene)-like coordination environment, in good agreement with the crystal structure (Figure 4.4). The LAl_2Me_3Cl moiety is calculated to be a *poorer* donor for Fe than real butadiene by approximately 17 kcal/mol.[10]

The structure calculated for the triplet state has C_s symmetry, with a mirror plane through the pyridine nitrogen, the Al and Fe atoms. The Fe atom is η^3-bound to the pyridine ring and approximately η^4-bound to the arene ring. The bonding situation is complex and is best described starting from a *triplet* ligand dianion (both π^* orbitals singly occupied) and high-spin (arene)$Fe^{(0)}$ (also a triplet). Of the pair-wise interactions between the unpaired fragment electrons, one is antiferromagnetic and one is ferromagnetic, leading to the triplet state for the molecule (the quintet state is much higher in energy). Due to the high-spin nature of $Fe^{(0)}$, its coordination number is lower than in the singlet state.[10]

The calculations predict the energy of the triplet to be ca. 6 kcal/mol lower than that of the singlet state. However, the observed X-ray structures of **4.4** and **4.5** agree much better with the singlet than with the triplet state. Spin state energies are notoriously difficult to calculate with high accuracy. At present, it is not clear whether the apparent disagreement is due to the choice of functional and basis-set, to the simplifications used to model the system, or to packing forces in the crystal. The most reasonable interpretation seems to be that for the real complexes **4.4** and **4.5** the singlet and triplet states are very close in energy, that the X-ray structure corresponds to the singlet state, and that the observed magnetism (too low for a pure triplet, but clearly not in agreement with a pure singlet) is due to thermal population of the triplet state.

Discussion

The initial aim of the research was to isolate the active species responsible for the catalytic activity of {2,6-[2,6-(^{i}Pr)$_2$PhN=C(CH_3)]$_2$(C_5H_3N)}$FeCl_2$ by reacting the divalent precursor with aluminum alkyls in the absence of ethylene. The results illustrated above indicate that the reaction has proceeded beyond the formation of the catalytically active species. Since complexes **4.1-4.5** are catalytically inactive, even upon further treatment with MAO or with other aluminum alkyls, these species must be regarded as the result of

catalyst deactivation. The formation of **4.1** and **4.2** from the reaction of the Fe catalyst with $AlMe_3$ is the result of both ligand transmetallation and reduction. Although we observed that traces of **4.1** ($\leq 0.5\%$) may be formed upon addition of $AlMe_3$ to a solution of the free ligand in toluene,[19] the reactivity of $AlMe_3$ with the free ligand is well understood and does not involve redox transformations to a significant extent.[20] Therefore, an obvious question arises about the source of the electrons necessary for the transformation (one electron or three, depending on the unknown fate of the Fe atom). The homolytic cleavage of an Al-Me bond from a hypothetical $LAlMe_3$ intermediate (as possibly arising from a simple transmetallation) is unlikely to provide the electrons necessary for the reduction. Conversely, as amply discussed in Chapter 3, alkylation, and methylation in particular, are certainly capable of affording mono- and di-reduction of the divalent precursor.[7] Since $AlMe_3$ is ultimately a methylating agent, it is entirely possible that its primary function is that of reducing the Fe center. The fact that the main products of the reaction are complexes **4.1** and **4.2**, while complex **4.3** is only formed in minor amounts, is in agreement with the fact that $AlMe_3$ is not as strong a reducing agent as MeLi (see Chapter 3), thus resulting mainly in a one electron reduction of the ligand.

Complexes **4.4** and **4.5** are very similar to complex **4.3**, except for the extruded Fe atom partially bonded to the pyridine ring. Regardless of how the oxidation states of Al and Fe are assigned, the formation of **4.4** and **4.5** is the result of a *four-electron reduction*. The fact that **4.4** and **4.5** are the major products suggests that a more extensive reduction occurs upon addition of $AlEt_3$ or Al^iBu_3 with respect to the case of $AlMe_3$. This could possibly be related to the more reducing nature of ethyl and isobutyl groups in hypothetical Fe-Et or Fe-^{i}Bu species in comparison to Fe-Me. In other words, the system undergoes a four electron reduction before the Fe center can migrate from the ligand system. As a result, the ligand transmetallation appears to have been arrested half-way, with the Fe atom remaining π-coordinated to the ligand. The absence of Fe in compound **4.3** suggests that Fe had the chance to migrate from the ligand system prior to its reduction. This proposal implies an initial reduction of the ligand system by two electrons, followed by the formation of a ligand-bound low-valent organo-Fe species. Bound to a methyl group, the Fe species is sufficiently stable to allow dissociation from the ligand, decomposing via reduction in solution. However, bound to ethyl or isobutyl

groups, the organo-Fe species becomes reduced immediately, prior to dissociation from the ligand, and hence the presence of a zerovalent Fe in the final compound.

Transmetallation of the ligand from Fe to Al may be explained by coordination of the Lewis acidic Al alkyl to the negatively charged ligand. In the case of complexes **4.1** and **4.2**, the ligand has been reduced by only one electron, therefore attracting only one unit of $AlMe_3$ (Scheme 4.3).

Scheme 4.3

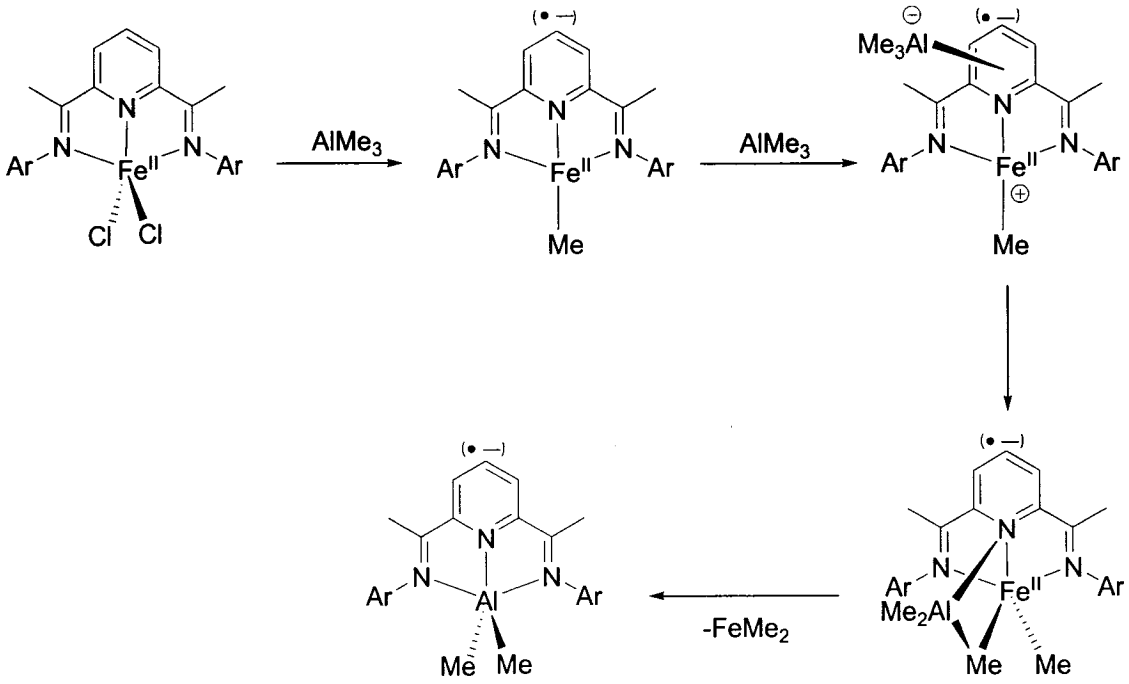

4.1

An obvious question arises regarding the location of Al when bound to the reduced Fe-complex. Although the electron density of the radical is delocalized over the π-backbone of the ligand, the coordination of the second Al in complexes **4.3-4.5** suggests a concentration of negative charge on the N of the pyridine ring. This places the Al moiety in close proximity to the Fe center, perhaps even favouring methylation via bridging intermediates. Upon loss of the $FeMe_2$ unit, the aluminum dimethyl moiety may then occupy the ideal tri-ligated position dictated by the geometry of the ligand (Scheme 4.3).

Conversely, complexes **4.3-4.5**, have undergone a two electron reduction of the ligand, therefore acquiring two Al moieties on the ligand backbone. Assuming complexation of one aluminum center to the nitrogen of the pyridine ring, the other Al may coordinate to one of the two imine-N atoms. Either way, coordination of an Al center to the reduced ligand once again places the Al and Fe centers near to one another and may lead to bridging-alkyl intermediates (similar to the Cl-bridge seen between the Al centers of complexes **4.3-4.5**). In substantiation of this proposal, the intensive NMR studies of Talsi *did* indicate the presence of Fe-Me-Al bridged species upon activation with $AlMe_3$.[5ab]

The scenario depicted above is purely speculative. However, it provides interesting implications with regards to the activation of the complex and mechanism of polymerization and is in fact substantiated by previous observations of the system. In chapter 3, activation of the complex was shown to involve an initial two electron reduction to a neutral species, in which the electrons can be found in the ligand π^* orbitals and the Fe is bound to a neutral donor.[7] This species is not the active species and requires additional activator to afford polymerization. Coordination of an Al unit to the negatively charged ligand would create a zwitterionic complex, generating a positive charge on the Fe center and a negative charge on Al (Scheme 4.4). Stabilization and neutralization of Fe could be achieved via a bridging methyl group between Al and Fe.[5ab] Coordination of a second Al unit to the ligand system would restore the zwitterionic nature of the complex, and hence also the positive charge on the Fe center (Scheme 4.4). The donor ligand is most likely to be labile and may be lost to reveal a coordinatively unsaturated cationic Fe methyl species. We believe that this species is the *active species* and the polymerization mechanism of the bis-iminopyridine Fe catalyst may follow a Ziegler-Natta pathway after all. In typical polymerization systems, the unsaturated metal may be stabilized by coordination of the anionic moiety. However, due to the zwitterionic nature of this species, there is the possibility that one of the imino-N atoms could dissociate from the metal center, to be replaced by a π-bound aryl ring (behaviour previously observed by Chirik).[21] From the coordinatively unsaturated active species ethylene can bind to the empty coordination site and insert into the Fe-C bond.

Scheme 4.4

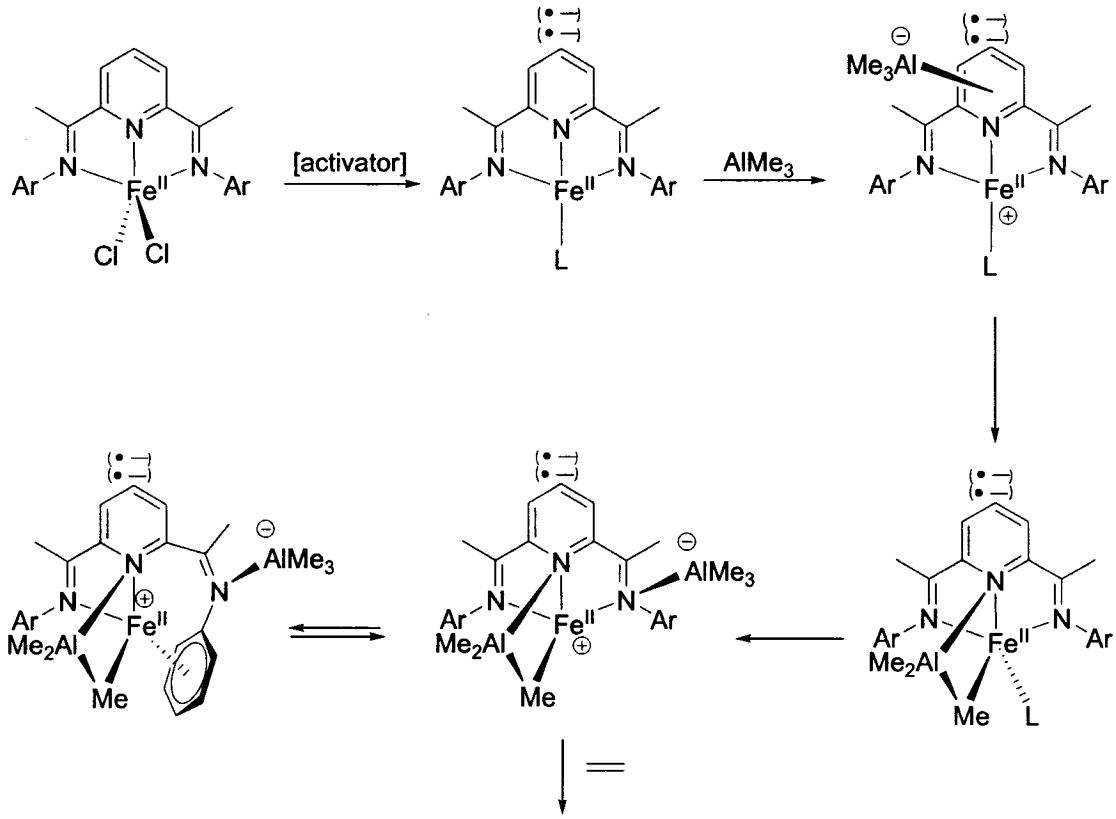

The particular nature of the resulting polymer may also be explained by this pathway. The majority of the polymer consists of saturated ends, indicative of chain transfer to aluminum as the chain termination pathway.[9] The propensity of the Fe-bound unit to bridge the Al center and the proximity of the two metals facilitates transfer of the growing polymer chain to Al. The bridging structure also explains why activation of the divalent precursor with chlorinated Al alkyls does not lead to polymer formation.[9] In this case, a Cl atom on the Al center may preferably bridge the Fe center instead of the alkyl group, preventing the formation of an Fe-C bond and therefore also polymer growth. Indeed, this preference is observed in complexes **4.3**-**4.5**.

Conclusion

With the intentions of isolating a possible active species in the bis-iminopyridine Fe catalytic system, the divalent precursor was reacted with aluminum alkyls. Unfortunately, the system appears to be much too unstable and only deactivation products were isolated. However, even the deactivated complexes give important insight into the activation pathway and molecular dynamism of these unique catalysts. These unprecedented findings clearly demonstrate that coordination of the aluminum activator to the reduced ligand system provides a possible activation mechanism.

References

(1) See Chapter 1 and references therein.

(2) (a) Small, B. L.; Brookhart, M.; Bennett, A. M. A. *J. Am. Chem. Soc.* **1998**, *120*, 4049. (b) Britovsek, G. J. P.; Gibson, V. C.; Kimberley, B. S.; Maddox, P. J.; McTavish, S. J.; Solan, G. A.; White, A. J. P.; Williams, D. J. *Chem. Commun.* **1998**, 849.

(3) Britovsek, G. J. P.; Gibson, V. C.; Spitzmesser, S. K.; Tellmann, K. P.; White, A. J. P.; Williams, D. J. *J. Chem. Soc., Dalton Trans.* **2002**, 1159.

(4) Britovsek, G. J. P.; Clentsmith, G. K. B.; Gibson, V. C.; Goodgame, D. M. L.; McTavish, S. J.; Pankhurst, Q. A. *Catal. Commun.* **2002**, *3*, 207.

(5) (a) Bryliakov, K. P.; Semikolenova, N. V.; Zudin, V. N.; Zakharov, V. A.; Talsi, E. P. *Catal. Commun.* **2004**, *5*, 45. (b) Bryliakov, K. P.; Semikolenova, N. V.; Zakharov, V. A.; Talsi, E. P. *Organometallics* **2004**, *23*, 5375. (c) Castro, P. M.; Lahtinen, P.; Axenov, K.; Viidanoja, J.; Kotiaho, T.; Leskelä, M.; Repo, T. *Organometallics* **2005**, *24*, 3664.

(6) Scott, J.; Gambarotta, S.; Korobkov, I.; Budzelaar, P. H. M. *J. Am. Chem. Soc.* **2005**, *127*, 13019.

(7) Scott, J.; Gambarotta, S.; Korobkov, I.; Budzelaar, P. H. M. *Organometallics* **2005**, *24*, 6298.

(8) (a) Bouwkamp, M. W.; Bart, S. C.; Hawrelak, E. J.; Trovitch, R. J.; Lobkovsky, E.; Chirik, P. J. *Chem. Commun.* **2005**, 3406. (b) Bouwkamp, M. W.; Lobkovsky, E.; Chirik, P. J. *J. Am. Chem. Soc.* **2005**, *127*, 9660.

(9) Britovsek, G. J. P.; Bruce, M.; Gibson, V. C.; Kimberley, B. S.; Maddox, P. J.; Mastroianni, S.; McTavish, S. J.; Redshaw, C.; Solan, G. A.; Strömberg, S.; White, A. J. P.; Williams, D. J. *J. Am. Chem. Soc.* **1999**, *121*, 8728.

(10) Scott, J.; Gambarotta, S.; Korobkov, I.; Knijnenburg, Q.; de Bruin, B.; Budzelaar, P. H. M. *J. Am. Chem. Soc.* **2005**, *127*, 17204.

(11) Blessing, R. *Acta Crystallogr.* **1995**, *A51*, 33.

(12) G. M. Sheldrick, Bruker AXS, Madison, WI, 2001.

(13) Addison, A. W.; Rao, T. N.; Reedijk, J.; van Rijn, J.; Verschoor, G. C. *J. Chem. Soc. Dalton Trans.* **1984**, 1349. The τ parameter helps to classify the geometry of five-coordinate complexes. The τ parameter is calculated by finding the difference between the two largest angles at the metal center and dividing by 60. For a perfect square pyramidal complex, τ = 0 and for a perfect trigonal bipyramidal complex, τ = 1. In cases where the actual geometry is ambiguous between square pyramidal and trigonal bipyramidal, the τ parameter helps to quantify the observed distortions.

(14) (a) Sugiyama, H.; Korobkov, I.; Gambarotta, S.; Möller, A.; Budzelaar, P. H. M. *Inorg. Chem.* **2004**, *43*, 5771. (b) Enright, D.; Gambarotta, S.; Yap, G. P. A.; Budzelaar, P. H. M. *Angew. Chem. Int. Ed.* **2002**, *41*, 3873.

(15) (a) de Bruin, B.; Bill, E.; Bothe, E.; Weyhermueller, T.; Wieghardt, K. *Inorg. Chem.* **2000**, *39*, 2936. (b) Budzelaar, P.H.M; de Bruin, B.; Gal A.W.; Wieghardt, K.; van Lenthe, J. H. *Inorg. Chem.*, **2001**, *40*, 4649. (c) Knijnenburg, Q.; Hetterscheid, D.; Kooistra, T. M.; Budzelaar, P. H. M. *Eur. J. Inorg. Chem.* **2004**, 6, 1204. (d) Bart, S. C.; Chlopek, K.; Bill, E.; Bouwkamp, M. W.; Lobkovsky, E.; Neese, F.; Wieghardt, K.; Chirik, P. J. *J. Am. Chem. Soc.* **2006**, *128*, 13901.

(16) Vidyaratne, I.; Gambarotta, S.; Korobkov, I.; Budzelaar, P. H. M. *Inorg. Chem.* **2005**, *44*, 1187.

(17) Bart, S. C.; Lobkovsky, E.; Chirik, P. J. *J. Am. Chem. Soc.* **2004**, *126*, 13794.

(18) Schumann, H.; Hummert, M.; Lukoyanov, A. N.; Fedushkin, I. L. *Organometallics* **2005**, *24*, 3891.

(19) Knijnenburg, Q.; Budzelaar, P. H. M. Internal results.

(20) (a) Bruce, M.; Gibson, V. C.; Redshaw, C.; Solan, G. A.; White, A. J. P.; Williams, D. J. *Chem. Commun.* **1998**, 2523. (b) Milione, S.; Cavallo, C.; Tedesco, C.; Grassi, A. *J. Chem. Soc. Dalton Trans.* **2002**, 1839. (c) Knijnenburg, Q.; Smits, J. M. M.; Budzelaar, P. H. M. *C. R. Chimie* **2004**, *7*, 865. (d) Knijnenburg, Q.; Smits, J. M. M.; Budzelaar, P. H. M *Organometallics* **2006**, *25*, 1036.

(21) Archer, A.; Bouwkamp, M. W.; Cortez, M.-P.; Lobkovsky, E.; Chirik, P. J. *Organometallics* **2006**, *25*, 4269.

Chapter Five

Reduction of Bis-iminopyridine-Cr Complexes to Give Highly Active Ethylene Polymerization Catalysts

---

Introduction

The initial discovery by Brookhart and Gibson that bis-iminopyridine ligands enable high activity for ethylene polymerization when coordinated to late transition metals[1] prompted extensive investigations towards unveiling the properties of this fascinating ligand system.[2-19] The choice of metal centers was expanded to include the mid-valent first row transition metals vanadium,[2] chromium[3b,20,21] and manganese.[3] Interestingly, the activity of these new systems could not compare to the Fe derivative. Nonetheless, mechanistic studies of these and other bis-iminopyridine-based systems (outlined in Chapter 1) gradually unveiled the remarkable reactivity of the ligand through its involvement in a variety of transformations, including attack at the imino-C atom[4,6] or any position of the pyridine ring,[2,3b,4,6cd,7] mono-[7bc,8] or double[3b,4,9,10] deprotonation of the imino-methyl protons and dimerization through either the ring *meta*-C atoms[3b,6cd] or the imino-methyl groups.[3b,4,5,11] Perhaps most fascinating is the possibility of storing up to three electrons in its delocalized π-system.[8] Chapters 3 and 4 have shown how this ability allows the preparation of complexes in which the metal deceivingly appears in unusually low oxidation states, where, in reality, the HOMO electrons are located in ligand-centered molecular orbitals.[11-16,19]

The involvement of the ligand system in electron transfer processes is perhaps the key to understanding why reduction of the metal center occurs so readily with various first row transition metals upon alkylation[2-4,16-18] or activation with Al-alkyls.[3b,18ab,19] As described in Chapter 3, the metal-to-ligand electron transfer does not necessarily imply quenching of the chemical reactivity. The "low-valent" Fe[16] and Co[18] complexes maintain the high activity and polymer quality when tested under similar conditions for ethylene polymerization as the divalent precursors, suggesting the presence of a reduced active species. In the case of V[2] and Cr,[3b] however, the facile reduction upon activation appears to be a deactivation pathway.

Chromium is the key element in the commercial silica-supported Phillips[22] and Unipol[23] catalytic systems for the polymerization of olefins. The importance of these catalysts has naturally provided a compelling rationale for the development of homogeneous Cr(III) catalysts supported by a variety of ligands, including both cyclopentadienyl-[24] and non-cyclopentadienyl-based systems.[3b,20,21,25-29] These catalysts are usually well-defined, and yet the metal oxidation state of the catalytically active species remains a matter of discussion, the most commonly accepted being either Cr(III) or Cr(II).

When tested in our lab, the Cr(III) bis-iminopyridine complex displayed extremely low catalytic activity upon activation with MAO at room temperature and under ethylene at atmospheric pressure.[3b] On the other hand, at higher temperatures and increased pressures of ethylene, Esteruelas[20] and Small[21] observed that the Cr(III) catalyst displays much higher, but varying, degrees of activity. Based on the results obtained with the Co[18] and Fe[16] analogues, it is possible that activation of the precursor with MAO involves an initial reduction to Cr(II). The Cr(II) derivative was also found to be catalytically active, initially as a polypropylene catalyst by DOW,[30] but also for ethylene polymerization by Small[21] and Esteruelas.[20] The observation by Esteruelas suggests that activation of the Cr(III) precursor does not involve reduction to Cr(II). However, by using UV-VIS and analysis of the resulting polymers, Small *et al.* instead came to the conclusion that the Cr(II) and Cr(III) precursors generate the same active species after reaction with MAO.

Explorations in our lab involving reaction of the bis-iminopyridine Cr(III) precursor with BzMgCl and $AlMe_3$ did indeed discover a facile reduction towards divalent complexes.[3b] The attempted alkylation with BzMgCl led to a slew of transformations, including alkylation and reduction of the metal center to Cr(II), alkylation of the pyridine ring *para*-C, and dimerization via the formation of two new C-C bonds between pyridine *meta*-Cs of two identical units. The reaction with $AlMe_3$ resulted in immediate reduction of the metal center. In this case, however, both final products were inactive.

In an attempt to understand the role of the oxidation state in the Cr catalysts, we explored the reactivity of the divalent Cr precursor. Herein, we describe the reduction of the $\{2,6\text{-}[2,6\text{-}(^{i}Pr)_2PhN{=}C(CH_3)]_2(C_5H_3N)\}CrCl_2$ catalyst with MeLi and NaH, deceivingly affording rare monovalent chromium species which unexpectedly provide extremely high levels of catalytic activity for ethylene polymerization. The work presented below was completed in collaboration with Indu Vidyaratne.[31]

Experimental Section

All operations were performed either under a nitrogen atmosphere using standard Schlenk techniques or in a purified nitrogen-filled dry-box. The THF complexes of $CrCl_3$ and $CrCl_2$ were prepared according to the standard procedure. The ligand 2,6-[2,6-$(^{i}Pr)_2PhN{=}C(CH_3)]_2(C_5H_3N)$,[1] the complex $\{2,6\text{-}[2,6\text{-}(^{i}Pr)_2PhN{=}C(CH_3)]_2(C_5H_3N)\}CrCl_3$[3b] and $LiCH_2Si(CH_3)_3$[32] were prepared according to published procedures. Solutions of 1.6 M MeLi in ether, 2.0 M $AlMe_3$ in toluene, and 10%w/w IBAO in toluene were purchased from Aldrich and used as received. Infrared spectra were recorded on a Mattson 9000 and Nicolet 750-Magna FT-IR instrument from Nujol mulls prepared in a dry box. Samples for magnetic susceptibility measurements were weighed inside a dry box equipped with an analytical balance and sealed into calibrated tubes and the measurements were carried out at room temperature with a Gouy balance (Johnson Matthey). Magnetic moments were calculated following standard methods and corrections for underlying diamagnetism were applied to the data. NMR spectra were recorded with a Varian AMX-500 spectrometer. Elemental analyses were performed with

a Perkin-Elmer 2400 CHN analyzer. Data for X-ray crystal structure determinations were obtained with a Bruker diffractometer equipped with a Smart CCD area detector.

Preparation of {2,6-[2,6-(^{i}Pr)$_2$PhN=C(CH$_3$)]$_2$(C$_5$H$_3$N)}CrCl$_2$•(THF)$_{0.75}$ (5.1).

A suspension of 2,6-[2,6-(^{i}Pr)$_2$PhN=C(CH$_3$)]$_2$(C$_5$H$_3$N) (0.902 g, 1.87 mmol) and CrCl$_2$(THF)$_2$ (0.5 g, 1.87 mmol) was refluxed in toluene (150 mL) overnight. The resulting purple solid was isolated by decanting the solution and washing with hexane. Excess fresh THF (200 mL) was added and the suspension boiled, followed by a hot filtration to obtain a clear purple solution. The purple solution was slowly cooled to room temperature, upon which time small purple crystals of **5.1** formed in 95% yield (1.07 g, 1.78 mmol). Anal. Calcd. (found after drying) for C$_{33}$H$_{43}$N$_3$Cl$_2$Cr (%): C, 65.55 (65.48) H, 7.17 (7.12); N, 6.95 (6.91). IR (Nujol mull, cm^{-1}): ν 3081 (w), 3062 (w), 2910 (s), 2853 (s), 1587 (m), 1553 (s), 1528 (s), 1409 (w), 1318 (s), 1277 (s), 1253 (m), 1242 (w), 1210 (s), 1187 (m), 1148 (w), 1117 (w), 1103 (m), 1069 (s), 1057 (m), 1041 (m), 1025 (m), 984 (w), 937 (m), 909 (m), 839 (w), 817 (s), 809 (s), 800 (s), 780 (s), 762 (m), 741 (m), 725 (s), 694 (m). [μ_{eff} = 3.6 μ_B]

Preparation of {2,6-[2,6-(^{i}Pr)$_2$PhN=C(CH$_3$)]$_2$(C$_5$H$_3$N)}CrMe(μ-Me)Li(THF)$_3$ (5.2).

A suspension of **5.1** (0.250 g, 0.41 mmol) in diethyl ether (20 mL) was cooled to -35°C and treated with a cold solution of MeLi (0.54 mL, 0.87 mmol) in ether (1.6 M). The resulting dark greenish-brown solution was allowed to warm to room temperature overnight. The solvent was evaporated to dryness and the residue re-suspended in hexane (15 mL). Most of the solid dissolved, affording a dark greenish-brown solution with a colourless precipitate. The solution was separated by centrifugation and stored at -35°C for two days, upon which time dark green-brown block crystals of **5.2** were isolated (0.114 g, 0.145 mmol, 35% yield). Anal. Calcd. (found) for C$_{47}$H$_{73}$CrLiN$_3$O$_3$ (%): C, 71.73 (71.66); H, 9.35 (9.31); N, 5.34 (5.28). IR (Nujol mull, cm^{-1}): ν 2973-2845 (b, s), 1575 (s), 1493 (w), 1469 (s), 1377 (m), 1355 (w), 1332 (m), 1316 (m), 1280 (w), 1244 (s), 1204 (s), 1176 (w), 1143 (m), 1133 (m), 1100 (w), 1078 (m), 1044 (s), 990 (s), 935 (m), 887 (s), 872 (s), 839 (w), 807 (s), 776 (s), 748 (s), 730 (s), 715 (w), 693 (w), 662 (m), 646 (w). [μ_{eff} = 4.2 μ_B]

Preparation of {2,6-[2,6-(^{i}Pr)$_2$PhN=C(CH$_3$)]$_2$(C$_5$H$_3$N)}CrCl (5.3).

Method A: A suspension of **5.1** (0.250 g, 0.413 mmol) with 2.2 equivalents of NaH (0.022 g, 0.910 mmol) in THF (25 mL) was stirred at room temperature for approximately 4 days. During this time, the colour of the mixture changed from purple to dark green. After 4 days, the solvent was evaporated *in vacuo* and the solids redissolved in toluene (20 mL). The dark green solution was centrifuged to remove a small amount of precipitate and concentrated to approximately 5 mL. Dark green crystals of **5.3** grew after standing at room temperature for 3 days (0.195 g, 0.34 mmol, 83% yield). Anal. Calcd. (found) for $C_{33}H_{43}N_3ClCr$ (%): C, 69.64 (69.59); H, 7.62 (7.61); N, 7.38 (7.40). IR (Nujol mull, cm^{-1}): ν 2854 (s), 1578 (w), 1501 (w), 1462 (s), 1377 (s), 1331 (w), 1315 (m), 1237 (s), 1185 (m), 1177 (m), 1106 (s), 1092 (s), 1024 (m), 948 (s), 827 (s), 756 (s), 727 (s), 693 (s). [μ_{eff} = 3.6 μ_B]

Method B: A suspension of {2,6-[2,6-(^{i}Pr)$_2$PhN=C(CH$_3$)]$_2$(C$_5$H$_3$N)}CrCl$_3$ (0.43 g, 0.67 mmol) in THF (15 mL) was reacted with 3.3 equivalents of NaH (0.05 g, 2.0 mmol) over a period of 1 week, during which time the colour of the mixture became dark green. After evaporating to dryness and adding toluene, the dark green solution was centrifuged to remove small amounts of insoluble solid and allowed to stand at room temperature. Dark green crystals of **5.3** precipitated after approximately 3 days (0.076 g, 0.15 mmol, 22%).

Preparation of {2-[2,6-(^{i}Pr)$_2$PhN=C(CH$_3$)]-6-[2,6-(^{i}Pr)$_2$PhN-C=CH$_2$](C$_5$H$_3$N)}Cr (THF) (5.4).

A solution of **5.3** (0.250 g, 0.439 mmol) in THF (15 mL) was cooled to -35°C and treated with a cold solution of LiCH$_2$Si(CH$_3$)$_3$ (0.045 g, 0.483 mmol) in THF (10 mL). After overnight stirring, the resulting brownish-green solution was evaporated to dryness and re-suspended in hexane (15 mL). The brownish-green supernatant was separated from a white precipitate by centrifugation and allowed to stand in the freezer at -35°C. Dark green crystals of **5.4** formed in two days (0.154 g, 0.225 mmol, 58% yield). Anal. Calcd. (found) for $C_{37}H_{50}CrN_3O$ (%): C, 73.48 (73.45); H, 8.33 (8.27); N, 6.95 (6.88). IR (Nujol mull, cm^{-1}): ν 2900 (s), 2854 (s), 1606 (m), 1574 (s), 1512 (s), 1464 (s), 1433 (s), 1402 (m), 1379 (s), 1357 (m), 1315 (m), 1300 (s), 1243 (s), 1221 (s), 1195 (m), 1174 (w), 1135

(w), 1091 (m), 1065 (m), 1052 (m), 1017 (m), 1003 (w), 978 (m), 925 (s), 899 (w), 871 (s), 859 (m), 824 (s), 804 (s), 774 (s), 755 (s), 738 (m), 725 (m), 690 (s). [$\mu_{eff} = 3.8\mu_B$]

Preparation of {2-[2,6-(^{i}Pr)$_2$PhN=C(CH$_3$)]-6-[2,6-(^{i}Pr)$_2$PhN-C=CH$_2$](C$_5$H$_3$N)}Cr(μ-Me) Li(THF)$_3$•(toluene)$_{0.66}$ (5.5).

A cold solution of MeLi in diethyl ether (1.6 M, 0.58 mL, 0.922 mmol) was added to a suspension of **5.3** (0.250 g, 0.439 mmol) in ether (25 mL) at -35°C. The resulting dark reddish-brown solution was stirred and allowed to warm to room temperature for 4 hours. After evaporating the solvent, the residue was washed with ether to remove a dark reddish-brown supernatant. The remaining precipitates were dissolved in THF and centrifuged. Dark reddish-brown crystals of **5.5** were grown from a THF/toluene solution (0.17 g, 0.21 mmol, 48%). Anal. Calcd. (found after drying) for $C_{46}H_{69}N_3O_3CrLi$ (%): C, 71.66 (71.61); H, 9.02 (8.97); N, 5.45 (5.44). IR (Nujol mull, cm^{-1}): ν 2975-2838 (b, s), 1602 (w), 1585 (m), 1563 (m), 1508 (w), 1468 (s), 1378 (s), 1302 (m), 1240 (s), 1193 (m), 1171 (m), 1155 (w), 1144 (m), 1110 (w), 1099 (m), 1044 (s), 967 (s), 910 (w), 887 (s), 828 (s), 799 (m), 770 (m), 742 (m), 726 (s), 693 (m), 666 (m). [$\mu_{eff} = 3.8\ \mu_B$]

Preparation of {2,6-[2,6-(^{i}Pr)$_2$PhN=C(CH$_3$)]$_2$(C$_5$H$_3$N)}Cr(μ-Cl)$_2$Al(CH$_3$)$_2$ (5.6).

A solution of AlMe$_3$ in toluene (2.0 M, 2.20 mL, 4.39 mmol) was added to a solution of complex **5.3** (0.250 g, 0.439 mmol) in the same solvent (20 mL) at -35°C. The colour of the mixture immediately changed from dark green to dark brownish-green. After stirring overnight, the solvent was evaporated and cold hexane (10 mL) added to the residue. The resulting suspension was centrifuged and the dark green solution, separated from the dark precipitates, afforded dark green crystals of **5.6** upon standing 2 days at -35°C (0.044 g, 0.066 mmol, 15% yield). Anal. Calcd. (found) for $C_{35}H_{49}AlCl_2CrN_3$ (%): C, 63.53 (63.47); H, 7.46 (7.41); N, 6.35 (6.33). IR (Nujol mull, cm^{-1}): ν 2963-2855 (s), 1576 (m), 1468 (s), 1377 (s), 1232 (s), 1147 (s), 1104 (s), 1093 (s), 1055 (s), 935 (s), 860 (s), 827 (s), 805 (m), 776 (s), 757 (m), 721 (m), 694 (s), 690 (s). [$\mu_{eff} = 3.9\ \mu_B$]

Preparation of {2,6-[2,6-(^{i}Pr)$_2$PhN=C(CH$_3$)]$_2$(C$_5$H$_3$N)}CrCH$_3$(hexane)$_{0.5}$ (5.7).

The preparation was carried out as for complex **5.6** except that the remaining hexane-insoluble portion was dissolved in toluene (15 mL). After centrifugation, the dark greenish-brown solution was concentrated to 5 mL and allowed to stand at room temperature for 4 days, upon which time dark brown crystals of **5.7** precipitated (0.180 g, 0.307 mmol, 70% yield). Anal. Calcd. (found after drying) for $C_{34}H_{46}N_3Cr$ (%): C, 74.42 (74.39); H, 8.45 (8.41); N, 7.66 (7.60). IR (Nujol mull, cm^{-1}): ν 2900-2849 (s, b), 1633 (m), 1584 (w), 1565 (w), 1464 (s), 1377 (s), 1318 (w), 1303 (w), 1222 (s), 1204 (m), 1150 (m), 1087 (s), 931 (s), 881 (w), 855 (s), 804 (w), 796 (w), 779 (w), 7556 (s), 726 (s), 705 (m), 665 (w). [μ_{eff} = 3.5 μ_B]

Preparation of {[η^4-{2,6-[2,6-(^{i}Pr)$_2$PhN=C(CH$_3$)]$_2$(C$_5$H$_3$N)}Al$_2$(^{i}Bu)$_3$(μ-Cl)]Cr(η^6-C$_7$H$_8$)}• (hexane)$_{0.66}$ (5.8).

A solution of IBAO in toluene (10%w/w, 6.55 g, 2.20 mmol) was added drop-wise to a solution of complex **5.3** (0.125 g, 0.220 mmol) in toluene (15 mL) at -35°C. The colour immediately turned deep brownish-red and the mixture was allowed to slowly reach room temperature. The solvent was evaporated *in vacuo* and the residue re-dissolved in hexane (20 mL), forming a deep brown-red solution which was separated by centrifugation from a substantial amount of insoluble material. Very dark block crystals of **5.8** were formed after standing for 5 days at room temperature. A non-characterizable oily material was also present. The crystals were isolated in pure form by careful washing with small portions of cold hexane to remove the oily contaminant. Anal. Calcd. (found upon drying) for $C_{48}H_{69}N_3ClCrAl_2$ (%): C, 69.50 (69.45); H, 8.38 (8.31); N, 5.07 (5.09). IR (Nujol mull, cm^{-1}): ν 2949-2861 (b, s), 1610 (w), 1564 (w), 1462 (s), 1405 (w), 1377 (s), 1318 (m), 1253 (w), 1230 (w), 1179 (s), 1161 (m), 1116 (w), 1066 (m), 1018 (s), 944 (w), 918 (w), 869 (m), 814 (m), 804 (m), 759 (w), 724 (m), 708 (m), 681 (s). [μ_{eff} = 1.7 μ_B]

X-ray Crystallography

All of the compounds consistently yielded crystals that diffracted weakly, and the results presented are the best of several trials. The crystals were mounted on thin glass fibers using paraffin oil and cooled to the data collection temperature. Data were

collected on a Bruker AXS SMART 1k CCD diffractometer. Data for the compounds **5.1, 5.2,** and **5.4-5.8** were collected with a sequence of 650 scans per set at 0.3° ω scans at 0, 120, and 240° in φ. To obtain acceptable redundancy data for compound **5.3**, the sequence of 650 scans per set with 0.3° ω scans at 0, 90, 180, and 270° in φ was used. Initial unit cell parameters were determined from 60 data frames collected at the different sections of the Ewald sphere. Semiempirical absorption corrections based on equivalent reflections were applied.[33] Systematic absences in the diffraction data-set and unit-cell parameters were consistent with monoclinic $P2_1/c$ for **5.1**, orthorhombic $Pna2_1$ for **5.2**, triclinic $P\bar{1}$ for **5.3**, orthorhombic $P2_12_12_1$ for **5.4**, monoclinic $P2_1/n$ for **5.5**, monoclinic $P2_1$ for **5.6**, monoclinic $C2/c$ for **5.7**, and monoclinic $P2_1/n$ for **5.8**. Solutions in centrosymmetric space groups for compounds **5.1, 5.3, 5.5, 5.7** and **5.8** and non-centrosymmetric for compounds **5.2, 5.4** and **5.6** yielded chemically reasonable and computationally stable results of refinement. The structures were solved by direct methods, completed with difference Fourier synthesis, and refined with full-matrix least-squares procedures based on F^2. The compound molecules were located in common positions in the structures of the complexes **5.1-5.6** and **5.8**. . In complex **5.7**, a half-occupancy ether solvent molecule is located on the 2-fold axis of the symmetry element and the Cr molecule is located in the common position (1/4 ether molecules per chromium center). In complex **5.5**, the initial solution suggested two cocrystallized, severely disordered, toluene solvent molecules. The data set was treated with the Squeeze routine of PLATON[34] with a refined void space per cell of 1246.2 Å^3 and an electron count per cell of 133, consistent with 8/3 toluene molecules per cell. In compound **5.6**, the asymmetric unit contains 2 molecules of the Cr complex, which brings the Z' number to 2. Complex **5.8** contains a partly occupied molecule of hexane. All non-hydrogen atoms were refined with anisotropic displacement coefficients. All hydrogen atoms were treated as idealized contributions. All scattering factors are contained in several versions of the SHELXTL program library, with the latest version used being v.6.12.[34] Crystallographic data and relevant bond distances and angles are reported in Tables 5.1 – 5.5.

Table 5.1. Crystal Data and Structure Analysis Results of Complexes 5.1-5.4

	5.1	**5.2**	**5.3**	**5.4**
formula	$C_{36}H_{49}Cl_2CrN_3O_{0.75}$	$C_{47}H_{73}CrLiN_3O_3$	$C_{33}H_{43}ClCrN_3$	$C_{37}H_{50}CrN_3O$
Mw	658.68	787.02	569.15	604.80
crystal system	Monoclinic	Orthorhombic	Triclinic	Orthorhombic
space group	P2(1)/c	Pna2(1)	P-1	P2(1)2(1)2(1)
a (Å)	13.644(4)	28.334(12)	8.528(19)	8.6512(18)
b (Å)	15.007(4)	12.367(5)	8.731(19)	19.119(4)
c (Å)	18.454(5)	13.407(6)	23.05(5)	20.720(4)
α (deg)	90	90	95.08(4)	90
β (deg)	100.880(5)	90	95.40(4)	90
γ (deg)	90	90	109.66(3)	90
V (Å^3)	3710.7(18)	4698(3)	1595(6)	3427.2(12)
Z	4	4	2	4
radiation (Kα, Å)	0.71073	0.71073	0.71073	0.71073
T (K)	213(2)	208(2)	210(2)	211(2)
D_{calcd} (g cm^{-3})	1.179	1.113	1.185	1.172
μ_{calcd} (mm^{-1})	0.481	0.283	0.467	0.365
F_{000}	1400	1708	606	1300
R, R_w[2 a]	0.0800, 0.1237	0.0762, 0.1130	0.0606, 0.1557	0.0643, 0.1264
GoF	1.009	1.012	1.031	1.025

[a] $R = \Sigma||F_0| - |F_c||/\Sigma|F|$, $R_w = [\Sigma(|F_0| - |F_c|)^2/\Sigma wF_0^2\}^{1/2}$

Table 5.2. Crystal Data and Structure Analysis Results of Complexes 5.5-5.8

	5.5	5.6	5.7	5.8
formula	$C_{50.62}H_{74.28}CrLiN_3O_3$	$C_{70}H_{98}Al_2Cl_4Cr_2N_6$	$C_{36.50}H_{52}CrN_3$	$C_{52}H_{78}Al_2ClCrN_3$
Mw	831.79	1323.30	584.81	886.58
crystal system	Monoclinic	Monoclinic	Monoclinic	Monoclinic
space group	P2(1)/n	P2(1)	C2/c	P2(1)/n
a (Å)	13.217(14)	14.337(17)	27.8(3)	10.895(6)
b (Å)	17.70(2)	14.879(17)	14.95(14)	19.206(11)
c (Å)	22.278(12)	17.38(2)	21.6(2)	23.981(14)
α (deg)	90	90	90	90
β (deg)	95.46(8)	98.86(2)	126.86(15)	101.029(11)
γ (deg)	90	90	90	90
V (Å^3)	5187(9)	3663(7)	7190(117)	4925(5)
Z	4	2	8	4
radiation (Kα, Å)	0.71073	0.71073	0.71073	0.71073
T (K)	203(2)	207(2)	208(2)	203(2)
D_{calcd} (g cm^{-3})	1.065	1.200	1.080	1.196
μ_{calcd} (mm^{-1})	0.260	0.509	0.344	0.359
F_{000}	1800	1404	2528	1912
R, R_w[2 a]	0.0588, 0.1426	0.0736, 0.1469	0.0666, 0.1548	0.0741, 0.1626
GoF	1.005	1.031	1.055	1.050

[a] $R = \Sigma||F_o| - |F_c||/\Sigma|F|$, $R_w = [\Sigma(|F_o| - |F_c|)^2/\Sigma wF_o^2\}^{1/2}$

Table 5.3. Selected Bond Distances (Å) and Angles (deg) of Complexes 5.1-5.4

5.1	5.2	5.3	5.4
Cr(1)-N(1) = 2.118(7)	Cr(1)-N(1) = 2.045(8)	Cr(1)-N(1) = 2.092(5)	Cr(1)-N(1) = 2.022(4)
Cr(1)-N(2) = 1.993(6)	Cr(1)-N(2) = 1.921(8)	Cr(1)-N(2) = 1.934(4)	Cr(1)-N(2) = 1.953(4)
Cr(1)-N(3) = 2.118(6)	Cr(1)-N(3) = 2.045(8)	Cr(1)-N(3) = 2.062(5)	Cr(1)-N(3) = 2.020(4)
Cr(1)-Cl(1) = 2.299(2)	Cr(1)-C(35) = 2.062(8)	Cr(1)-Cl = 2.287(4)	Cr(1)-O(1) = 2.071(3)
Cr(1)-Cl(2) = 2.416(3)	Cr(1)-C(34) = 2.134(9)	C(1)-C(2) = 1.504(6)	C(1)-C(2) = 1.416(7)
C(1)-C(2) = 1.470(10)	Li(1)-C(34) = 2.362	C(8)-C(9) = 1.497(6)	C(8)-C(9) = 1.443(7)
C(8)-C(9) = 1.495(10)	C(1)-C(2) = 1.473(12)	N(1)-C(2) = 1.311(5)	N(1)-C(2) = 1.374(6)
N(1)-C(2) = 1.294(9)	C(8)-C(9) = 1.477(12)	N(3)-C(8) = 1.331(5)	N(3)-C(8) = 1.372(6)
N(3)-C(8) = 1.298(9)	N(1)-C(2) = 1.376(10)	N(1)-Cr(1)-N(2) = 76.66(16)	N(1)-Cr(1)-N(2) = 79.18(15)
N(1)-Cr(1)-N(2) = 75.4(3)	N(3)-C(8) = 1.379(10)	N(2)-Cr(1)-N(3) = 77.95(13)	N(2)-Cr(1)-N(3) = 78.47(16)
N(2)-Cr(1)-N(3) = 76.2(3)	N(1)-Cr(1)-N(2) = 77.8(4)	N(3)-Cr(1)-Cl(1) = 102.29(11)	N(3)-Cr(1)-O(1) = 101.21(16)
N(3)-Cr(1)-Cl(1) = 99.2(2)	N(2)-Cr(1)-N(3) = 77.2(4)	N(1)-Cr(1)-Cl(1) = 103.24(13)	N(1)-Cr(1)-O(1) = 101.16(15)
N(1)-Cr(1)-Cl(1) = 101.77(19)	N(3)-Cr(1)-C(34) = 101.1(3)	N(1)-Cr(1)-N(3) = 154.46(14)	N(1)-Cr(1)-N(3) = 157.62(16)
N(2)-Cr(1)-Cl(1) = 160.95(19)	N(1)-Cr(1)-C(34) = 100.5(4)	N(2)-Cr(1)-Cl(1) = 175.61(10)	N(2)-Cr(1)-O(1) = 178.20(17)
N(1)-Cr(1)-N(3) = 146.5(3)	N(1)-Cr(1)-N(3) = 149.3(3)		
N(1)-Cr(1)-Cl(2) = 98.11(18)	N(2)-Cr(1)-C(34) = 168.6(3)		
N(2)-Cr(1)-Cl(2) = 93.16(18)	C(35)-Cr(1)-N(1) = 98.2(3)		
N(3)-Cr(1)-Cl(2) = 100.89(18)	C(35)-Cr(1)-N(2) = 94.3(3)		
Cl(1)-Cr(1)-Cl(2) = 105.88(10)	C(35)-Cr(1)-N(3) = 101.1(3)		
	C(35)-Cr(1)-C(34) = 97.1(4)		
	Cr(1)-C(34)-Li(1) = 166.73		

Table 5.4. Selected Bond Distances (Å) and Angles (deg) of Complexes 5.5-5.7

5.5	5.6	5.6 (cont'd)	5.7
Cr(1)-N(1) = 2.034(4)	Cr(1)-N(1) = 2.105(8)	N(1)-Cr(1)-Cl(2) = 99.9(2)	Cr(1)-N(1) = 1.944(16)
Cr(1)-N(2) = 1.993(3)	Cr(1)-N(2) = 1.923(8)	N(2)-Cr(1)-N(3) = 77.6(3)	Cr(1)-N(2) = 1.877(12)
Cr(1)-N(3) = 2.028(4)	Cr(1)-N(3) = 2.131(8)	N(3)-Cr(1)-Cl(1) = 99.2(2)	Cr(1)-N(3) = 1.929(12)
Cr(1)-C(34) = 2.129(4)	Cr(1)-Cl(1) = 2.468(4)	N(3)-Cr(1)-Cl(2) = 99.9(3)	Cr(1)-C(34) = 1.959(13)
C(34)-Li(1) =	Cr(1)-Cl(2) = 2.526(4)	Cl(1)-Al(1)-Cl(2) = 94.11(16)	C(1)-C(2) = 1.522(15)
C(13)-C(14) = 1.465(6)	Cl(1)-Al(1) = 2.248(5)	Cl(1)-Al(1)-C(34) = 106.3(4)	C(8)-C(9) = 1.496(10)
C(20)-C(21) = 1.387(6)	Cl(2)-Al(1) = 2.233(5)	Cl(1)-Al(1)-C(35) = 109.8(4)	N(1)-C(2) = 1.363(12)
N(1)-C(14) = 1.383(5)	Al(1)-C(34) = 1.957(11)	Cl(2)-Al(1)-C(34) = 109.7(4)	N(3)-C(8) = 1.360(10)
N(3)-C(20) = 1.381(5)	Al(1)-C(35) = 1.948(12)	Cl(2)-Al(1)-C(35) = 110.0(4)	N(1)-Cr(1)-N(2) = 81.5(7)
C(14)-C(15) = 1.409(6)	C(1)-C(2) = 1.497(14)	C(34)-Al(1)-C(35) = 123.0(5)	N(2)-Cr(1)-N(3) = 81.7(8)
C(19)-C(20) = 1.461(6)	C(8)-C(9) = 1.509(13)		N(3)-Cr(1)-C(34) = 98.5(8)
N(2)-C(15) = 1.372(5)	N(1)-C(2) = 1.327(12)		N(1)-Cr(1)-C(34) = 98.3(7)
N(2)-C(19) = 1.359(5)	N(3)-C(8) = 1.334(11)		N(1)-Cr(1)-N(3) = 163.18(16)
N(1)-Cr(1)-N(2) = 77.72(16)	N(2)-Cr(1)-Cl(1) = 144.7(2)		N(2)-Cr(1)-C(34) = 179.09(19)
N(2)-Cr(1)-N(3) = 77.55(16)	N(2)-Cr(1)-Cl(2) = 133.2(2)		
N(3)-Cr(1)-C(34) = 101.54(16)	Cl(1)-Cr(1)-Cl(2) = 82.11(11)		
N(1)-Cr(1)-C(34) = 103.32(17)	N(1)-Cr(1)-N(3) = 154.9(3)		
N(1)-Cr(1)-N(3) = 155.13(14)	N(1)-Cr(1)-N(2) = 77.6(3)		
N(2)-Cr(1)-C(34) = 172.97(16)	N(1)-Cr(1)-Cl(1) = 98.6(2)		

Table 5.5. Selected Geometrical Parameters of Complex 5.8

Bond Distances (Å)	Angles (deg)
Al(1)-N(1) = 2.140(5)	N(2)-C(7) = 1.457(7)
Al(1)-N(2) = 2.002(5)	C(7)-C(8) = 1.343(8)
Al(1)-N(3) = 1.924(5)	C(8)-C(9) = 1.508(9)
Al(1)-C(41) = 1.967(6)	N(3)-C(8) = 1.378(8)
Al(1)-Cl = 2.393(3)	N(2)-Al(1)-C(41) = 172.3(3)
Al(2)-Cl = 2.291(3)	N(1)-Al(1)-N(3) = 142.7(2)
Al(2)-N(2) = 1.963(5)	N(3)-Al(1)-Cl = 104.56(17)
Al(2)-C(45) = 1.968(7)	N(1)-Al(1)-Cl = 104.55(16)
Al(2)-C(49) = 1.952(7)	N(2)-Al(1)-Cl = 85.09(16)
Cr(1)-C(3) = 2.119(6)	N(2)-Al(1)-N(1) = 77.5(2)
Cr(1)-C(4) = 1.952(7)	N(2)-Al(1)-N(3) = 82.4(2)
Cr(1)-C(5) = 2.000(7)	C(41)-Al(1)-Cl = 98.2(2)
Cr(1)-C(6) = 2.158(7)	C(41)-Al(1)-N(1) = 94.9(2)
Cr(1)-C(34) = 2.094(7)	C(41)-Al(1)-N(3) = 103.4(3)
Cr(1)-C(35) = 2.064(7)	Al(1)-Cl-Al(2) = 82.97(8)
Cr(1)-C(36) = 2.083(7)	N(2)-Al(2)-Cl = 88.80(16)
Cr(1)-C(37) = 2.060(7)	N(2)-Al(2)-C(45) = 111.9(3)
Cr(1)-C(38) = 2.073(7)	N(2)-Al(2)-C(49) = 116.3(3)
Cr(1)-C(39) = 2.088(7)	Cl-Al(2)-C(45) = 108.5(2)
C(1)-C(2) = 1.512(9)	Cl-Al(2)-C(49) = 104.0(2)
N(1)-C(2) = 1.300(7)	C(45)-Al(2)-C(49) = 121.4(3)
C(2)-C(3) = 1.435(9)	C(3)-N(2)-C(7) = 108.6(5)
N(2)-C(3) = 1.459(8)	C(3)-N(2)-Al(1) = 116.1(4)
C(3)-C(4) = 1.428(8)	C(3)-N(2)-Al(2) = 113.7(4)
C(4)-C(5) = 1.395(9)	C(7)-N(2)-Al(1) = 109.7(4)
C(5)-C(6) = 1.438(10)	C(7)-N(2)-Al(2) = 105.1(4)
C(6)-C(7) = 1.440(9)	Al(1)-N(2)-Al(2) = 103.0(2)

Complex 5.1. The structure of complex **5.1** (Figure 5.1) is very similar to the Fe,[1] Co[1] and Mn[3] bis-iminopyridine analogues. The coordination geometry around the Cr center is defined by the three N atoms of the ligand [Cr(1)-N(1) = 2.118(7) Å, Cr(1)-N(2) = 1.993(6) Å, Cr(1)-N(3) = 2.118(6) Å] and two terminal Cl atoms [Cr(1)-Cl(1) = 2.299(2) Å, Cr(1)-Cl(2) = 2.416(3) Å] in an overall distorted square-pyramidal arrangement. The basal plane is occupied by the nitrogen donor atoms of the tridentate ligand and one chlorine atom [N(1)-Cr(1)-N(2) = 75.4(3)°, N(2)-Cr(1)-N(3) = 76.2(3)°, N(3)-Cr(1)-Cl(1) = 99.2(2)°, N(1)-Cr(1)-Cl(1) = 101.77(19)°, N(2)-Cr(1)-Cl(1) = 160.95(19)°]. The second Cl atom is located in the apical position [N(1)-Cr(1)-Cl(2) = 98.11(18)°, N(2)-Cr(1)-Cl(2) = 93.16(18)°, N(3)-Cr(1)-Cl(2) = 100.89(18)°, Cl(1)-Cr(1)-Cl(2) = 105.88(10)°]. The other bond distances and angles do not show any distinguishing features and compare well with those found in the Fe, Co and Mn derivatives.[1,3]

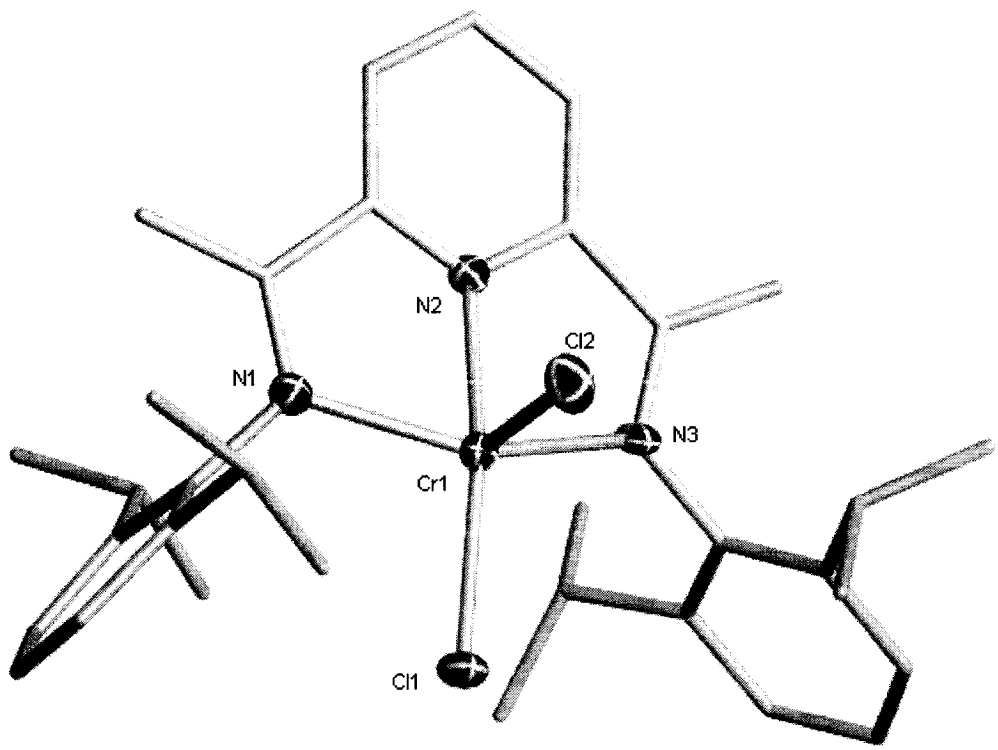

Figure 5.1. Partial thermal ellipsoid plot of **5.1**, drawn at the 30% probability level. Hydrogen atoms have been omitted for clarity.

Complex 5.2. The complex consists of a pentacoordinate Cr center surrounded by the ligand's three donor atoms [Cr(1)-N(1) = 2.045(8) Å, Cr(1)-N(2) = 1.921(8) Å, Cr(1)-N(3) = 2.045(8) Å] and two methyl groups in an overall distorted square pyramidal geometry (τ = 0.31)[35] (Figure 5.2). One methyl group, located in the axial position [C(35)-Cr(1)-N(1) = 98.2(3)°, C(35)-Cr(1)-N(2) = 94.3(3)°, C(35)-Cr(1)-N(3) = 101.1(3)°, C(35)-Cr(1)-C(34) = 97.1(4)°], is terminally bound [Cr(1)-C(35) = 2.062(8) Å]. The carbon of a second methyl group [Cr(1)-C(34) = 2.134(9) Å] occupies the fourth equatorial position [N(1)-Cr(1)-N(2) = 77.8(4)°, N(2)-Cr(1)-N(3) = 77.2(4)°, N(3)-Cr(1)-C(34) = 101.1(3)°, N(1)-Cr(1)-C(34) = 100.5(4)°, N(1)-Cr(1)-N(3) = 149.3(3)°, N(2)-Cr(1)-C(34) = 168.6(3)°] and is bridging a THF-solvated lithium cation forming an almost linear Li-C-Cr array [Li(1)-C(34) = 2.362 Å, Cr(1)-C(34)-Li(1) = 166.73°]. An examination of the ligand parameters shows a slight shortening in the C_{Me}-C_{imino} bonds [C(1)-C(2) = 1.473(12) Å, C(8)-C(9) = 1.477(12) Å], paralleled by a lengthening in the imino C-N bonds [N(1)-C(2) = 1.376(10) Å, N(3)-C(8) = 1.379(10) Å]. Other modifications include a shortening of the C_{imine}-C_{ortho} bond lengths [C(2)-C(3) = 1.417(11) Å, C(7)-C(8) = 1.403(13) Å] and a lengthening of the C_{ortho}-N_{pyr} bond distances [N(2)-C(3) = 1.380(11) Å, N(2)-C(7) = 1.392(11) Å] relative to the divalent precursor.

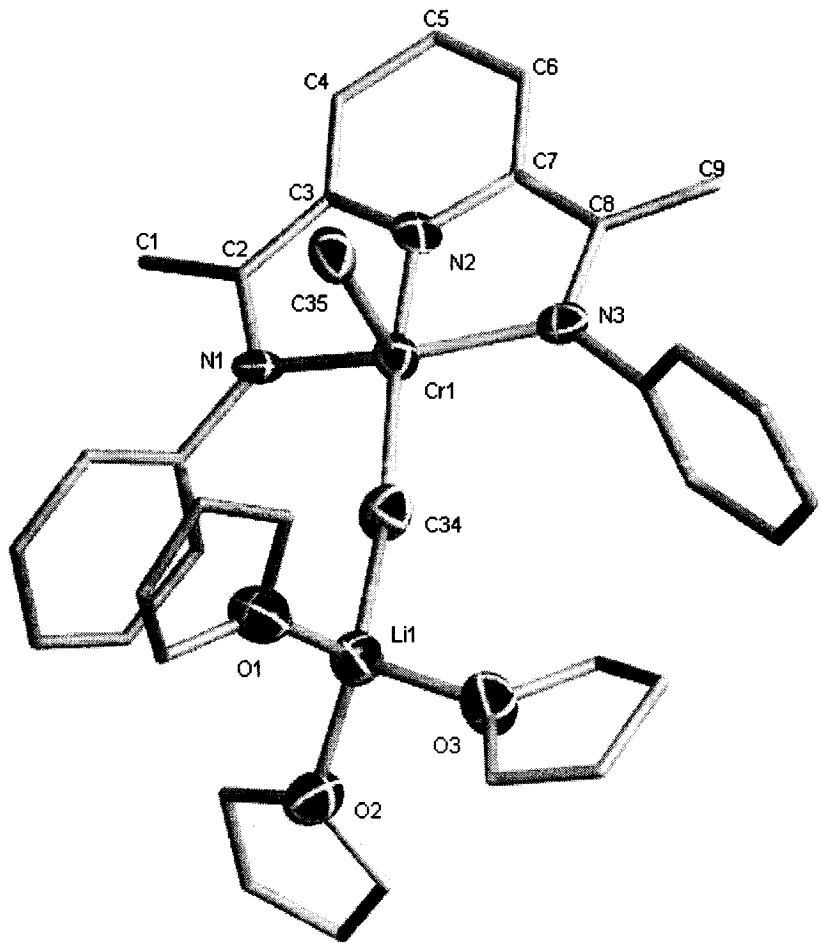

Figure 5.2. Partial thermal ellipsoid plot of **5.2**, drawn at the 30% probability level. The isopropyl groups of the ligand and the H atoms have been removed for clarity.

Complex 5.3. Complex **5.3** (Figure 5.3) consists of a Cr center bound to the three N atoms of the ligand [Cr(1)-N(1) = 2.092(5) Å, Cr(1)-N(2) = 1.934(4) Å, Cr(1)-N(3) = 2.062(5) Å] and a terminal Cl atom [Cr(1)-Cl(1) = 2.287(4) Å] in an overall distorted square planar geometry [N(1)-Cr(1)-N(2) = 76.66(16)°, N(2)-Cr(1)-N(3) = 77.95(13)°, N(1)-Cr(1)-N(3) = 154.46(14)°, N(1)-Cr(1)-Cl(1) = 103.24(13)°, N(3)-Cr(1)-Cl(1) = 102.29(11)°, N(2)-Cr(1)-Cl(1) = 175.61(10)°]. Some of the bond distances and angles of the ligand backbone are different from complex **5.2**. The C=N and the N_{pyr}-C_{ortho} bonds have been lengthened, by an average of approximately 0.025 Å and 0.035 Å respectively, and the C_{imine}-C_{ortho} bonds has been lengthened correspondingly, by approximately 0.035 Å.

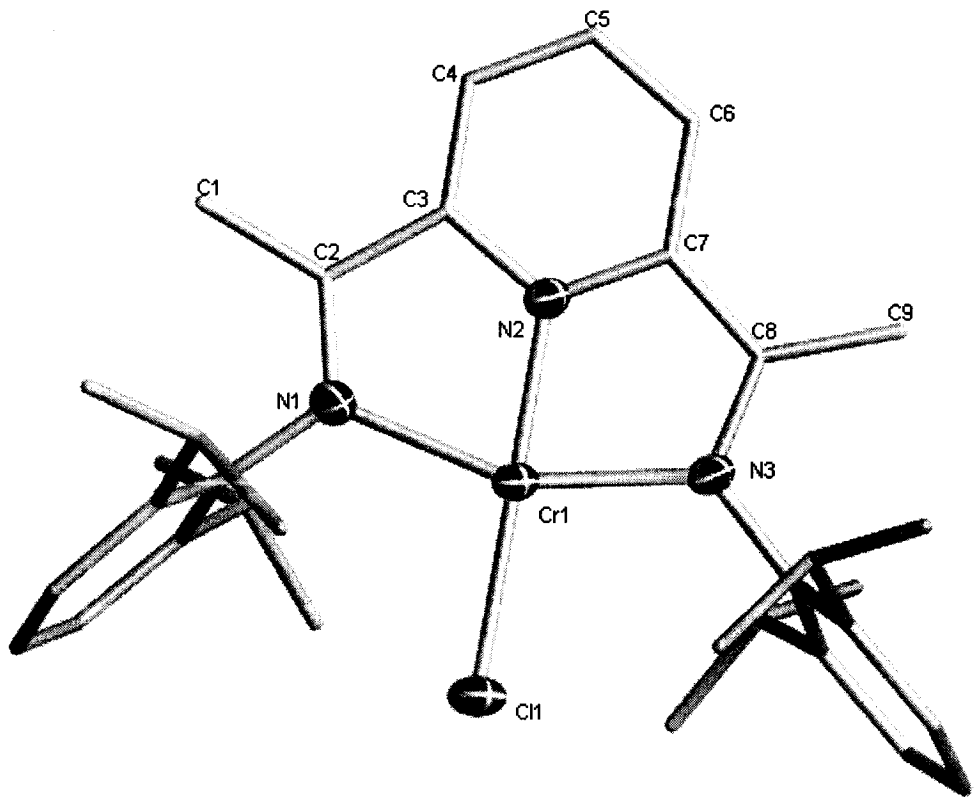

Figure 5.3. Partial thermal ellipsoid plot of **5.3**, drawn at the 30% probability level. Hydrogen atoms have been omitted for clarity.

Complex 5.4. The structure of complex **5.4** contains a tetracoordinate Cr center in a distorted square planar geometry (Figure 5.4), surrounded by the tridentate ligand [Cr(1)-N(1) = 2.022(4) Å, Cr(1)-N(2) = 1.953(4) Å, Cr(1)-N(3) = 2.020(4) Å] and a molecule of THF [Cr(1)-O(1) = 2.071(3) Å, N(1)-Cr(1)-N(2) = 79.18(15)°, N(2)-Cr(1)-N(3) = 78.47(16)°, N(3)-Cr(1)-O(1) = 101.21(16)°, N(1)-Cr(1)-O(1) = 101.16(15)°, N(1)-Cr(1)-N(3) = 157.62(16)°, N(2)-Cr(1)-O(1) = 178.20(17)°]. The shortness of the C_{imino}-C_{Me} bond lengths [C(1)-C(2) = 1.416(7) Å, C(8)-C(9) = 1.443(7) Å] clearly diagnoses deprotonation of one of the two methyl groups with formation of a $C{=}CH_2$ unit which is disordered over the two positions. Accordingly, the two C=N bond distances of the imino functions have been lengthened [N(1)-C(2) = 1.374(6) Å, N(3)-C(8) = 1.372(6) Å]. The other geometrical parameters of the ligand show only slight modifications and are in-between those of complex **5.1** and **5.3**.

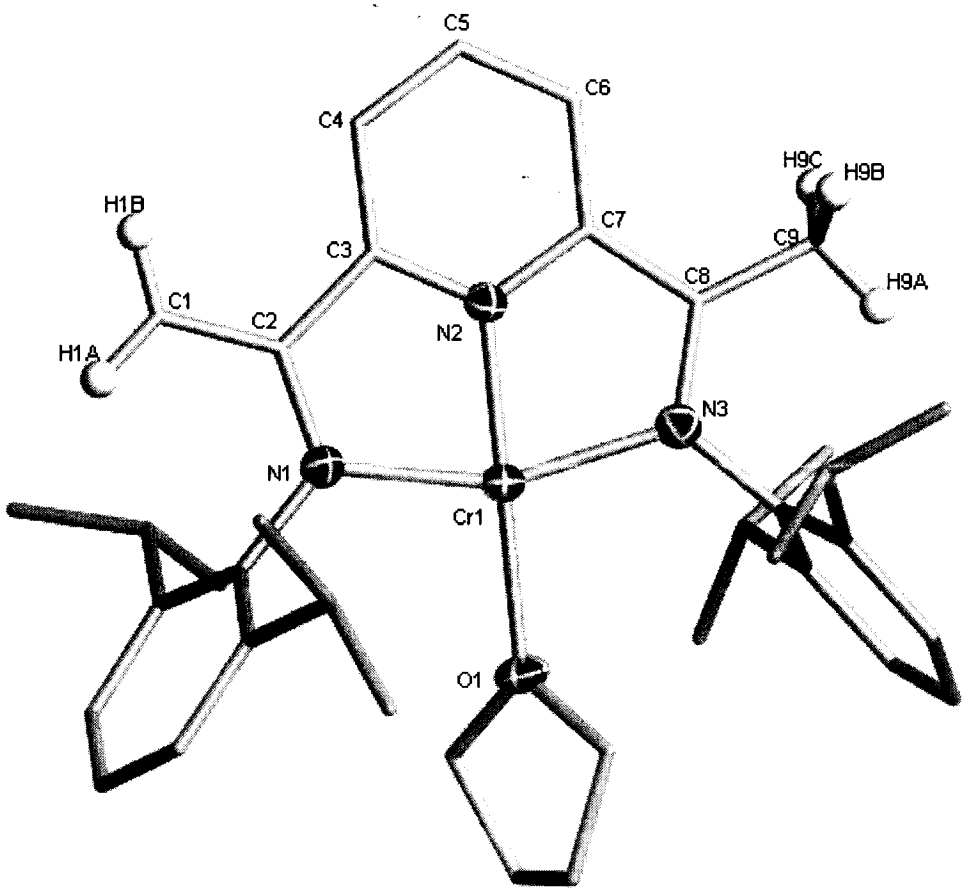

Figure 5.4. Partial thermal ellipsoid plot of **5.4**, drawn at the 30% probability level. Selected H atoms have been omitted for clarity.

Complex 5.5. Complex **5.5** (Figure 5.5) consists of a tetracoordinate Cr center bound to the three nitrogen atoms of the ligand system [Cr(1)-N(1) = 2.034(4) Å, Cr(1)-N(2) = 1.993(3) Å, Cr(1)-N(3) = 2.028(4) Å] and a methyl group [Cr(1)-C(34) = 2.129(4) Å]. In turn, the methyl group bridges a THF-solvated Li cation [Li(1)-C(34) = 2.391 Å, Cr(1)-C(34)-Li(1) = 172.28°]. The geometry about the Cr center is distorted square planar with the methyl group raised slightly from the plane defined by the ligand [N(1)-Cr(1)-N(2) = 77.72(16)°, N(1)-Cr(1)-N(3) = 155.13(14)°, N(1)-Cr(1)-C(34) = 103.32(17)°, N(2)-Cr(1)-N(3) = 77.55(16)°, N(2)-Cr(1)-C(34) = 172.97(16)°, N(3)-Cr(1)-C(34) = 101.54(16)°]. Similar to complex **5.4**, the C_{methyl}-C_{imine} bond lengths have been shortened to an average of 1.426 Å [C(13)-C(14) = 1.465(6) Å, C(20)-C(21) = 1.387(6) Å]. Consequently, the C=N bond distances have also been lengthened [N(1)-C(14) = 1.383(5) Å, N(3)-C(20) = 1.381(5) Å]. Other modifications to the ligand backbone include a slightly larger degree

of elongation and contraction than seen for complex **5.4** in the Np_{yr}-C_{ortho} and C_{imine}-C_{ortho} distances.

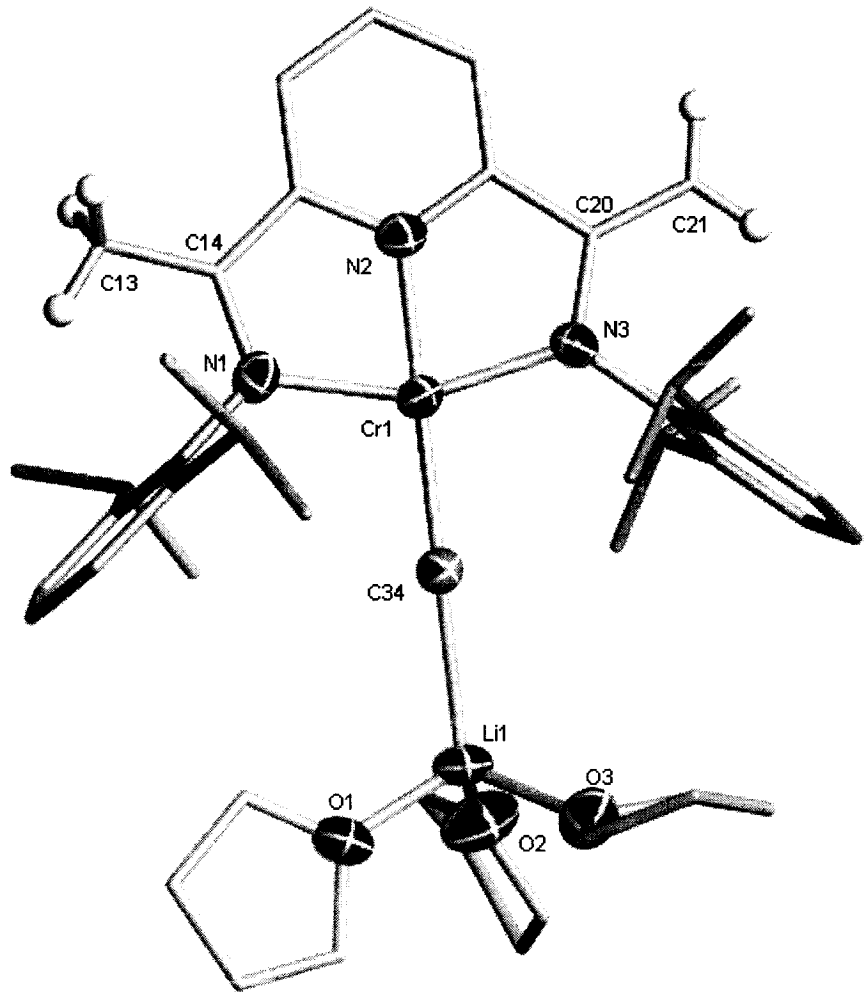

Figure 5.5. Partial thermal ellipsoid plot of **5.5**, drawn at the 30% probability level. Selected hydrogen atoms have been omitted for clarity.

Complex 5.6. The structure of complex **5.6** (Figure 5.6) consists of a pentacoordinate Cr center bound to the tridentate ligand [Cr(1)-N(1) = 2.105(8) Å, Cr(1)-N(2) = 1.923(8) Å, Cr(1)-N(3) = 2.131(8) Å] and two Cl atoms [Cr(1)-Cl(1) = 2.468(4) Å, Cr(1)-Cl(2) = 2.526(4) Å] in a severely distorted square pyramidal geometry ($\tau = 0.17$).[35] The axial site is occupied by the second Cl atom [N(1)-Cr(1)-Cl(2) = 99.9(2)°, N(2)-Cr(1)-Cl(2) = 133.2(2)°, N(3)-Cr(1)-Cl(2) = 99.9(3)°] even though the angle subtended at the chromium center by the two Cl atoms is narrow [Cl(1)-Cr(1)-Cl(2) = 82.11(11)°]. The other atoms occupy the equatorial positions [N(1)-Cr(1)-N(2) = 77.6(3)°, N(1)-Cr(1)-N(3) =

154.9(3)°, N(1)-Cr(1)-Cl(1) = 98.6(2)°, N(2)-Cr(1)-N(3) = 77.6(3)°, N(2)-Cr(1)-Cl(1) = 144.7(2)°, N(3)-Cr(1)-Cl(1) = 99.2(2)°]. In turn, the Cl atoms are bridging one -$AlMe_2$ unit [Cl(1)-Al(1) = 2.248(5) Å, Cl(2)-Al(1) = 2.233(5) Å, Al(1)-C(34) = 1.957(11) Å, Al(1)-C(35) = 1.948(12) Å] in which the Al center is found in a distorted tetrahedral geometry [Cl(1)-Al(1)-Cl(2) = 94.11(16)°, Cl(1)-Al(1)-C(34) = 106.3(4)°, Cl(1)-Al(1)-C(35) = 109.8(4)°, Cl(2)-Al(1)-C(34) = 109.7(4)°, Cl(2)-Al(1)-C(35) = 110.0(4)°, C(34)-Al(1)-C(35) = 123.0(5)°]. The bond distances of the backbone are similar to those of complex **5.3**.

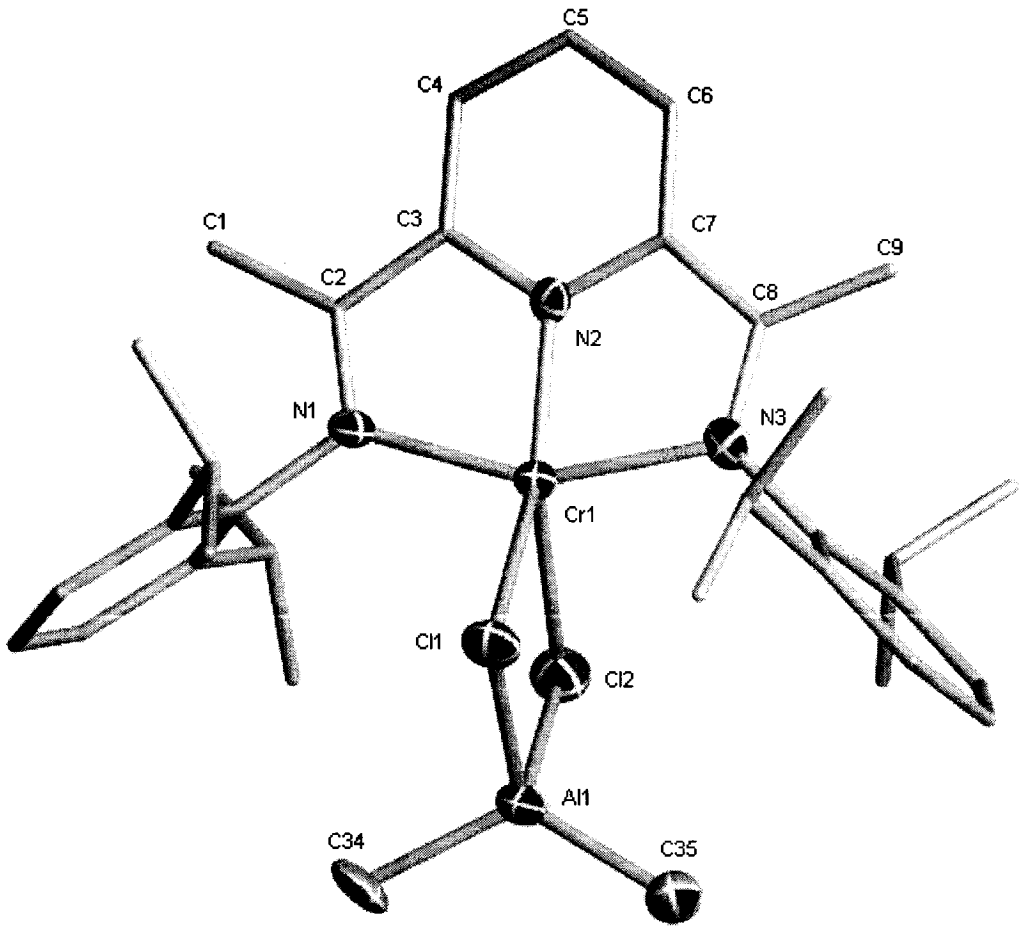

Figure 5.6. Partial thermal ellipsoid plot of **5.6**, drawn at the 30% probability level. Hydrogen atoms have been omitted for clarity.

Complex 5.7. The Cr center of complex **5.7** adopts a distorted square planar arrangement (Figure 5.7) very similar to those observed in **5.3** and **5.4**. The square plane is formed by the three nitrogen donor atoms of the ligand [Cr(1)-N(1) = 1.944(16) Å, Cr(1)-N(2) =

1.877(12) Å, Cr(1)-N(3) = 1.929(12) Å] and a terminal methyl group [Cr(1)-C(34) = 1.959(13) Å, N(1)-Cr(1)-N(2) = 81.5(7)°, N(2)-Cr(1)-N(3) = 81.7(8)°, N(3)-Cr(1)-C(34) = 98.5(8)°, N(1)-Cr(1)-C(34) = 98.3(7)°, N(1)-Cr(1)-N(3) = 163.18(16)°, N(2)-Cr(1)-C(34) = 179.09(19)°]. The ligand system appears to deviate slightly from complex **5.3** showing a curious lengthening of all bonds of the backbone. The largest stretch is in the C=N bond distance, from an average of 1.321 Å to 1.362 Å. However, the most extreme modification is a parallel elongation of approximately 0.03 Å in the C_{imine}-C_{ortho} bond length, as opposed to an equivalent contraction of the distance.

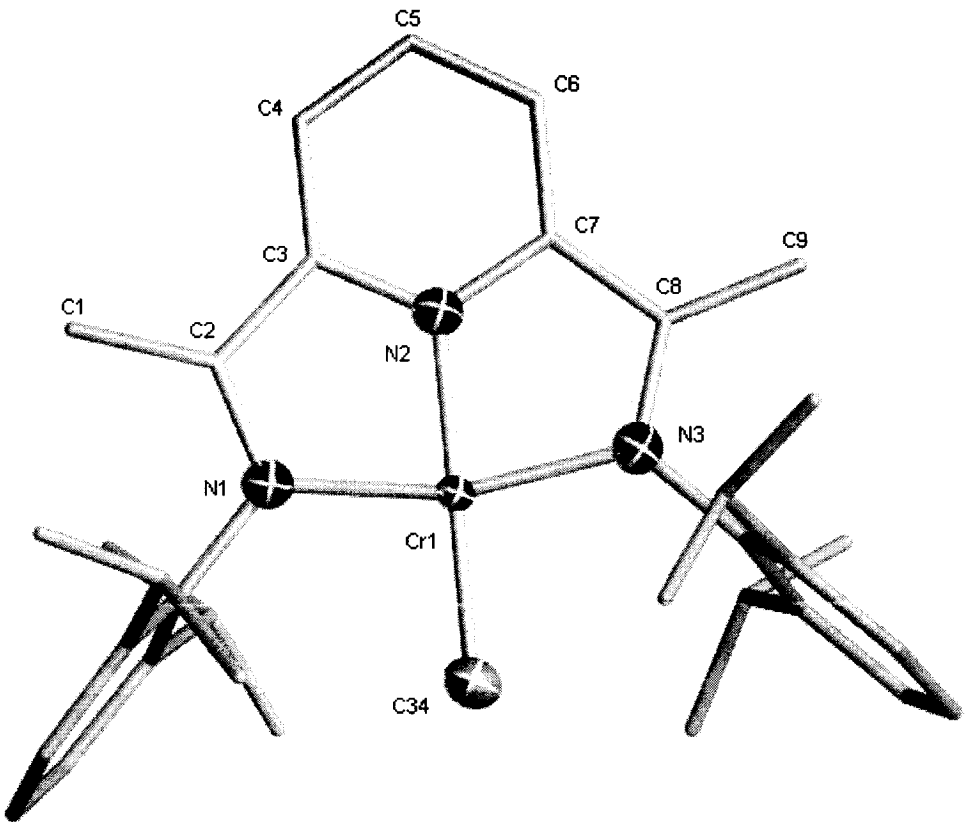

Figure 5.7. Partial thermal ellipsoid plot of **5.7**, drawn at the 30% probability level. Hydrogen atoms have been omitted for clarity.

Complex 5.8. The crystal structure of **5.8** is very similar to the Fe analogue (complex **4.5** in Chapter 4),[19] showing the ligand system connected to a toluene-solvated chromium atom and to a $^{i}Bu_2Al(\mu\text{-}Cl)Al^{i}Bu$ unit bound to the nitrogen atoms of the folded ligand (Figure 5.8). One Al is found coordinated to all three nitrogens of the ligand [Al(1)-N(1)

= 2.140(5) Å, Al(1)-N(2) = 2.002(5) Å, Al(1)-N(3) = 1.924(5) Å], an ^{i}Bu moiety [Al(1)-C(41) = 1.967(6) Å] and a chlorine atom [Al(1)-Cl = 2.393(3) Å] in a geometry intermediate between trigonal bipyramidal and square pyramidal (τ = 0.493)[35] [N(1)-Al(1)-N(2) = 77.5(2)°, N(1)-Al(1)-N(3) = 142.7(2)°, N(1)-Al(1)-Cl(1) = 104.55(16)°, N(1)-Al(1)-C(41) = 94.9(2)°, N(2)-Al(1)-N(3) = 82.4(2)°, N(2)-Al(1)-Cl(1) = 85.09(16)°, N(2)-Al(1)-C(41) = 172.3(3)°, N(3)-Al(1)-Cl(1) = 104.56(17)°, N(3)-Al(1)-C(41) = 103.4(3)°, Cl(1) -Al(1)-C(41) = 98.2(2)°]. The Cl atom and the N of the pyridine ring in turn bridge the second Al atom [Al(2)-Cl = 2.291(3) Å, Al(2)-N(2) = 1.963(5) Å], whose coordination is completed by two ^{i}Bu groups [Al(2)-C(45) = 1.968(7) Å, Al(2)-C(49) = 1.952(7) Å] in a distorted tetrahedral arrangement [N(2)-Al(2)-Cl = 88.80(16)°, N(2)-Al(2)-C(45) = 111.9(3)°, N(2)-Al(2)-C(49) = 116.3(3)°, Cl-Al(2)-C(45) = 108.5(2)°, Cl-Al(2)-C(49) = 104.0(2)°, C(45)-Al(2)-C(49) = 121.4(3)°]. The ligand appears folded and the major distortion is observable around the pyridine ring, which adopts an η^4 coordination with a Cr atom [Cr(1)-C(3) = 2.119(6) Å, Cr(1)-C(4) = 1.952(7) Å, Cr(1)-C(5) = 2.000(7) Å, Cr(1)-C(6) = 2.158(7) Å]. In turn, the Cr atom is η^6-bound to a molecule of toluene with a distance to the centroid of 1.541(7) Å. The pyridine ring is no longer planar [N(2)-C(3)-C(4) = 117.4(5)°, C(3)-C(4)-C(5) = 112.8(6)°, C(4)-C(5)-C(6) = 117.7(6)°, C(5)-C(6)-C(7) = 121.1(6)°, C(6)-C(7)-N(2) = 113.9(5)°, C(3)-N(2)-C(7) = 108.6(5)°], with the largest deviation occurring at the N of the ring. Bound to the ring and two Al atoms, the N is now clearly sp^3 [C(3)-N(2)-C(7) = 108.6(5)°, C(3)-N(2)-Al(1) = 116.1(4)°, C(3)-N(2)-Al(2) = 113.7(4)°, C(7)-N(2)-Al(1) = 109.7(4)°, C(7)-N(2)-Al(2) = 105.1(4)°, Al(1)-N(2)-Al(2) = 103.0(2)°]. In comparison to the bond distances observed in all other complexes, drastic modifications are apparent in the ligand backbone. First of all, the disruption of aromaticity in the pyridine ring, due to the sp^3 nature of the N atom and the η^4-coordination of the Cr atom, has resulted in lengthening of all bonds in the pyridine ring [N(2)-C(3) = 1.459(8) Å, C(3)-C(4) = 1.428(8) Å, C(4)-C(5) = 1.395(9) Å, C(5)-C(6) = 1.438(10) Å, C(6)-C(7) = 1.440(9) Å, N(2)-C(7) = 1.457(7) Å]. The fact that the Cr atom is only bound to two thirds of the ring creates an asymmetric localization of the electron density throughout the rest of the ligand backbone. On the half of the ligand in which the pyridine *ortho*-C is bound to the Cr, the C=N and C_{imine}-C_{ortho} bonds assume semi-normal distances [N(1)-C(2) = 1.300(7) Å, C(2)-C(3) = 1.435(9) Å], as expected for

localization of the double bond on the imine function. However, the other half of the ligand backbone, that further away from the Cr coordination, assumes the opposite arrangement [N(3)-C(8) = 1.378(8) Å, C(8)-C(7) = 1.343(8) Å].

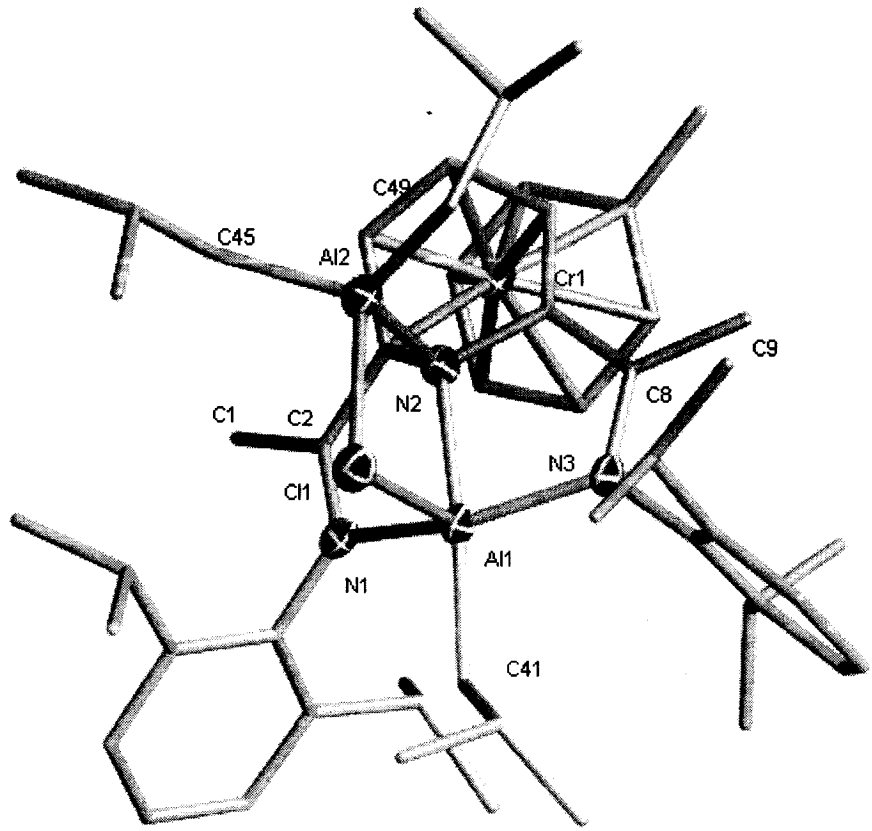

Figure 5.8. Partial thermal ellipsoid plot of **5.8**, drawn at the 30% probability level. Hydrogen atoms have been omitted for clarity.

Results and Discussion

Alkylation of trivalent chromium compounds very commonly affords reduction to the divalent state.[36] The trivalent bis-iminopyridine Cr(III) complexes seem to follow the same trend in spite of the unique electronic flexibility of this particular ligand system. We have previously described that treatment with a mild reducing agent such as Me_3Al affords a divalent complex in crystalline form.[3b] Therefore, in collaboration with Indu Vidyaratne, we turned our attention towards investigating the divalent oxidation state as a prerequisite to catalytically active species. The synthesis of the divalent {2,6-[2,6-(^{i}Pr)$_2$PhN=C(CH$_3$)]$_2$(C$_5$H$_3$N)}CrCl$_2$ (**5.1**) was carried out in a straight forward manner by

refluxing $CrCl_2(THF)_2$ in toluene and in the presence of the 2,6-diisopropylphenyl-bis-iminopyridine ligand. Purple microcrystals of **5.1** were isolated in 95% yield from THF while slow crystallization afforded X-ray quality crystals. The crystal structure (Figure 5.1) confirms that the complex possesses the same structure as the previously reported $FeCl_2$ and $CoCl_2$ adducts with an overall square pyramidal arrangement of the metal center.[1] The magnetic moment at room temperature [μ_{eff} = 3.6 μ_B] was substantially lower than expected for the d^4 configuration of high-spin divalent chromium, diagnosing the same phenomenon of charge transfer and consequent internal coupling previously observed with this ligand.[11,12,16,19]

As mentioned above, the reaction of the trivalent chromium derivative with $AlMe_3$ affords reduction to a divalent complex where two $AlMe_3$ residues are bridged to the metal center via bridging chlorine atoms.[3b] Different from the case of vanadium,[2] we find no evidence for direct alkylation of the divalent center. Conversely, the use of BzMgCl afforded attack of the pyridine ring *para*-position, which in turn triggered a dimerization process.[3b] Therefore, we have now attempted to form Cr-C bonds with MeLi.

The reaction with 2 equivalents of MeLi was carried out at -35°C in ether (Scheme 5.1) affording $\{2,6\text{-}[2,6\text{-}(^i Pr)_2PhN{=}C(CH_3)]_2(C_5H_3N)\}CrMe(\mu\text{-}Me)Li(THF)_3$ (**5.2**) in crystalline form (Figure 5.2). Formally speaking, the presence of two Me groups and one lithium cation assigns the monovalent state to the chromium atom. Similar to the case of Fe however,[16] the appearance of this complex as a rare case of monovalent chromium is probably deceiving and complex **5.2** can more realistically be described as a divalent chromium center coupled to a ligand radical anion. Inspection of the ligand backbone reveals slight modifications to the bond distances, representative of a one electron reduction of the ligand.[12] Table 5.6 compares selected ligand bond distances for all compounds discussed herein. In going from the $LCrCl_2$ derivative [L = $2,6\text{-}[2,6\text{-}(^i Pr)_2PhN{=}C(CH_3)]_2(C_5H_3N)$] to the reduced complex **5.2**, the C=N imine and the N_{pyr}-C_{ortho} bonds have lengthened by approximately 0.08 Å and 0.04 Å respectively, paralleled by a decrease in the C_{imine}-C_{ortho} bond lengths by approximately 0.06 Å. The observed contraction and elongation of the selected bonds in the ligand backbone is characteristic of ligand reduction towards a radical anion. In turn, the measured magnetic moment of

4.2 μ_B is in agreement with a high spin d^4 electronic configuration of a Cr(II) center antiferromagnetically coupled to a ligand radical anion.

Table 5.6. Comparative Distances of Selected Bonds (Å)

Complex	Cr-N	N_{imine}-C_{imine}	C_{imine}-C_{ortho}	C_{ortho}-N_{pyr}	C_{methyl}-C_{imine}
1	1.993(6)	1.294(9)	1.484(10)	1.329(9)	1.470(10)
	2.118(7)	1.298(9)	1.463(10)	1.359(9)	1.495(10)
	2.118(6)				
2	1.921(8)	1.376(10)	1.417(11)	1.380(11)	1.473(12)
	2.045(8)	1.379(10)	1.403(13)	1.392(11)	1.477(12)
	2.045(8)				
3	1.934(4)	1.311(5)	1.447(6)	1.374(5)	1.504(6)
	2.062(5)	1.331(5)	1.429(6)	1.384(5)	1.497(6)
	2.092(5)				
4	1.953(4)	1.374(6)	1.459(6)	1.360(6)	1.416(7)
	2.020(4)	1.372(6)	1.436(6)	1.366(6)	1.443(7)
	2.022(4)				
5	1.993(3)	1.383(5)	1.409(6)	1.359(5)	1.465(6)
	2.028(4)	1.381(5)	1.461(6)	1.372(5)	1.387(6)
	2.034(4)				
6	1.923(8)	1.327(12)	1.422(13)	1.377(11)	1.497(14)
	2.105(8)	1.334(11)	1.417(13)	1.404(11)	1.509(13)
	2.131(8)				
7	1.877(12)	1.363(12)	1.473(12)	1.388(10)	1.522(15)
	1.929(12)	1.360(10)	1.460(17)	1.394(15)	1.496(10)
	1.944(16)				
8		1.300(7)	1.435(9)	1.459(8)	1.512(9)
		1.378(8)	1.343(8)	1.457(7)	1.508(9)

Regardless of how we consider the oxidation state of the chromium center, the result of the alkylation reaction is the formation of a "reduced" species containing one additional electron with respect to the initial divalent complex. Previous work has demonstrated that deliberate reduction of the $FeCl_2$[14] and VCl_3[15] precursors may lead to the formation of species with an overall zerovalent appearance. However, in spite of the electron accepting ability of this remarkable ligand, the chemical reactivity in those cases remained that of a legitimately reduced metal species. The repetition of dinitrogen fixation by Fe,[14] V[15], Co[5,18b] and even Cr[37] displays the genuine low-valent type of behaviour of these reduced complexes. Furthermore, the catalytic activity was not

affected since the highly reduced Fe species produced the same type of polymer as its divalent precursor.[16]

Scheme 5.1

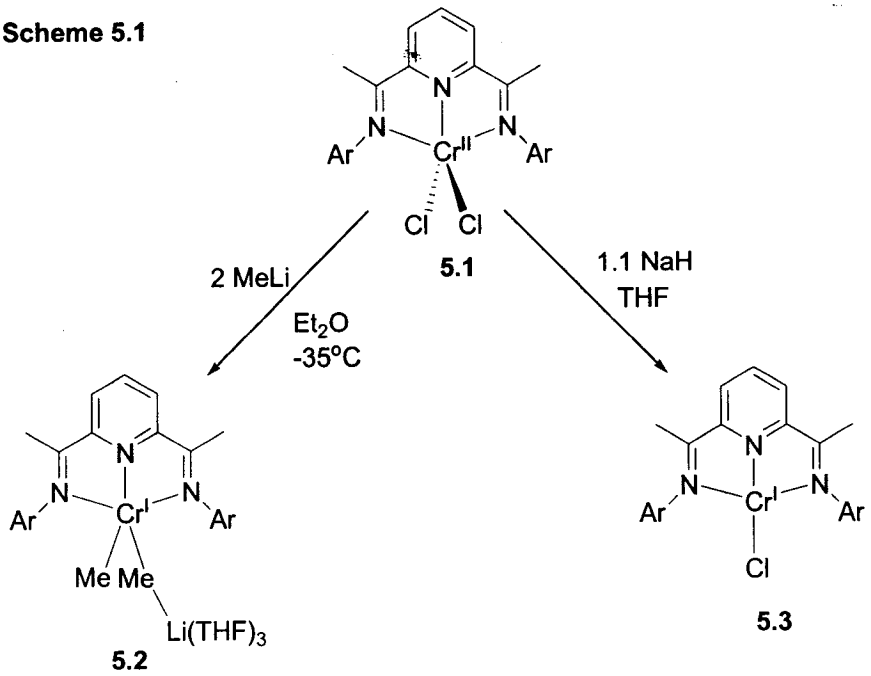

Reduction of complex **5.1** was further attempted with 2.2 equivalents of NaH as a reductant. The reaction was carried out in THF over a period of one week and gave a rather straightforward reduction yielding dark green X-ray quality crystals of {2,6-[2,6-(^{i}Pr)$_2$PhN=C(CH$_3$)]$_2$(C$_5$H$_3$N)}CrCl (**5.3**) (Scheme 5.1) in good yield. Complex **5.3**, whose appearance is that of a monovalent chromium complex (Figure 5.3), could also be prepared, albeit in much lower yield, by reducing the $CrCl_3$ derivative with 3.3 equivalents of NaH. The room temperature magnetic moment of 3.6 μ_B is in agreement with the description of the metal center as a high spin d^4 Cr(II) center in a square planar ligand field magnetically coupled to a radical anion. In accord, deviations in the ligand backbone distances, to a lesser extent than those seen for complex **5.2** (Table 5.6), suggest partial reduction of the ligand instead of the metal center.

In line with the behaviour of the Fe analogue,[16] and in spite of its low-valent appearance, **5.3** is an extremely active polymerization catalyst when treated with MAO (*vide infra*). Thus, we have attempted further alkylation in order to verify the stability of the "monovalent" oxidation state while in the presence of alkylating agents (as for

example during the polymerization reaction). The results of the alkylation of **5.3** with 1 equivalent of $LiCH_2Si(CH_3)_3$ or MeLi afforded {2-[2,6-(^{i}Pr)$_2$PhN=C(CH_3)]-6-[2,6-(^{i}Pr)$_2$PhN-C=CH_2](C_5H_3N)}Cr(THF) (**5.4**) and {2-[2,6-(^{i}Pr)$_2$PhN=C(CH_3)]-6-[2,6-(^{i}Pr)$_2$PhN-C=CH_2](C_5H_3N)}CrCH_3] [Li(THF)$_4$] (**5.5**) respectively (Scheme 5.2). The comparable crystal structures can be seen in Figures 5.4 and 5.5. In both of these new species one of the two methyl groups has undergone deprotonation, as witnessed by a decrease in the ketimine bond lengths corresponding to an increase in the C=N bond distances (Table 5.6). The fourth coordination site of **5.4** contains a molecule of THF and complex **5.5** is bound by a bridging methyl-Li unit. Therefore, it appears that the oxidation state has remained unmodified, at least with these particular alkylating agents. Accordingly, the magnetic moments [μ_{eff} = 3.5 and 3.8 μ_B] are very similar to that of **5.3** and in agreement with the d^5 intermediate-spin electronic configuration or a d^4 metal antiferromagnetically coupled to a ligand radical. However, as in **5.3**, the remaining bond distances of the ligand backbone are still altered with respect to the divalent precursor. A contraction in the C_{imine}-C_{ortho} bond distances, paralleled by an elongation of the N_{pyr}-C_{ortho} bond lengths suggests partial reduction of the ligand. In this case, the ligand system may retain the reduced state of complex **5.3**, as well as undergo mono-deprotonation to form a ligand mono-radical dianion.

The involvement of the imino-methyl groups in acid-base types of reactions with alkylating agents towards the formation of mono- and di-deprotonated forms of the ligand is documented in the chemical reactivity of this particular ligand system.[3b,4,7bc,8-10] In most of the cases, the mono-deprotonation preludes a curious dimerization reaction. This process engages the redox chemistry of the metal center. Conversely, the isolation of a complex in which the ligand has undergone only mono-deprotonation is a rare event, having only been witnessed for Li[7bc] and Ga.[38]

Scheme 5.2

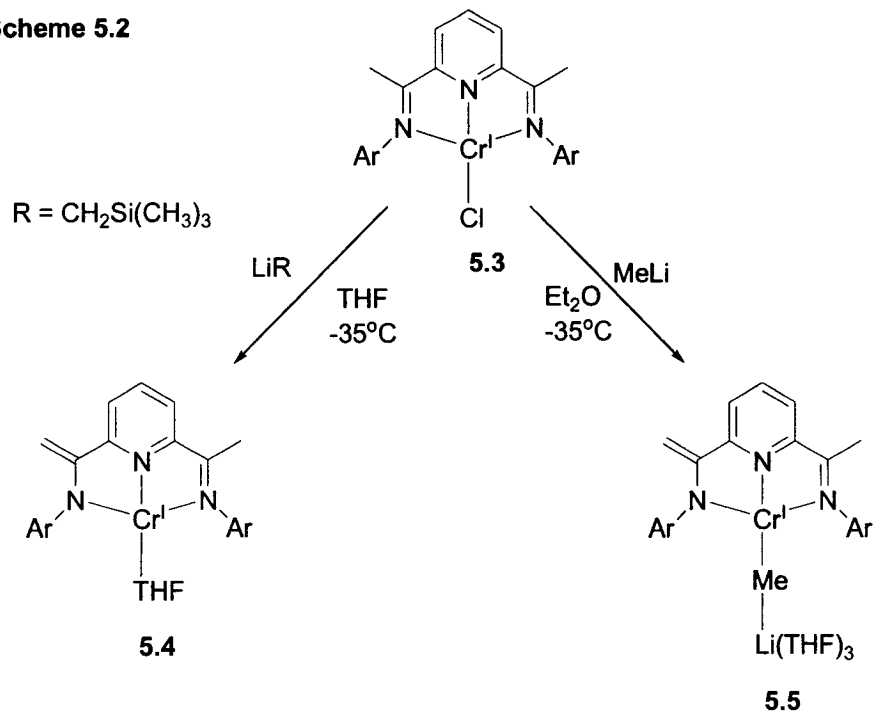

5.3 **5.4** **5.5**

As briefly mentioned above, complex **5.3** is a potent polymerization catalyst in combination with MAO. Because the reaction with MAO did not lead to isolable products, the reaction of **5.3** with $AlMe_3$ is a viable surrogate in the pursuit of a potential active species for the polymerization reaction. When complex **5.3** was reacted with excess $AlMe_3$ in toluene two products, $\{2,6\text{-}[2,6\text{-}(^{i}Pr)_2PhN{=}C(CH_3)]_2(C_5H_3N)\}Cr(\mu\text{-}Cl)_2Al(CH_3)_2$ (**5.6**) and $\{2,6\text{-}[2,6\text{-}(^{i}Pr)_2PhN{=}C(CH_3)]_2(C_5H_3N)\}CrCH_3$ (**5.7**), were isolated and separated by fractional crystallization from hexane and toluene respectively (Scheme 5.3). Both complexes have been characterized by X-ray crystallography and their representative structures can be found in Figures 5.6 and 5.7.

Complex **5.6** features the Cr center surrounded by the ligand and bound to two bridging Cl atoms. From the formal point of view, the connectivity suggests a formal oxidation state of +1 for the Cr center and therefore the formation of **5.6** is most likely the result of coordination of an $AlClMe_2$ unit to complex **5.3**, substantiated by a similar magnetic moment of 3.9 μ_B. The Al-bound Cl atom may be produced during the formation of complex **5.7**, which is a result of direct replacement of the Cl atom on the metal center with a CH_3 unit. Again, the ligand backbone deformations of both compounds suggest reduction of the ligand by one electron (Table 5.6)[12] and can

therefore be described as Cr(II) centers bound to ligand radical anions. The magnetic moment of 3.5 μ_B is in agreement with this description.

Scheme 5.3

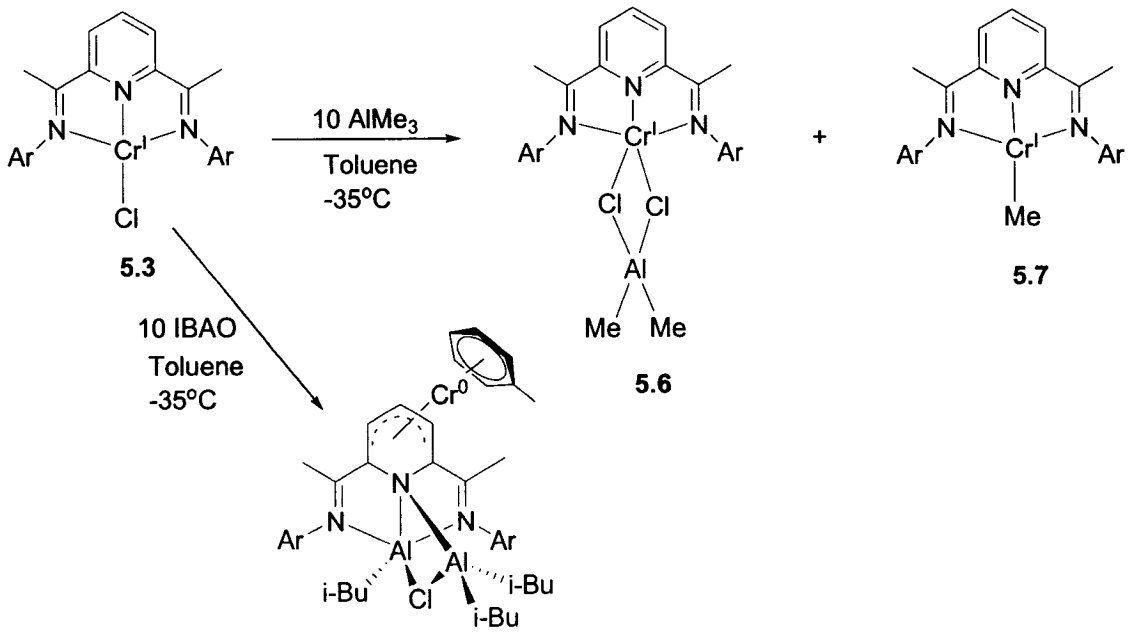

It is interesting to note that addition of activator to the highly active Cr(I) precatalyst (**5.3**) does not result in reduction of the metal center, contrary to the case of Co[18ab] or Fe.[19] However, addition of a different activator, namely IBAO, led to reduction of the metal center and partial transmetallation (Scheme 5.3), forming [η^4-{2,6-[2,6-(^{i}Pr)$_2$PhN=C(CH$_3$)]$_2$(C$_5$H$_3$N)} Al$_2$(^{i}Bu)$_3$(μ-Cl)]Cr-(η^6-C$_7$H$_8$) (**5.8**) (Figure 5.8).

The connectivity of **5.8** was revealed by single crystal X-ray diffraction (Figure 5.8) and is nearly identical to the analogous Fe structure described in Chapter 4.[19] The structure comprises three metal centers: two aluminum atoms and one chromium atom. The chromium atom has been partially dislodged from the ligand system and appears to be exclusively η^4-bound to part of the pyridine ring but not to the N donor atom. The three ligand donor atoms are instead used to hold an Al$_2$(^{i}Bu)$_3$Cl unit. The fact that the Al-containing unit is dicationic suggests that the ligand system is dianionic. The Cr center, on the other hand, could reasonably be present in the zerovalent state. The η^6-coordination of one molecule of toluene is also another indicating factor, given the well-

established ability of zerovalent chromium to form arene complexes. Taken together, the formation of **5.8** is the result of a three-electron reduction, two electrons housed on the ligand, the other one on the Cr center (assuming a *formally* monovalent **5.3**), and a partial transmetallation of the ligand system from Cr to Al. Similar to the analogous Fe compound,[19] complex **5.8** is paramagnetic, with a room temperature value of the magnetic moment of 1.7 μ_B. Calculations performed on the Fe system indicate that the electrons stored on the ligand can be found either in the singlet or triplet state,[19] and the paramagnetism in this case also suggests the presence of a mixture of the two states at room temperature. Although the NMR spectrum of **5.8** is contained within the range expected for a diamagnetic system, the peaks are very broad and overlapping, making their convincing assignment based on position and integration extremely difficult.

In Chapter 4, reaction of the bis-iminopyridine-$FeCl_2$ precursor with $AlEt_3$ or Al^iBu_3 resulted in the formation of similar compounds, including a species with the Fe atom partially extruded from the ligand, describing a possible deactivation pathway for the catalyst.[19] Having observed the partial transmetallation of the transition metal for the second time, and with a metal of a very different nature, it is tempting to speculate that this might be a general behaviour for complexes of this ligand system. The reaction pathway leading to the final metal extrusion and formation of (bis-iminopyridine)Al derivatives certainly may be, rather than metal reduction, responsible for catalyst deactivation and decomposition in these highly active systems. It is also interesting to note that, unlike the Cr complexes described herein, activation of the Fe-derivative with $AlMe_3$ also leads to deactivation products by reduction and transmetallation. Perhaps the greater stability of Cr-alkyls over Fe-alkyls may define the difference in reactivity with $AlMe_3$ and allow the isolation of active species, whereas the facile deactivation by IBAO may be a result of the more reducing nature of ^{i}Bu groups over Me groups.

Catalysis Results

The catalytic testing of each complex was performed under two sets of conditions for the purpose of comparison. The trivalent precursor $LCrCl_3$ was also prepared and tested for comparison under the same conditions. Polymerization under atmospheric ethylene pressure at room temperature proceeded in a Schlenk flask on a vacuum-

nitrogen line. Samples were also tested at 40 atm ethylene and 50°C in a high pressure reactor. In both cases, a pre-weighed amount of catalyst was dissolved in 100mL of toluene under N_2 prior to loading the reaction vessel. A solution of 500 equivalents of MAO in toluene was added to the catalyst and allowed to stir for 10 minutes. The Schlenk-line polymerizations were run for 60 minutes under a continuous flow of ethylene, after first evacuating the nitrogen. High-pressure polymerizations were heated to 50°C in an oil bath and charged with 40 atm of ethylene, maintaining the pressure throughout the run. Both polymerizations were quenched by addition of MeOH and HCl. The resulting polymer was collected by filtration and dried thoroughly prior to obtaining the mass. Table 5.7 outlines the results of the catalytic testing.

Each compound was tested under two sets of conditions: 1) atmospheric ethylene pressure at room temperature and 2) 40 atm ethylene at 50°C. Numerous comparisons can be made from the results outlined in Table 5.7. In all cases, raising the pressure and temperature of the reaction increased the activity of the catalyst significantly, normally by at least one order of magnitude or greater. The most fascinating observation, however, is the increase in activity with a decrease in oxidation state (runs 1/2, 3/4, and 7/8). The activity of the Cr(III) precursor under 40 atm ethylene, 357 gPE/mmol·h·atm, is only half that of the Cr(I) catalyst at atmospheric pressure, 759 gPE/mmol·h·atm. However, the decrease in activity in going from complex **5.3** to **5.2**, both of which contain Cr in the formally monovalent oxidation state, could be ascribed either to the different geometry and coordination number of the metal centers, with square planar being more active than square pyramidal, or to the presence of a weakly-bound MeLi unit able to afford other transformations. The highest activity recorded was accomplished by complex **5.7**, 4202 gPE/mmol·h·atm. Interestingly, complex **5.7** also displays an extremely high activity at atmospheric ethylene pressure, even higher than that of the corresponding bis-iminopyridine $FeCl_2$ precursor (~650 gPE/mmol·h·atm) under identical conditions.[4] Runs 10 and 11 compare the results of varying the amount of cocatalyst, showing a slight decrease in the catalytic activity upon doubling the MAO concentration. The increased amount of MAO may lead to an increase in the rate of deactivation or possibly coordination of excess TMA to a dormant species of the type $[Cr](\mu\text{-}Me)_2AlMe_2$.[39]

Table 5.7. Ethylene Polymerization Results

Run	Complex	Amount of Catalyst (μmol)	MAO (equivs)	$P(C_2H_4)$ (atm)	Temp. (°C)	Time (mins)	Yield PE (g)	Activity (gPE/mmol·hr·atm)	Mw	Mn	PDI
1	**$LCrCl_3$**	15.6	500	1	23	60	1.39	89	28,500	1,640	17.4
2	**$LCrCl_3$**	20.3	500	40	50	60	7.24	357	57,400	2,060	27.9
3	**5.1**	19.7	500	1	23	60	3.05	155	8,250	1,100	7.5
4	**5.1**	22.8	500	40	50	30	28.24	2477	9,280	2,650	3.5
5	**5.2**	15.2	500	1	23	60	1.74	114	26,600	1,580	16.8
6	**5.2**	10.2	500	40	50	60	9.82	966	34,200	1,970	17.4
7	**5.3**	13.2	500	1	23	60	10.04	759	8,010	3,090	2.6
8	**5.3**	22.8	500	40	50	60	68.71	3014	41,000	1,710	24.0
9	**5.4**	16.5	500	1	23	60	2.72	165			
10	**5.4**	23.1	500	40	50	60	61.23	2645	202,100	1,810	111.7
11	**5.4**	31.4	1000	40	50	60	67.8	2160			
12	**5.7**	17.1	500	1	23	60	19.2	1200			
13	**5.7**	18.8	500	40	50	60	79	4202	27,600	1,650	16.7

Most of the polymer samples were analyzed by GPC and selected results can be seen in Figure 5.9. All samples display a broad distribution in the molecular weights, sometimes even exhibiting bimodal nature. The major trends to be observed are an increase in the molecular weight of the polymer with an increase in pressure for the Cr(III) and Cr(II) adducts, both displaying very similar GPC traces. The GPC of complex **5.3**, the analogous Cr(I) catalyst, is also very similar to the Cr(III) and Cr(II) traces, but undergoes a decrease in molecular weight upon an increase in ethylene pressure. The similarities in the GPC and the increase in activity from Cr(III) to Cr(I) suggest potentially the same active species in all three cases. However, from previous results we know that the Cr(III) adduct is easily reduced to an inactive state upon addition of $AlMe_3$. The formation of the active species in this case may only be a minor product, therefore accounting for the low activity. However, the Cr(II) complex may undergo a more facile transformation into the active species than Cr(III), and therefore be more active. Of course these are mere speculations and more research is needed into determining the active species of the Cr(III) and Cr(II) adducts. Interestingly, complex **5.7**, the main product of activation of **5.3** with $AlMe_3$, shows almost identical polymer molecular weight distribution to **5.3**, suggesting the formation of the same active species. Therefore complex **5.3** is a precursor to complex **5.7**, which is a precursor to the active species. Complexes **5.2** and **5.4**, on the other hand, have a similar bimodal distribution, indicative of competing active species, or a change in the active species with time. According to previous results, the newly-formed C=C double bond is susceptible to reductive dimerization,[3-5] with the potential of transforming during the catalytic cycle. The presence of a weakly-bound MeLi unit could result in deprotonation of one of the methyl wings, as witnessed in the formation of complex **5.5**, thereby producing a similar complex to **5.4** and undergoing the same type of catalyst activation and producing similar polymers.

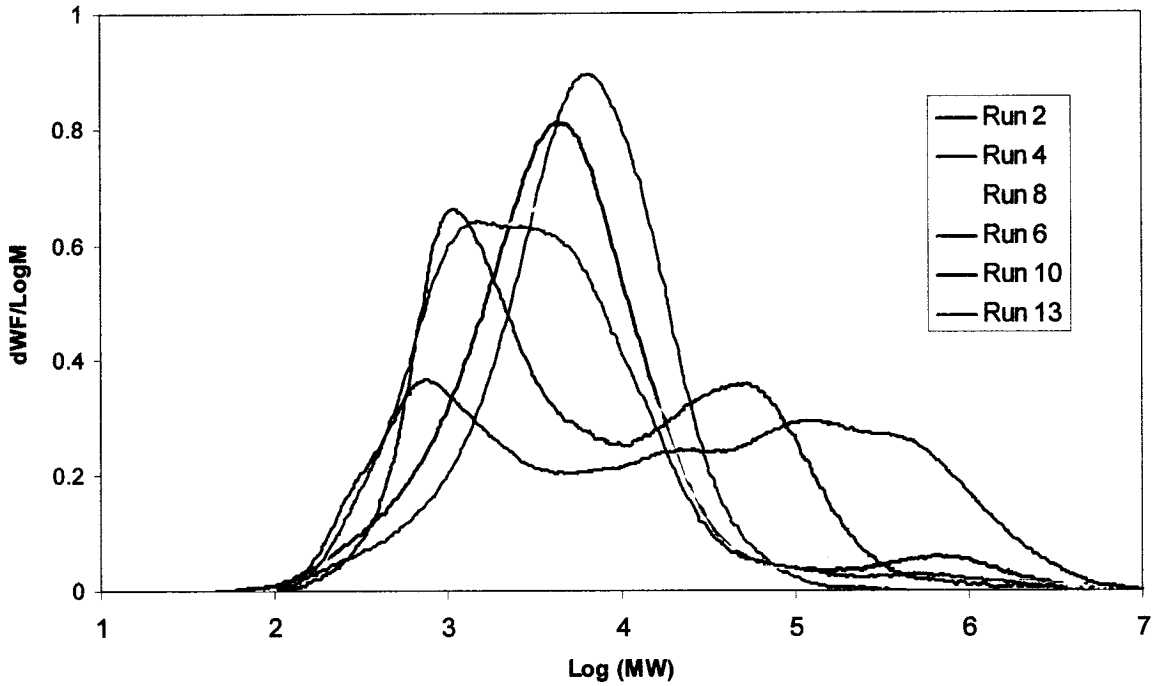

Figure 5.9. Gel permeation chromatogram of selected polymer samples.

From the results presented above, it appears that reduction of the system, with isolation of the electron on the ligand system at the expense of the metal center, leads to a more active catalyst precursor. The active species appears to involve reduction of the ligand system, similar to that seen for the Fe and Co systems, as well as alkylation.[16,18,19] It therefore appears that the catalytic activity is governed by the ability of the ligand to accept negative charge, and formation of active species requires the presence of electron density on the ligand backbone.

The main conclusion that can be put forth regarding catalysis is that activation towards the best catalytic system involves reduction and alkylation of the precursor. This scenario is very similar to that reported for Co, where activation of the $CoCl_2$ precursor involves an initial one electron reduction of the system, followed by alkylation of the square planar metal center. In both cases, the electron resides on the ligand backbone, maintaining the divalent oxidation state of the metal center. Accordingly, the polymer samples produced by Cr and Co have very similar molecular weight distributions. The activation scenario is distinctly different from the $FeCl_2$ derivative, which involves an initial two electron reduction of the system, with both electrons residing on the ligand

backbone. Consequently, a completely different polymer sample is produced by the Fe precursor, characterized by a much higher molecular weight and a majority of saturated end groups, hence suggesting a different activation mechanism.

Conclusion

In summary, low valent Cr species have been isolated, supported by the bis-iminopyridine ligand system, and shown to be highly active ethylene polymerization precatalysts. The activity of the monovalent Cr complexes were found to be much higher than the Cr(III) or Cr(II) precursors, suggesting that reduction of the system enhances the catalytic activity. The presence of the electron on the ligand backbone seems to be an important factor for increased activity by bis-iminopyridine catalysts. Similar to Fe, the deactivation pathway has been established, involving reduction and transmetallation of the ligand system to the Al cocatalyst.

References

(1) (a) Small, B. L.; Brookhart, M.; Bennett, A. M. A. *J. Am. Chem. Soc.* **1998**, *120*, 4049. (b) Britovsek, G. J. P.; Gibson, V. C.; Kimberley, B. S.; Maddox, P. J.; McTavish, S. J.; Solan, G. A.; White, A. J. P.; Williams, D. J. *Chem. Commun.* **1998**, 849.

(2) Reardon, D.; Conan, F.; Gambarotta, S.; Yap, G.; Wang, Q. *J. Am. Chem. Soc.* **1999**, *121*, 9318.

(3) (a) Reardon, D.; Aharonian, G.; Gambarotta, S.; Yap, G. P. A. *Organometallics* **2002**, *21*, 786. (b) Sugiyama, H.; Aharonian, G.; Gambarotta, S.; Yap, G. P. A.; Budzelaar, P. H. M. *J. Am. Chem. Soc.* **2002**, *124*, 12268.

(4) (a) Scott, J.; Gambarotta, S.; Korobkov, I.; Budzelaar, P. H. M. *J. Am. Chem. Soc.* **2005**, *127*, 13019. (b) See also Chapter 2.

(5) (a) Scott, J.; Gambarotta, S.; Korobkov, I. *Can. J. Chem.* **2005**, *83*, 279. (b) See also Chapter 8.

(6) (a) Bruce, M.; Gibson, V. C.; Redshaw, C.; Solan, G. A.; White, A. J. P.; Williams, D. J. *Chem. Commun.* **1998**, 2523. (b) Milione, S.; Cavallo, C.; Tedesco, C.; Grassi, A. *J. Chem. Soc. Dalton Trans.* **2002**, 1839. (c) Knijnenburg, Q.; Smits, J. M. M.; Budzelaar, P. H. M. *C. R. Chimie* **2004**, *7*, 865. (d) Knijnenburg, Q.; Smits, J. M. M.; Budzelaar, P. H. M *Organometallics* **2006**, *25*, 1036.

(7) (a) Clentsmith, G. K. B.; Gibson, V. C.; Hitchcock, P. B.; Kimberley, B. S.; Rees, C. W. *Chem. Commun.* **2002**, 1498. (b) Khorobkov, I.; Gambarotta, S.; Yap, G. P. A. *Organometallics* **2002**, *21*, 3088. (c) Blackmore, I. J.; Gibson, V. C.; Hitchcock,

P. B.; Rees, C. W.; Williams, D. J.; White, A. J. P. *J. Am. Chem. Soc.* **2005**, *127*, 6012.

(8) Enright, D.; Gambarotta, S.; Yap, G. P. A.; Budzelaar, P. H. M. *Angew. Chem. Int. Ed.* **2002**, *41*, 3873.

(9) Sugiyama, H.; Gambarotta, S.; Yap, G. P. A.; Wilson, D. R.; Thiele, S. K.-H. *Organometallics* **2004**, *23*, 5054.

(10) Bouwkamp, M. W.; Lobkovsky, E.; Chirik, P. J. *Inorg. Chem.* **2006**, *45*, 2.

(11) Sugiyama, H.; Korobkov, I.; Gambarotta, S.; Möller, A.; Budzelaar, P. H. M. *Inorg. Chem.* **2004**, *43*, 5771.

(12) (a) de Bruin, B.; Bill, E.; Bothe, E.; Weyhermüller, T.; Wieghardt, K. *Inorg. Chem.* **2000**, *39*, 2936. (b) Budzelaar, P. H. M.; de Bruin, B.; Gal, A. W.; Wieghardt, K.; van Lenthe, J. H. *Inorg. Chem.* **2001**, *40*, 4649. (c) Bart, S. C.; Chlopek, K.; Bill, E.; Bouwkamp, M. W.; Lobkovsky, E.; Neese, F.; Wieghardt, K.; Chirik, P. J. *J. Am. Chem. Soc.* **2006**, *128*, 13901.

(13) Knijnenburg, Q.; Hetterscheid, D.; Kooistra, T. M.; Budzelaar, P. H. M. *Eur. J. Inorg. Chem.* **2004**, 1204.

(14) (a) Bart, S. C.; Lobkovsky, E.; Chirik, P. J. *J. Am. Chem. Soc.* **2004**, *126*, 13794. (b) Scott, J. Chapter 6.

(15) Vidyaratne, I.; Gambarotta, S.; Korobkov, I.; Budzelaar, P. H. M. *Inorg. Chem.* **2005**, *44*, 1187.

(16) (a) Scott, J.; Gambarotta, S.; Korobkov, I.; Budzelaar, P. H. M. *Organometallics* **2005**, *24*, 6298. (b) See also Chapter 3.

(17) Bouwkamp, M. W.; Bart, S. C.; Hawrelak, E. J.; Trovitch, R. J.; Lobkovsky, E.; Chirik, P. J. *Chem. Commun.* **2005**, 3406.

(18) (a) Kooistra, T. M.; Knijnenburg, Q.; Smits, J. M. M.; Horton, A. D.; Budzelaar, P. H. M.; Gal, A. W. *Angew. Chem. Int. Ed.* **2001**, *40*, 4719. (b) Gibson, V. C.; Humphries, M. J.; Tellmann, K. P.; Wass, D. F.; White, A. J. P.; Williams, D. J. *Chem. Commun.* **2001**, 2252. (c) Steffen, W.; Blömker, T.; Kleigrewe, N.; Kehr, G.; Fröhlich, R.; Erker, G. *Chem. Commun.* **2004**, 1188. (d) Kleigrewe, N.; Steffen, W.; Blömker, T.; Kehr, G.; Fröhlich, R.; Wibbeling, B.; Erker, G.; Wasilke, J.-C.; Wu, G.; Bazan, G. C. *J. Am. Chem. Soc.* **2005**, *127*, 13955.

(19) (a) Scott, J.; Gambarotta, S.; Korobkov, I.; Knijnenburg, Q.; de Bruin, B.; Budzelaar, P. H. M. *J. Am. Chem. Soc.* **2005**, *127*, 17204. (b) See also Chapter 4.

(20) Esteruelas, M. A.; López, A. M.; Méndez, L.; Oliván, M.; Oñate, E. *Organometallics* **2003**, *22*, 395.

(21) Small, B. L.; Carney, M. J.; Holman, D. M.; O'Rourke, C. E.; Halfen, J. A. *Macromolecules* **2004**, *37*, 4375.

(22) Hogan, J. P.; Banks, R. L. Phillips Petroleum Co., U.S. Patent No. 2825721, 1958.

(23) (a) Karapinka, G. L. Union Carbide Corp., DE. 1808388, **1970**. (b) Karol, F. J.; Karapinka, G. L.; Wu, C.; Dow, A. W.; Johnson, R. N.; Carrick, W. L. *J. Polym.*

Sci., Polym. Chem. Ed. **1972**, *10*, 2621. (c) Karapinka, G. L. Union Carbide Corp., US. 3709853, **1973**.

(24) (a) Thomas, B. J.; Noh, S. K.; Schulte, G. K.; Sendlinger, S. C.; Theopold, K. H. *J. Am. Chem. Soc.* **1991**, *113*, 893. (b) Bhandari, G.; Kim, Y.; McFarland, J. M.; Rheingold, A. L.; Theopold, K. H. *Organometallics* **1995**, *14*, 738. (c) Liang, Y.; Yap, G. P. A.; Rheingold, A. L.; Theopold, K. H. *Organometallics* **1996**, *15*, 5284. (d) White, P. A.; Calabrese, J.; Theopold, K. H. *Organometallics* **1996**, *15*, 5473. (e) Theopold, K. H. *CHEMTECH* **1997**, *27*, 26. (f) Emrich, R.; Heinemann, O.; Jolly, P. W.; Krüger, C.; Verhownik, G. P. J. *Organometallics* **1997**, *16*, 1511. (g) Theopold, K. H. *Eur. J. Inorg. Chem.* **1998**, 15. (h) Döhring, A.; Göhre, J.; Jolly, P. W.; Kryger, B.; Rust, J.; Verhownik, G. P. J. *Organometallics* **2000**, *19*, 388. (i) Jensen, V. R.; Angermund, K.; Jolly, P. W.; Børve, K. J. *Organometallics* **2000**, *19*, 403. (j) Döhring, A.; Jensen, V. R.; Jolly, P. W.; Thiel, W.; Weber, J. C. *Organometallics* **2001**, *20*, 2234. (k) Enders, M.; Fernández, P.; Ludwig, G.; Pritzkow, H. *Organometallics* **2001**, *20*, 5005. (l) Döhring, A.; Jensen, V. R.; Jolly, P. W.; Thiel, W.; Weber, J. C. In *Organometallic Catalysts and Olefin Polymerization*; Blom, R., Follestad, A., Rytter, E., Tilset, M., Ystenes, M., Eds.; Springer-Verlag: Berlin, 2001; p 127.

(25) (a) Coles, M. P.; Gibson, V. C. *Polym. Bull.* **1994**, *33*, 529. (b) Coles, M. P.; Dalby, C. I.; Gibson, V. C.; Little, I. R.; Marshall, E. L.; Ribeiro da Costa, M. H.; Mastroianni, S. *J. Organomet. Chem.* **1999**, *591*, 78.

(26) (a) Gibson, V. C.; Maddox, P. J.; Newton, C.; Redshaw, C.; Solan, G. A.; White, A. J. P.; Williams, D. J. *Chem. Commun.* **1998**, 1651. (b) Kim, W.-K.; Fevola, M. J.; Liable-Sands, L. M.; Rheingold, A. L.; Theopold, K. H. *Organometallics* **1998**, *17*, 4541. (c) Gibson, V. C.; Newton, C.; Redshaw, C.; Solan, G. A.; White, A. J. P; Williams, D. J. *Eur. J. Inorg. Chem.* **2001**, 1895. (d) McAdams, L. A.; Kim, W.-K.; Liable-Sands, L. M.; Guzei, A. I.; Rheingold, A. L.; Theopold, K. H. *Organometallics* **2002**, *21*, 952.

(27) (a) Gibson, V. C.; Newton, C.; Redshaw, C.; Solan, G. A.; White, A. J. P.; Williams, D. J. *J. Chem. Soc., Dalton Trans.* **1999**, 827. (b) Gibson, V. C.; Mastroianni, S.; Newton, C.; Redshaw, C.; Solan, G. A.; White, A. J. P.; Williams, D. J. *J. Chem. Soc., Dalton Trans.* **2000**, 1969. (c) Jones, D. J.; Gibson, V. C.; Green, S. M.; Maddox, P. J. *Chem. Commun.* **2002**, 1038.

(28) (a) Köhn, R. D.; Haufe, M.; Mihan, S.; Lilge, D. *Chem. Commun.* **2000**, 1927. (b) Köhn, R. D.; Haufe, M.; Kociok-Köhn, G.; Grimm, S.; Wasserscheid, P.; Keim, W. *Angew. Chem., Int. Ed.* **2000**, *39*, 4337. (c) Köhn, R. D.; Seifert, G; Kociok-Köhn, G.; Mihan, S.; Lilge, D.; Mass, H. In *Organometallic Catalysts and Olefin Polymerization*; Blom, R., Follestad, A., Rytter, E., Tilset, M., Ystenes, M., Eds.; Springer-Verlag, Berlin, 2001; p 147.

(29) Ikeda, H.; Manoi, T.; Nakayama, Y.; Yasuda, H. *J. Organomet. Chem.* **2002**, *648*, 226.

(30) Devore, D.; Feng, S. S.; Frazier, K. A.; Patton, J. T. (Dow Chemical) WO0069923, 2000.

(31) Vidyaratne, I.; Scott, J.; Gambarotta, S.; Korobkov, I.; Duchateau, R. R. J. *Organometallics* accepted.

(32) Tessier-Youngs, C.; Beachley Jr., O. T. *Inorg. Synth.* **1986**, *24*, 95.

(33) Blessing, R. *Acta Crystallogr.* **1995**, *A51*, 33.

(34) G. M. Sheldrick, Bruker AXS, Madison, WI, 2001.

(35) Addison, A. W.; Rao, T. N.; Reedijk, J.; van Rijn, J.; Verschoor, G. C. *J. Chem. Soc. Dalton Trans.* **1984**, 1349. The τ parameter helps to classify the geometry of five-coordinate complexes. The τ parameter is calculated by finding the difference between the two largest angles at the metal center and dividing by 60. For a perfect square pyramidal complex, $\tau = 0$ and for a perfect trigonal bipyramidal complex, $\tau = 1$. In cases where the actual geometry is ambiguous between square pyramidal and trigonal bipyramidal, the τ parameter helps to quantify the observed distortions.

(36) (a) Bhandari, G.; Kim, Y.; McFarland, J. M.; Rheingold, A. L.; Theopold, K. H. *Organometallics* **1995**, *14*, 738. b) MacAdams, L. A.; Buffone, G. P.; Incarvito, C. D.; Golen, J. A.; Rheingold, A. L.; Theopold, K. H. *Chem. Commun.* **2003**, 1164.

(37) (a) Vidyaratne, I.; Scott, J.; Gambarotta, S.; Budzelaar, P. H. M.; Korobkov, I. *manuscript submitted.* (b) See also Chapter 7.

(38) Scott, J.; Phull, H,; Gambarotta, S.; Korobkov, I. *manuscript in preparation.*

(39) Kissin, Y. V.; Qian, C.; Xie, G.; Chen, Y. *J. Polym. Sci. A: Polym. Chem.* **2006**, *44*, 6159.

Chapter Six

Reduction of Bis-iminopyridine-$FeCl_2$ and Subsequent Dinitrogen Fixation

---

Introduction

Throughout history, serendipity has intervened in many of the most important chemical discoveries. Still others have been achieved through dedication and hard work towards preconceived ideas. And yet, despite decades of research, there are some chemical objectives that long remain the ambition of numerous scientists. Understanding and mimicking the nitrogenase enzyme in its ability to catalytically fixate and incorporate dinitrogen into useful nitrogen-containing molecules, such as ammonia, is one such aspiration.[1] Taunted by the facility with which nature performs this feat,[2] an even remotely equivalent level of human accomplishment has gone unrequited to date. Relying on the Haber-Bosch synthesis of ammonia from N_2 and H_2 under extreme conditions, humans have managed to overcome the difficulties associated with this transformation,[3] exploiting the reaction to its fullest throughout the world. In fact, the production of ammonia from N_2 has been cited as one of the most significant discoveries of the twentieth century, and is allegedly responsible for sustaining 50% of the world's population.[4] On the other hand, the energy demands for this synthesis are purported to utilize just less than 2% of the world's energy consumption.[5] The importance of discovering a catalytic process employing mild conditions becomes obvious not only from an energy conservation perspective but also as an intellectual challenge.

The inherent difficulty with this transformation lies not only in the fixation and activation of this exceedingly inert molecule, but also in the cleavage of the extremely strong N-N triple bond (dissociation energy = 945 kJ/mol).[6] Nature has devised a unique system for the incorporation of N_2 into the biosphere, involving the catalytic reduction of N_2 by the nitrogenase enzymes.[2] Upon fixation of the dinitrogen moiety to the Fe-Mo-S core, a series of steps involves the transfer of six electrons from the pyruvate electron pool towards the complete reduction of the N-N triple bond and subsequent cleavage.[7] Recently, the design of a catalytic cycle capable of producing ammonia from dinitrogen under very mild conditions was ingeniously devised by Schrock *et al.* via a cobaltocene-promoted reduction of the molybdenum-coordinated dinitrogen complex $[HIPTN_3N]MoN_2$, $\{[HIPTN_3N]^{3-} = [\{3,5\text{-}(2,4,6\text{-}i\text{-}Pr_3C_6H_2)_2C_6H_3NCH_2CH_2\}_3N]^{3-}\}$.[8] The system relies on similar concepts as those employed by nitrogenase, separating the source of electrons and the source of protons through the judicious use of suitable reagents. The step-wise reduction and protonation of the dinitrogen moiety has allowed for the study of numerous intermediates involved in the coveted transformation to ammonia. Recent results by our lab in thorium chemistry[9] suggest another possible strategy whereby the radical nature of the reduced, metal-bound dinitrogen moiety is enhanced enough to encourage hydrogen atom abstraction from the solvent.

Although the fixation of dinitrogen has been observed with almost all metals, research has been mainly focused on the use of strongly reducing, low-valent, early metal systems.[8-11] The large volume and variety of transformations involving early metal dinitrogen complexes, including partial reduction followed by elemental modifications or incorporation into the ligand system, has made early metal complexes the most popular targets for these studies and several recent reviews have detailed the latest developments in this area.[12] Dinitrogen chemistry involving late transition metals is substantially less developed than early metal or f-block systems, even though, interestingly, Fe is the protagonist in the unique performance of nitrogenase. Although late metal complexes seem inclined towards labile coordination of dinitrogen, it is now established that nitrogenase initially forms a dinitrogen complex, possibly *weakly*-bound, which then undergoes a step-wise reduction via multiple association-dissociation rounds between the Fe-protein and the Fe-Mo protein.[7] Indeed, dinitrogen complexes of Fe have been

observed on several occasions; in most cases displaying minimal activation of the N-N triple bond.[13-16] However, Holland *et al.* have described an end-on bridging dinitrogen complex of Fe supported by the *nacnac* ligand which, upon subsequent reduction, undergoes a two electron reduction of the triple bond.[14] To date, reduction towards a double bond is the greatest amount of activation witnessed for an Fe-bound N_2 moiety. Of note, the group of Peters demonstrated the ability to generate a bridging triple-bound Fe-dinitrogen complex through the six electron redox reaction between two $Fe^{IV}\equiv N$ complexes.[15a] By microscopic reversibility, the reverse reaction involving the six electron reduction of a bridging dinitrogen ligand towards two nitrido moieties should be kinetically possible.

The use of late transition metal complexes, and of Fe in particular, incorporating a ligand capable of accepting electrons and funneling the charge density towards a metal-bound dinitrogen unit may have potential as a reduction catalyst for dinitrogen. The possibility of dinitrogen fixation by late transition metal bis-iminoyridine complexes was discovered by Gibson with a cationic bis-iminopyridine Co(I) complex.[17] In this case, the dinitrogen unit was coordinated in an end-on terminal fashion and displayed very little activation of the triple bond, as indicated by the minimal lengthening of the N-N distance. The expected lability of the dinitrogen ligand was demonstrated by the ready exchange with a π-bound ethylene molecule.[17] A similar case of dinitrogen fixation obtained with a neutral Co(I) compound supported by a dimerized form of the ligand is reported in Chapter 8 and exhibits the shortest N-N bond of a cobalt-coordinated N_2 ligand published to date.[18] Unfortunately, further reduction of this complex has only led to intractable materials. Nonetheless, the first step of fixating the dinitrogen moiety has been accomplished.

Recently, fixation and two electron reduction of a bound dinitrogen unit was obtained upon addition of NaH to bis-iminopyridineVCl_3.[19] Unlike the Co complexes described above, the N_2 moiety assembles an end-on bridge between two metal centers, forming a dimer in which the N-N unit has been reduced by two electrons (Scheme 6.1). This type of multimetallic cooperative activation is more promising for reductive cleavage because the six electrons necessary for the complete reduction of the N-N triple

bond may be supplied by two metal centers instead of only one. However, once again, the addition of external reductants did not lead to isolable products.

Scheme 6.1

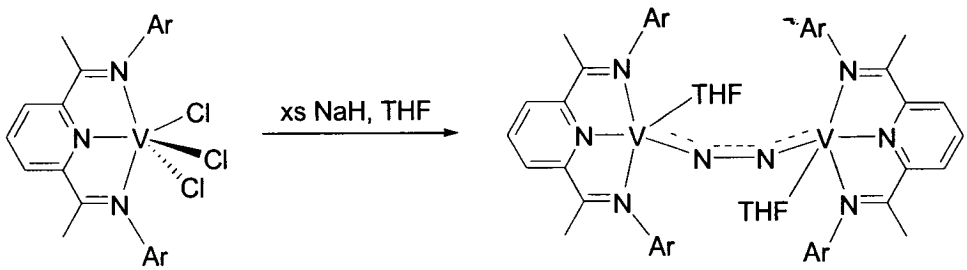

Concurrent to portions of the work described herein, the group of Chirik published the reduction of the bis-iminopyridine $FeCl_2$ complex with Na/Hg or $NaBEt_3H$.[16] The reaction afforded a double-dinitrogen complex with the formal appearance of a zerovalent Fe species (Scheme 6.2). Both dinitrogen moieties are terminally bound to the metal center in an end-on fashion and exhibit minimal activation of the triple bond. Studies have shown the coordination to be weak and easily replaced with other suitable donors like CO. A more accurate electronic description of the system is that of a divalent Fe center bound to a diradical ligand.[16,20] It is therefore curious that the electrons have not been made available to the N_2 ligand, suggesting a dimeric formation as a prerequisite to further reduction.

Scheme 6.2

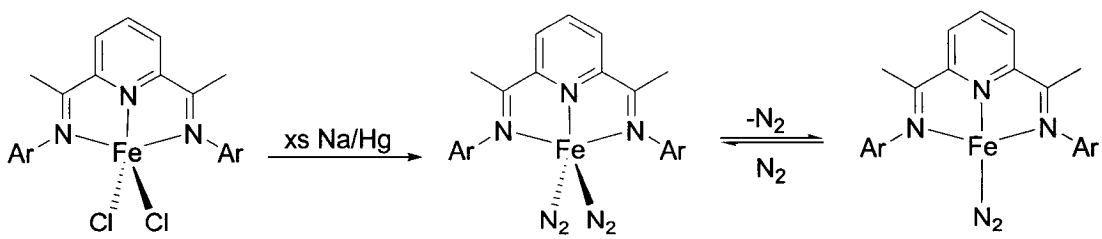

According to this hypothesis, work was carried out in collaboration with Indumathi Vidyaratne to attempt reduction of the chromium species (Chapter 7). As a

result, an unprecedented case of fixation, cleavage and partial hydrogenation was obtained with the chromium derivative of the same ligand system.[21]

Herein, we report the preliminary results of our exploration of the reduction of the bis-iminopyridine $FeCl_2$ complex using NaH as a reducing agent. Several complexes have been isolated, depending on the concentration of reducing agent, length of reaction time and other as-yet-unidentified variables. Work is being continued in this area by Indu Vidyaratne.

Experimental Section

All operations were performed either under a nitrogen atmosphere using standard Schlenk techniques or in a purified nitrogen-filled dry-box. The THF complex of $FeCl_2$ was prepared according to the standard procedure and the ligand 2,6-[2,6-(^{i}Pr)$_2$PhN=C(CH_3)]$_2$(C_5H_3N)[22] was prepared according to published procedures. Metallic sodium and NaH were purchased from Aldrich and washed with hexane under nitrogen to remove the oil. Infrared spectra were recorded on a Mattson 9000 and Nicolet 750-Magna FT-IR instrument from Nujol mulls prepared in a dry box. Samples for magnetic susceptibility measurements were weighed inside a dry box equipped with an analytical balance and sealed into calibrated tubes and the measurements were carried out at room temperature with a Gouy balance (Johnson Matthey). Magnetic moments were calculated following standard methods and corrections for underlying diamagnetism were applied to the data. NMR spectra were recorded on a Varian INOVA 500 spectrometer. Data for X-ray crystal structure determinations were obtained with a Bruker diffractometer equipped with a Smart CCD area detector.

Preparation of {2-[2,6-(^{i}Pr)$_2$PhN=C(CH_3)]-6-[2,6-(^{i}Pr)$_2$PhN-C=CH_2](C_5H_3N)}Fe(μ-N_2)Na(THF) (6.1).

A suspension of $FeCl_2(THF)_{1.5}$ (0.15 g, 0.64 mmol) and 2,6-[2,6-(^{i}Pr)$_2$PhN=C(CH_3)]$_2$(C_5H_3N) (0.306 g, 0.64 mmol) in THF (10 mL) was added to a suspension of 3.1 equivalents of NaH (0.048 g, 1.98 mmol) in THF (5 mL). The colour of the solution slowly changed from dark blue to dark brownish-red over the period of two days. Stirring was continued for an additional 5 days, the solvent was evaporated *in vacuo* and fresh

ether was added to the dark residue. Centrifugation allowed the separation of a dark brown solution from a mass of dark precipitates. Crystals of **6.1** grew from the mother liquor upon standing for a few days at room temperature (0.089 g, 0.13 mmol, 21% yield). IR (Nujol mull, cm^{-1}): ν 2956 (s), 2925 1(s), 2855 (s), 1912 (s), 1630 (m), 1573 (s), 1513 (w), 1463 (s), 1378 (s), 1366 (w), 1340 (w), 1324 (m), 1242 (m), 1211 (w), 1195 (w), 1099 (w), 1084 (w), 1056 (m), 1021 (w), 998 (m), 959 (w), 936 (w), 881 (m), 805 (s), 767 (w),759 (w), 740 (w), 727 (m), 693 (w). Anal. Calcd. (found) for $C_{37}H_{50}FeN_5NaO$ (%): C, 67.36 (66.72); H, 7.63 (7.15); N, 10.62 (10.23). [μ_{eff} = 6.5 μ_B].

Preparation of {2,6-[2,6-(^{i}Pr)$_2$PhN=C(CH$_3$)]$_2$(C$_5$H$_3$N)}Fe(μ-N$_2$)Na(Na(THF)$_2$) (6.2).

Method A: The $LFeCl_2$ complex was prepared *in situ* by mixing $FeCl_2(THF)_{1.5}$ (0.100 g, 0.43 mmol) with 2,6-[2,6-(^{i}Pr)$_2$PhN=C(CH$_3$)]$_2$(C$_5$H$_3$N) (0.205 g, 0.43 mmol) in THF (10 mL) overnight. The dark blue suspension was added to a suspension of NaH (6 equivalents, 0.062 g, 2.58 mmol) in THF (5 mL) and stirred for 5 days. The solvent was evaporated and the dark residue washed with ether to remove a bright magenta-coloured solution. Fresh THF was added to the remaining precipitates and the resulting suspension was centrifuged and layered with hexane. After 2 days at room temperature, dark brown crystals of **6.2** were isolated in 25 % yield (0.076 g, 0.10 mmol). IR (Nujol mull, cm^{-1}): ν 3048 (m), 2852 (s), 1899 (s), 1819 (w), 1584 (w), 1540 (w), 1462 (s), 1377 (s), 1356 (m), 1300 (s), 1258 (s), 1201 (w), 1174 (w), 1157 (w), 1095 (m), 1048 (s), 1000 (m), 972 (w), 953 (w), 939 (w), 915 (m), 892 (m), 807 (m), 795 (w), 776 (m), 755 (s), 708 (s), 658 (m). Anal. Calcd. (found) for $C_{41}H_{59}FeN_5Na_2O_2$ (%): C, 65.15 (64.79); H, 7.86 (7.85); N, 9.27 (8.90). [μ_{eff} = 5.6 μ_B].

Method B: The complex precursor $LFeCl_2$ was prepared *in situ* as described above and 4 equivalents of metallic Na (0.060 g, 2.58 mmol) were added to the THF suspension (15 mL). The mixture was allowed to stir for 1 week, upon which time the colour of the solution changed from dark blue to dark orange-brown. The solution was evaporated to dryness and fresh THF was added to the dark residue. The dark brown solution was centrifuged, concentrated and layered with hexanes to obtain dark brown crystals of **6.2** after 2 days at room temperature (0.177 g, 0.23 mmol, 55% yield).

Preparation of [{2,6-[2,6-(^{i}Pr)$_2$PhN=C(CH$_3$)]$_2$(C$_5$H$_3$N)}Fe-N$_2$]$_2$(μ-Na)[Na(THF)$_2$]$_2$ (6.3).

The *in situ*-prepared LFeCl$_2$ (FeCl$_2$(THF)$_{1.5}$ (0.100 g, 0.43 mmol) and 2,6-[2,6-(^{i}Pr)$_2$PhN=C(CH$_3$)]$_2$(C$_5$H$_3$N) (0.205 g, 0.43 mmol) in THF (15 mL)) was reacted with 12 equivalents of NaH (0.124 g, 5.16 mmol) in THF (5 mL). The mixture was allowed to stir for 1 week before removing the solvent *in vacuo* and washing the residue with ether. Fresh THF was added and the dark brown-orange solution was centrifuged prior to concentrating and layering with hexanes. Dark brown crystals of **6.3** grew at room temperature within several days (0.048 g, 0.064 mmol, 15% yield per Fe). IR (Nujol mull, cm^{-1}) ν: 2850 (s), 1910 (m), 1868 (m), 1751 (w), 1644 (m), 1586 (w), 1580 (m), 1494 (m), 1466 (s), 1379 (s), 1252 (s), 1179 (m), 1140 (m), 1111 (s), 1094 (s), 1018 (m), 947 (s), 863 (s), 826 (s), 802 (m), 774 (s), 757 (s), 744 (s), 733 (s), 719 (s), 634 (m), 599 (m).

Preparation of {2,6-[2,6-(^{i}Pr)$_2$PhN=C(CH$_3$)]$_2$(C$_5$H$_3$N)}Fe(η^1-N$_2$)(κ^1-{2,6-[2,6-(^{i}Pr)$_2$PhN=C(CH$_3$)]$_2$(NC$_5$H$_2$)}Na(THF)$_2$) (6.4).

Solid samples of FeCl$_2$(THF)$_{1.5}$ (0.200 g, 0.85 mmol), 2,6-[2,6-(^{i}Pr)$_2$PhN=C(CH$_3$)]$_2$(C$_5$H$_3$N) (0.820 g, 1.70 mmol), and NaH (0.62 g, 2.55 mmol) were mixed in 30 mL of THF and allowed to stir for 1 week. The colour of the solution became dark brown. Evaporation of the solvent afforded a dark brown residue. Addition of fresh hexane and centrifugation lead to the separation of a dark magenta solution. Upon allowing the solution to stand for several days at -35°C, dark magenta crystals of **6.4** were formed in low yield (0.052 g, 0.043 mmol, 5% yield). IR (Nujol mull, cm^{-1}) ν: 2919 (s), 2853 (s), 2009 (s), 1648 (m), 1614 (s), 1530 (s),1488 (w), 1461 (s), 1377 (s), 1279 (m), 1237 (m), 1192 (m), 1158 (m), 1120 (s), 1101 (s), 1055 (s), 968 (s), 857 (m), 832 (w), 774 (s), 740 (s), 724 (s), 698 (s), 665 (w), 611 (s). Anal. Calcd. (found) for C$_{74}$H$_{101}$FeN$_8$NaO$_2$ (%) solvent-free: C, 73.24 (72.98); H, 8.38 (8.24); N, 9.24 (8.97).

Preparation of {2,6-[2,6-(^{i}Pr)$_2$PhN=C(CH$_3$)]$_2$(C$_5$H$_3$N)}Fe(κ^1-{2,6-[2,6-(^{i}Pr)$_2$PhN=C(CH$_3$)]$_2$(NC$_5$H$_2$)}Na(THF)$_2$) (6.5).

The reaction was performed as above for the preparation of complex **6.4** and the work-up completed as usual to obtain the dark brown solution in hexanes. If the solution is allowed to crystallize at room temperature instead of -35°C, crystals of **6.5** may be isolated in about 20% yield. Ether can also be added to the left-over insoluble material and a dark brown solution can be separated by centrifugation. Crystallization at room temperature over the period of a few days afforded more crystals of **6.5** in about 20% yield, identical in connectivity but displaying a different unit cell than those grown from hexane (0.42 g, 0.33 mmol, combined yield approximately 40%). IR (Nujol mull, cm^{-1}): ν 2956 (s), 2928 (s), 2855 (s), 1642 (w), 1629 (m), 1617 (m), 1590 (m), 1530 (s), 1461 (s), 1377 (s), 1364 (s), 1327 (m), 1274 (b, m), 1253 (w), 1238 (s), 1190 (m), 1157 (w), 1098 (b, s), 1056 (m), 990 (m), 965 (s), 936 (w), 887 (w), 856 (w), 821 (w), 803 (w), 789 (w), 771 (s), 759 (s), 744 (w), 726 (m), 695 (m), 640 (m). Anal. Calcd. (found) for C$_{74}$H$_{101}$FeN$_6$NaO$_2$ (%) solvent-free: C, 81.93 (81.49); H, 9.38 (9.22); N, 7.75 (7.48). [μ_{eff} = 4.5 μ_B]

Preparation of {2-[2,6-(^{i}Pr)$_2$PhN=C(CH$_3$)]-6-[2,6-(^{i}Pr)$_2$PhN-C=CH$_2$](C$_5$H$_3$N)}Na(THF) (6.6).

To a solid mixture of Fe(0) powder (0.020 g, 0.36 mmol), 2,6-[2,6-(^{i}Pr)$_2$PhN=C(CH$_3$)]$_2$(C$_5$H$_2$N) (0.173 g, 0.36 mmol) and NaH (0.009 g, 0.38 mmol) were added with 15 mL of THF and the suspension allowed to stir for 3 weeks. Removal of the solvent *in vacuo* revealed a dark green-brown residue. The mass was washed with hexane before fresh ether was added. The soluble portion was centrifuged to remove any precipitates and dark brown crystals of **6.6** grew upon standing at room temperature for 2 days (0.16 g, 0.28 mmol, 74 % yield). IR (Nujol mull, cm^{-1}): ν 3100 (w), 2950-2850 (s), 1644 (s), 1629 (s), 1584 (s), 1559 (m), 1537 (s), 1464 (s), 1434 (w), 1405 (m), 1376 (w), 1366 (m), 1353 (w), 1344 (w), 1322 (m), 1302 (m), 1264 (s), 1246 (s), 1208 (w), 1193 (m), 1170 (w), 1147 (m), 1121 (w), 1106 (m), 1094 (m), 1056 (m), 1042 (s), 997 (s), 986 (w), 934 (m), 911 (w), 892 (m), 883 (m), 848 (m), 822 (w), 812 (s), 802 (m), 793 (s), 768 (s), 753 (s), 733 (s), 713 (m), 684 (m), 676 (m). ^{1}H NMR (200 MHz, d$_6$-benzene, 23°C) δ (ppm):

C***H***$(CH_3)_2$: two septets, 2H each at 3.88 (J = 7.1 Hz) and 2.45 (J = 7.0 Hz); CH(C***H***$_3)_2$: four doublets, 6H each at 1.61 and 1.32 (J = 7.1 Hz) and at 0.98 and 0.91 (J = 6.9 Hz); N=CC***H***$_3$(imine): one singlet, 3H at 1.68; NC=C***H***$_2$: two singlets, 1H each at 4.52 and 3.83; C***H***(pyridine): two doublets, 1H each at 8.16 and 6.89 and one pseudo triplet, 1H at 7.02 (J = 7.6 Hz); C***H***(aryl): one doublet, 2H at 7.41 (J = 7.6 Hz) and partly overplapping multiplets at 7.21-7.04; ether: one quadruplet at 2.98 and one triplet at 1.20. ^{13}C NMR (125.72 MHz, benzene-d^6, 23°C) (ppm): C***H***$(CH_3)_2$: 29.2 and 28.9; CH(C***H***$_3)_2$: 23.6, 23.5, 25.7, and 25.6; Me(imine): 33.2; NC=C***H***$_2$: 76.6; C***H***(pyridine): 120.1, 123.9, 126.0; C***H***(aryl): 122.1, 123.8, 137.4; ether: 62.8, 20.5.

X-ray Crystallography

All of the compounds consistently yielded crystals that diffracted weakly, and the results presented are the best of several trials. The crystals were mounted on thin glass fibers using paraffin oil and cooled to the data collection temperature. Data were collected on a Bruker AXS SMART 1k CCD diffractometer. Data for the compounds **6.1-6.3** and **6.5** were collected with a sequence of 650 scans per set at 0.3° ω scans at 0, 120, and 240° in φ. To obtain acceptable redundancy data for compounds **6.4** and **6.6**, the sequence of 650 scans per set with 0.3° ω scans at 0, 90, 180, and 270° in φ was used. Initial unit cell parameters were determined from 60 data frames collected at the different sections of the Ewald sphere. Semiempirical absorption corrections based on equivalent reflections were applied.[23] Systematic absences in the diffraction data-set and unit-cell parameters were consistent with monoclinic ***P2$_1$/c*** for **6.1**, orthorhombic ***P2$_1$2$_1$2$_1$*** for **6.2**, monoclinic ***P2$_1$/n*** for **6.3**, triclinic $P\bar{1}$ for **6.4**, orthorhombic ***Pbcn*** for **6.5**, and orthorhombic ***Pbca*** for **6.6**. Solutions in centrosymmetric space groups for compounds **6.1** and **6.3-6.6,** and non-centrosymmetric for compounds **6.2,** yielded chemically reasonable and computationally stable results of refinement. The structures were solved by direct methods, completed with difference Fourier synthesis, and refined with full-matrix least-squares procedures based on F^2. All non-hydrogen atoms were refined with anisotropic displacement coefficients. All hydrogen atoms were treated as idealized contributions. All scattering factors are contained in several versions of the SHELXTL

program library, with the latest version used being v.6.12.[24] Crystallographic data and relevant bond distances and angles are reported in Tables 6.1-6.6.

Table 6.1. Crystal Data and Structure Analysis Results of Complexes 6.1-6.3

	6.1	6.2	6.3
formula	$C_{37}H_{50}FeN_5NaO$	$C_{41}H_{59}FeN_5Na_2O_2$	$C_{82}H_{118}Fe_2N_{10}Na_3O_4$
Mw	659.66	755.76	1488.53
Crystal system	Monoclinic	Orthorhombic	Monoclinic
space group	P2(1)/c	P2(1)2(1)2(1)	P2(1)/n
a (Å)	11.816(4)	12.6462(15)	18.343(3)
b (Å)	16.736(5)	13.2223(15)	22.444(3)
c (Å)	18.701(6)	24.765(3)	20.117(3)
α (deg)	90	90	90
β (deg)	98.545(6)	90	95.840(2)
γ (deg)	90	90	90
V (Å^3)	3657(2)	4141.0(8)	8239(2)
Z	4	4	4
radiation (Kα, Å)	0.71073	0.71073	0.71073
T (K)	213(2)	203(2)	203(2)
D_{calcd} (g cm^{-3})	1.198	1.212	1.200
μ_{calcd} (mm^{-1})	0.459	0.424	0.421
F_{000}	1408	1616	3188
R, $R_w{}^{2\,a}$	0.0723, 0.1507	0.0492, 0.1044	0.0744, 0.1745
GoF	1.085	1.051	1.005

[a] $R = \Sigma||F_0| - |F_c||/\Sigma|F|$, $R_w = [\Sigma(|F_0| - |F_c|)^2/\Sigma wF_0^2\}^{1/2}$

Table 6.2. Crystal Data and Structure Analysis Results of Complexes 6.4-6.6

	6.4	6.5	6.6
formula	$C_{74}H_{101}FeN_8NaO_2$	$C_{81.13}H_{117.63}FeN_6NaO_2$	$C_{37}H_{50}N_3NaO$
Mw	1213.47	1287.78	575.79
Crystal system	Triclinic	Orthorhombic	Orthorhombic
space group	P-1	Pbcn	Pbca
a (Å)	13.396(4)	20.938(3)	18.470(10)
b (Å)	15.014(5)	25.133(3)	16.728(9)
c (Å)	23.226(7)	30.776(4)	22.266(12)
α (deg)	71.351(5)	90	90
β (deg)	77.270(5)	90	90
γ (deg)	68.453(6)	90	90
V (Å^3)	4089(2)	16195(3)	6879(6)
Z	2	8	8
radiation (Kα, Å)	0.71073	0.71073	0.71073
T (K)	206(2)	206(2)	293(2)
D_{calcd} (g cm^{-3})	0.986	1.056	1.112
μ_{calcd} (mm^{-1})	0.232	0.237	0.077
F_{000}	1308	5595	2496
R, R_w[2 a]	0.0895, 0.2030	0.0759, 0.1677	0.1054, 0.2615
GoF	1.002	1.061	1.090

[a] $R = \Sigma|F_0| - |F_c|/\Sigma|F|$, $R_w = [\Sigma(|F_0| - |F_c|)^2/\Sigma wF_0^2\}^{1/2}$

Table 6.3. Selected Bond Distances (Å) and Angles (deg) of Complexes 6.1 and 6.2

6.1	6.2
Fe(1)-N(1) = 1.904(2)	Fe(1)-N(1) = 1.895(4)
Fe(1)-N(2) = 1.874(2)	Fe(1)-N(2) = 1.855(4)
Fe(1)-N(3) = 1.894(3)	Fe(1)-N(3) = 1.882(4)
Fe(1)-N(4) = 1.750(3)	Fe(1)-N(4) = 1.723(5)
N(4)-N(5) = 1.090(5)	N(4)-N(5) = 1.149(6)
N(4)-Na(1) = 2.954(4)	Na(1)-N(5) = 2.333(5)
N(5)-Na(1) = 2.287(5)	Na(1)-C(24) = 3.050(6)
Na(1)-C(11) = 2.887(4)	Na(1)-C(25) = 2.740(6)
Na(1)-C(12) = 2.764(4)	Na(1)-C(26) = 3.055(6)
Na(1)-C(13) = 2.884(4)	Na(1)-C(2A) = 2.945(6)
Na(1)-C(14) = 3.123(4)	Na(1)-C(3A) = 2.628(5)
Na(1)-O(1) = 2.203(4)	Na(1)-N(2A) = 2.507(5)
Na(1)-C(4a) = 2.797(4)	Na(1)-C(7A) = 3.100(5)
Na(1)-C(5a) = 2.772(4)	Na(1)-Fe(1A) = 3.089(2)
N(1)-C(2) = 1.376(4)	Na(2)-O(1) = 2.349(5)
N(3)-C(8) = 1.371(4)	Na(2)-O(2) = 2.328(5)
N(2)-C(3) = 1.365(4)	Na(2)-N(2) = 2.469(5)
N(2)-C(7) = 1.367(4)	Na(2)-C(3) = 2.942(6)
C(1)-C(2) = 1.446(5)	Na(2)-C(7) = 2.732(6)
C(2)-C(3) = 1.436(4)	Na(2)-Fe(1) = 3.163(3)
C(7)-C(8) = 1.442(4)	N(1)-C(8) = 1.404(7)
C(8)-C(9) = 1.426(5)	N(3)-C(2) = 1.403(6)
N(1)-Fe(1)-N(2) = 80.97(11)	N(2)-C(3) = 1.433(6)
N(1)-Fe(1)-N(3) = 162.29(11)	N(2)-C(7) = 1.414(6)
N(1)-Fe(1)-N(4) = 98.33(12)	C(1)-C(2) = 1.487(8)
N(2)-Fe(1)-N(3) = 81.33(11)	C(2)-C(3) = 1.389(7)
N(2)-Fe(1)-N(4) = 177.33(13)	C(7)-C(8) = 1.403(7)
N(3)-Fe(1)-N(4) = 99.31(12)	C(8)-C(9) = 1.478(8)
Fe(1)-N(4)-N(5) = 177.3(4)	N(1)-Fe(1)-N(2) = 81.22(18)
Fe(1)-N(4)-Na(1) = 136.17(14)	N(1)-Fe(1)-N(3) = 161.94(19)
N(4)-N(5)-Na(1) = 117.6(3)	N(1)-Fe(1)-N(4) = 101.3(2)
N(5)-N(4)-Na(1) = 43.3(3)	N(2)-Fe(1)-N(3) = 80.79(18)
N(4)-Na(1)-N(5) = 19.09(12)	N(2)-Fe(1)-N(4) = 177.43(19)
	N(3)-Fe(1)-N(4) = 96.67(19)
	Fe(1)-N(4)-N(5) = 174.3(4)
	N(4)-N(5)-Na(1) = 143.4(4)

Table 6.4. Selected Bond Distances (Å) and Angles (deg) of Complex 6.3

6.3	6.3
Fe(1)-N(1) = 1.880(6)	C(7)-C(8) = 1.388(11)
Fe(1)-N(2) = 1.865(6)	C(8)-C(9) = 1.458(10)
Fe(1)-N(3) = 1.883(6)	N(6)-C(35) = 1.386(9)
Fe(1)-N(4) = 1.716(7)	N(8)-C(41) = 1.352(9)
Fe(2)-N(6) = 1.881(6)	N(7)-C(36) = 1.388(9)
Fe(2)-N(7) = 1.834(6)	N(7)-C(40) = 1.387(9)
Fe(2)-N(8) = 1.909(6)	C(34)-C(35) = 1.482(11)
Fe(2)-N(9) = 1.782(7)	C(35)-C(36) = 1.389(11)
N(4)-N(5) = 1.163(8)	C(40)-C(41) = 1.411(11)
N(9)-N(10) = 1.112(9)	C(41)-C(42) = 1.513(11)
Na(1)-Fe(1) = 3.034(4)	N(1)-Fe(1)-N(2) = 80.8(3)
Na(1)-O(1) = 2.289(8)	N(1)-Fe(1)-N(3) = 161.4(3)
Na(1)-O(2) = 2.374(8)	N(1)-Fe(1)-N(4) = 97.0(3)
Na(1)-N(2) = 2.506(7)	N(2)-Fe(1)-N(3) = 80.8(3)
Na(1)-C(7) = 2.737(8)	N(2)-Fe(1)-N(4) = 177.7(3)
Na(1)-C(8) = 3.114(9)	N(3)-Fe(1)-N(4) = 101.5(3)
Na(2)-Fe(1) = 3.045(4)	N(2)-Fe(1)-Na(1) = 55.5(2)
Na(2)-O(3) = 2.256(10)	N(2)-Fe(1)-Na(2) = 55.4(2)
Na(2)-O(4) = 2.376(9)	N(4)-Fe(1)-Na(1) = 124.3(2)
Na(2)-N(2) = 2.511(7)	N(4)-Fe(1)-Na(2) = 125.6(2)
Na(2)-C(3) = 3.092(9)	Na(1)-Fe(1)-Na(2) = 107.49(11)
Na(2)-C(7) = 2.626(9)	Fe(1)-N(4)-N(5) = 174.6(7)
Na(2)-C(8) = 2.954(9)	N(4)-N(5)-Na(3) = 135.4(6)
Na(3)-Fe(2) = 3.049(4)	N(5)-Na(3)-N(7) = 126.3(3)
Na(3)-N(5) = 2.336(8)	N(5)-Na(3)-C(13) = 112.7(3)
Na(3)-C(12) = 3.105(10)	N(6)-Fe(2)-N(7) = 80.7(3)
Na(3)-C(13) = 2.799(9)	N(6)-Fe(2)-N(8) = 159.1(3)
Na(3)-C(14) = 3.006(9)	N(6)-Fe(2)-N(9) = 97.7(3)
Na(3)-N(7) = 2.557(7)	N(7)-Fe(2)-N(8) = 80.4(3)
Na(3)-C(36) = 3.056(9)	N(7)-Fe(2)-N(9) = 167.5(3)
Na(3)-C(40) = 2.815(8)	N(8)-Fe(2)-N(9) = 98.8(3)
N(1)-C(2) = 1.380(9)	Fe(2)-N(9)-N(10) = 178.6(8)
N(3)-C(8) = 1.402(9)	
N(2)-C(3) = 1.409(9)	
N(2)-C(7) = 1.409(9)	
C(1)-C(2) = 1.492(10)	
C(2)-C(3) = 1.384(10)	

Table 6.5. Selected Bond Distances (Å) and Angles (deg) of Complex 6.4

6.4	6.4
Fe(1)-N(4) = 1.957(4)	C(46)-C(47) = 1.396(6)
Fe(1)-N(6) = 1.832(4)	C(47)-C(48) = 1.383(7)
Fe(1)-N(14) = 1.947(4)	C(48)-C(49) = 1.506(7)
Fe(1)-N(2) = 1.807(6)	C(49)-C(50) = 1.498(7)
Fe(1)-C(46) = 1.953(5)	N(4)-Fe(1)-N(6) = 80.3(2)
Na(39)-N(40) = 2.522(5)	N(4)-Fe(1)-N(14) = 157.29(18)
Na(39)-N(44) = 2.350(5)	N(4)-Fe(1)-N(2) = 98.2(2)
Na(39)-N(51) = 2.512(5)	N(4)-Fe(1)-C(46) = 98.88(19)
Na(39)-O(76) = 2.350(5)	N(6)-Fe(1)-N(14) = 80.02(19)
Na(39)-O(81) = 2.288(5)	N(6)-Fe(1)-N(2) = 162.55(18)
N(2)-N(3) = 1.133(6)	N(6)-Fe(1)-C(46) = 102.1(2)
N(4)-C(5) = 1.355(7)	N(14)-Fe(1)-N(2) = 97.26(19)
N(14)-C(12) = 1.360(6)	N(14)-Fe(1)-C(46) = 96.16(18)
N(6)-C(7) = 1.373(7)	N(2)-Fe(1)-C(46) = 95.3(2)
N(6)-C(11) = 1.398(6)	Fe(1)-N(2)-N(3) = 178.7(5)
C(6)-C(5) = 1.525(8)	N(40)-Na(39)-N(44) = 67.02(15)
C(5)-C(7) = 1.408(8)	N(40)-Na(39)-N(51) = 132.85(16)
C(11)-C(12) = 1.387(7)	N(40)-Na(39)-O(76) = 97.10(17)
C(12)-C(13) = 1.492(7)	N(40)-Na(39)-O(81) = 106.69(17)
N(40)-C(41) = 1.282(7)	N(44)-Na(39)-N(51) = 67.28(15)
N(51)-C(49) = 1.290(6)	N(44)-Na(39)-O(76) = 101.21(18)
N(44)-C(43) = 1.369(6)	N(44)-Na(39)-O(81) = 159.0(2)
N(44)-C(48) = 1.347(6)	N(51)-Na(39)-O(76) = 102.44(17)
C(42)-C(41) = 1.508(7)	N(51)-Na(39)-O(81) = 111.73(18)
C(41)-C(43) = 1.501(7)	O(76)-Na(39)-O(81) = 99.4(2)
C(43)-C(45) = 1.373(7)	
C(45)-C(46) = 1.411(7)	

Table 6.6. Selected Bond Distances (Å) and Angles (deg) of Complexes 6.5 and 6.6

6.5	6.5	6.6
Fe(1)-N(1) = 1.916(5)	C(38)-C(39) = 1.427(7)	Na(1)-N(1) = 2.371(4)
Fe(1)-N(2) = 1.866(4)	C(39)-C(40) = 1.389(7)	Na(1)-N(2) = 2.358(4)
Fe(1)-N(3) = 1.922(4)	C(40)-C(41) = 1.500(7)	Na(1)-N(3) = 2.386(4)
Fe(1)-C(38) = 1.939(6)	C(41)-C(42) = 1.514(7)	Na(1)-O(1) = 2.291(4)
Na(1)-N(4) = 2.508(5)	N(1)-Fe(1)-N(2) = 80.6(2)	N(1)-C(2) = 1.309(6)
Na(1)-N(5) = 2.334(5)	N(1)-Fe(1)-N(3) = 159.84(19)	N(3)-C(8) = 1.308(6)
Na(1)-N(6) = 2.501(5)	N(1)-Fe(1)-C(38) = 101.0(2)	N(2)-C(3) = 1.366(6)
Na(1)-O(1) = 2.283(5)	N(2)-Fe(1)-N(3) = 80.4(2)	N(2)-C(7) = 1.332(6)
Na(1)-O(2) = 2.318(6)	N(2)-Fe(1)-C(38) = 169.0(2)	C(1)-C(2) = 1.40(3)
N(1)-C(8) = 1.379(7)	N(3)-Fe(1)-C(38) = 99.0(2)	C(2)-C(3) = 1.497(7)
N(3)-C(2) = 1.367(7)	N(4)-Na(1)-N(5) = 66.58(16)	C(7)-C(8) = 1.511(7)
N(2)-C(3) = 1.373(7)	N(4)-Na(1)-N(6) = 129.87(17)	C(8)-C(9) = 1.49(2)
N(2)-C(7) = 1.362(7)	N(4)-Na(1)-O(1) = 114.25(19)	N(1)-Na(1)-N(2) = 68.73(14)
C(1)-C(2) = 1.498(8)	N(4)-Na(1)-O(2) = 102.3(2)	N(1)-Na(1)-N(3) = 136.46(16)
C(2)-C(3) = 1.420(8)	N(5)-Na(1)-N(6) = 66.56(16)	N(1)-Na(1)-O(1) = 109.46(16)
C(7)-C(8) = 1.398(8)	N(5)-Na(1)-O(1) = 157.9(2)	N(2)-Na(1)-N(3) = 67.86(15)
C(8)-C(9) = 1.522(8)	N(5)-Na(1)-O(2) = 98.4(2)	N(2)-Na(1)-O(1) = 172.01(18)
N(4)-C(35) = 1.282(6)	N(6)-Na(1)-O(1) = 102.76(18)	N(3)-Na(1)-O(1) = 113.05(16)
N(6)-C(41) = 1.275(6)	N(6)-Na(1)-O(2) = 101.10(19)	
N(5)-C(36) = 1.353(6)	O(1)-Na(1)-O(2) = 102.8(2)	
N(5)-C(40) = 1.332(6)		
C(34)-C(35) = 1.511(7)		
C(35)-C(36) = 1.489(7)		
C(36)-C(37) = 1.381(7)		
C(37)-C(38) = 1.397(7)		

Complex 6.1. Complex **6.1** consists of a tetracoordinate Fe center surrounded by the ligand system [Fe(1)-N(1) = 1.904(2) Å, Fe(1)-N(2) = 1.874(2) Å, Fe(1)-N(3) = 1.894(3) Å] and a linearly end-on bound unit of dinitrogen [Fe(1)-N(4) = 1.750(3) Å, Fe(1)-N(4)-N(5) = 177.3(4)°] in a distorted square planar geometry [N(1)-Fe(1)-N(2) = 80.97(11)°, N(1)-Fe(1)-N(3) = 162.29(11)°, N(1)-Fe(1)-N(4) = 98.33(12)°, N(2)-Fe(1)-N(3) = 81.33(11)°, N(2)-Fe(1)-N(4) = 177.33(13)°, N(3)-Fe(1)-N(4) = 99.31(12)°]. In turn, the dinitrogen moiety forms a distorted side-on bridge to a Na atom [N(4)-Na(1) = 2.954(4) Å, N(5)-Na(1) = 2.287(5) Å, Fe(1)-N(4)-Na(1) = 136.17(14)°, N(4)-N(5)-Na(1) = 117.6(3)°, N(5)-N(4)-Na(1) = 43.3(3)°, N(4)-Na(1)-N(5) = 19.09(12)°]. The Na cation is π-bonded to one of the aryl rings (approximately η^4) [Na(1)-C(11) = 2.887(4) Å, Na(1)-C(12) = 2.764(4) Å, Na(1)-C(13) = 2.884(4) Å, Na(1)-C(14) = 3.123(4) Å] and a molecule of THF [Na(1)-O(1) = 2.203(4) Å], as well as being loosely coordinated to the *para* and one *meta*-C of the pyridine ring of a second identical molecule [Na(1)-C(4a) = 2.797(4) Å, Na(1)-C(5a) = 2.772(4) Å] in an overall polymeric array. The N-N bond distance of the bound N_2 unit is 1.090(5) Å, very similar to that reported for free dinitrogen and therefore indicating minimal or no extent of reduction of the triple bond. The ligand system maintains its planarity but displays modified bond distances throughout the backbone. Most notably, the C_{imine}-C_{methyl} bond lengths have been substantially shortened to 1.446(5) Å and 1.426(5) Å, indicative of deprotonation of one of the methyl groups, averaged over the molecule. As expected, the imino functions have also been lengthened in response to the deprotonation [N(1)-C(2) = 1.376(4) Å, N(3)-C(8) = 1.371(4) Å]. However, the degree of elongation is more than expected for this type of transformation, compared to the elongations witnessed in the pure mono-deprotonated Ga complex[25] [N(1)-C(2) = 1.329(6) Å, N(3)-C(8) = 1.334(6) Å]. Similarities can be found, however, to the imine lengths of the mono-deprotonated Cr complex of Chapter 5 [N(1)-C(2) = 1.374(6) Å, N(3)-C(8) = 1.372(6) Å].[26] In addition, elongations are also apparent in the N_{pyr}-C_{ortho} bonds of the pyridine ring [N(2)-C(3) = 1.365(4) Å, N(2)-C(7) = 1.367(4) Å], along with similar contractions in the C_{imine}-C_{ortho} bond lengths [C(2)-C(3) = 1.436(4) Å, C(7)-C(8) = 1.442(4) Å]. These measured distances are indicative of reduction of the ligand by one electron, as well as

deprotonation, forming a dianionic ligand monoradical. A representative model is shown in Figure 6.1.

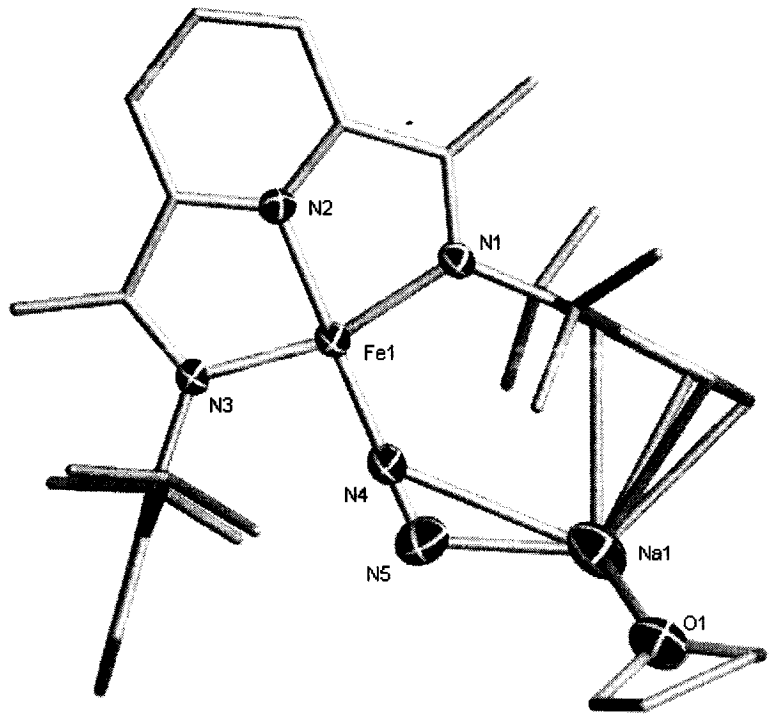

Figure 6.1. Partial thermal ellipsoid plot of complex **6.1**, drawn at the 30% probability level. Hydrogen atoms have been omitted for clarity.

Complex 6.2. Figure 6.2 displays the partial thermal ellipsoid plot of complex **6.2**, showing similarities to the structure of complex **6.1**. The ligand system chelates the Fe center in a distorted square planar arrangement [Fe(1)-N(1) = 1.895(4) Å, Fe(1)-N(2) = 1.855(4) Å, Fe(1)-N(3) = 1.882(4) Å]. The fourth coordination site is occupied by an end-on dinitrogen unit [Fe(1)-N(4) = 1.723(5) Å, N(1)-Fe(1)-N(2) = 81.22(18)°, N(1)-Fe(1)-N(3) = 161.94(19)°, N(1)-Fe(1)-N(4) = 101.3(2)°, N(2)-Fe(1)-N(3) = 80.79(18)°, N(2)-Fe(1)-N(4) = 177.43(19)°, N(3)-Fe(1)-N(4) = 96.67(19)°]. The N-N distance is longer than that of complex **6.2**, at 1.149(6) Å, but is still extremely short and displays only a small degree of activation of the triple bond. The bonding of the dinitrogen unit to the metal center is slighty bent from linear [Fe(1)-N(4)-N(5) = 174.3(4)°] and forms a bridge to a Na atom [Na(1)-N(5) = 2.333(5) Å, N(4)-N(5)-Na(1) = 143.4(4)°]. Unlike complex **6.1**, in this case the dinitrogen unit forms a slightly bent end-on bridge to the Na, as opposed to the distorted side-on binding seen in **6.1**. The Na atom is stabilized via an η^3-

bond to the *meta* and *para*-carbons of one of the aryl groups of the ligand [Na(1)-C(24) = 3.050(6) Å, Na(1)-C(25) = 2.740(6) Å, Na(1)-C(26) = 3.055(6) Å], as well as η^3 to the N_{pyr}, C_{ortho} and C_{imine} of a second molecule [Na(1)-N(2A) = 2.507(5) Å, Na(1)-C(3A) = 2.628(5) Å, Na(1)-C(2A) = 2.945(6) Å], with a weak bond to the other *ortho*-C also appearing [Na(1)-C(7A) = 3.100(5) Å], thereby assembling a polymeric array. A second Na atom is present, η^3-bound to the pyridine N and *ortho*-C's of the ligand [Na(2)-N(2) = 2.469(5) Å, Na(2)-C(3) = 2.942(6) Å, Na(2)-C(7) = 2.732(6) Å] and solvated by two molecules of THF [Na(2)-O(1) = 2.349(5) Å, Na(2)-O(2) = 2.328(5) Å]. Each Na atom is in close proximity to an Fe center, close enough to potentially be considered metal-metal bonds [Na(1)-Fe(1A) = 3.089(2) Å, Na(2)-Fe(1) = 3.163(3) Å]. The coordination of two Na atoms to the delocalized π-system of the ligand is reflected by modifications to the ligand bond distances. The imine bond distances have been lengthened substantially compared to the neutral ligand [N(1)-C(8) = 1.404(7) Å, N(3)-C(2) = 1.403(6) Å], as have the N_{pyr}-C_{ortho} bond lengths [N(2)-C(3) = 1.433(6) Å, N(2)-C(7) = 1.414(6) Å]. These elongations are paralleled by a contraction in the C_{imine}-C_{ortho} bonds [C(2)-C(3) = 1.389(7) Å, C(7)-C(8) = 1.403(7) Å]. The C_{imine}-C_{methyl} bond lengths are similar to those of the neutral ligand.

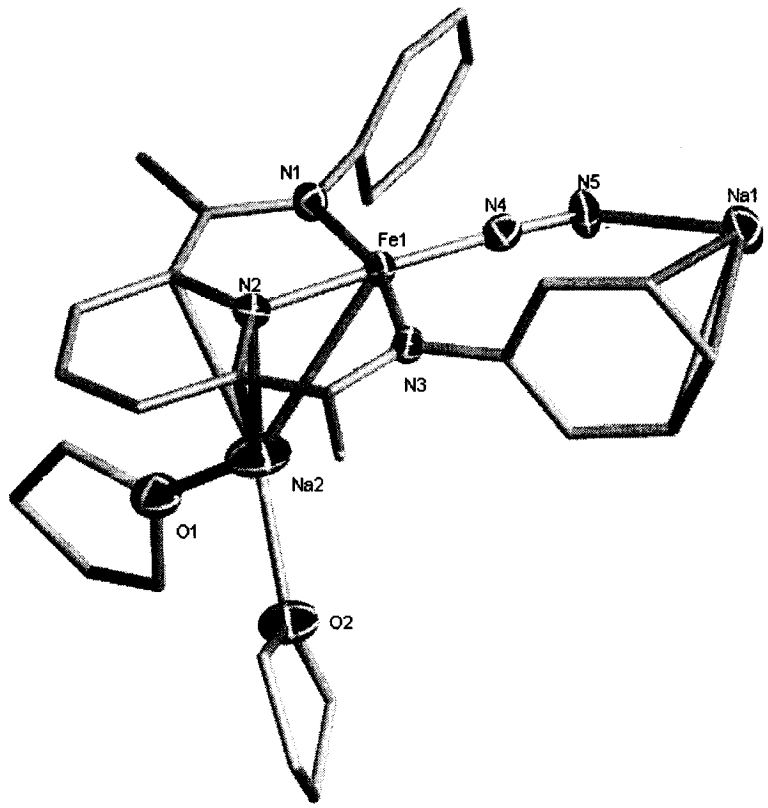

Figure 6.2. Partial thermal ellipsoid plot of complex **6.2**, drawn at the 30% probability level. ^{i}Pr substituents on the aryl rings and all hydrogen atoms have been omitted for clarity.

Complex 6.3. The structure of complex **6.3** features a distinct dimeric molecule involving two ligand systems, two Fe centers, three Na atoms and two end-on bound dinitrogen moieties (Figure 6.3). The first Fe center adopts a distorted square planar geometry completed by the three N atoms of the first ligand system [Fe(1)-N(1) = 1.880(6) Å, Fe(1)-N(2) = 1.865(6) Å, Fe(1)-N(3) = 1.883(6) Å] and an end-on unit of dinitrogen [Fe(1)-N(4) = 1.716(7) Å, N(1)-Fe(1)-N(2) = 80.8(3)°, N(1)-Fe(1)-N(3) = 161.4(3)°, N(1)-Fe(1)-N(4) = 97.0(3)°, N(2)-Fe(1)-N(3) = 80.8(3)°, N(2)-Fe(1)-N(4) = 177.7(3)°, N(3)-Fe(1)-N(4) = 101.5(3)°]. The dinitrogen unit is not exactly linear to the Fe center [Fe(1)-N(4)-N(5) = 174.6(7)°] and displays a N-N bond length of 1.163(8) Å, less than a two electron reduction but suggesting a degree of activation. Two doubly-THF-solvated Na atoms [Na(1)-O(1) = 2.289(8) Å, Na(1)-O(2) = 2.374(8) Å, Na(2)-O(3) = 2.256(10) Å, Na(2)-O(4) = 2.376(9) Å] coordinate to the first ligand system on opposite sides of the plane defined by the backbone. The first Na atom appears to be η^3-bound to the N_{pyr},

C_{ortho} and adjacent C_{imine} [Na(1)-N(2) = 2.506(7) Å, Na(1)-C(7) = 2.737(8) Å, Na(1)-C(8) = 3.114(9) Å] and the second Na atom coordinates to the opposite side of the same atoms and involves the other *ortho*-C atom in an η^4-bond [Na(2)-N(2) = 2.511(7) Å, Na(2)-C(3) = 3.092(9) Å, Na(2)-C(7) = 2.626(9) Å, Na(2)-C(8) = 2.954(9) Å]. The dimeric structure is realized by the third Na atom, connected to the first molecule via an end-on dinitrogen bridge to the Fe center [Na(3)-N(5) = 2.336(8) Å, N(4)-N(5)-Na(3) = 135.4(6)°] and an η^3-bond to the aryl group of the first ligand [Na(3)-C(12) = 3.105(10) Å, Na(3)-C(13) = 2.799(9) Å, Na(3)-C(14) = 3.006(9) Å] and assembling the dimer by η^3-coordination to the pyridine ring of the second unit [Na(3)-N(7) = 2.557(7) Å, Na(3)-C(36) = 3.056(9) Å, Na(3)-C(40) = 2.815(8) Å]. All three Na atoms are in close proximity to an Fe center [Na(1)-Fe(1) = 3.034(4) Å, Na(2)-Fe(1) = 3.045(4) Å, Na(3)-Fe(2) = 3.049(4) Å]. The second Fe center is found in a distorted square planar arrangement coordinated to the three nitrogen atoms of the second ligand [Fe(2)-N(6) = 1.881(6) Å, Fe(2)-N(7) = 1.834(6) Å, Fe(2)-N(8) = 1.909(6) Å] and another end-on dinitrogen unit [Fe(2)-N(9) = 1.782(7) Å, N(6)-Fe(2)-N(7) = 80.7(3)°, N(6)-Fe(2)-N(8) = 159.1(3)°, N(6)-Fe(2)-N(9) = 97.7(3)°, N(7)-Fe(2)-N(8) = 80.4(3)°, N(7)-Fe(2)-N(9) = 167.5(3)°, N(8)-Fe(2)-N(9) = 98.8(3)°]. The coordination of the N_2 ligand to the second Fe center is more linear than that to the first Fe center [Fe(2)-N(9)-N(10) = 178.6(8)°] but is also a terminal N_2 unit, unlike above, with only a small degree of activation of the triple bond [N(9)-N(10) = 1.112(9) Å]. Close inspection of the two ligand systems shows slight differences in the bond lengths in the backbone. Both exhibit elongated N_{imine}-C_{imine} [N(1)-C(2) = 1.380(9) Å and N(3)-C(8) = 1.402(9) Å for ligand(1) and N(6)-C(35) = 1.386(9) Å and N(8)-C(41) = 1.352(9) Å for ligand(2)] and N_{pyr}-C_{ortho} bond distances [N(2)-C(3) = 1.409(9) Å and N(2)-C(7) = 1.409(9) Å for ligand(1) and N(7)-C(36) = 1.388(9) Å and N(7)-C(40) = 1.387(9) Å for ligand(2)] and shortened C_{imine}-C_{ortho} bonds [C(2)-C(3) = 1.384(10) Å and C(7)-C(8) = 1.388(11) Å for ligand(1) and C(35)-C(36) = 1.389(11) Å and C(40)-C(41) = 1.411(11) Å for ligand(2)], but the deviations occur to a larger extent on the first ligand system, characteristic of increased electron density in the ligand π^* orbitals.[20,27]

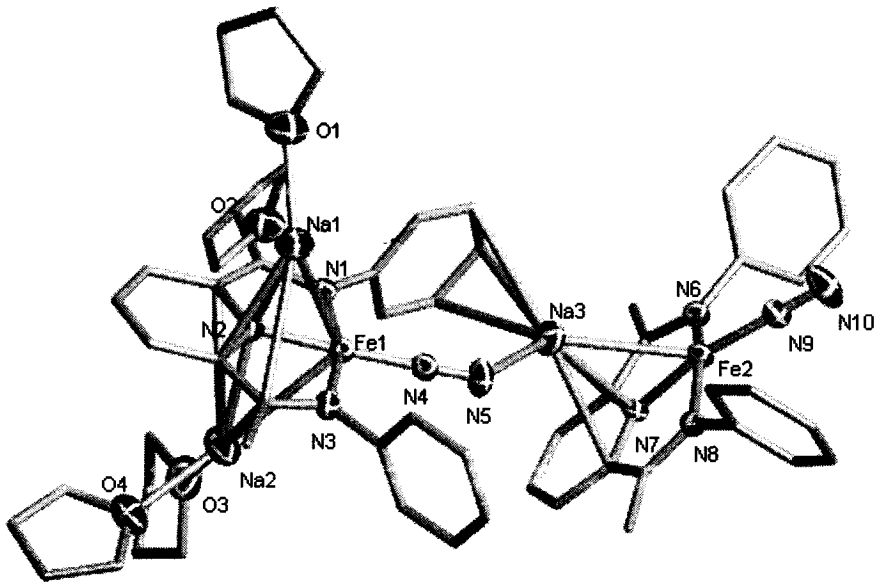

Figure 6.3. Partial thermal ellipsoid plot of complex **6.3**, drawn at the 30% probability level. ^{i}Pr substituents on the aryl rings and all hydrogen atoms have been omitted for clarity.

Complex 6.4. The connectivity of complex **6.4** shows a large dinuclear molecule containing two ligand systems surrounding one Fe atom and one Na atom respectively (Figure 6.4). The Fe center adopts a square pyramidal geometry ($\tau = 0.09$)[28] in which the three nitrogen atoms of the ligand backbone [Fe(1)-N(4) = 1.957(4) Å, Fe(1)-N(6) = 1.832(4) Å, Fe(1)-N(14) = 1.947(4) Å] and one N atom of a terminal end-on dinitrogen unit [Fe(1)-N(2) = 1.807(6) Å] complete the basal plane [N(4)-Fe(1)-N(6) = 80.3(2)°, N(4)-Fe(1)-N(14) = 157.29(18)°, N(4)-Fe(1)-N(2) = 98.2(2)°, N(6)-Fe(1)-N(14) = 80.02(19)°, N(6)-Fe(1)-N(2) = 162.55(18)°, N(14)-Fe(1)-N(2) = 97.26(19)°]. The apical position is occupied by a σ-bond to the *para*-position of a second ligand [Fe(1)-C(46) = 1.953(5) Å], which has been deprotonated in that position. The planar backbone of the second ligand is oriented orthogonally to the first ligand plane and coordinates a di-THF-solvated Na atom [Na(39)-N(40) = 2.522(5) Å, Na(39)-N(44) = 2.350(5) Å, Na(39)-N(51) = 2.512(5) Å, Na(39)-O(76) = 2.350(5) Å, Na(39)-O(81) = 2.288(5) Å]. The geometry about the Na atom is somewhere between square pyramidal and trigonal bipyramidal ($\tau = 0.44$)[28] [N(40)-Na(39)-N(44) = 67.02(15)°, N(40)-Na(39)-N(51) = 132.85(16)°, N(40)-Na(39)-O(76) = 97.10(17)°, N(40)-Na(39)-O(81) = 106.69(17)°,

N(44)-Na(39)-N(51) = 67.28(15)°, N(44)-Na(39)-O(76) = 101.21(18)°, N(44)-Na(39)-O(81) = 159.0(2)°, N(51)-Na(39)-O(76) = 102.44(17)°, N(51)-Na(39)-O(81) = 111.73(18)°, O(76)-Na(39)-O(81) = 99.4(2)°]. In the case of the second ligand system, the bond lengths of the backbone are barely changed with respect to the free ligand and do not require further discussion. However, the bond distances of the ligand surrounding the Fe center have been modified in comparison to the neutral ligand, characterized by elongations in the imine C=N and N_{pyr}-C_{ortho} bond lengths [N(4)-C(5) = 1.355(7) Å, N(14)-C(12) = 1.360(6) Å, N(6)-C(7) = 1.373(7) Å, N(6)-C(11) = 1.398(6) Å], and contractions in the C_{imine}-C_{ortho} bond lengths [C(5)-C(7) = 1.408(8) Å, C(11)-C(12) = 1.387(7) Å], compared to others in Table 6.7. The degree of modification suggests a two electron reduction of the ligand system.[20,27] The C_{imine}-C_{methyl} bonds are unmodified and are therefore intact. The end-on bound dinitrogen unit displays a fairly short N-N bond (1.133(6) Å) indicative of little or no activation of the triple bond.

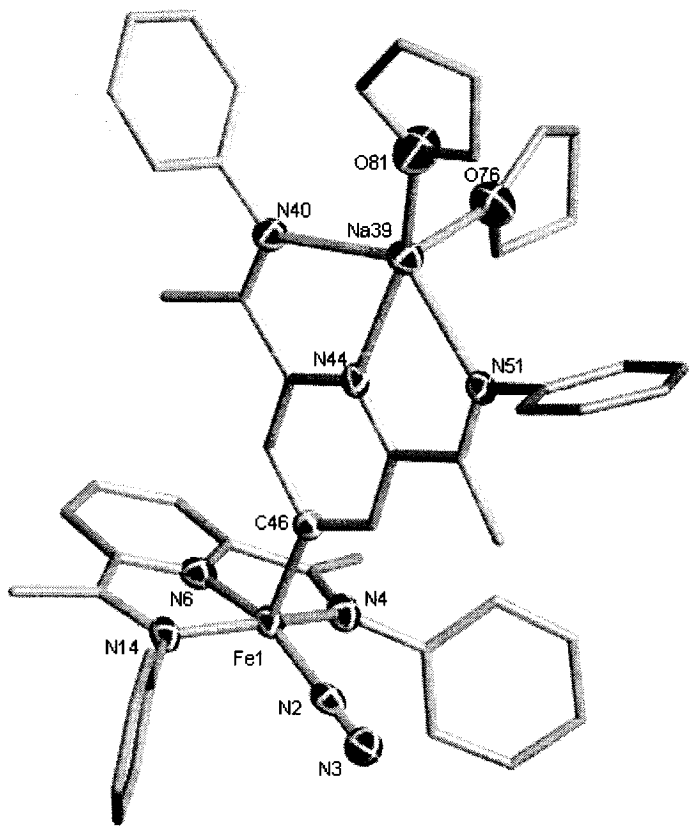

Figure 6.4. Partial thermal ellipsoid plot of complex **6.4**, drawn at the 30% probability level. ^{i}Pr substituents on the aryl rings and all hydrogen atoms have been omitted for clarity.

Complex 6.5. The structure of complex **6.5** is very similar to that of complex **6.4** in that it is comprised of two ligand systems in the same molecule, surrounding one Fe atom and a Na cation (Figure 6.5). The Fe center forms bonds to the three nitrogen atoms of the first ligand system [Fe(1)-N(1) = 1.916(5) Å, Fe(1)-N(2) = 1.866(4) Å, Fe(1)-N(3) = 1.922(4) Å] and the *para*-C of the second pyridine ring [Fe(1)-C(38) = 1.939(6) Å] in a distorted square planar geometry [N(1)-Fe(1)-N(2) = 80.6(2)°, N(1)-Fe(1)-N(3) = 159.84(19)°, N(1)-Fe(1)-C(38) = 101.0(2)°, N(2)-Fe(1)-N(3) = 80.4(2)°, N(2)-Fe(1)-C(38) = 169.0(2)°, N(3)-Fe(1)-C(38) = 99.0(2)°]. The Na center coordinates to the three nitrogen atoms of the second ligand [Na(1)-N(4) = 2.508(5) Å, Na(1)-N(5) = 2.334(5) Å, Na(1)-N(6) = 2.501(5) Å] and two molecules of THF [Na(1)-O(1) = 2.283(5) Å, Na(1)-O(2) = 2.318(6) Å] in a pentacoordinate arrangement midway between square pyramidal and trigonal bipyramidal ($\tau = 0.47$)[28] [N(4)-Na(1)-N(5) = 66.58(16)°, N(4)-Na(1)-N(6) = 129.87(17)°, N(4)-Na(1)-O(1) = 114.25(19)°, N(4)-Na(1)-O(2) = 102.3(2)°, N(5)-Na(1)-N(6) = 66.56(16)°, N(5)-Na(1)-O(1) = 157.9(2)°, N(5)-Na(1)-O(2) = 98.4(2)°, N(6)-Na(1)-O(1) = 102.76(18)°, N(6)-Na(1)-O(2) = 101.10(19)°, O(1)-Na(1)-O(2) = 102.8(2)°]. The sp^2 hybridization of the *para*-C on the second ligand implies that it has been deprotonated. No other ligand modifications are apparent in the distances and angles of the backbone, however, the first ligand system surrounding the Fe atom, displays bond distance modifications to the ligand backbone as expected for a two electron reduction (Table 6.7).[20,27]

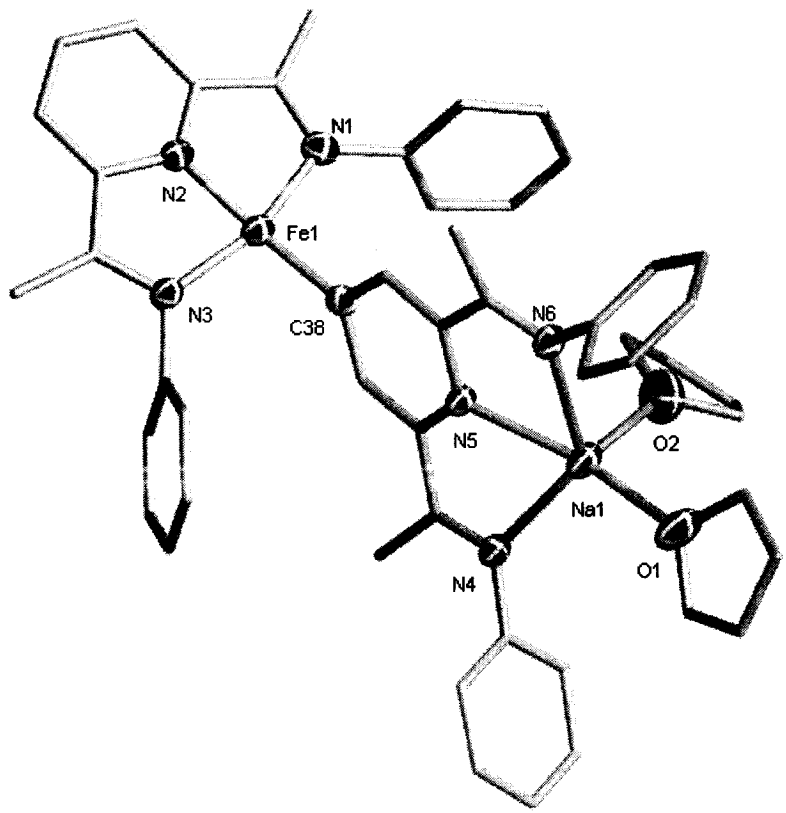

Figure 6.5. Partial thermal ellipsoid plot of complex **6.5**, drawn at the 30% probability level. ^{i}Pr substituents on the aryl rings and all hydrogen atoms have been omitted for clarity.

Complex 6.6. Complex **6.6** (Figure 6.6) consists of a ligand bound Na atom [Na(1)-N(1) = 2.371(4) Å, Na(1)-N(2) = 2.358(4) Å, Na(1)-N(3) = 2.386(4) Å] solvated by a molecule of THF [Na(1)-O(1) = 2.291(4) Å] in a distorted square planar geometry [N(1)-Na(1)-N(2) = 68.73(14)°, N(1)-Na(1)-N(3) = 136.46(16)°, N(1)-Na(1)-O(1) = 109.46(16)°, N(2)-Na(1)-N(3) = 67.86(15)°, N(2)-Na(1)-O(1) = 172.01(18)°, N(3)-Na(1)-O(1) = 113.05(16)°]. The distance between the C of the imine function and the ketimine methyl group has been shortened with respect to the free ligand [C(1)-C(2) = 1.40(3) Å, C(8)-C(9) = 1.49(2) Å]. The double bond of the imino function has been slightly lengthened in response [N(1)-C(2) = 1.309(6) Å, N(3)-C(8) = 1.308(6) Å]. The other bond distances of the ligand backbone have not been altered compared to the neutral ligand and display no particular features.

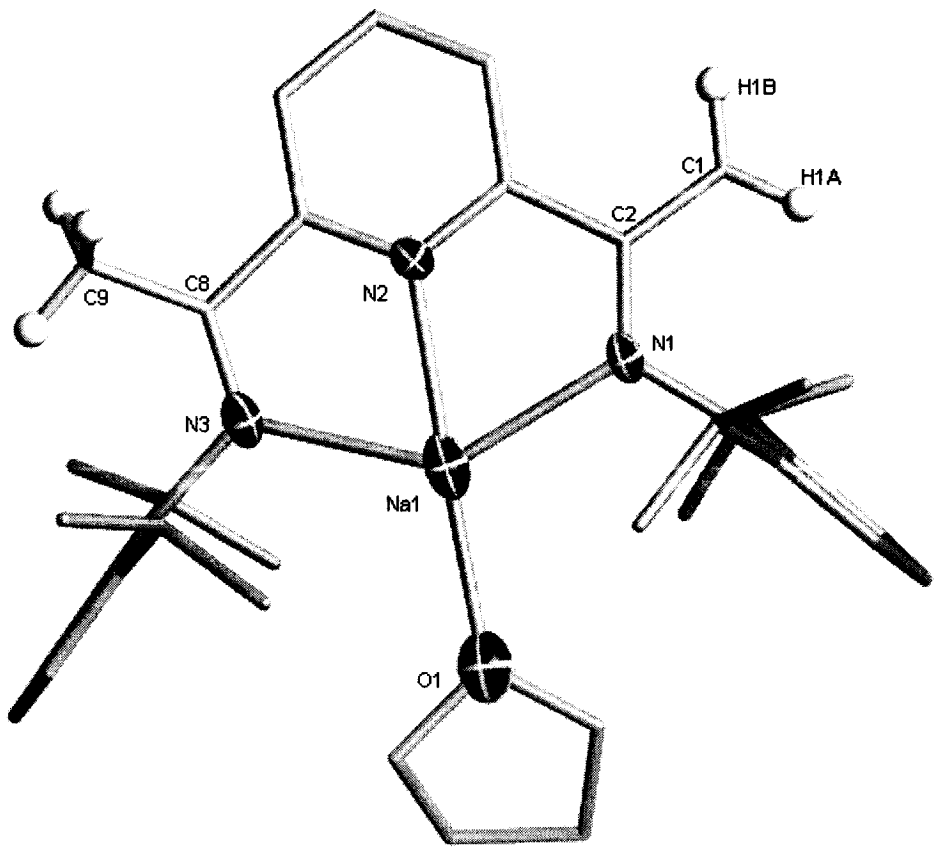

Figure 6.6. Partial thermal ellipsoid plot of complex **6.6**, drawn at the 30% probability level. Relevant H atoms have been added in their most probable positions.

Table 6.7. Comparative Bond Distances (Å) of Selected Compounds

Compounds	Fe-N	N_{imine}-C_{imine}	C_{imine}-C_{ortho}	C_{ortho}-N_{pyr}
	2.222(4)	1.301(7)	1.466(8)	1.356(7)
L[a]FeCl$_2$	2.091(4)	1.295(7)	1.482(8)	1.323(7)
	2.225(5)			
	1.968(5)	1.337(7)	1.432(8)	1.349(7)
LFeMe[b]	1.893(4)	1.332(7)	1.442(8)	1.368(7)
	1.952(5)			
	1.917(6)	1.356(8)	1.404(10)	1.391(9)
[LFeMe][Li(THF)$_4$][c]	1.849(6)	1.377(9)	1.421(11)	1.372(8)
	1.915(5)			
		1.400(4)	1.373(4)	1.421(4)
Li$_3$L[d]		1.409(4)	1.380(4)	1.412(4)
	1.904(2)	1.376(4)	1.436(4)	1.365(4)
6.1	1.874(2)	1.371(4)	1.442(4)	1.367(4)
	1.894(3)			
	1.895(4)	1.404(7)	1.389(7)	1.433(6)
6.2	1.855(4)	1.403(6)	1.403(7)	1.414(6)
	1.882(4)			
	1.880(6)	1.380(9)	1.384(10)	1.409(9)
6.3: Fe(1)	1.865(6)	1.402(9)	1.388(11)	1.409(9)
	1.883(6)			
	1.881(6)	1.386(9)	1.389(11)	1.388(9)
6.3: Fe(2)	1.834(6)	1.352(9)	1.411(11)	1.387(9)
	1.909(6)			
	1.957(4)	1.355(7)	1.408(8)	1.373(7)
6.4	1.832(4)	1.360(6)	1.387(7)	1.398(6)
	1.947(4)			
	1.916(5)	1.379(7)	1.420(8)	1.373(7)
6.5	1.866(4)	1.367(7)	1.398(8)	1.362(7)
	1.922(4)			

[a] L = 2,6-[2,6-(^{i}Pr)$_2$PhN=C(CH$_3$)]$_2$(C$_5$H$_3$N)
[b] Reference 29.
[c] Complex **3.1**.[30]
[d] Reference 31.

Results and Discussion

Upon reduction of $LFeCl_2$ [L = 2,6-[2,6-(^{i}Pr)$_2$PhN=C(CH$_3$)]$_2$(C$_5$H$_3$N)] with 3 equivalents of NaH in THF, the colour of the solution changes from dark blue to bright burgundy over the period of a few days. Work up of the reaction mixture suggests an untidy distribution of products. From an ether soluble portion of the reaction mixture, it was possible to crystallize and isolate {2-[2,6-(^{i}Pr)$_2$PhN=C(CH$_3$)]-6-[2,6-(^{i}Pr)$_2$PhN-C=CH$_2$](C$_5$H$_3$N)}Fe(μ-N$_2$)Na(THF) (**6.1**) in moderate yield (Scheme 6.3). Crystals suitable for X-ray diffraction were removed from the mother liquor and shown to be very prone towards spontaneous loss of nitrogen, as witnessed by a continuous evolution of gas from the solid surface of the crystals, even at low temperature. Rapid deterioration of the crystals made it very difficult to obtain a satisfactory data collection. However, in one case the data were sufficient to provide the connectivity displayed in Figure 6.1. From the formal point of view, the complex can be described as resulting from the combination of a zerovalent Fe center surrounded by a mono-deprotonated mono-anionic ligand with its Na countercation. In fact, the square planar coordination geometry about Fe is as expected for a d^8 zerovalent Fe metal. However, given the established ability of this particular ligand system to accept electronic density into the delocalized π-system and to form radical anions,[20,27,30-33] a higher oxidation state cannot be excluded at this stage. The main feature of this complex is the presence of a dinitrogen molecule end-on bonded to Fe and in turn side-on bonded to a Na cation. The extremely short N-N distance, 1.090(5) Å, indicates minimal, if any, reduction of the triple bond. In sharp contrast however, the IR stretching frequency of the N-N bond is clearly visible at 1912 cm^{-1}. This value is remarkably lower than in other terminally bonded dinitrogen complexes,[13a-g,i,j] which is of course indicative of at least some extent of reduction in the N-N bond order. On the other hand, it is important to note that coordination of dinitrogen to transition metals and especially to f-block elements may often display strange and unexplained features, such as a further shortening of the N-N bond distance with respect to free dinitrogen as result of the coordination.[34] In the present case, the bond distance of the N atom to the Fe center of 1.750(3) Å is also surprisingly short and thus suggests possible Fe-N multiple bond character. At this stage, we have no explanation for this apparently contradictory behaviour. Assuming the dinitrogen unit has been the recipient of one electron and the

ligand system is dianionic, the oxidation state of the metal center is most likely +2. The measured magnetic moment of 6.5 μ_B is very similar to that obtained for complex **3.1** and indicates a substantial degree of unpaired electron density.[30] It is also important to note that the formation of small amounts of elemental Fe during the reduction may lead anomalous readings.

Scheme 6.3

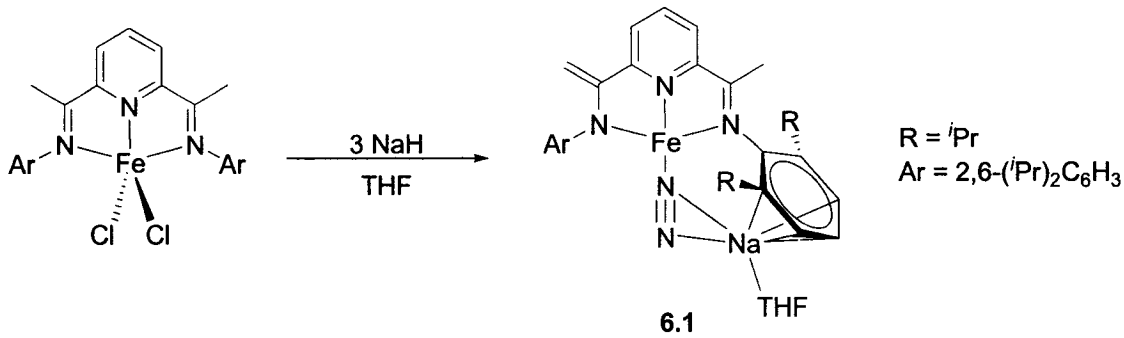

6.1

Given the apparent complexity of the reaction above, as suggested by the solubility properties of the reaction mixture, reduction reactions were also examined with different stoichiometric ratios and reducing agents. Reduction of the dichloride precursor with 6 equivalents of either Na or NaH for one week in THF afforded another dinitrogen complex $\{2,6\text{-}[2,6\text{-}(^{i}Pr)_2PhN{=}C(CH_3)]_2(C_5H_3N)\}Fe(\mu\text{-}N_2)Na(Na(THF)_2)$ (**6.2**) in crystalline form and acceptable yield from either toluene or a THF/hexane solution (Scheme 6.4).

The structure of complex **6.2** (Figure 6.2) bears resemblance to complex **6.1**, also consisting of an Fe center surrounded by the ligand system and a molecule of dinitrogen in an end-on coordination mode. In turn, the dinitrogen unit is end-on bonded to a Na atom. The presence of a second Na atom, solvated by two molecules of THF and η^3-bound to the pyridine ring of the ligand, provides the major visible difference with complex **6.1**. Also different from **6.1**, the values of the C_{imine}-C_{methyl} bond distances imply that the methyl groups have not been deprotonated during the reduction. As expected however, the other bond lengths of the ligand backbone have been modified in such a way to suggest a greater extent of reduction than in complex **6.1**. From the formal point of view, since the ligand displays no particularly visible modifications, and given the

presence of the two Na atoms, the complex might be regarded as containing Fe in the negative divalent state. However, the square planar coordination geometry of the Fe atom more realistically diagnoses a d^8 zerovalent Fe coupled to a radical dianion. The N-N bond [1.149(6) Å], although still short, is significantly longer than in complex **6.1**, and is also paralleled by a decrease in the Fe-N bond length and the IR stretching frequency (1899 cm^{-1}). Altogether, this suggests that a larger extent of reduction indeed results in a larger degree of activation, but only to a minor extent. In turn, this indicates that once again the ligand system is the most preferred target of the reduction. This behaviour is not unprecedented in Fe chemistry, given that further reduction of the Fe-*nacnac* dinitrogen complex gives only a minor extent of N_2 reduction, according to the N-N distance.[14] The measured magnetic moment of complex **3** (5.6 μ_B) once again diagnoses a significant amount of unpaired electron density that may be explained by the combination of a high spin Fe(II) metal center and a triplet ligand with a small amount of antiferromagnetic coupling. Regardless of how we consider the metal oxidation state, the formation of **6.2** is the result of a four electron reduction.

Scheme 6.4

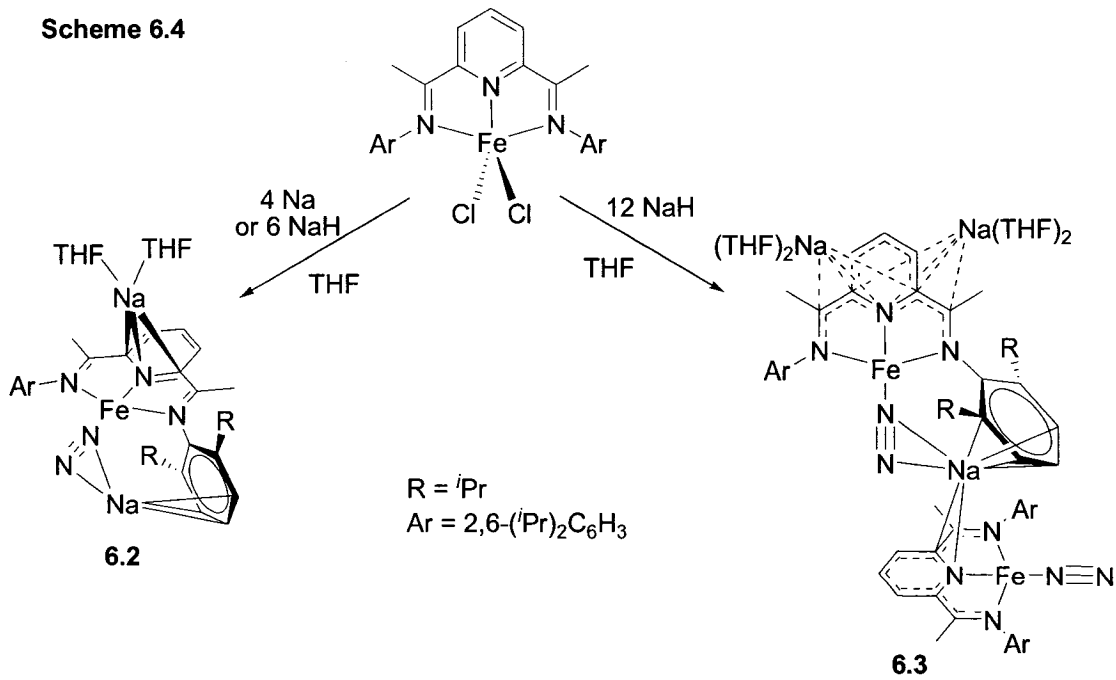

By increasing the amount of reducing agent (up to 12 equivalents of NaH), the isolation of a new species [{2,6-[2,6-(i-Pr)$_2$PhN=C(CH$_3$)]$_2$(C$_5$H$_3$N)}Fe-N$_2$]$_2$(μ-Na)

$[Na(THF)_2]_2$ (**6.3**) was made possible (Scheme 6.4). X-ray diffraction of the crystals revealed the structure displayed in Figure 6.3. Although complex **6.3** appears to be a minor product, as indicated by the very poor yield, to date no other species have been crystallized from this reaction mixture.

The dinuclear structure of **6.3** may be regarded, from the formal point of view, as resulting from the additional one-electron reduction of **6.2**, and further coordination to a simple (ligand)FeN_2 unit. The interaction of the Na cation with the aromatic ring of one unit and the pyridine ring of the second is responsible for assembling the dinuclear structure. Of the two dinitrogen moieties, one is involved in completing a bridge from the first Fe center to the second ligand system via a Na atom, and the other is found terminally bound to the second Fe center. The bridging Na atom is bound side-on to the first dinitrogen ligand, η^4-bound to one aryl ring of the first ligand and π-bound to the N and *ortho*-position of the pyridine ring of a second ligand. Two additional Na atoms are present in the molecule, π-bound to each side of the delocalized backbone of the first ligand in η^4 fashion.

Indirect evidence regarding the oxidation state of the two metal centers is provided by the degree of reduction in the ligand backbones.[20,27] Considering the first ligand (bound to the three Na atoms), the coordination of two Na atoms to opposite sides of the ligand plane suggests a larger extent of reduction. Indeed, the essential backbone bond lengths have been shortened or lengthened to suggest the presence of three additional electrons in the π^* orbitals. Table 6.7 compares the relative bond lengths for a number of compounds and those of the first ligand are similar to the tri-lithiated complex[31] in which three electrons have been shown to occupy the ligand orbitals. On the other hand, the second ligand displays modifications like those observed in the case of a two-electron reduction. The second Fe center (bound to the terminal dinitrogen unit) is most likely present in the +2 oxidation state. The similarities in geometry and trends in this chemistry also suggest a divalent state for the first Fe center, but the presence of three Na atoms requires that the dinitrogen unit be the recipient of two electrons to obtain neutrality. Although the bridging N-N bond is the longest among the complexes reported in this chapter, the distance of 1.163(8) Å is still relatively short and hard to reconcile with a two electron reduction. However, the Fe-N bond length is indeed very short

[Fe(1)-N(4) = 1.716(7) Å] and clearly indicative of a substantial amount of Fe-N multiple bond character. This phenomenon is perhaps similar to that observed by the group of Holland upon reduction of an N_2-bridged Fe dimer, in which the N-N bond remained rather short in response to the added electron density, as opposed to visibly reducing the bond order.[14] Another explanation may involve delocalization of the electron density across the Fe-N-N-Na bridge.

During the isolation of complex **6.1** from the reaction mixture, small amounts of another complex could occasionally be crystallized from hexane. The formulation of this new species as $\{2,6\text{-}[2,6\text{-}(^{i}Pr)_2PhN{=}C(CH_3)]_2(C_5H_3N)\}Fe(\eta^1\text{-}N_2)(\kappa^1\text{-}\{2,6\text{-}[2,6\text{-}(^{i}Pr)_2PhN{=}C(CH_3)]_2(NC_5H_2)\}Na(THF)_2)$ (**6.4**) was yielded by a crystal structure. Unfortunately, the crystals were small and diffracted weakly, but in one case sufficient data were collected to enable structural determination (Figure 6.4). The structure of complex **6.4** contains two tridentate ligand systems, one of which surrounds one Fe atom and the other which coordinates a Na cation. The two units are connected together via an Fe-C bond with the *para*-C of the pyridine ring on the Na-centered ligand. The pentacoordination of the Fe center is completed by an end-on dinitrogen unit displaying a short N-N distance of 1.133(6) Å, typical of a small amount of activation of the triple bond. The formation and orientation of the Fe-C σ-bond implies an initial deprotonation of the *para*-position of that pyridine ring, evidently forming a monoanionic ligand. Other bond distances and angles of this ligand backbone are similar to those of the neutral ligand, showing no other modifications to the system. The presence of the Na cation implies a zerovalent oxidation state for the Fe center. However, the bond distances of the Fe-centered ligand system have undergone elongations and contractions related to reduction by two electrons.[20,27] As previously observed in the other formally zerovalent complexes of this ligand system (see Chapter 3),[30] the electronic structure of complex **6.4** is more likely to consist of a ligand diradical dianion bound to a divalent metal center.

Formation of a complex containing two ligand systems per Fe center suggests either ligand dissociation in solution or alternatively transmetallation of the ligand to Na. In addition, the formation of **6.4** requires 3 equivalents of NaH per Fe (assuming two equivalents act as reducing agents for the Fe-centered ligand and one acts to deprotonated the second ligand in the *para*-position). In an attempt to form complex **6.4** in higher

yields, the reaction of one equivalent of $FeCl_2$ starting material with two equivalents of ligand and 3 equivalents of NaH was pursued in THF over the period of one week. After work-up of the reaction mixture, complex **6.4** could still only be crystallized in trace amounts upon freezing the hexane fraction. However, upon crystallization at room temperature, or from ether, a similar compound could be made in significant yield. The new complex appears to be similar to **6.4** minus the dinitrogen unit (Scheme 6.5). X-ray diffraction determined the precise formulation of complex **6.5** as {2,6-[2,6-(^{i}Pr)$_2$PhN=C(CH$_3$)]$_2$(C$_5$H$_3$N)}Fe(κ^1-{2,6-[2,6-(^{i}Pr)$_2$PhN=C(CH$_3$)]$_2$(NC$_5$H$_2$)}Na(THF)$_2$.

Scheme 6.5

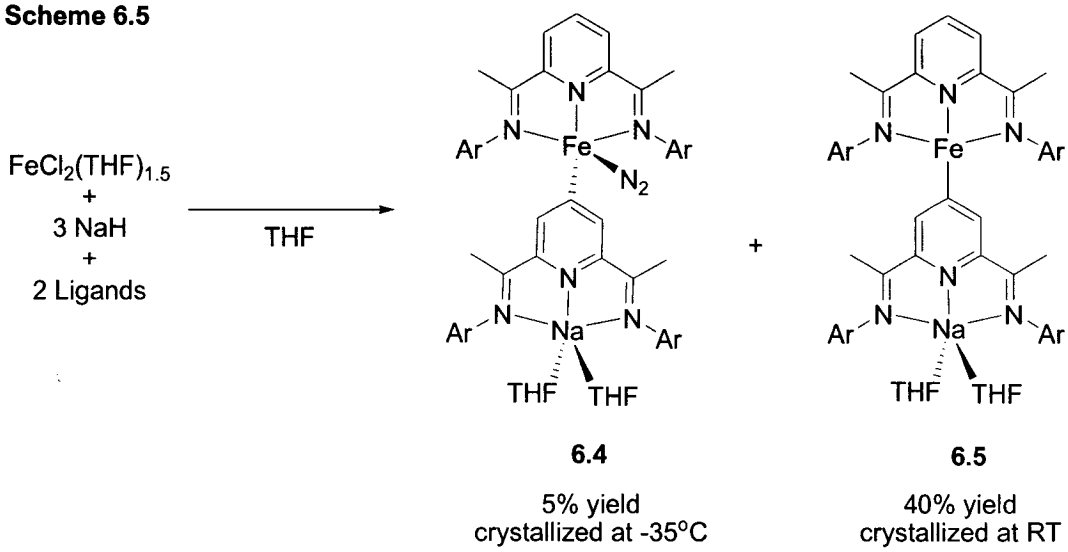

6.4

5% yield
crystallized at -35°C

6.5

40% yield
crystallized at RT

Complex **6.5** contains a distorted square planar Fe center bound to one ligand system and the *para*-position of a second ligand system (Figure 6.5). In turn, the nitrogen atoms of the second ligand surround a THF-solvated Na atom. Besides the *para*-deprotonation of the second ligand, other bond distances and angles compare well to those of the starting $LFeCl_2$ or neutral ligand.[22] On the other hand, the bond distances of the ligand tri-coordinated to Fe suggest the presence of two electrons in the delocalized π-system, once again indicating the presence of a divalent Fe atom bound to a ligand diradical and a monoanionic deprotonated Na-centered ligand. The measured magnetic moment of 4.5 μ_B is in fact as expected for a low-spin square planar d^6 Fe coupled to a ligand diradical (or a high spin square planar d^6 Fe with the two electrons on the ligand paired).

The preparation of complexes **6.4** and **6.5** involves reduction of one ligand by two electrons and deprotonation of a second ligand at the *para*-position of the pyridine ring to form a monoanionic ligand, most likely due to NaH attack at the *para*-position of a free ligand present in the reaction mixture. The formation of **6.4** and **6.5** therefore appear to be related and a possible mechanism in the formation of **6.4** may involve the fixation of dinitrogen by **6.5**. The concentration of atmospheric dinitrogen in solution increases with a decrease in temperature, hence the sequestration of dinitrogen by **6.4** upon crystallization at -35°C. The barrier to inversion from an assumed square pyramidal geometry with the N_2 ligand in the apical position (which would be expected upon initial fixation to a square planar complex) to the current *para*-C in the apical position is most likely small. As a result, the stronger bond assumes the apical site. However, an alternate reaction pathway involves σ-coordination of a monoanionic *para*-deprotonated ligand to an initial square planar Fe-N_2 complex, similar to that described by Chirik in solution.[16] Considering the isolation of complex **6.5** in much higher yields than **6.4**, and the lack of isolable Chirik-like Fe-N_2 compound, the former scenario is more plausible.

The reduction of the ligand at the expense of the metal center is a fascinating event, one that takes place either via direct reduction of the ligand system, or via a rapid metal to ligand charge transfer from a primarily reduced Fe center to the π* orbitals of the ligand. Preliminary results with gallium have demonstrated MLCT upon coordination of a Ga(II) species to the neutral ligand, creating a $L^{\bullet-}Ga^{III}$ situation.[25] A similar attempt, involving the reaction between metallic Fe and the free ligand, was not successful in forming a complex. However, upon addition of NaH to the vessel, a reaction did take place (Scheme 6.6) and crystals of {2-[2,6-(^{i}Pr)$_2$PhN=C(CH$_3$)]-6-[2,6-(^{i}Pr)$_2$PhN-C=CH$_2$](C$_5$H$_3$N)} Na(THF) (**6.6**) were isolated in good yield (Figure 6.6).

Scheme 6.6

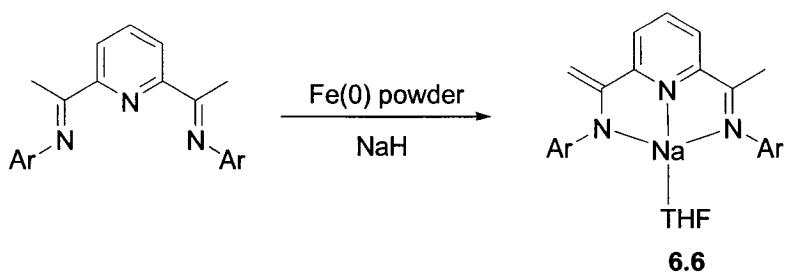

6.6

The simple mononuclear unit of **6.6** is characterized by a square planar Na atom bound to the ligand system and solvated by a molecule of THF. The only distinguishable features concerning the ligand system are the shortened C_{imine}-C_{methyl} bond distances and the correspondingly lengthened N=C_{imine} bonds, indicative of mono-deprotonation of one imino-methyl group. The newly formed monoanionic ligand has precedent in the reaction of the ligand with MeLi,[35] and deprotonation of the methyl group has become a relatively common transformation under certain circumstances.[21,25,26,31,33,36,37] Fascinatingly, the Fe powder appears to be a necessary reagent in the formation of **6.6**, since reaction of the ligand and NaH in the absence of metallic Fe yields only unreacted starting material after stirring for several weeks. However, it is deprotonation of the *para*-position of the pyridine ring that is achieved during the formation of **6.4** and **6.5**. Hence, some unknown factor may encourage attack instead at the *para*-position. Perhaps π-coordination of a hypothetically formed L^{2-}Fe(II) to the pyridine ring of a free ligand increases the susceptibility of the *para*-position towards deprotonation by excess NaH, in turn forming a new Fe-C σ-bond.

Conclusion

Reduction of the $LFeCl_2$ precursor is an extremely complex reaction, with the formation of a slew of Fe-dinitrogen products, most of which have not been isolated. It appears that added electron density occupies primarily the ligand system, enabling the fixation of dinitrogen by the Fe center. However, the antibonding orbitals of the ligand can only accept a finite number of electrons, at which point additional electrons may act towards reducing the triple bond of the activated dinitrogen moiety. It is interesting to note that fixation of dinitrogen by late transition metal bis-iminopyridine systems (Fe[16] and Co[17,18]) results in weakly-activated, end-on dinitrogen units, whereas dinitrogen complexes of V[19] and Cr[21] bis-iminopyridine systems adopt bimetallic structures defined by an end-on N_2 bridge. The immobilization of the dinitrogen unit between the two metal centers allows for a greater degree of reduction of the triple bond. In fact, the V-N_2 unit undergoes a two electron reduction[19] and the Cr-N_2 unit may accept 6 electrons and result in complete cleavage of the triple bond.[21] The ideal situation therefore appears to involve

a bimetallic attack of the associated dinitrogen moiety, an outcome that is curiously not easy to attain with the late metal systems.

References

(1) For recent reviews see: (a) MacLachlan, E. A.; Fryzuk, M. D. *Organometallics* **2006**, *25*, 1530. (b) Gambarotta, S. *J. Organomet. Chem.* **1995**, *500*, 117. (c) Gambarotta, S.; Scott, J. *Angew. Chem. Int. Ed.* **2004**, *43*, 5289. (d) MacKay, B. A.; Fryzuk, M. D. *Chem. Rev.* **2004**, *104*, 385. (e) Hidai, M.; Mizobe, Y. *Chem. Rev.* **1995**, *95*, 1115. (f) Hidai, M. *Coord. Chem. Rev.* **1999**, *185-186*, 99. (g) Fryzuk, M. D.; Johnson, S. A. *Coord. Chem. Rev.* **2000**, *200-202*, 379.

(2) (a) Leigh, G. J. *Acc. Chem. Res.* **1992**, *25*, 177. (b) Howard, J. B.; Rees, D. C. *Chem. Rev.* **1996**, *96*, 2965. (c) Burgess, B. K.; Lowe, D. J. *Chem. Rev.* **1996**, *96*, 2983. (d) Burgess, B. K. *Chem. Rev.* **1990**, *90*, 1377.

(3) (a) Ertl, G. *Catalytic Ammonia Synthesis* Ed. Jennings, J. R., Plenum, New York, **1991**. (b) Schlogl, R. *Angew. Chem. Int. Ed.* **2003**, *42*, 2004.

(4) (a) Tamaru, K. In *Catalytic Ammonia Synthesis* Ed. Jennings, J. R., Plenum, New York, **1991**, 1-18. (b) Campbell, C. T. *Science* **2001**, *294*, 1471. (c) Fryzuk, M. D. *Nature* **2004**, *427*, 498. (d) Smil, V. *Nature* **1999**, *400*, 415.

(5) (a) Statistics from the International Fertilizer Industry Association: http://www.fertilizer.org/ifa/statistics/indicators/ind_reserves.asp. (b) The Haber-Bosch synthesis is reported to use 8-12 GCal of energy per Ton of ammonia produced: Lababidi, H. M. S.; Alatiqi, I.; Nayfeh, L. J. *Applied Thermal Engineering* **2000**, *20*, 1495.

(6) In *CRC Handbook of Chemistry and Physics: 73rd Ed.* Ed. In Chief: Lide, D. R., CRC Press, **1992**.

(7) (a) Seefeldt, L. C.; Dance, I. G.; Dean, D.R. *Biochemistry* **2004**, *43*, 1401. (b) Seefeldt, L. C.; Dean, D.R. *Acc. Chem. Res.* **1997**, *30*, 260.

(8) (a) Yandulov, D. V.; Schrock, R. R. *Science* **2003**, *301*, 76. (b) Schrock, R. R. *Acc. Chem. Res.* **2005**, *38*, 955.

(9) Korobkov, I.; Gambarotta, S.; Yap, G. P. A. *Angew. Chem. Int. Ed.* **2003**, *42*, 4958.

(10) Pool, J. A.; Lobkovsky, E.; Chirik, P. J. *Nature* **2004**, *427*, 527.

(11) (a) Berno, P.; Gambarotta, S. *Angew. Chem. Int. Ed.* **1995**, *34*, 822. (b) Laplaza, C. E.; Cummins, C. C. *Science* **1995**, *268*, 861. (c) Cui, Q.; Musaev, D. G.; Svensson, M.; Sieber, S.; Morokuma, K. *J. Am. Chem. Soc.* **1995**, *117*, 12366. (d) Laplaza, C. E.; Johnson, M. J. A.; Peters, J. C.; Odom, A. L.; Kim, E.; Cummins, C. C.; George, G. N.; Pickering, I. J. *J. Am. Chem. Soc.* **1996**, *118*, 8623. (e) Zanotti-Gerosa, A.; Solari, E.; Giannini, L.; Floriani, C.; Cheisi-Villa, A.; Rizzoli, C. *J. Am. Chem. Soc.* **1998**, *120*, 437. (f) Ishino, H.; Tokunaga, S.; Seino, H.; Ishii, Y.; Hidai, M. *Inorg. Chem.* **1999**, *38*, 2489. (g) Peters, J. C.; Cherry, J. P. F.; Thomas, J. C.; Baraldo, L.; Mindiola, D. J.; Davis, W. M.; Cummins, C. C. *J. Am. Chem. Soc.* **1999**, *121*,

10053. (h) Tsai, Y. C.; Johnson, M. J. A.; Mindiola, D. J.; Cummins, C. C.; Klooster, W. T.; Koetzle, J. F. *J. Am. Chem. Soc.* **1999**, *121*, 10426. (i) Clentsmith, G. K. B.; Bates, V. M. E.; Hitchcock, P. B.; Cloke, F. G. N. *J. Am. Chem. Soc.* **1999**, *121*, 10444. (j) Caselli, A.; Solari, E.; Scopelliti, R.; Floriani, C.; Re, N.; Rizzoli, C.; Chiesi-Villa, A. *J. Am. Chem. Soc.* **2000**, *122*, 3652. (k) Mindiola, D. J.; Meyer, K.; Cherry, J. P. F.; Baker, T. A.; Cummins, C. C. *Organometallics* **2000**, *19*, 1622. (l) Solari, E.; Silva, C. D.; Iacono, B.; Hesschenbrouck, J.; Rizzoli, C.; Scopelliti, R.; Floriani, C. *Angew. Chem. Int. Ed.* **2001**, *40*, 3907. (m) Yandulov, V.; Schrock, R. R. *J. Am. Chem. Soc.* **2002**, *124*, 6252. (n) Fryzuk, M. D.; Kozak, C. M.; Bowdridge, M. R.; Patrick, B. O.; Rettig, S. J. *J. Am. Chem. Soc.* **2002**, *124*, 8389. (o) Kawaguchi, H.; Matsuo, T. *Angew. Chem. Int. Ed.* **2002**, *41*, 2792. (p) Fryzuk, M. D.; MacKay, B. A.; Johnson, S. A.; Patrick, B. O. *Angew. Chem. Int. Ed.* **2002**, *41*, 3709. (q) Tsai, Y.-C.; Cummins, C. C. *Inorg. Chim. Acta.* **2003**, *345*, 63. (r) Fryzuk, M. D.; MacKay, B. A.; Patrick, B. O. *J. Am. Chem. Soc.* **2003**, *125*, 3234. (s) Shaver, M. P.; Fryzuk, M. D. *Adv. Synth. Catal.* **2003**, *345*, 1061.

(12) (a) Kozak, C. M.; Mountford, P. *Ang. Chem. Int. Ed.* **2004**, *43*, 1186. (b) Fryzuk, M. D.; Love, J. B.; Rettig, S. J.; Young, V. G. *Science* **1997**, *275*, 1445. (c) Basch, H.; Musaev, D. G.; Morokuma, K.; Fryzuk, M. D.; Love, J. B.; Seidel, W. W.; Albinati, A.; Koetzle, T. F.; Klooster, W. T.; Mason, S. A.; Eckert, J. *J. Am. Chem. Soc.* **1999**, *121*, 523. (d) Fryzuk, M. D.; Johnson, S. A.; Rettig, S. J. *J. Am. Chem. Soc.* **1998**, *120*, 11024. (e) Fryzuk, M. D.; Johnson, S. A.; Patrick, B. O.; Albinati, A.; Mason, S. A.; Koetzle, T. F. *J. Am. Chem. Soc.* **2001**, *123*, 3960.

(13) (a) Hills, A.; Hughes, D. L; Jimenez-Tenorio, M.; Leigh, G. J. *J. Organomet. Chem.* **1990**, *391*, C41. (b) Komiya, S.; Akita, M.; Yoza, A.; Kasuga, N.; Fukuoka, A.; Kai, Y. *J. Chem. Soc., Chem. Commun.* **1993**, 787. (c) Hills, A.; Hughes, D. L.; Jimenez-Tenorio, M.; Leigh, G. L. *J. Chem. Soc., Dalton Trans.* **1993**, 3041. (d) Leal, A. D.; Jimenez-Tenorio, M.; Puerta, M. C.; Valerga, P. *Organometallics* **1995**, *14*, 3839. (e) George, T. A.; Rose, D. J.; Chang, Y.; Chen, Q.; Zubieta, J. *Inorg. Chem.* **1995**, *34*, 1295. (f) Hirano, M.; Akita, M.; Morikita, T.; Kubo, H.; Fukuoka, A.; Komiya, S. *J. Chem. Soc., Dalton Trans.* **1997**, 3453. (g) Wiesler, B. E.; Lehnert, N.; Tuczek, F.; Neuhausen, J.; Tremel, W. *Angew. Chem. Int. Ed.* **1998**, *37*, 815. (h) Berke, H.; Bankhardt, W.; Huttner, G.; von Seyerl, J.; Zsolnai, L. *Chem. Ber.* **1981**, *114*, 2754. (i) Kandler, H.; Gauss, C.; Bidell, W.; Rosenberger, S.; Bürgi, T.; Eremenko, I. L.; Veghini, D.; Orama, O.; Burger, P.; Berke, H. *Chem. Eur. J.* **1995**, *1*, 541. (j) Danopoulos, A. A.; Wright, J. A.; Motherwell, W. B. *Chem. Commun.* **2005**, 784.

(14) Smith, J. M.; Lachicotte, R. J.; Pittard, K. A.; Cundari, T. R.; Lukat-Rodgers, G.; Rodgers, K. R.; Holland, P. L. *J. Am. Chem. Soc.* **2001**, *123*, 9222.

(15) (a) Betley, T. A.; Peters, J. C. *J. Am. Chem. Soc.* **2004**, *126*, 6252. (b) Mankad, N. P.; Whited, M. T.; Peters, J. C. *Angew. Chem. Int. Ed.* **2007**, *46*, 5768.

(16) Bart, S. C.; Lobkovsky, E.; Chirik, P. J. *J. Am. Chem. Soc.* **2004**, *126*, 13794.

(17) Gibson, V. C.; Humphries, M. J.; Tellmann, K. P.; Wass, D. F.; White, A. J. P.; Williams, D. J. *Chem. Commun.* **2001**, 2252.

(18) (a) Scott, J.; Gambarotta, S.; Korobkov, I. *Can. J. Chem.* **2005**, *83*, 279. (b) See also Chapter 8.

(19) Vidyaratne, I.; Gambarotta, S.; Korobkov, I.; Budzelaar, P. H. M. *Inorg. Chem.* **2005**, *44*, 1187.

(20) Bart, S. C.; Chlopek, K.; Bill, E.; Bouwkamp, M. W.; Lobkovsky, E.; Neese, F.; Wieghardt, K.; Chirik, P. J. *J. Am. Chem. Soc.* **2006**, *128*, 13901.

(21) (a) Vidyaratne, I.; Scott, J.; Gambarotta, S.; Budzelaar, P. H. M.; Korobkov, I. *manuscript submitted.* (b) See also Chapter 7.

(22) (a) Small, B. L.; Brookhart, M.; Bennett, A. M. A. *J. Am. Chem. Soc.* **1998**, *120*, 4049. (b) Britovsek, G. J. P.; Gibson, V. C.; Kimberley, B. S.; Maddox, P. J.; McTavish, S. J.; Solan, G. A.; White, A. J. P.; Williams, D. J. *Chem. Commun.* **1998**, 849.

(23) Blessing, R. *Acta Crystallogr.* **1995**, *A51*, 33.

(24) Sheldrick, G. M. Bruker AXS, Madison, WI, 2001.

(25) Scott, J.; Phull, H,; Gambarotta, S.; Korobkov, I. *manuscript in preparation.*

(26) (a) Vidyaratne, I.; Scott, J.; Gambarotta, S.; Korobkov, I.; Duchateau, R. R. J. *Accepted in Organometallics.* (b) See also Chapter 5.

(27) (a) de Bruin, B.; Bill, E.; Bothe, E.; Weyhermueller, T.; Wieghardt, K. *Inorg. Chem.* **2000**, *39*, 2936. (b) Budzelaar, P.H.M; de Bruin, B.; Gal A.W.; Wieghardt, K.; van Lenthe, J. H. *Inorg. Chem.*, **2001**, *40*, 4649. (c) Knijnenburg, Q.; Hetterscheid, D.; Kooistra, T. M.; Budzelaar, P. H. M. *Eur. J. Inorg. Chem.* **2004**, 6, 1204.

(28) Addison, A. W.; Rao, T. N.; Reedijk, J.; van Rijn, J.; Verschoor, G. C. *J. Chem. Soc. Dalton Trans.* **1984**, 1349. The τ parameter helps to classify the geometry of five-coordinate complexes. The τ parameter is calculated by finding the difference between the two largest angles at the metal center and dividing by 60. For a perfect square pyramidal complex, $\tau = 0$ and for a perfect trigonal bipyramidal complex, $\tau = 1$. In cases where the actual geometry is ambiguous between square pyramidal and trigonal bipyramidal, the τ parameter helps to quantify the observed distortions.

(29) Bouwkamp, M. W.; Bart, S. C.; Hawrelak, E. J.; Trovitch, R. J.; Lobkovsky, E.; Chirik, P. J. *Chem. Commun.* **2005**, 3406.

(30) (a) Scott, J.; Gambarotta, S.; Korobkov, I.; Budzelaar, P. H. M. *Organometallics* **2005**, *24*, 6298. (b) See also Chapter 3.

(31) Enright, D.; Gambarotta, S.; Yap, G. P. A.; Budzelaar, P. H. M. *Angew. Chem. Int. Ed.* **2002**, *41*, 3873.

(32) (a) Scott, J.; Gambarotta, S.; Korobkov, I.; Knijnenburg, Q.; de Bruin, B.; Budzelaar, P. H. M. *J. Am. Chem. Soc.* **2005**, *127*, 17204. (b) See also Chapter 4.

(33) (a) Sugiyama, H.; Korobkov, I.; Gambarotta, S.; Möller, A.; Budzelaar, P. H. M. *Inorg. Chem.* **2004**, *43*, 5771.

(34) (a) Roussel, P.; Scott, P. *J. Am. Chem. Soc.* **1998**, *120*, 1070. (b) Roussel, P.; Errington, W.; Kaltsoyannis, N.; Scott, P. *J. Organomet. Chem.* **2001**, *635*, 69. (c) Evans, W. J.; Ulibarri, T. A.; Ziller, J. W. *J. Am. Chem. Soc.* **1988**, *110*, 6877. (d) Guan, J.; Dubé, T.; Gambarotta, S.; Yap, G. P. A. *Organometallics* **2000**, *19*, 4820.

(35) (a) Khorobkov, I.; Gambarotta, S.; Yap, G. P. A. *Organometallics* **2002**, *21*, 3088. (b) Blackmore, I. J.; Gibson, V. C.; Hitchcock, P. B.; Rees, C. W.; Williams, D. J.; White, A. J. P. *J. Am. Chem. Soc.* **2005**, *127*, 6012.

(36) (a) Scott, J.; Gambarotta, S.; Korobkov, I.; Budzelaar, P. H. M. *J. Am. Chem. Soc.* **2005**, *127*, 13019. (b) See also Chapter 2.

(37) Bouwkamp, M. W.; Lobkovsky, E.; Chirik, P. J. *Inorg. Chem.* **2006**, *45*, 2.

Chapter Seven

Dinitrogen Fixation, Partial Hydrogenation and Formation of Coordinated Cr-imide.

Introduction

Dinitrogen fixation and activation by transition metal centers has been a continuing saga since the initial discovery of the ability of transition metals to form dinitrogen complexes.[1] As a result of considerable research, the immobilized dinitrogen unit may be guided towards a few diversified stoichiometric transformations.[2] It has only been in the past few years that tremendous advances have been made towards understanding the elementary steps by which this exceedingly stable molecule is reduced, cleaved and protonated.[3] Today, dinitrogen activation is documented with almost all of the metals but it is trivalent molybdenum[1e3ab,4] and tantalum,[5] and divalent samarium[6] which provide the largest variety of reduced species.

Chapter 6 highlighted the ability of the bis-iminopyridine ligand to afford a slew of dinitrogen complexes of Fe.[7] The dinitrogen units in these complexes all appear to have undergone minimal reduction, emphasizing the trend for late transition metals to only engage in labile, or weak, fixation of dinitrogen. Despite increasing amounts of reducing agent, the added electron density chose to reside in the π^* orbitals of the ligand system, instead of the dinitrogen moiety. In contrast, the dimeric vanadium complexes prepared in our lab display a two-electron reduction of the dinitrogen unit.[8] The main difference between the Fe and V systems, besides the nature of the metal center, is the

bonding mode of the dinitrogen to the metal ions. Most of the N_2 ligands on Fe are found terminally bound, with the others engaged in bridging to a Na countercation. On the other hand, in the V system, the N_2 unit bridges two V centers. The multimetallic cooperative activation of two metal centers appears to be the driving force to encourage further reduction of the N-N triple bond.

In sharp contrast to the unique versatility of molybdenum,[1e3ab,4] chromium appears to be one of the most reluctant elements to interact with dinitrogen. The only chromium dinitrogen complexes reported so far are in fact less than a handful of Chatt-type zerovalent derivatives containing phosphine[9] or arene ligands.[10] Chapter 5 reported the synthesis and characterization of several low-valent chromium complexes of the bis-iminopyridine ligand.[11] In the present work, we describe how further reduction of these complexes in the presence of nitrogen leads to a dinitrogen complex and subsequent cleavage of the N-N bond. The chemistry presented herein was completed with the generous help and collaboration of Indu Vidyaratne.[12]

Experimental Section

All preparations were performed under an inert atmosphere by using standard Schlenk techniques and a nitrogen-atmosphere glove box. $CrCl_2(THF)_2$ was prepared following the standard procedure and $\{2,6\text{-}[2,6\text{-}(^{i}Pr)_2PhN{=}C(CH_3)]_2(C_5H_3N)\}CrCl_3$,[13] $\{2,6\text{-}[2,6\text{-}(^{i}Pr)_2PhN{=}C(CH_3)]_2(C_5H_3N)\}CrCl_2$,[11] and $\{2,6\text{-}[2,6\text{-}(^{i}Pr)_2PhN{=}C(CH_3)]_2(C_5H_3N)\}CrCl$[11] were prepared according to published procedures. Infrared spectra were recorded on a Mattson 9000 and Nicolet 750-Magna FT-IR instrument from Nujol mulls prepared in a dry-box. Samples for magnetic susceptibility measurements were weighed inside a dry box equipped with an analytical balance and sealed into calibrated tubes. Magnetic measurements were carried out with a Gouy balance (Johnson Matthey) at room temperature and calculated following standard methods and applying corrections for underlying diamagnetism to the data. Elemental analyses were carried out with a Perkin Elmer 2400 CHN analyzer. Data for X-ray crystal structure determinations were obtained with a Bruker diffractometer equipped with a SMART CCD area detector. NMR spectra were recorded with a Varian AMX-500 spectrometer.

Preparation of {[{2,6-[2,6-(^{i}Pr)$_2$PhN=C(CH$_3$)]$_2$(C$_5$H$_3$N)}Cr(THF)]$_2$(μ-N$_2$)}•(ether) (7.1).

Method A. A solution of {2,6-{2,6-(^{i}Pr)$_2$PhN=C(CH$_3$)}$_2$(C$_5$H$_3$N)}CrCl$_2$ (1.31 g, 2.0 mmol) in THF (100 mL) was treated with NaH (0.100 g, 4.2 mmol) in THF (20 mL) or metallic Na (4.1 mmol). The resulting purple mixture was stirred for 7 days at room temperature and the colour of solution changed from purple to dark green. The solvent was evaporated *in vacuo* and the dark green solid was re-dissolved in hexane (80 mL). Dark green crystals of **7.1** were isolated upon cooling (0.255 g, 0.19 mmol, 19 % yield). Suitable crystals for X-ray diffraction were grown from ether and were found to contain ether of crystallization (*vide infra*). Anal. Calcd. (found) for C$_{78}$H$_{112}$Cr$_2$N$_8$O$_3$ (%): C 71.31 (71.27); H 8.59 (8.55); N 8.53 (8.48). IR (Nujol mull, cm^{-1}): ν. 1868 (m), 1644 (m), 1580 (m), 1494 (m), 1466 (s), 1379 (s), 1252 (s), 1179 (m), 1140 (w), 1111 (s), 1094 (s), 1018 (m), 947 (s), 863 (s), 826 (s), 802 (m), 774 (s), 757 (w), 744 (w), 733 (w), 719 (w), 695 (s). [μ_{eff} = 5.7 μ_B]

Method B. A solution of {2,6-{2,6-(^{i}Pr)$_2$PhN=C(CH$_3$)}$_2$(C$_5$H$_3$N)}CrCl (1.138 g, 2.0 mmol) in THF (100 mL) was treated with either NaH (0.053 g, 2.2 mmol) in THF (20 mL) or metallic Na (0.048 g, 2.1 mmol). The resulting green solution was stirred for 7 days at room temperature and the solution became dark black-green. The solvent was evaporated *in vacuo* and the dark green solid was re-dissolved in hexane (80 mL). Dark-green crystals of **7.1** were obtained upon cooling (0.235 g, 0.179 mmol, 18% yield).

Preparation of {2-[2,6-(^{i}Pr)$_2$PhN=C(CH$_3$)]-6-[2,6-(^{i}Pr)$_2$PhN-C=CH$_2$](C$_5$H$_3$N)}Cr (THF) (7.2).

A solution of {2,6-{2,6-(^{i}Pr)$_2$PhN=C(CH$_3$)}$_2$(C$_5$H$_3$N)}CrCl (1.138 g, 2.0 mmol) in THF (100 mL) was treated with a suspension of NaH (0.053 g, 2.2 mmol) in THF (20 ml) under Ar atmosphere. The resulting green coloured suspension was stirred for 7 days at room temperature, during which the colour of solution changed from green to dark brown. The solvent was evaporated *in vacuo* and the dark brown solid was re-dissolved in hexane (60 mL) and centrifuged. Dark green crystals of **7.2** were isolated upon cooling the resulting solution (0.967 g, 1.6 mmol, 80% yield). Anal. Calcd. (found) for C$_{37}$H$_{50}$CrN$_3$O (%): C 73.48 (73.45); H 8.33 (8.29); N 6.95 (6.93). IR (Nujol mull, cm^{-1}):

ν 2900 (s), 2854 (s), 1606 (m), 1574 (s), 1512 (s), 1464 (s), 1433 (s), 1402 (m), 1379 (s), 1357 (m), 1315 (m), 1300 (s), 1243 (s), 1221 (s), 1195 (m), 1174 (w), 1135 (w), 1091 (m), 1065 (m), 1052 (m), 1017 (m), 1003 (w), 978 (m), 925 (s), 899 (w), 871 (s), 859 (m), 824 (s), 804 (s), 774 (s), 755 (s), 738 (m), 725 (m), 690 (s). [μ_{eff} = 3.8 μ_B]

Preparation of [{2,6-[2,6-(^{i}Pr)$_2$PhN=C(CH$_3$)]$_2$(C$_5$H$_3$N)}Cr(THF)][{2-[2,6-(^{i}Pr)$_2$ PhN=C(CH$_3$)]-6-[2,6-(^{i}Pr)$_2$PhN-C=CH$_2$](C$_5$H$_3$N)}Cr(THF)](μ-N$_2$H)(μ-Na)$_2$ (7.3).

A solution of **7.1** (0.550 g, 0.42 mmol) was treated with NaH (0.024 g, 1.0 mmol) in toluene (15 mL) under nitrogen atmosphere. The resulting mixture was stirred for 5 days at room temperature, during which time the colour of the solution changed from dark green to dark brown. The excess of NaH was removed by centrifugation and the resulting solution was evaporated to dryness. The solid residue was redissolved in toluene (25 mL). Dark brown crystals of **7.3** were isolated at room temperature after standing for one week. (0.167 g, 0.13 mmol, 31 % yield). Anal. Calcd. (found) for $C_{74}H_{102}Cr_2N_8Na_2O_2$ (%): C 69.13 (68.92); H 8.00 (8.11); N 8.72 (8.66). IR (Nujol mull, cm^{-1}): 3399 (s) (3343 (s) for ^{15}[N]), 2917 (s), 1907 (m), 1850 (m), 1599 (m), 1572 (m), 1540 (w), 1463 (s), 1426 (s), 1377 (s), 1354 (w), 1337 (w), 1306 (m), 1279 (m), 1232 (s), 1194 (m), 1337 (w), 1306 (m), 1279 (m), 1232 (s), 1194 (m), 1178 (m), 1155 (w), 1109 (m), 1094 (m), 1052 (w), 1029 (m), 1004 (w), 984 (m), 975 (m), 951 (w), 930 (w), 879 (s), 862 (s), 793 (m), 787 (m), 756 (s), 727 (s), 694 (m), 666 (w). [μ_{eff} = 1.9 μ_B].

Preparation of {2-[2,6-(^{i}Pr)$_2$PhN=C(CH$_3$)]-6-[2,6-(^{i}Pr)$_2$PhN-C=CH$_2$](C$_5$H$_3$N)}Cr (μ-NH)][Na(THF)] (7.4).

Method A. A solution of **7.1** (1.138 g, 0.86 mmol) in THF (100 mL) was treated with a suspension of NaH (0.065 g, 2.7 mmol) in THF (15 mL). The resulting green solution was stirred for 7 days at room temperature. The colour of the solution changed to dark brown. After centrifugation the solvent was evaporated *in vacuo* and the dark brown solid was redissolved in hexane (65 mL). Dark-brown crystals of **7.4** were isolated from a concentrated solution upon standing at room temperature for 10 days (0.141 g, 0.22 mmol, 13 %). Anal. Calcd. (found) for $C_{37}H_{52}CrN_4NaO$ (%): C 69.02 (68.88); H 8.14 (8.25); N 8.70(8.66). IR (Nujol mull, cm^{-1}): ν 3413 (m) [3366 (m) for ^{15}[N]), 2855 (s), 1617 (w),

1572 (s), 1512 (s), 1463 (s), 1402 (w), 1378 (m), 1355 (m), 1317 (w), 1261 (w), 1227 (m), 1195 (w), 1164 (w), 1149 (w), 1134 (w), 1092 (m), 1051 (m), 1016 (s), 973 (s), 932 (w), 871 (s), 803 (s), 761 (m), 750 (m), 724 (s), 695 (w), 665 (w), 634 (m).

Method B. A solution of {2,6-{2,6-(^{i}Pr)$_2$PhN=C(CH$_3$)}$_2$(C$_5$H$_3$N)}CrCl (0.750 g, 1.3 mmol) was treated with a suspension of NaH (0.206 g, 8.6 mmol) in THF (15 mL) and the resulting mixture was stirred for 7 days at room temperature, upon which time the colour of the solution became dark black-brown. Excess NaH was removed by centrifugation. After evaporation of the THF, the residue was redissolved in hexane (25 mL). Dark brown crystals of **7.4** (0.276 g, 0.43 mmol, 33%) were isolated at room temperature after standing for one week.

Method C. A solution of **7.3** (0.530 g, 0.41 mmol) was treated with suspension of NaH (0.042 g, 1.7 mmol) in THF (20 mL) and the dark brown mixture was allowed to stir for 10 days at room temperature. Excess NaH was removed by centrifuged and evaporated to dryness. The residue was redissolved in hexane (25 ml) and dark brown crystals of **7.4** were isolated upon slow cooling at –35°C (0.084 g, 0.13 mmol, 16 % yield).

Degradation of 7.4 and Isolation of NH_4BPh_4[14]

An analytically pure sample of **7.4** (0.200 g) was treated with a 9% HCl/H$_2$O solution. After centrifugation of the solution and addition of NaBPh$_4$, a white solid was collected, washed and identified by IR, NMR and MS as NH_4BPh_4 and compared to those spectra of an analytically pure sample. The degradation test was also performed on the ^{15}N adduct of complex **7.4.** The IR displays the characteristic isotopic shift of NH stretching band from 3218 to 3148 cm^{-1}. The mass spectrum also exhibits the ammonium ion peak at 19 m/z compared to the 18 m/z peak for the non-isotopically enriched sample. The ^{15}N-NMR resonance was located at 140.1 ppm.

X-ray Crystallography

Suitable crystals were selected, mounted on a thin, glass fiber with paraffin oil, and cooled to the data collection temperature. Data were collected on a Bruker AXS SMART 1 k CCD diffractometer. For all the compounds data collection was performed with three batch runs at phi = 0.00 deg (650 frames), at phi = 120.00 deg (650 frames), and at phi = 240.00 deg (650 frames). Initial unit-cell parameters were determined from 60 data frames collected at different sections of the Ewald sphere. Semiempirical absorption corrections based on equivalent reflections were applied.[15] The systematic absences and unit-cell parameters were consistent for the reported space groups. The structures were solved by direct methods, completed with difference Fourier syntheses, and refined with full-matrix least-squares procedures based on *F*2. A cocrystallized solvent molecule in the structure of **7.1** was refined isotropically. All the other non-hydrogen atoms in all the structures were refined with anisotropic displacement parameters. All hydrogen atoms were treated as idealized contributions. All scattering factors and anomalous dispersion factors are contained in the SHELXTL 6.12 program library.[16] Complex **7.1** has one molecule of diethyl ether per 2 chromium atoms in the lattice which gives the best result when refined with half occupancy. Relevant crystal data and bond distances and angles are given in Tables 7.1 and 7.2.

Table 7.1. Crystal Data and Structure Analysis Results of 7.1, 7. 3 and 7.4

	7.1	**7.3**	**7.4**
formula	$C_{39}H_{56}CrN_4O_{1.50}$	$C_{74}H_{102}Cr_2N_8Na_2O_2$	$C_{37}H_{52}CrN_4NaO$
Mw	656.88	1287.63	644.82
crystal system	Monoclinic	Monoclinic	Monoclinic
space group	C2/c	P2/n	P2(1)/c
a (Å)	25.143(3)	18.148(3)	12.024(3)
b (Å)	11.5634(14)	18.561(3)	16.623(5)
c (Å)	30.241(4)	21.219(3)	18.556(5)
α	90	90	90
β	113.095(2)	103.198(2)	99.425(5)
γ	90	90	90
V (Å^3)	8087.7(17)	6958.6(16)	3658.8(17)
Z	8	4	4
radiation (Kα, Å)	0.71073	0.71073	0.71073
T (K)	213(2)	203(2)	208(2)
D_{calcd} (g cm^{-3})	1.079	1.229	1.171
μ_{calcd} (mm^{-1})	0.316	0.375	0.357
F_{000}	2832	2760	1384
R, *Rw*^{2} [a]	0.0674, 0.1757	0.0541, 0.1363	0.0764, 0.1653
GoF	1.086	1.054	1.045

[a] *R*) Σj*F*oj - j*F*cj/Σj*F*j. *R*w) [Σ(j*F*oj - j*F*cj)2/Σ*w*Fo2]$^{1/2}$.

Table 7.2. Selected Bond Distances (Å) and Angles (deg) of 7.1, 7.3 and 7.4

7.1	7.3	7.4
Cr(1)-N(1) = 2.141(3)	Cr(1)-N(1) = 2.054(4)	Cr(1)-N(1) = 2.010(6)
Cr(1)-N(2) = 1.940(3)	Cr(1)-N(2) = 1.953(4)	Cr(1)-N(2) = 1.958(6)
Cr(1)-N(3) = 2.083(3)	Cr(1)-N(3) = 2.086(4)	Cr(1)-N(3) = 2.010(6)
Cr(1)-N(4) = 1.781(3)	Cr(1)-N(7) = 1.770(4)	Cr(1)-N(4) = 1.911(10)
Cr(1)-O(1) = 2.182(3)	Cr(1)-O(1) = 2.124(3)	Na(1)-N(4) = 2.157(10)
N(4)-N(4a) = 1.241(6)	Cr(2)-N(4) = 2.079(3)	Na(1)-O(1) = 2.239(7)
N(1)-C(2) = 1.338(5)	Cr(2)-N(5) = 1.944(4)	Na(1)-C(22) = 2.962(8)
N(3)-C(8) = 1.366(5)	Cr(2)-N(6) = 2.060(3)	Na(1)-C(23) = 2.991(8)
C(1)-C(2) = 1.512(5)	Cr(2)-N(8) = 1.765(4)	Na(1)-C(24) = 3.021(8)
C(8)-C(9) = 1.505(6)	Cr(2)-O(2) = 2.147(3)	Na(1)-C(25) = 3.041(8)
C(2)-C(3) = 1.424(5)	N(1)-C(2) = 1.400(6)	Na(1)-C(26) = 2.989(8)
C(7)-C(8) = 1.406(5)	N(3)-C(8) = 1.426(6)	Na(1)-C(27) = 2.936(8)
N(2)-C(3) = 1.372(5)	N(2)-C(3) = 1.387(6)	Na(1)-C(5A) = 2.951(9)
N(2)-C(7) = 1.404(5)	N(2)-C(7) = 1.396(6)	Na(1)-C(6A) = 2.879(8)
N(1)-Cr(1)-N(2) = 75.33(12)	C(1)-C(2) = 1.465(6)	N(1)-C(2) = 1.377(9)
N(1)-Cr(1)-N(3) = 137.88(12)	C(2)-C(3) = 1.405(7)	N(3)-C(8) = 1.373(9)
N(1)-Cr(1)-N(4) = 109.51(12)	C(3)-C(4) = 1.415(7)	N(2)-C(3) = 1.366(9)
N(1)-Cr(1)-O(1) = 91.84(11)	C(4)-C(5) = 1.352(7)	N(2)-C(7) = 1.378(9)
N(2)-Cr(1)-N(3) = 76.61(12)	C(5)-C(6) = 1.437(7)	C(1)-C(2) = 1.484(10)
N(2)-Cr(1)-N(4) = 103.46(13)	C(6)-C(7) = 1.470(7)	C(2)-C(3) = 1.408(10)
N(2)-Cr(1)-O(1) = 151.88(12)	C(7)-C(8) = 1.383(6)	C(7)-C(8) = 1.434(10)
N(3)-Cr(1)-N(4) = 107.13(13)	C(8)-C(9) = 1.470(7)	C(8)-C(9) = 1.452(10)
N(3)-Cr(1)-O(1) = 98.56(11)	N(1)-Cr(1)-N(2) = 77.62(15)	N(1)-Cr(1)-N(2) = 78.1(3)
N(4)-Cr(1)-O(1) = 104.41(12)	N(1)-Cr(1)-N(3) = 138.31(15)	N(1)-Cr(1)-N(3) = 156.0(3)
Cr(1)-N(4)-N(4a) = 161.95(15)	N(1)-Cr(1)-N(7) = 109.52(15)	N(1)-Cr(1)-N(4) = 102.6(3)
	N(1)-Cr(1)-O(1) = 95.04(14)	N(2)-Cr(1)-N(3) = 77.8(3)
	N(2)-Cr(1)-N(3) = 77.93(15)	N(2)-Cr(1)-N(4) = 178.9(4)
	N(2)-Cr(1)-N(7) = 101.55(15)	N(3)-Cr(1)-N(4) = 101.4(3)
	N(2)-Cr(1)-O(1) = 155.28(13)	Cr(1)-N(4)-Na(1) = 128.7(5)
	N(3)-Cr(1)-N(7) = 108.12(15)	
	N(3)-Cr(1)-O(1) = 93.31(13)	
	N(7)-Cr(1)-O(1) = 103.15(14)	
	Cr(1)-N(7)-N(8) = 163.5(3)	
	Cr(2)-N(8)-N(7) = 159.7(3)	

Complex 7.1. The structure consists of a symmetry generated dimer with two identical {2,6-{2,6-(^{i}Pr)$_2$PhN=C(Me)}$_2$(C_5H_3N)}Cr(THF) units connected by one bridging end-on ligated dinitrogen unit (Figure 7.1). The coordination geometry around the metal center can be best described as distorted square pyramidal (τ = 0.23).[17] The basal plane is comprised of the three nitrogen atoms of the ligand system [Cr(1)-N(1) = 2.141(3) Å, Cr(1)-N(2) = 1.940(3) Å, Cr(1)-N(3) = 2.083(3) Å] and the coordinated THF oxygen atom [Cr(1)-O(1) = 2.182(3) Å, N(1)-Cr(1)-N(2) = 75.33(12)°, N(1)-Cr(1)-N(3) = 137.88(12)°, N(1)-Cr(1)-O(1) = 91.84(11)°, N(2)-Cr(1)-N(3) = 76.61(12)°, N(2)-Cr(1)-O(1) = 151.88(12)°, N(3)-Cr(1)-O(1) = 98.56(11)°]. The bridging dintrogen unit is located on the apical position [Cr(1)-N(4) = 1.781(3) Å, N(4)-Cr(1)-N(1) = 109.51(12)°, N(4)-Cr(1)-N(2) = 103.46(13)°, N(4)-Cr(1)-N(3) = 107.13(13)°, N(4)-Cr(1)-O(1) = 104.41(12)°]. The N-N distance is longer than in free N_2 [N(4)-N(4a) = 1.241(6) Å] and the geometry about the Cr_2N_2 unit deviates substantially from linearity [Cr(1)-N(4)-N(4a) = 161.95(15)°]. The long bonding distance formed by the two methyl groups with the imine carbon atoms [C(1)-C(2) = 1.512(5) Å, C(8)-C(9) = 1.505(6) Å] is consistent with the presence of C-C single bonds. However, the bond lengths of the imine functions have been lengthened with respect to the neutral ligand [N(1)-C(2) = 1.338(5) Å, N(3)-C(8) = 1.366(5) Å] which is also paralleled by a shortening in the C_{imine}-C_{ortho} bond distances [C(2)-C(3) = 1.424(5) Å, C(7)-C(8) = 1.406(5) Å] and a lengthening in the N_{pyr}-C_{ortho} bond distances [N(2)-C(3) = 1.372(5) Å, N(2)-C(7) = 1.404(5) Å].

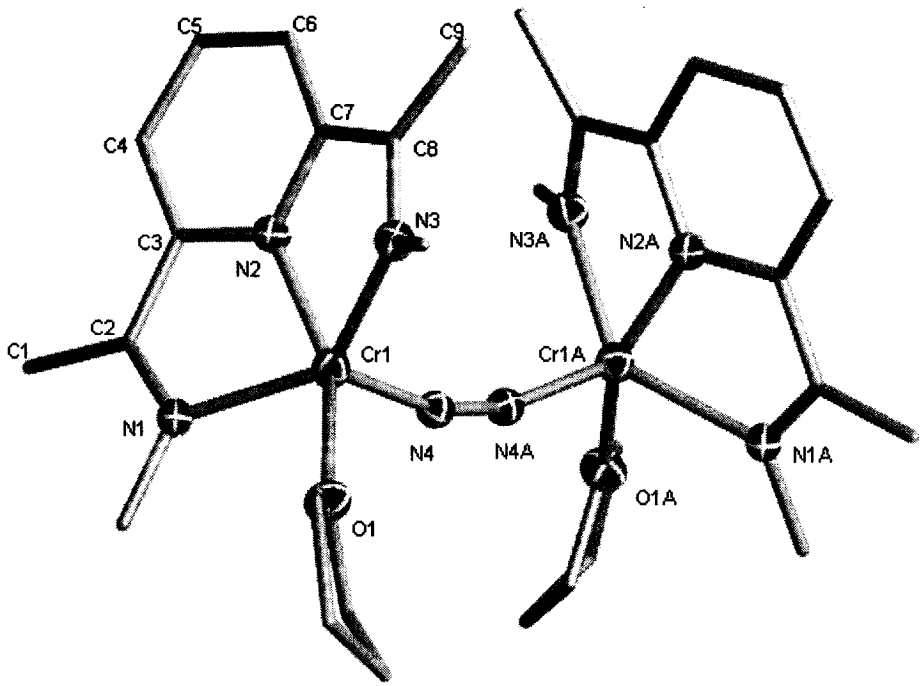

Figure 7.1. Partial thermal ellipsoid plot of **7.1** with ellipsoids drawn at the 30% probability level. Aryl groups on the imine-N atoms and all hydrogen atoms have been omitted for clarity.

Complex 7.3. The molecular structure of **7.3** is closely related to **7.1**, featuring a Cr-dimer bridged by a N_2 unit (Figure 7.2). Each Cr center adopts a severely distorted square pyramidal geometry in which the two imine nitrogen donor atoms of the ligand and the N atom of the dinitrogen residue are bound in the equatorial pane [Cr(1)-N(1) = 2.054(4) Å, Cr(1)-N(3) = 2.086(4) Å, Cr(1)-N(7) = 1.770(4) Å, N(1)-Cr(1)-N(3) = 138.31(15)°, N(1)-Cr(1)-N(7) = 109.52(15)°, N(7)-Cr(1)-N(3) = 108.12(15)°]. The THF oxygen atom and pyridine N atom occupy the axial positions [Cr(1)-N(2) = 1.953(4) Å, Cr(1)-O(1) = 2.124(3) Å, N(2)-Cr(1)-O(1) = 155.28(13)°, N(1)-Cr(1)-O(1) = 95.04(14)°, N(1)-Cr(1)-N(2) = 77.62(15)°, N(2)-Cr(1)-N(3) = 77.93(15)°, N(3)-Cr(1)-O(1) = 93.31(13)° N(7)-Cr(1)-N(2) = 101.55(15)°, N(7)-Cr(1)-O(1) = 103.15(14)°]. The Cr_2N_2 unit shows a folding comparable to that of **7.1** [Cr(1)-N(7)-N(8) = 163.5(3)°, Cr(2)-N(8)-N(7) = 159.7(3)°], and the N-N distance [N(7)-N(8) = 1.288(5) Å] seems to be in agreement with the presence of a double bond, similar to that seen in complex **7.1**. The folding along the N-N vector could be the result of the presence of hydrogen atoms on one or both nitrogen

atoms, although the large Cr-N-N angles make this rather unlikely. The precise nature of the bridging N_2 unit will be discussed in more detail later on. Different from **7.1,** two Na atoms are side-on bonded to the dinitrogen unit [Na(1)-N(7) = 2.618(4) Å, Na(1)-N(8) = 2.478(4) Å] forming a puckered Na_2N_2 moiety. Each of the two Na atoms is bonded to one imine nitrogen atom [Na(1)-N(4) = 2.587(4) Å] as well as weakly π-bound to the pyridine ring of the opposite ligand. The coordination geometry of each Na atom is completed by an agostic interaction with the Me unit of one isopropyl group of one aromatic ring [Na(1)...C(54) = 3.079(6) Å]. The imine Me groups show C-C distances [1.465(6) Å, 1.470(7) Å, 1.486(6) Å and C(45)-C(46) = 1.435(6) Å; for an average of 1.464 Å] which are shorter than expected for C_{sp2}-C_{sp3} single bonds (usually around 1.50 Å, as found in the neutral ligand), but not short enough for the typical scenario of one deprotonated Me group equally disordered over two positions (around 1.43 Å, as found in **7.2**).[11] In this particular case, a single deprotonation may have occurred in the dimer: one double bond disordered over four positions may well account for the observed C-C distances.

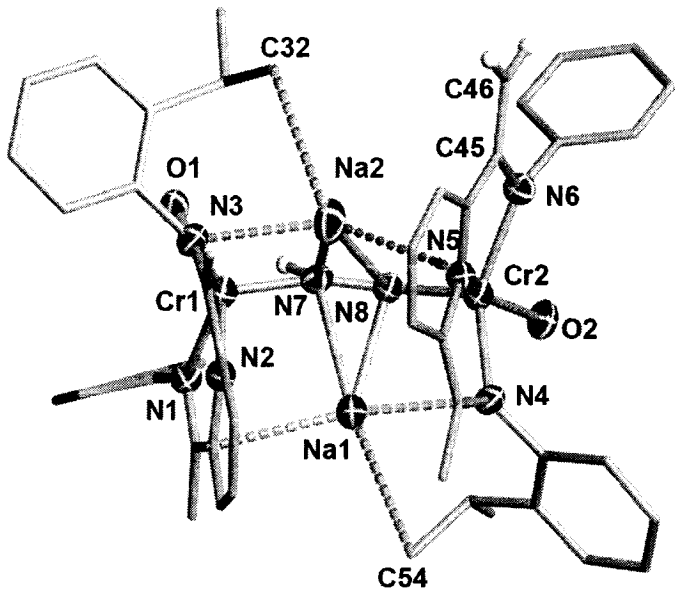

Figure 7.2. Partial thermal ellipsoid plot with ellipsoids of **7.3** drawn at the 30% probability level. Some of the ^{i}Pr groups, the THF carbon atoms and almost all of the hydrogen atoms have been omitted for clarity.

Complex 7.4. The structure of complex **7.4** (Figure 7.3) is comprised of a mononuclear, square planar Cr center surrounded by the ligand system [Cr(1)-N(1) = 2.010(6) Å, Cr(1)-N(2) = 1.958(6) Å, Cr(1)-N(3) = 2.010(6) Å]. An NH or NH_2 group occupies the fourth coordination site [Cr(1)-N(4) = 1.911(10) Å, N(1)-Cr(1)-N(2) = 78.1(3)°, N(1)-Cr(1)-N(3) = 156.0(3)°, N(1)-Cr(1)-N(4) = 102.6(3)°, N(2)-Cr(1)-N(3) = 77.8(3)°, N(2)-Cr(1)-N(4) = 178.9(4)°, N(3)-Cr(1)-N(4) = 101.4(3)°], forming a bridge to a Na atom [N(4)-Na(1) = 2.157(10) Å]. In turn, the Na cation carries one molecule of THF and is π-bound to one aryl ring of the ligand [Na(1)-O(1) = 2.239(7) Å], assembling an infinite array via bonding to the *meta* and *para* carbons of an identical unit [Na(1)-C(5a) = 2.951(9) Å, Na(1)-C(6a) = 2.879(8) Å]. The C_{methyl}-C_{imine} bonds are rather short for C-C single bonds and suggest that one of the two Me groups might in fact have undergone deprotonation with consequent formation of a double bond. The other bond distance alterations are characteristic of reduction by two electrons [N(1)-C(2) = 1.377(9) Å, N(3)-C(8) = 1.373(9) Å, N(2)-C(3) = 1.366(9) Å, N(2)-C(7) = 1.378(9) Å, C(2)-C(3) = 1.408(10) Å, C(7)-C(8) = 1.434(10) Å].

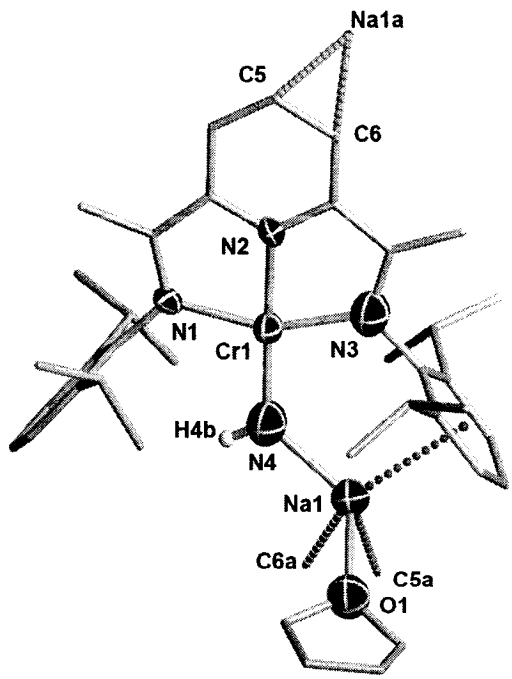

Figure 7.3. Partial thermal ellipsoid plot of **7.4** with ellipsoids drawn at the 30% probability level. Most hydrogen atoms have been omitted for clarity.

Results and Discussion

The divalent 2,6-{[2,6-(^{i}Pr)$_2$C$_6$H$_5$]N=C(CH$_3$)}$_2$(C$_5$H$_3$N)CrCl$_2$ is readily formed via straightforward reaction of the neutral ligand with CrCl$_2$(THF)$_2$.[11] Its reduction with NaH in THF (Scheme 7.1) affords the reduced species 2,6-{[2,6-(^{i}Pr)$_2$C$_6$H$_5$]N=C(CH$_3$)}$_2$(C$_5$H$_3$N)CrCl discussed in Chapter 5, which forms a potent ethylene polymerization catalyst upon activation with MAO.[11] In spite of the connectivity, suggesting a rare case of monovalent non-cyclopentadienyl chromium, the fairly regular square planar coordination geometry around the metal center strongly suggests that, similar to the cases of Al[18] and Fe,[7,19] the complex contains a *higher valent* metal center magnetically coupled to one or more ligand-centered unpaired electrons. This observation prompted further attempts to reduce both LCrCl$_2$ and LCrCl [L = 2,6-{[2,6-(^{i}Pr)$_2$C$_6$H$_5$]N=C(CH$_3$)}$_2$(C$_5$H$_3$N)].

The reaction of both LCrCl$_2$ and LCrCl with an appropriate amount of either metallic sodium or sodium hydride in THF under a nitrogen atmosphere afforded the corresponding dinuclear dinitrogen complex [2,6-{[2,6-(^{i}Pr)$_2$C$_6$H$_5$]N=C(CH$_3$)}$_2$ (C$_5$H$_3$N)Cr(THF)]$_2$(μ-N$_2$) (**7.1**). The connectivity of **7.1**, as yielded by an X-ray crystal structure (Figure 7.1), showed a dinuclear complex with the two square pyramidal chromium atoms bridged by one end-on bonded dinitrogen unit and each surrounded by one ligand and one molecule of coordinated THF. The complex is basically isostructural with the vanadium analogue.[8] The N-N distance [N(4)-N(4a) = 1.241 Å] of the coordinated N$_2$ unit also compares well with that of the vanadium complex, possibly suggesting that the dinitrogen unit has undergone a two-electron reduction. To the best of our knowledge, only one dinitrogen-bridged dichromium complex has been reported before, [(arene)Cr(CO)$_2$]$_2$(μ-N$_2$). This complex contains an end-on bonded N$_2$ unit (Chatt type) with a very short N-N bond 1.110(18) Å.[10] The elongation in **7.1** of the C$_{imine}$=N$_{imine}$ bond together with the shortening of the C$_{ortho}$-C$_{imine}$ bonds suggests significant reduction of the ligand system.[7,20] This, together with the partial reduction of dinitrogen, suggests the possibility of regarding the complex as bearing two divalent (or trivalent) chromium centers bound to monoanionic (or dianionic) ligands and bridged by an N_2^{2-} unit. Complex **7.1** is paramagnetic and displays a room temperature magnetic moment per molecule of μ_{eff} = 5.7 μ_B. This value is certainly lower than expected for two high-spin d^4

Cr(II) centers. On the other hand, the internal coupling between the metal center and the ligand radical anion, as normally observed in the reduced species of this ligand system,[19-21] as well as possible coupling between the two metal centers, may well result in a rather non-diagnostic value of the magnetic moment. Regardless of how we consider the metal oxidation state in **7.1**, its formation can be easily rationalized in terms of reduction of the metal center followed by intramolecular re-oxidation at the expense of both the coordinated N_2 unit and the ligand system.

Scheme 7.1

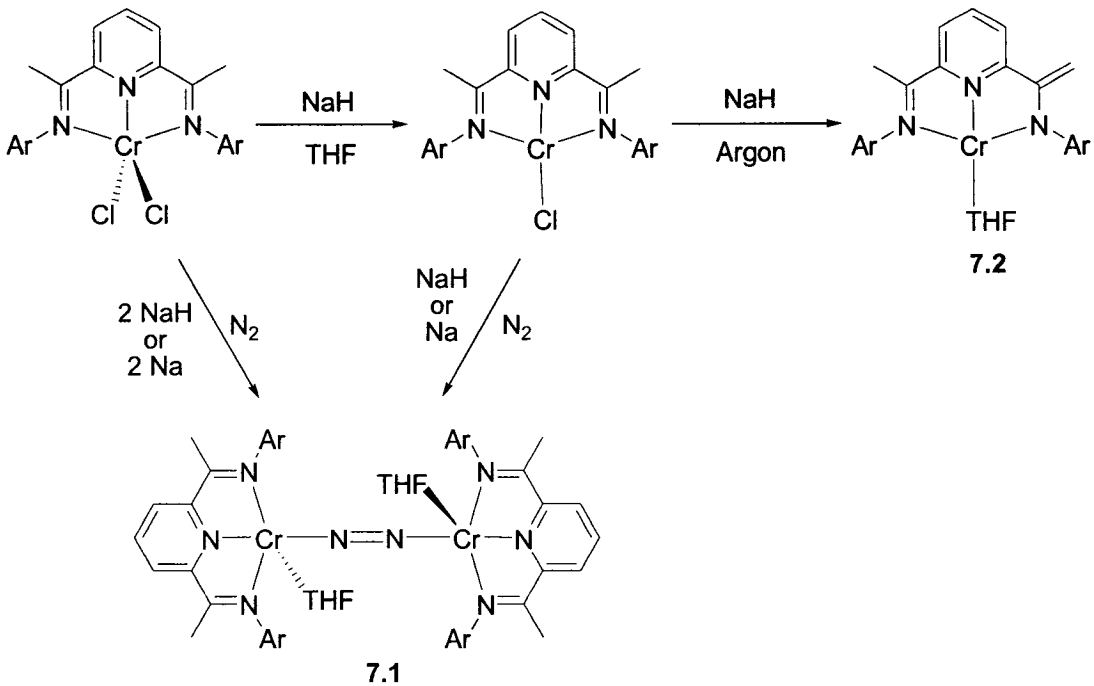

Treatment of LCrCl with NaH under argon (with careful exclusion of dinitrogen from the reaction medium) afforded the complex formulated as {2-[2,6-(^{i}Pr)$_2$PhN=C(CH$_3$)]-6-[2,6-(^{i}Pr)$_2$PhN-C=CH$_2$](C$_5$H$_3$N)}Cr(THF) (**7.2**) (Scheme 7.1), in which the formally Cr(I) atom is surrounded by the mono-deprotonated form of the ligand and one molecule of THF in an overall square planar geometry. The formation of **7.2** arises from the deprotonation of one of the two methyl groups attached to the imino function, implying that, in the absence of N_2, NaH acts as a base. Complex **7.2** was also shown to arise upon addition of Li-alkyls to LCrCl in Chapter 5, and a full description of

the complex can be found therein (complex **5.4**).[11] The oxidation state of **7.2** is most likely the same as in the starting complex LCrCl, as strongly suggested by the similar square planar coordination geometry and very comparable values of the magnetic moment. Although the magnetic values are not completely in agreement with the d^4 electronic configuration of divalent chromium, they can be reasonably explained in terms of a divalent chromium atom coupled to a ligand radical dianion.

The partial reduction of the N_2 unit in **7.1** is intriguing and suggests that further reduction of the dinitrogen moiety may be possible. Accordingly, the reaction of **7.1** with NaH afforded dark brown paramagnetic crystals of a complex formulated as [{2,6-[2,6-(^{i}Pr)$_2$PhN=C(CH$_3$)]$_2$(C$_5$H$_3$N)}Cr(THF)][{2-[2,6-(^{i}Pr)$_2$PhN=C(CH$_3$)]-6-[2,6-(^{i}Pr)$_2$PhN-C=CH$_2$](C$_5$H$_3$N)}Cr(THF)](μ-N$_2$H)(μ-Na)$_2$ (**7.3**) on the basis of the X-ray crystal structure (Figure 7.2) and spectroscopic evidence. The dinuclear structure of the complex is surprisingly similar to that of **7.1**, with each Cr center surrounded by the ligand and a molecule of THF and the two Cr entities apparently bridged through an end-on bonded N_2 moiety. Different from complex **7.1**, however, is the presence of two Na atoms bonded to each side of the N_2 unit, forming a folded N_2Na_2 unit. In addition, each Na atom is π-bound to one pyridine ring and forms an agostic contact with one of the four Me isopropyl groups of one aryl substituent. The severe puckering of the N_2Na_2 moiety and consequent pyramidalization of the nitrogen atom suggests that protonation may have occurred. Accordingly, the IR spectrum of complex **7.3** did show one single medium/weak resonance at 3399 cm^{-1} that shifted to 3343 cm^{-1} in the sample prepared with $^{15}N_2$. This clearly indicates the presence of one N-H function. In addition, the C-C distances to the imine methyl groups are somewhat shorter than expected for a normal C_{sp3}-C_{sp2} single bond but longer than expected for the scenario (previously observed with other complexes[11,22,23]) of one deprotonated imine group disordered over the two positions. The values observed in this structure would agree well with the presence of only one CH_2=C function disordered over the *four* positions provided by the two ligands of the dinuclear complex. The room temperature magnetic moment is surprisingly low [μ_{eff} = 1.9 μ_B]. In spite of having been generated in THF and crystallized from toluene, the complex, once crystallized, shows no solubility in any solvent with which it does not react, thus regrettably preventing spectroscopic investigations in solution.

From the formal point of view, the formation of **7.3** from **7.1** implies a two-electron reduction followed by one hydrogen atom transferred from one of the four imine Me groups to the N_2 moiety. Calculations on this complex (discussed below) could only be reconciled with the observed structure if it was assumed that the crystal shows disorder between Cr-NH=N-Cr and Cr-N=NH-Cr orientations of the N_2H bridge: an ordered bridge would be sharply angled at the NH moiety (ca 130°) and much closer to linear at the other nitrogen atom (Scheme 7.2). If the structure is indeed disordered, the observed N-N distance may not be meaningful. The large Cr-N-N angles appear to rule out the possibility of having a μ-N_2H_2 unit in the structure.

Scheme 7.2

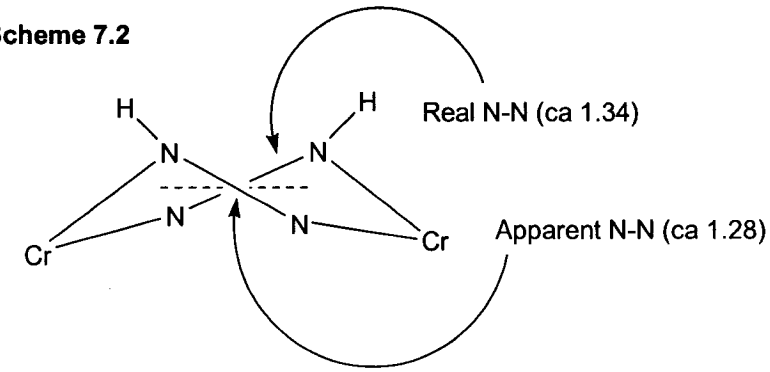

Further treatment of **7.3**, or more conveniently of either **7.1** or [{2,6-[2,6-(^{i}Pr)$_2$PhN=C(CH$_3$)]$_2$(C$_5$H$_3$N)}CrCl, with NaH in appropriate amounts (Scheme 7.3) afforded a new paramagnetic complex [μ_{eff} = 3.6 μ_B] formulated as {2-[2,6-(^{i}Pr)$_2$PhN=C(CH$_3$)]-6-[2,6-(^{i}Pr)$_2$PhN-C=CH$_2$](C$_5$H$_3$N)}Cr(μ-NH)][Na(THF)] (**7.4**) on the basis of the X-ray crystal structure, spectroscopic data and chemical degradation experiments.

The structure reveals a Cr center in a square planar environment defined by the three donor atoms of the ligand system and a non-hydrogen light atom. This atom in turn bridges a Na atom, π-bound to one of the aryl substituents (Figure 7.3). The thermal parameters of the bridging atom could be satisfactorily refined as either carbon or nitrogen. The hydrogen atom(s) at N could not be located, but the IR spectrum of **7.4** displays one sharp peak at 3413 cm^{-1}, in the area typical for NH stretching bands. Crystalline samples with identical cell parameters obtained by carrying out the same

reaction under $^{15}N_2$ displayed an isotopic shift to 3366 cm^{-1}. In addition, chemical degradation with diluted HCl followed by precipitation with $NaBPh_4$ afforded analytically pure samples of $^{15}NH_4BPh_4$ therefore conclusively demonstrating that the bridging atom is nitrogen and its origin is N_2 gas.[14]

Scheme 7.3

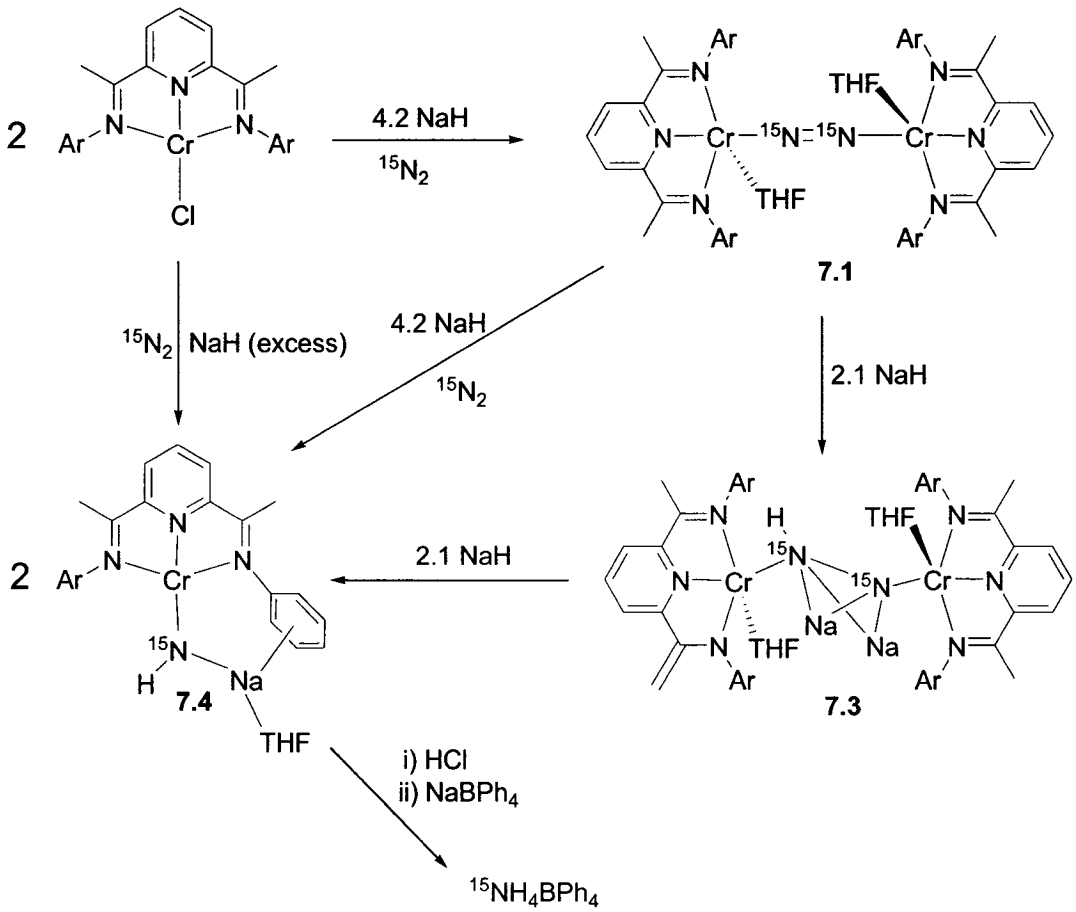

Just as in **7.3**, the imine C-Me bond lengths (1.465 Å av.) are somewhat shorter than expected for a C_{sp2}-C_{sp3} single bond, but not short enough for one deprotonated ($C{=}CH_2$) group disordered over two sites (as in **7.2**). There are at least two probable interpretations. The first possibility is that the complex is a (co-crystallized) mixture of a mono-deprotonated and a non-deprotonated complex. The two complexes might even have different numbers of hydrogen atoms at N, although the observation of a single sharp NH stretch vibration makes this unlikely. As a second possibility, the deviation

from the expected 1.43 Å (for a disordered mono-deprotonated complex, such as **7.2**) or 1.50 Å (for a non-deprotonated complex, like **7.1**) is but an artifact.

The isotope enrichment demonstrates that the formation of **7.4** is the result of dinitrogen cleavage. The fact that **7.4** could be obtained from LCrCl, **7.1** or **7.3** suggests that **7.1** and **7.3** may be regarded as intermediates in the formation of **7.4**, with **7.3** being the immediate precursor. The square planar geometry of the Cr center is very comparable to that of **7.2**, thus indicating that even in this case the metal center is present in the divalent state, i.e. reduction of **7.3** has taken place at nitrogen, *not* at the metal centre. The low magnetic moment [μ_{eff} = 3.6 μ_B] is not compatible with straight square planar Cr^{II}, but rather suggests that the complex contains high-spin Cr^{II} antiferromagnetically coupled to a ligand-centered unpaired electron. There are two formulations that would be consistent with these arguments (Scheme 7.4). The first is a complex containing a non-deprotonated ligand (as a radical anion) and a uni-negative NHNa(THF) fragment. Electronically, this variation (**7.4a**) would be similar to complex LCrCl. As a second possibility, the complex may contain a mono-deprotonated ligand (as a radical dianion) and a neutral $NH_2Na(THF)$ fragment. Electronically, this variation (**7.4b**) would be similar complex **7.2**.

Scheme 7.4

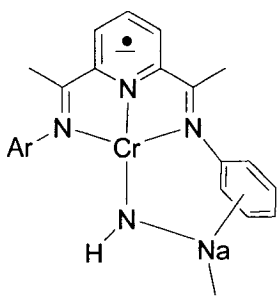

7.4a

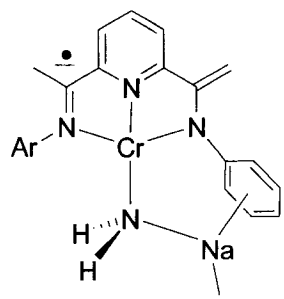

7.4b

Calculations confirm the electronic similarities mentioned above, and have been unsuccessful in determining the probability of one structure over the other. Co-crystallization of **7.4a** and **7.4b**, with the observed Cr-N bond length being an average of those belonging to **7.4a** and **7.4b**, remains of course a distinct possibility as well.

However, the presence of the sharp N-H resonance in the I.R. spectrum seems to suggest that perhaps structure **7.4a** is the main contributor to the description of what appears to be a tautomeric mixture.

A possible rationalization for the formation of **7.4** could start with **7.3** reacting with an additional equivalent of NaH, resulting in cleavage of the N-N bond to produce one mono-sodium amide and one di-sodium amide complex (Scheme 7.5). The latter should easily be basic enough to deprotonate any solvent and form a mono-sodium amide. Scheme 7.5 shows a possible sequence producing equimolar quantities of **7.4a** and **7.4b**, but of course this is pure speculation.

Scheme 7.5

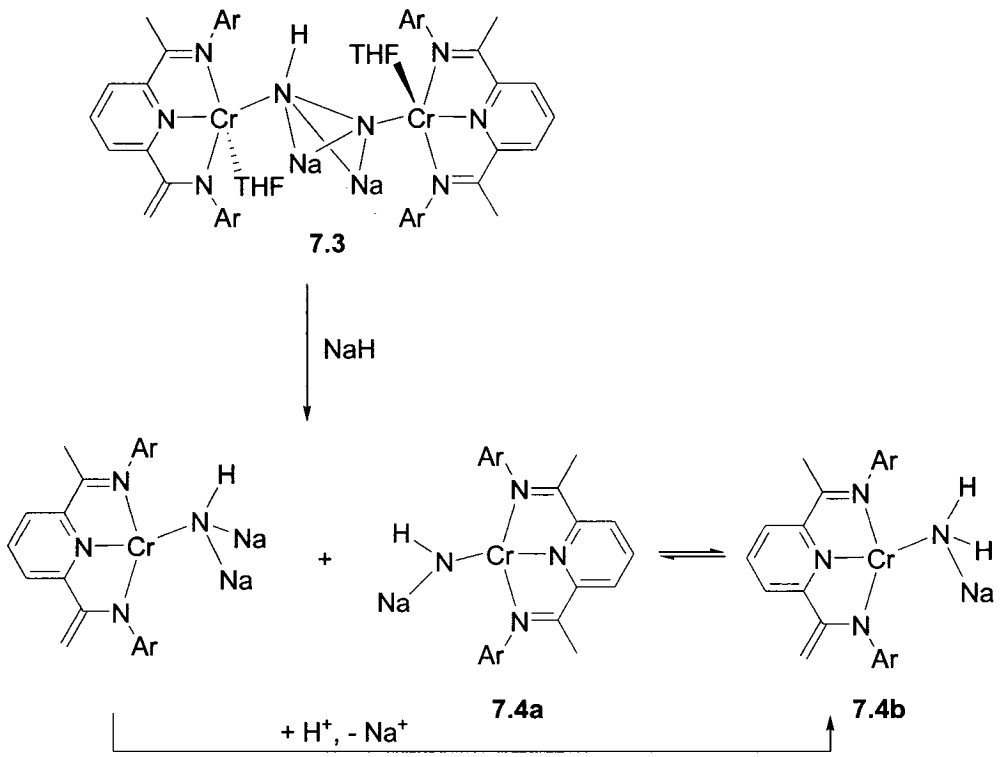

Calculations and Discussion

In collaboration with Peter Budzelaar from the University of Manitoba, calculations were performed on the complexes described herein.[12] For calculations on mononuclear model systems, the 2,6-$^{i}Pr_2C_6H_3$ groups were replaced by methyl groups

and THF was replaced by Me_2O. Spin states up to S = 5/2 were considered for each species and geometries were fully optimized for each individual spin state. The full system was then optimized assuming the spin state that was lowest for the model system. Vibrational analyses were not feasible for these large, open-shell systems.

All calculations were carried out with the Turbomole program[24] coupled to the PQS Baker optimizer.[25] All calculations used the spin-unrestricted formalism; even for "S = 0" systems, spin-unrestricted calculations gave significantly lower energies than spin-restricted calculations. Geometries were fully optimized at the B3-LYP level[26] level using the Turbomole SV(P) basis set [24a,c] on all atoms. Orbital drawings were created using Molden.[27]

Electronic structure of mononuclear Cr complexes

DFT calculations were performed for various spin states of simplified models of $L'CrCl_3$ (**7A**), $L'CrCl_2$ (**7B**), L'CrCl (**7C**) and complex **7.2** [L' = 2,6-$\{CH_3N{=}C(CH_3)\}_2(C_5H_3N)$].[12] For the lowest-energy spin state, geometry optimizations were then performed for the complete molecule. Calculated geometrical parameters are collected and compared with experimental values in Table 7.3. The agreement was generally satisfactory, although calculated bond lengths to Cr are systematically long.

The trivalent $L'CrCl_3$ prefers the expected high-spin (S = 3/2) ground state. It has an approximately octahedral metal environment, with the apical chlorides bent backward towards the pyridine ring. The calculated ligand C=N and C_{im}-C_{py} distances are close to those of the free ligand and, as expected, indicate that there is no significant electron transfer to ligand π^* orbitals.

Complex $L'CrCl_2$ prefers a triplet (S = 1) ground state by a small margin (ca 0.5 kcal/mol for the simplified model). This preference already indicates that the complex is *not* an ordinary Cr^{II} complex (which would normally prefer a high-spin S = 2 ground state). Rather, the orbital analysis of the triplet state shows occupied d_{xz}, d_{yz} and d_{xy} orbitals in the α manifold, but a mostly ligand π^*-type occupied orbital of β-spin (of the same symmetry as d_{xz}). Thus, this complex is best described as having Cr^{III} antiferromagnetically coupled to a ligand radical anion. In agreement with this description, it shows elongated C=N bonds and shortened C_{im}-C_{py} bonds.

Interestingly, calculations indicate that complex L'CrCl contains Cr^{II} antiferromagnetically coupled to a ligand radical anion. Thus, whereas the reduction of the trivalent precursor to the divalent $L'CrCl_2$ is ligand-centered, further reduction to L'CrCl is metal-centered. The α manifold of L'CrCl contains occupied d_{xz}, d_{yz} and d_{xy} and d_{z2} orbitals, whereas a single occupied ligand π*-like orbital is found in the β-manifold.

The deprotonated complex **7.2** also features Cr^{II}, now antiferromagnetically coupled to a ligand-centered unpaired electron mainly located in the intact imine-pyridine portion of the mono-deprotonated ligand. In earlier work, we observed easy dimerization of similar mono-deprotonated ligand complexes through coupling of the terminal methylene groups.[28] Dimerization might be made more difficult here by the presence of the additional unpaired electron on the ligand: the hypothetical dimer would contain two formally zero-valent chromium atoms.

The ligand C=N and C_{im}-C_{py} distances can be used to estimate the amount of metal-to-ligand electron transfer.[7,20] Because of the small changes in bond lengths involved, this requires either highly accurate X-ray data or the use of calculated distances (which suffer much less from random errors). Figure 7.4 shows calculated average distances for the above complexes (and for **7.4**), together with the "standard values" for transfer of zero to three electrons.[29] The positions of complexes $L'CrCl_3$, $L'CrCl_2$ and L'CrCl in the graph are indeed consistent with the transfer of 0, 1 and 1 electron, respectively. Complexes **7.2** and **7.4b** do not follow the trend of the other points, which is to be expected since they contain a deprotonated ligand.

Table 7.3. Calculated and observed bond lengths for mononuclear Cr complexes

	7A		7B		7C		7.2	
Bond[a]	Calc'd	Exp[b]	Calc'd	Exp[c]	Calc'd	Exp[c]	Calc'd	Exp
Cr-N	2.211	2.142	2.120	2.118	2.131	2.077	2.067	2.020
	2.026	1.991	1.931	1.993	1.964	1.934	1.974	1.945
C=N	1.292	1.301	1.318	1.296	1.323	1.321	1.377	1.381
C_{im}-C_{py}	1.495	1.468	1.452	1.484	1.450	1.438	1.457	1.431
C_{im}-"Me"	1.505	1.489	1.506	1.477	1.508	1.501	1.436	1.435
Cr-Cl/O	2.358	2.314	2.266	2.299	2.307	2.287	2.134	2.084
	2.265	2.282	2.269	2.416				

[a] Averaged where appropriate. [b] ref 30. [c] ref 11.

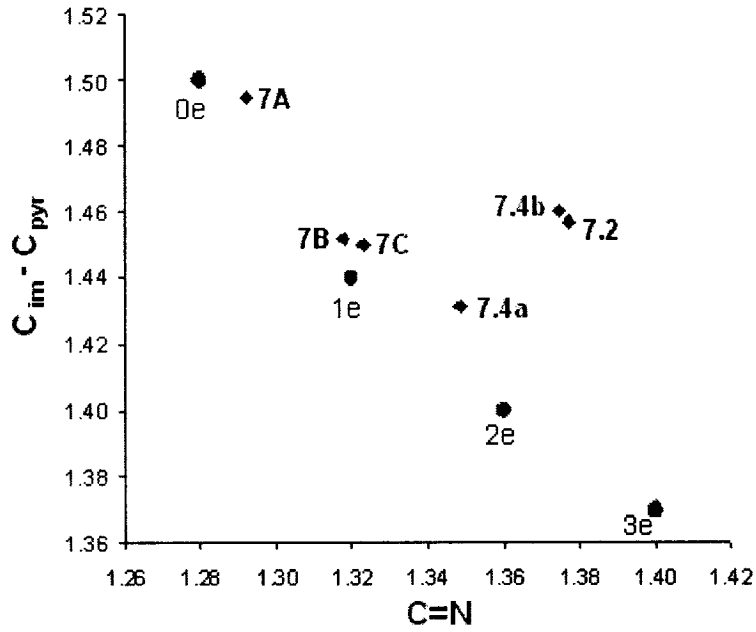

Figure 7.4. Calculated (◆) C=N and C_{im}-C_{py} distances for complexes L'$CrCl_3$, L'$CrCl_2$, L'CrCl, **7.2** and **7.4a/b**, compared to reference values (●) for transfer of 0-3 electrons.[29]

Electronic structure of dinuclear Cr complexes

In view of the uncertainties surrounding the formulation of **7.3**, we considered both N_2H-bridged (**7.3a**: [{2,6-[2,6-(^{i}Pr)$_2$PhN=C(CH_3)]$_2$(C_5H_3N)}Cr(THF)][{2-[2,6-(^{i}Pr)$_2$PhN=C(CH_3)]-6-[2,6-(^{i}Pr)$_2$PhN-C=CH_2](C_5H_3N)}Cr](μ-N_2H)(μ-Na)$_2$) and N_2-bridged (**7.3b**: [{2,6-[2,6-(^{i}Pr)$_2$PhN=C(CH_3)]$_2$(C_5H_3N)}Cr(THF)]$_2$(μ-N_2)(μ-Na)$_2$) structures. Structure **7.3a**, assumed above for complex **7.3**, seems the most likely in view of the observation of an N-H stretch vibration in the IR spectrum. Structure **7.3b** corresponds to a simple 2-electron reduction of **7.1**, and is of interest in itself even if it would not correspond to the actual structure of complex **7.3**.

Constructing satisfactory theoretical descriptions of dinuclear complexes **7.1** and **7.3b** turned out to be surprisingly difficult. Several spin states, differing mainly in the coupling between the electrons on different Cr atoms, are close in energy. Surprisingly, nearly all models constructed of both **7.1** and **7.3b** spontaneously eliminated the bridging N_2 molecule during geometry optimization. The only model of **7.1** in which N_2 remained bound was one containing water molecules (as models for THF), where hydrogen bridges from these waters to the negatively charged N_2 fragment artificially strengthens the Cr-N_2 interaction somewhat.

It seems likely that the methods used (several functionals were tried) do not describe the balance between donation to the highly delocalized ligand π* system and to the rather compact N_2 π* orbitals *versus* occupation of metal 3*d* orbitals very well.[31] In order to arrive at some sort of theoretical description nonetheless, we constrained both Cr-N_2 bonds to their experimental (X-ray) values. For complex **7.1**, this produces an electronic structure in which each chromium centre is essentially Cr^{III}, each ligand has *one* π*-orbital *doubly* occupied, and one 3*d* electron antiferromagnetically coupled to an electron in an N_2 π*-orbital, i.e. we have a doubly reduced N_2 molecule, iso-electronic with dioxygen. Other spin states show different couplings between the Cr centers and ligand π*-orbitals, and also sometimes occupation of two *different* ligand π*-orbitals. In view of the problems mentioned above, we think that our results, in particular as regards coupling between Cr and ligand orbitals, should be treated with caution. Even the amount of electron transfer to the diiminepyridine ligand cannot be considered very reliable, since an incorrect balance between metal and ligand orbitals seems to be the cause of the computational problems. However, a description as $[L^{2-}Cr^{III}(THF)]_2(N_2^{2-})$ seems reasonable based on the results mentioned earlier for mononuclear complexes. The alternative $[L^{-}Cr^{II}(THF)]_2(N_2^{2-})$ description seems less likely, since the Cr^{II} centers in such a complex would have their d_{z2} orbitals occupied and hence should not bind ligands in apical positions.[32]

For hypothetical structure **7.3b**, the tendency to eliminate N_2 is strong. Calculations with Cr-N distances constrained to their experimental values produce an electronic structure which still is most easily described as containing two Cr^{III}, each bound to a ligand tri-anion (one π*-orbital doubly and the other one singly occupied) and to N_2^{2-}. The role of the sodium atoms is just to provide electrons to the π*-systems of the diiminepyridine ligands. Dissociation of N_2 allows rearrangement and occupation of the Cr d_{z2} orbitals, which (as for **7.1**) is the driving force for expulsion of N_2.

Our preferred model **7.3a** does not dissociate in the calculation. The pronounced asymmetry of the complex makes unambiguous interpretation of the orbital occupation pattern difficult. The structure, like **7.1** and **7.3b**, appears to contain two Cr^{III} centres, one bound to a ligand tri-anion monoradical (as in **7.3b**), and the other one to the mono-deprotonated closed-shell ligand trianion. The bridging N_a=N_bH fragment is effectively

2-, and is nearly linear around N_a but sharply angled around N_b. This structure can only be reconciled with the observed structure of **7.3** if we assume disorder in the N_2H bridge (and possibly also in the ligand deprotonation site), as explained above.

Neither the X-ray structure nor the calculations allow completely unambiguous assignment of the structure of **7.3**. However, we feel that a structure similar to **7.3a** is the most likely one. It is compatible with the observed N-H stretch vibration, would explain the somewhat shortened imine C-CH_3 bonds, and is less likely than the "over-reduced" structure **7.3b** to spontaneously expel N_2. However, more variations remain possible, differing in deprotonation state of one or both ligands, nature of the bridge (N_2 vs N_2H) or even presence of one or two hydrides at Na.

Conclusion

The formation of an unprecedented chromium-dinitrogen complex, its partial reduction and protonation and eventual cleavage to an imide product have been reported in this chapter. Given the unusual paucity of dinitrogen chemistry among chromium complexes, it seems plausible that the electron-storage capabilities of the bis-iminopyridine ligand play an important role in this sequence of reactions. The chemistry is complex, with several reactions occurring in parallel, and even with the aid of calculations some uncertainties remain in the structures assigned to intermediate and final products. Given that chromium seems to have no inclination for dinitrogen fixation/activation, these transformations can only be ascribed to the remarkable ability of the bis-iminopyridine ligand to act as an electron reservoir in multi-step reductive transformations.

References

(1) Allen, A. D.; Senoff, C. V. *J. Chem. Soc., Chem. Commun.* **1965**, 621.

(2) (a) MacLachlan, E. A.; Fryzuk, M. D. *Organometallics* **2006**, *25*, 1530. (b) Gambarotta, S. *J. Organomet. Chem.* **1995**, *500*, 117. (c) Gambarotta, S.; Scott, J. *Angew. Chem. Int. Ed.* **2004**, *43*, 5289. (d) MacKay, B. A.; Fryzuk, M. D. *Chem. Rev.* **2004**, *104*, 385. (e) Hidai, M.; Mizobe, Y. *Chem. Rev.* **1995**, *95*, 1115. (f) Hidai, M. *Coord. Chem. Rev.* **1999**, *185-186*, 99. (g) Fryzuk, M. D.; Johnson, S. A. *Coord. Chem. Rev.* **2000**, *200-202*, 379.

(3) (a) Yandulov, D. V.; Schrock, R. R. *Science* **2003**, *301*, 76. (b) Schrock, R. R. *Acc. Chem. Res.* **2005**, *38*, 955. (c) Pool, J. A.; Lobkovsky, E.; Chirik, P. J. *Nature* **2004**, *427*, 527. (d) Korobkov, I.; Gambarotta, S.; Yap, G. P. A. *Angew. Chem. Int. Ed.* **2003**, *42*, 4958.

(4) (a) Laplaza, C. E.; Cummins, C. C. *Science* **1995**, *268*, 861. (b) Laplaza, C. E.; Johnson, M. J. A.; Peters, J. C.; Odom, A. L.; Kim, E.; Cummins, C. C.; George, G. N.; Pickering, I. J. *J. Am. Chem. Soc.* **1996**, *118*, 8623. (c) Yandulov, D. V.; Schrock, R. R. *J. Am. Chem. Soc.* **2002**, *124*, 6252. (d) Mindiola, D. J.; Meyer, K.; Cherry, J.-P. F.; Baker, T. A.; Cummins, C. C. *Organometallics* **2000**, *19*, 1622. (e) Solari, E.; Da Silva, C.; Iacono, B.; Hesschenbrouck, J.; Rizzoli, C.; Scopelliti, R.; Floriani, C. *Angew. Chem. Int. Ed.* **2001**, *40*, 3907.

(5) (a) Fryzuk, M. D.; Johnson, S. A.; Rettig, S. J. *J. Am. Chem. Soc.* **1998**, *120*, 11024. (b) Fryzuk, M. D.; Johnson, S. A.; Patrick, B. O.; Albinati, A.; Mason, S. A.; Koetzle, T. F. *J. Am. Chem. Soc.* **2001**, *123*, 3960. (c) Fryzuk, M. D.; MacKay, B. A.; Johnson, S. A.; Patrick, B. O. *Angew. Chem. Int. Ed.* **2002**, *41*, 3709. (d) Fryzuk, M. D.; MacKay, B. A.; Patrick, B. O. *J. Am. Chem. Soc.* **2003**, *125*, 3234. (e) MacKay, B. A.; Patrick, B. O.; Fryzuk, M. D. *Organometallics* **2005**, *24*, 3836.

(6) (a) Jubb, J.; Gambarotta, S. *J. Am. Chem. Soc.* **1994**, *116*, 4477. (b) Dubé, T.; Conoci, S.; Gambarotta, S.; Yap, G. P. A.; Vasapollo, G. *Angew. Chem. Int. Ed.* **1999**, *38*, 3657. (c) Dube, T.; Ganesan, M.; Conoci, S.; Gambarotta, S.; Yap, G. P. A. *Organometallics* **2000**, *19*, 3716. (d) Guan, J.; Dube, T.; Gambarotta, S.; Yap, G. P. A. *Organometallics* **2000**, *19*, 4820.

(7) (a) See Chapter 6. (b) Bart, S. C.; Lobkovsky, E.; Chirik, P. J. *J. Am. Chem. Soc.* **2004**, *126*, 13794. (c) Bart, S. C.; Chlopek, K.; Bill, E.; Bouwkamp, M. W.; Lobkovsky, E.; Neese, F.; Wieghardt, K.; Chirik, P. J. *J. Am. Chem. Soc.* **2006**, *128*, 13901.

(8) Vidyaratne, I.; Gambarotta, S.; Korobkov, I.; Budzelaar, P. H. M. *Inorg. Chem.* **2005**, *44*, 1187.

(9) (a) Girolami, G. S.; Salt, J. E.; Wilkinson, G.; Thornton-Pett, M.; Hursthouse, M. B. *J. Am. Chem. Soc.* **1983**, *105*, 5954. (b) Sellman, D.; Maisel, G. *Z. Naturforsch., B* **1972**, *27B*, 465. (c) Karsch, H. H. *Angew. Chem. Int. Ed.* **1977**, *16*, 56. (d) Sobota, P.; Jezowski-Trzebiatowskq, B. *J. Organomet. Chem.* **1977**, *131*, 341.

(10) Denholm, S.; Hunter, G.; Weakley, T. J. R. *J. Chem. Soc., Dalton Trans.* **1987**, 2789.

(11) (a) Vidyaratne, I.; Scott, J.; Gambarotta, S.; Korobkov, I.; Duchateau, R. R. J. *Accepted in Organometallics.* (b) See also Chapter 5.

(12) (a) Vidyaratne, I.; Scott, J.; Gambarotta, S.; Budzelaar, P. H. M.; Korobkov, I. *manuscript submitted.*

(13) Sugiyama, H.; Aharonian, G.; Gambarotta, S.; Yap, G. P. A.; Budzelaar, P. H. M. *J. Am. Chem. Soc.* **2002**, *124*, 12268.

(14) Skoog, D. A.; West, D. M.; Holler, F. J. *Fundamentals of Analytical Chemistry, 7th Ed.* Saunders College Publishing, Philadelphia, **1996**.

(15) Blessing, R. *Acta Crystallogr.* **1995**, *A51*, 33.

(16) Sheldrick, G. M. Bruker AXS, Madison, WI, 2001.

(17) Addison, A. W.; Rao, T. N.; Reedijk, J.; van Rijn, J.; Verschoor, G. C. *J. Chem. Soc. Dalton Trans.* **1984**, 1349. The τ parameter helps to classify the geometry of five-coordinate complexes. The τ parameter is calculated by finding the difference between the two largest angles at the metal center and dividing by 60. For a perfect square pyramidal complex, $\tau = 0$ and for a perfect trigonal bipyramidal complex, $\tau = 1$. In cases where the actual geometry is ambiguous between square pyramidal and trigonal bipyramidal, the τ parameter helps to quantify the observed distortions.

(18) (a) Scott, J.; Gambarotta, S.; Korobkov, I.; Knijnenburg, Q.; de Bruin, B.; Budzelaar, P. H. M. *J. Am. Chem. Soc.* **2005**, *127*, 17204. (b) See also Chapter 4.

(19) (a) Scott, J.; Gambarotta, S.; Korobkov, I.; Budzelaar, P. H. M. *Organometallics* **2005**, *24*, 6298. (b) See also Chapter 3.

(20) (a) de Bruin, B.; Bill, E.; Bothe, E.; Weyhermüller, T.; Wieghardt, K. *Inorg. Chem.* **2000**, *39*, 2936. (b) Budzelaar, P. H. M.; de Bruin, B.; Gal, A. W.; Wieghardt, K.; van Lenthe, J. H. *Inorg. Chem.* **2001**, *40*, 4649. (c) Knijnenburg, Q.; Hetterscheid, D.; Kooistra, T. M.; Budzelaar, P. H. M. *Eur. J. Inorg. Chem.* **2004**, 1204.

(21) Sugiyama, H.; Korobkov, I.; Gambarotta, S.; Möller, A.; Budzelaar, P. H. M. *Inorg. Chem.* **2004**, *43*, 5771.

(22) (a) Khorobkov, I.; Gambarotta, S.; Yap, G. P. A. *Organometallics* **2002**, *21*, 3088. (b) Blackmore, I. J.; Gibson, V. C.; Hitchcock, P. B.; Rees, C. W.; Williams, D. J.; White, A. J. P. *J. Am. Chem. Soc.* **2005**, *127*, 6012.

(23) Scott, J.; Phull, H,; Gambarotta, S.; Korobkov, I. *manuscript in preparation.*

(24) (a) Ahlrichs, R. *et al* Turbomole Version 5, January **2002**. Theoretical Chemistry Group, University of Karlsruhe. (b) Treutler, O.; Ahlrichs, R. *J. Chem. Phys.* **1995**, *102*, 346. (c) Schäfer, A.; Horn, H.; Ahlrichs, R. *J. Chem. Phys.* **1992**, *97*, 2571. (d) Schäfer, A.; Huber, C.; Ahlrichs, R. *J. Chem. Phys.* **1994**, *100*, 5829. (e) Andrae, D.; Haeussermann, U.; Dolg, M.; Stoll, H.; Preuss, H. *Theor. Chim. Acta* **1990**, *77*, 123.

(25) (a) PQS version 2.4, **2001**, Parallel Quantum Solutions, Fayetteville, Arkansas, USA (the Baker optimizer is available separately from PQS upon request). (b) Baker J. *J. Comput. Chem.* **1986**, *7*, 385.

(26) (a) Lee, C.; Yang, W.; Parr, R. G. *Phys. Rev. B* **1988**, *37*, 785. (b) Becke, A. D. *J. Chem. Phys.* **1993**, *98*, 1372. (c) Becke, A. D. *J. Chem. Phys.* **1993**, *98*, 5648. (d) All calculations were performed using the Turbomole functional "b3 lyp", which is not identical to the Gaussian "B3LYP" functional.

(27) Schaftenaar, G.; Noordik, J. H. *J. Comput.-Aided Mol. Design* **2000**, *14*, 123.

(28) (a) Sugiyama, H.; Aharonian, G.; Gambarotta, S.; Yap, G. P. A.; Budzelaar, P. H. M. *J. Am. Chem. Soc.* **2002**, *124*, 12268. (b) Scott, J.; Gambarotta, S.; Korobkov, I.; Budzelaar, P. H. M. *J. Am. Chem. Soc.* **2005**, *127*, 13019. (c) Scott, J.; Gambarotta, S.; Korobkov, I. *Can. J. Chem.* **2005**, *83*, 279. (d) Sugiyama, H.; Gambarotta, S.; Yap, G. P. A.; Wilson, D. R.; Thiele, S. K.-H. *Organometallics* **2004**, *23*, 5054.

(29) Knijnenburg, Q.; Gambarotta, S.; Budzelaar, P. H. M. *Dalton Trans.* **2006**, 5442.

(30) Esteruelas, M. A.; López, A. M.; Méndez, L.; Oliván, M.; Oñate, E. *Organometallics*, **2003**, *22*, 395.

(31) The alternative possibility that the actual structure of **7.3** differs from the one we tried to model in having fewer or more hydrogen atoms cannot be entirely excluded at this stage.

(32) In fact, on elongating the Cr-N_2 distance the d_{z2} orbital becomes occupied, and this seems to cause the dissociation of the N_2 molecule in the calculation.

Chapter Eight

Spontaneous Reductive Dimerization of Cobalt and Subsequent Dinitrogen Fixation

---

Introduction

Preceding chapters have shown that the bis-iminopyridine ligand is not merely a good supporting ligand for transition metal complexes, but that it experiences a significant amount of participation in the reactivity of the complex and plays a very dominant role in determining the chemical behaviour of these systems.[1-8] The fact that the various transition metal complexes of this system display diverse activities towards ethylene polymerization and produce polymers of a very different nature must be ascribed not only to the electronic configurations of the metal center, but also to the variety of possible ligand transformations.

Different transition metal precursors appear to be prone to certain transformations over others, and those predispositions can act to either aid or hinder the activity of the catalyst. The availability of certain ligand transformations may determine the nature of the active species and therefore also the polymerization mechanism followed by that particular system. For example, the catalytic activity and polymer quality produced by the Fe and Co analogues are very different, indicating the involvement of two separate polymerization mechanisms.[9] Chapter 2 describes the variety of possible alkylation products of the divalent Fe precursor, including nucleophilic attack at the *ortho*-position or the imino-C atom, deprotonation of the ketimine methyl groups, or even dimerization

and reduction.[4a] On the other hand, previous studies of the analogous cobalt system have unveiled a relatively straightforward reduction of the system upon similar alkylation, with no visible alterations to the ligand backbone.[10]

The prominence of the ligand in the chemistry of these systems suggests that it may be possible to alter the reactivity of the complex by changing the electronic structure of the ligand backbone. Previous work in our lab has revealed the possibility of creating a dianionic version of the ligand via deprotonation of both ketimine methyl groups.[6] Although the 'new' ligand is very analogous in structure to the bis-iminopyridine molecule, the electronic characteristics have been altered. Preliminary investigations of the properties of the dianionic ligand with lanthanide metals revealed extremely high activity for butadiene polymerization and, even more desirable, outstanding stereoselectivity of the polymerization process.[6] Reduction of the lanthanide complexes demonstrated that the electron-accepting ability is still very strong in the dianionic version of this ligand. However, instead of housing electron density in the delocalized π-system, the electron density goes towards C-C bond formation to assemble a dinuclear structure.[6b]

In Chapter 2, the dianionic ligand was shown to coordinate to the divalent Fe center, resulting in the expected neutral species weakly retaining a molecule of LiCl.[4a] Although the catalytic activity of this species doubled in comparison to the neutral ligand derivative, the polymer, while similarly bimodal like that obtained by the neutral complex, contained a larger portion of the higher molecular weight fraction. To recap, the lower molecular weight fraction stems from chain termination by chain transfer to aluminum, whereas the higher molecular weight fraction undergoes β-hydride elimination as the main chain termination pathway.[9] Therefore, the relatively minor modification of the electronic configuration of the ligand system is sufficient to substantially interfere with the catalytic activity and polymerization mechanism.

Although not as well-performing as the Fe catalyst, the cobalt precursor is a fascinating system in its own right. Prior to our work on Fe, the groups of Gal, Gibson and Erker published independent investigations on the reactivity of the divalent Co precursor.[10] Upon activation with MAO or other aluminum activator, the metal center underwent one electron reduction to Co(I). Even though the ligand system may be the

recipient of the added electron density,[11] the metal ion behaves as a reduced, highly reactive Co(I) center, capable of forming stable dinitrogen or ethylene complexes.[10b] Since the electron accepting ability of the ligand appears to be at the basis of this behaviour, it will be interesting to observe how changes to the ligand backbone will affect the catalytic system. We have therefore attempted the reaction of the dianionic version of the ligand, {[2,6-[2,6-(^{i}Pr)$_2$PhN-C=(CH$_2$)]$_2$(C$_5$H$_3$N)]Li(THF)}{Li(THF)$_4$}, with divalent cobalt. Herein, the formation of a monovalent, dimeric cobalt complex is presented, together with its ability to polymerize ethylene and coordinate dinitrogen.[5]

Experimental Section

All operations were performed either under an argon atmosphere using standard Schlenk techniques or in a purified nitrogen-filled dry-box. The THF complex of $CoCl_2$ was prepared according to the standard procedure and 2,6-[2,6-(^{i}Pr)$_2$PhN-C(CH$_3$)]$_2$(C$_5$H$_3$N),[12] LiCH$_2$Si(CH$_3$)$_3$,[13] and {[2,6-[2,6-(^{i}Pr)$_2$PhN-C=(CH$_2$)]$_2$(C$_5$H$_3$N)] Li(THF)}{Li(THF)$_4$}[6] were prepared following published procedures. NaH was purchased from Aldrich and washed with hexane under nitrogen to remove the oil. Infrared spectra were recorded on a Mattson 9000 and Nicolet 750-Magna FT-IR instrument from Nujol mulls prepared in a dry box. Samples for magnetic susceptibility measurements were weighed inside a dry box equipped with an analytical balance and sealed into calibrated tubes and the measurements were carried out at room temperature with a Gouy balance (Johnson Matthey). Elemental analyses were performed on a Perkin-Elmer 2400 CHN analyzer. Data for X-ray crystal structure determinations were obtained with a Bruker diffractometer equipped with a Smart CCD area detector. NMR spectra were recorded on a Bruker AMX-500 spectrometer.

Preparation of {[2,6-(^{i}Pr)$_2$PhN-C=(CH$_2$)](C$_5$H$_3$N)[2,6-(^{i}Pr)$_2$PhN=C(CH$_2$)]}$_2$[Co(μ-Cl)Li(THF)$_3$]$_2$·(THF)$_4$ (8.1).

A solution of {[2,6-[2,6-(^{i}Pr)$_2$PhN-C=(CH$_2$)]$_2$(C$_5$H$_3$N)]Li(THF)}{Li(THF)$_4$} (1.25 g, 1.5 mmol) in THF was added to a stirred suspension of CoCl$_2$(THF)$_{1.5}$ (0.35 g, 1.5 mmol) in THF. The solution instantly became dark burgundy. The reaction was allowed to stir for 5 minutes and centrifuged to remove small amounts of insoluble material. The solvent was

evaporated *in vacuo* until a small volume and the resulting solution was allowed to stand at room temperature for 24 hours upon which large, dark-burgundy crystals of **8.1** were isolated (0.92 g, 0.48 mmol, 65%). Anal. Calcd. (found) for $C_{106}H_{164}N_6Cl_2Li_2O_{10}Co_2$ (%): C, 67.54 (67.78); H, 8.77 (9.01); N, 4.46 (4.55). IR (Nujol mull, cm^{-1}): ν 3058 (w), 2895 (s), 1640 (m), 1565 (vs), 1517 (m), 1466 (vs), 1399 (m), 1378 (m), 1323 (w), 1304 (m), 1260 (s), 1200 (w), 1174 (s), 1160 (w), 1099 (vs), 1048 (vs), 1026 (vs), 1003 (vs), 936 (m), 913 (s), 892 (m), 801 (vs), 778 (m), 764 (m), 748 (m), 726 (s), 694 (m).

Preparation of {[2,6-(^{i}Pr)$_2$PhN-C=(CH$_2$)](C$_5$H$_3$N)[2,6-(^{i}Pr)$_2$PhN=C(CH$_2$)]}$_2$[Co(N$_2$)]$_2$·2(toluene) (8.2).

A solution of {[2,6-[2,6-(^{i}Pr)$_2$PhN-C=(CH$_2$)]$_2$(C$_5$H$_3$N)]Li(THF)}{Li(THF)$_4$} (1.25 g, 1.5 mmol) in toluene was added to a stirred suspension of $CoCl_2(THF)_{1.5}$ (0.35 g, 1.5 mmol) in toluene under an argon atmosphere. The solution instantly became dark-burgundy red. The mixture was stirred overnight and centrifuged to remove small amounts of insoluble residue. The solution was then exposed to nitrogen gas causing an extreme deepening of the colour with standing overnight. The black-coloured solution was evaporated *in vacuo* down to a small volume. Small dark brown crystals of **8.2** were obtained after allowing the solution to stand at room temperature for 48 hours (0.59 g, 0.45 mmol, 60%). Anal. Calcd. (found) for $C_{80}H_{98}Co_2N_{10}$ (%): C, 72.93 (72.71); H, 7.50 (7.83); N, 10.63 (10.88). ^{1}H NMR (C_6D_6), 500MHz, 25°C) δ (ppm): 0.917 (d, 12H, (C***H***$_3$)$_2$CH), 1.21 (m, 24H, (C***H***$_3$)$_2$CH), 1.42 (d, 12H, (C***H***$_3$)$_2$CH), 2.47 (quint, 4H, (CH$_3$)$_2$C***H***), 3.16 (quint, 4H, (CH$_3$)$_2$C***H***), 3.53 (br s., 4H, N=C-C***H***$_2$-C***H***$_2$-C=N), 4.01 (s, 2H, NC=C***H***$_2$), 4.67 (s, 2H, NC=C***H***$_2$), 6.74 (d, 4H, *m*-C$_6$***H***$_3$^{i}Pr$_2$), 6.88 (d, 4H, *m*-C$_6$***H***$_3$^{i}Pr$_2$), 7.01 (t, 2H, *p*-C$_6$***H***$_3$^{i}Pr$_2$), 7.10 (t, 2H, *p*-C$_6$***H***$_3$^{i}Pr$_2$), 7.30 (t, 2H, *p*-C$_5$***H***$_3$N), 7.41 (d, 2H, *m*-C$_5$***H***$_3$N), 8.26 (d, 2H, *m*-C$_5$***H***$_3$N). IR (Nujol mull, cm^{-1}): ν 3057 (w), 2895 (s), 2153 (vs), 1598 (w), 1583 (m), 1548 (m), 1533 (m), 1494 (m), 1464 (vs), 1418 (w), 1372 (vs), 1323 (s), 1250 (s), 1203 (w), 1176 (s), 1142 (w), 1098 (m), 1073 (m), 1057 (m), 1038 (m), 1006 (s), 935 (m), 915 (m), 894 (w), 869 (w), 800 (s), 780 (vs), 762 (m), 747 (s), 729 (vs), 694 (m).

Preparation of [{2,6-[2,6-(^{i}Pr)$_2$PhN=C(CH$_3$)]$_2$(C$_5$H$_3$N)}Co(η^1-N$_2$)][Na(THF)$_5$] (8.3). Solid $CoCl_2(THF)_{1.5}$ (0.100 g, 0.42 mmol), 2,6-[2,6-(^{i}Pr)$_2$PhN=C(CH$_3$)]$_2$(C$_5$H$_3$N) (0.205 g, 0.42 mmol) and 6 equivalents of NaH (0.061 g, 2.52 mmol) were mixed together and suspended in THF. After stirring for 1 week, the colour of the solution became dark green. The THF was evaporated and the ether-soluble materials were separated. Fresh THF was added to the dark residue and a dark green solution in THF was centrifuged and layered with hexane. Dark green crystals of **8.3** precipitated after concentration and standing undisturbed for two days at room temperature (0.095 g, 0.10 mmol, 24% yield). IR (Nujol mull, cm^{-1}): ν 2950-2849 (s, b), 2144 (m), 2097 (m), 2039 (s), 2014 (m), 2002 (m), 1974 (s), 1579 (w), 1462 (s), 1377 (s), 1358 (w), 1310 (m), 1243 (s), 1090 (m), 1047 (m), 964 (m), 890 (w), 806 (w), 775 (w), 758 (m), 739 (m), 725 (m), 664 (w). [μ_{eff} = 2.4 μ_B]

X-ray Crystallography

Compounds **8.1-8.3** consistently yielded crystals that diffracted weakly and the results presented are the best of several trials. The crystals were mounted on thin glass fibers using paraffin oil and cooled to the data collection temperature. Data were collected on a Bruker AXS SMART 1k CCD diffractometer. To obtain acceptable redundancy data compounds **8.1-8.3** were collected with the sequence of 0.3° ω-scans at 0, 120 and 240° in φ. Initial unit cell parameters were determined from 50 data frames collected at the different sections of the Ewald sphere. Semi-empirical absorption corrections based on equivalent reflections were applied.[14] Systematic absences in the diffraction data-set and unit-cell parameters were consistent with monoclinic $P2_1/n$ for **8.1**, triclinic $P\bar{1}$ for **8.2**, and triclinic $P\bar{1}$ for **8.3**. Solutions in the centrosymmetric space groups yielded chemically reasonable and computationally stable results of refinement. The structures were solved by direct methods, completed with difference Fourier syntheses and refined with full-matrix least-squares procedures based on F^2. The compound molecule was located in the inversion center in structure of **8.1**. Two molecules of THF with full occupancy not located on any symmetry operators were found in the lattice of **8.1**. Two molecules of toluene with a full occupancy not located on any symmetry operators were found in the asymmetric unit of **8.2**. All non-hydrogen

atoms, except those of the THF solvent molecules in **8.1** were refined with anisotropic displacement coefficients. THF solvent molecules in the structure of **8.1** were refined isotropically. All hydrogen atoms were treated as idealized contributions. All scattering factors are contained in several versions of the SHELXTL program library with the latest version v.6.12.[15] Crystallographic data and relevant bond distances and angles are reported in Table 8.1 and 8.2.

Table 8.1. Crystal Data and Structure Analysis Results for Complexes 8.1-8.3

	8.1	**8.2**	**8.3**
formula	$C_{106}H_{164}Cl_2Co_2Li_2N_6O_{10}$	$C_{80}H_{98}Co_2N_{10}$	$C_{106}H_{166}Co_2N_{10}Na_2O_{10}$
Mw	1885.07	1317.54	1904.33
Crystal system	Monoclinic	Triclinic	Triclinic
space group	P2(1)/n	P-1	P-1
a (Å)	12.193(4)	10.6951(18)	12.392(3)
b (Å)	17.861(5)	15.299(3)	21.639(5)
c (Å)	24.904(7)	24.071(4)	22.065(5)
α (deg)	90	74.320(3)	103.224(3)
β (deg)	99.632(6)	89.344(3)	91.013(3)
γ (deg)	90	69.659(3)	105.849(3)
V (Å^3)	5347(3)	3540.5(10)	5520(2)
Z	2	2	2
radiation (Kα, Å)	0.71073	0.71073	0.71073
T (K)	203(2)	125(2)	200(2)
D_{calcd} (g cm^{-3})	1.171	1.236	1.146
μ_{calcd} (mm^{-1})	0.417	0.520	0.366
F_{000}	2032	1404	2056
R, R_w[2 a]	0.0804, 0.2319	0.0772, 0.1845	0.0639, 0.1504
GoF	1.107	1.022	1.052

[a] $R = \Sigma||F_0| - |F_c||/\Sigma|F|$, $R_w = [\Sigma(|F_0| - |F_c|)^2/\Sigma wF_0^2\}^{1/2}$

Table 8.2. Selected Bond Distances (Å) and Angles (deg) of Complexes 8.1-8.3

8.1	8.2	8.3
Co-N(1) = 1.902(5)	Co(1)-N(1) = 1.850(4)	Co(1)-N(1) = 1.869(3)
Co-N(2) = 1.816(5)	Co(1)-N(2) = 1.821(4)	Co(1)-N(2) = 1.813(3)
Co-N(3) = 1.882(5)	Co(1)-N(3) = 1.856(4)	Co(1)-N(3) = 1.863(3)
Co-Cl = 2.2677(19)	Co(1)-N(4) = 1.808(5)	Co(1)-N(4) = 1.754(3)
Cl-Li = 2.397(14)	N(4)-N(5) = 1.095(6)	N(4)-N(5) = 1.131(4)
N(1)-C(2) = 1.388(8)	N(1)-C(2) = 1.372(6)	N(1)-C(2) = 1.360(5)
C(1)-C(2) = 1.359(9)	C(1)-C(2) = 1.341(7)	N(3)-C(8) = 1.387(4)
N(3)-C(8) = 1.359(8)	N(3)-C(8) = 1.353(6)	N(2)-C(3) = 1.385(5)
C(8)-C(9) = 1.498(9)	C(8)-C(9) = 1.492(6)	N(2)-C(7) = 1.395(5)
C(9)-C(9') = 1.554(13)	C(9)-C(42) = 1.536(7)	C(1)-C(2) = 1.505(6)
N(2)-C(3) = 1.369(8)	N(2)-C(3) = 1.326(15)	C(2)-C(3) = 1.398(5)
N(2)-C(7) = 1.374(8)	N(2)-C(7) = 1.346(19)	C(7)-C(8) = 1.385(5)
C(2)-C(3) = 1.484(9)	C(2)-C(3) = 1.48(2)	C(8)-C(9) = 1.498(6)
C(7)-C(8) = 1.419(9)	C(7)-C(8) = 1.41(2)	Na(1)-O(1) = 2.331(4)
N(2)-Co-N(3) = 82.1(2)	N(4)-Co(1)-N(2) = 177.6(2)	Na(1)-O(2) = 2.349(4)
N(2)-Co-N(1) = 83.0(2)	N(4)-Co(1)-N(1) = 96.88(18)	Na(1)-O(3) = 2.305(5)
N(3)-Co-N(1) = 165.1(2)	N(2)-Co(1)-N(1) = 82.95(17)	Na(1)-O(4) = 2.321(4)
N(2)-Co-Cl = 177.29(17)	N(4)-Co(1)-N(3) = 98.14(18)	Na(1)-O(5) = 2.305(4)
N(3)-Co-Cl = 98.05(17)	N(2)-Co(1)-N(3) = 82.00(18)	N(1)-Co(1)-N(2) = 81.07(14)
N(1)-Co-Cl = 96.76(16)	N(1)-Co(1)-N(3) = 164.95(18)	N(1)-Co(1)-N(3) = 162.94(13)
Co-Cl-Li = 155.2(4)	N(5)-N(4)-Co(1) = 178.9(5)	N(1)-Co(1)-N(4) = 98.63(15)
		N(2)-Co(1)-N(3) = 81.88(14)
		N(2)-Co(1)-N(4) = 179.40(16)
		N(3)-Co(1)-N(4) = 98.43(14)
		Co(1)-N(4)-N(5) = 179.6(4)

Complex 8.1. The molecule consists of a symmetry-generated dimer (Figure 8.1) where the metal ion is surrounded by the ligand system [Co-N(1) = 1.902(5) Å, Co-N(2) = 1.816(5) Å, Co-N(3) = 1.882(5) Å] and one chlorine atom [Co-Cl = 2.2677(19) Å] in a lightly-folded square planar arrangement [N(1)-Co-N(2) = 83.0(2)°, N(2)-Co-N(3) = 82.1(2)°, N(1)-Co-N(3) = 165.1(2)°, N(1)-Co-Cl = 96.76(16)°, N(3)-Co-Cl = 98.05(17)°, N(2)-Co-Cl = 177.29(17)°]. The chlorine atom bridges one Li cation solvated by three molecules of THF [Cl-Li = 2.397(14) Å]. Of the two –ene functions originally present in the dilithium salt, only one remained intact after the reaction, exhibiting a short C-C bond distance [C(1)-C(2) = 1.359(9) Å] as expected for a C-C double bond. The other –ene

function was reduced to a single bond [C(8)-C(9) = 1.498(9) Å]. The terminal C atom of this function now forms a C-C single bond with an identical C atom of a second unit [C(9)-C(9A) = 1.554(13) Å], thereby assembling the dinuclear structure. Consequently, the adjacent C-N distance was shortened to a length exhibiting substantial double bond character [N(3)-C(8) = 1.359(8) Å]. The slightly large values of the final convergence parameters are due to the disorder encountered in the THF molecules, which could not be properly modeled.

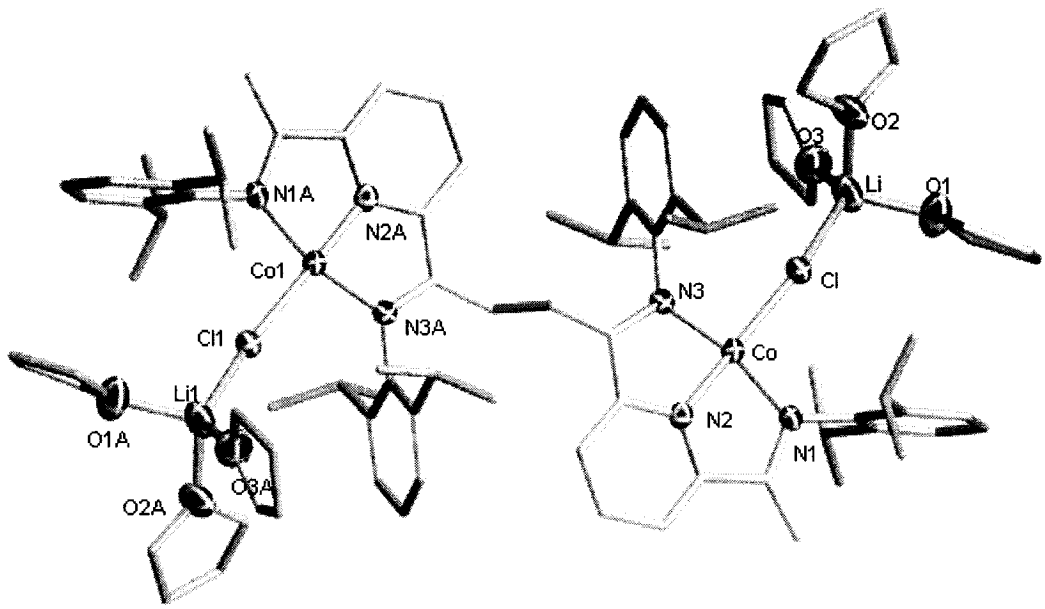

Figure 8.1. Partial thermal ellipsoid plot of **8.1**, drawn at the 30% probability level. Hydrogen atoms have been omitted for clarity.

Complex 8.2. The basic structure of complex **8.2** (Figure 8.2) is very similar to that of **8.1** where each cobalt center is connected to one moiety of the binucleating ligand [Co(1)-N(1) = 1.850(4) Å, Co(1)-N(2) = 1.821(4) Å, Co(1)-N(3) = 1.856(4) Å]. The dinuclear structure is realized through the coupling of one methylene unit with that of a second identical entity. The bond distances and angles are comparable to those found for complex **8.1**. The geometry around the cobalt is once again distorted square planar [N(1)-Co(1)-N(2) = 82.95(17)°, N(2)-Co(1)-N(3) = 82.00(18)°, N(1)-Co(1)-N(3) = 164.95(18)°, N(1)-Co(1)-N(4) = 96.88(18)°, N(3)-Co(1)-N(4) = 98.14(18)°, N(2)-Co(1)-N(4) = 177.6(2)°] the only difference being that the pendant Cl-Li(THF)$_3$ unit has been replaced by a terminally bound N_2 unit [Co(1)-N(4) = 1.808(5) Å]. The bond length of the

coordinated dinitrogen unit [N(4)-N(5) = 1.095(6) Å] is characteristic of a N≡N triple bond, suggesting minimal activation of the triple bond. The bond lengths in the ligand system are similar to those of complex **8.1**. However, the C=N adjacent to the dimerization has been contracted to a much larger extent than above [N(3)-C(8) = 1.306(18) Å], while maintaining a similar degree of contraction in the C_{imine}-C_{methyl} bond [C(7)-C(8) = 1.41(2) Å].

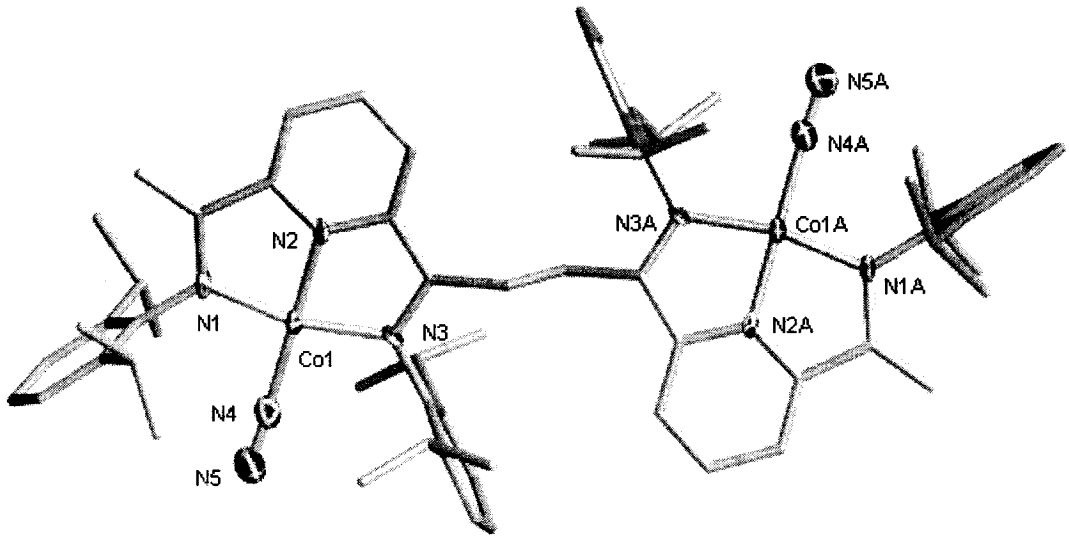

Figure 8.2. Partial thermal ellipsoid plot of **8.2**, drawn at the 30% probability level. Hydrogen atoms have been omitted for clarity.

Complex 8.3. The structure of complex **8.3** is shown in Figure 8.3 and consists of a solvent separated ion pair. The ligand system is found coordinated to a cobalt center in the anionic unit, occupying three of the four coordination sites of the metal center [Co(1)-N(1) = 1.869(3) Å, Co(1)-N(2) = 1.813(3) Å, Co(1)-N(3) = 1.863(3) Å]. The distorted square planar metal center is completed by an end-on dinitrogen moiety [Co(1)-N(4) = 1.754(3) Å, N(1)-Co(1)-N(2) = 81.07(14)°, N(1)-Co(1)-N(3) = 162.94(13)°, N(1)-Co(1)-N(4) = 98.63(15)°, N(2)-Co(1)-N(3) = 81.88(14)°, N(2)-Co(1)-N(4) = 179.40(16)°, N(3)-Co(1)-N(4) = 98.43(14)°]. The corresponding cationic unit involves an atom of Na solvated by five molecules of THF in a distorted trigonal bipyramidal geometry (τ = 0.68).[16] Coordination of the dinitrogen molecule to the metal center results only in weak activation of the triple bond, as witnessed by the short N-N bond distance of 1.131(4) Å. In addition, the Co-N-N line is very linear [Co(1)-N(4)-N(5) = 179.6(4)°]. The bond

distances of the ligand backbone have undergone modifications compared to the $CoCl_2$ and CoCl complexes.

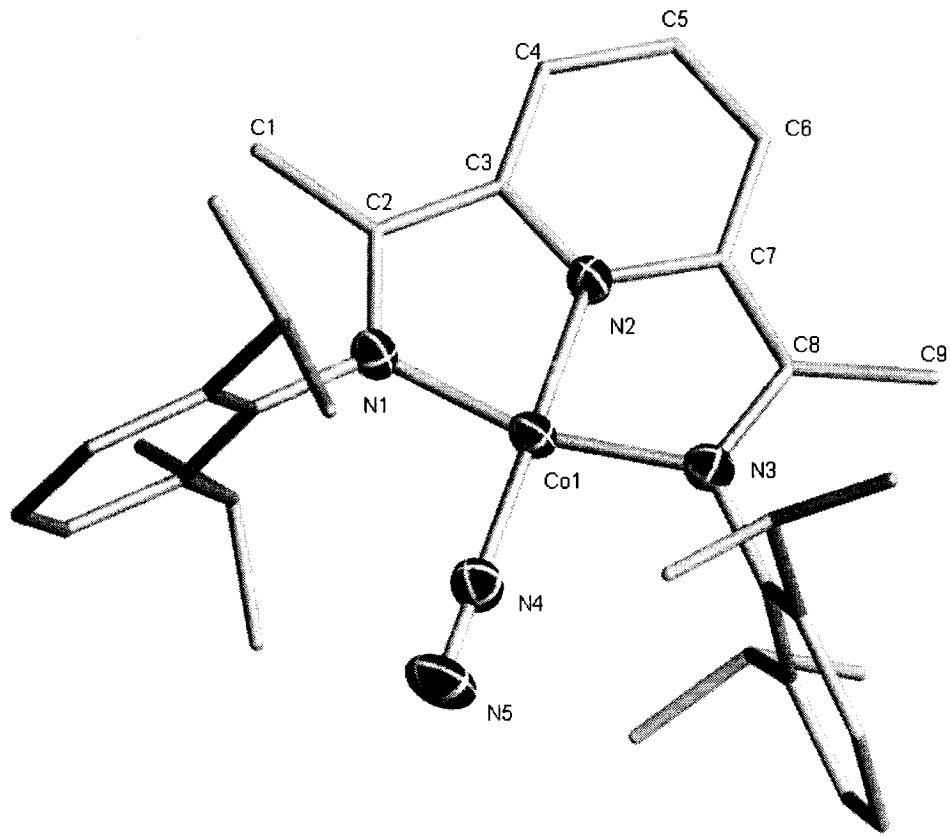

Figure 8.3. Partial thermal ellipsoid plot of the anionic unit of **8.3**, drawn at the 30% probability level. Hydrogen atoms have been omitted for clarity.

Results and Discussion

The reaction of $CoCl_2(THF)_{1.5}$ with the dilithium salt of the bis-aminopyridine dianion $\{[2,6\text{-}[2,6\text{-}(^i Pr)_2PhN\text{-}C{=}(CH_2)]_2(C_5H_3N)]Li(THF)\}\{Li(THF)_4\}$ was carried out in THF under an argon atmosphere, affording a dark burgundy solution. Dark red crystals of the dimeric $\{[2,6\text{-}(^i Pr)_2PhN\text{-}C{=}(CH_2)](C_5H_3N)[2,6\text{-}(^i Pr)_2PhN{=}C(CH_2)]\}_2[Co(\mu\text{-}Cl)Li(THF)_3]_2\cdot 4(THF)$ (**8.1**) were isolated in 65% yield after slow concentration at room temperature. The formula and connectivity of **8.1** were elucidated by elemental analysis and an X-ray crystal structure (Figure 8.1).

The chemical connectivity, as summarized in Scheme 8.1, doubtlessly assigns the monovalent state to the two Co atoms. Accordingly, complex **8.1**, which is extremely air-

sensitive and turns brown immediately upon exposure to air, is diamagnetic in the solid state, as expected for a d^8 species in a square planar environment. Unfortunately, the near-to-zero solubility of **8.1** in most common NMR solvents prevented the recording of informative spectra.

Scheme 8.1

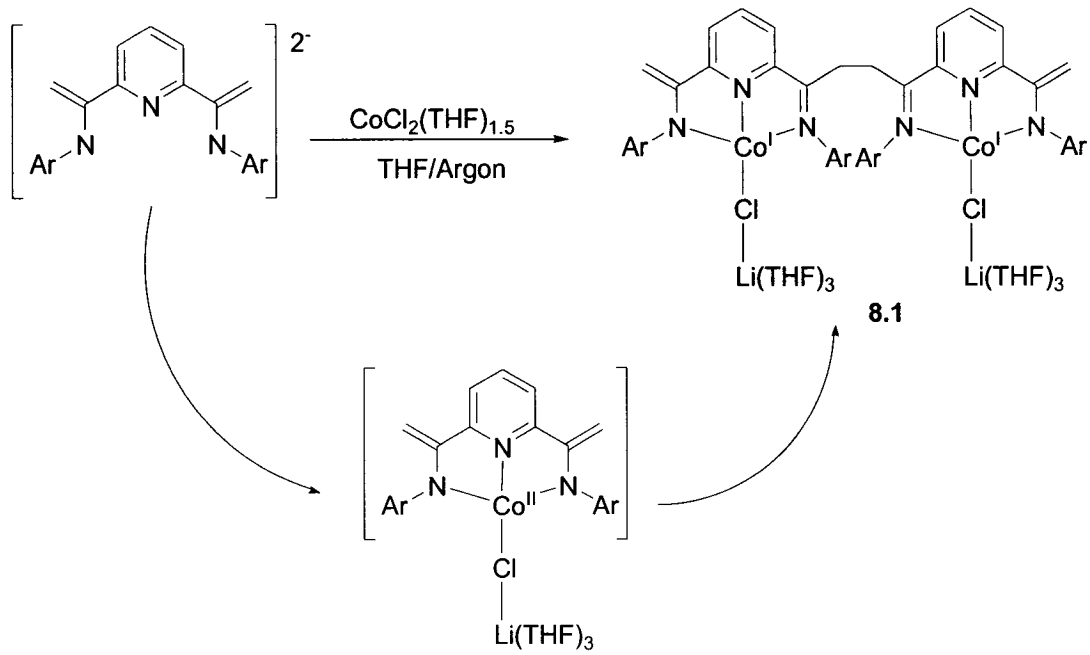

The coupling of the ligand at the expense of a C=C double bond, as observed during the formation of **8.1**, has a precedent in the chemistry of Fe,[4a] Mn[2a] and Ln[6] [Ln = Nd, La]. In the case of the lanthanides, the presence of a strong reducing agent was required to afford the coupling. In the case of Fe and Mn, the dimerization was most likely initiated via the reductive coupling of two intermediate mono-deprotonated species, formed upon alkylation of the neutral divalent complexes. By contrast, the coupling affording complex **8.1** occurred via *spontaneous reduction* to Co(I) upon coordination of the dianionic ligand to the metal center. The electron necessary for the reduction is supplied by the homolytic cleavage of the C=C double bond. This is particularly striking considering that Co(I) is a strongly reducing metal center and is usually regarded as far more reactive than the divalent congener. According to the J. Halpern analogy and simple isolobality arguments, a d^8 Co(I) ion in a square planar ligand field must be regarded as

the analogue of an organic carbene.[17] The tremendous tendency of these species to perform oxidative addition types of attack can only be explained in this view. However, considering the rather general ability of the neutral ligand to host electrons in the delocalized π-system (see Chapters 3-7),[4bd,6a,8,11,18] one could reasonably expect that even in this case a Co(II) antiferromagnetically coupled to a ligand radical anion may in fact be a more realistic description. Besides the obvious bond length modifications upon restoring the imino function, the C_{imine}-C_{methyl} bond length adjacent to the new C-C bond has also been contracted, in comparison to the analogous bond on the other side of the ligand [C(7)-C(8) = 1.419(9) Å vs C(2)-C(3) = 1.484(9) Å], suggesting delocalization of the electron density and possible reduction of the ligand by one electron.

During the preparation of **8.1** in toluene and under a dinitrogen atmosphere, a much deeper colour and precipitation of a dark-coloured microcrystalline solid was observed (Scheme 8.2). The solid state IR of the new material showed the presence of a sharp and intense band at 2153 cm^{-1} possibly diagnosing the presence of a terminally-bound dinitrogen molecule with minimal extent of reduction. Recrystallization of this new compound was successful and small crystals were obtained from the reaction mixture, proving the chemical connectivity and formula of this new species as a double dinitrogen complex $\{[2,6\text{-}(^{i}Pr)_2PhN\text{-}C=(CH_2)](C_5H_3N)[2,6\text{-}(^{i}Pr)_2PhN=C(CH_2)]\}_2[Co(N_2)]_2\cdot 2(toluene)$ (**8.2**). The connectivity of **8.2** is very similar to that of **8.1**, where the weakly bound LiCl moiety has been replaced by an end-on dinitrogen unit (Figure 8.2). The N-N distance of the coordinated N_2 unit of **8.2** [N(4)-N(5) = 1.095(6) Å] suggests very little, if no, activation of the N-N triple bond. This is in good agreement with the stretching frequency of the coordinated dinitrogen, which displays an unusually high value (ν = 2153 cm^{-1}). From these observations, it is conceivable to expect that the coordination of N_2 in **8.2** might be especially labile. In sharp contrast with these expectations, the dinitrogen moiety could *not* be expelled from the complex, even in boiling toluene or THF. The ^{1}H-NMR spectrum of **8.1** showed the terminal $=CH_2$ groups as two rather broad singlets at 4.67 ppm and 4.01 ppm coupled to the same resonance at 72.53 ppm of the ^{13}C-NMR spectrum. Two sets of ^{i}Pr groups are present while the CH_2CH_2 bridge between the two units gives a broad resonance at 3.53 ppm.

Scheme 8.2

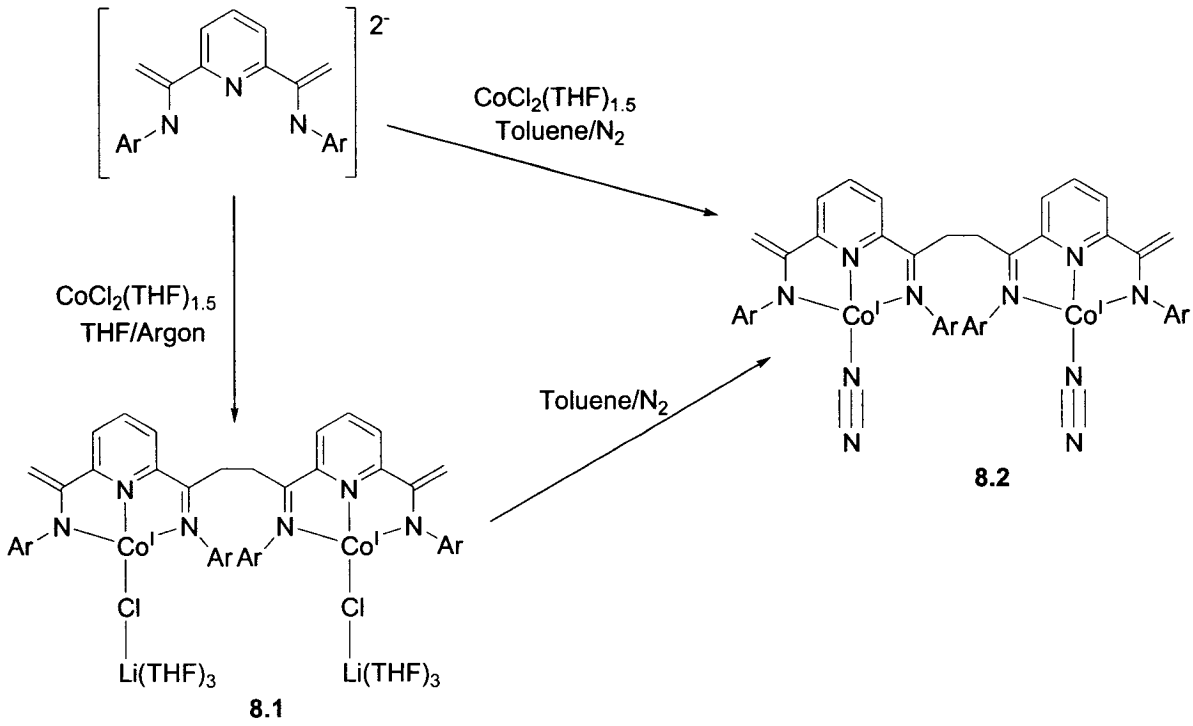

Dinitrogen fixation by reduced complexes of the bis-iminopyridine ligand system is rapidly becoming a trend.[5,10b,19] Considering the exciting results described in Chapter 6 regarding dinitrogen fixation upon reduction of the divalent Fe precursor, the similar reduction with NaH was attempted on the divalent Co analogue. Upon mixing the brownish-green $LCoCl_2$ complex with NaH over the period of a few weeks in THF, the colour of the suspension became dark burgundy. Crystals of the well-known LCoCl complex were isolated from THF. The formation of this complex has been seen upon alkylation of the divalent precursor with various Li-alkyls, as well as upon reduction with Mg or Zn.[10] A further reduction of the system was therefore attempted, beginning with the addition of 6 equivalents of NaH to the $LCoCl_2$ starting complex. After stirring for 1 week, the solution became dark green and dark green crystals of [{2,6-[2,6-(^{i}Pr)$_2$PhN=C(CH$_3$)]$_2$(C$_5$H$_3$N)}Co(η^1-N$_2$)][Na(THF)$_5$] (**8.3**) were isolated from a THF/hexane layer of the reaction mixture in fairly good yield (Scheme 8.3). The connectivity of the product was yielded by single crystal X-ray diffraction and a representative model of the anionic unit can be seen in Figure 8.3. Complex **8.3** consists

of a cobalt center surrounded by the ligand system and a weakly activated, end-on molecule of dinitrogen and is completed by a THF-solvated Na atom in the lattice. The molecule of dinitrogen displays only weak activation, as determined by the short N-N distance [1.131(4) Å]. However, the bond length of the nitrogen to the Co center is relatively short [1.754(3) Å], indicating possible electron delocalization throughout the Co-N-N bonds. The presence of one Na atom per Co unit indicates a formally -1 oxidation state for the Co atom. However, the bond distances of the ligand backbone have been modified to suggest a two or possibly even three electron reduction. The magnetic moment at room temperature of the bulk solid sample was measured as 2.4 μ_B, corresponding either to a three electron reduced ligand (two electrons paired) bound to a low spin square planar Co(II) d^7 metal center or the presence of two unpaired electrons on the ligand backbone coordinated to a closed-shell Co(I) d^8 center. Attempts to reduce the dinitrogen unit further by using an excess of NaH have been thus far unsuccessful.

Scheme 8.3

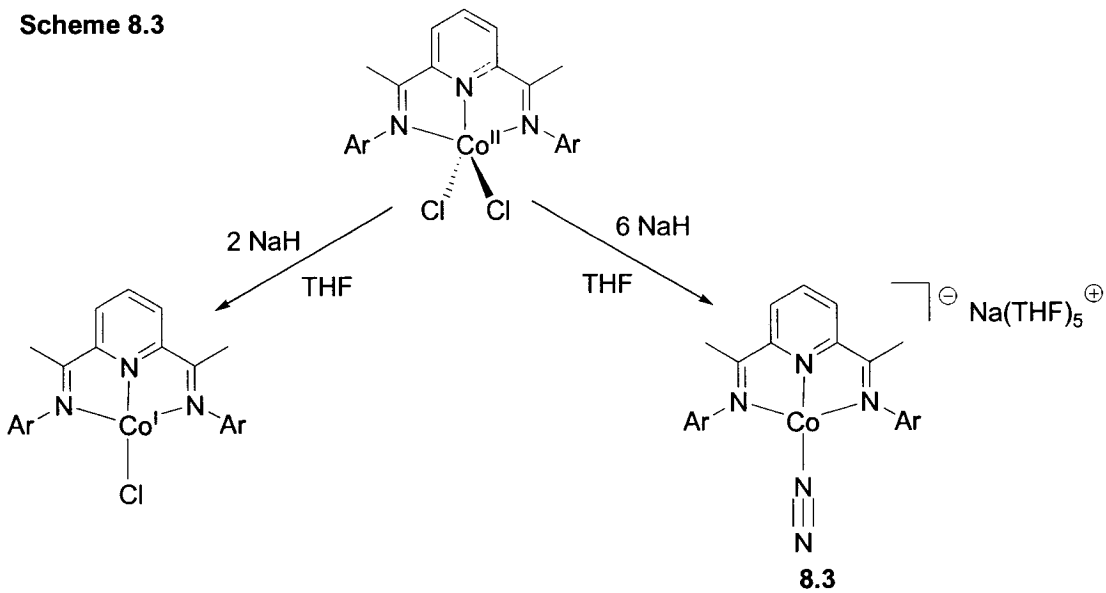

8.3

Dinitrogen complexes of cobalt are scarce.[5,10b,20-32] In addition, the few reported complexes all appear to be rather similar, the main differences arising from the skeleton of the supporting phosphine ligand and the oxidation state of the Co center, which varies from -1 to +1. In some cases, the coordination of dinitrogen is assisted by another metal center.[22-27,30,31] The result of a database search on existing cobalt dinitrogen complexes is

summarized in Table 8.3. Of the eighteen complexes listed, nine contain cobalt in the formal monovalent state. All of these species display stretching frequencies substantially lower than that of **8.2**, thus indicating the lowest level of activation among all of the cobalt-N_2 complexes reported to date. Closely related to complexes **8.2** and **8.3** is Gibson's cationic bis-iminopyridinato dinitrogen complex.[10b] However, the ligand is formally neutral in this compound and it is the Lewis acidity of a Co(I) cationic complex which is regarded as the driving force for the labile coordination of dinitrogen. Unfortunately, no IR data were reported for this complex. However, the N-N distance [N-N = 1.112(6)Å] is midway between those observed for **8.2** and **8.3**.

Table 8.3. Known Co-N_2 complexes

Complex	ν_{NN} (cm^{-1})	d_{NN} (Å)	Ref.
$CoH(PPh_3)_3N_2$	2088	1.112(11)	20
$[Co(PPh_3)_3N_2]Mg(THF)_2$	1840	NS[a]	21
$[Co(PPh_3)_3N_2]_2Mg(THF)_4$	1840	NS	22
$[Co(PPh_3)_3N_2]Li(Et_2O)_3$	1900	1.167(16)	22
$[Co(PPh_3)_3N_2]Li(THF)_3$	1890	1.19(4)	22
$[Co(PPh_3)_3N_2]Na(THF)_3$	1910	NS	22,23
$[Co(PPh_3)_3]_2N_2$	sym	NS	23
$\{[Co(PMe_3)_3N_2]K\}_6$	2056	1.16	24
$[Co(PMe_3)_3N_2]_2Mg(THF)_4$	1830	1.18	25
$[Co(PMe_3)_3N_2MgC(CH_3)_3(Et_2O)]_2$	1660	1.211(4)	26
$[Co(PMe_3)_3N_2Al(CH_3)_2]_2$	Not given	1.252(6)	27
$[CoP(CH_2CH_2PPh_2)_3N_2]PF_6/BPh_4$	2125	1.084	28
$[Co(PMe_3)(N_2)(\mu\text{-}t\text{-}Bu_2P)]_2$	1910	1.092(5)	29
$[Co\{(PPh_2CH_2)_3CCH_3\}]_2N_2$	sym	1.18(2)	30
$\{Co[(P\text{-}i\text{-}Pr_2CH_2)_3BPh]N_2\}_2Mg(THF)_4$	1863	1.155(3)	31
$[\{Co[(P\text{-}i\text{-}Pr_2CH_2)_3BPh]\}_2N_2]Na(THF)_6$	Not given	1.147(4)	31
$CoTp'N_2$	2046	NS	32
$[CoLN_2][MeB(C_6F_5)_3]$	Not given	1.112(6)	10b

Tp' = hydridotris(3-*t*-butyl-5-methylpyrazolyl)borate
L = 2,6-[CMe=N(2,6-C_6H_3-*i*-Pr_2)]$_2C_5H_3N$
[a] No structure reported to date

In lieu of the remarkable polymerization activity of the neutral ligand Co and Fe complexes,[12] ethylene polymerization was attempted with the Co(I) dimer. Studies by Gibson and Budzelaar on the original Co(II) system with the neutral ligand have discovered that prior to polymerization, the Co(II) is reduced to Co(I) by the presence of

MAO, or other alkylating agents, leading to the assumption that it is a Co(I) complex, rather than a Co(II) species, that is responsible for the activity of the precatalyst.[10] In our polymerization testing of complex **8.1**, an activity of 428 gPE/mmol·h·atm was determined. This value is surprisingly comparable to those reported by Brookhart and Gibson for their cobalt (II) precatalyst tested under similar conditions.[12] Catalytic testing was also completed with the dinitrogen complex **8.2**, resulting in an activity of 200 gPE/mmol·h·atm, half that of its LiCl counterpart. The fact that compound **8.2** is able to polymerize ethylene emphasizes the fact that the dinitrogen unit must be labile, in order to free a coordination site for the ensuing polymerization.

Interestingly, the polymer collected from complexes **8.1** and **8.2** is completely different from that produced by Brookhart and Gibson's bis-iminopyridine Co(I) species. Their polymer displays a broad molecular weight distribution centered at 25 000,[12] whereas the molecular weight peak of our polymer is very sharp, centered at 45 000, and corresponds to a polydispersity of 1.1. This remarkable increase in polymer quality implies a different mechanism of polymerization, besides an obviously different active species. Studies by Gibson have shown that the active species in the bis-iminopyrdine Co(II) catalyst is most likely a cationic LCo(I) compound, trapped with ethylene after the removal of the methyl group by a Lewis acid.[10b] Polymerization may proceed by attack of the LA-bound methyl group on the Co center, and coordination of the LA to the ethylene unit, oxidizing the metal center to Co(III).[33] However, with complex **8.1**, removal of the weakly coordinating LiCl moiety results in an alkyl-free, neutral, coordinatively unsaturated metal complex. It is unknown at this time what the active species could be in this case. Possibilities for a polymerization mechanism may be oxidative addition via the cyclization of two ethylene units and the metal center, followed by a typical Ziegler-Natta mechanism upon addition of activator; or perhaps a similar zwitterionic mechanism like that described in Chapter 4 for Fe. Further research is required in order to elucidate the actual mechanism at play.

Conclusion

In this preliminary study, aimed at assessing the ability of the bis-aminopyridine ligand to support catalytic activity, dimeric Co(I) complexes have been prepared from the

reaction of Co(II) with the dianionic ligand via the reductive coupling of two identical units. This species is active for ethylene polymerization, with a different activity and polymer quality than the divalent neutral ligand precursor, once more reiterating how subtle differences in the electronic structure of the ligand can lead to widespread differences in terms of reactivity and polymer quality. Also of interest in this chapter, is the fixation of dinitrogen by cobalt. The fact that only terminal dinitrogen complexes may be isolated and the degree of reduction of the triple bond remains minimal lends some support to the hypothesis put forth in Chapters 6 and 7, requiring the participation of two metal centers to afford further reduction and cleavage of the dinitrogen moiety. The emerging trend appears to suggest that late transition metals, Fe and Co, are unable to form bridging structures and prefer to coordinate terminal dinitrogen units, whereas the earlier transition metals, V and Cr, may assemble dinuclear systems and promote a larger degree of reduction in the N-N triple bond

References

(1) Reardon, D.; Conan, F.; Gambarotta, S.; Yap, G. P. A.; Wang, Q. *J. Am. Chem. Soc.* **1999**, *121*, 9318.

(2) (a) Sugiyama, H.; Aharonian, G.; Gambarotta, S.; Yap, G. P. A.; Budzelaar, P. H. M. *J. Am. Chem. Soc.* **2002**, *124*, 12268. (b) Reardon, D.; Aharonian, G.; Gambarotta, S.; Yap, G. P. A. *Organometallics* **2002**, *21*, 786.

(3) (a) Clentsmith, G. K. B.; Gibson, V. C.; Hitchcock, P. B.; Kimberley, B. S.; Rees, C. W. *Chem. Commun.* **2002**, 1498. (b) Khorobkov, I.; Gambarotta, S.; Yap, G. P. A. *Organometallics* **2002**, *21*, 3088. (c) Blackmore, I. J.; Gibson, V. C.; Hitchcock, P. B.; Rees, C. W.; Williams, D. J.; White, A. J. P. *J. Am. Chem. Soc.* **2005**, *127*, 6012.

(4) (a) Scott, J.; Gambarotta, S.; Korobkov, I.; Budzelaar, P. H. M. *J. Am. Chem. Soc.* **2005**, *127*, 13019. (b) (b) Scott, J.; Gambarotta, S.; Korobkov, I.; Budzelaar, P. H. M. *Organometallics* **2005**, *24*, 6298. (c) Bouwkamp, M. W.; Lobkovsky, E.; Chirik, P. J. *Inorg. Chem.* **2006**, *45*, 2. (d) Scott, J.; Gambarotta, S.; Korobkov, I.; Knijnenburg, Q.; de Bruin, B.; Budzelaar, P. H. M. *J. Am. Chem. Soc.* **2005**, *127*, 17204.

(5) Scott, J.; Gambarotta, S.; Korobkov, I. *Can. J. Chem.* **2005**, *83*, 279.

(6) (a) Sugiyama, H.; Gambarotta, S.; Yap, G. P. A.; Wilson, D. R.; Thiele, S. K.-H. *Organometallics* **2004**, *23*, 5054. (b) Sugiyama, H.; Korobkov, I.; Gambarotta, S.; Möller, A.; Budzelaar, P. H. M. *Inorg. Chem.* **2004**, *43*, 5771.

(7) (a) Clentsmith, G. K. B.; Gibson, V. C.; Hitchcock, P. B.; Kimberley, B. S.; Rees, C. W. *Chem. Commun.* **2002**, 1498. (b) Khorobkov, I.; Gambarotta, S.; Yap, G. P. A.

Organometallics **2002**, *21*, 3088. (c) Blackmore, I. J.; Gibson, V. C.; Hitchcock, P. B.; Rees, C. W.; Williams, D. J.; White, A. J. P. *J. Am. Chem. Soc.* **2005**, *127*, 6012.

(8) Enright, D.; Gambarotta, S.; Yap, G. P. A.; Budzelaar, P. H. M. *Angew. Chem. Int. Ed.* **2002**, *41*, 3873.

(9) Britovsek, G. J. P.; Bruce, M.; Gibson, V. C.; Kimberley, B. S.; Maddox, P. J.; Mastroianni, S.; McTavish, S. J.; Redshaw, C.; Solan, G. A.; Strömberg, S.; White, A. J. P.; Williams, D. J. *J. Am. Chem. Soc.* **1999**, *121*, 8728.

(10) (a) Kooistra, T. M.; Knijnenburg, Q.; Smits, J. M. M.; Horton, A. D.; Budzelaar, P. H. M.; Gal, A. W. *Angew. Chem. Int. Ed.* **2001**, *40*, 4719. (b) Gibson, V. C.; Humphries, M. J.; Tellmann, K. P.; Wass, D. F.; White, A. J. P.; Williams, D. J. *Chem. Commun.* **2001**, 2252. (c) Steffen, W.; Blömker, T.; Kleigrewe, N.; Kehr, G.; Fröhlich, R.; Erker, G. *Chem. Commun.* **2004**, 1188. (d) Kleigrewe, N.; Steffen, W.; Blömker, T.; Kehr, G.; Fröhlich, R.; Wibbeling, B.; Erker, G.; Wasilke, J.-C.; Wu, G.; Bazan, G. C. *J. Am. Chem. Soc.* **2005**, *127*, 13955.

(11) Knijnenburg, Q.; Hetterscheid, D.; Kooistra, T. M.; Budzelaar, P. H. M. *Eur. J. Inorg. Chem.* **2004**, 1204.

(12) (a) Small, B. L.; Brookhart, M.; Bennett, A. M. A. *J. Am. Chem. Soc.* **1998**, *120*, 4049. (b) Britovsek, G. J. P.; Gibson, V. C.; Kimberley, B. S.; Maddox, P. J.; McTavish, S. J.; Solan, G. A.; White, A. J. P.; Williams, D. J. *Chem. Commun.* **1998**, 849.

(13) Tessier-Youngs, C.; Beachley Jr., O. T. *Inorg. Synth.* **1986**, *24*, 95.

(14) Blessing, R. *Acta Crystallogr.* **1995**, *A51*, 33.

(15) Sheldrick, G. M. Bruker AXS, Madison, WI, 2001.

(16) Addison, A. W.; Rao, T. N.; Reedijk, J.; van Rijn, J.; Verschoor, G. C. *J. Chem. Soc. Dalton Trans.* **1984**, 1349.

(17) Halpern, J. *C&EN* **1966**, *Oct. 31.*, 68.

(18) (a) de Bruin, B.; Bill, E.; Bothe, E.; Weyhermüller, T.; Wieghardt, K. *Inorg. Chem.* **2000**, *39*, 2936. (b) Budzelaar, P. H. M.; de Bruin, B.; Gal, A. W.; Wieghardt, K.; van Lenthe, J. H. *Inorg. Chem.* **2001**, *40*, 4649. (c) Bart, S. C.; Chlopek, K.; Bill, E.; Bouwkamp, M. W.; Lobkovsky, E.; Neese, F.; Wieghardt, K.; Chirik, P. J. *J. Am. Chem. Soc.* **2006**, *128*, 13901.

(19) (a) Vidyaratne, I.; Gambarotta, S.; Korobkov, I.; Budzelaar, P. H. M. *Inorg. Chem.* **2005**, *44*, 1187. (b) Bart, S. C.; Lobkovsky, E.; Chirik, P. J. *J. Am. Chem. Soc.* **2004**, *126*, 13794. (c) Scott, J. Chapter 6. (d) Vidyaratne, I.; Scott, J.; Gambarotta, S.; Budzelaar, P. H. M.; Korobkov, I. *manuscript submitted.*

(20) (a) Enemark, J. H;. Davis, B. R.; McGinnety, J. A.; Ibers, J. A. *Chem. Commun.* **1968**, 96. (b) Davis, B. R.; Payne, N. C.; Ibers, J. A. *Inorg. Chem.* **1969**, *8*, 2719.

(21) Miura, Y.; Yamamoto, A. *Chem. Lett.* **1978**, 937.

(22) Yamamoto, A.; Miura, Y.; Ito, T.; Chen, H.-L.; Iri, K.; Ozawa, F.; Miki, K.; Sei, T.; Tanaka, N.; Kasai, N. *Organometallics* **1983**, *2*, 1429.

(23) Aresta, M.; Nobile, C. F.; Rossi, M.; Sacco, A. *Chem. Commun.* **1971**, 781.

(24) Klein, H.-F.; Hammer, R.; Wenninger, J.; Friedrich, P.; Huttner, G. *Z. Naturforsch* **1978**, *33b*, 1267.

(25) Hammer, R.; Klein, H.-F.; Schubert, U.; Frank, A.; Huttner, G. *Angew. Chem. Int. Ed.* **1976**, *15*, 612.

(26) Klein, H.-F.; Koenig, H.; Koppert, S.; Ellrich, K.; Riede, J. *Organometallics* **1987**, *6*, 1341.

(27) Klein, H.-F.; Ellrich, K.; Ackermann, K. *J. Chem. Soc., Chem. Commun.* **1983**, 888.

(28) (a) Bianchini, C.; Peruzzini, M.; Zanobini, F. *Organometallics* **1991**, *10*, 3415. (b) Bianchini, C.; Mealli, C.; Meli, A.; Peruzzini, M.; Zanobini, F. *J. Am. Chem. Soc.* **1988**, *110*, 8725.

(29) Jones, R. A.; Stuart, A. L.; Atwood, J. L.; Hunter, W. E. *Organometallics* **1983**, *2*, 1437.

(30) Cecconi, F.; Ghilardi, C. A.; Midollini, S.; Moneti, S.; Orlandini, A.; Bacci, M. *J. Chem. Soc., Chem. Commun.* **1985**, 731.

(31) Betley, T. A.; Peters, J. C. *J. Am. Chem. Soc.* **2003**, *125*, 10782.

(32) Egan Jr., J. W.; Haggerty, B. S.; Rheingold, A. L.; Sendlinger, S. C.; Theopold, K. H. *J. Am. Chem. Soc.* **1990**, *112*, 2445.

(33) Humphries, M. J.; Tellmann, K. P.; Gibson, V. C.; White, A. J. P.; Williams, D. J. *Organometallics* **2005**, *24*, 2039.

Chapter Nine

Late Transition Metal Complexes of Dipyrrole and Schiff Base Pyrrole Ligands

---

Introduction

The previous chapters have engaged the reactivity of Fe, Co and Cr complexes of the bis-iminopyridine ligand with various alkylating agents, aluminum activators and reducing agents, showing the susceptibility of the ligand towards both nucleophilic and radical attack to afford a variety of transformations.[1-3] However, at the basis of the exceptional catalytic activity is the ability of the π-system to accept negative charge at the expense of the metal center.[1c-f,4,5] Chapter 3 demonstrated that formation of the active Fe species involves an initial reduction of the ligand by two electrons, forming an alkyl-free neutral complex comprised of a dianionic ligand bound to a divalent Fe center.[1cd] Chapter 4 expanded on these results, demonstrating facile ligand transmetallation from the Fe to Al as a possible deactivation pathway.[1ef] A proposed mechanism based on the combined results of Chapters 3 and 4 suggests that the active species involves coordination of two $AlMe_3$ molecules to the dianionic ligand backbone and partial alkylation of the Fe center towards a zwitterionic Fe(II) alkyl (Scheme 9.1).[1f]

Scheme 9.1

Thus, essential properties of the ligand system appear to be a multi-chelating, dianionic, N-donor backbone in combination with a large delocalized π-system. The ligand system must also be capable of assembling a bi- or trimetallic structure, bound to the Al activator and the metal center simultaneously. Is it possible, therefore, to recreate the favourable conditions for zwitterionic activation of late metal systems? Can the unique properties of the bis-iminopyridine ligand be duplicated in the design of new catalysts?

A promising platform based on the characteristics described above is the dipyrrolide system (Chart 9.1: **9.1a,b,c**). Our previous work with low-valent *f*-block elements has shown that primary characteristics of these ligands are:[6] 1) an enhanced tendency to increase the reactivity of the metal center,[7] 2) the ability to assemble large cyclic flat cluster structures,[8] 3) the availability of a variety of bonding modes and 4) the possibility of fine-tuning the metal redox potential in anionic metallate structures.[9] The ligand is dianionic and bidentate, containing two pyrrole N atoms for coordination to the metal center. The obvious coordination mode is σ-bound through the N atoms. However, being isoelectronic with Cp, the deprotonated pyrrole rings can also π-bond via η^5-coordination to the metal center. The delocalized π-system of pyrrole, in addition to the negatively charged N atom, allows utilization of both bonding modes simultaneously.[6-9]

The drawbacks of the dipyrrolides, in terms of the desired characteristics of the bis-iminopyridine ligand, are its lack of steric bulk and its lack of extended delocalization. In an effort to include these properties, as well as to exploit of the advantages of pyrroles, a variation of the Schiff base salen ligand, comprised of the typical salen C=N-C-C-N=C backbone (with various possible substituents on the ethylene

bridge) bound on each side to the α-position of a pyrrole, was also considered in addition to the variations on the pyrrolide theme.[10] Chosen examples are highlighted in Chart 9.1.

Chart 9.1

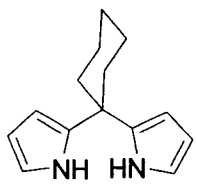

9.1a

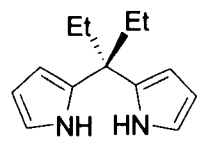

9.1b

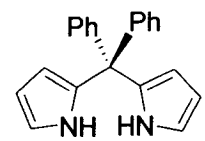

9.1c

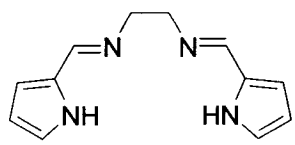

9.2a

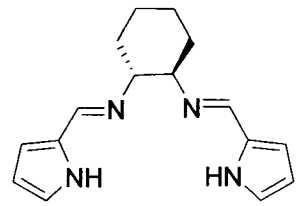

9.2b

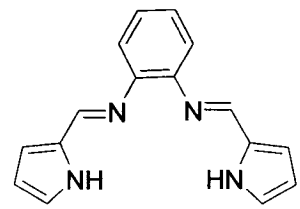

9.2c

Herein, we describe the attempt to isolate novel late transition metal ethylene polymerization catalysts supported by the dipyrrolide dianion[11] and its Schiff-base counterpart.

Experimental Section

All operations were performed under an inert atmosphere using standard Schlenk techniques or a nitrogen-filled dry box. THF complexes of $FeCl_2$, Cr_3Cl_3 and $CoCl_2$ were prepared according to standard procedures. The ligands 1,1'-(2-$C_4H_3NH)_2C_6H_{10}$ (**9.1a**),[8a] (2-$C_4H_3NH)_2C(C_2H_5)_2$ (**9.1b**),[8a] (2-$C_4H_3NH)_2C(C_6H_5)_2$ (**9.1c**),[8a] 1,2-[(2-$C_4H_3NH)CH{=}N]_2C_2H_4$ (**9.2a**),[10d] 1,2-[(2-$C_4H_3NH)CH{=}N]_2C_6H_{10}$ (**9.2b**)[10d] and 1,2-[(2-$C_4H_3NH)CH{=}N]_2C_6H_4$ (**9.2c**)[10d] were prepared following literature procedures. Methyl lithium (1.4 M solution in ether) was obtained from Aldrich and used as received. NaH and KH (suspension in mineral oil) were also obtained from Aldrich and were washed with hexane to remove the oil. Infrared spectra were recorded on a Mattson 9000 and Nicolet 750-Magna FTIR instrument from Nujol mulls prepared in a dry-box. Samples

for magnetic susceptibility measurements were weighed inside a dry-box equipped with an analytical balance and sealed into calibrated tubes. Room temperature magnetic measurements were carried out with a Gouy balance (Johnson Matthey) at room temperature. Samples for magnetic susceptibility measurements at variable temperatures were pre-weighed inside a dry-box equipped with an analytical balance and flame sealed into calibrated 5 mm 'od' quartz tubes. Magnetic measurements were carried out using a Quantum Design MPMS5S SQUID magnetometer at 1.0 T, in the temperature range 2-300 K. Accurate sample mass was determined by difference by breaking the tube after data collection. Background data on the cleaned, empty tube were obtained under identical experimental conditions. Standard corrections for underlying diamagnetism were applied to data.[12] Elemental analyses were carried out with a Perkin Elmer 2400 CHN analyzer. Data for X-ray crystal structure determination were obtained with a Bruker diffractometer equipped with a Smart CCD area detector. The ^{57}Fe Mössbauer spectra were collected at room temperature in constant acceleration mode on a velocity range of +/- 11 mm/s, to identify the possible presence of impurities. The raw spectra were folded to produce a flat background and a zero velocity corresponding to the CS of metallic iron at room temperature. The folded spectra were fitted using symmetric (equal areas and equal widths) quadrupole doublets of Lorentzian lines. The absorbers were loaded anoxically in gas tight holders and had 235 mg of sample per half inch diameter windows.[13]

Preparation of $([1,1\text{-}(2\text{-}C_4H_3N)_2C_6H_{10}]_2Fe[K(THF)]_2\}_n$ (9.3).

A solution of 1,1'-dipyrrolylcyclohexane (**9.1a**) (1.8 g, 8.5 mmol) in THF was added drop-wise to a stirred suspension of KH (0.72 g, 17.9 mmol) in THF. A vigorous reaction took place resulting in a cloudy solution. After 1 hour of stirring, a suspension of $FeCl_2(THF)_{1.5}$ (1.0 g, 4.2 mmol) was added and the colour became slightly yellow. The reaction was allowed to stir overnight and then filtered. The clear yellow solution was concentrated and layered with hexanes. Large, clear crystals of **9.3** were formed upon standing at room temperature for a few days (1.87 g, 3.0 mmol, 63%). Anal. Calcd (found) for $C_{36}H_{48}N_4O_2FeK_2$ (%): C, 61.52 (61.48); H, 6.88 (6.80); N, 7.97 (7.91). IR (Nujol mull, cm^{-1}): ν 3091 (w), 2917 (s), 1461 (vs), 1435 (s), 1401 (w), 1377 (s), 1297

(w), 1278 (w), 1263 (w), 1228 (w), 1213 (w), 1157 (m), 1127 (w), 1104 (w), 1038 (s), 959 (m), 906 (m), 872 (w), 829 (w), 769 (m), 734 (vs), 724 (s). [μ_{eff} = 5.6 μ_B]

Preparation of {[1,1-(2-C_4H_3N)$_2C_6H_{10}$]$_2$Co][K(THF)]$_2$}$_n$ (9.4).

A solution of **9.1a** (1.80 g, 8.4 mmol) in THF was added drop-wise to a suspension of KH (0.71 g, 17.7 mmol) in THF. A vigorous reaction took place resulting in a cloudy solution. After 1 hour of stirring, the addition of a suspension of $CoCl_2(THF)_{1.5}$ (1.0 g, 4.2 mmol) afforded a deep purple colour. The reaction was allowed to stir overnight and then centrifuged. The dark purple solution was concentrated and layered with hexanes. Large, purple crystals of **9.4** were formed upon standing at room temperature for two days (2.22 g, 3.1 mmol, 75%). Anal. Calcd (found) for $C_{36}H_{48}N_4O_2CoK_2$ (%): C, 61.25 (61.18); H, 6.85 (6.83); N, 7.94 (7.89). IR (Nujol mull, cm^{-1}): ν 3084 (w), 2906 (vs), 1461 (vs), 1440 (s), 1401 (w), 1377 (s), 1341 (w), 1298 (m), 1277 (w), 1265 (w), 1228 (w), 1214 (w), 1198 (w), 1159 (m), 1127 (m), 1106 (m), 1093 (w), 1038 (s), 961 (m), 906 (m), 890 (w), 872 (w), 841 (w), 828 (w), 781 (m), 769 (m), 733 (vs), 724 (s). [μ_{eff} = 4.5 μ_B]

Preparation of [μ,η^5-{[1,1-(2-C_4H_3N)$_2C_6H_{10}$]$_2$Fe}Fe]$_2$ (9.5).

A solution of **9.1a** (0.91 g, 4.2 mmol) in THF was added to a stirred suspension of either KH or NaH (0.21 g, 8.7 mmol) in THF. After stirring for 24 hours, the addition of a suspension of $FeCl_2(THF)_{1.5}$ (1.0 g, 4.2 mmol) in THF turned the colour dark orange. The reaction mixture was stirred for 30 minutes, filtered, slowly evaporated and allowed to stand at room temperature to yield bright orange pyramidal crystals of **9.5** (0.78 g, 6.4 mmol, 60%). Anal. Calcd (found) for $C_{64}H_{80}N_8O_2Fe_4$ (%): C, 63.17 (63.03); H, 6.62 (6.57); N, 9.21 (9.18). IR (Nujol mull, cm^{-1}): ν 3091 (w), 3042 (s), 1462 (vs), 1377 (s), 1302 (w), 1282 (w), 1264 (w), 1245 (w), 1226 (w), 1213 (w), 1187 (w), 1169 (m), 1129 (s), 1143 (w), 1048 (m), 1035 (m), 1017 (m), 976 (w), 938 (w), 906 (w), 828 (s), 772 (m), 721 (vs). [μ_{eff} = 7.5 μ_B]

Preparation of [μ,η^5-{[1,1-(2-C_4H_3N)$_2$C(C_2H_5)$_2$]$_2$Fe}Fe]$_2$ (9.6).

A suspension of NaH (0.021 g, 0.88 mmol) in THF (3 mL) was added dropwise to a solution of **9.1b** (0.086 g, 0.43 mmol) in THF (10 mL). The mixture was stirred for 24

hours at room temperature and became opaque and white. The deprotonated ligand was added to a suspension of $FeCl_2(THF)_{1.5}$ (0.100 g, 0.43 mmol) in THF (10 mL). The brick orange solution was stirred overnight, filtered to remove beigy-white solids, concentrated and layered with toluene. After a couple of days, large, dark orange crystals of **9.6** were isolated in 38% yield (0.050 g, 0.041 mmol). IR (Nujol mull, cm^{-1}): ν 3091 (w), 2916 (s), 2853 (s), 1458 (s), 1377 (m), 1324 (w), 1292 (w), 1269 (w), 1247 (m), 1209 (w), 1180 (m), 1144 (s), 1123 (m), 1090 (w), 1041 (s), 976 (m), 941 (m), 903 (w), 848 (w), 862 (w), 830 (s), 788 (m), 770 (m), 727 (w), 718 (s), 673 (w).

Preparation of $[\mu,\eta^5$-{[1,1-(2-$C_4H_3N)_2C(C_6H_5)_2]_2Fe\}Fe]_2$ (9.7).

A suspension of KH (0.114 g, 2.84 mmol) in THF (10 mL) was added dropwise and very slowly to a solution of **9.1c** (0.381 g, 1.28 mmol) in THF (10 mL). The suspension was stirred for 4 hours and added to $FeCl_2(THF)_{1.5}$ (0.300 g, 1.28 mmol) in THF (5 mL). The colour slowly darkened with stirring from beige to brown and dark orangy-brown overnight. The THF was evaporated and the dark orange solid redissolved in toluene and filtered. After concentrating and freezing the toluene solution, small orange crystals of **9.7** could be isolated in poor yield (0.075 g, 0.038 mmol, 12% yield).

Preparation of $[\mu,\eta^5$-{[1,1-(2-$C_4H_3N)_2C_6H_{10}]_2Co\}Fe]_2$ (9.8).

A solution of **9.4** (0.300 g, 0.40 mmol) in THF was added to a stirred suspension of $FeCl_2(THF)_{1.5}$ (1.00 g, 0.4 mmol). The dark burgundy solution was stirred for an additional two hours and then allowed to stand at room temperature for 2 days. Large dark orange crystals of **8** were isolated from the white residue by repeated decantation with THF (0.14 g, 0.11mmol, 53%). Anal. Calcd (found) for $C_{64}H_{80}Co_2Fe_2N_8O_2$ (%): C, 62.85 (62.78); H, 6.59 (6.54); N, 9.16 (9.09). IR (Nujol mull, cm^{-1}): ν 3091 (w), 3042 (s), 1462 (vs), 1377 (s), 1302 (w), 1282 (w), 1264 (w), 1245 (w), 1226 (w), 1213 (w), 1187 (w), 1169 (m), 1129 (s), 1143 (w), 1048 (m), 1035 (m), 1017 (m), 976 (w), 938 (w), 906 (w), 828 (s), 772 (m), 721 (vs). [$\mu_{eff} = 6.6\ \mu_B$]

Preparation of [1,1-(2-$C_4H_3N)_2C_6H_{10}$]Fe(pyridine)$_3$ (9.9).

A solid sample of **9.5** (0.100 g, 0.082 mmol) was treated with hot pyridine. The resulting bright orange solution was filtered and allowed to stand at -37°C for two days, upon which orange-yellow crystals of **9.9** separated (0.089 g, 0.16 mmol, 50%). Anal. Calcd (found) for $C_{31.5}H_{33.5}FeN_{5.5}$ (%): C, 69.42 (69.38); H, 6.20 (6.17); N, 14.14 (14.09).

Preparation of {1,2-[(2-C_4H_3N)CH=N]$_2C_2H_4$}$_2Co_2$ (9.10).

A suspension of KH (0.035 g, 0.87 mmol) in THF (5 mL) was added dropwise to a solution of **9.2a** (0.090 g, 0.42 mmol) in THF (10 mL), with visible gas evolution. The mixture was stirred for two hours, upon which time it was added to a suspension of $CoCl_2(THF)_{1.5}$ (0.100 g, 0.42 mmol) in THF (5 mL), immediately becoming dark reddish-brown. After stirring overnight, the solution was centrifuged to separate a dark red solution from grey precipitates. Layering a semi-concentrated solution with hexanes resulted in a harsh precipitation of more grayish-coloured solids after sitting overnight. The red solution was separated from the precipitates and dark red crystals of **9.10** grew upon standing at room temperature for several days (0.043 g, 0.076 mmol, 36% yield).

Preparation of {1,2-[(2-C_4H_3N)CH=N]$_2C_6H_{10}$}$_2Co_2$ (9.11).

The ligand **9.2b** (0.113 g, 0.42 mmol) was reacted with 2 equivalents of KH (0.035 g, 0.87 mmol) in THF (10 mL) for two hours. Addition of the resulting solution to a suspension of $CoCl_2(THF)_{1.5}$ (0.100 g, 0.42 mmol) in THF (5 mL) produces a dark reddish-brown solution. After stirring overnight, the suspension was centrifuged to remove a dark red solution from dark grey precipitates. Dark red crystals of complex **9.11** grew upon standing at room temperature in THF (0.059 g, 0.091 mmol, 43% yield).

Preparation of [{1,2-[(2-C_4H_3N)CH=N]$_2C_6H_4$}$_2$Cr]K (9.12).

A suspension of KH (0.033 g, 0.82 mmol) in THF (5 mL) was added dropwise to a solution of the ligand **9.2c** (0.105 g, 0.40 mmol) in THF (10 mL), evolving gas. After two hours of stirring, the solution was added to a suspension of $CrCl_3(THF)_3$ (0.150 g, 0.40 mmol) in THF (5 mL) at room temperature. After stirring overnight, the solution was a dark orange colour. Centrifugation separated out a dark orange solution and crystals of

complex **9.12** grew after leaving the concentrated THF solution at room temperature for several days (0.069 g, 0.10 mmol, 25% yield). IR (Nujol mull, cm^{-1}): ν 2920 (s), 2854 (s), 1580 (m), 1550 (s), 1512 (w), 1460 (s), 1429 (w), 1385 (s), 1348 (w), 1328 (w), 1286 (s), 1222 (w), 1193 (m), 1174 (w), 1139 (m), 1078 (m), 1036 (s), 980 (m), 950 (w), 894 (w), 879 (w), 852 (m, b), 796 (w), 784 (w), 748 (s), 686 (w), 665 (w), 628 (m).

X-Ray Crystallography

All of the compounds consistently yielded crystals that diffracted weakly, and the results presented are the best of several trials. The crystals were mounted on thin glass fibers using paraffin oil and cooled to the data collection temperature. Data were collected on a Bruker AXS SMART 1k CCD diffractometer. Data for the compounds **9.3-9.5** and **9.7-9.12** were collected with a sequence of 650 scans per set at 0.3° ω scans at 0, 120, and 240° in φ. To obtain acceptable redundancy data for compound **9.6**, the sequence of 650 scans per set with 0.3° ω scans at 0, 90, 180, and 270° in φ was used. Initial unit cell parameters were determined from 60 data frames collected at the different sections of the Ewald sphere. Semiempirical absorption corrections based on equivalent reflections were applied.[14] Systematic absences in the diffraction data-set and unit-cell parameters were consistent with monoclinic $P2_1/c$ for **9.3** and **9.4**, orthorhombic *Fddd* for **9.5**, triclinic $P\bar{1}$ for **9.6**, monoclinic *C2/c* for **9.7**, orthorhombic *Aba2* for **9.8**, monoclinic $P2_1/n$ for **9.9**, monoclinic, *C2/c* for **9.10**, orthorhombic *Pccn* for **9.11**, and monoclinic *C2/c* for **9.12**. Solutions in centrosymmetric space groups for compounds **9.3-9.5** and **9.7-9.12** and non-centrosymmetric for compound **9.6** yielded chemically reasonable and computationally stable results of refinement. The structures were solved by direct methods, completed with difference Fourier synthesis, and refined with full-matrix least-squares procedures based on F^2. For each of the isomorphous structure pairs, **9.3** and **9.4**, and **9.5** and **9.8**, the atomic coordinates of the first solved were used as a trial solution for the second. The compound molecule is located on a two-fold rotation axis for **9.8** and **9.5**. The compound exists as an infinite chain for **9.3** and **9.4.** A half-molecule of co-crystallized pyridine solvent was located disordered at an inversion centre in **9.9**. A molecule of co-crystallized tetrahydrofuran solvent was located in each asymmetric unit of **9.8** and **9.9**. All non-hydrogen atoms, except the disordered pyridine molecule in **9.9**

which was treated as a rigid hexagon with isotropically refined atoms, were refined with anisotropic displacement parameters. All hydrogen atoms were treated as idealized contributions. All non-hydrogen atoms were refined with anisotropic displacement coefficients. All hydrogen atoms were treated as idealized contributions. All scattering factors are contained in several versions of the SHELXTL program library, with the latest version used being v.6.12.[15] Crystallographic data and relevant bond distances and angles are reported in Tables 9.1-9.5.

Table 9.1. Crystal Data and Structure Analysis Results of Complexes 9.3-9.7

	9.3	**9.4**	**9.5**	**9.6**	**9.7**
formula	$C_{36}H_{48}FeK_2N_4O_2$	$C_{36}H_{48}CoK_2N_4O_2$	$C_{64}H_{80}Fe_4N_8O_2$	$C_{66}H_{80}Fe_4N_8$	$C_{126}H_{112}Fe_4N_8$
Mw	702.83	705.91	1216.76	1208.78	1961.64
crystal system	Monoclinic	Monoclinic	Orthorhombic	Triclinic	Monoclinic
space group	P2(1)/c	P2(1)/c	Fddd	P-1	C2/c
a (Å)	10.9890(8)	11.0006(13)	22.057(2)	12.4135(10)	21.788(3)
b (Å)	20.4952(14)	20.395(3)	25.329(3)	15.7314(13)	20.896(3)
c (Å)	16.1207(11)	16.051(2)	25.558(3)	16.6567(14)	22.575(3)
α (deg)	90	90	90	78.3550(10)	90
β (deg)	101.3950(10)	101.811(3)	90	87.3470(10)	104.322(3)
γ (deg)	90	90	90	72.5230(10)	90
V (Å^3)	3559.2(4)	3525.0(8)	14279(3)	3038.4(4)	9959(2)
Z	4	4	8	2	4
radiation (Kα, Å)	0.71073	0.71073	0.71073	0.71073	0.71073
T (K)	203(2)	203(2)	203(2)	203(2)	203(2)
D_{calcd} (g cm^{-3})	1.312	1.330	1.132	1.321	1.308
μ_{calcd} (mm^{-1})	0.694	0.760	0.839	0.982	0.628
F_{000}	1488	1492	5120	1272	4112
R, R_w[2 a]	0.0554, 0.0868	0.0549, 0.0767	0.0895, 0.2590	0.0418, 0.0916	0.0751, 0.0837
GoF	1.059	1.029	1.048	1.016	1.053

[a] $R = \Sigma||F_0| - |F_c||/\Sigma|F|$, $R_w = [\Sigma(|F_0| - |F_c|)^2/\Sigma wF_0^2\}^{1/2}$

Table 9.2. Crystal Data and Structure Analysis Results of Complexes 9.8-9.12

	9.8	**9.9**	**9.10**	**9.11**	**9.12**
formula	$C_{64}H_{80}Co_2Fe_2N_8O_2$	$C_{31.50}H_{33.50}FeN_{5.50}$	$C_{51}H_{54}Co_4N_{16}O_{0.75}$	$C_{32}H_{36}Co_2N_8$	$C_{36}H_{32}CrKN_8O$
Mw	1222.92	544.99	1138.82	650.55	683.80
crystal system	Orthorhombic	Monoclinic	Monoclinic	Orthorhombic	Monoclinic
space group	Aba2	P2(1)/n	C2/c	Pccn	C2/c
a (Å)	20.7800(14)	8.6212(15)	34.813(8)	19.460(6)	10.972(2)
b (Å)	19.5453(13)	17.778(3)	23.351(5)	10.216(3)	18.129(4)
c (Å)	14.2942(10)	18.306(3)	13.362(3)	15.641(4)	17.188(4)
α (deg)	90	90	90	90	90
β (deg)	90	100.949(2)	103.757(4)	90	103.859(3)
γ (deg)	90	90	90	90	90
V (Å^3)	5805.6(7)	2754.6(8)	10551(4)	3109.5(16)	3319.5(12)
Z	4	4	8	4	4
radiation (Kα, Å)	0.71073	0.71073	0.71073	0.71073	0.71073
T (K)	223(2)	203(2)	213(2)	200(2)	200(2)
D_{calcd} (g cm^{-3})	1.399	1.314	1.434	1.390	1.368
μ_{calcd} (mm^{-1})	1.103	0.578	1.289	1.102	0.513
F_{000}	2568	1148	4688	1352	1420
R, R_w[2 a]	0.0335, 0.0814	0.0549, 0.0932	0.0468, 0.1234	0.0514, 0.1004	0.0433, 0.1172
GoF	1.026	1.027	1.054	1.021	1.037

[a] $R = \Sigma||F_0| - |F_c||/\Sigma|F|$, $R_w = [\Sigma(|F_0| - |F_c|)^2/\Sigma wF_0^2\}^{1/2}$

Table 9.3. Selected Bond Distances (Å) and Angles (deg) of Complexes 9.3-9.6

9.3	9.4	9.5	9.6
Fe-N(1) = 2.057(2)	Co-N(1) = 2.014(3)	Fe(1)-N(1) = 2.018(8)	Fe(1)-(N1) = 1.994(3)
Fe-N(2) = 2.043(2)	Co-N(2) = 2.003(3)	Fe(1)-C(1) = 2.030(12)	Fe(1)-(N2) = 2.140(3)
Fe-N(3) = 2.051(2)	Co-N(3) = 2.013(3)	Fe(1)-C(2) = 2.033(13)	Fe(1)-(N7) = 2.147(3)
Fe-N(4) = 2.079(2)	Co-N(4) = 2.031(3)	Fe(1)-C(3) = 2.050(10)	Fe(1)-N(8) = 2.009(3)
K(1)-N(4) = 3.234(2)	K(1)-N(4) = 3.106(3)	Fe(1)-C(4) = 2.022(11)	Fe(2)-N(2) = 2.023(3)
K(1)-C(19) = 3.079(3)	K(1)-C(19) = 3.086(3)	Fe(2)-N(1) = 2.136(9)	Fe(2)-C(5) = 2.029(4)
K(1)-C(20) = 3.122(3)	K(1)-C(20) = 3.120(3)	Fe(2)-N(2) = 1.974(10)	Fe(2)-C(6) = 2.089(4)
K(1)-C(21) = 3.288(3)	K(1)-C(21) = 3.301(3)	N(1)-Fe(2)-N(2) = 91.7(4)	Fe(2)-C(7) = 2.073(4)
K(1)-O(1) = 2.617(2)	K(1)-O(1) = 2.610(3)	N(1)-Fe(2)-N(2A) = 101.1(4)	Fe(2)-C(8) = 2.047(4)
K(2)-N(3) = 3.095(2)	K(2)-N(3) = 3.090(3)	N(1)-Fe(2)-N(1A) = 132.0(5)	N(1)-Fe(1)-N(2) = 92.36(12)
K(2)-C(15) = 3.209(3)	K(2)-C(15) = 3.220(4)	N(2)-Fe(2)-N(2A) = 148.5(5)	N(1)-Fe(1)-N(7) = 100.29(12)
K(2)-C(16) = 3.194(3)	K(2)-C(16) = 3.211(4)	N(2)-Fe(2)-N(1A) = 101.1(4)	N(1)-Fe(1)-N(8) = 150.25(13)
K(2)-C(17) = 3.038(3)	K(2)-C(17) = 3.046(3)	N(2A)-Fe(2)-N(1A) = 91.7(4)	N(2)-Fe(1)-N(7) = 134.80(11)
K(2)-C(18) = 2.980(3)	K(2)-C(18) = 2.976(3)		N(2)-Fe(1)-N(8) = 98.55(12)
K(2)-N(4) = 3.034(2)	K(2)-N(4) = 3.016(4)		N(7)-Fe(1)-N(8) = 91.49(12)
K(2)-C(19) = 3.176(3)	K(2)-C(19) = 3.161(3)		
K(2)-C(20) = 3.292(3)	K(2)-C(20) = 3.300(4)		
K(2)-C(21) = 3.206(3)	K(2)-C(21) = 3.208(3)		
K(2)-C(22) = 3.028(3)	K(2)-C(22) = 3.026(3)		
K(2)-O(2) = 2.650(2)	K(2)-O(2) = 2.644(3)		
N(1)-Fe-N(2) = 90.20(9)	N(1)-Co-N(2) = 91.04(10)		
N(1)-Fe-N(3) = 125.71(9)°	N(1)-Co-N(3) = 123.45(11)		
N(1)-Fe-N(4) = 124.05(9)°	N(1)-Co-N(4) = 124.92(10)		
N(2)-Fe-N(3) = 111.88(9)°	N(2)-Co-N(3) = 111.06(11)		
N(2)-Fe-N(4) = 118.17(9)°	N(2)-Co-N(4) = 117.55(11)		
N(3)-Fe-N(4) = 89.14(8)°	N(3)-Co-N(4) = 90.61(1)		

Table 9.4. Selected Bond Distances (Å) and Angles (deg) of Complexes 9.7-9.9

9.7	9.8	9.9
Fe(1)-N(1)/N(1A) = 1.995(6)	Co-N(1) = 2.079(2)	Fe-N(1) = 2.101(2)
Fe(1)-N(2)/N(2A) = 2.172(6)	Co-N(2) = 1.961(3)	Fe-N(2) = 2.040(2)
Fe(2)-N(2) = 2.003(6)	Co-N(3) = 2.077(2)	Fe-N(3) = 2.411(2)
Fe(2)-C(5) = 2.015(7)	Co-N(4) = 1.958(3)	Fe-N(4) = 2.192(2)
Fe(2)-C(6) = 2.076(7)	Fe-N(1) = 2.016(2)	Fe-N(5) = 2.140(2)
Fe(2)-C(7) = 2.061(7)	Fe-C(1) = 2.027(3)	N(1)-Fe-N(2) = 89.89(8)
Fe(2)-C(8) = 2.039(8)	Fe-C(2) = 2.076(3)	N(1)-Fe-N(3) = 173.61(8)
N(1)-Fe(1)-N(2) = 88.2(2)	Fe-C(3) = 2.073(3)	N(1)-Fe-N(4) = 96.25(9)
N(1)-Fe-N(1A) = 151.8(4)	Fe-C(4) = 2.041(3)	N(1)-Fe-N(5) = 97.97(8)
N(1)-Fe-N(2A) = 105.7(2)	N(1)-Co-N(2) = 92.13(9)	N(2)-Fe-N(3) = 83.73(8)
N(1A)-Fe-N(2) = 105.7(2)	N(1)-Co-N(3) = 130.70(9)	N(2)-Fe-N(4) = 142.39(9)
N(1A)-Fe-N(2A) = 88.2(2)	N(1)-Co-N(4) = 101.71(10)	N(2)-Fe-N(5) = 114.56(9)
N(2)-Fe-N(2A) = 121.2(3)	N(2)-Co-N(3) = 100.65(10)	N(3)-Fe-N(4) = 88.66(8)
	N(2)-Co-N(4) = 147.06(11)	N(3)-Fe-N(5) = 85.03(8)
	N(3)-Co-N(4) = 92.74(10)	N(4)-Fe-N(5) = 101.31(8)°

Table 9.5. Selected Bond Distances (Å) and Angles (deg) of Complexes 9.10-9.12

9.10	9.11	9.12
Co(1)-N(1) = 1.990(3)	Co(1)-N(1) = 1.963(5)	Cr(1)-N(2) = 2.134(2)
Co(1)-N(2) = 2.038(3)	Co(1)-N(2) = 2.046(5)	Cr(1)-N(3) = 2.011(2)
Co(1)-N(5) = 1.987(3)	Co(2)-N(3) = 2.055(5)	Cr(1)-N(4) = 2.007(2)
Co(1)-N(6) = 2.040(3)	Co(2)-N(4) = 1.984(5)	K(1)-N(1) = 3.143(3)
Co(2)-N(3) = 2.044(3)	N(1)-Co(1)-N(2) = 84.2(2)	K(1)-C(12) = 3.441(3)
Co(2)-N(4) = 1.979(3)	N(1)-Co(1)-N(1A) = 141.8(3)	N(2)-C(5) = 1.295(4)
Co(2)-N(7) = 2.048(3)	N(1)-Co(1)-N(2A) = 114.1(2)	N(3)-C(12) = 1.311(4)
Co(2)-N(8) = 2.000(3)	N(2)-Co(1)-N(2A) = 124.1(3)	N(2)-Cr(1)-N(3) = 78.37(9)
N(1)-Co(1)-N(2) = 84.02(13)	N(3)-Co(2)-N(4) = 83.8(2)	N(2)-Cr(1)-N(4) = 157.82(9)
N(1)-Co(1)-N(5) = 133.63(13)	N(3)-Co(2)-N(3A) = 123.0(3)	N(2)-Cr(1)-N(2A) = 88.71(12)
N(1)-Co(1)-N(6) = 118.82(13)	N(3)-Co(2)-N(4A) = 113.3(2)	N(2)-Cr(1)-N(3A) = 109.57(9)
N(2)-Co(1)-N(5) = 119.53(13)	N(4)-Co(2)-N(4A) = 144.9(3)	N(2)-Cr(1)-N(4A) = 94.87(9)
N(2)-Co(1)-N(6) = 122.56(12)		N(3)-Cr(1)-N(4) = 79.81(9)
N(5)-Co(1)-N(6) = 83.45(13)		N(3)-Cr(1)-N(2A) = 109.57(9)
N(3)-Co(2)-N(4) = 83.57(13)		N(3)-Cr(1)-N(3A) = 169.29(13)
N(3)-Co(2)-N(7) = 123.74(12)		N(3)-Cr(1)-N(4A) = 92.58(9)
N(3)-Co(2)-N(8) = 127.80(13)		N(4)-Cr(1)-N(2A) = 94.87(9)
N(4)-Co(2)-N(7) = 116.17(13)		N(4)-Cr(1)-N(3A) = 92.58(9)
N(4)-Co(2)-N(8) = 126.50(13)		N(4)-Cr(1)-N(4A) = 90.03(13)
N(7)-Co(2)-N(8) = 83.75(13)		

Complex 9.3. The structure (Figure 9.1) consists of one Fe atom surrounded by the four N atoms of two σ-ligated dipyrrolyl dianions [Fe-N(1) = 2.057(2) Å, Fe-N(2) = 2.043(2) Å, Fe-N(3) = 2.051(2) Å, Fe-N(4) = 2.079(2) Å], defining a distorted tetrahedral environment [N(1)-Fe-N(2) = 90.20(9)°, N(1)-Fe-N(3) = 125.71(9)°, N(1)-Fe-N(4) = 124.05(9)°, N(2)-Fe-N(3) = 111.88(9)°, N(2)-Fe-N(4) = 118.17(9)°, N(3)-Fe-N(4) = 89.14(8)°]. Two inequivalent potassium atoms also occupy the unit cell. One is π-bonded to one pyrrole ring of one ligand [K(1)-N(4) = 3.234(2) Å, K(1)-C(19) = 3.079(3) Å, K(1)-C(20) = 3.122(3) Å, K(1)-C(21) = 3.288(3) Å] and the second is π-bound to two pyrrole rings of one ligand [K(2)-N(3) = 3.095(2) Å, K(2)-C(15) = 3.209(3) Å, K(2)-C(16) = 3.194(3) Å, K(2)-C(17) = 3.038(3) Å, K(2)-C(18) = 2.980(3) Å, K(2)-N(4) = 3.034(2) Å, K(2)-C(19) = 3.176(3) Å, K(2)-C(20) = 3.292(3) Å, K(2)-C(21) = 3.206(3) Å, K(2)-C(22) = 3.028(3) Å]. In turn, each potassium atom is bound to a molecule of THF and π-bonded to the pyrrole ring of a second identical unit, thus assembling an infinite array.

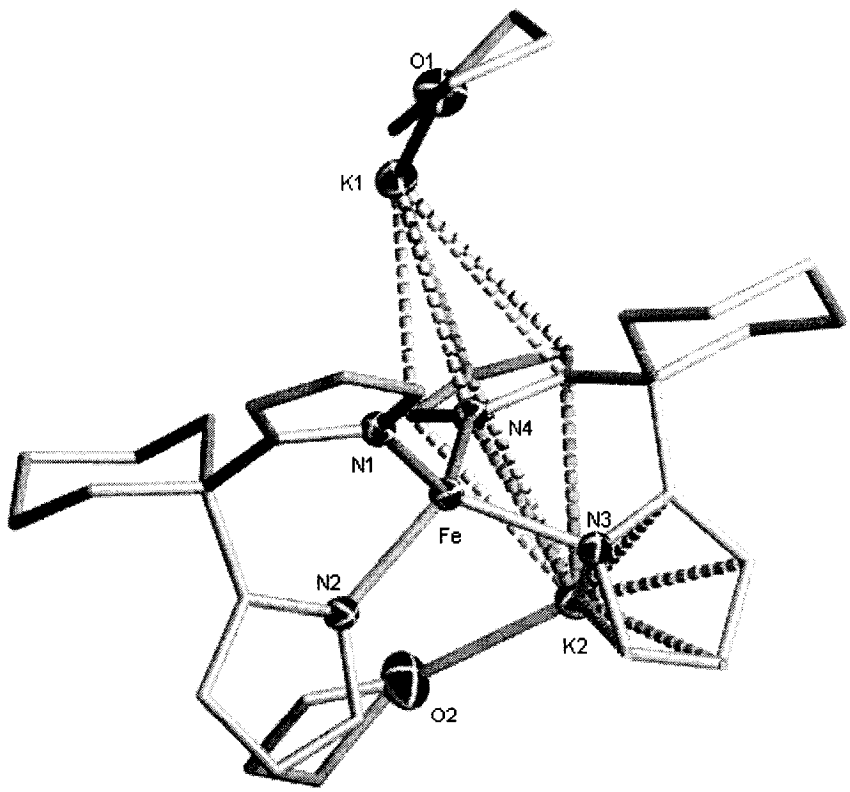

Figure 9.1. Partial thermal ellipsoid plot of **9.3**, drawn at the 30% probability level. Hydrogen atoms have been omitted for clarity.

Complex 9.4. The structure of complex **9.4** is basically identical to **9.3**, with a Co center surrounded by two ligands in a distorted tetrahedral geometry [N(1)-Co-N(2) = 91.04(10)°, N(1)-Co-N(3) = 123.45(11)°, N(1)-Co-N(4) = 124.92(10)°, N(2)-Co-N(3) = 111.06(11)°, N(2)-Co-N(4) = 117.55(11)°, N(3)-Co-N(4) = 90.61(1)°]. Once again, both ligands are bichelating and σ-bound through the N of the pyrrole rings [Co-N(1) = 2.014(3) Å, Co-N(2) = 2.003(3) Å, Co-N(3) = 2.013(3) Å, Co-N(4) = 2.031(3) Å]. Completing the structure are two inequivalent K atoms, one π-bound to one pyrrole ring of one ligand [K(1)-N(4) = 3.106(3) Å, K(1)-C(19) = 3.086(3) Å, K(1)-C(20) = 3.120(3) Å, K(1)-C(21) = 3.301(3) Å] and the second π-bound to two pyrrole rings of the same ligand [K(2)-N(3) = 3.090(3) Å, K(2)-C(15) = 3.220(4) Å, K(2)-C(16) = 3.211(4) Å, K(2)-C(17) = 3.046(3) Å, K(2)-C(18) = 2.976(3) Å, K(2)-N(4) = 3.016(4) Å, K(2)-C(19) = 3.161(3) Å, K(2)-C(20) = 3.300(4) Å, K(2)-C(21) = 3.208(3) Å, K(2)-C(22) = 3.026(3) Å]. Each K atom is also coordinated to a molecule of THF, and like above, assemble an infinite array via π-bonding with pyrrole rings from adjacent molecules (Figure 9.2).

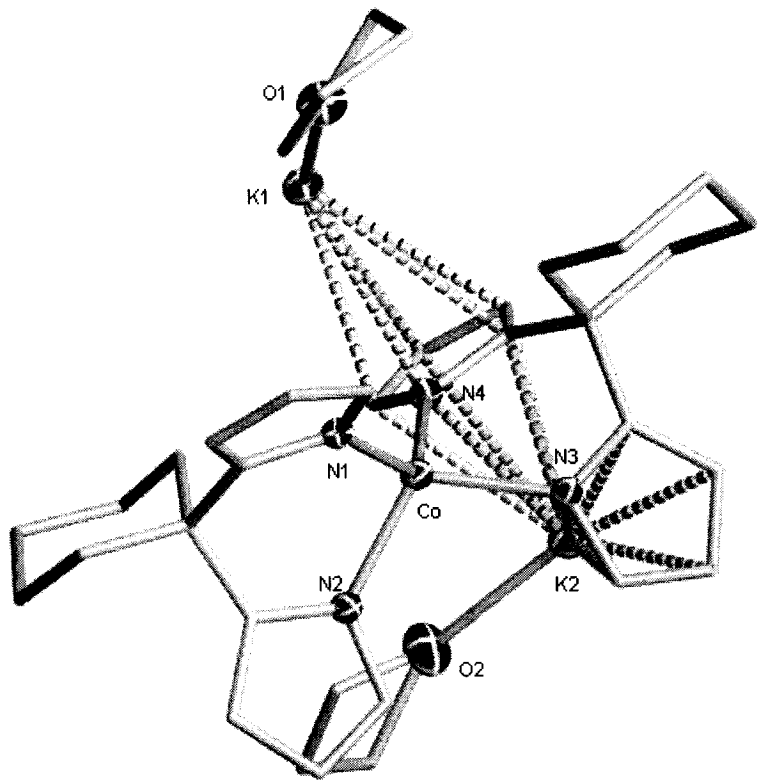

Figure 9.2. Partial thermal ellipsoid plot of **9.4**, drawn at the 30% probability level. Hydrogen atoms have been omitted for clarity.

Complex 9.5. The molecular structure of **9.5** is a symmetry generated tetramer, consisting of four Fe atoms and four dianionic ligands (Figure 9.3). There are two types of Fe centers, adopting a diamond-shaped planar arrangement, with each set of opposite Fe centers assuming identical coordination environments. Two of the iron centers display a severely flattened tetrahedral coordination geometry [N(1)-Fe(2)-N(2) = 91.7(4)°, N(1)-Fe(2)-N(2A) = 101.1(4)°, N(1)-Fe(2)-N(1A) = 132.0(5)°, N(2)-Fe(2)-N(2A) = 148.5(5)°, N(2)-Fe(2)-N(1A) = 101.1(4)°, N(2A)-Fe(2)-N(1A) = 91.7(4)°] defined by the four N atoms of two σ-bonded dipyrrolide dianions [Fe(2)-N(1) = 2.136(9) Å, Fe(2)-N(2) = 1.974(10) Å, Fe(2)-N(1A) = 2.136(9) Å, Fe(2)-N(2A) = 1.974(10) Å]. The other two Fe centers form the bridges, connecting the two identical units by π-bonding to two pyrrole rings from opposite units in a ferrocenoid-type structure [Fe(1)-N(1) = 2.018(8) Å, Fe(1)-C(1) = 2.030(12) Å, Fe(1)-C(2) = 2.033(13) Å, Fe(1)-C(3) = 2.050(10) Å, Fe(1)-C(4) = 2.022(11) Å]. Two unit cells have been found for complex **9.5**. One is found in Table 9.1 and the other can be found in reference 16.

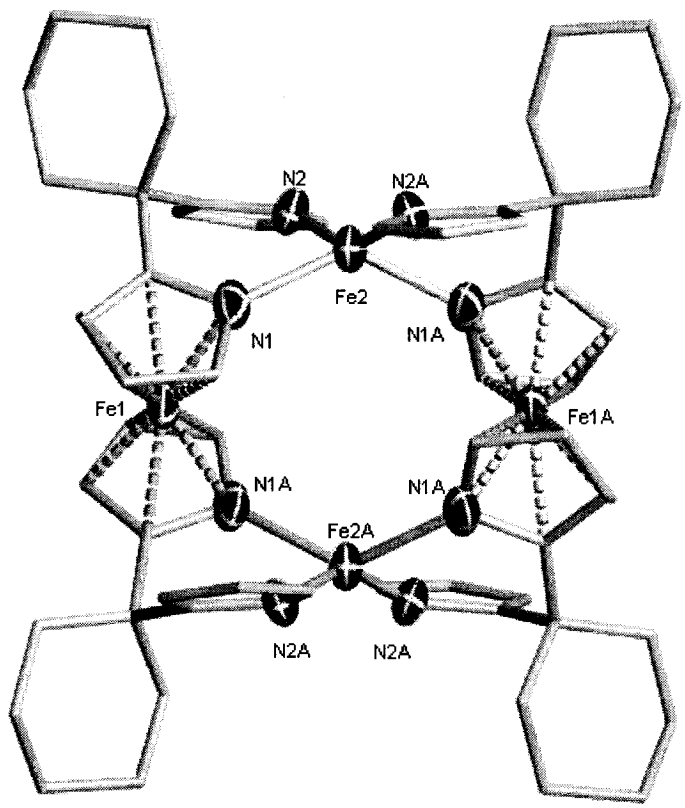

Figure 9.3. Partial thermal ellipsoid plot of **9.5**, drawn at the 30% probability level. Hydrogen atoms have been omitted for clarity.

Complex 9.6. The structure of complex **9.6** is very similar to that of **9.5**, containing four Fe centers (in two separate coordination geometries) and four dianionic ligands (bridging the metal centers) in a tetrameric cluster (Figure 9.4). The first set of Fe centers (located opposite each other) are nearly identically σ-bound to four N atoms from two ligand system [Fe(1)-(N1) = 1.994(3) Å, Fe(1)-(N2) = 2.140(3) Å, Fe(1)-(N7) = 2.147(3) Å, Fe(1)-N(8) = 2.009(3) Å] in a severely distorted tetrahedral geometry [N(1)-Fe(1)-N(2) = 92.36(12)°, N(1)-Fe(1)-N(7) = 100.29(12)°, N(1)-Fe(1)-N(8) = 150.25(13)°, N(2)-Fe(1)-N(7) = 134.80(11)°, N(2)-Fe(1)-N(8) = 98.55(12)°, N(7)-Fe(1)-N(8) = 91.49(12)°]. The two units are then bridged by two other Fe center, π-bound to two pyrrole rings from two separate units in a metallocenic structure [Fe(2)-N(2) = 2.023(3) Å, Fe(2)-C(5) = 2.029(4) Å, Fe(2)-C(6) = 2.089(4) Å, Fe(2)-C(7) = 2.073(4) Å, Fe(2)-C(8) = 2.047(4) Å]. Two unit cells have been found for complex **9.6**. One is found in Table 9.1 and the other can be found in reference 17.

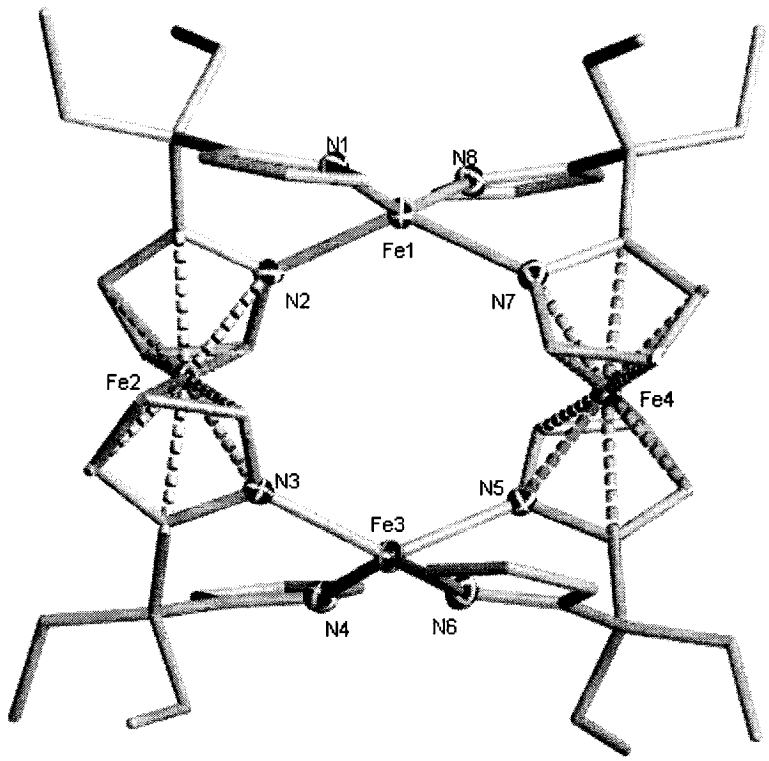

Figure 9.4. Partial thermal ellipsoid plot of **9.6**, drawn at the 30% probability level. Hydrogen atoms have omitted for clarity.

Complex 9.7. Complex **9.7** adopts a very similar tetranuclear structure to complexes **9.5** and **9.6** (displayed in Figure 9.5). The four Fe centers are bridged by four ligand systems, σ-bound to one set of distorted tetrahedral Fe atoms [Fe(1)-N(1)/N(1A) = 1.995(6) Å, Fe(1)-N(2)/N(2A) = 2.172(6) Å, N(1)-Fe(1)-N(2) = 88.2(2)°, N(1)-Fe-N(1A) = 151.8(4)°, N(1)-Fe-N(2A) = 105.7(2)°, N(1A)-Fe-N(2) = 105.7(2)°, N(1A)-Fe-N(2A) = 88.2(2)°, N(2)-Fe-N(2A) = 121.2(3)°] and π-bound to the other two ferrocenic Fe's [Fe(2)-N(2) = 2.003(6) Å, Fe(2)-C(5) = 2.015(7) Å, Fe(2)-C(6) = 2.076(7) Å, Fe(2)-C(7) = 2.061(7) Å, Fe(2)-C(8) = 2.039(8) Å]. In this case, a plane of symmetry bisects the molecule through the tetrahedrally coordinated –ate Fe centers.

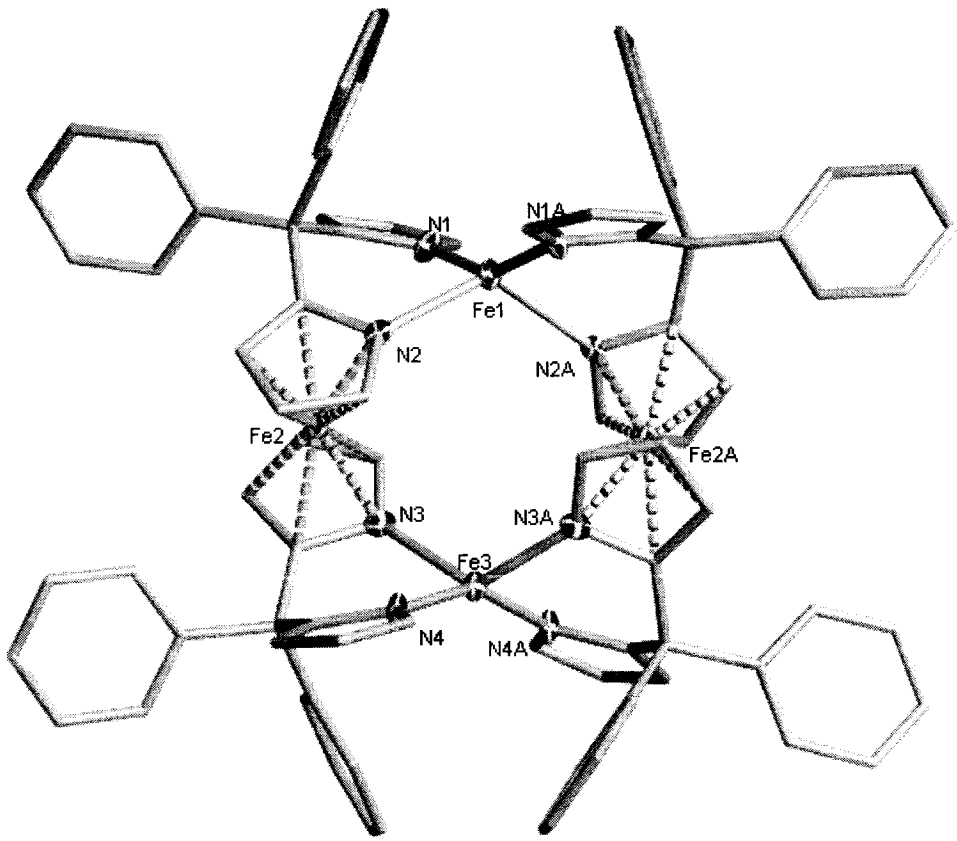

Figure 9.5. Partial thermal ellipsoid plot of **9.7**, drawn at the 30% probability level. Hydrogen atoms have omitted for clarity.

Complex 9.8. The X-ray structure of **9.8** is very similar to that of complex **9.5**. However, the tetranuclear cluster is now comprised of two Co centers, occupying the distorted tetrahedral sites, and two Fe centers in the metallocenic sites, shown in Figure 9.6. The bond distances and angles are also very similar [Co-N(1) = 2.079(2) Å, Co-N(2) = 1.961(3) Å, Co-N(3) = 2.077(2) Å, Co-N(4) = 1.958(3) Å, N(1)-Co-N(2) = 92.13(9)°, N(1)-Co-N(3) = 130.70(9)°, N(1)-Co-N(4) = 101.71(10)°, N(2)-Co-N(3) = 100.65(10)°, N(2)-Co-N(4) = 147.06(11)°, N(3)-Co-N(4) = 92.74(10)°, Fe-N(1) = 2.016(2) Å, Fe-C(1) = 2.027(3) Å, Fe-C(2) = 2.076(3) Å, Fe-C(3) = 2.073(3) Å, Fe-C(4) = 2.041(3) Å].

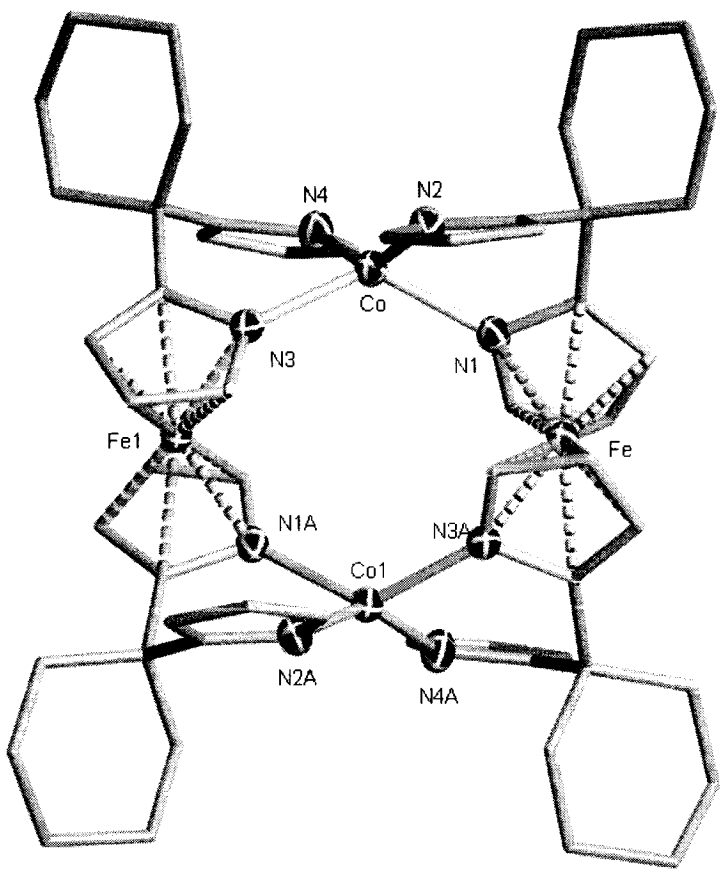

Figure 9.6. Partial thermal ellipsoid plot of **9.8**, drawn at the 30% probability level. Hydrogen atoms have been omitted for clarity.

Complex 9.9. The structure of complex **9.9** is monomeric with the Fe metal in a severely distorted pentacoordinate arrangement, midway between trigonal bipyramidal and square pyramidal (τ = 0.52)[18] [N(1)-Fe-N(2) = 89.89(8)°, N(1)-Fe-N(3) = 173.61(8)°, N(1)-Fe-N(4) = 96.25(9)°, N(1)-Fe-N(5) = 97.97(8)°, N(2)-Fe-N(3) = 83.73(8)°, N(2)-Fe-N(4) = 142.39(9)°, N(2)-Fe-N(5) = 114.56(9)°, N(3)-Fe-N(4) = 88.66(8)°, N(3)-Fe-N(5) = 85.03(8)°, N(4)-Fe-N(5) = 101.31(8)°], bound to the N atoms of three coordinated molecules of pyridine [Fe-N(3) = 2.411(2) Å, Fe-N(4) = 2.192(2) Å, Fe-N(5) = 2.140(2) Å] and the N atoms of two σ-bonded pyrrolyl rings of one ligand [Fe-N(1) = 2.101(2) Å, Fe-N(2) = 2.040(2) Å] (Figure 9.7).

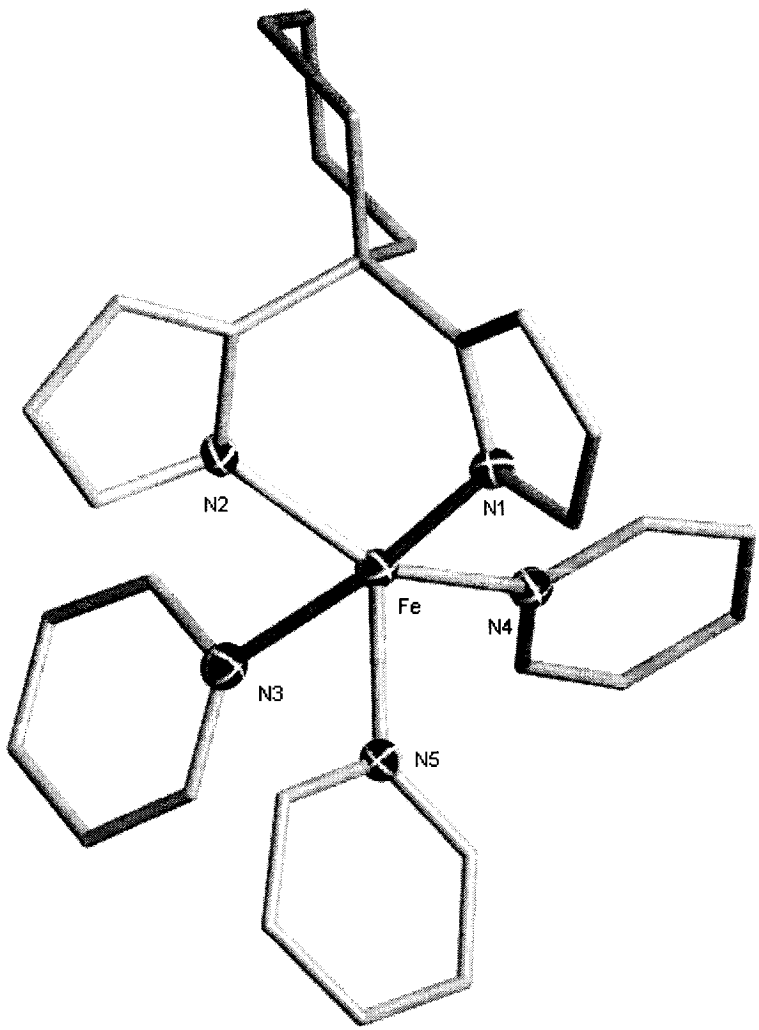

Figure 9.7. Partial thermal ellipsoid plot of **9.9**, drawn at 30% probability. Hydrogen atoms have been omitted for clarity.

Complex 9.10. Complex **9.10** is a dinuclear structure containing two ligands, shown in Figure 9.8. Each ligand system surrounds two metal centers, κ^2-bound to each Co through the pyrrole nitrogen and its adjacent imino-N. In such a way, four nitrogen atoms from two separate ligand systems surround the metal center [Co(1)-N(1) = 1.990(3) Å, Co(1)-N(2) = 2.038(3) Å, Co(1)-N(5) = 1.987(3) Å, Co(1)-N(6) = 2.040(3) Å, Co(2)-N(3) = 2.044(3) Å, Co(2)-N(4) = 1.979(3) Å, Co(2)-N(7) = 2.048(3) Å, Co(2)-N(8) = 2.000(3) Å] in a severely distorted tetrahedral geometry [N(1)-Co(1)-N(2) = 84.02(13)°, N(1)-Co(1)-N(5) = 133.63(13)°, N(1)-Co(1)-N(6) = 118.82(13)°, N(2)-Co(1)-N(5) = 119.53(13)°, N(2)-Co(1)-N(6) = 122.56(12)°, N(5)-Co(1)-N(6) = 83.45(13)°]. The two Co centers are separated by a distance of 4.096 Å. The crystal structure contains two virtually identical dimeric units and a molecule of THF disordered in the lattice.

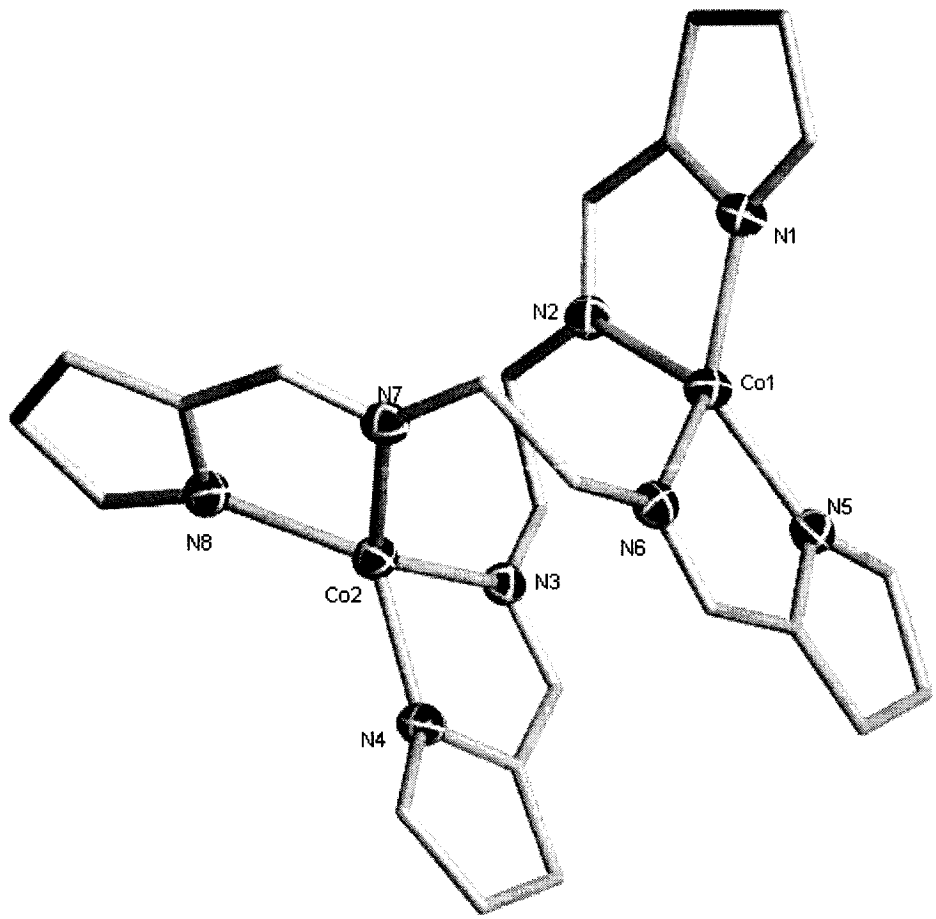

Figure 9.8. Partial thermal ellipsoid plot of complex **9.10**, drawn at the 30% probability level. Hydrogen atoms have been omitted for clarity.

Complex 9.11. The symmetry-generated dimeric structure of **9.11** is very similar to complex **9.10**. Each Co center adopts a severely distorted tetrahedral environment [N(1)-Co(1)-N(2) = 84.2(2)°, N(1)-Co(1)-N(1A) = 141.8(3)°, N(1)-Co(1)-N(2A) = 114.1(2)°, N(2)-Co(1)-N(2A) = 124.1(3)°] defined by coordination to two pyrrole N atoms and two imine N atoms from two separate ligands [Co(1)-N(1) = 1.963(5) Å, Co(1)-N(2) = 2.046(5) Å, Co(2)-N(3) = 2.055(5) Å, Co(2)-N(4) = 1.984(5) Å]. The twisted ligand systems assemble the dimer, bringing the Co centers within 3.851 Å of each other (Figure 9.9).

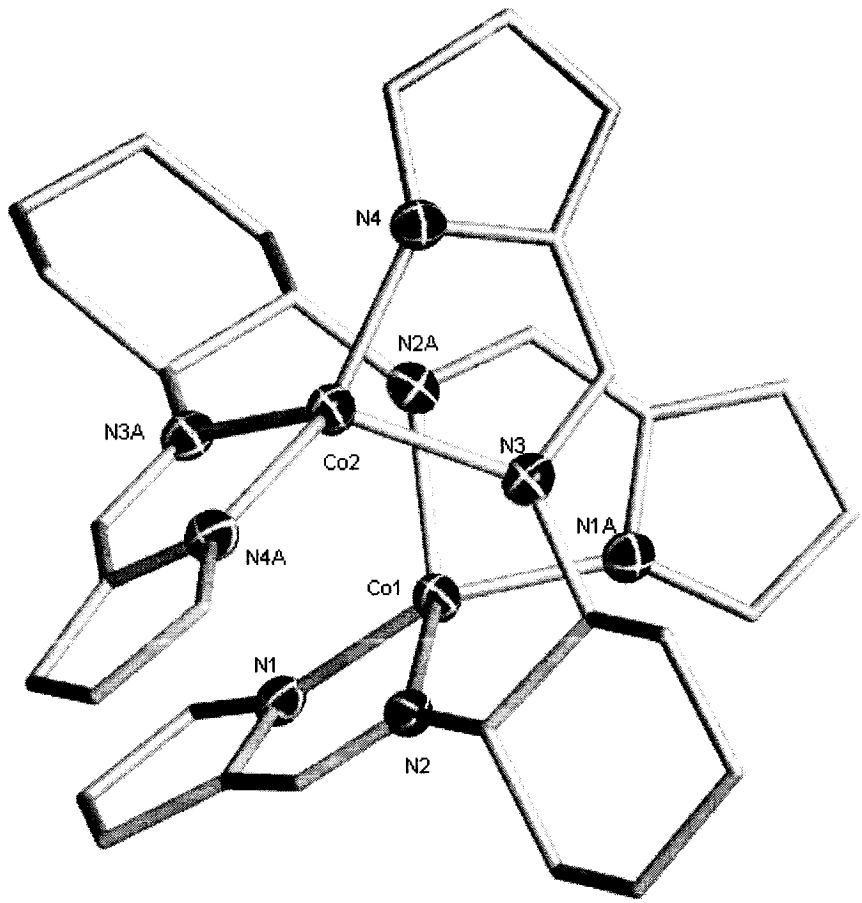

Figure 9.9. Partial thermal ellipsoid plot of complex **9.11**, drawn at the 30% probability level. Hydrogen atoms have been omitted for clarity.

Complex 9.12. The symmetry-generated structure of complex **9.12** (Figure 9.10) contains one Cr center surrounded by two κ^3-bound ligands [Cr(1)-N(2) = 2.134(2) Å, Cr(1)-N(3) = 2.011(2) Å, Cr(1)-N(4) = 2.007(2) Å] in a distorted octahedral geometry [N(2)-Cr(1)-N(3) = 78.37(9)°, N(2)-Cr(1)-N(4) = 157.82(9)°, N(3)-Cr(1)-N(4) = 79.81(9)°, N(2)-Cr(1)-N(2A) = 88.71(12)°, N(2)-Cr(1)-N(3A) = 109.57(9)°, N(2)-Cr(1)-N(4A) = 94.87(9)°, N(3)-Cr(1)-N(3A) = 169.29(13)°, N(3)-Cr(1)-N(4A) = 92.58(9)°, N(4)-Cr(1)-N(4A) = 90.03(13)°]. Each ligand system coordinates meridionally to the metal with three of its N atoms, while its free pyrrole ring engages in σ-bonding with a K counteraction [K(1)-N(1) = 3.143(3) Å]. The solvent-free K is in turn tetrahedrally coordinated to two other molecules via the imino function adjacent to the Cr-bound pyrrole ring [K(1)-C(12) = 3.441(3) Å].

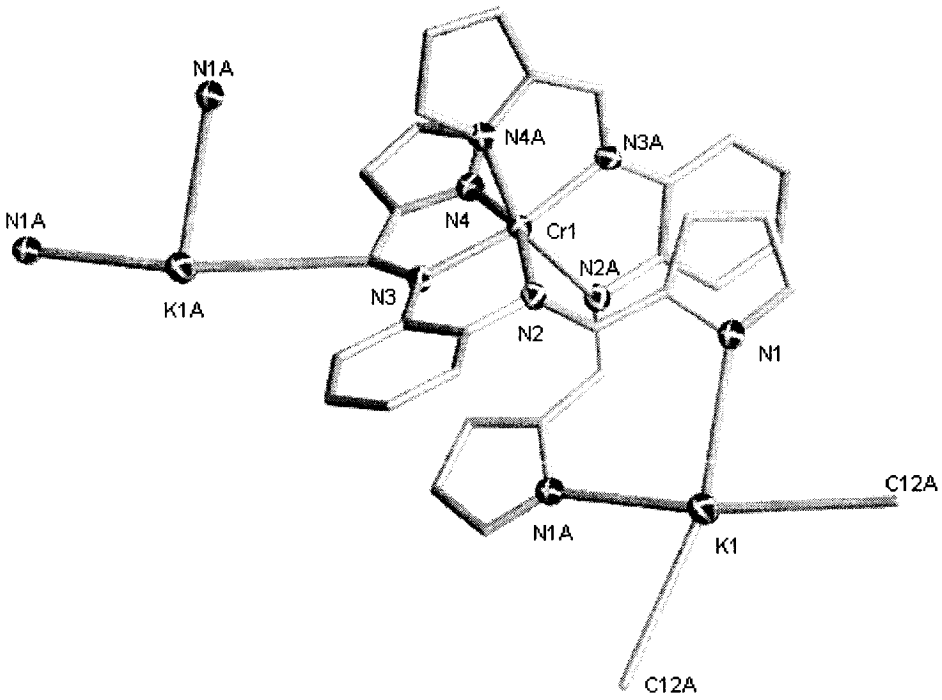

Figure 9.10. Partial thermal ellipsoid plot of complex **9.12**, drawn at the 30% probability level. Hydrogen atoms have been omitted for clarity.

Results and Discussion

The dipyrrole ligands can be readily deprotonated upon treatment with two equivalents of either KH, NaH or MeLi to give the dipyrrolide dianions $[1,1\text{-}(2\text{-}C_4H_3N)_2CR_2]^{2-}$ (R = $-(CH_2)_5-$ (**9.1a**), C_2H_5 (**9.1b**), C_6H_5 (**9.1c**)) (the reaction with NaH requires stirring overnight to afford complete deprotonation, whereas the reaction with KH or MeLi takes only 4 hours). Addition of 2 equivalents of the deprotonated ligand (R_2 = $-(CH_2)_5-$) to a suspension of $FeCl_2(THF)_{1.5}$ in THF does not result in a visible colour change, with the solution remaining beige to colourless. However, work-up of the reaction mixture allowed the isolation of $\{[1,1\text{-}(2\text{-}C_4H_3N)_2C_6H_{10}]_2Fe[K(THF)]_2\}_n$ (**9.3**), collected in good yield as large colourless crystals from a THF/hexane layer (Scheme 9.3). A series of metallate complexes can be prepared according to this procedure, since the nature of both the ligand substituents and alkali cations did not significantly modify the results of the reaction. The analogous reaction of 2 equivalents of the dianionic ligand (R_2 = $-(CH_2)_5-$) with $CoCl_2(THF)_{1.5}$ lead to the isolation of $\{[1,1\text{-}(2\text{-}C_4H_3N)_2C_6H_{10}]_2Co[K(THF)]_2\}_n$ (**9.4**) as dark purple crystals in 75% yield. Both complexes **9.3** and **9.4** were characterized by X-ray analysis and the formulae and connectivity are displayed in Figures 9.1 and 9.2. Analytical data in agreement with the proposed formulations were also obtained.

Scheme 9.3

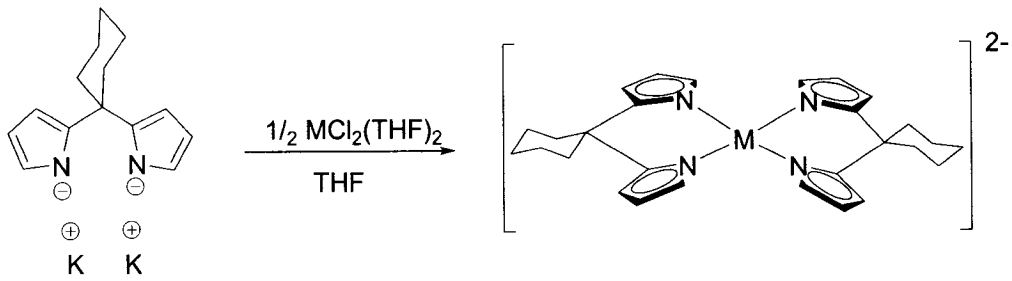

M = Fe, **9.3**
M = Co, **9.4**

The structures of the Fe and Co metallates (**9.3** and **9.4**) are basically identical. Both consist of a tetradentate metal center surrounded by two σ-bound ligands in a distorted tetrahedral geometry. Two potassium atoms can also be found in the unit cell, π-bound to the pyrrole rings and σ-bound to a molecule of THF. The bond distances and angles are

very similar for both complexes **9.3** and **9.4**, including the deviation in the tetrahedral geometry of the metal center. This suggests that the geometrical distortion is an artifact of structural optimization, as opposed to the nature of the metal center. The room temperature magnetic moments of 5.6 μ_B for **9.3** and 4.5 μ_B for **9.4** are slightly higher than expected for tetracoordinate d^6 and d^7 metal centers and may indicate large orbital contributions and a significant degree of temperature independent paramagnetism (TIP).

Anionic -ate types of structures similar to **9.3** and **9.4** are commonly encountered in the chemistry of dipyrrolide dianions. Previous work in *f*-block[8a,19] and transition metal[7] chemistry has clearly demonstrated an enhanced tendency to form either tetrahedral or octahedral structures, where alkali cations are retained at the exterior of the molecule.

With the goal of forming complexes containing only one ligand system and a neutral Fe moiety, the 1:1 reaction was carried out (Scheme 9.4). Addition of 1 equivalent of the dipyrrolide dianion $[1,1\text{-}(2\text{-}C_4H_3N)_2C_6H_{10}]^{2-}$ to $FeCl_2(THF)_{1.5}$ in THF resulted in an immediate colour change from colourless to orange. Crystals of $[\mu,\eta^5\text{-}\{[1,1\text{-}(2\text{-}C_4H_3N)_2C_6H_{10}]_2Fe\}Fe]_2$ (**9.5**) were grown from a THF solution at room temperature and a representative structure can be seen in Figure 9.3.

Scheme 9.4

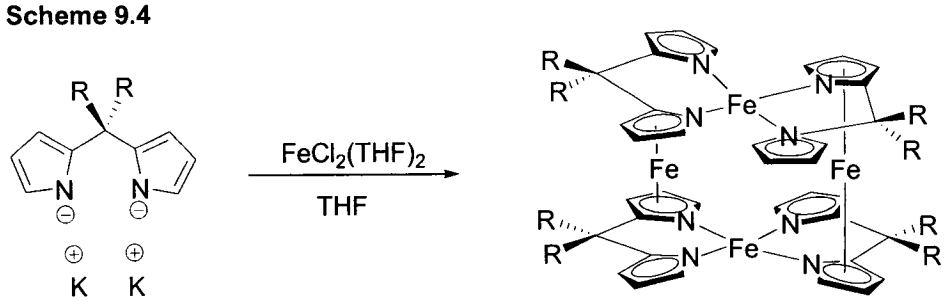

2R = -$(CH_2)_5$ -, **9.5**
R = C_2H_5, **9.6**
R = C_6H_5, **9.7**

Complex **9.5** consists of a tetrameric cyclic cluster, where the four Fe atoms are found in a planar diamond-shaped core, bridged by four dianionic ligands. Interestingly, the Fe centers occupy two completely different coordination environments. Two of the Fe atoms, located opposite one another in the tetranuclear core, adopt a similar geometry to

that seen in complex **9.3**, where each one is surrounded by two σ-bound bidentate ligands in a distorted tetrahedral geometry. The connection between the two identical units is realized by the other two Fe atoms, which are π-coordinated to two pyrrole rings from two separate metallate units in a symmetric ferrocenoid-type arrangement, thereby assembling the tetramer.

The magnetic moment of **9.5** shows only a minor variation in the temperature range 55-300 K (μ_{eff} = 7.23-7.47 μ_B). At lower temperatures the moment drops rapidly to 3.9 μ_B (Figure 9.11). Although this is a considerably large effect for a simple Zero Field Splitting, the data were nicely fitted by a d^6-d^6 model with a weak antiferromagnetic exchange (J = -0.84 cm^{-1}, g = 2.14). This is based of course on the assumption that the two metals present in a metallocenic type of arrangement are diamagnetic, which is fairly reasonable given their 18-electron configuration.

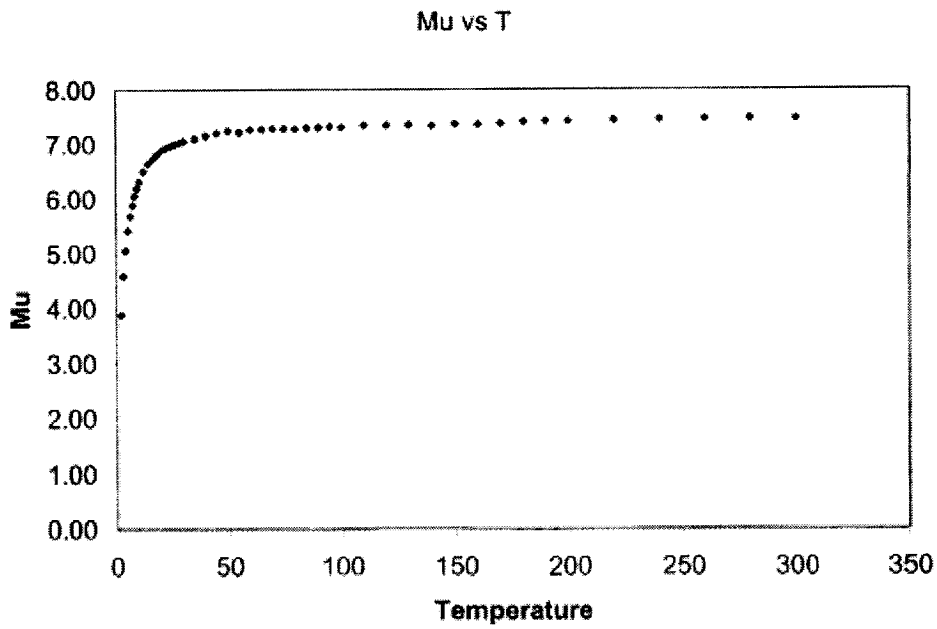

Figure 9.11. Plot of the magnetic moment of **9.5** at variable temperatures.

Formation of tetrameric Fe clusters appears to be a general reaction and does not depend on the ligand substituents. As such, compounds of the general formula $[\mu,\eta^5$-{[1,1-(2-$C_4H_3N)_2CR_2]_2Fe\}Fe]_2$ have been isolated, where R = Et (**9.6**) and C_6H_5 (**9.7**). Complexes **9.6** and **9.7** have also been characterized by X-ray diffraction and can be seen in Figures 9.4 and 9.5. A change in the electronics or sterics of the ligand substituents does

not appear to affect the assembly of the cluster, since all three tetramers adopt very similar structures.

Tetranuclear species such as these, containing two Fe atoms in different coordination environments and magnetic states, are rather unique. Although the dual bonding ability of the ligand (σ versus π) appears to be the driving force for the construction of the tetranuclear cluster, the analogous 1:1 reaction of ligand to metal with $CoCl_2(THF)_{1.5}$ does not result in the formation of a multinuclear species. In this case, the only isolable products are unreacted $CoCl_2(THF)_{1.5}$ and complex **9.4**. Therefore, the driving force for the formation of complexes **9.5-9.7** is conceivably provided by the 18 electron configuration of the two diamagnetic ferrous nodes.

In principle, the assembly of clusters due to the inherent stability provided by ferrocenoid-like Fe centers may be applied towards the production of heteropolymetallic cluster structures. With that in mind, the anionic Co-metallate (**9.4**) was reacted with one equivalent of $FeCl_2(THF)_{1.5}$ (Scheme 9.5). The reaction afforded dark orange crystals of the heterometallic $[\mu,\eta^5\text{-}\{[1,1\text{-}(2\text{-}C_4H_3N)_2C_6H_{10}]_2Co\}Fe]_2$ (**9.8**) (Figure 9.6). Not surprisingly, the measured crystallographic cell parameters are identical to those of complex **9.5**, and the bond distances and angles are also very similar. The only apparent difference was a slightly less flattened tetrahedral environment.

Scheme 9.5

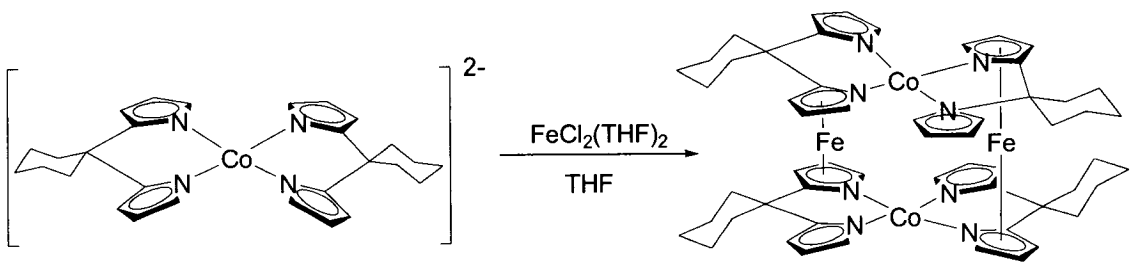

9.4 **9.8**

As expected, the identity of the metal centers in the tetramer could not be confirmed by crystallography. However, the presence of Fe and Co in the ratio 1:1 was established by X-ray fluorescence. In addition, the room T magnetic moment (μ_{eff} = 6.6 μ_B) was substantially lower than in the case of **9.5,** as expected for two divalent Co centers in a distorted tetrahedral environment with minimal magnetic exchange, thereby supporting the

idea that the two atoms present in the metallocenic type of environment are indeed two Fe atoms.

Strong support for the presence of Fe in the π-bound sites was obtained from ^{57}Fe Mössbauer spectroscopy. In collaboration with Denis Rancourt, both complexes **9.5** and **9.8** were measured at room temperature and their spectra are displayed in Figure 9.12.[11] The four-line spectrum of complex **9.5** is actually considered as two sharp symmetric doublets of equal spectral area (within experimental error of 0.6% of the total spectral area) having center shift (CS, with respect to metallic Fe at room temperature), quadrupole splitting (QS), and Lorentzian half width (G) at half maximum values of CS/QS/G = 0.52/2.51/0.126 and 0.68/1.30/0.139 mm/s. The presence of the doublets is indicative of two separate coordination environments for Fe, consistent with the X-ray structure. The distorted tetrahedral site is expected to experience larger local strain distortions than the more symmetric ferrocenoid irons, and is therefore ascribed to the doublet with broader lines (and a smaller quadrupole splitting). Interestingly, and as expected, the spectrum of **9.8** shows only the doublet of the diamagnetic ferrous nodes, with CS/QS/G = 0.50/2.46/0.129 mm/s, therefore demonstrating the absence of Fe in the tetrahedrally N-coordinated sites.

The robustness of the tetranuclear cluster was probed by attempting the reduction of **9.5** with two equivalents of Na-naphthalenide. The idea was to leave the two ferrous nodes intact while reducing the other two metal centers to the highly reactive monovalent state. In line with the behaviour of related tetranuclear clusters of low-valent samarium,[6] the cyclic structure was disrupted, affording elemental iron and the metallate **9.3**. Although the two ferrous nodes provide the stability necessary to assemble the tetranuclear structure, they are in reality the primary target of the reductant. Furthermore, the cluster could be cleaved by simple attack with coordinating solvents such as pyridine. For example, simple treatment of **9.5** with pyridine afforded a high yield of $[1,1\text{-}(2\text{-}C_4H_3N)_2C_6H_{10}]Fe(pyridine)_3$ (**9.9**). The formation of **9.9** under mild conditions implies that the ferrocenoid Fe atoms may regain the ligand system, switching from π to the σ-coordination mode.

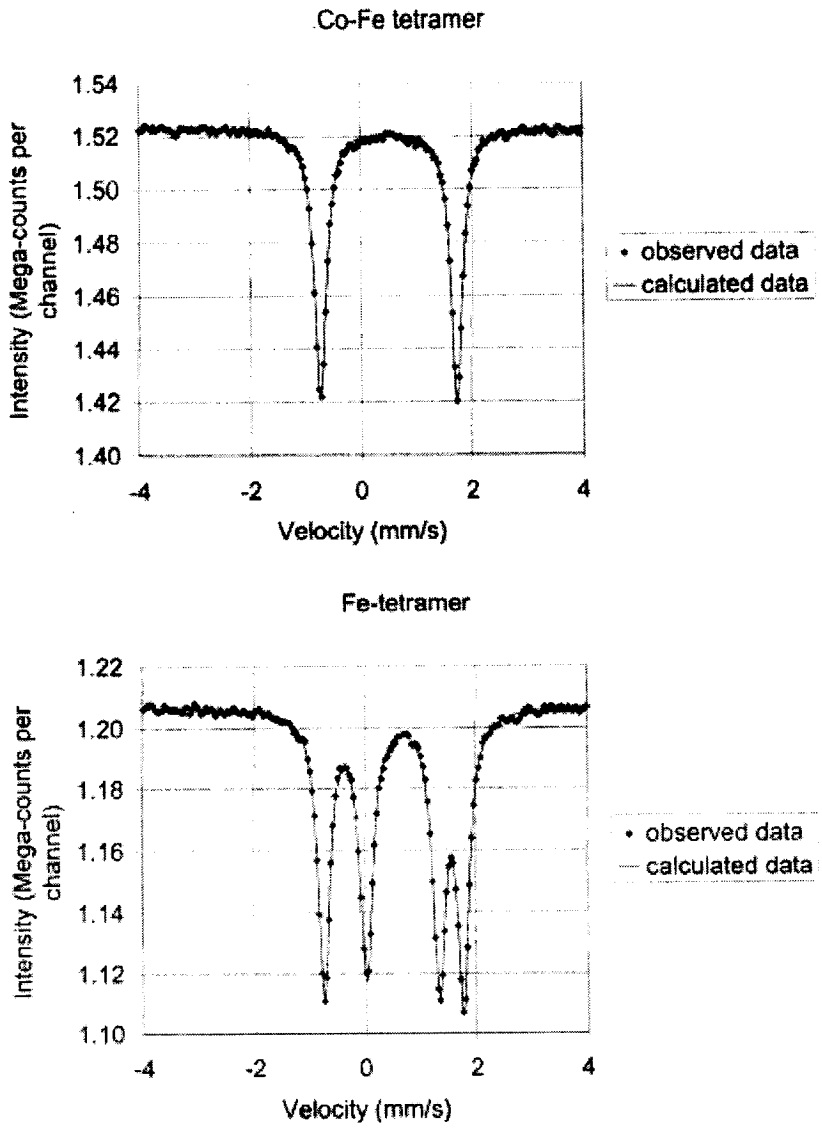

Figure 9.12. ^{57}Fe Mossbauer spectra of complexes **9.5** and **9.8**.

Unfortunately, complexes **9.3-9.9**, although structurally very interesting, are inactive for ethylene polymerization when activated by MAO at room temperature and one atmosphere of ethylene. The formation of the target molecule, a monomeric complex surrounded by only one ligand, was only possible in the presence of a suitably-stabilizing donor, such as pyridine. The coordination of three molecules of pyridine suggests the steric bulk and bi-chelating nature of the ligand are insufficient for our purposes. Therefore, expanding on the pyrrole-theme, a family of salen-pyrrole (dipyrrole-diimine) ligands was

chosen for study, shown in Chart 9.1. The results presented below are still in their preliminary form due to time constraints.

The salen-pyrrole dianion is a much larger ligand than the dipyrroles, containing four nitrogen donor atoms, two of which are pyrroles. To date, only a few complexes of this ligand system exist in the literature.[10] Three ligands were prepared by altering the substituents on the backbone, and they may be seen in Chart 9.1. Similar to the dipyrroles, the salen-pyrrole functions can be deprotonated easily with KH in THF. Reaction of one equivalent of either the ethylene or cyclohexyl derivative with $CoCl_2(THF)_{1.5}$ (Scheme 9.6) resulted in an immediate colour change from royal blue to dark reddish-brown. Dark crystals of **9.10** and **9.11** were grown from a THF solution layered with hexanes. The formulae and connectivity were determined by X-ray diffraction and representative structures can be seen in Figures 9.8 and 9.9.

Scheme 9.6

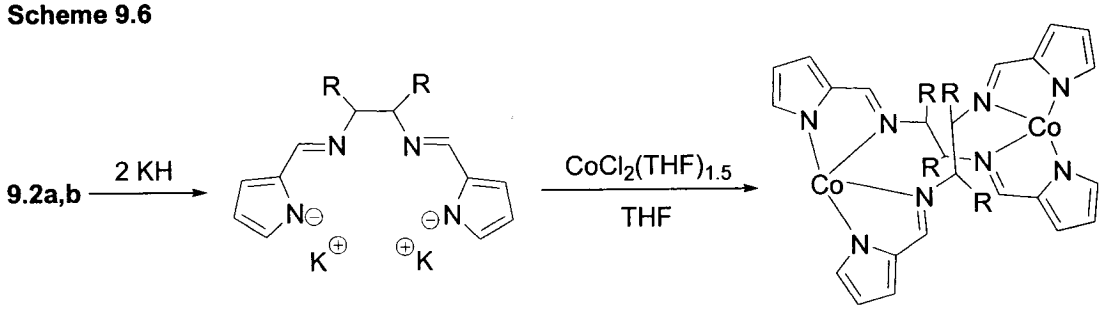

9.10: R = H
9.11: R_2 = -$(CH_2)_4$-

The backbone of the ligand is flexible enough for complexes **9.10** and **9.11** to be dimeric with two ligands, each of which surrounds two metal centers. Each cobalt atom adopts a distorted tetrahedral geometry which is relatively flattened on the outside, creating a very open face on the metal center. Although the ligands force the metal centers into close proximity, there is no interaction between them and the distance is far too great to consider a metal-metal bonding scenario. This bonding situation is similar to that seen for analogous compounds of Mg, Cu and Zn.[10c]

The structure of the Co dimer may provide the ideal scaffold for the zwitterionic Ziegler-Natta polymerization mechanism described above. Considering the ability of the

pyrrole rings to interact with more than one metal center in a variety of bonding modes, it would not be too far-fetched to envisage one or two pyrrole-π-bound $AlMe_3$ moieties per Co center. Also, there is no ligand bulk enveloping the coordinatively unsaturated metal center, leaving it susceptible for coordination of small molecules, or perhaps methylation through an $AlMe_3$ bridge. The formation of complexes **9.10** and **9.11** demonstrate the ability to form a coordinatively unsaturated neutral late metal complex bearing pyrrole functions, thereby achieving the objectives discussed above. It remains to be seen whether the complexes are inclined towards zwitterion formation, and whether they will actually be catalysts for the polymerization of ethylene.

The phenyl-backboned ligand, **9.2c**, has a delocalized π-system throughout the molecule. As such, it is expected to be very rigid and most likely not inclined to form dimers like **9.2a** and **9.2b**. Unfortunately, reactions with Fe and Co have not been promising so far. The behaviour of this ligand system has therefore been investigated with chromium. The reason for selecting chromium was based on the impressive catalytic activity observed while in combination with the bis-iminopyridine ligand. When ligand **9.2c** was deprotonated and reacted with one equivalent of $CrCl_3(THF)_3$ in THF, the mononuclear complex **9.12** was formed as dark orange crystals from a concentrated THF solution at room temperature (Scheme 9.7).

Scheme 9.7

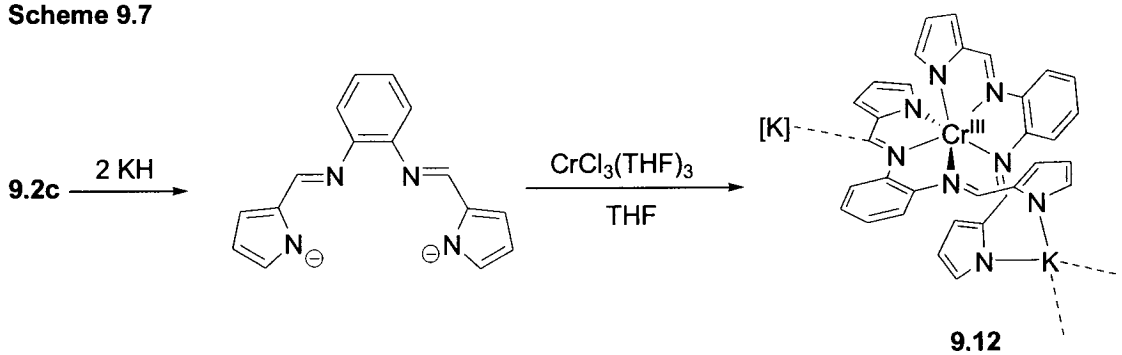

9.12

Crystal structure determination of complex **9.12** revealed the formation of a mononuclear, diligated complex (Figure 9.10) in which each ligand is meridionally κ^3-bound to the distorted octahedral metal center. The presence of a pyrrole-bound K countercation assigns the trivalent state to the Cr center.

The catalytic activity of complex **9.12** (13 μmol) was tested in a Schlenk flask at room temperature with 500 equivalents of MAO in toluene and for 30 minutes. After quenching, 0.37 g of polymer was recovered, giving a modest activity of 57 gPE/mmol·h·atm. Regardless of the decreased activity compared to the bis-iminopyridine Cr catalyst, optimized catalytic conditions, including pressurized runs, could increase the activity tremendously. However, the positive polymerization results show that the ligand system is indeed capable of supporting catalytic activity when bound to transition metals and further research is therefore promising in this area. Although complexes **9.10-9.12** have not been fully characterized, their formation is very preliminary, and very interesting, and studies are underway to test these systems (**9.10-9.12**) under varying catalytic conditions and explore their reactivity with various aluminum activators.

Conclusion

In summary, a family of late transition metal dipyrrolide complexes has been prepared. The ability of the pyrrole ligands to engage in multiple bonding modes has allowed the formation of mono- and bimetallic cluster structures. Unfortunately unsuccessful as ethylene polymerization catalysts, they are of academic interest due to the prospects of cluster compounds to engage in multimetallic cooperative activation of small molecules. Although the particular complexes described herein were ineffective towards this end, the use of Fe to assemble more highly reactive metal centers may be an attractive approach. Preliminary results also highlight the ability of the Schiff base pyrrole ligands to construct dinuclear complexes. The ability of the pyrrole ligands to engage in σ and π bonds simultaneously makes these systems extremely promising as scaffolds for the coordination of aluminum activators and formation of zwitterionic ethylene polymerization catalysts. Perhaps someday the catalytic activity of late transition metal Schiff base pyrrole compounds may rival even those of the bis-iminopyridine system.

References

(1) (a) Scott, J.; Gambarotta, S.; Korobkov, I.; Budzelaar, P. H. M. *J. Am. Chem. Soc.* **2005**, *127*, 13019. (b) See Chapter 2. (c) Scott, J.; Gambarotta, S.; Korobkov, I.; Budzelaar, P. H. M. *Organometallics* **2005**, *24*, 6298. (d) See Chapter 3. (e) Scott, J.; Gambarotta, S.; Korobkov, I.; Knijnenburg, Q.; de Bruin, B.; Budzelaar, P. H. M. *J. Am. Chem. Soc.* **2005**, *127*, 17204. (f) See Chapter 4.

(2) Scott, J.; Gambarotta, S.; Korobkov, I. *Can. J. Chem.* **2005**, *83*, 279.

(3) (a) Vidyaratne, I.; Scott, J.; Gambarotta, S.; Korobkov, I.; Duchateau, R. R. J. *Accepted in Organometallics.* (b) See also Chapter 5. (c) Vidyaratne, I.; Scott, J.; Gambarotta, S.; Budzelaar, P. H. M.; Korobkov, I. *manuscript submitted.* (d) See Chapter 7.

(4) (a) Enright, D.; Gambarotta, S.; Yap, G. P. A.; Budzelaar, P. H. M. *Angew. Chem. Int. Ed.* **2002**, *41*, 3873. (b) Sugiyama, H.; Gambarotta, S.; Yap, G. P. A.; Wilson, D. R.; Thiele, S. K.-H. *Organometallics* **2004**, *23*, 5054.

(5) (a) de Bruin, B.; Bill, E.; Bothe, E.; Weyhermüller, T.; Wieghardt, K. *Inorg. Chem.* **2000**, *39*, 2936. (b) Budzelaar, P. H. M.; de Bruin, B.; Gal, A. W.; Wieghardt, K.; van Lenthe, J. H. *Inorg. Chem.* **2001**, *40*, 4649. (c) Bart, S. C.; Chlopek, K.; Bill, E.; Bouwkamp, M. W.; Lobkovsky, E.; Neese, F.; Wieghardt, K.; Chirik, P. J. *J. Am. Chem. Soc.* **2006**, *128*, 13901. (d) Knijnenburg, Q.; Hetterscheid, D.; Kooistra, T. M.; Budzelaar, P. H. M. *Eur. J. Inorg. Chem.* **2004**, 1204.

(6) Dubé, T.; Conoci, S.; Gambarotta, S.; Yap, G. P. A.; Vasapollo, G. *Angew. Chem., Int. Ed.* **1999**, *38*, 3657.

(7) (a) Aharonian, G.; Gambarotta, S.; Yap, G. P. A. *Organometallics* **2002**, *21*, 4257; (b) Ganesan, M.; Gambarotta, S.; Yap, G. P. A. *Angew. Chem., Int. Ed.* **2001**, *40*, 766; (c) Dubé, T.; Ganesan, M.; Conoci, S.; Gambarotta, S.; Yap, G. P. A. *Organometallics* **2000**, *19*, 3716.

(8) (a) Freckmann, D. M. M.; Dubé, T.; Bérubé, C. D.; Gambarotta, S.; Yap, G. P. A. *Organometallics* **2002**, *21*, 1240; (b) Dubé, T.; Freckmann, D. M. M.; Conoci, S.; Gambarotta, S.; Yap, G. P. A. *Organometallics* **2000**, *19*, 209; (c) Dubé, T.; Conoci, S.; Gambarotta, S.; Yap, G. P. A. *Organometallics* **2000**, *19*, 115.

(9) Dubé, T.; Conoci, S.; Gambarotta, S.; Yap, G. P. A. *Organometallics* **2000**, *19*, 1182.

(10) (a) Wu, Z.; Yang, G.; Chen, Q.; Liu, J.; Yang, S.; Ma, J. S. *Inorg. Chem. Commun.* **2004**, *7*, 249. (b) Bacchi, A.; Carcelli, M.; Gabba, L.; Ianelli, S.; Pelagatti, P.; Pelizzi, G.; Rogolino, D. *Inorg. Chim. Acta* **2003**, *342*, 229. (c) Liang, L.-C.; Lee, P.-Y.; Lan, W.-L.; Hung, C.-H. *J. Organomet. Chem.* **2004**, *689*, 947. (d) Berube, C. D.; Gambarotta, S.; Yap, G. P. A. *Organometallics* **2003**, *22*, 434. (e) van Stein, G. C.; van Koten, G.; Passenier, H.; Steineback, O.; Vrieze, K. *Inorg. Chim. Acta* **1984**, *89*, 79. (f) Franceschi, F.; Guillemot, G.; Solari, E.; Floriani, C.; Re, N.; Birkedal, H.; Pattison, P. *Chem. Eur. J.* **2001**, *7*, 1468. (g) Kikuchi, T.; Kabuto, C.; Yokoi, H.; Iwaizumi, M.; Mori, W. *Chem. Commun.* **1983**, 1306. (h) Mohamadou, A.; Barbier, J. P. *Inorg. Chim. Acta* **1990**, *169*, 17. (i) Weber, J. H. *Inorg. Chem.* **1967**, *6*, 258. (j)

Stern, C.; Franceschi, F.; Solari, E.; Floriani, C.; Re, N.; Scopelliti, R. *J. Organomet. Chem.* **2000**, *593-594*, 86. (k)

(11) Scott, J.; Gambarotta, S.; Yap, G. P. A.; Rancourt, D. G. *Organometallics* **2003**, *22*, 2325.

(12) Foese, G.; Gorter, C. J.; Smits, L. J. *Constantes Selectionnes, Diamagnetisme, Paramagnetisme, Relaxation Paramagnetique;* Mason: Paris, France, **1957**.

(13) Rancourt, D. G. *Hyperfine Interact.* **1998**, *117*, 3.

(14) Blessing, R. *Acta Crystallogr.* **1995**, *A51*, 33.

(15) Sheldrick, G. M. Bruker AXS, Madison, WI, 2001.

(16) Alternate unit cell for complex **9.5**: orthorhombic, a = 20.552(3) Å, b = 19.537(2) Å, c = 14.2842(16) Å, V = 5735.4(13) Å^3.

(17) Alternate unit cell for complex **9.6**. orthorhombic, a = 35.885(3) Å, b = 16.6818(14) Å, c = 17.6981(15) Å, V = 10594.5(15) Å^3.

(18) Addison, A. W.; Rao, T. N.; Reedijk, J.; van Rijn, J.; Verschoor, G. C. *J. Chem. Soc. Dalton Trans.* **1984**, 1349. The τ parameter helps to classify the geometry of five-coordinate complexes. The τ parameter is calculated by finding the difference between the two largest angles at the metal center and dividing by 60. For a perfect square pyramidal complex, $\tau = 0$ and for a perfect trigonal bipyramidal complex, $\tau = 1$. In cases where the actual geometry is ambiguous between square pyramidal and trigonal bipyramidal, the τ parameter helps to quantify the observed distortions.

(19) Ganesan, M.; Lalonde, M. P.; Gambarotta, S.; Yap, G. P. A. *Organometallics* **2001**, *20*, 2443.

Conclusion

The original goal of this thesis, naively simple in its design, was the isolation of the active species in the bis-iminopyridine-Fe catalytic system. The only sound conclusion to be drawn regarding this objective is that the bis-iminopyridine ligand plays a significant role in the activation and polymerization mechanism of these systems. The reactivity studies completed in this thesis support any number of possible reaction mechanisms, all pivoting on the ability of the ligand to become involved in the reactivity at the metal center, via chemical or electronic transformations. The ligand backbone is susceptible to nucleophilic attack by alkylating agents, deprotonation, dimerization and even reduction, and any of these transformations may be responsible for the high degree of catalytic activity witnessed by these systems. Nevertheless, low-lying π^* orbitals appear to be at the basis of most observed transformations, and it may be this characteristic ability to accept negative charge that sets this ligand apart from the rest and turns relatively placid metal centers into highly active catalysts. Although we did not accomplish our thesis objectives by isolating the active species, results gathered from numerous chapters and separate publications led to the proposal discussed in Chapter 4. Our unusual activation and polymerization mechanism is based on the formation of a zwitterionic Al-Fe species, similar to Ziegler-Natta polymerization in the presence of a

divalent Fe alkyl, but encompassing a zwitterionic metal pair instead of a solvent-separated ion pair.

Learning from our results and applying our knowledge of the bis-iminopyridine ligand system, we can assemble a few desired characteristics necessary for the implementation of potential ligands for the zwitterionic polymerization of ethylene, including the ability to bind more than one metal center, the possibility of zwitterion formation and stability through steric hindrance at the metal center. Prospective ligands include pyrrole-based scaffolds, capable of engaging in multiple bonding modes simultaneously to assemble multimetallic structures. Preliminary results indicate polymerization is possible with Cr complexes of the larger Schiff base pyrroles but more work is necessary to explore the activation modes of these complexes in order to design a more optimal system.

Not only is this ligand beneficial for supporting ethylene polymerization catalysts, but its propensity for electron storage has resulted in the preparation of reduced complexes capable of fixating and even reducing dinitrogen. Although the electron density resides mainly on the ligand backbone, the complex undergoes reactivity as expected of a low-valent metal center. Significantly, the nature of the metal center plays a role in determining the bonding mode adopted by the dinitrogen moiety, where late transition metals (Fe and Co) are susceptible to weak, terminal fixation and earlier metals (V and Cr) show a preference for assembling end-on bridging dinitrogen complexes. The bimetallic cooperative interaction of two metal centers on one unit has allowed the reduction and partial hydrogenation of the dinitrogen moiety towards complete cleavage of the triple bond by a reduced Cr complex.

An interesting prospect for future work could involve combining the electron storage capabilities of the bis-iminopyridine ligand with a metal center known for its ability to reduce and cleave dinitrogen; namely molybdenum or tungsten. However, in its neutral state the bis-iminopyridine ligand has refrained from coordinating to larger metal centers, like the second and third row transition metals and the lanthanides. However, once reduced, or anionized through deprotonation, the ligand has been shown to engage in coordination to lanthanide metals. Therefore, the preparation of complexes in which the ligand system is already the bearer of added electron density may be the key to the

formation of second and third row transition metal complexes, which remain unexplored to this day. The availability of several oxidation states, coupled with the ligand's penchant for electrons, may be the ideal conditions for the facile transformation of dinitrogen into desired products. Considering the wealth of chemistry already provided by this ligand system, it's complexes are sure to be found in the literature for years to come.

When Brookhart and Gibson introduced Fe and Co bis-iminopyridine complexes to the world of catalysis, they were most likely unaware of the fascinating chemistry just waiting to be unearthed. Some might say their breakthrough was serendipitous, as late transition metal systems had been virtually written-off as potential catalysts for ethylene polymerization. Nonetheless, the remarkably diversified chemistry uncovered by their discovery was definitely opportune, opening a veritable "can of worms" of exciting reactivity. It is this world, full of mystery and intrigue, unexpected outcomes, strange transformations, and too many products, into which this thesis delves. At times it has been frustrating, but it has also never been dull and I am very fortunate to have been exposed to this world and had the opportunity to explore its chemistry face-to-face. The bis-iminopyridine ligand has truly become my *idée fixe*; at times haunting, always irresistible, infusing the chapters of this thesis with its allure. We may never fully understand this ligand, but hopefully we will have the chance to appreciate it for everything it has to offer. To future explorers in this area: perceived innocence is just that, always expect the unexpected.